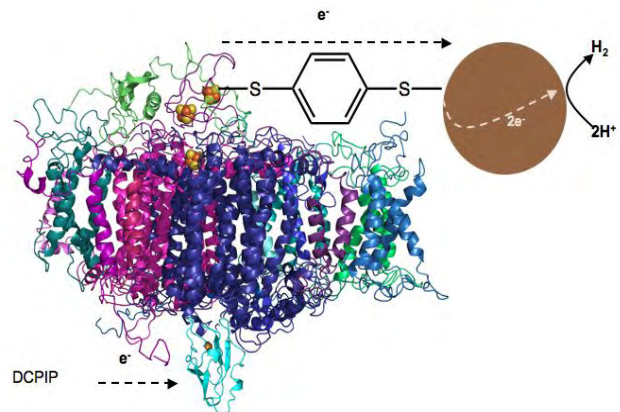
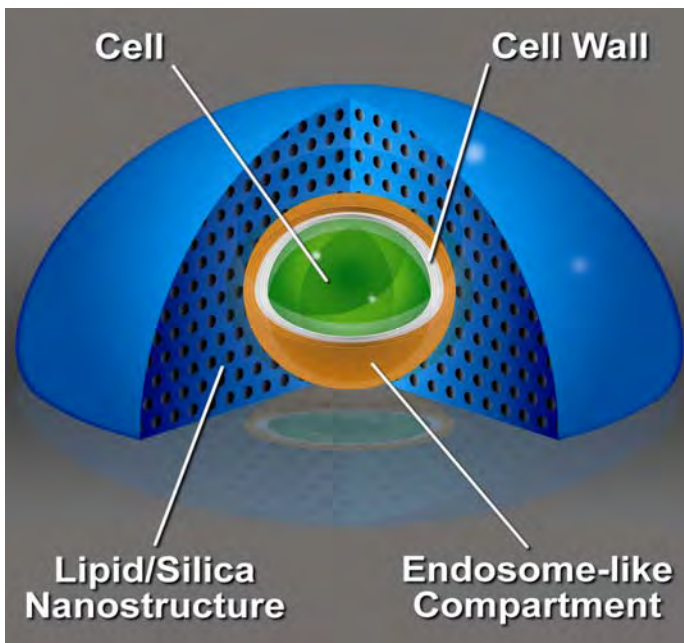
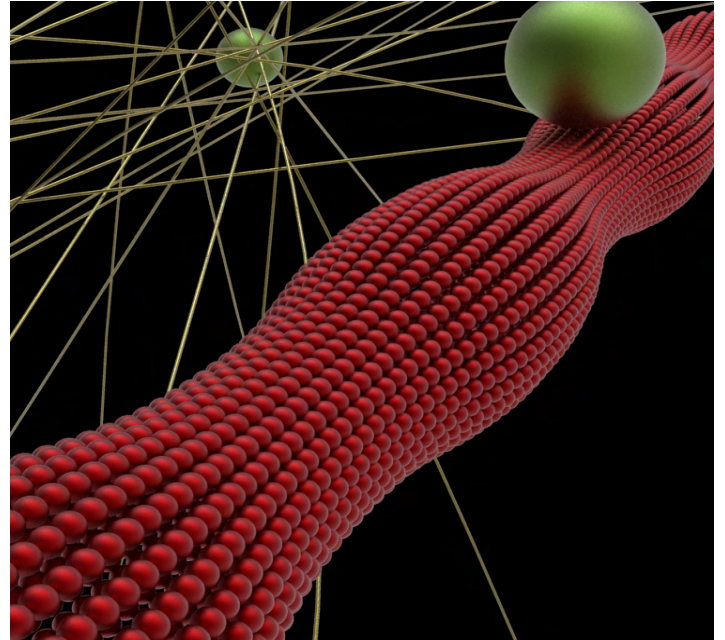
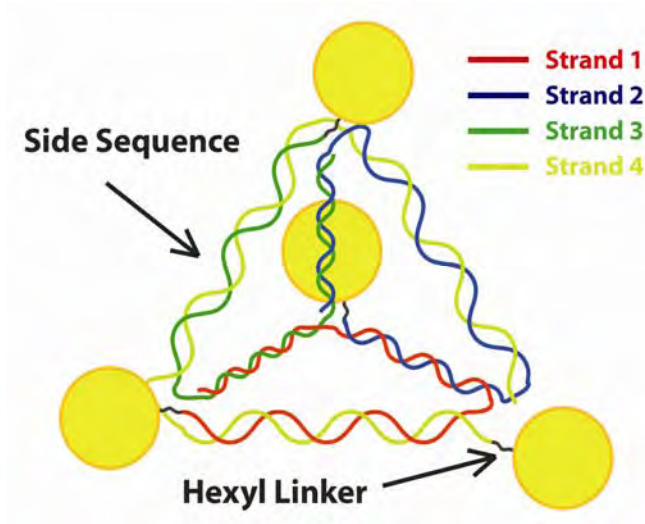


# Biomolecular Materials Contractors' Meeting–2009

October 11–14, 2009

Airlie Conference Center, Warrenton, VA



U.S. DEPARTMENT OF  
**ENERGY**

Office of Basic Energy Sciences  
Division of Materials Sciences and Engineering

## On the Cover

- Top Left: Schematic of gold nanoparticle labeled DNA pyramid formed by self-assembly.  
**Courtesy:** Sassan Sheikholeslami and Paul Alivisatos, *Lawrence Berkeley National Laboratory*
- Top Right: Single-particle fluorescence tracking shows surprisingly non-classical, non-Gaussian statistics combined with mundane Fickian displacement when colloidal beads (green) diffuse on phospholipid tubes (red) and through networks of actin filaments (beige).  
**Courtesy:** Steve Granick and Rui Lu, *University of Illinois-Urbana Champaign*
- Bottom Left: Schematic of physical system to isolate individual *S. aureus* within a nanostructured droplet and study quorum sensing at the single cell level. Self-assembly of cell plus lipids and silica precursors results in lipid multilayer localized at cell surface, mimicking features of endosomal entrapment.  
**Courtesy:** Carol Ashley and Jeff Brinker, *Sandia National Laboratories*
- Bottom Right: Photosystem I-molecular wire-Pt nanoparticle bioconjugate designed for light-driven evolution of hydrogen.  
**Courtesy:** John Golbeck and Donald Bryant, *Pennsylvania State University*

## Foreword

This volume comprises the scientific content of the 2009 Biomolecular Materials Contractors' Meeting sponsored by the Division of Materials Sciences and Engineering (DMS&E) in the Office of Basic Energy Sciences (BES) of the U. S. Department of Energy (DOE). The meeting, held on October 11–14, 2009 at the Airlie Conference Center, Warrenton, VA, is the third Contractors' Meeting on this topic and is one of several research theme-based Contractors' Meetings conducted by DMS&E. The meeting's focus is on research at the intersection of materials sciences and biology, and it also features research that cuts across several other DMS&E core research program areas where appropriate and relevant.

The Biomolecular Materials Core Research Activity (CRA) formally came into existence following the recommendations of a workshop sponsored by the Basic Energy Sciences Advisory Committee (BESAC) in 2002. The major programmatic emphasis is on exploring the molecules, processes, and concepts of the biological world that could be utilized or mimicked in designing novel materials, processes, and devices with potential energy significance in support of DOE's mission.

The purpose of the Biomolecular Materials Contractors' Meetings is to bring together researchers funded by DMS&E in this area on a periodic basis (currently once every two years), in order to facilitate the discussion of new results and research highlights, to nucleate new ideas and collaborations among the participants, and to identify new research opportunities. The meeting will also help DMS&E in assessing the state of the program, identifying new research directions, and recognizing programmatic needs. The agenda at this year's meeting exemplifies some of the major research themes covered within the broad, expanding field of biomolecular materials.

Many of the BES Contractors' Meetings are passing the quarter-century mark in longevity and are very highly regarded by their participants. We earnestly hope that the Biomolecular Materials Contractors' Meetings will continue to be just as successful and uphold this long-standing BES tradition.

It is a great pleasure to express sincere thanks to all of the meeting attendees, including the invited plenary speakers, for their active participation and sharing their ideas and new research results. The advice and help of Meeting Chairs, Anna Balazs and Jeff Brinker, in organizing this meeting are deeply appreciated. Our hearty thanks also go to Christie Ashton in DMS&E and Joreé O'Neil and her colleagues at the Oak Ridge Institute of Science and Education (ORISE) for their outstanding work in taking care of all the logistical aspects of the meeting.

Mike Markowitz and Arvind Kini  
Division of Materials Sciences and Engineering  
Office of Basic Energy Sciences  
U.S. Department of Energy

**U. S. Department of Energy**  
**Office of Basic Energy Sciences**  
***Biomolecular Materials Contractors' Meeting***  
Airlie Conference Center, Warrenton, VA  
October 11–14, 2009  
Anna Balazs and Jeff Brinker, *Meeting Chairs*

**SUNDAY, OCTOBER 11**

3:00 – 6:00 pm	Arrival and Registration
5:00 – 6:00 pm	Reception (No Host)
6:00 – 7:00 pm	***** Dinner *****
7:00 – 7:30 pm	<b>Introductory Remarks</b> Linda Horton <i>Director, Division of Materials Sciences and Engineering</i> Mike Markowitz <i>Program Manager, Biomolecular Materials</i>
<b>Session I</b>	<b>Topic: Biology as Source and Inspiration for Materials</b> <b>Chairs:</b> Anna Balazs and Jeff Brinker
7:30 – 8:00 pm	Peter Schultz, The Scripps Research Institute <i>Biopolymers Containing Unnatural Amino Acids</i>
8:00 – 8:30 pm	Dan Morse, University of California-Santa Barbara <i>Biological and Biomimetic Low-Temperature Routes to Materials for Energy Applications</i>
8:30 – 9:00 pm	Robert Ritchie, Lawrence Berkeley National Laboratory <i>Damage Tolerance in Biological Materials: Can This Be Mimicked in Engineering Structural Materials?</i>
9:00 – 9:30 pm	George Whitesides, Harvard University <i>Dynamic Self-Assembly, Emergence, and Complexity</i>
9:30 – 10:00 pm	Sheril Kirshenbaum, Duke University (Invited Plenary Lecture) <i>Unscientific America</i>
10:00 – 11:00 pm	<b>Interactions and Discussions</b>

## MONDAY, OCTOBER 12

7:00 – 8:00 am	Breakfast
8:00 – 8:30 am	Mike Markowitz/Arvind Kini <i>Highlights, Acknowledgements and Delineation</i>
<b>Session II</b>	<b>Topic: Self-Assembly and Directed Assembly</b> <b>Chair:</b> Cyrus Safinya
8:30 – 9:00 am	Sam Stupp, Northwestern University <i>Self-Assembly of Hierarchical Structures: Filaments, Artificial Cells, and Hybrids</i>
9:00 – 9:30 am	Atul Parikh, University of California-Davis and Sunil Sinha, University of California-San Diego <i>Dynamic Self-Assembly: Structure-Dynamics-Function Relations in Heterogeneous Phospholipid Bilayers</i>
9:30 – 10:00 am	John Rogers, University of Illinois-Urbana Champaign <i>Programming Function via Soft Materials</i>
10:00 – 10:30 am	***** Break *****
<b>Session III</b>	<b>Topic: Self-Assembly and Directed Assembly (Contd.)</b> <b>Chair:</b> Surya Mallapragada
10:30 – 11:00 am	Matt Francis, Lawrence Berkeley National Laboratory <i>Using Viral Capsids to Build Integrated Photocatalytic Systems</i>
11:00 – 11:30 am	Bruce Bunker, Sandia National Laboratories <i>Programmable Microtubule Assemblies</i>
11:30 – 12:00 Noon	David Deamer, University of California-Santa Cruz (Invited Plenary Lecture) <i>Biological Pores and Channels: Single Molecule Nanopore Analysis of Nucleic Acids, Exonucleases and Polymerases</i>
12:00 Noon – 1:00 pm	***** Lunch *****
1:00 – 4:00 pm	<b>Interactions and Discussions</b>
4:00 – 6:00 pm	<b>Poster Session I</b>
6:00 – 7:00 pm	***** Dinner *****

**Session IV**

**Topic: Simulation and Computational Approaches to Functional Materials**

Chair: Phillip Geissler

7:00 – 7:30 pm

Sharon Glotzer, University of Michigan  
*Strategies for Self-Assembly: Simulation Studies and Design of Tethered Nanoparticle “Shape Amphiphiles” as Building Blocks for Next-Generation Materials*

7:30 – 8:00 pm

Monica Olvera de la Cruz, Northwestern University  
*Electrostatic Driven Self-Assembly Design of Functional Nanostructures*

8:00 – 8:30 pm

Sohail Murad, University of Illinois-Chicago  
*Observation and Simulations of Transport of Molecules and Ions Across Model Membranes*

8:30 – 9:00 pm

Anna Balazs, University of Pittsburgh  
*Designing Colonies of Communicating Microcapsules that Exhibit Collective Behavior*

9:00 – 9:30 pm

Ken Showalter, West Virginia University (Invited Plenary Lecture)  
*Dynamical Quorum Sensing and Synchronization in Populations of Excitable and Oscillatory Catalytic Particles*

9:30 – 11:00 pm

*Continuation of Poster Session I*

**TUESDAY, OCTOBER 13**

7:00 – 8:00 am

Breakfast

**Session V**

**Topic: Novel Tools and Techniques for Studying Biomolecular Materials**

Chair: Geraldine Richmond

8:00 – 8:30 am

Nigel Browning, Lawrence Livermore National Laboratory and Jim DeYoreo, Lawrence Berkeley National Laboratory  
*Observing Biomolecular Materials Assembly in the Dynamic TEM*

8:30 – 9:00 am

Roger Pynn, Indiana University  
*Development of New Methods for Studying Nanostructures using Neutron Scattering*

9:00 – 9:30 am	Harald Ade, North Carolina State University and Advanced Light Source <i>Soft X-ray Imaging and Spectroscopic Tools- Organic Heterojunction Devices: Structure, Composition, and Performance at Length Scales &lt; 20 nm</i>
9:30 – 10:00 am	Charles Rosenblatt, Case Western Reserve University <i>Nanomanipulation and Optical Nanotomography of Anisotropic Fluids</i>
10:00 – 10:30 am	***** Break *****
<b>Session VI</b>	<b>Topic: Bio/Non-bio Materials Integration</b> <b>Chair:</b> Jean Fréchet
10:30 – 11:00 am	Matthew Parsek, University of Washington (Invited Plenary Lecture) <i>What is a Quorum in the “Real World”? Chemical, Physical, and Biological Parameters that Influence Quorum Sensing in Pseudomonas aeruginosa</i>
11:00 – 11:30 am	Jeff Brinker, Sandia National Laboratories <i>Molecular Nanocomposites: Biotic/Abiotic Interfaces, Materials, and Architectures</i>
11:30 – 12:00 Noon	Michael Strano, Massachusetts Institute of Technology <i>Photoelectrochemical Complexes for Solar Energy Conversion that Chemically and Autonomously Regenerate</i>
12:00 Noon – 1:00 pm	***** Lunch *****
1:00 – 4:00 pm	<b>Interactions and Discussions</b>
4:00 – 6:00 pm	<b>Poster Session II</b>
6:00 – 7:00 pm	***** Dinner *****
<b>Session VII</b>	<b>Title: Biomimetic Materials and Structures</b> <b>Chair:</b> John Golbeck
7:00 – 7:30 pm	Marc Baldo, Massachusetts Institute of Technology <i>High Efficiency Biomimetic Organic Solar Cells</i>

- 7:30 – 8:00 pm                      Zhibin Guan, University of California at Irvine  
*Biomimetic 3D Network Polymers Containing Reversibly  
Unfoldable Modules (RUMs) for Strong and Tough  
Materials*
- 8:00 – 8:30 pm                      Y. Elaine Zhu, University of Notre Dame  
*Water-Immersed Polymer Interfaces and the Roles of Their  
Materials Properties on Biolubrication*
- 8:30 – 9:00 pm                      Helmut Strey, Stony Brook University  
*Electrostatically Self-Assembled Amphiphiles*
- 9:00 – 9:30 pm                      Christine Keating, Pennsylvania State University (Invited  
Plenary Lecture)  
*Artificial Cells and Cytomimetic Environments*
- 9:30 – 11:00 pm                      ***Continuation of Poster Session II***

## **WEDNESDAY, OCTOBER 14**

- 7:00 – 8:00 am                      Breakfast
- Session VIII**                      **Topic: Biotemplated Synthesis**  
Chair: Trevor Douglas
- 8:00 – 8:30 am                      Hiroshi Matsui, CUNY, Hunter College  
*Room-Temperature Synthesis of Semiconductor Nanowires  
by Templating Collagen Triple Helices and Their Precise  
Assembly into Electrical Circuits by Biomolecular  
Recognition*
- 8:30 – 9:00 am                      Arun Gupta and Peter Prevelige, University of Alabama  
*Protein-Templated Synthesis and Assembly of  
Nanostructures for Efficient Hydrogen Production  
Using Visible Light*
- 9:00 – 9:30 am                      Sarah Heilshorn, SLAC/Stanford University  
*Protein Biotemplates for Self-Assembly of Nanostructures  
from Clathrin Materials*
- 9:30 – 10:00 am                      \*\*\*\*\* Break \*\*\*\*\*

**Session IX**

**Topic: Biomolecular Assemblies**

Chair: Steve Granick

10:00 – 10:30 am

Millicent Firestone, Argonne National Laboratory  
*Design and Synthesis of Biologically-Inspired Materials*

10:30 – 11:00 am

Andrew Shreve, Los Alamos National Laboratory  
*Molecularly Engineered Biomimetic Nanoassemblies*

11:00 – 11:30 am

Jun Liu and Greg Exarhos, Pacific Northwest National  
Laboratory  
*Molecularly Organized Nanostructural Materials*

11:30 – 12:00 Noon

Closing Remarks  
Anna Balazs and Jeff Brinker, *Meeting Chairs*  
Mike Markowitz, *Program Manager, Biomolecular  
Materials*

12:00 Noon

\*\*\*\*\* Lunch and Adjourn \*\*\*\*\*  
(Optional box lunches available)



***TABLE OF  
CONTENTS***

## Table of Contents

<b>Foreword</b> .....	i
<b>Agenda</b> .....	ii
<b>Table of Contents</b> .....	ix
 <b>Laboratory Projects</b>	
<i>DNA Directed Nanocrystals: Assemblies, Properties and Applications</i>	
<b>Paul Alivisatos, Sassan Sheikholeslami, Shelley Claridge, Alex Mastroianni Bjoern Reinhard, and Youngwook Jun</b> .....	1
<i>Collective Dynamics, Self-Assembly, and Mixing in Active Microparticle Ensembles</i>	
<b>Igor S. Aronson and Raymond E. Goldstein</b> .....	4
<i>Kinesin-Driven Dynamic Self-Assembly of Nanocomposite Rings</i>	
<b>George Bachand, Haiqing Liu, Marlene Bachand, Bruce Bunker, and Erik Spoerke</b> .....	8
<i>Functional Interfacing of Biological Components and Synthetic Materials</i>	
<b>Carolyn R. Bertozzi and Kamil Godula</b> .....	12
<i>Molecular Nanocomposites: Biotic/Abiotic Interfaces, Materials, and Architectures</i>	
<b>C. Jeffrey Brinker, Eric C. Carnes, and Carlee Ashley</b> .....	15
<i>Observing Biomolecular Materials Assembly in the Dynamic TEM</i>	
<b>N. D. Browning and J. J. DeYoreo</b> .....	19
<i>Programmable Microtubule Assemblies</i>	
<b>Erik Spoerke, George Bachand, Andrew Boal, Judy Hendricks, and Bruce Bunker</b> .....	23
<i>Design and Synthesis of Biologically-Inspired Materials</i>	
<b>Millicent A. Firestone, Sungwon Lee, Simonida Grubjesic, Omar Green, Gregory Becht, and Philip D. Laible</b> .....	27
<i>Using Viral Capsids to Build Integrated Photocatalytic Systems</i>	
<b>Matthew B. Francis</b> .....	31
<i>Bio-inspired Catalytic Assemblies</i>	
<b>Jean M. J. Fréchet</b> .....	35

<i>Biology-Inspired Programmable Assembly of Hybrid Nanosystems</i> <b>Oleg Gang and Daniel van der Lelie</b> .....	39
<i>Statistical Mechanics of Biomolecular Materials</i> <b>Phillip Geissler</b> .....	43
<i>Hybrid Static/Fluidic Synthetic Substrates to Interface Living and Nonliving</i> <b>Theobald Lohmueller, Jay T. Groves, Matt Francis, Phil Geissler, and Carolyn Bertozzi</b> .....	47
<i>Protein Biotemplates for Self-Assembly of Nanostructures from Clathrin Materials</i> <b>Sarah Heilshorn, Nicholas Melosh, Seb Doniach, and Andrew Spakowitz</b> .....	50
<i>Molecularly Organized Nanostructural Materials</i> <b>Jun Liu, Gregory J. Exarhos, Li-Qiong Wang, Yongsoon Shin, Maria Sushko, Praveen Thallapally, and Donghai Wang</b> .....	54
<i>Bioinspired Materials</i> <b>Surya Mallapragada, Mufit Akinc, George Kraus, Monica Lamm, Balaji Narasimhan, Marit Nilsen-Hamilton, Tanya Prozorov, Klaus Schmidt-Rohr, Alex Travesset, and David Vaknin</b> .....	58
<i>Directed Organization of Functional Materials at Inorganic-Macromolecular Interfaces</i> <b>Aleksandr Noy, James J. DeYoreo, Raymond W. Friddle, Nipun Misra, Julio Martinez, George Gilmer, and Matt Francis</b> .....	62
<i>Directed Self-Assembly of Soft-Matter and Biomolecular Materials</i> <b>Benjamin Ocko, Antonio Checco, Masa Fukuto, and Lin Yang</b> .....	66
<i>Damage Tolerance in Biological Materials: Can This Be Mimicked in Engineering Structural Materials?</i> <b>Robert O. Ritchie</b> .....	70
<i>Adaptive and Reconfigurable Nanocomposites</i> <b>Bruce C. Bunker, Todd M. Alam, David R. Wheeler, Dale L. Huber, Mark J. Stevens, Andrew M. Dattelbaum, Andrew P. Shreve, Darryl Y. Sasaki</b> .....	72
<i>Solid-State NMR of Complex Materials</i> <b>Klaus Schmidt-Rohr, E. M. Levin, Yan-Yan Hu, and Xueqian Kong</b> .....	76
<i>Molecularly Engineered Biomimetic Nanoassemblies</i> <b>Andrew P. Shreve, Hsing-Lin Wang, Jennifer Martinez, Srinivas Iyer, Reginaldo Rocha, James Brozik, Darryl Sasaki, Atul N. Parikh, and Sunil K. Sinha</b> .....	80
<i>Design Principles for Self-Assembly of Monomers into Tubules</i> <b>Mark J. Stevens</b> .....	84

## University Grant Projects

<i>Organic Heterojunction Devices: Structure, Composition, and Performance at Length Scales &lt; 20 nm</i> <b>Harald W. Ade</b> .....	88
<i>Nanoscale Organic Hybrid Materials (NOHMs)</i> <b>Lynden A. Archer</b> .....	92
<i>Designing Colonies of Communicating Microcapsules that Exhibit Collective Behavior</i> <b>Anna C. Balazs</b> .....	96
<i>High Efficiency Biomimetic Organic Solar Cells</i> <b>Marc Baldo and Troy Van Voorhis</b> .....	100
<i>Self Assembling Biological Springs: Force Transducers on the Micron and Nanoscale</i> <b>Natalia Kozlova, Boris Khaykovich, Aleksey Lomakin, and George B. Benedek</b> .....	104
<i>Design, Synthesis and Characterization of Novel Electronic and Photonic Biomolecular Materials</i> <b>J. K. Blasie, W. F. DeGrado, J. G. Saven, and M. J. Therien</b> .....	108
<i>Hyperbranched Conjugated Polymers and Their Nanodot Composites</i> <b>Uwe Bunz and Vincent M. Rotello</b> .....	112
<i>Protein Architecture for Photo-Catalytic Hydrogen Production</i> <b>Trevor Douglas, Mark Young, and John Peters</b> .....	116
<i>In Situ Studies of Nucleation and Assembly at Soft-Hard Interfaces</i> <b>Pulak Dutta</b> .....	120
<i>Modular Designed Protein Constructions for Solar Generated H<sub>2</sub> from Water</i> <b>P. Leslie Dutton</b> .....	124
<i>Material Lessons of Biology: Structure-Function Studies of Protein Sequences Involved in Inorganic-Organic Composite Material Formation</i> <b>John Spencer Evans</b> .....	128
<i>In Vitro Evolution of Catalysts for the Production and Utilization of Alternative Fuels</i> <b>Dan Feldheim and Bruce Eaton</b> .....	132
<i>Strategies for Self-Assembly: Simulation Studies and Design of Tethered Nanoparticle “Shape Amphiphiles” as Building Blocks for Next-Generation Materials</i> <b>Sharon C. Glotzer</b> .....	136

<i>A PS I-Molecular Wire-H<sub>2</sub>ase Construct for Light-Induced H<sub>2</sub> Generation</i> <b>John H. Golbeck and Donald A. Bryant</b> .....	140
<i>Structured, Stabilized Phospholipid Vesicles</i> <b>Steve Granick</b> .....	144
<i>Biomimetic 3D Network Polymers Containing Reversibly Unfoldable Modules (RUMs) for Strong and Tough Materials</i> <b>Zhibin Guan</b> .....	148
<i>Protein-Templated Synthesis and Assembly of Nanostructures for Efficient Hydrogen Production Using Visible Light</i> <b>Arunava Gupta and Peter E. Prevelige</b> .....	152
<i>Virus Assemblies as Templates for Nanocircuits</i> <b>Michael T. Harris and James N. Culver</b> .....	156
<i>Designing Two-Level Biomimetic Fibrillar Interfaces</i> <b>Anand Jagota and Chung-Yuen Hui</b> .....	160
<i>(Bio)Chemical Tailoring of Biogenic 3-D Nanopatterned Templates with Energy-Relevant Functionalities</i> <b>Nils Kröger and Kenneth H. Sandhage</b> .....	164
<i>Structure-Property Relationships of Polymer Brushes in Restricted Geometries and Their Utilization as Ultra-Low Lubricants</i> <b>Tonya L. Kuhl and Roland Faller</b> .....	168
<i>Structure and Dynamics of Vesicles in Solution</i> <b>Erik Luijten</b> .....	172
<i>Room-Temperature Synthesis of Semiconductor Nanowires by Templating Collagen Triple Helices and Their Precise Assembly into Electrical Circuits by Biomolecular Recognition</i> <b>Hiroshi Matsui</b> .....	175
<i>Biological and Biomimetic Low-Temperature Routes to Materials for Energy Applications</i> <b>Daniel E. Morse</b> .....	179
<i>Observation and Simulations of Transport of Molecules and Ions across Model Membranes</i> <b>Sohail Murad and Cynthia Jameson</b> .....	183
<i>Electrostatic Driven Self-Assembly Design of Functional Nanostructures</i> <b>Graziano Vernizzi, Samuel I. Stupp, Michael J. Bedzyk, and Monica Olvera de la Cruz</b> .....	187

<i>Dynamic Self-Assembly: Structure-Dynamics-Function Relations in Heterogeneous Phospholipid Bilayers</i> <b>Atul N. Parikh and Sunil K. Sinha</b> .....	191
<i>Development of New Methods for Studying Nanostructures using Neutron Scattering</i> <b>Roger Pynn</b> .....	195
<i>Wet Interfaces: Developing a Molecular Framework for Understanding the Behavior of Materials in Aqueous Solutions</i> <b>Geraldine L. Richmond</b> .....	199
<i>Programming Function via Soft Materials</i> <b>John A. Rogers</b> .....	203
<i>Nanomanipulation and Optical Nanotomography of Anisotropic Fluids</i> <b>Charles Rosenblatt</b> .....	207
<i>Miniaturized Hybrid Materials Inspired by Nature</i> <b>C. R. Safinya, Y. Li, and K. Ewert</b> .....	211
<i>Bio-gating a Physical Nanosystem by Metabolic Activity of Microorganisms</i> <b>Ravi F. Saraf</b> .....	215
<i>Biopolymers Containing Unnatural Amino Acids</i> <b>Peter G. Schultz</b> .....	219
<i>Theoretical Research Program on Bio-inspired Inorganic Hydrogen Generating Catalysts and Electrodes</i> <b>Annabella Selloni and Roberto Car</b> .....	223
<i>Photoelectrochemical Complexes for Solar Energy Conversion that Chemically and Autonomously Regenerate</i> <b>Michael S. Strano, Stephen G. Sligar, Colin A. Wraight</b> .....	227
<i>Electrostatically Self-Assembled Amphiphiles</i> <b>Helmut H. Strey and Vesna Stanic</b> .....	231
<i>Self-Assembly of Hierarchical Structures: Filaments, Artificial Cells, and Hybrids</i> <b>Samuel I. Stupp</b> .....	235
<i>Water-Immersed Polymer Interfaces and the Roles of Their Materials Properties on Biolubrication</i> <b>Y. Elaine Zhu</b> .....	239

<i>Dynamic Self-Assembly, Emergence and Complexity</i> <b>George M. Whitesides</b> .....	243
---	-----

**Invited Talks**

<i>Single Molecule Nanopore Analysis of Nucleic Acids, Exonucleases and Polymerases</i> <b>David Deamer and Mark Akeson</b> .....	247
--	-----

<i>Artificial Cells and Cytomimetic Environments</i> <b>Christine D. Keating</b> .....	251
---	-----

<i>Unscientific America</i> <b>Sheril Kirshenbaum</b> .....	252
--	-----

<i>What is a Quorum in the “Real World”? Chemical, Physical, and Biological Parameters that Influence Quorum Sensing in Pseudomonas aeruginosa</i> <b>Matthew R. Parsek</b> .....	253
--	-----

<i>Dynamical Quorum Sensing and Synchronization in Populations of Excitable and Oscillatory Catalytic Particles</i> <b>Kenneth Showalter</b> .....	254
---	-----

<b>Author Index</b> .....	256
---------------------------	-----

<b>Participant List</b> .....	257
-------------------------------	-----



***LABORATORY  
PROJECTS***

# DNA Directed Nanocrystals: Assemblies, Properties and Applications

Paul Alivisatos, Sassan Sheikholeslami, Shelley Claridge, Alex Mastroianni,  
Bjoern Reinhard, Youngwook Jun

University of California Berkeley  
Department of Chemistry  
Berkeley, CA 94720-1460

Lawrence Berkeley National Laboratory  
Materials Science Division  
Berkeley, CA 94720

[PAAlivisatos@lbl.gov](mailto:PAAlivisatos@lbl.gov), [SNSheikholeslami@lbl.gov](mailto:SNSheikholeslami@lbl.gov)

**Program Scope:** The goals of this project are to further the fundamental understanding and develop applications of DNA directed nanocrystal assemblies. We are developing solution based processes for the biomolecular assembly of nanocrystals with increasing complexity. Our methods for preparing and studying the physical properties of these assemblies include: gel electrophoresis, high performance liquid chromatography, single particle darkfield scattering spectroscopy, and small angle x-ray scattering. We are studying the applicability of these assemblies as bio-sensors for in vitro and live cell studies.

**Recent Progress:** Metal and semiconductor nanocrystals are the subject of intense research activity across the fields of chemistry, physics, biology and materials science. In particular, the optical and electronic properties of these materials are attractive for a range of applications including: single electron transistors, advanced photonic devices, and extremely sensitive biosensors. In order to exploit the unique properties of these nanocrystals, reliable methods for precise assembly of single nanocrystals into more complicated structures is required. To that end, we focus on the DNA directed assembly of nanocrystals into higher order structures, where the resultant properties are a function

of the ordering and coupling between adjacent particles.

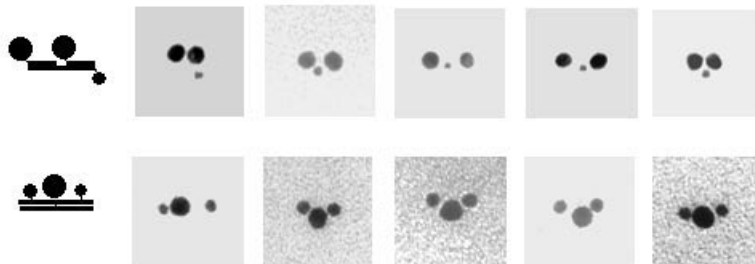
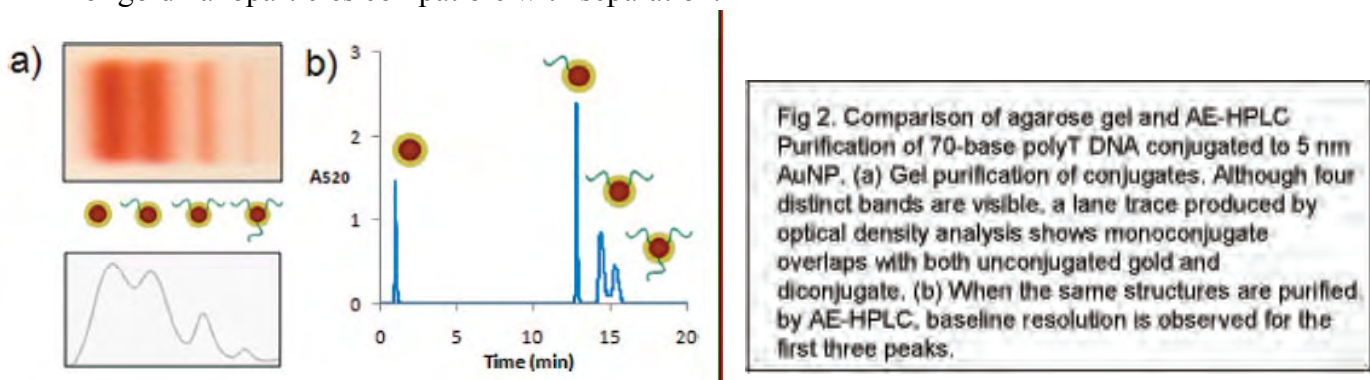


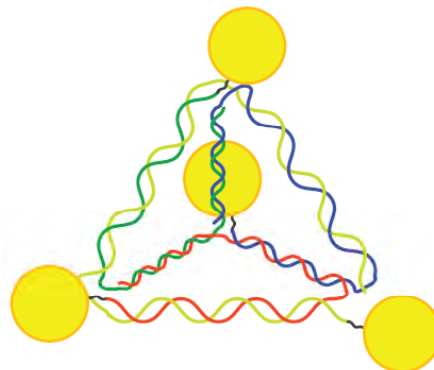
Fig. 1. Examples of 5 and 10 nm diameter Au nanocrystals grouped together by DNA

One major area of focus in our lab is the synthesis and isolation of metal nanoparticles functionalized with discrete numbers of single-stranded DNA molecules. These nanoparticle-DNA (NP-DNA) conjugates serve as the elementary building blocks for the creation of topologically connected structures in any geometry permitted by the Watson-Crick base pairing capabilities of the templating DNA molecules. Earlier work in our group focusing on the electrophoretic isolation of NP-DNA conjugates was recently extended by the use of high performance liquid chromatography (HPLC). HPLC is a general analytical separation technique that makes use of the differential interaction between the analytes of interest and the column packing material. We used an ion-exchange column and a salt gradient procedure to separate a mixture of NP-DNA conjugates into bands corresponding to nanoparticles with exact numbers of DNA molecules covalently attached. The HPLC technique proved capable of separating NP-DNA conjugates with higher resolution than electrophoresis and extended the size range of gold nanoparticles compatible with separation.



The analytical separation techniques pioneered in our group are critical to the self-assembly of higher order structures with designed functionalities. One example of this is our ongoing development of a new kind of molecular ruler based on the plasmon coupling between adjacent metal nanoparticles. In a manner similar to Fluorescence Resonance Energy Transfer (FRET), the nanoparticle rulers report the end to end distance of a biomolecule of interest based on the light scattering properties of the nanoparticles. Our “plasmon ruler” has been used to study, at the single molecule level, the hybridization kinetics of DNA, the bending and cleavage kinetics of the restriction enzyme EcoRV, and the signaling processes involved in cellular apoptosis.

More recent progress in the self-assembly of nanoparticles by DNA into three dimensional structures is exemplified in our work on DNA nanoparticle pyramids. These pyramid structures were synthesized with 4 different sizes of particles at each junction, and also in the 2 different stereoisomers, R and S. These results suggest that we might be able to synthesize optically active nanoparticle systems for potential use in high performance optical filters.



**Future Plans:** We will continue to explore and design more complicated three dimensional nanoparticle-DNA structures with unique optical properties. The NP-DNA pyramids will be expanded upon and constructed with larger gold and silver nanoparticles to enhance the optical activity of the structure. Also, we will pursue our work on plasmon rulers, focusing on 3D structures constructed with metal nanoparticles for the purpose of creating a molecular ruler that can sense orientational changes in addition to distance changes. Furthermore, the plasmon rulers will be used in more live cell studies to evaluate the potential for long term stable imaging of cellular events.

**Publications 2007-2009:**

Claridge, S.A., et al., *Isolation of discrete nanoparticle - DNA conjugates for plasmonic applications*. Nano Letters, 2008. 8(4): p. 1202-1206.

Claridge, S.A., et al., *Enzymatic ligation creates discrete multinanoparticle building blocks for self-assembly*. Journal of the American Chemical Society, 2008. 130(29): p. 9598-9605.

Reinhard, B.M., et al., *Use of plasmon coupling to reveal the dynamics of DNA bending and cleavage by single EcoRV restriction enzymes*. Proceedings of the National Academy of Sciences of the United States of America, 2007. 104(8): p. 2667-2672.

Mastroianni, A.J., S.A. Claridge, and A.P. Alivisatos, *Pyramidal and Chiral Groupings of Gold Nanocrystals Assembled Using DNA Scaffolds*. Journal of the American Chemical Society, 2009. 131(24): p. 8455-8459.

Mastroianni, A., et al., *Probing the Conformational Distributions of Sub-Persistence Length DNA*. Biophysical Journal, 2009  
(In Press).

Jun, Y., et al., *Continuous imaging of plasmon rulers in live cells reveals early stage caspase-3 activation at the single molecule level*. Proceedings of the National Academy of Sciences of the United States of America (Submitted), 2009.

## Collective Dynamics, Self-Assembly, and Mixing in Active Microparticle Ensembles

Igor S. Aronson, Materials Science Division, Argonne National Laboratory, 9700 S Cass Av, Argonne, IL60439, [aronson@msd.anl.gov](mailto:aronson@msd.anl.gov)

Raymond E. Goldstein, Department of Applied Mathematics and Theoretical Physics, Centre for Mathematical Sciences, University of Cambridge, Wilberforce Road, CB3 0WA, United Kingdom [R.E.Goldstein@damtp.cam.ac.uk](mailto:R.E.Goldstein@damtp.cam.ac.uk)

**Program Scope.** This project focuses on the emergent coherent dynamics found in ensembles of active microparticles at high volume fraction, where recent experiments have revealed novel, large-scale coherent structures which arise from hydrodynamic interactions between the particles. These structures are found in two complementary systems - electromagnetically-driven metallic microparticles and self-propelled microorganisms such as bacteria and algae. They provide fundamental challenges to our understanding of collective flows, mixing, and transport in nonequilibrium systems. High-speed imaging, particle imaging velocimetry, optical coherence tomography, and microrheology are used to characterize the dynamics and correlations in these systems, to provide benchmarks for the refinement of theories of such behavior, and to explore possible applications in nanoscale self-assembly, microfluidic mixing, and targeted drug delivery. Current activities include experimental and theoretical studies of the properties of collective behavior in ensembles of the swimming bacterium *Bacillus subtilis* in the confined geometry of thin film samples, viscosity of bacteria-laden fluids, and fundamental studies of flagella-driven flows, mixing and transport in unicellular and multicellular algae. Future directions encompass ac-microrheology of bacterial films, rectification of chaotic bacterial motion, mechanism of active transport of melanosomes, dynamics of metachronal waves, quorum sensing, flagellar synchronization.

### Recent progress

**Enhanced Transport.** High-resolution optical coherence tomography is used to study the onset of a large-scale convective motion in free-standing thin films of adjustable thickness containing suspensions of swimming aerobic bacteria *Bacillus subtilis*. Clear evidence is found that beyond a threshold film thickness there exists a transition from quasi-two-dimensional collective swimming to three-dimensional turbulent behavior, see Fig. 1a. The latter state, qualitatively different from bioconvection in dilute bacterial suspensions, is characterized by enhanced diffusivities of oxygen and bacteria [4]. These results emphasize the impact of self-organized bacterial locomotion on the onset of three-dimensional dynamics, and suggest key ingredients necessary to extend standard models of bioconvection to incorporate effects of large-scale collective motion. Using *Chlamydomonas* swimming algae, we have completed a precise and controlled study of the statistics of enhanced diffusion of tracer particles, with particular emphasis on the probability distribution function of particle displacements [13]. We find a novel self-similar form to the time-dependent pdfs which includes exponential tails (often seen in the study of turbulent flows), and systematics with concentration that are amenable to theoretical analysis. The role of unsteadiness in the flows is clear, a point that overturns conventional wisdom in the marine biology context of suspension feeding.

**Viscosity reduction.** Measurements of the shear viscosity in suspensions of swimming *Bacillus subtilis* in free standing liquid films have revealed that the viscosity can decrease by up to **a factor of seven** compared to the viscosity of the same liquid without bacteria or with non-motile bacteria [3]. The reduction in viscosity is observed in two complimentary experiments: one studying the decay of a large vortex induced by a moving microprobe and another measuring the viscous torque on a rotating magnetic particle immersed in the film (see Fig. 1b). The viscosity depends on the concentration and swimming speed of the bacteria which is in turn controlled by the concentration of oxygen permeating the liquid film. The viscosity reduction is attributed to the effect of self-propulsion of swimming bacteria and reorientation due to applied shear flow, Fig. 1c. We derive the effective viscosity of dilute suspensions of such bacteria. An individual bacterium propels itself forward by rotating its flagella and reorients itself randomly by tumbling [5,6]. Due to the bacterium's asymmetric shape, interactions with a prescribed generic (such as pure shear or planar shear) background flow cause the bacteria to preferentially align in directions in which self-propulsion produces a significant reduction in the effective viscosity, in agreement with recent experiments.

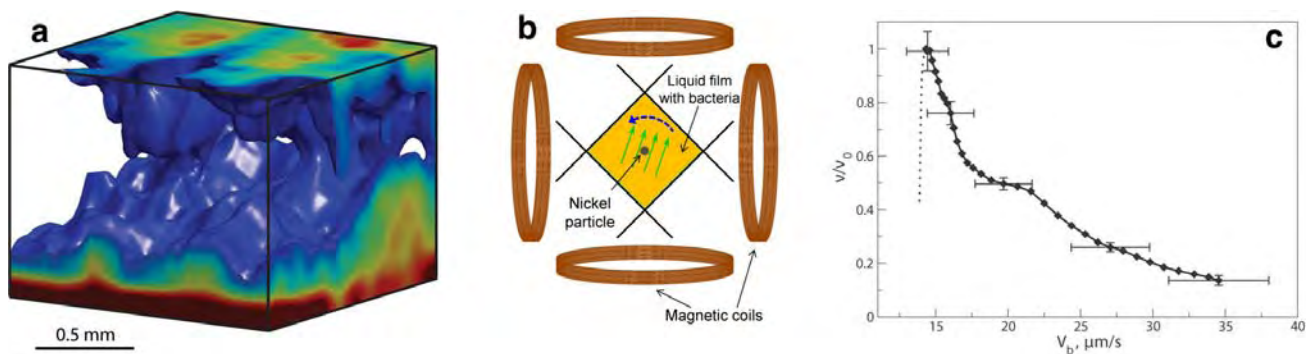


**Figure 1.** (a) Three-dimensional scan of the bacterial concentration obtained by optical coherence tomography. (b). Schematics of bacterial microrheometer: a thin liquid film containing a bacterial suspension and submersed *Nickel* microparticle spanning between four movable fibers. Two pairs of magnetic coils create a rotating magnetic field (four green arrows). (c) Results of measurements: viscosity  $\nu$  vs. speed of the bacteria  $V_b$ ,  $\nu_0$  is viscosity of solution of immobilized bacteria.

**Hydrodynamic bound states:** In the process of searching for hydrodynamic interactions between swimming multicellular algae we accidentally discovered [11] the existence of bound states of these organisms (see Fig. 2). These orbiting pairs of *Volvox* are held together by a fluid dynamical effect associated with proximity to a wall, a process that can be completely understood analytically through a combination of singularity methods and lubrication theory in Stokes flow. The existence of these states, which can include hundreds of organisms, may have a biological consequence in facilitating fertilization during the sexual phase of their life cycle.

**Flagellar synchronization:** One of the outstanding problems in eukaryotic cell biology is the nature of flagellar synchronization, a dynamics that underlies many important biological functions ranging from development to respiratory function, reproduction, and eye functioning. Using the model organism *Chlamydomonas reinhardtii* we have studied this problem in great detail and have discovered some remarkable phenomena [11]. We found that a single cell stochastically switches back and forth between synchronous and asynchronous beating of its two flagella, that synchronous and asynchronous beating result in straight-line motion and abrupt turns, respectively, and that as a consequence a cell population diffuses in much the same manner as peritrichously flagellated bacteria which execute “run-and-tumble” locomotion. These results also serve to highlight the role of biochemical noise in the synchronization dynamics of eukaryotic flagella.



**Figure 2.** Two colonies of the multicellular algae *Volvox carteri* orbiting each other in a hydrodynamic bound state near a glass surface. These are viewed from above, swimming up against the surface. Overlaid images several seconds apart depict the sense and speed of rotation

### Future Plans

Argonne group will focus on ac-microrheology of bacterial films. We anticipate nontrivial elastic properties of the bio-suspension and will study the dynamics of bacterial suspensions in systems of different sizes (from 50 microns to 2 mm) confined in fluid films (open film geometry) and thin microchannels. We also plan to explore the dynamics of self-starting bacterial micromotors. These micromotors are asymmetric 100-200 micron microgears immersed in the suspensions of swimming bacteria. According to recent theoretical predictions, these microgears can be set into desired rotational motion due to rectification of the bacterial chaotic motion. We plan to fabricate these microgears using soft lithography method.

We plan to initiate a new research direction: fundamental aspects of active transport and emergent behavior in model biomolecular system consisting of polar filaments and molecular motors. This model system includes nature-provided bio-assay based on the melanophore cells, the skin cells found in frogs and some fish. These cells contain pigment spherical organelles termed melanosomes (typical size is of the order of  $0.5 \mu\text{m}$ ). The melanophores are able to redistribute these melanosomes along microtubules and actin filaments. The advantage of this system is that primary biological mechanisms of movement of melanosomes along microtubules and actin filaments are well-characterized. The fundamental questions to address: the mechanism of correlated motion of the organelles and their relation with kinetics of the molecular motors. .

Cambridge group will focus on two main thrusts to the next stage of research. The first concerns the phenomenon of “metachronal waves,” which are long-wavelength modulations of the beating patterns of flagellated organisms. These have been known for decades, but not well understood at all. We have recently discovered that *Volvox* colonies display such waves and afford a particularly good context for systematic study. At the same time, a preliminary theoretical analysis suggests the importance of unsteady effects within the Stokes equation. The second thrust involves the phenomenon of quorum sensing in bacterial systems, wherein bacteria secrete and detect chemicals and can determine from the concentration exterior to the cell when they are among others. When the external concentration exceeds a threshold it can trigger a change in behavior. Our studies of collective dynamics and mixing in bacterial suspensions suggest a potentially important role for these processes in the spread of quorum sensing signals, and we are gearing up for experiments and theory to ascertain their significance.

#### **DOE Sponsored Publications in 2008-2009.**

1. **Self-Assembled Magnetic Surface Swimmers**, A. Snezhko, M. Belkin, I. S. Aranson, and W.-K. Kwok, *Phys. Rev. Lett.* **102**, 118103 (2009)
2. **Magnetically Driven Surface Mixing**, M. Belkin, A. Snezhko, I. S. Aranson, and W.-K. Kwok, *Phys. Rev. E* **80**, 011310 (2009)
3. **Reduction of viscosity in suspension of swimming bacteria**, A. Sokolov and I.S. Aranson, submitted to *Phys. Rev. Lett.* (2009)
4. **Enhanced mixing and spatial instability in concentrated bacterial suspensions**, A. Sokolov, F.I. Feldchtein, R.E. Goldstein, and I.S. Aranson, *Phys. Rev E* (2009)
5. **Effective viscosity of dilute bacterial suspensions: a two-dimensional model**, B. M. Haines, I. S. Aranson, L. V. Berlyand, and D.A. Karpeev, *Phys. Biology*, **5**, 046003 (2008)
6. **Three-dimensional model for the effective viscosity of bacterial suspensions**, B. M. Haines, A. Sokolov, I. S. Aranson, L. V. Berlyand, and D.A. Karpeev, submitted to *Phys. Rev. E.* (2009)
7. **A Model of Hydrodynamic Interaction Between Swimming Bacteria**, V. Gyrya, I. S. Aranson, L. V. Berlyand and D. A. Karpeev, *Bulletin of Mathematical Biology*, DOI 10.1007/s11538-009-9442-6 (2009)
8. **Microfluidics of Cytoplasmic Streaming and its Implications for Intracellular Transport**, R. E. Goldstein, I. Tuval, and J.-W. van de Meent, *Proceedings of the National Academy of Sciences USA* **105**, 3663 (2008).
9. **Nature's Microfluidic Transporter: Rotational Cytoplasmic Streaming at High Péclet Numbers**, J.-W. van de Meent, I. Tuval, R. E. Goldstein, *Phys. Rev. Lett.* **101**, 178102 (2008).
10. **How to Track Protists in Three Dimensions**, Knut Drescher, Kyriacos Leptos, and Raymond E. Goldstein, *Review of Scientific Instruments* **80**, 014301 (2009).
11. **Dancing *Volvox*: Hydrodynamic Bound States of Swimming Algae**, K. Drescher, K. Leptos, T. Ishikawa, T. J. Pedley, R. E. Goldstein, *Phys. Rev Lett.* **102**, 168101 (2009).
12. ***Chlamydomonas* Swims With Two ‘Gears’ in a Eukaryotic Version of Run-and-Tumble Locomotion**, M. Polin, I. Tuval, K. Drescher, J.P. Gollub, R. E. Goldstein, *Science* **325**, 487 (2009).
13. **Dynamics of Enhanced Tracer Diffusion in Suspensions of Eukaryotic Microorganisms**, Kyriacos C. Leptos, Jeffrey S. Guasto, Jerry P. Gollub, Adriana I. Pesci, and Raymond E. Goldstein, *submitted* (2009).

# Kinesin-driven dynamic self-assembly of nanocomposite rings

George Bachand, Haiqing Liu, Marlene Bachand, Bruce Bunker, Erik Spoerke  
gdbacha@sandia.gov, bcbunke@sandia.gov, edspoer@sandia.gov  
Sandia National Laboratories, Albuquerque, NM 87185

## Program Scope

Complex nanomaterials formed through self-assembly are ubiquitous in living systems.<sup>1</sup> While many of these structures are static,<sup>2</sup> there is also a plethora of biological materials that exhibit emergent properties such as adaptive or quasi-intelligent behaviors and self-replication.<sup>3,4</sup> Such materials rely on dynamic self-assembly processes where structural organization is directly dependent on the amount energy distributed in the system, and often driven by the dissipation of chemical energy in enzymatic reactions. For example, dynamic instability (i.e., spontaneous assembly/disassembly) of microtubule filaments (MTs) within a cell is regulated by the catalysis of guanosine triphosphate (GTP), and enables the cell to continuously reconfigure the MT networks based on changing physiological needs.<sup>5</sup> The power of such dynamic assembly processes in biological systems has spurred considerable interest in the understanding and applications of such processes for developing advanced nanomaterials.

Our overall project, *Active Assembly of Dynamic and Adaptable Materials*, examines fundamental materials science issues at the intersection of biology, nanomaterials, and integrated systems. More specifically, research activities involve the exploitation of active biomolecules to perform tasks associated with living materials including the active transport, assembly, reconfiguration, healing, and disassembly of nanomaterials. Organisms use cooperative interactions between motor proteins (e.g., kinesin) and MTs for processes ranging from cell division to melanophore reorganization. Our work is focused on understanding and exploiting energy-consuming proteins (i.e., tubulin and kinesin) to assemble synthetic nanomaterials into complex structures that are not constrained by limitations associated with standard diffusion or equilibrium processes. This abstract will specifically discuss recent work on a project subtask focused on nanocomposites formed through kinesin-driven dynamic self-assembly.

## Recent Progress

Self-assembly of nanostructured materials through energy-dissipating process has been well-documented in Nature. We reported an interesting phenomenon in which nanocomposite ring structures (Fig. 1) self-assemble from the interaction of biotinylated MT filaments (bMTs) and streptavidin-coated quantum dots (QDs).<sup>6</sup> The overall assembly principles in this system closely mimic biological self-assembly, in which energy-dissipating and thermodynamic components drive the self-assembly. Under conditions of thermal equilibrium, QDs and bMTs self-assemble into

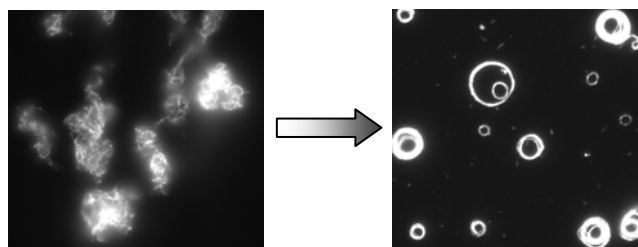


**Fig. 1: Assembly of nanocomposite rings.** In the absence of kinesin transport, biotinylated MT filaments and streptavidin-coated QDs form random aggregate structures (left). In contrast, ordered ring structures emerge (right) when MTs are being transported by kinesin and streptavidin-coated QDs are introduced.

disordered, aggregate structures (Fig. 1, left). When kinesin transport is added to the system, bMTs and QDs self-assemble into ordered ring structures (Fig. 1, right), based on a balanced interaction between thermodynamic (i.e., biotin-streptavidin bond formation) and energy-dissipating (i.e., kinesin-based transport) processes. The ring nanocomposites store considerable elastic energy based on the relatively high stiffness of the MTs, which possess an intrinsic flexural rigidity ( $\kappa = 2.0 \times 10^{-24} \text{ N m}^2$ ;  $L_p = \sim 500 \mu\text{m}$ ). The measured size of the ring structures ranged from 2.5 to 11  $\mu\text{m}$ , with an average inner and outer diameter of  $3.4 \pm 0.2 \mu\text{m}$  and  $5.2 \pm 0.2 \mu\text{m}$ , respectively. Using these averages, a typical composite stores  $\sim 33,000 K_B T$  (135 aJ) in elastic energy.

#### Mechanism of self-assembly

We recently described the nucleation and growth mechanism by which the ring nanocomposite self-assembles.<sup>6</sup> Nucleation is initiated by the introduction of QDs to actively moving bMTs, which serves to “glue” together bMTs into extended oligomeric structures (Figure 2i). These structures continue to be transported by kinesin motors, but also rotate axially based on the intrinsic helicity of a sub-set of bMT filaments. Rotation drives the formation of kinked and coiled domains (Figure 2ii) that induce mechanical strain and bending (Fig. 2iii) of the QD-bMTs. The bent oligomers then form closed rings and continue rotation. Ring growth proceeds as QD-bMTs collide with existing rings and are wound up (Fig. 2iv) into larger and larger structures (Fig. 2v).

#### Kinetics of self-assembly and disassembly

The nanocomposite rings represent non-equilibrium structures that self-assemble and self-disassemble. Self-assembly (nucleation and growth) of the ring nanocomposite occurs immediately upon addition of QDs, and ceases at  $\sim 15$  min following QD addition, marking a

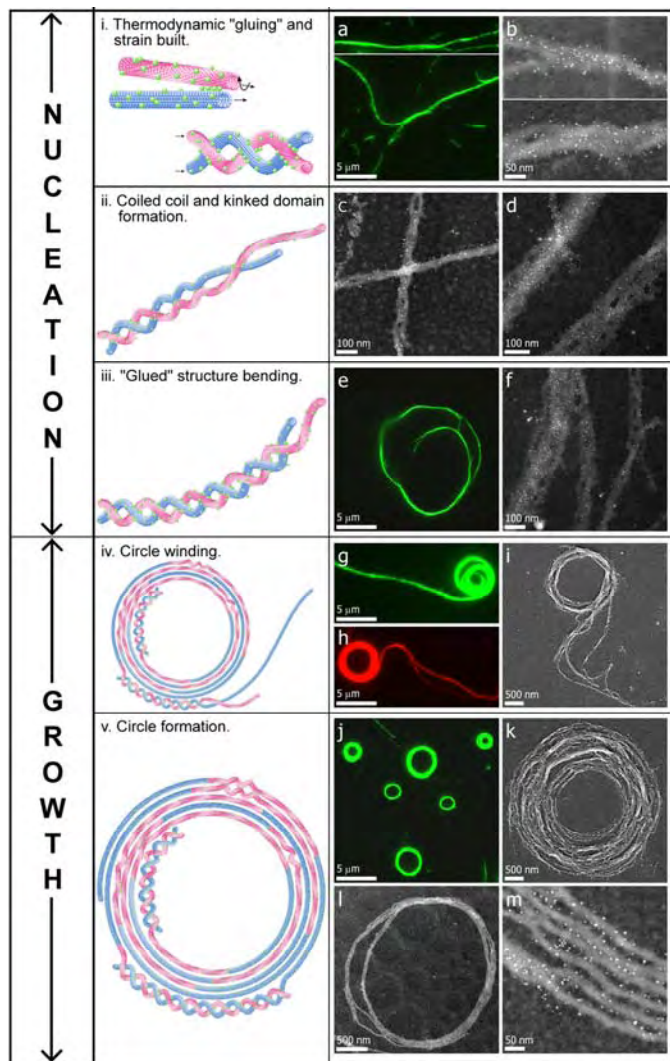


**Fig.2: Growth and nucleation of ring nanocomposites.** During nucleation, thermodynamic gluing of QD-carrying bMTs drives the self-assembly of extended oligomers that are transported and rotated (axially) by kinesin motors. Kinked and coiled domains emerge based on axial rotation, which in turn induce mechanical strain and bending. The bent QD-bMTs then form closed circles, ending the nucleation stage. Growth of the rings occurs as bMTs collide with existing rings and are added to the outer most part of the structure. Left – artistic representation; Right – Fluorescence, scanning electron and scanning transmission electron photomicrographs. (Taken from Liu et al.<sup>7</sup>).

brief metastable stage (Fig. 3). This stage can be maintained for extended periods of time (i.e., >4 hrs) by removing the energy-dissipative component by adding AMP-PNP, a non-hydrolyzable analog of ATP that inhibits kinesin transport. When ATP is maintained, the nanocomposite rings spontaneously disassemble within 30 minutes after addition of the QDs. Shortened tubulin oligomers and monomers remain moving on the surface, and are incapable of reassembling into ring structures again. We hypothesize that the mechanical strain that builds within the structures ultimately leads to bMT fracture, likely at regions with structural defects. The ends of these fractured bMTs may then be pulled by kinesin motors and removed from the larger structure.

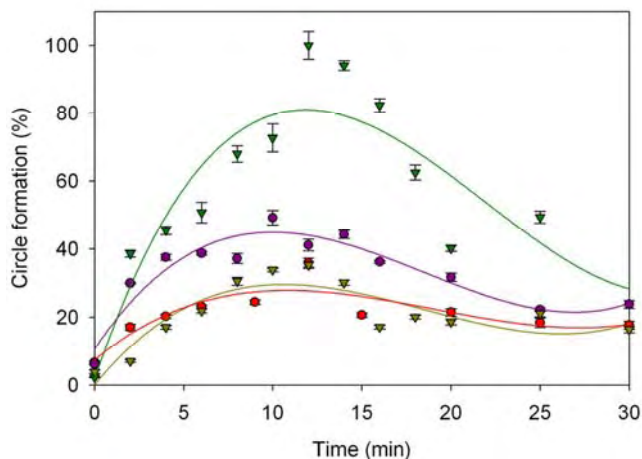


**Fig. 3: Kinetics of ring self-assembly and disassembly.** The assembly stage occurred rapidly upon introduction of SQDs to the system, and reached a maximum density at ~15 min. Following a brief metastable stage, the nanocomposite rings disassembled into linear oligomeric composites. This process followed a cubic polynomial curve, and was dependent on the level of biotinylated tubulin: 20% (●),  $R^2=0.76$ ,  $P<0.03$ ; 50% (●),  $R^2=0.89$ ,  $P<0.01$ ; 70% (▼),  $R^2=0.80$ ,  $P<0.01$ ; 90% (▼),  $R^2=0.79$ ,  $P<0.01$ .

Reversible disassembly may be controllably induced by the addition of excess biotin to the system. The mechanical strain associated with bMT bending within the composites also creates considerable strain on each biotin-streptavidin bond, which significantly changes the off-rate of this non-covalent bond. As the bonds between the QDs and bMTs disassociate, free biotin bonds to the QDs, which in turn destabilizes the rings. Within ~15 min, the majority of QDs are removed, leaving linear bMTs moving on the surface. Assembly of ring nanocomposites can then be re-initiated by adding new QDs to the system.

### Future Plans

The ring composites offer a unique system for studying the dynamic assembly of nanostructured materials. We are continuing to study this model system to further understand how the interaction of the thermodynamic and energy-dissipating components drives the various stages of assembly and disassembly. For example, we can change the “phase” of the bMT-QD composites by varying the level of thermodynamic input (e.g., SQD concentration) and holding the energy-dissipating input constant. In addition, the nanocomposite phase may also be changed by altering the rate of energy-dissipation (i.e., rate of kinesin transport). Lastly, we will study how physical confinement in microfluidic channels and within post-arrays influence ring formation with the goal of forming more complex integrated assemblies.

### References

1. Whitesides, G. M.; Grzybowski, B. *Science* **2002**, *295*, 2418.
2. Bhushan, B. *Philos. Trans. R. Soc. A-Math. Phys. Eng. Sci.* **2009**, *367*, 1445.
3. Kroger, N. *Curr. Opin. Chem. Biol.* **2007**, *11*, 662.
4. Copeland, M. F.; Weibel, D. B. *Soft Matter* **2009**, *5*, 1174.

5. Bouchard, A. M.; Warrender, C. E.; Osbourn, G. C. *Phys. Rev. E: Stat., Nonlinear, Soft Matter Phys.* **2006**, *74*, 41902.
6. Bachand, M.; Trent, A.; Bunker, B.; Bachand, G. *J. Nanosci. Nanotech.* **2005**, *5*, 718.
7. Liu, H.; Spoerke, E.D.; Bachand, M.; Koch, S.J.; Bunker, B.C.; Bachand, G.D. *Adv. Mater.* **2008**, *20(23)*, 4476.

#### DOE-Sponsored Publications (2007-2009)

- Liu, H., Spoerke, E.D., Bachand, M., Koch, S.J., Bunker, B.C., and Bachand, G.D. (2008). Dynamic self-assembly of nanocomposite structures through the interaction of thermodynamic and energy-dissipating processes. *Adv. Mater.* **20(23)**: 4476–4481. *(Cover)*
- Spoerke, E.D., Bachand, G.D., Liu, J., Sasaki, D.Y., and Bunker, B.C. (2008). Assembly of polar-oriented synthetic microtubule organizing centers. *Langmuir* **24(14)**: 7039-7043.
- Greene, A.C., Trent, A.M., and Bachand, G.D. (2008). Controlling kinesin motor transport through an engineered metal switch. *Biotechnol. Bioeng.* **101(3)**: 478-486.
- Liu, H., Bachand, G.D., Kim, H., Hayden, C.C., and Sasaki, D.Y. (2008). “Lipid nanotube formation via streptavidin-membrane binding interactions.” *Langmuir* **24**: 3686-3689.
- Rivera, S.B., Koch, S.J., Bauer, J.M., Edwards, J.M., and Bachand, G.D. (2007). Temperature dependent properties of a kinesin-3 motor protein from *Thermomyces lanuginosus*. *Fungal Genet. Biol.* **44**: 1170-1179.

## FUNCTIONAL INTERFACING OF BIOLOGICAL COMPONENTS AND SYNTHETIC MATERIALS

The broad objective of this program is to develop new functional materials with design elements derived from nature. A key aspect of the program involves development of technologies that interface synthetic materials with biological materials, and to generate hybrid materials with functions related to energy and biological inquiry.

**PRINCIPAL INVESTIGATOR:** Carolyn R. Bertozzi  
Molecular Foundry  
Lawrence Berkeley National Laboratory  
and  
Departments of Chemistry and  
Molecular and Cell Biology and  
Howard Hughes Medical Institute  
University of California  
Berkeley, CA 94720 ([crb@berkeley.edu](mailto:crb@berkeley.edu))

### CONSTRUCTION OF MODULAR NANOSCALE GLYCOMIMETICS FOR APPLICATIONS IN MICROARRAY TECHNOLOGIES

Kamil Godula and Carolyn R. Bertozzi

Glycans are vital components involved in biochemical processes across all domains of life. In eukaryotes, glycans decorate cell surface and secreted proteins where they are poised to mediate a variety of molecular recognition events.<sup>1-3</sup> For example, they can serve as points of attachment for viruses, bacteria and other cells. Glycans also participate in many facets of the vertebrate immune system and in organ development. Inside the cell, they can mediate protein trafficking and serve as regulatory switches for protein function. Transferring the functional capabilities of glycans into man-made materials offers new technological opportunities in areas as diverse as biosensing, drug delivery or tissue engineering (schematically shown in Fig. 1).

In nature, glycans are commonly found in glycoconjugates, such as glycoproteins, where they are presented to their protein receptors in spatially well-organized ensembles. Such multivalent glycan display is often required for proper biological function. For instance, mucins – a family of cell membrane bound glycoproteins – contain repeating regions of densely clustered serine and/or threonine residues bearing O-linked glycans that initiate with an  $\alpha$ -N-acetylgalactosamine core sugar (GalNAc).<sup>4,5</sup> Mucins accommodate a characteristic rod-like molecular architecture, which is the result of such an arrangement, as the closely packed glycans force the polypeptide backbone into an extended structure. We have successfully recreated the architecture of mucins in synthetic polymers and so obtained physiologically relevant glycomimetics of nanoscale dimensions with tunable functionality. Our synthetic design enables interfacing of these mucin mimetics with synthetic materials, such as

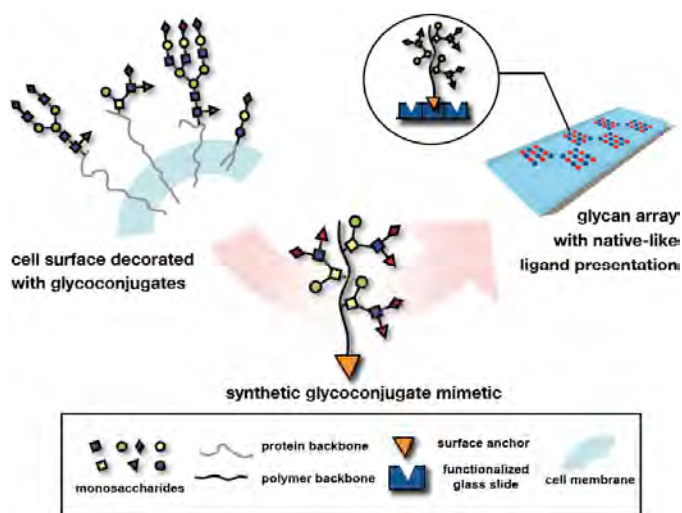


**Figure 1.** Strategy for integrating structural and functional features of native cell-surface glycoconjugates with man-made materials.

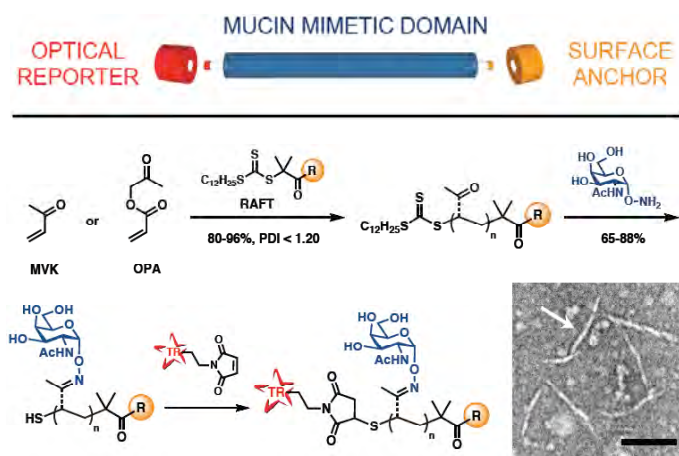


**Figure 2.** Design of a synthetic mucin mimetic. A) Modular approach for the assembly of dual end-functionalized mucin mimetics. B) Synthetic scheme for the preparation of a fluorescent mucin mimetic and a TEM image of the resulting rod-like glycopolymer (scale bar = 100 nm).

The glycopolymers possessed extended rod-like structures in solution and hydrodynamic properties similar to native mucins. TEM analysis of  $\alpha$ -GalNAc-modified poly(OPA) polymers revealed extended rigid structures similar to natural mucin glycoproteins of comparable length (Fig. 2).<sup>14</sup>

Mucinous glycoproteins are often thought of as extending out from cell surfaces and towering over other membrane-associated molecules, where their glycan ligands are positioned in specific geometries and made available for interactions with their protein receptors. We used fluorescence interference contrast (FLIC) imaging to investigate whether our mucin mimetic polymers possessed similar capability to project away from membrane surfaces. FLIC is an interferometric imaging technique developed to achieve z-resolution on the nanometer scale by measuring the interference between emitted and deflected waves of light originating from a fluorescent object positioned over a reflective surface (e.g., silicon oxide).<sup>15</sup> First, we synthesized a glycopolymer furnished with a phospholipid tail for anchoring in supported lipid bilayers and terminated with a fluorescent probe Alexa Fluor 488 (Fig. 3A). We incorporated the resulting polymer into a lipid bilayer supported by reflective silicon oxide surface and then imaged by FLIC (Fig. 3B). We found that the approximately 30 nm long glycopolymers projected away from the synthetic membrane by  $11 \pm 1$  nm, consistent with entropy-dominated sampling of the membrane-proximal space (Fig. 3B).<sup>8</sup> This result was indicative of the preference of the membrane-bound glycopolymers to assume spatial arrangements similar to those proposed for native cell surface mucins. Presumably, glycopolymers attached to solid supports, such as silicon oxide, might show similar behavior and serve as a physiologically relevant platform for biosensors.

To assemble glycopolymer microarrays we synthesized fluorescent

synthetic lipid membranes,<sup>6,7,8</sup> glass and silicon chips,<sup>9</sup> carbon nanotubes<sup>10,11</sup> or live cells, that are central to numerous existing or emerging biosensing and drug-delivery technologies (Fig. 1).<sup>12</sup>

The mucin mimetics comprise a poly(methyl vinyl ketone) (poly(MVK)) or a poly(2-oxopropylacrylate) (poly(OPA)) backbone, generated by reversible addition-fragmentation (RAFT) polymerization,<sup>13</sup> to which synthetic glycans were appended via oxime linkages (Fig. 2). Through the use of the RAFT technique, we achieved excellent control over size and chain-length uniformity of the resulting mucin mimetic polymers (polydispersity index < 1.15) and introduced two orthogonal end-functional groups suitable for the attachment of a number of different surface anchors and fluorophores (Fig. 2).

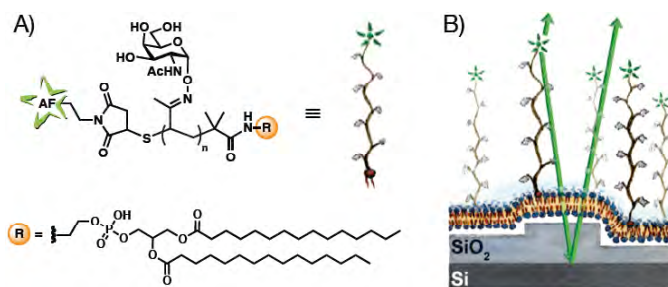


**Figure 3.** Schematic of an experimental setup for FLIC analysis of the molecular orientation of mucin mimetics at synthetic lipid membranes.

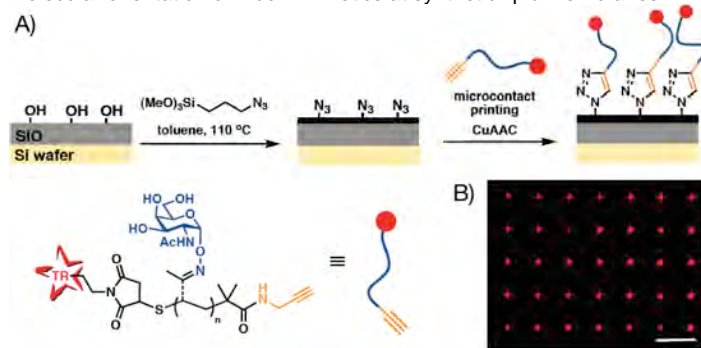


**Figure 4.** Microcontact printing of alkyne-terminated mucin mimetics on azide-functionalized silicon oxide chips.

glycopolymers terminated with an alkyne group that can be “clicked” to azide-functionalized silicon oxide surfaces (Fig. 4).<sup>9</sup> The glycopolymers were subsequently arrayed using microcontact printing on silicon oxide chips pretreated with (3-azidopropyl)trimethoxy silane (Fig. 4A). When the ink contained a copper catalyst, the terminal alkyne groups underwent a cycloaddition reaction with the surface azides to provide stable patterns of glycopolymers covalently attached via a triazol linkage (fluorescence micrograph in Fig. 4B). The printed glycopolymers bound lectins specific for their pendant glycans. A key characteristic of these glycan microarrays was that the density and orientation of glycans was determined by the polymer structure rather than by poorly understood features of the underlying surface. These microarrays are ideally suited for a high-throughput analysis of glycan specificities toward their cognate receptors, for detection of biomarkers and pathogens or for patterning of live cells.

Our future work will focus on developing strategies for facile and high-throughput “on-chip” glycopolymer construction using natural glycans. We will exploit the ability of sugars with a free reducing terminus to react with hydrazide nucleophiles to form stable hydrazones.<sup>19</sup> In these adducts, the reducing terminal monosaccharide exists primarily (>95%) in the cyclic pyranose form and as the  $\beta$ -anomer. Our preliminary work suggests that this approach is indeed feasible, thus, alleviating the burden of glycan functionalization that is currently required for the synthesis of glycopolymers. We will also employ imaging techniques, such as the FLIC or the Scanning Ion-Conductance Microscopy (SICM) to determine the molecular orientation of the surface bound mucin mimetics and to gain a better understanding of how the spatial presentation of glycans affects their interactions with cognate protein receptors.

## BIBLIOGRAPHY AND REFERENCES CITED

1. Reuter, G.; Gabius, H. J. *Cell. Mol. Life Sci.* **1999**, *55*, 368-422.
2. Spiro, R. G. *Glycobiology* **2002**, *12*, 43R-56R.
3. Varki, A. *Glycobiology* **1993**, *3*, 97-130.
4. Hang, H. C.; Bertozzi, C. R. *Bioorg. Med. Chem.* **2005**, *13*, 5021-5034.
5. Shogren, R.; Gerken, T. A.; Jentoft, N. *Biochemistry* **2002**, *28*, 5525-5536.
6. Rabuka, D.; Parthasarathy, R.; Lee, G. S.; Chen, X.; Groves, J. T.; Bertozzi, C. R. *J. Am. Chem. Soc.* **2007**, *129*, 5462-5471. **(WORK SUPPORTED BY DOE)**
7. Parthasarathy, R.; Rabuka, D.; Bertozzi, C. R.; Groves, J. T. *J. Phys. Chem. B* **2007**, *111*, 12133-12135. **(WORK SUPPORTED BY DOE)**
8. Godula, K.; Umbel, M. L.; Rabuka, D.; Botyanszki, Z.; Bertozzi, C. R.; Parthasarathy, R. *J. Am. Chem. Soc.* **2009**, *131*, 10263-10268. **(WORK SUPPORTED BY DOE)**
9. Godula, K.; Rabuka, D.; Nam, K. T.; Bertozzi, C. R. *Angew. Chem. Int. Ed.* **2009**, *48*, 4973-4976. **(WORK SUPPORTED BY DOE)**
10. Chen, X.; Tam, U. C.; Czlapiński, J. L.; Lee, G. S.; Rabuka, D.; Zettl, A.; Bertozzi, C. R. *J. Am. Chem. Soc.* **2006**, *128*, 6292-6293. **(WORK SUPPORTED BY DOE)**
11. Chen, X.; Lee, G. S.; Zettl, A.; Bertozzi, C. R. *Angew. Chem. Int. Ed.* **2004**, *43*, 6111-6116. **(WORK SUPPORTED BY DOE)**
12. Rabuka, D.; Forstner, M. B.; Groves, J. T.; Bertozzi, C. R. *J. Am. Chem. Soc.* **2008**, *130*, 5947-5953. **(WORK SUPPORTED BY DOE)**
13. Chiefari, J.; Chong, Y. K.; Ercole, F.; Krstina, J.; Jeffery, J.; Le, T. P. T.; Mayadunne, R. T. A.; Meijs, G. F.; Moad, C. L.; Moad, G.; Rizzardo, E.; Thang, S. H. *Macromolecules* **1998**, *31*, 5559-5562.
14. McMaster, T. J.; Berry, M.; Corfield, A. P.; Miles, M. J. *Biophys. J.* **1999**, *77*, 533-541.
15. Ajo-Franklin, C. M.; Yoshina-Ishii, C.; Boxer, S. G. *Langmuir* **2005**, *21*, 4976-4983.

# Molecular Nanocomposites Biotic/Abiotic Interfaces, Materials, and Architectures

C. Jeffrey Brinker<sup>1,2</sup>, Eric C. Carnes<sup>2</sup>, Carlee Ashley<sup>2</sup>

<sup>1</sup> Sandia National Laboratories, <sup>2</sup> The University of New Mexico  
Advanced Materials Lab  
1001 University Blvd SE,  
Albuquerque, NM 87106,  
cjbrink@sandia.gov,  
<http://www.unm.edu/~solgel>

**Program Scope:** Our bio-molecular nanocomposites research focuses on two complementary, interrelated goals: 1) the use of living cells and bio-interfaces to direct the formation of new classes of complex, symbiotic, 'living' materials and 2) the use of cell-directed materials and architectures to understand environmental influences on cellular behavior. Our work builds on our work on evaporation-induced self-assembly and its extension to cell directed assembly.

**Recent Progress:** We have discovered and continue to explore a unique metabolically and optically controlled lithography approach that allows patterned integration of live cells into nominally solid-state devices and maintains their viability under extreme conditions of desiccation and starvation. We observe that yeast, bacterial, and mammalian cells deposited on lipid/silica thin film mesophases actively reconstruct the surface to create a fully 3D bio/nano interface composed of localized lipid bilayers enveloped by a lipid /silica mesophase. Remarkably this integration process selects exclusively for living cells over the corresponding apoptotic cells (those undergoing programmed cell death). The localized lipid interface maintains fluidity,

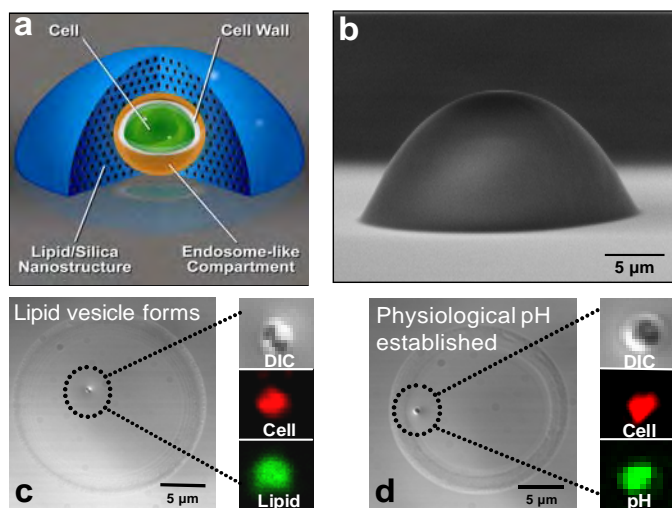


**Figure 1.** Isolation of individual *S. aureus* within a nanostructured droplet. (a) schematic of physical system (not to scale) showing a cell incorporated in an endosome-like lipid vesicle within a surrounding nanostructured lipid/silica droplet deposited on glass substrate and (b) SEM image of physical system. The nanostructure maintains cell viability under dry external conditions and allows complete chemical and physical isolation of one cell from all others. c and d show plan-view optical microscope images of individual cells in droplets (large outer circular areas). Magnified areas show differential interference contrast image and red fluorescence image of individual stained, isolated cells (both c and d) and green fluorescence image of NBD-labeled lipid localization at cell surface (c) or localized pH (d), using Oregon Green pH-sensitive dye. We find that, within the droplet, the cells become enveloped in an endosome-like lipid vesicle (c), and establish a localized pH consistent with physiological early endosomal conditions (~5.5) (d).

accessibility, and functionality of the cellular surface and viability of the cell. Optical definition of cellular integration is achieved by dose-dependent UV exposure of the lipid/silica mesophase film. Short exposures reduce the film contact angle with water and promote integration. Longer exposures solidify the lipid/silica mesophase, preventing integration. Double exposures define first patterns of cellular integration and second high diffusivity pathways to or between cells via photolytic degradation of the lipid mesophase template and attendant formation of ordered monosized, mesopores. Temperature dependent studies along with those employing sodium azide to interfere with ATP production confirm that integration is metabolically controlled. Overall this 'lithography with life' approach provides the first demonstration of optically-defined 3D cellular immobilization. It promises a new means to integrate 'bio' with 'nano' into platforms useful to study and manipulate cellular behavior at the individual cell level and to interface living organisms with electronics, photonics, and fluidics.

We used our cellular integration approach to explore quorum sensing at the individual cell level. Many bacteria emit and sense small, diffusible 'signaling' molecules (autoinducers) whose extracellular

concentration regulates gene expression through a positive feedback system, controlling important functions including virulence and biofilm formation<sup>1</sup>. The prevailing view of why this signaling takes place is that it allows populations of cells to assess their density. If a ‘quorum’ exists, bacteria coordinate their gene expression to function as a community, thereby providing group benefits exceeding those of individual cells. This idea that bacteria act cooperatively for the social good is so appealing that the potential benefits of quorum sensing at the individual cell level have not yet been fully explored. We used cell-directed assembly to develop a physical system that simulates endosomal or phagosomal bacterial entrapment during infection and maintains cell viability under conditions of complete chemical and physical isolation.

*S. aureus* were immobilized, individually within a matrix fabricated at a sufficiently small physical scale (~20 μm diameter, physically isolated hemispherical droplets, see Fig. 1a-b) so that the overall cell density exceeded the reported QS threshold ( $10^7 - 10^9$  cells mL<sup>-1</sup>). The matrix was formed by adaptation of our cell-directed assembly approach to an aerosol procedure we developed previously to form ordered porous silica nanospheres. It results in cells incorporated within a dihexanoylphosphatidylcholine (*diC*<sub>6</sub>PC) lipid vesicle (Fig. 1c) maintained at a pH of ~5.5 (Fig. 1d), approximating that of the early endosome, and surrounded by an ordered silicon dioxide nanostructure (Fig. 1a and b) that serves as a reservoir for any added buffer and media. This construct mimics some of the physical and chemical features of a bacterium entrapped within an intracellular membrane-bound compartment (endosome or phagosome). Importantly, this architecture, *viz* a vesicle-enveloped cell incorporated in a much larger nanostructured silica bead (Fig. 1a-b), allows individual cells to be maintained in a viable state under externally dry conditions that establish complete physical and chemical isolation of one cell from all others. This reduced physical system is biologically relevant, because *Staphylococcus aureus* is known to become trapped in such intracellular compartments, and it is proposed that they employ a QS strategy to induce new gene expression, promoting intracellular survival and/or escape. However it is presently unknown whether confinement alone can promote QS or whether other factors within the endosomal organelle are required. We use our system to test confinement alone as a mechanism for inducing QS.

To optically monitor the onset and kinetics of auto-induced QS, we used *S. aureus* strains ALC1743 (*agr* group 1 RN6390 containing reporter *agr*: P3-gfp) and ALC1740 (RN6390 containing reporter *hla*-gfp) at an early exponential phase prior to QS induction. Expression of green fluorescent protein (GFP) by ALC1743 reports quorum sensing-dependent *agr* P3-promoter

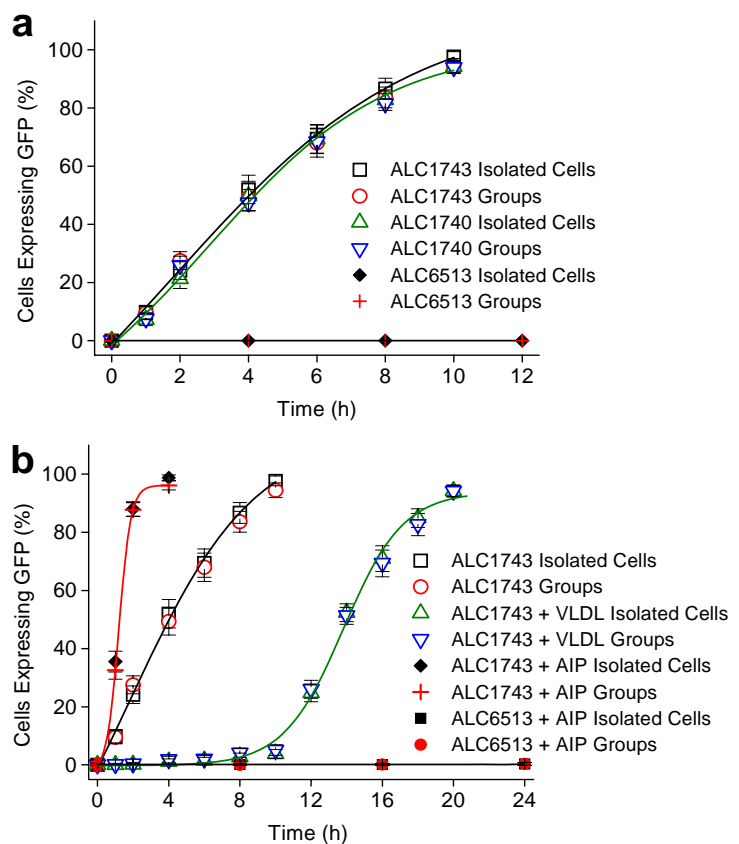


**Figure 2 a)** Percentage of individual *S. aureus* cells (or small groups of cells, n=2-8, see Supplementary Fig. 1 online) expressing GFP as function of incubation time at 37°C (at least 600 cells were counted for each time point). Data are presented as % of cells expressing GFP +/- the 95% confidence interval, with sigmoidal fit of only isolated cell data for clarity. No statistical difference can be seen between individual and small group (2-8 cells) behavior (Chi square analysis shows no P-value < 0.05). The absence of expression in ALC6513 (an *agrA*(-) mutant containing the same *gfp* reporter, *agr*: P3-gfp, as for strains ALC1743, ALC 1740 but lacking *AgrA*, one component of the two component regulatory pair), shows there to be no non-AIP induced GFP expression. **(b)** Percentage of individual cells (or small groups of cells) expressing GFP as function of incubation time at 37°C for samples prepared with exogenous addition of cyclic AIP (AIP1) or very low density lipoprotein (VLDL), a proven inhibitor of QS in *S. aureus*<sup>21</sup>. For strain ALC6513, the samples were maintained at 37°C for 24 hours prior to addition of exogenous AIP1. The ALC1743 data without exogenous additions is re-plotted as a reference.

activation, while in ALC1740 it reports QS-mediated downstream synthesis of the pore-forming toxin,  $\alpha$ -hemolysin. As a negative control we used strain ALC6513 (an *agrA*(-) mutant containing reporter *agr*: P3-gfp) – because this strain uses the exact same reporter construct as ALC1743 but lacks AgrA, one component of the two component regulatory pair, it tests for the possibility of non-AIP induced GFP expression. As shown in the kinetic plot (Fig. 2a), GFP expression follows a sigmoidal curve. It initiates over one hour and increases progressively with time to over 90% at ten hours where it begins to level off. Over the 24 hour time course we observed no measurable GFP expression from strain ALC6513.

Figure 2b depicts the time course for GFP expression of ALC1743 isolated in droplets to which exogenous type 1 AIP or the QS inhibitor, very low density lipoprotein (VLDL), was added immediately prior to the aerosol assembly process. We observe cyclic AIP1 to accelerate significantly GFP expression relative to the corresponding ALC1743 sample prepared without exogenous AIP. In contrast VLDL suppresses GFP expression for 10 hours, after which expression kinetics paralleling those of ALC1743 are recovered. The mechanism of VLDL inhibition of quorum sensing in *S. aureus* involves binding of the major structural protein of this lipoprotein, apolipoprotein B, to AIP1 preventing binding to the AgrC receptor and antagonizing the QS signaling cascade. For isolated cells, GFP expression presumably commences once the local extracellular AIP concentration becomes comparable to that of VLDL. Fig. 2b also plots GFP expression for the *agrA*(-) mutant strain isolated for 24 hours and then dosed with exogenous AIP1. No GFP expression was observed for times up to 24 hours.

Fig. 2a shows the time course of GFP expression of isolated, individual *S. aureus* strain ALC1740. The progressively increasing GFP expression over 10 hours mirrors that of QS (Fig. 2a) and shows activation of the RNAIII-dependent pathway that induces expression of secreted virulence factors. Here we specifically detect activation of the  $\alpha$ -hemolysin promoter. Although there are data that suggest that small numbers of intracellular *S. aureus* quorum sense, the combined data in Figures 2a and b provide the first proof of auto-induction of an individual, physically and chemically isolated organism. Additionally these data provide the first evaluation of gene expression kinetics for a large population of isolated individual cells. We postulate that quorum sensing allows isolated *S. aureus* to sense confinement through increased extracellular concentration of autoinducer and to activate virulence factor pathways and initiate new gene expression needed to survive in such confined environments. To demonstrate the benefit of discrete quorum sensing to individuals, we compared the viability of isolated, individual RN6390 to that of RN6911, a RN6390 mutant unable to initiate QS due to deletion of the *agr* operon. We found that, over an 18-day incubation period confined within the media-containing nanostructured lipid/silica droplet at 37°C, the viability of RN6390 (*agr*+) was significantly greater than that of the isolated mutant RN6911 (*agr*-). A plausible explanation for the viability difference is that confinement-induced QS and attendant up-regulation of a spectrum of genes affecting virulence and metabolism enhances utilization of external nutrients.

**Future Directions: Implications for Induced Dormancy and Drug Resistance** – Beyond QS, there is now overwhelming evidence of environmental influences on cellular behavior, and these epigenetic effects are currently being recognized as crucial to the understanding of a diverse spectrum of problems including cancer metastasis, drug resistance, TB dormancy, and nanoparticle toxicology. For example, it has recently been proposed that cancer cells may use a quorum sensing mechanism, similar to bacteria, to regulate gene expression and control steps in metastatic colonization. Progress on addressing these problems, however, is currently hindered by an inability to incorporate cells into three-dimensional architectures that better represent the nanostructured extracellular matrix (ECM), tissues, or niches (e.g. capillaries), where cells may reside *in vivo*. Using a derivative of the cell-directed assembly approach developed by our team, we immobilized Human hepatocarcinoma (Hep3B) cells within a coherent 3D lipid/silica matrix qualitatively similar to that used in the bacterial entrapment studies discussed above. Our initial results demonstrate that integration of Hep3B within a silica matrix induces cellular dormancy within four hours and that dormant cells re-enter the cell cycle as a homogeneous, synchronized population once the matrix is suspended in serum-containing growth medium and begins to dissolve. We find that, by simply controlling the amount of time that cells remain integrated within the silica film, they become arrested at various points in the cell cycle and can be

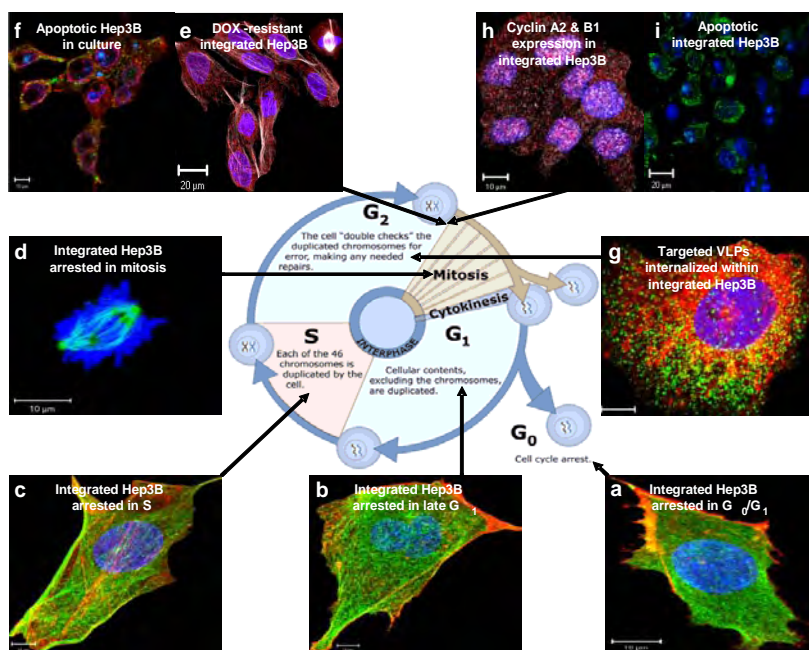


**Figure 3.** Cancer cell cycle arrest, dormancy, and drug resistance can be directed by integration. (a) cells integrated for >72 hours remain dormant ( $G_0/G_1$ ), (b) cells integrated for 24-72 hours arrest in  $G_1/S$ , (c) cells integrated for 12-24 hours arrest in S, and (d) cells integrated for 4-12 hours arrest at  $G_2/M$ . Integrated Hep3B arrested in  $G_2/M$  are resistant to high concentrations of doxorubicin (e), while cells grown in tissue culture rapidly become apoptotic (f), while cells integrated for 24-72 hours arrest in  $G_1/S$  are resistant to high concentrations of doxorubicin (e), while cells grown in tissue culture rapidly become apoptotic (f). VLPs bearing the SP94 targeting peptide bind to integrated Hep3B cells arrested in  $G_0/G_1$  and are endocytosed as the cells re-enter the growth cycle (g). Targeted VLPs that encapsidate a siRNA cocktail against cyclin A2 (h, expression prior to delivery in red), B1 (h, white), and B2 are capable of inducing apoptosis in integrated Hep3B once cells re-enter the cell cycle and progress through  $G_2$  (i).

maintained under ‘normal’ growth conditions with minimal loss of viability for several weeks (see Fig. 3 a-d). Additionally, we observe that confinement of individual Hep3B induces resistance to chemotherapeutic agents (e.g. doxorubicin and camptothecin) that interfere in DNA replication and, therefore, normally target proliferating cells during the S-phase of the cell cycle. Integrated Hep3B cells can be exposed to a high concentration of doxorubicin ( $\sim 70 \mu\text{M}$ , 1000 times the  $\text{IC}_{50}$  value for DOX-sensitive cells) for 7 days without induction of apoptosis (see Fig. 3 e; the absence of a signal from a FITC-labeled substrate for caspase-3 indicates that the cells are not apoptotic), suggesting that confinement within our nanostructure can induce and preserve drug resistance and other specific cellular states not accessible in tissue culture or *in vivo*. Our future research will address whether cell-signaling pathways analogous to those used by quorum sensing bacteria underlie these intriguing behaviors.

### Publications Acknowledging DOE-BES Support Since 2007 (Partial List)

1. “Confinement-Induced Quorum Sensing of Individual *Staphylococcus aureus* Bacteria.” Carnes, EC; Lopez, DM; Cheung, A; Gresham, H; Timmins, GS; and Brinker, CJ. *Nature Chemical Biology*. *In Press* (August 2009).
2. “Characterization of Lipid-Templated Silica and Hybrid Thin Film Mesophases by Grazing Incidence Small-Angle X-ray Scattering.” Dunphy DR, Alam TM, Tate MP, et al. *Langmuir* 25 (16) 9500-9509 (August 2009).
3. “Nanoporous silica-water interfaces studied by sum-frequency vibrational spectroscopy.” Zhang, L; Singh, S; Tian, CY; Shen, R; Wu, Y; Shannon, MA; and C. Jeffery Brinker. *J. Chem Phys* 130, 154702 (2009)
4. “Dynamic Investigation of Gold Nanocrystal Assembly using *in situ* Grazing-Incidence Small-Angle X-ray Scattering.” Dunphy D; Fan HY; Li XF; Wang J, Brinker, CJ. *Langmuir* 24 (19)10575-1057 (October 2008).
5. “In-Situ Fluorescence Probing of the Chemical and Structural Changes during Formation of Hexagonal Phase Cetyltrimethylammonium Bromide (CTAB) and Lamellar Phase CTAB/Poly(dodecylmethacrylate) Sol-Gel Silica Thin Films.” Huang MH; Soyez, HM; Dunn, BS; Zink, JI; Sellinger, AS; Brinker, CJ. *Journal of Sol-Gel Science and Technology*, Sep 2008, v. 47(3) pp. 300-310
6. “Free-Standing, Patternable Nanoparticle/Polymer Monolayer Arrays Formed by Evaporation Induced Self-Assembly at a Fluid Interface.” Pang, J.; Xiong, S.; Jaeckel, F.; Sun, Z.; Dunphy, D.; Brinker, C. J. *J. Am. Chem. Soc.*; (Communication); 2008; March 19, 2008; v. 130 (11) pp. 3284+.
7. “Directed aerosol writing of ordered silica nanostructures on arbitrary surfaces with self-assembling inks.” J. Pang, JN Stuecker, YB Jiang, AJ Bhakta, P Li, J Cesarano, D Sutton, P. Calvert and CJ Brinker. *Small*, January 2008; v. 4(7) pp. 982-989.
8. “Sub-10 nm thick microporous membranes made by plasma-defined atomic layer bridged silsesquioxane precursor.” YB Jiang, G. Xomeritakis, Z. Chen, C. Dunphy, DJ Kissel, JL Cecchi, and CJ Brinker. *J. Am. Chem. Soc* 2007, v. 129, p. 15446-15447.
9. “Cell-directed assembly of bio/nano interfaces – a new scheme for cell immobilization.” HK Baca, EC Carnes, S. Singh, CE Ashley, DM Lopez, CJ Brinker. *Accounts of Chemical Research*, 2007, vol. 40 (9), p. 836-845.
10. Modulus-density scaling behavior and framework architecture of nanoporous self-assembled silicas. H. Fan, C. Hartshorn, T. Buchheit, D. Tallant, R. Assink, R. Simpson, D. Kissel, D. Lacks, S. Torquato, and C.J. Brinker. *Nature Materials*, June 2007, vol. 6, no. 6, p. 418-423

## Observing Biomolecular Materials Assembly in the Dynamic TEM

N. D. Browning (PI)<sup>1</sup>, J. J. DeYoreo<sup>2</sup>

<sup>1</sup>Condensed Matter and Materials Division, Physical and Life Sciences Directorate, Lawrence Livermore National Laboratory, PO Box 808, Livermore, Ca 94550.

<sup>2</sup> Lawrence Berkeley National Laboratory, Mail Stop: 67R3207,  
One Cyclotron Road, Berkeley, CA 94720

[browning20@llnl.gov](mailto:browning20@llnl.gov), [jjdeyoreo@lbl.gov](mailto:jjdeyoreo@lbl.gov)

### Program Scope

The presence of an interface between a macromolecular component and inorganic materials is a hallmark of biomolecular materials. The organic side of the interface can play an active role in directing the formation and organization of the inorganic materials, while the inorganic component often becomes the substrate for assembly of macromolecules. In both, our understanding of assembly is extremely limited because of a lack of an experimental tool with the spatial and temporal resolution needed to capture the formative events in the process. The development of the dynamic transmission electron microscope (DTEM) with an *in situ* fluid-cell offers the potential to observe these systems on the required spatial and temporal scale. We will utilize this new capability to directly image mineralization in ferritin cages. In doing so, we believe we can open a new window on biomolecular materials that promises dramatic advances in our understanding of the underlying thermodynamic and kinetic factors that lead to organization of macromolecules and drive assembly at macromolecular-inorganic interfaces.

### Recent Progress

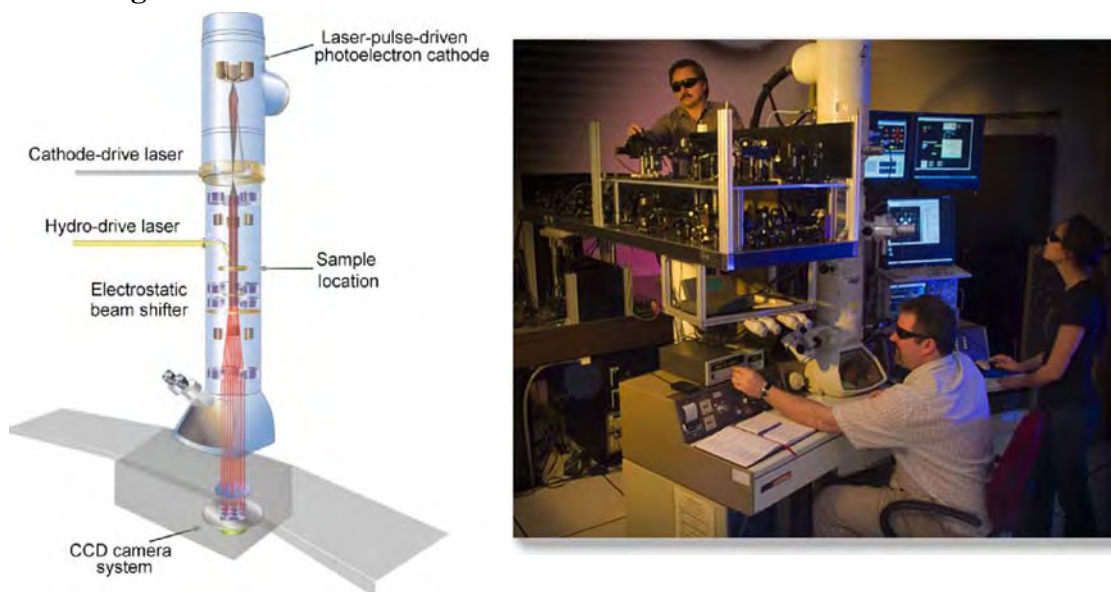


**Figure 1:** (a) Schematic of LLNL DTEM (b) Installed and operating DTEM at LLNL

This is a newly funded research project that makes use of the recent development of the DTEM at Lawrence Livermore National Laboratory (LLNL) [1]. In the DTEM, very high time resolution is achieved by producing a short burst of electrons to illuminate the specimen, coupled

with single electron sensitive CCD image recording technology (Figure 1). A photocathode source is irradiated with a pulsed UV laser with photon energy greater than the target work function. A flux of electrons is then produced via photoemission with approximately the same time duration as the stimulating laser pulse. After this photoemission process, the microscope processes the emitted electron “packet” in the traditional way (acceleration, focusing, magnification, detection, etc.). This means that images can be obtained with the same time resolution as the electron pulse duration – which is currently ~10ns. If the photoemission pulse is synchronized with a second laser that stimulates the sample, *in situ* reactions can also be initiated and studied with high time precision. Using this approach, a combined <10nm and 10ns spatio-temporal resolution can be achieved. These are precisely the imaging parameters needed for the study dynamic biomolecular processes.

The ability to perform *in situ*, dynamic, TEM experiments is further enabled by a custom-built stage and fluid cell [2]. This combination offers electrochemical and/or temperature control over the system of study and is suitable for a wide range of experiments in the DTEM. A schematic of the core design for an experimental cell is presented in figure 2 and the important features are summarized as follows: first, each cell is hermetically sealed, thereby isolating the experimental sample and solution from the high vacuum environment of the TEM chamber. Second, the cell contains a narrow solution reservoir, which provides a

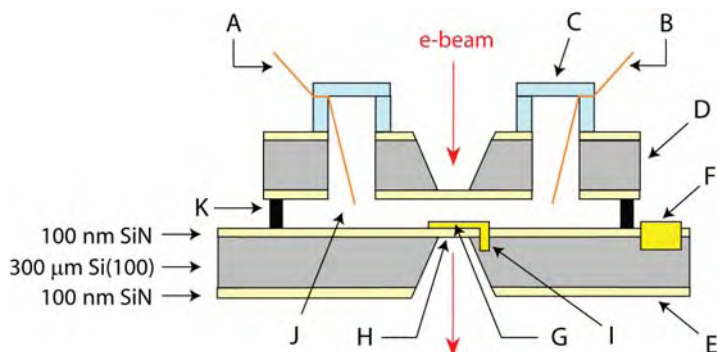


**Figure 2:** Schematic cross-section of the *in situ* TEM cell viewed from the side. Components: **A:** Reference electrode, **B:** Counter electrode, **C:** Glass tower, **D:** Upper SiN<sub>x</sub>/Si(100)/ SiN<sub>x</sub> wafer, **E:** Lower wafer, **F:** Au contact to working electrode via the Si(100) wafer, **G:** 20 nm Au working electrode, **H:** 100 x 100 μm SiN<sub>x</sub> ‘window’, **I:** Electrical contact between Si(100) and Au, **J:** Solution reservoir, **K:** SiO<sub>2</sub> spacer (200 nm at closest approach)

path of limited e-beam attenuation and enables high resolution imaging. In general, the depth of the reservoir is within the 200-500 nm range. Third, the incorporation of a three electrode system facilitates electrochemical control of the sample. Following assembly, the experimental cell is fastened to a mount at the end of the TEM holder. A Peltier heater/cooler adjacent to the cell enables temperature control between 0-70°C with a precision of ±0.5°C. This temperature range is ideally suited for the study of biological and bio-mimetic systems in aqueous environments. The holder offers considerable flexibility in the rate of heating and cooling of the experimental sample (between 0.1-5°C/min). Although the over thickness of the cell exceeds more traditional TEM samples, it is still possible to tilt the holder by ±15°.

To date, we have tested the fluid cell in a conventional TEM over a range of liquid layer thicknesses from ~100 nm to 10 microns. The results have demonstrated that a resolution of ~ 1 nm is attainable when imaging through liquid layers a few hundred nm thick. Using the temperature control stage, we have driven growth of gold nanoparticles and aggregation of iron oxide nanocrystals. We have also shown that the electron beam can be used to induce growth of low-Z colloidal particles (figure 3). We have tested the ability of the electrochemical circuit to drive nucleation of calcite from an undersaturated solution by installing the lower wafer of the cell within the fluid cell of an AFM. The creation of OH<sup>-</sup> ions through application of a voltage to

the lower electrode raises the pH, thus creating a condition of supersaturation. The sequence of images in figure 4 shows the progressive transformation of a film of amorphous calcium carbonate deposited by this method into a film of oriented calcite crystals.

### Research Plan

The DTEM will be used to study the crystallization of  $\text{Fe}_3\text{O}_4/\gamma\text{-Fe}_2\text{O}_3$  within the cage protein ferritin. Among the methods for biomimetic synthesis of inorganic nanostructures, mineralization within protein cages has been identified as particularly promising. The architecture of the cages is central to their suitability for

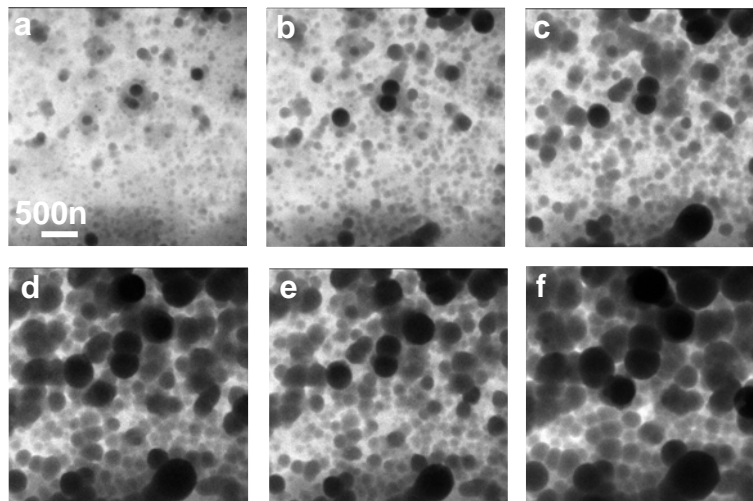


**Figure 3:** Time sequence of TEM images showing nucleation and growth of low-Z colloids in solution collected at 25 s intervals through a 1  $\mu\text{m}$  cell.

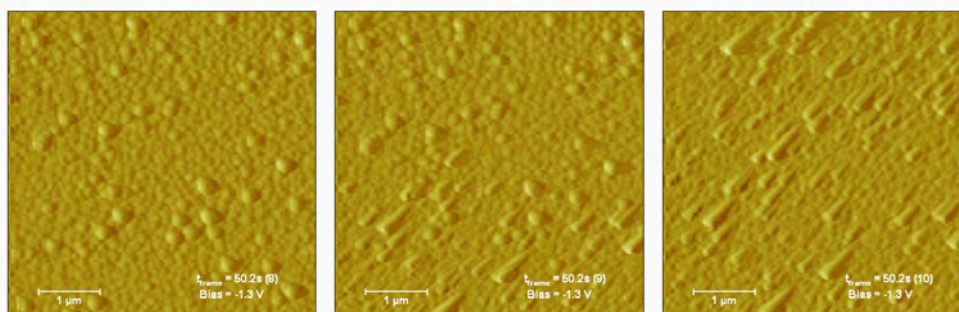


**Figure 4:** Time sequence of AFM images showing ACC-to-calcite transition on base plate of TEM fluid cell collected at 30 s intervals.

nanomaterial synthesis: they are constructed via combination of a specific number of protein subunits and exhibit a well-defined interior (and exterior) surface structure and a cavity of precise nm-scale dimensions. As such, the interior surface of the cages provides a bio-template for controlled nucleation and the empty cavity acts as a container for subsequent mineral growth. Since the cavity is of defined dimensions, the resulting inorganic nanocrystals have narrow size and shape distributions, features that are desirable for any technological application. Naturally occurring cage architectures also adopt a variety of shapes and sizes (figure 5), which provide significant flexibility for tailoring the final nanocrystalline product. Moreover, the interior surface of the cage can be

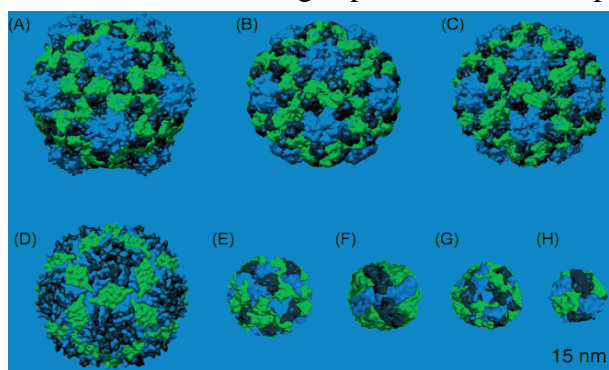


**Figure 5:** Space-filling images of a series of protein cage architectures, including ferritin (F), which is 12 nm in diameter [3].

genetically/chemically modified to create sites for selective, controlled, nucleation.

The nucleation and growth of  $\text{Fe}_3\text{O}_4$  within the ferritin cage protein provides an excellent system of study for several reasons: (1) ferritin was one of the first cage proteins used for the synthesis of inorganic nanocrystals and is known to nucleate a wide range of materials within its core (e.g.  $\text{Fe}_3\text{O}_4$ , CdS, CdSe, ZnSe,  $\text{In}_2\text{O}_3$ ,  $\text{Ni}(\text{OH})_3$ , Ag, Pd, and CoPt). As a consequence, it is canonical among the cage proteins used for biomimetic crystallization; (2) the experiments will be conducted in collaboration with Prof. Trevor Douglas at Montana State University, who will provide the ferritin samples to ensure that the *in situ* DTEM measurements are directly comparable with studies conducted concurrently by his group; (3) the insight obtained from these experiments will have value within the bio-medical field for Fe sequestration in living species.

The  $\text{Fe}_3\text{O}_4$ /ferritin system also offers three important experimental benefits: (1) the high-Z Fe ions within the iron oxide will yield excellent contrast with the cell components and enable high resolution imaging throughout the nucleation and growth of the  $\text{Fe}_3\text{O}_4$  phase (ferritin can contain up to 4,000 Fe ions). (2) it has been demonstrated [2] that a combination of heating ( $\sim 60^\circ\text{C}$ ), basic (pH $\sim 8.5$ ) and oxidative conditions are required to induce the nucleation of  $\text{Fe}_3\text{O}_4$  (or  $\gamma\text{-Fe}_2\text{O}_3$ ) within the proteins and, as a result, the heating capabilities of the experimental holder can be used to control the onset of specific mineral formation. Initially, the experimental cell will be held at  $\sim 5^\circ\text{C}$  to minimize/inhibit the nucleation of ferrihydrite. Heating to  $60^\circ\text{C}$  will then act as a ‘trigger’ for  $\text{Fe}_3\text{O}_4$  nucleation, which can be synchronized with the DTEM image to minimize e-beam damage of the organic protein; (3) the ferritin cages can be immobilized within the field of view by tethering them to the surface of the Au WE with a self assembled monolayer of cysteine.

The DTEM studies of mineralization within the ferritin cage will focus upon determining the evolution in size, structure and phase (determined from electron diffraction data) of the mineral component from formation of the incipient nuclei to the final suite of crystals and the associated rates of nucleation and growth. Time-resolved imaging and diffraction will be conducted at a range of temperatures and solution supersaturations (set by the electrode potentials for the hydrocerrusite system). These will be selected based upon the conditions and protocols successfully implemented in reported studies of hydrocerrusite/monolayer and  $\text{Fe}_3\text{O}_4$ /ferritin systems. While the previous studies provide a framework for our initial measurements, we note that experimental feedback will enable optimization of the conditions required for successful *in situ* DTEM measurements of each system. For example, the exact potential necessary to induce mineral nucleation on a SAM surface will be determined by gradually decreasing the applied voltage (towards -1V and beyond) and allowing the system to reach equilibrium while imaging. The required bias for nucleation can then be applied in future experiments, which ensures non-equilibrium and uncontrolled crystallization does not occur. We anticipate that the *in situ* DTEM measurements will answer key questions about the dynamics and, therefore, the mechanisms of templated mineralization, which cannot be addressed using traditional experimental techniques.

## References

- [1] LaGrange, T., et al, *Single-shot dynamic transmission electron microscopy*. Applied Physics Letters, 2006. **89**(4): p. -.
- [2] Uchida, M., et al, *Biological containers: Protein cages as multifunctional nanoplatfoms*. Advanced Materials, 2007. **19**(8): p. 1025-1042.
- [3] Wong, K.K.W., et al, *Biomimetic synthesis and characterization of magnetic proteins (magnetoferritin)*. Chemistry of Materials, 1998. **10**(1): p. 279-285.

## Programmable Microtubule Assemblies

Erik Spoerke, George Bachand, Andrew Boal, Judy Hendricks, and Bruce Bunker

Sandia National Laboratories  
Albuquerque, NM 87185  
[bcbunke@sandia.gov](mailto:bcbunke@sandia.gov)

**Program Scope:** The work described here is a subtask on a program entitled *Active Assembly of Dynamic and Adaptable Materials*. The goal of the overall program is to explore the extent to which energy-consuming proteins such as fiber-forming tubulin and motor proteins can be used for the active transport, assembly, and reconfiguration of nanomaterials in artificial environments. These energy-consuming components allow us move beyond self-assembly and to manipulate materials via mechanisms that are not constrained by standard diffusion or equilibrium processes. The goal of the Microtubule subtask involves learning how to create networks of microtubules that can be programmed to polymerize and depolymerize via a process called dynamic instability. The programmable networks can then be used to pull or push objects, to provide scaffolds for other nanomaterials (via biomineralization or mimicking diatom skeleton formation) or as “train tracks” for materials transport via mobile motor proteins.

**Recent Progress:** To provide cellular functionality, microtubules must be oriented and anchored to desired objects and be placed in environments where they can be made to grow or shrink on command. We have been learning how to create dynamic microtubule assemblies in artificial systems by importing or duplicating biological constructs to meet our needs.

Here, we report on the use of: 1) artificial microtubule organizing centers (AMOCs) as anchors, and 2) microtubule associated proteins (MAPs) that regulate the adsorption and polymerization of dynamic microtubule assemblies (Fig. 1).

The combined use of organizing centers and MAPs is illustrated by constructs we have created in which MAPs (Cytoskeleton, Inc.) have been covalently linked to amine-functionalized microspheres. When tubulin monomers are polymerized in the presence of these structures, surface-bound MAPs bind growing microtubules to the organizing center, while MAPs in solution help to stabilize the growing microtubule by inhibiting the depolymerization cycle of the dynamic instability process. The

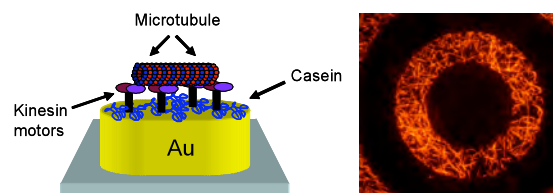


Figure 1: Fluorescent images showing MAP-stabilized microtubules (bright fibers) anchored to an AMOC consisting of a lithographically-defined gold ring (ring width = 10 microns).

resulting structures are asters of microtubules bound and arrayed around the central microsphere (Fig. 2).

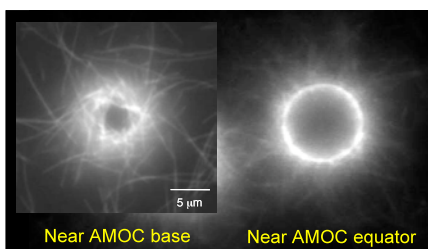


Figure 2: A fluorescent image of a MAP-assembled AMOC: a microtubule aster formed around a polymer bead.

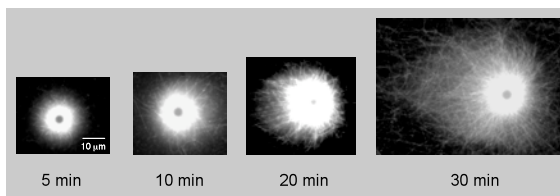


Figure 3: Fluorescent images showing the increased size of MAP-stabilized AMOCs as a function of growth time.

Because the MAPs stabilize the microtubules, the microtubules continue to grow as long as there is a critical concentration of tubulin in solution. This allows us to systematically vary the size of the asters.

We have also demonstrated that the microtubule aster arrays can be dynamically assembled and disassembled. Although the MAPs stabilize against depolymerization of the microtubules at room temperature, lowering the

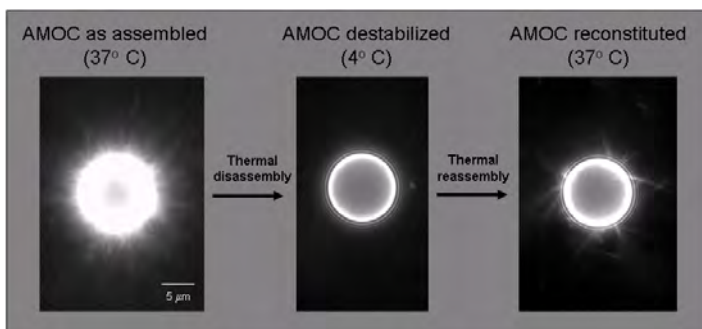


Figure 4: Fluorescent images showing the dynamic, programmable assembly of AMOCs. Images depict the initial assembly, disassembly through thermal destabilization, and ultimate reassembly of AMOC asters.

temperature to 4°C sufficiently destabilizes the microtubules to induce disassembly of the asters. However, the MAPs that are covalently attached to the beads insure that the asters reform on warming the system back to room temperature. (Note: Full recovery requires the addition of fresh MAPs to the solution.)

Finally, we have demonstrated that we can utilize lithographically patterned and functionalized substrates as artificial microtubule organizing centers, and control the formation, disappearance, and movement of microtubules in an “on-chip” environment. In this case, the objects serving as microtubule organizing centers are gold electrodes that have been functionalized with the motor protein kinesin as the MAP. In the presence of the non-hydrolyzable ATP analogue (5’-adenylyl-beta,gamma-imidodiphosphate or AMPPMP), the kinesin motors are capable of binding and stabilizing microtubules, but are incapable of active transport, allowing kinesin to behave just like the other MAPs described here. We have used this AMPPMP-modified kinesin to form microtubule networks that bridge between two gold electrodes (Fig. 5). The bridges can be reversibly removed via two distinct strategies: 1) Cooling to 4°C destabilizes and eliminates the bound microtubules

just as it does when other MAPs are used (Fig. 5, left). 2) The microtubules can also be removed by adding ATP to the solution. Here, ATP displaces the AMPPMP and provides fuel that activates the motor proteins. The kinesin motors then propel the bound microtubules to electrode edges, where they are launched into solution (Fig. 5, right).

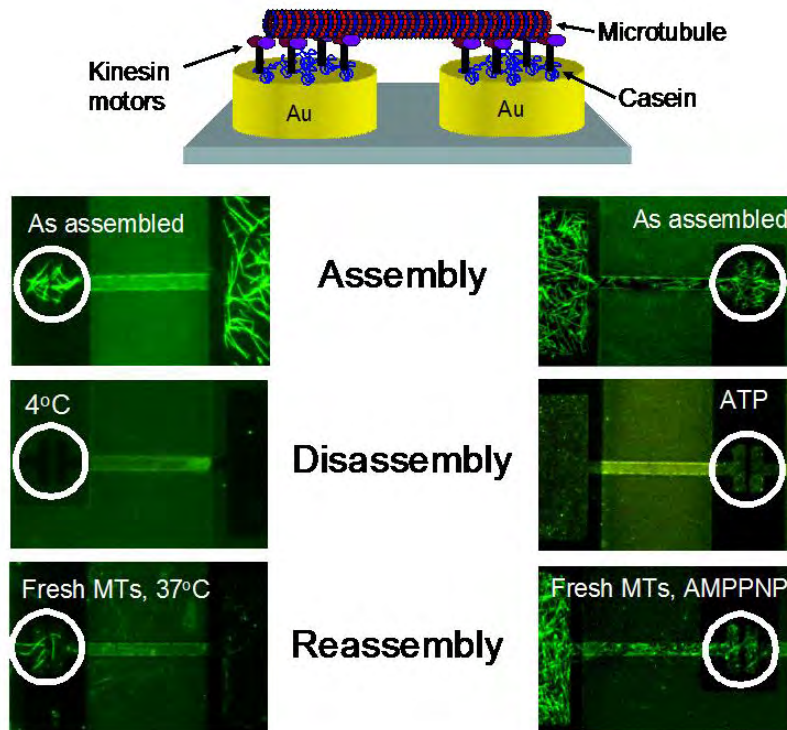


Figure 4: Fluorescent images showing the dynamic, programmable assembly of MT interconnects using thermal instability (left) and ATP-fueled kinesin motility (right). In each case, kinesin motors on the patterned gold selectively capture MTs to form interconnect bridges. Introduction of the programmable stimulus (cooling to destabilize MTs or ATP to activate kinesin motors) in each system resulted in the annihilation of the MT interconnects. Reversing this stimulation (warming with fresh MTs or adding AMPPNP) effectively reconstituted the MT bridge formation.

**Future Plans:** Work on the Microtubule subtask will continue to examine how to create and manipulate two-dimensional patterns of microtubules on substrates. We will also be exploring how to exploit the resulting networks as templates for the deposition of active nanomaterials, as well as for supporting active transport processes involving motor proteins. In the future, we plan to extend these dynamic, programmable materials into three-dimensional architectures such as hydrogel and aerogel constructs. Additional work will investigate creating multiple levels of dynamic assembly. For example, we plan to encapsulate microtubule-organizing centers within lipid vesicles to create constructs such as the artificial amoeba.

## Publications 2007-2009:

E. D. Spoerke, Judy K. Hendricks, George D. Bachand, and Bruce C. Bunker. "Bio-Organization of Microtubule Templates for Metallic Nanointerconnect Synthesis." Submitted to *Nano Letters* (2009).

E.D. Spoerke, Judy K. Hendricks, George D. Bachand, Eleya Bekyarova, Robert C. Haddon, and Bruce C. Bunker. "Dynamic Biomolecular Assembly of Carbon Nanotube Interconnects." Submitted to *Nature Nanotech* (2009).

E.D. Spoerke, Andrew K. Boal, and Bruce C. Bunker, "Dynamic Assembly of Artificial Microtubule Organizing Centers." Submitted to *Langmuir* (2009).

E. D. Spoerke, G.D. Bachand, J. Jiu, D. Y. Sasaki, and B.C. Bunker. "Assembly of polar-oriented synthetic microtubule organizing centers." *Langmuir* **24**(14): 7039-7043 (2008).

A. K. Boal, B. C. Bunker, and T. J. Headley, "Microtubule Templated Synthesis of Metal Sulfide Nanomaterials," *Adv. Funct. Mater.*, in review.

H. Liu, G.D. Bachand, H. Kim, C.C. Hayden, E.A. Abate, and D.Y. Sasaki. "Lipid nanotube formation via streptavidin-membrane binding interactions." *Langmuir* **24**: 3686-3689. (2008).

C.M. Yip, M.S. Kent, and D.Y. Sasaki, "Protein Membrane Interactions on Supported Lipid Membranes." H.S. Nalwa (ed.), vol 2. American Scientific Publishers, Stevenson Ranch. Pp67-121. (2009).

H. Liu, E.D. Spoerke, M. Bachand, S.J. Koch, B.C. Bunker, and G.D. Bachand. "Dynamic self-assembly of nanocomposite structures through the interaction of thermodynamic and energy-dissipating processes." *Adv. Mater.* **20**(23): 4476-4481. (2008). (**Cover**)

A.C. Greene, A.M. Trent, and G.D. Bachand. "Controlling kinesin motor transport through an engineered metal switch. *Biotechnol. Bioeng.* **101**(3): 478-486. (2008).

S. B. Rivera, S. J. Koch, J. M. Bauer, J. M. Edwards, and G.D. Bachand. "Temperature dependent properties of a kinesin-3 motor protein from *Thermomyces lanuginosus*. *Fungal Genet. Biol.* **44**: 1170-1179. (2007).

Sandia is a multiprogram laboratory operated by Sandia Corporation, a Lockheed Martin Company, for the United States Department of Energy's National Nuclear Security Administration under Contract DE-AC04-94AL85000.

## Design and Synthesis of Biologically-Inspired Materials

Millicent A. Firestone<sup>1</sup>, Sungwon Lee<sup>1</sup>, Simonida Grubjesic<sup>1</sup>, Omar Green<sup>1</sup>,  
Gregory Becht<sup>1</sup>, Philip D. Laible<sup>2</sup>

<sup>1</sup>Materials Science and <sup>2</sup>Biosciences Divisions  
Argonne National Laboratory, Argonne, IL 60439  
firestone@anl.gov

**Program Scope:** The *Nanostructured Biocomposite Materials for Energy Transduction* research program has as its overarching goal the design, synthesis, and characterization of a new class of functional nanoscale materials that exploit the native capabilities of biological molecules to store and transduce energy. A major research thrust in this work is the development of biologically-inspired synthetic materials that stabilize and organize proteins and regulate their function.

**Recent Progress:** Membrane proteins give rise to some of Nature's most intricate and important processes, ranging from metabolism to energy transduction. The ability to harness this evolutionarily-optimized functionality outside of the cell could lead to the development of protein-based systems useful for advancing alternative or renewable energy storage or production. The future of protein-based materials (and ultimately devices), however, requires the further development of a suitable supporting and insulating matrix that will preserve, order/orient and control the activity of the proteins. To more fully mimic the complexity of natural systems, additional capabilities should be incorporated into these materials. Specific requirements include: (i) a structured material that contains segregated hydrophilic and hydrophobic regions for the co-integration and spatial organization of both membrane and water-soluble molecules, (ii) a membrane protein sequestering region (i.e., biomembrane) that possesses fluidity suitable for maintenance of protein integrity and dynamics while being impervious to movement of charged species and small soluble entities, (iii) a transport mechanism (i.e., either passive or active) to facilitate the diffusion of essential molecules involved in energy conversion and other metabolic/catalytic processes, and (iv) an approach for the repair of damaged (mis-folded, denatured) proteins. For the full realization of protein-based functional materials in the fabrication of devices, additional criteria must be met including: (i) architectures that ensure assembly of the proteins into high density, ordered arrays for signal amplification and addressability, (ii) matrices that contain components for interfacing with traditional materials or device platforms and (iii) materials with the proper balance of mechanical strength and chemical resistance for use in real world applications but without detriment to the biological components. *Toward this end, our research has emphasized the design, synthesis and characterization of hierarchical, self-assembled, soft nanospace architectures that fulfill these criteria.*

Previously, we reported the development of biomimetic materials that self-assemble into three-dimensional matrices that allow for the compartmentalization, organization and integration of a variety of membrane proteins and accessory molecules. During this funding period, we have worked to chemically modify the composition of these materials so as to both improve their mechanical durability and to allow for functional integration with traditional device materials.

The first of the two soft materials platforms that we have worked to develop is a family of polymer-grafted, lipid-based complex fluids. The complex fluids are composed of mixtures of molecular amphiphiles, whose composition and properties have been shown to be readily tuned to allow for the incorporation of a wide variety of biomolecules (e.g., soluble and membrane proteins). Our work has focused on studying light-transducing integral membrane proteins such as the bacterial photosynthetic reaction center (RC). The RC, whose native function is to convert light into electrochemical energy through generation of stabilized, transmembrane charge separation is of interest since it will provide the basis for the development of a wide variety of light-transducing materials such as solar cells, photodetectors, and photodiodes. During this funding period, we have carried out studies evaluating the co-integration of light-harvesting complexes, both synthetic and natural, that serve to collect and funnel energy to the RCs. These antenna complexes dramatically increase the absorption cross-section of an RC and efficiently transfer energy to it.

In addition, we have also worked to successfully modify the current complex fluid composition so as to improve its mechanical properties. We have synthesized and integrated diacrylate block copolymers, and shown that introduction of the end-reactive groups on the hydrophilic block produces both inter- and intra-lamellar crosslinks within the complex fluid upon brief UV- irradiation, serving to stabilize the self-assembled structure (Figure 1). This compositional modification converts the complex fluid from a physical gel to a durable chemical gel. SAXS studies have shown that integration of the block copolymers allow for the capture of a particular architecture in a

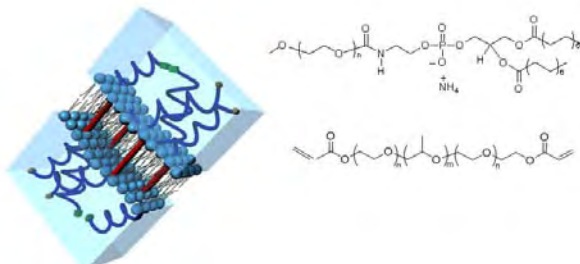


**Figure 1.** Molecular composition and schematic illustration of crosslinked, lamellar structured complex fluid.

durable form. Studies evaluating protein reconstitution and their integrity as a function of crosslinking density are currently underway.

In addition to our studies on complex fluids, a second family of responsive soft nanostructures based upon polymerized ionic liquids (poly(ILs)) have been developed. These nanostructured chemical (polymeric) gels are formed by the spontaneous organization of a binary mixture of water and polymerizable analogues of *N*-alkylimidazolium-based ionic liquids. Photopolymerization of the pre-assembled IL monomers results in the formation of ductile, mechanically

robust gels that have the ability to spatially localize guests within defined compartments in the anisotropic matrix. Many of the polymer architectures resemble those found in cellular environments, featuring amphiphilic bilayers separated by water channels, thus offering the possibility of sequestering both lipophilic (e.g., membrane proteins) and water-soluble guests into the segregated domains. During this funding period we have worked to incorporate components that will facilitate the interfacing and coupling of protein output (light-generated electron flow) to traditional device architectures. Specifically, we have modified these polymers in two ways so as to promote electrical communication between the encapsulated proteins and an external circuit. In the first approach, a hybrid material that organizes Au nanoparticles into columns within a hexagonally perforated lamellar structured poly(IL) was shown to behave as a conduction pathway or conduit (Figure 2). In the second approach, a thiophene moiety was incorporated into the ionic liquid monomer, yielding a nanostructured electrically conductive polymer. Efforts are underway to examine approaches for the co-integration and electrical interfacing of the RCs in these materials.

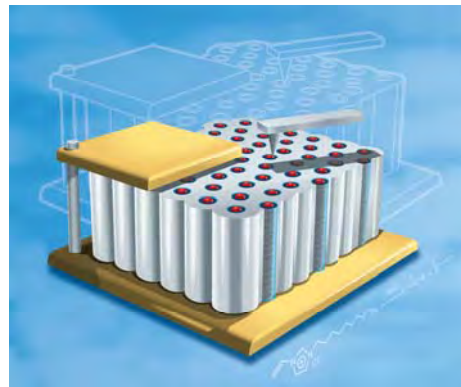


Figure 2. Schematic illustration of the hexagonal perforated lamellar structured poly(1-decyl-3-vinylimidazolium chloride). Au nanoparticles (red) are organized within the hydrophilic columns which function as an electronic conduction pathway to the external circuit.

**Future Plans:** Our recent accomplishment of improving the mechanical properties of the biomimetic materials is significant and will now allow for us to focus our efforts on addressing the challenge of coupling multi-protein activity and connecting their output into traditional device architectures. This work will build upon our prior efforts on photosynthetic proteins by furthering their integration into electronic devices for generating photocurrent. The Au nanoparticle-poly(IL) composite and the thiophene-derived IL polymer will be used to enable an electrical connection between the nanoscopically-organized biomolecules and macroscopic electrodes. Success in this work will permit adaption of the RCs as the basis for a photoelectric device. The fundamental outcome of this work will address three important materials challenges: stabilization of the protein(s) outside its native biomembrane, unidirectional orientation of the protein(s), and efficient means to couple the internal electron transfer cycle to an external electrode system.

Another area of future investigation will examine materials approaches for mimicking Nature's ability to repair or replace damaged proteins. The objective of this work will be to devise materials that mimic the function of molecular chaperones. As a first approach we will explore the use of colloids to control the local electrostatic environment of the proteins within the scaffolds. By controlling the local protein chemical environment it may be possible to inhibit protein unfolding or degradation thereby increasing the operating lifetime of the protein-

based material. Ultimately, materials that possess the ability to repair or remove inactive forms of the proteins will be pursued.

#### DOE Sponsored Publications in 2007-2009

- Green, O.; Grubjesic, S.; Lee, S.; Firestone, M. A. "*The design of polymeric ionic liquids for the preparation of functional materials*", Polymer Reviews 2009, In press. INVITED
- Lee, S.; Cummins, M. D.; Willing, G. A.; Firestone, M. A. "*Conductivity of ionic liquid-derived polymers with internal gold nanoparticle conduits*". J. Mater. Chem. 2009, In press.
- Crisci, A.; Hay, D. N. T.; Seifert, S.; Firestone, M. A. "*pH and ionic strength-induced structural changes in poly(acrylic acid)-lipid based self-assembled materials*", Macromol. Symp. (2009), 281, 126-134.
- Grubjesic, S.; Seifert, S.; Firestone, M. A. "*Cytoskeleton mimetic reinforcement of a self-assembled N, N'-dialkylimidazolium ionic liquid monomer by copolymerization*" Macromolecules (2009), 42, 5461-5470.
- Burns, C. T.; Lee, S.; Seifert, S.; Firestone, M. A., "*Thiophene-based ionic liquids: synthesis, physical properties, self-assembly, and oxidative polymerization*", Polymers for Adv. Tech. (2008), 19(10), 1369-1382. INVITED
- Burns, C. T.; Choi S. Y.; Dietz, M. L.; Firestone, M. A., "*Acidichromic spiropyran-functionalized mesoporous silica: Towards stimuli-responsive metal ion separations media*", Separation Science & Technology, (2008), 43, 2503-2519.
- Lee, B.; Firestone, M. A., "*Electron density mapping of triblock copolymers associated with model biomembranes: Insights into conformational states and effect on bilayer structure*", Biomacromolecules, (2008), 9, 1541-1550.
- Batra, D.; Hay, D. N. T.; Firestone, M. A., "*Formation of a biomimetic, liquid-crystalline hydrogel by self-assembly and polymerization of an ionic liquid*", Chem. Mater. (2007) 19, 4423-4431
- Batra, D.; Seifert, S.; Firestone, M. A., "*The effect of cation structure on the mesophase architecture of self-assembled and polymerized imidazolium-based ionic liquids*", Macromolec. Chem. Phys. (2007) 208, 1416-1427.
- Reiss, B. D.; Hanson, D. K.; Firestone, M. A., "*Evaluation of the photosynthetic reaction center protein as a bioelectronic circuit element*", Biotechnol. Prog. (2007) 23, 985-987.
- Batra, D.; Seifert, S.; Varela, L.; Firestone, M. A., "*Solvent-mediated plasmon-tuning in a gold nanoparticle-poly (ionic liquid) composite*", Adv. Func. Mat. (2007) 17, 1279-1287.
- Reiss, B.; Auciello, O.; Ocola, L. E.; Firestone, M. A., "*Integration of biomolecules with inorganic ferroelectrics: A novel approach to nanoscale devices*" in *Biosurfaces and Biointerfaces*, edited by M. Firestone, J. Schmidt, N. Malmstadt (Mater. Res. Soc. Symp. Proc. 950E, Warrendale, PA, 2007).
- Adiga, S. P.; Zapol, P.; Firestone, M. A., "*Modeling block copolymer interactions with biomimetic membranes*", in *Biosurfaces and Biointerfaces*, edited by M. Firestone, J. Schmidt, N. Malmstadt (Mater. Res. Soc. Symp. Proc. 950E, Warrendale, PA, 2007), 0950-D15-25.

# Using Viral Capsids to Build Integrated Photocatalytic Systems

Matthew B. Francis

University of California, Berkeley, and

Materials Sciences Division, Lawrence Berkeley National Lab

Berkeley, CA 94720-1460

francis@cchem.berkeley.edu

**Program Scope:** The protein capsids of viruses provide a convenient source of rigid, nanoscale scaffolds for the construction of complex multifunctional materials. These proteins can be produced in large quantities through expression in *E. coli*, and can be genetically tailored to possess reactive groups for the positioning of synthetic molecules on their surfaces. Through this program, we have explored the use of two capsid-forming proteins to build light harvesting systems and connect them to photocatalytic groups. In one example, we have developed chemical strategies to attach the rod-like protein shell of the tobacco mosaic virus to polymers,<sup>1</sup> carbon nanotubes,<sup>2</sup> light harvesting chromophores,<sup>3</sup> and porphyrins. We have also developed methods to transfer the modified viral capsids into organic media for the purposes of embedding them into polymeric films. As a second target, methods have been developed to append new functionality to both the external and internal surfaces of MS2 viral capsids. These spherical assemblies have been used to house chromophores that collect light and transfer the energy to catalysts located on the exterior surface. Taken together, these new scaffolds provide many new avenues for the integration of multiple functional components with defined spatial relationships. Equally important for these studies is the set of chemical strategies that has been developed to modify biomolecules with high site selectivity and yield.

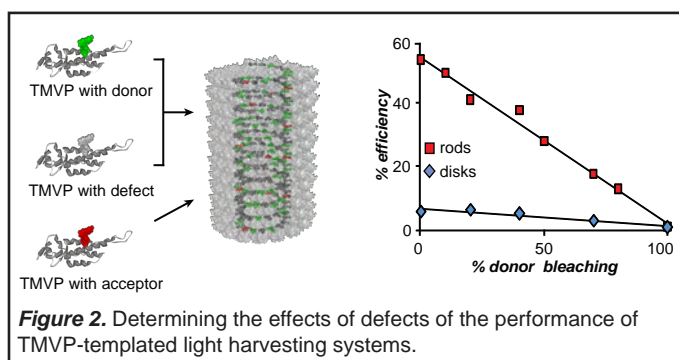
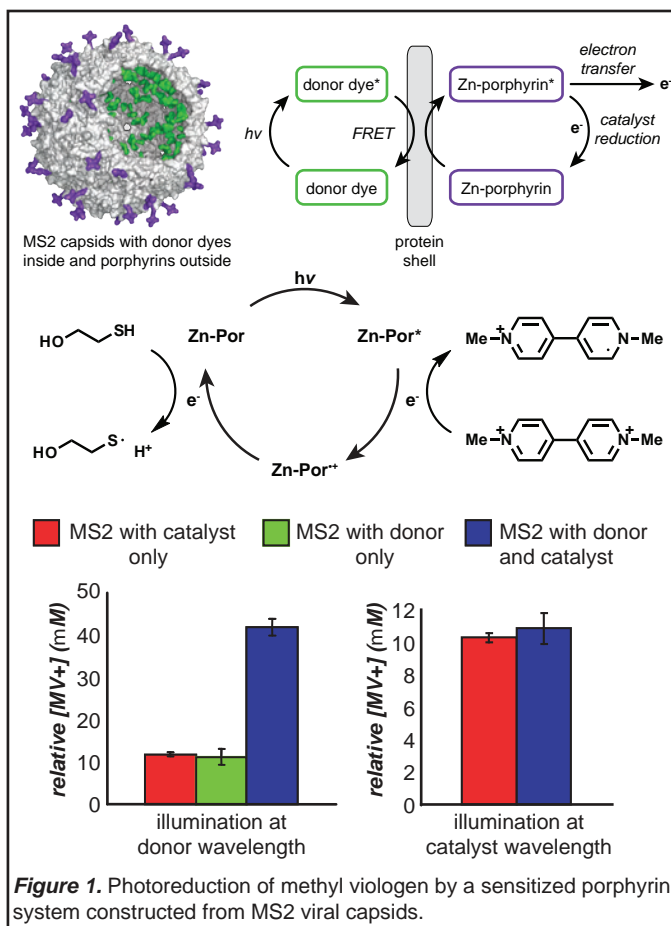
**Recent Progress:** During the past two years, we have developed a new strategy that attaches synthetic groups to artificial amino acids introduced into proteins.<sup>4</sup> Using the *in vivo* amber codon suppression technique developed by Prof. Peter Schultz (Scripps Research Inst.), we can now introduce reactive aniline groups into specific locations on viral capsid proteins. We have also developed a new chemical reaction that can target these residues with high chemoselectivity.<sup>5</sup> In the context of this program, we have used this strategy to attach 30-60 porphyrins to the external surface of MS2 capsids.<sup>6</sup> We have also introduced cysteine residues inside the capsid to allow the installation of fluorescein and other chromophores for light collection, Figure 1. The resulting capsids collect broad spectrum light and transfer the energy through the protein shell to the external catalysts. We have also demonstrated that the photoexcited porphyrins can transfer electrons to soluble carriers, and that the light harvesting systems allow them to work at illumination wavelengths that were previously unusable. We are currently adding phthalocyanines to these systems, as their increased absorption at longer wavelengths (relative to porphyrins) should lead to further improvements in system efficiency.

## Other Highlights:

- A significant amount of effort has been directed toward the synthesis of new porphyrins and phthalocyanines that possess the proper chemical functional groups for protein bioconjugation. In particular, we have synthesized a number of new structures that possess alkoxyamine groups, which can be attached to reactive carbonyls. Several methods are now available for the introduction of ketone and aldehyde groups on proteins, including our oxidative coupling strategy that targets artificial amino acids. With these new molecules and strategies, we can now dictate the position of photocatalytic groups on the genetic level.

- We have previously reported the covalent attachment of chromophores to TMV coat protein monomers (TMVP) and the subsequent self assembly of these proteins to access highly efficient light harvesting systems.<sup>3</sup> These systems have been characterized using steady-state and time-resolved spectroscopic methods.<sup>7</sup> One unique aspect of TMVP-templated light harvesting arrays is the fact that they are inherently three-dimensional, and thus could possess redundant energy transfer pathways that could circumvent defect sites better than two-dimensional systems. To test this possibility, we have recently developed a chemical strategy to introduce well-defined numbers of “bleached” chromophores into the arrays, Figure 2. These studies have shown that the three-dimensional structures do indeed have an improved tolerance for defects, showing a linear decrease in efficiency as photoinactive sites are introduced. In contrast, two-dimensional systems would be expected to show an exponential decrease due to increased exciton trapping. This very promising result that suggests that the three-dimensional TMVP-based systems will be substantially more resistant to photobleaching in device applications. With a view toward building photovoltaic devices, we are developing a new strategy for the attachment of our light harvesting systems to conductive surfaces through the intermediacy of phthalocyanine monolayers. We will then measure the photocurrents that these systems can generate.

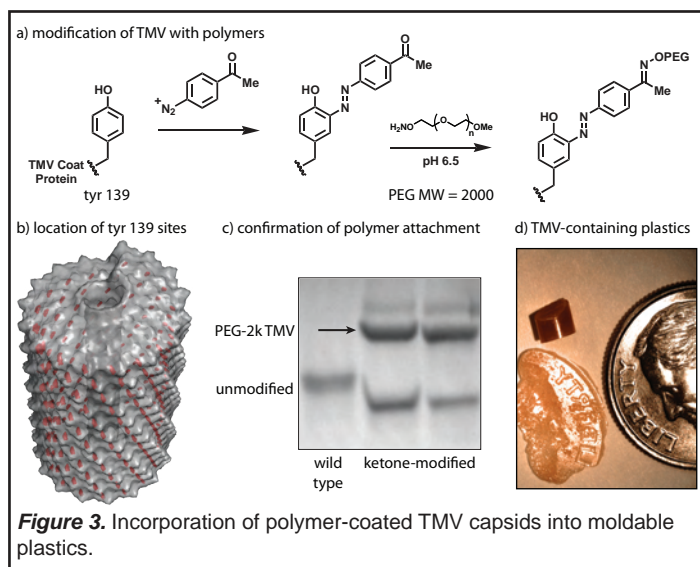
- From our first studies, the assembly



state of TMV-based light harvesting systems has been observed to exert a dramatic effect of light harvesting performance, with rod assemblies consistently significantly outperforming disks, Figure 2. Using computer modeling, we first determined that the principal transition dipole of the chromophores is oriented along the long axis of assembled rods, suggesting that energy transfer is much more efficient in this direction. Disks lack this transfer orientation. Secondly, we have developed a computational simulation of these systems in collaboration with Prof. Phillip Geissler (UC Berkeley). This model tracks the fate of large numbers of absorbed photons as they transfer from donor to donor, and finally to the acceptor groups. The transfer rate constants in these simulations were based on our previous data from time-resolved studies.<sup>7</sup> By changing the format of the chromophore matrix (and thus the rate constants for energy transfer), we can mimic the arrangement in our rod and disk systems. These studies have revealed an important difference in the energy dissipation rates of the donors in the two systems, and they have shown that the small number of chromophores in disk systems is more subject to statistical variations during the assembly process. We are now using these simulations to guide the choice of appropriate photocatalysts for use in these systems.

- Previously we have shown that TMV capsids can be transferred to a variety of aprotic organic solvents after polymer chains have been attached to their external surfaces, Figure 3.<sup>1</sup> In addition to displaying increased thermal stability,<sup>8</sup> the use of these solvents allows an expanded set of processing conditions to be applied for the creation of TMV-containing polymer films. The ability to dissolve these capsids in hydrophobic solvents suggested that they might also be soluble in styrene and other polymerizable aromatic monomers. We have recently found that solutions of PEG-2k TMV can be prepared in neat styrene, and we have added AIBN as a thermal polymerization initiator. Upon heating the styrene polymerizes to yield TMV-containing plastic materials. These polymers can then be heated past the glass transition temperature of the polystyrene and cast into different shapes, Figure 3. In current experiments we are microtoming samples of the TMV-containing plastics and analyzing them using SEM to see how the rod-like assemblies are distributed in this material.

- In a new project area, we have furthered our exploration of the use of well-defined protein modification strategies to integrate proteins into polymer frameworks. In particular, we have developed a tandem modification strategy to add ketone groups to both the N- and the C-terminus of proteins.<sup>9</sup> When combined with soluble polymers possessing alkoxyamine groups, the proteins crosslink the chains to form hydrogels. This preparation method directly couples the folding state of the protein to the hydrodynamic swelling properties of the gel, allowing conformational changes to be reported by size changes in the



material. As one example, we have shown that polymers crosslinked with metallothioneins can efficiently bind toxic heavy metals in ocean water, simultaneously producing a change in gel size that reports the concentration that is present.<sup>10</sup> We are currently incorporating other metal binding proteins into these materials to develop gels that can test and remediate water that is believed to be contaminated with actinides and PCBs, two pollutants that are commonly associated with energy-related activities.

**Reference List (all of these publications have credited this program)**

1. Schlick, T. L.; Ding, Z.; Francis, M. B. "Dual Surface Modification of the Tobacco Mosaic Virus" *J. Am. Chem. Soc.* **2005**, *127*, 3718-3723.
2. Holder, P. G.; Francis, M. B. "Integration of a Self-Assembling Protein Scaffold with Water-Soluble Single-Walled Carbon Nanotubes" *Angewandte Chemie* **2007**, *23*, 4370-4373.
3. Miller, R. A.; Presley, A. D.; Francis, M. B. "Self-Assembling Light Harvesting Systems From Tobacco Mosaic Virus Capsid Proteins" *J. Am. Chem. Soc.* **2007**, *129*, 3104-3109.
4. Carrico, Z. M.; Romanini, D. W.; Mehl, R. A.; Francis, M. B. "Oxidative Coupling of Peptides to a Virus Capsid Containing Unnatural Amino Acids" *Chemical Communications* **2008**, 1205-1207.
5. Hooker, J. M.; Esser-Kahn, A. P.; Francis, M. B. "Modification of Aniline-Containing Proteins Using a Chemoselective Oxidative Coupling Reaction" *J. Am. Chem. Soc.* **2006**, *128*, 15558-15559.
6. Stephanopoulos, N.; Carrico, Z. M.; Francis, M. B. "Nanoscale Integration of Sensitizing Chromophores and Photocatalytic Groups Using Bacteriophage MS2" *Angewandte Chemie Int. Ed.* **2009**, *25*, in press.
7. Ma, Y. Z.; Miller, R. A.; Fleming, G. R.; Francis, M. B. "Energy Transfer Dynamics in Light-Harvesting Assemblies Templated by the Tobacco Mosaic Virus Coat Protein" *J. Phys. Chem. B.* **2008**, *112*, 6887-6892.
8. Johnson, H. R.; Hooker, J. M.; Clark, D. S.; Francis, M. B. "Solubilization and Stabilization of Bacteriophage MS2 in Organic Solvents" *Biotechnology and Bioprocess Engineering* **2007**, 224-233.
9. Esser-Kahn, A. P.; Francis, M. B. "Protein-Crosslinked Polymeric Materials Through Site-Selective Bioconjugation" *Angewandte Chemie Int. Edition* **2008**, *47*, 3751-3754.
10. Esser-Kahn, A. P.; Iavarone, A. I.; Francis, M. B. "Metallothionein-Crosslinked Hydrogels for the Selective Removal of Heavy Metals from Water" *J. Am. Chem. Soc.* **2008**, *130*, 15820-15822.

## Bio-inspired catalytic assemblies

Jean. M.J. Frechet  
Division of Materials Research  
Lawrence Berkeley National Laboratory  
718 Latimer Hall  
Berkeley, CA 94720-1460  
[J\\_Frechet@lbl.gov](mailto:J_Frechet@lbl.gov)

### Program Scope:

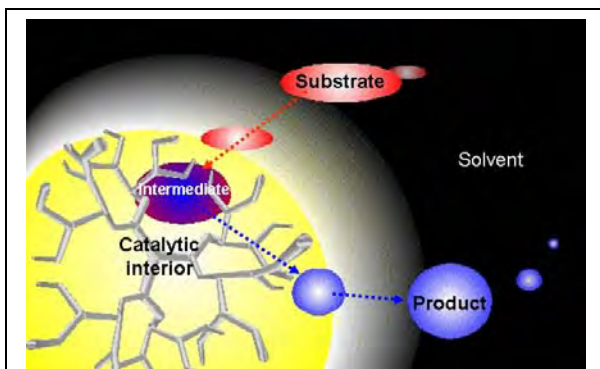


Figure 1. Schematic representation of a bio-inspired catalytic nanoparticle and its mode of action.

As part of a fundamental study of bioinspired catalysts this program explores the design and function of synthetic macromolecules and nanoparticulate assemblies thereof that mimic the shape and function of natural enzymes. The fundamental design of the macromolecules mimics that of enzymes as it incorporates the concepts of site isolation and or free energy driven processes into synthetic macromolecules, about the same size and shape as enzymes, that act as individual nanometer sized reactors with

an active catalytic center surrounded by molecular components that contribute to mass transport in and out of the active center (Figure 1).

### Funding level:

2008-2009 \$76K; 2007-2008: \$140K; 2006-2007: \$140K

### Research Progress

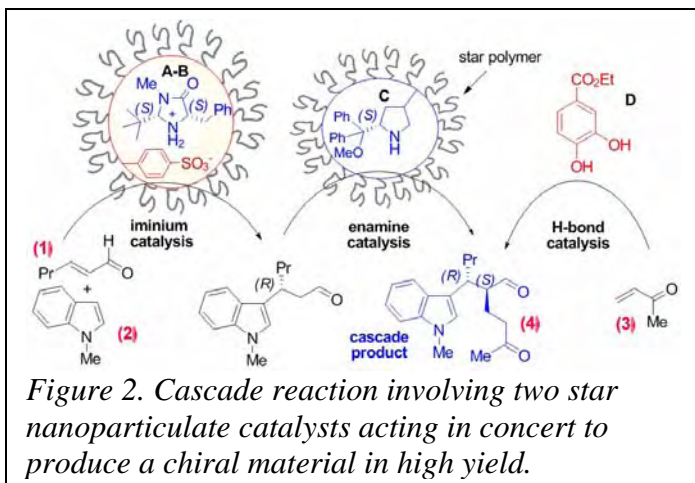


Figure 2. Cascade reaction involving two star nanoparticulate catalysts acting in concert to produce a chiral material in high yield.

#### 1. Star nanoparticles as multi-enzyme mimic in asymmetric reactions.

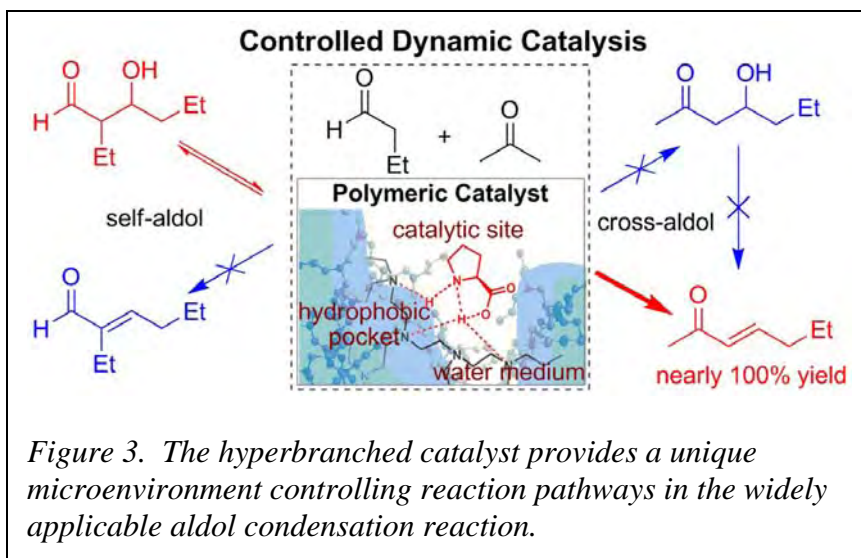
In 2008 we completed the first phase of our work on our asymmetric cascade mimic of multi-enzyme catalysis. Excellent results were obtained with our enzyme-like star nanoparticles enabling the one-pot preparation of complex organic molecules with two stereocenters from a mixture of three very common achiral

starting materials. The reaction shown in the Figure 2 involved two star nanoparticle

catalysts, which, just like enzymes, provided both a chiral environment and site-isolation of the reactive centers. In this reaction three achiral starting materials (1), (2) and (3) are combined in one pot in the presence of enzyme-like star nanoparticle catalysts (A-B) and (C) as well as H-bond donor (D) to produce complex product (4) in 89% isolated yield! The reaction, which creates TWO asymmetric centers proceeds with remarkably high enantioselectivity (99% ee). Unfortunately our plans to continue this project along a very ambitious line have now been discontinued as a result of the 50% funding cutback for this project, and the subsequent departure of uniquely qualified personnel.

## 2. Catalytic control of aldol reaction pathways through catalyst-provided microenvironment: controlled dynamic catalysis.

A fundamental chemoselectivity challenge that remains intrinsically unsolved in aldol-type reactions is the suppression of self-aldol reactions with enolizable aldehydes in reactions such as cross-aldol processes. Contrasting with the usual practice of using large excesses of one component to compete with the undesired self aldehyde condensation reactions, we have developed an enzyme-like polymer catalyst consisting of a



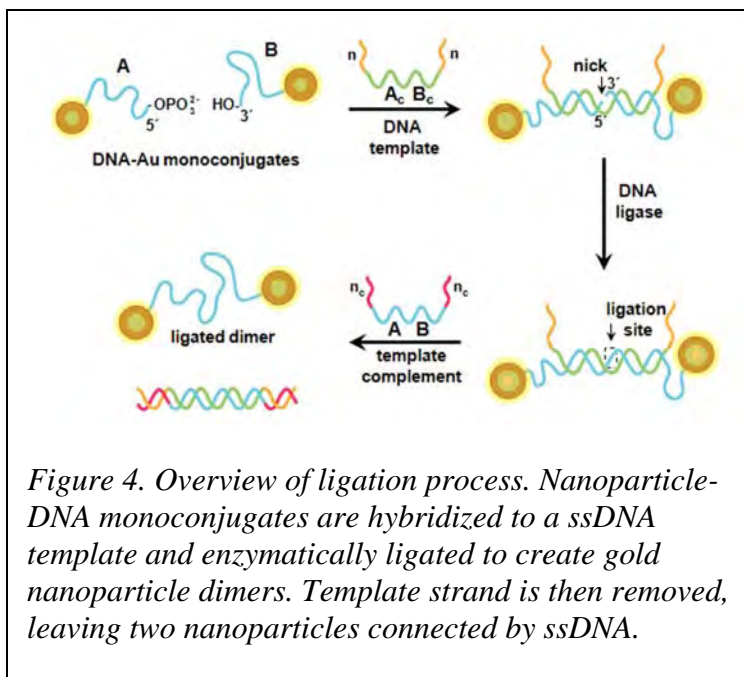
hyperbranched polyethyleneimine derivative and proline that can eliminate the self-aldol reactions by suppressing an irreversible aldol condensation pathway. Control experiments and preliminary mechanistic studies suggest that the polymer catalyst provides an

optimum environment for the aldol reaction to proceed selectively in water, and the catalytic conditions provided by the polymer are difficult to duplicate with typical small molecule analogs. This polymer catalyst system or its modified version have potential applications in developing new or more efficient synthesis, as demonstrated in a dynamic catalytic process for the preparation of  $\alpha,\beta$ -unsaturated ketones using cross ketone/aldehyde reactions without the need for excess substrates.

## 3. Nanoparticle-DNA conjugates. (Collaboration with Paul Alivisatos).

Enzymatic ligation of discrete nanoparticle-DNA conjugates creates nanoparticle dimer and trimer structures in which the nanoparticles are linked by single-stranded DNA, rather than by double-stranded DNA as in previous experiments (Figure 4). Ligation was verified by agarose gel and small-angle X-ray scattering. This capability was utilized in two ways: first, to create a new class of multiparticle building blocks for nanoscale self-

assembly and, second, to develop a system that can amplify a population of discrete nanoparticle assemblies.



Discrete DNA-gold nanoparticle conjugates with DNA lengths as short as 15 bases for both 5 and 20 nm gold particles have been purified by anion-exchange HPLC. Conjugates comprising short DNA (<40 bases) and large gold particles (>20 nm) are difficult to purify by other means and are potential substrates for plasmon coupling experiments. Conjugate purity is demonstrated by hybridizing complementary conjugates to form discrete structures,

which are visualized by TEM. The DNA-nanoparticle conjugates project in collaboration with Paul Alivisatos has now been terminated with the graduation of our joint student Dr. Shelley Claridge.

### Future Plans.

We propose to explore a new modular route to catalytic polymer nanoparticles as enzyme mimics based on the development of a universal core moiety to which a variety of catalytic species can be appended in a single step using for example “click” chemistry. Such an approach would greatly simplify the rather demanding syntheses of our enzyme mimics. In a first phase we plan to synthesize three distinct families of “clickable” polymer carriers differing by their polarity properties:

1. Non-polar periphery, non-polar core
2. Polar periphery, non-polar core
3. Non-polar periphery, polar core

For example, polystyrene may be used as a non-polar component for all of the proposed polymer carriers, due to the fact it has a relatively high chemical inertness while also providing for a rather facile introduction of “clickable” functionalities. Polystyrene is also readily accessible in a variety of topological forms (such as linear chains, stars, or crosslinked nanoscale particles). Polar components may include poly(ethylene oxide), poly(acrylamide), poly(ethyleneimine), and suitably functionalized polyester dendrons. Once this modular approach is established it will be tested in a variety of organocatalytic processes.

## **Publications.**

755. Chi, Y.; Scroggins, S. T.; Boz, E.; Fréchet, J. M. J.. Control of Aldol Reaction Pathways of Enolizable Aldehydes in an Aqueous Environment with a Hyperbranched Polymeric Catalyst. *J. Am. Chem. Soc.*; 2008, 130, 17287-17289.

748 Claridge, S. A.; Mastroianni, A. J.; Au, Y. B.; Liang, H. W.; M., Christine M.; Fréchet, J. M. J.; Alivisatos, A. Paul. Enzymatic Ligation Creates Discrete Multi-nanoparticle Building Blocks for Self-Assembly. *J. Am. Chem. Soc.* 2008, 130, 9598-9605.

745. Chi, Y.; Scroggins, S.T.; Fréchet, J. M. J. One-Pot Multi-Component Asymmetric Cascade Reactions Catalyzed by Soluble Star Polymers with Highly Branched Non-Interpenetrating Catalytic Cores. *J. Am. Chem. Soc.*, 2008, 130, 6322-6323.

741. Zhao, M.; Helms, B.; Slonkina, E.; Friedle, S.; Lee, D.; Dubois, J.; Hedmann, B.; Hodgson, K.O.; Fréchet, J.M.J; Lippard, S.J.; Iron Complexes of Dendrimer-Appended Carboxylates for Activating Dioxygen and Oxidizing Hydrocarbons; *J. Am. Chem. Soc.*, 2008, 130, 4352-4363

737. Claridge, S.A.; Liang, H.W.; Basu, S.R.; Fréchet, J.M.J; Alivisatos, A.P.; Isolation of Discrete Nanoparticle–DNA Conjugates for Plasmonic Applications. *Nanoletters*, 2008, 8, 1202-1206.

## **Biology-Inspired Programmable Assembly of Hybrid Nanosystems**

Oleg Gang (ogang@bnl.gov) and Daniel van der Lelie (vdlelie@bnl.gov)  
Brookhaven National Laboratory, Upton, NY, 11973

*Program scope:* Incorporation of biomolecules into nano-object designs provides a unique opportunity to establish highly selective and reversible interactions between the components of nanosystems, a property previously intrinsic only to biological matter. The encoding, provided by biomolecules, can allow for self-assembly of nanoscale objects of multiple types and functionalities into well determined architectures. The strategies based on using biomolecules as site-specific scaffolds, smart assembly guides and selective glue agents are appealing for the creation of new classes of nanomaterials with potential uses for novel optical and electrical devices, biomedical applications and as an effective way for material fabrication.

The main focus of our interdisciplinary effort is the development of novel biomimetic approaches for the creation of well defined nanoscale architectures that incorporate inorganic nano-objects and biological molecules into hybrid systems. The central areas of this effort include (i) an understanding of the interplay between selective biological interactions and non-selective physical factors for the bio-programmable assembly of hybrid systems; (ii) development of methods for the assembly of inorganic nano-components into well defined nanostructures using biomolecular mediators, cooperative effects, and bio-directed reactions. In addition, underlying all work in assembly is the need for a broader library of biological approaches that provide the required selectivity of interaction, and methods for linking the biological elements to the inorganic nano-materials. Our research strategy combines a characterization of the microscopic structure of nanoscale objects and their systems with a range of methods for the assembly of such systems, including both biochemical and physiochemical approaches.

*Recent progress:* Spatial organization of nanoscale systems by means of self-assembly relies on effective control of inter-component interactions and entropic effects. An encoded addressability of the interactions between system components using biomolecules is especially lucrative for the creation of rationally designed multicomponent systems, since it allow for establishing interaction rules, thus leading to rational and predictable methods for nanosystem assembly. Approaches based on DNA programmability for a pre-designed placement of nanoparticles in one- and two-dimensions have demonstrated a great potential of this strategy. However, in three dimensions, experimental realization of nanoparticle ordering using DNA motifs has remained elusive until recently, with nanoscale systems forming amorphous aggregates. At the same time, theoretical works predicted a rich phase behavior of DNA mediated assemblies even for relatively simple binary systems. We have focused our efforts on understanding the relationship between factors related to the design of DNA mediated nano-objects, involved interactions and thermodynamic pathways and a phase formation of assembled systems.

Recently, we achieved an important breakthrough by discovering a crystalline ordering in DNA mediated nanoparticle assemblies, i.e. superlattices. We have systematically studied a structure of self-assembled aggregates in a binary system of DNA coated nanoparticle for various single stranded (ss) DNA lengths. In each assembly system, a set of DNA-capped gold nanoparticles with different DNA structures were allowed to assemble via DNA hybridization into mesoscale

aggregates. The complementary outer recognition sequences of the DNA-capping provided the driving force for A and B particle assembly. The length of the recognition sequence sets the scale of adhesion (per hybridized linker), while attraction energy varies from  $\sim 30$  kT at room temperature, to  $\sim 0$  kT at DNA melting temperature. In a “brush” regime, the length, of DNA and the flexibility of the non-complementary internal spacer allowed for tuning the range of repulsive interaction and its strength. Thus, the use of systems with constant recognition sequence and varied spacer length allowed for effective tuning of interparticle potential. For sufficiently soft interaction potentials (long ssDNA), we discovered the formation of 3D nanoparticle assemblies with crystalline long range ( $\sim$ micron) order using synchrotron SAXS measurements (Fig. 1). The crystalline assemblies are thermodynamically reversible and temperature-tunable, with body centered cubic (BCC) lattices, where particles occupy only  $\sim 4\%$  of the unit cell. The DNA design and thermodynamic pathway leading to the crystallization of particles has been explored, thus, opening the way for creation of new classes of nanoscale metamaterials.

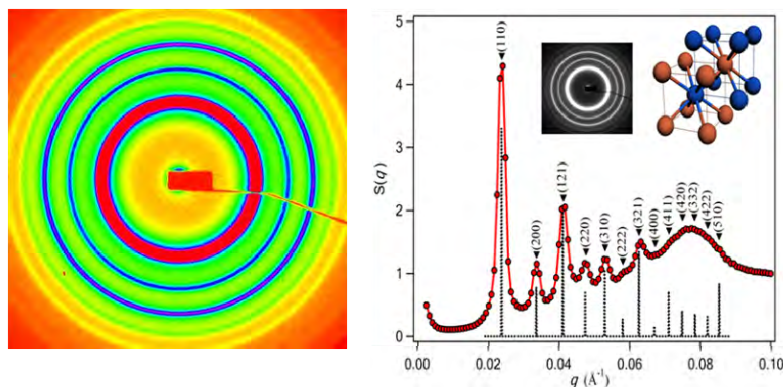


Figure 1. Small angle x-ray scattering (SAXS) pattern of assembly of nanoparticles functionalized with complementary DNA (left) reveals a crystalline structure (right) with BCC lattice organization. (D. Nykypanchuk, M. M. Maye, D. van der Lelie, and O. Gang, Nature **451**, 549, 2008).

The use of interparticle DNA linker, whose two ends are complimentary to the respective mutually non-complementary ssDNAs is particularly attractive due to its potential for building various architectures from a given set of nanoparticle via different linker designs. Our recent efforts were focused on a systematic, structural study of nanoparticle assemblies with flexible ssDNAs linkers of different lengths and fixed DNA recognition ends. We found that that formation of crystalline organization is evidently favored for longer and more flexible ssDNA linker. Our results indicates that relative ratio  $r$  of DNA linkers vs. particle has a dramatic effect on the crystallization behavior. For example no crystalline structure is obtained if  $r \sim 6$ , while particle self-assemble in a BCC structure when  $r \sim 10$ . At the same time, the observed correlation between a length of DNA linker and onset of crystallization is strongly depends on  $r$ . We investigated how phase formation depends on  $r$  for DNA linkers of various lengths and explored if by regulating a fraction of linkers we can control of the coordination number.

The phase diagram of DNA linker mediated nanoparticle assemblies was experimentally investigated and constructed (Fig. 2). Using small angle x-ray scattering we studied the dependence of the internal structure of assembly on two main system parameters: DNA linker length and the number of linkers per particle. The formation of a crystalline BCC phase was observed for a limited range of linker lengths, while the number of linkers per particle controlled the onset of system crystallization. We also investigated the influence of linkage defects on

crystalline structure of assembled superlattice. The observed phase behavior of DNA mediated nanoparticles correlates with predictions for star-polymers systems.

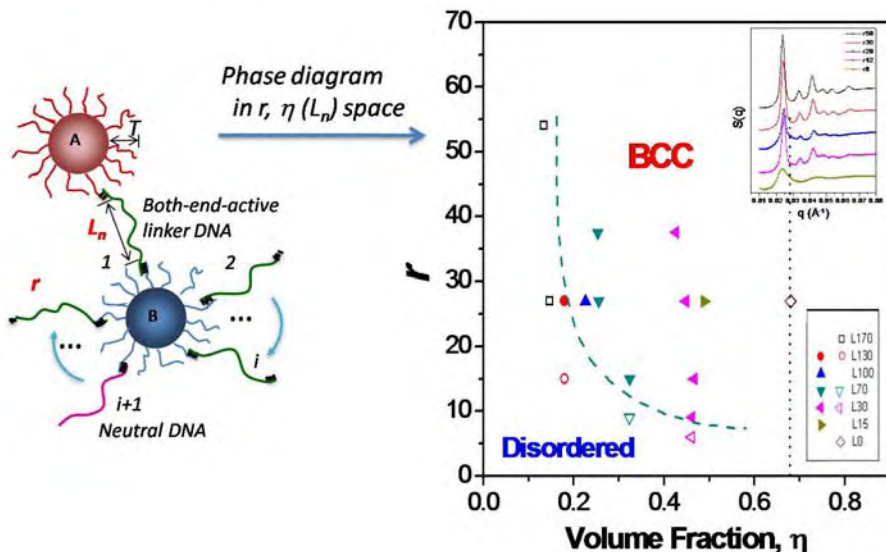


Figure 2. Experimental phase diagram of DNA covered gold nanoparticles (AuNP) in terms of linker/AuNP ratio  $r$  and volume fraction  $\eta$  determined by a linker length. Open and solid symbols correspond to disordered and ordered states, respectively. Vertical dotted line represents maximum volume fraction of BCC phase of touching core-shell NPs. (Inset) The structure factor of system connected with 30 bases linker for different linker/AuNP ratio  $r$ . (H. M. Xiong, D. van der Lelie, and O. Gang, PRL **102**, 015504, 2009)

The inherent temperature dependence of DNA hybridization limits the use of temperature sensitive biological molecules, including proteins. We therefore developed an alternative method for controllable assembly and disassembly of single stranded DNA (ssDNA) conjugated nanoparticles, using the gene 5 protein as the molecular glue via binding to two anti-parallel ssDNAs. The g5p protein is encoded by filamentous bacteriophages where it cooperatively binds to ssDNA to form precursors for the assembly of phage particles. We demonstrated that ssDNA functionalized nano sized particles could be assembled into aggregates by the addition of g5p. The entire process was controlled tightly by the concentration of the g5p protein and the presence of double-stranded DNA. The g5p-ssDNA aggregate was successfully disintegrated by hybridization with complementary ssDNA that triggers the dissociation of the complex. This permits to control both assembly and disassembly of nanoparticles at room temperature without thermal treatment.

Our future studies will be focused on further investigation of phase behavior of hybrid systems with recognition interactions and understanding underlying phenomena, and development of novel approaches for assembly of well-ordered nanoscale systems using biomolecular motifs. Specifically, we will conduct:

- Investigation of assembly, phase behavior and elastic properties of 3D nanoparticle/DNA structures with regulated DNA assembly motifs, including systems with binary set of particles and with more complex (non-spherical) particle's geometry.

- Study on behavior and self-organization processes of bio-functionalized nanoparticles at interfaces, where we will explore how a competition between particle-particle and particle-surface interactions, effect of multiple bio-recognition events and cooperative phenomena of DNA chains affect structure formation. Our studies also aim to reveal structural, thermal and reaction behavior of DNA in confined geometries.
- Application of engineered DNA binding proteins, such as the gene 5 protein of filamentous bacteriophages and the MecP2 methyl-CpG binding protein for design biological scaffolds by formation of complexes with double stranded DNA and is to use the scaffolds for programmed self-assembly of nanoparticles.

### **Publications during 2007-2009:**

M. M. Maye, D. Nykypanchuk, D. van der Lelie, and O. Gang, "DNA-Regulated micro- and nanoparticle assembly", *Small* **3**, 1678 (2007).

D. Nykypanchuk, M. M. Maye, D. van der Lelie, and O. Gang, "DNA-based approach for interparticle interaction control", *Langmuir* **23**, 6305 (2007).

H. Kang, M. Maye, D. Nykypanchuk, M. Clarke, P. Yim, K. Briggman, O. Gang, and J. Hwang, "Optical properties of single DNA-conjugated quantum dots by single molecule confocal microscopy and spectroscopy", *Biophysical Journal*, 337A (2007).

D. Nykypanchuk, M. M. Maye, D. van der Lelie, and O. Gang, "DNA-guided crystallization of colloidal nanoparticles", *Nature* **451**, 549 (2008). (featured on the cover; selected in the Nature Editors favorite list for 2008; highlighted in Science and in various media)

B. J. Panessa-Warren, J. B. Warren, M. M. Maye, D. Van der Lelie, O. Gang, S. S. Wong, B. Ghebrehiwet, G. T. Tortora, and J. A. Misewich, "Human epithelial cell processing of carbon and gold nanoparticles", *International Journal of Nanotechnology* **5**, 55 (2008).

H. M. Xiong, D. van der Lelie, and O. Gang, "DNA linker-mediated crystallization of nanocolloids", *Journal of the American Chemical Society* **130**, 2442 (2008).

M. M. Maye, P. Freumuth, and O. Gang, "Adenovirus Knob Trimers as Tailorable Scaffolds for Nanoscale Assembly", *Small* **4**, 1941 (2008).

S. K. Lee, M. M. Maye, Y. B. Zhang, O. Gang, and D. van der Lelie, "Controllable g5p-Protein-Directed Aggregation of ssDNA-Gold Nanoparticles", *Langmuir* **25**, 657 (2009).

Y. B. Zhang, S. Monchy, B. Greenberg, M. Mergeay, O. Gang, S. Taghavi, D. van der Lelie, "ArsR arsenic-resistance regulatory protein from *Cupriavidus metallidurans* CH34", *Antonie Van Leeuwenhoek International Journal of General and Molecular Microbiology* **96**(2): 161-170, (2009)

M. M. Maye, D. Nykypanchuk, M. Cusiner, D. van der Lelie, and O. Gang, "Stepwise surface encoding for high-throughput assembly of nanoclusters", *Nature Materials*, **8**, 388 (2009) (media coverage ABCNews.com, Science News)

H. M. Xiong, D. van der Lelie, and O. Gang, "Phase Behavior of Nanoparticles Assembled by DNA Linkers", *Physical Review Letters* **102**, 015504 (2009).

# Statistical mechanics of biomolecular materials

Phillip Geissler

Lawrence Berkeley National Laboratory

Materials Sciences Division

Biomolecular Materials Program

1 Cyclotron Rd.

Berkeley, CA 94720

[plgeissler@lbl.gov](mailto:plgeissler@lbl.gov)

**Program Scope:** Biomolecular materials differ fundamentally from their solid state counterparts not only in the origin of their components but also in how they organize. Noncovalent forces governing intra- and inter-molecular arrangements of proteins and nucleic acids are hardly stronger than random thermal noise at room temperature. The resulting softness and fluxionality of these arrangements greatly complicate rational design of biomolecular materials, but they also enrich the possible sensitivity, adaptivity, and functional diversity that can be achieved. This project uses theoretical tools of statistical mechanics to examine how microscopic fluctuations shape structure, response, and dynamics of solutions comprising many biological molecules and other nanometer-scale components. Specific focus is on the use of DNA hybridization to construct nanoparticle arrays, on tailoring protein complexes to achieve robust and adaptive self-assembly, and on exploiting the statistical mechanics of lipid bilayers to organize membrane-associated molecules.

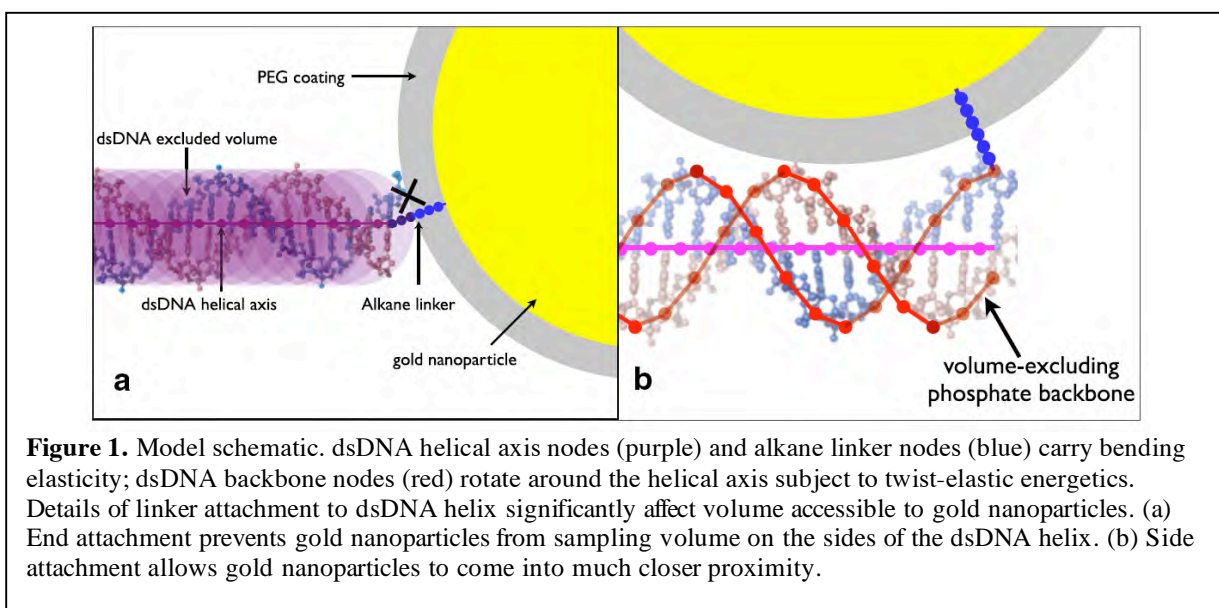
## Recent Progress:

### *Building nanoparticle super-molecules with DNA*

The sequence-specific hybridization of nucleic acids appears to offer a unique opportunity for structural design at nanometer- to micron-length scales. In principle, connections between nanoparticle components (e.g., colloidal nanocrystals) can be programmed in detail through the nucleotide sequences of single-stranded DNA (ssDNA) segments to which they are attached. Small clusters, in effect nanoparticle “molecules”, have been built in this fashion. Synthesizing more complex superstructures, from large intricately shaped clusters to extended ordered arrays, relies on overcoming several challenges. Among them are (1) understanding in quantitative detail the physical properties of their “covalent bonds,” i.e., subpersistence-length segments of double-stranded DNA (dsDNA), and (2) preventing nonspecific hybridization events that can generate prohibitive kinetic barriers to self-assembly.

In the last two years we have made significant progress on the first of these issues, working closely with Paul Alivisatos’s laboratory. In experiments nanoparticle dimers are assembled from gold particles labeled with complementary ssDNA segments. X-ray scattering from these constructs yields an unambiguous characterization of fluctuations in the dots’ separation distance. Our theoretical contributions provide a basis for molecular inferences through geometrically, mechanically, and statistically sound models. Fig. 1 illustrates our approach, calling attention to details of gold-DNA attachment we have found to critically affect model predictions and implications for anomalous dsDNA elasticity.

We have performed Monte Carlo simulations of a model based upon the worm-like chain description of semiflexible polymers. We find that this simple mechanical description, with a standard persistence length 50 nm, is quite accurate in describing dsDNA conformational statistics for constructs comprising tens of basepairs. We regard the success of this simple semiflexible polymer model as an indication that correlations in local bending angle (in contrast to those in local

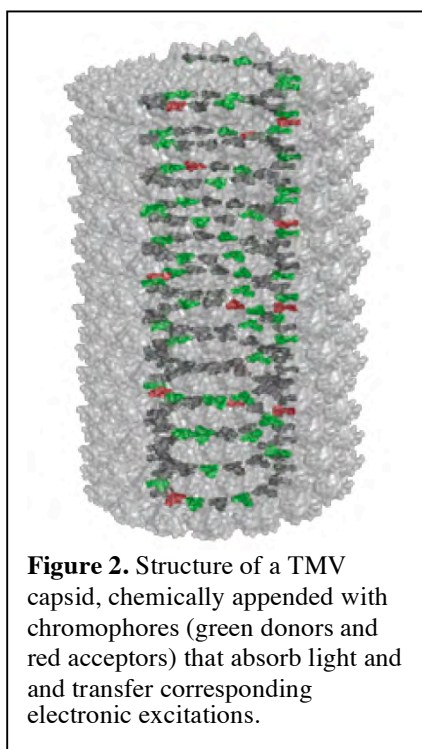


orientation) do not extend much beyond a few basepairs. Our computer simulations highlight the consequences of such a limited correlation length: for chain conformations determined by tens of statistically independent bending angles, even highly nonlinear elaborations in bending potential (e.g., that proposed to describe disruption of local basepairing) influence distributions of typical end-to-end distance fluctuations in barely perceptible ways, provided they are consistent with the well-established mechanics of dsDNA at large scales. The computational results we present are thus robust to changes in the fine details of bending energetics. They are quite sensitive, however, to the way certain aspects of the DNA-nanoparticle attachment geometry are treated, emphasizing the importance of scrutinizing how indirect measurement methods report on macromolecular structure at the nanometer length scale.

These results argue against suggestions that dsDNA becomes unexpectedly flexible on length scales of tens of nanometers, and against suggestions that unexpectedly soft stretching modes are needed to rationalize scattering data of this sort. They emphasize instead the limitations of conventional notions that caricature subpersistence-length chains as effectively rigid. In related work we have used similar models to investigate kinetics of dsDNA cyclization that focus more directly on structural response to tight bending. That work indicates that new experimental approaches are still needed to establish the circumstances under which localized disruptions of Watson-Crick basepairing become important.

### *Light harvesting with viral capsids*

The photosynthetic apparatus is uniquely able to convert the energy of absorbed sunlight into chemical bonds. This complex collection of proteins, pigments, and electron transfer centers functions to create a transmembrane potential that drives the synthesis of high energy metabolites. While detailed spectroscopic studies of the natural system have yielded fundamental insight into its energy transfer processes, similarly efficient synthetic systems have been difficult to prepare due to the lack of available methods that can localize the multiple components in the positions that these mechanisms dictate. The primary goal of our studies together with Matt Francis's laboratory is to develop biomolecule-based scaffolds that can template artificial photosynthetic systems with unparalleled efficiency and control. The realization of this goal requires both an expanded set of chemical methods for the attachment of synthetic groups to proteins and a detailed understanding of



the cooperative interplay between the chromophores and photocatalysts involved in energy transduction.

The ways in which the heterogeneous environment presented by a biomolecular scaffold influences efficiencies of energy transfer and catalytic activity can be very difficult to anticipate. Chromophores embedded within self-assembling structures such as TMV rods are likely not free to rotate but are instead orientationally biased by the scaffold. In turn, these moieties can affect the assembly properties and overall structure of the scaffold itself. Chromophore-labeled TMV monomers, for example, exhibit an enhanced tendency to assemble relative to their unlabeled counterparts. The strength of dipolar coupling between energy transfer units, which ultimately dictates light-harvesting efficiency, is thus an emergent property of the synthetic architecture. We have begun to develop multi-scale theoretical models to rationalize observed energy collection behavior in terms of molecular structure and dynamics, and eventually to predict synthetic modifications that could improve device performance dramatically.

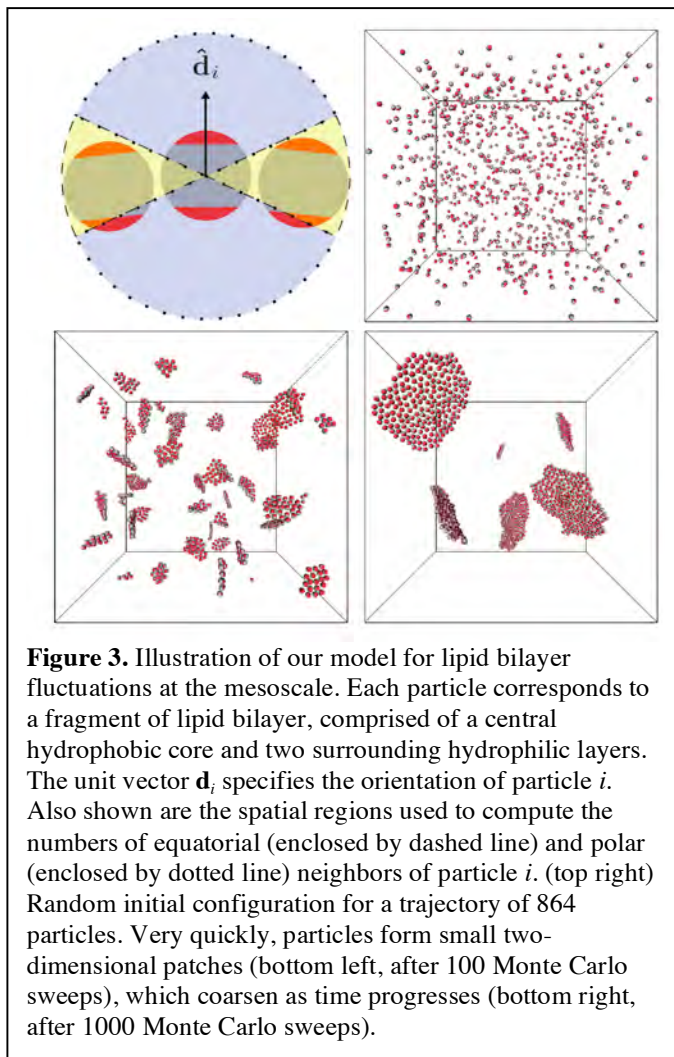
At the coarsest level we represent TMV-based light-harvesting arrays as networks of photoactive centers that can each absorb light, accept excitations from neighboring chromophores, dissipate energy, bleach, and as a result shuttle excitations to catalytic sites. We have carried out Monte Carlo computer simulations of excitation dynamics within networks of various donor densities, rates of transfer and energy loss, and geometries. The results of these studies bear out the defect tolerance of three-dimensional architectures shown in Fig. 2 as a consequence of pathway redundancy, thus establishing a key principle for future scaffold designs. They also suggest that incorporation within the capsid scaffold greatly suppresses energy dissipation routes that impair collection efficiencies in free solution and even in isolated capsid subunits (i.e., TMV disks).

### *Patterning within lipid bilayers*

The membranes of living cells feature richly organized lipids and protein inclusions. Recent experiments, for example in Jay Groves’s laboratory, suggest that the origin of these spatial patterns can lie not in detailed regulation or protein binding but instead in natural correlations among compositional fluctuations and those in membrane shape.

We have developed a new simulation model at the many-lipid scale to scrutinize such correlations and their patterning capabilities. Our description follows transparently from the statistical mechanics of hydrophobicity underlying membrane thermodynamics. Coarse-grained features that have proved difficult to capture by other approaches arise quite naturally from this microscopically grounded perspective. Despite its simplicity, our model successfully captures several important properties of lipid bilayer physics, such as intrinsic fluidity and the ability to spontaneously assemble into two-dimensional sheets. It is furthermore sufficiently versatile to reproduce a wide range of experimentally relevant elastic properties.

We envision the lipid bilayer as a collection of small membrane patches of size  $d \approx 5$  nm, roughly the thickness of a typical bilayer, each comprising  $\approx 100$  phospholipid molecules. For geometric simplicity, we represent each patch as a volume-excluding sphere with an axis of rotational symmetry pointing from one polar head group region to the other. Cohesion of such patches is due of



applications are underway. In the case of lipid membranes we are poised to examine how membrane shape fluctuations mediate aggregation of inclusions, making direct connection with Jay Groves's experiments. In the case of artificial light-harvesting apparatus, we plan computer simulations that will explore detailed mechanisms of energy transfer and dissipation within synthetic matrices, supporting the rational design of Matt Francis's artificial capsid-based systems. In the case of dsDNA elasticity, we have begun atomistically detailed molecular dynamics calculations to elucidate the relationship between bending strain and dehybridization, informing a next generation of coarse-grained models. We further plan coarse-grained studies of hybridization kinetics in the self-assembly of complex nanoparticle arrays.

### Publications:

A.J. Mastroianni, D.A. Sivak, P.L. Geissler, and A.P. Alivisatos, "Probing the conformational distributions of subpersistence length DNA," *Biophysical Journal*, in press (2009).

A. Pasqua, L. Maibaum, G. Oster, D.A. Fletcher, P.L. Geissler, "Large-scale simulations of fluctuating biological membranes," arXiv:0904.2245 (2009).

R.A. Miller, N. Stephanopoulos, J.M. McFarland, A.S. Rosko, P.L. Geissler, and M.B. Francis, "The impact of assembly state on the defect tolerance of TMV-based light harvesting arrays," in preparation (2009).

course to the presence of water: Exposing the hydrophobic portion (i.e., the equatorial region of our model spheres) to solvent incurs a free energetic cost, while exposing the hydrophilic portion (i.e., the polar caps of our model spheres) is thermo-dynamically advantageous. At length scales  $> 1$  nm both of these contributions should be proportional to the exposed area. Remarkably, these considerations alone are sufficient to successfully mimic the flexibility and fluidity of natural bilayers.

The advantage of our model lies in a facile ability to address mesoscale response without sacrificing the microscopic basis of corresponding fluctuations. As a representative biophysical example that calls for these capabilities, we considered the resistance of a fluctuating membrane to impingement of a nanorod oriented perpendicular to the lipid bilayer. Experimental realizations of this situation include extension of polymerizing actin filaments close to a cell membrane and external forcing of a carbon nanotube against a cell wall.

### Future Plans:

In each of the areas described above we have developed new theoretical capabilities whose

# Hybrid static/fluidic synthetic substrates to interface living and nonliving

Theobald Lohmueller and Jay T. Groves

Matt Francis, Phil Geissler, Carolyn Bertozzi

## Biomolecular Materials Program

Materials Sciences Division  
Lawrence Berkeley National Laboratory  
408 Stanley Hall  
Berkeley, CA 9720  
[tlohmueller@gmail.com](mailto:tlohmueller@gmail.com)  
[JTGroves@lbl.gov](mailto:JTGroves@lbl.gov)

**Program Scope:** The long-term goal of our project is the development of novel nano-patterned synthetic materials to establish functional interfaces between living cells and nonliving devices. In particular, we focus on spatial and mechanical aspects of how cells interact with specific signaling molecules. Arrays of micro- and nano-patterned adhesion molecules have been used to show that structural differences of a few nanometers can influence cell fate. However, fixed surface patterning is known to fall far short of achieving long-term stable interfaces needed for technological applications. Consequently there is a high demand on further developments in material science and nanotechnology to mimic biological interfaces with defined chemical composition and physical properties. In this project we aim to characterize the coupling mechanisms that link cytoskeletal dynamics to chemical signaling pathways inside living cells by patterning certain proteins while others are able to freely diffuse within the interface.

**Recent Progress:** Block Copolymer Nanolithography (BCL) will be used as a bottom-up approach to create quasi-hexagonal arrays of noble metal nanoparticles on a rigid support, such as glass or silica. Polystyrene (PS)-*block*-poly(2-vinylpyridine) (P2VP) diblock copolymers are dissolved in toluene, forming micelles that can be loaded with a defined amount of a metallic precursor. When a solid substrate is dip-coated in the solution, solvent evaporation causes the micelles to self-assemble into a hexagonally-packed monolayer. Subsequent oxygen plasma treatment of the sample leads to a complete removal of the polymer shell, leaving behind an array of periodically-spaced metal particles on the substrate's surface. The separation distance between the nanoparticles can be adjusted in a range between 50 and 200 nm by varying the molecular weight of the diblock copolymer, the concentration of the polymer solution and the dipping speed respectively. The gold nanoparticles can be functionalized with specific proteins or molecules. Particle sizes in the range of 2-50 nm produce pattern dimensions that match the structural dimensions of membrane receptors in a living cell.

The deposition of lipid bilayers between biofunctionalized gold nanoparticles would thus result in a system where one specific molecule is tethered at the interface, while membrane bound molecules are able to diffuse freely on the surface. This system allows the patterning of an area of several  $\text{cm}^2$  with defined density of adhesion molecules and high sample throughput which is advantageous for biological studies.

We performed first experiments for the development of an artificial platform that allows static and dynamic patterning of proteins by combining supported lipid bilayers (SLBs) with biofunctionalized nanoparticles. Recent activities include:

- Fabrication of quasi-hexagonal arrays of gold nanoparticles with variable particle size and density using Block Copolymer Nanolithography (BCL).
- Selective immobilization of proteins to gold nanoparticles by using a mono-thiol- (Ni-nitrilotriacetic acid) NTA-histidine tag (His-tag) linker system.
- Formation of supported lipid bilayers between the nanoparticles.
- First life cell experiments of biofunctionalized nanoparticle/lipid bilayer substrates.

**Future Plans:** We are aiming to develop an innovative biomimetic platform that combines both, static and dynamic components suitable for quantitative studies on living cells. The system will be realized by deposition of supported lipid bilayers (SLB) between hexagonal arrays of gold nanoparticles. Intracellular adhesion molecule-1 (ICAM-1) will be statically bound to the particles while membrane-linked major histocompatibility complex molecules (MHCs) are able to diffuse within the lipid bilayer.

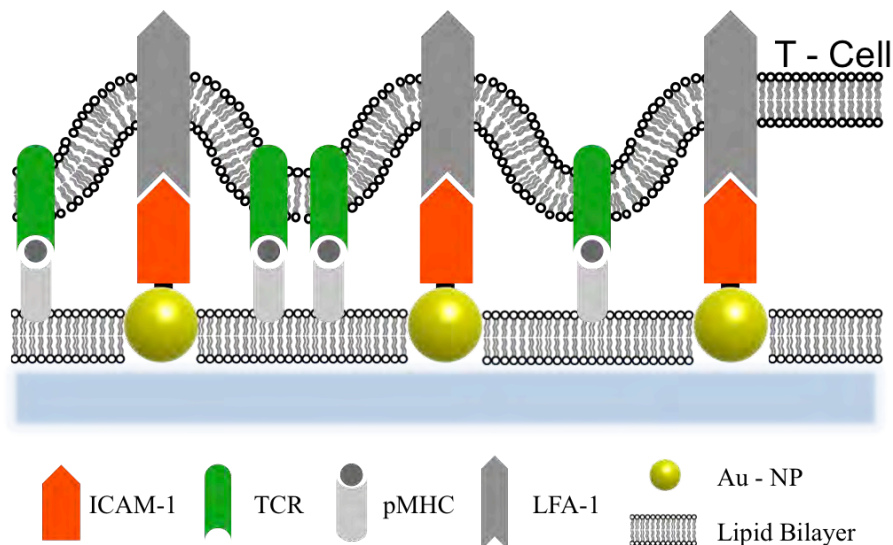


**Fig.1:** Schematic overview of the aspired approach: Gold nanoparticles are selectively functionalized with ICAM-1 molecules. The particle diameter as well as the interparticle spacing is thereby controlled within a range of several hundred nanometers. At the same time a supported membrane containing pMHC molecules is deposited between the gold dots. Within this approach, ICAM-1 is fixed on the platform with

single molecule precision, while unperturbed pMHC-TCR movement within the bilayer allows the formation of the designated supramolecular activation cluster.

The application of the system to immune cell studies allows to investigate how nanopatterning of adhesion molecules in a background of mobile activating ligands does affect cell adhesion and signaling *in vivo*. Epifluorescence and total internal reflection microscopy will be used to reveal how molecular reorganization and clustering is altered by predefined pattern on a molecular level. Experimental work to accomplish this includes:

- AFM studies will be performed to characterize the formation of nanoparticle/lipid bilayer interfaces. In particular we wish to determine whether the SLB is covering the gold nanoparticles and if this is dependent on the interparticle spacing and/or the particle size. Furthermore AFM measurements should reveal the binding of single proteins to the nanoparticles
- Selective immobilization of ICAM-1 to gold nanoparticles and pMHC to the lipid bilayer by using thiol chemistry and (Ni-nitrilotriacetic acid) NTA-histidine tag (His-tag) linker system.
- The dynamics of the TCR movement during synapse formation can be tracked by using total internal reflection fluorescence microscopy (TIRF). TCR microclusters will be imaged by staining the TCR clusters and LFA-1 with anti-TCR Fab H57 fragments and anti-LFA-1 antibody, respectively.
- Utilization of top-down lithography in combination with BCL to generate aperiodic micro-/nanostructured pattern over a large surface area.
- T-Cell activation will be quantified by measuring the relative cytoplasmatic  $Ca^{2+}$  levels of individual cells using Fura-2 as a ratiometric fluorescent dye. Related to the calcium levels the secretion of interferons (INF) will be measured to quantify the activation of T cells using Enzyme-linked Immunosorbent Assay (ELISA) analysis.

Besides looking at T-Cell activation, this project should yield to a general approach for an artificial platform, suitable for controlling interactions with living cells in hybrid synthetic environments. By varying the receptor molecules, this approach can be translated to many different cell types with different utilitarian applications in energy and materials science.

The present approach is an important advance of established methods in chemistry and material science by combining self-assembly based nanotechnology with fluid membrane patterning to probe reorganization and clustering of receptor proteins in the cell membrane with nanoscopic precision. This combination has not been realized up to date and should thus offer exciting new opportunities to investigate how cellular communications are regulated on the molecular level.

## Task Title: Protein Biotemplates for Self-Assembly of Nanostructures from Clathrin Materials

**Investigators:** Sarah Heilshorn, Nicholas Melosh, Seb Doniach, and Andrew Spakowitz

476 Lomita Mall, McCullough 246, Stanford University, Stanford, CA 94305. Heilshorn@stanford.edu

**Program Scope:** Self-assembly has become a powerful method to create highly-ordered structures with spatial and temporal patterning on two-dimensional substrates. However, the divide between our current technological capabilities and the power demonstrated by biological systems to assemble both organic and inorganic species into intricate three-dimensional structures is still vast. The ultimate goal of this program is to identify the necessary combination of assembly mechanisms and building-block properties for deterministic formation of complex three-dimensional organic/inorganic constructs. By appropriate selection of architecture, materials, and morphology; these materials will lead to fundamentally new designs for bio-inorganic devices for energy storage, catalysis, and fuel cells. This collaborative effort has focused on the remarkable self-assembling protein, clathrin. Clathrin is composed of three-armed “triskelion” monomers, with three-fold symmetry, semi-flexible arms, and specific binding sites for adaptor peptide sequences. Clathrin is a highly unusual self-assembling material, as it occurs naturally in 2-D sheets, 3-D cubes, tetragons, and geodesic spheres. Because of the rich diversity of structure and dimensionality, clathrin is an ideal model for understanding how natural systems controllably transform from inherently two-dimensional materials into the third dimension. Our program is designed to demonstrate clathrin as a controllable 2-D and 3-D assembly system, identify the key self-assembly characteristics that make it successful, and finally template inorganic species to the clathrin networks.

### Recent Progress and Future Plans:

**1: Developed protocols to isolate and purify significant quantities of clathrin.** Since clathrin is not synthetically available, we developed isolation protocols to derive clathrin from natural sources. Three potential sources (murine liver, murine brain, and bovine brain) were characterized for purity and quantity of yield. Our optimized purification protocol consists of three steps: differential centrifugation to obtain clathrin-coated vesicles from bovine brain tissue, depolymerization of the protein coats from the vesicles, and purification of clathrin monomers by size exclusion chromatography. From ~2 kg of brain tissue, we obtain ~5 mg of >95% pure clathrin, Fig. 1.

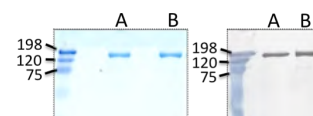


**Figure 1:** SDS-PAGE of purified clathrin protein from bovine brain tissue (left) with corresponding western blot (right). A & B are separate samples.

**2: Measured the fluctuation dynamics of clathrin monomers using X-ray scattering.** The self-assembly of clathrin monomers into specific structures relies on interactions between molecules at specific environmental conditions (pH, temperature, ionic strength). Small angle x-ray scattering (SAXS) provides a means of determining these interaction potentials via the concentration dependence of the scattering profiles for relatively dilute solutions of clathrin. We made a series of SAXS measurements of purified clathrin solutions and have a first determination of the interparticle interference effects. The concentration dependence of the SAXS profiles  $I(q,c)$ , where  $q$  is the wave vector ( $q$  proportional to  $\sin(\varphi)$  where  $\varphi$  is the scattering angle) and  $c$  is the concentration is shown in Fig. 2. To analyze this data we make use of the fact that the scattering in the dilute limit principally determines the single molecule scattering profile  $I_0(q)$ . The concentration dependence may be used to extract the interference term via the relation shown, Fig. 2. We used a least squares analysis to overlay the scattering profiles at concentration  $c_i$  with the profile of the lowest concentration data measured at larger angles where the interference term is negligible. This allows us to obtain a precise determination of the relative concentrations of the succeeding curves. Then by subtraction we are able to separate out the interference term as shown in Fig 3. This result

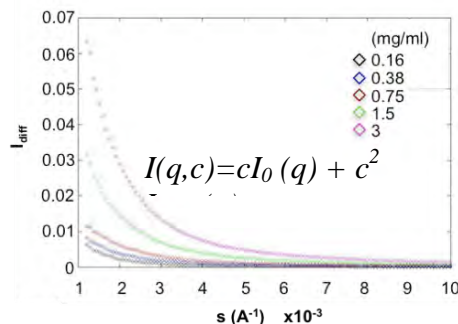


**Fig 2.** Concentration dependence of SAXS profiles for clathrin solutions.

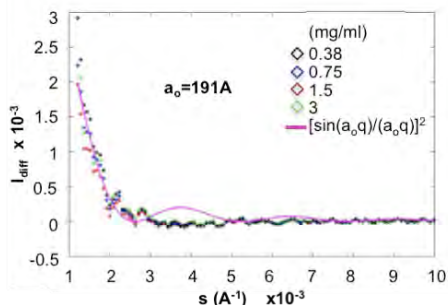


**Fig 3.** Plot of differences  $(I(s,c) - a(c)I(s,c_0))/(a(c))^2$  where  $c_0$  is the lowest concentration profile.  $a(c)$  is adjusted to give a best least squares fit for  $(6 \cdot 10^{-3} < s < 10^{-2})$ . Difference curves are overlaid with the function  $[\sin(a_0 q)/a_0 q]^2$  where  $q=2ps$ , to allow qualitative estimation of the interparticle scattering,  $a_0$ .

provides direct evidence of attraction between the clathrin molecules, as a repulsive term would lead to a negative interference term. To relate these results to clathrin-clathrin interparticle scattering, we are currently running simulations of the scattering dependence on the phenomenological colloidal DLVO (Derjaguin-Landau-Verwey-Overbeek) potential. We are using a simplified model of clathrin in terms of a series of “blobs” joined together to form the legs of the clathrin triskelia. By Monte Carlo averaging the dependence of the pair distribution function on the DLVO potential parameters and comparing the results with the above data, we will extract effective charges leading to the observed attraction between clathrin legs. By extending the above measurements to buffers of varying pH and salt concentration, we will predict parameters that explore the

entire phase diagram of clathrin assembly, allowing formation of clathrin structures of varying topology.

### 3: Constructed a theoretical framework to understand how molecular shape and flexibility lead to different 2-D aggregates.

We simultaneously developed theoretical models that could accommodate 3-fold symmetry of the clathrin molecule and triskelion flexibility. Initial development has focused on two simpler 2-D models before including a third spatial dimension. The first model is a lattice model with 3-fold symmetry leading to three near-neighbor interactions on a hexagonal lattice. Using dynamic mean field theory, we constructed the full phase diagram (Fig. 4, left) of the 2-D ordered assembly consisting of the stability, metastability, and instability regions. Utilizing this predictive model, we predicted 2-D conformations and structural defects (Fig. 4, right) for various quench depths into the two-phase region of the phase diagram. This model has yielded critical information about the shape of the phase diagram for clathrin assembly and the relationship between assembly dynamics and structural morphology. These features will be compared directly to the results rendered from pressure-area isotherms from Langmuir-Blodgett trough experiments and used as guidance for controlling the experimental assembly.

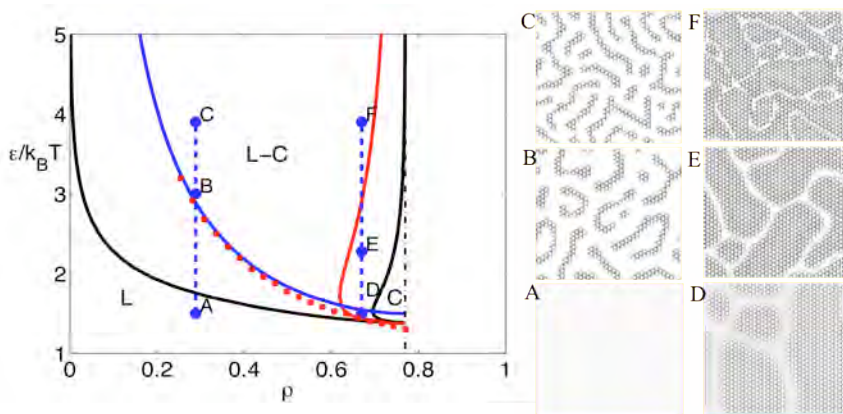


**Figure 4:** (left) Phase diagram for clathrin self-assembly using lattice model. The black lines are binodal coexistence curves between a disordered-liquid state (L) and an ordered crystal state (C). The red line is the crystal spinodal curve, and the blue line is the disordered-liquid spinodal curve. (right) Dynamic mean field solution after 2000 steps for states A, B, and C at density=0.29, and states D, E, and F at density=0.66 shown on the phase diagram.

We then developed a more detailed, mesoscale model of clathrin that incorporates molecular flexibility of the triskelion, resulting in a treatment addressing the ability for clathrin to assemble into 2-D lattices with rings of different number of sides. Our novel model combines Brownian dynamics and dynamic Monte Carlo simulations into a framework that tracks the trajectory of tens to hundreds of clathrin triskelia undergoing assembly with minimal computational power. Furthermore, it is straightforward to extend this model to study 3-D assembly, clathrin-nanoparticle co-assembly, and membrane assembly. In Fig. 5A,B, we show two example structures that arise from our model for assembly. Here, we demonstrate that the interaction strength and elastic properties lead to vastly different

morphological characteristics. The interaction strength and elastic properties both have likely experimental handles (salt, pH, temperature, lipid content, and adaptor protein concentration); thus, our predictions will provide direct guidance to the experiments toward the morphologies of interest. The cluster-size distribution (Fig. 5C) exhibits a clear bimodal shape that is indicative of coexistence between phases that have a first-order transition. This prediction is qualitatively consistent with our simplified lattice model.

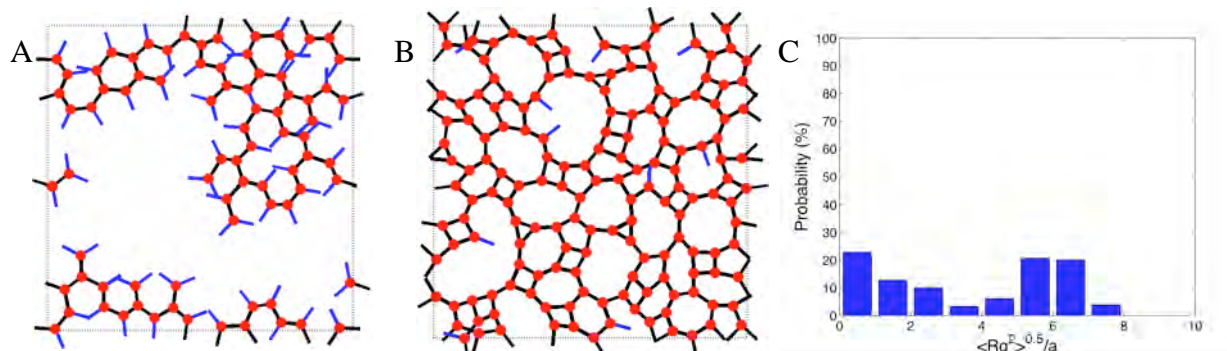


**Figure 5:** (left) Self-assembly configurations after 100 time steps for 80 pinwheels, with bending and stretching stiffness of legs  $2a^2/k_B T$ , and  $100a^2/k_B T$ , respectively (A), and 160 pinwheels with bending and stretching stiffness of legs are  $50a^2/k_B T$ , and  $100a^2/k_B T$ , respectively (B). In these simulations, binding affinity is  $9k_B T$ . (C) Distribution of radius of gyration for binding affinity  $3k_B T$ ,  $N=80$ , where bending and stretching stiffness of legs are  $50a^2/k_B T$ , and  $100a^2/k_B T$ , respectively.

**4: Measured 2-D clathrin assembly in Langmuir-Blodgett films.** Measuring the 2-D clathrin network structure will provide direct validation of the theoretical models and provide a well-defined starting material for inorganic decoration and 3-D assembly. In biological cells, the clathrin network is visualized by cryo freeze-fraction, which is inappropriate for following the dynamic and mechanical response of an assembling clathrin network. We developed a miniaturized Langmuir-Blodgett (LB) trough (Fig. 6a) to measure the mechanical changes as clathrin associates with a lipid monolayer and assembles into aggregates. After clathrin injection it is recruited to the lipid monolayer surface over time, eventually coming to equilibrium with monomers in the subphase, Fig. 6b. The mechanical properties were measured from the surface pressure during areal compression, Fig. 6c. The two dimensional stiffness of the film is calculated from:  $\kappa = -A_0 d\Pi/dA$ , where  $A_0$  is the original area,  $\Pi$  the pressure, and  $A$  area. The lipid layer has a modulus of  $\kappa=0.07$  N/m, while lipid plus clathrin has  $\kappa=0.10$  N/m, a 42% increase in stiffness, Fig. 6c. Our calculations suggest that a fully densified clathrin lattice would be six times stiffer than the lipid monolayer; thus we are measuring smaller, likely non-percolating aggregates. Cryo-TEM and theory will be combined with further mechanical measurements to relate mechanical response to network structure. Measurements of both the elastic and inelastic response will be performed using micro-LB rheology, providing a richer view of the dynamic self-assembly process.

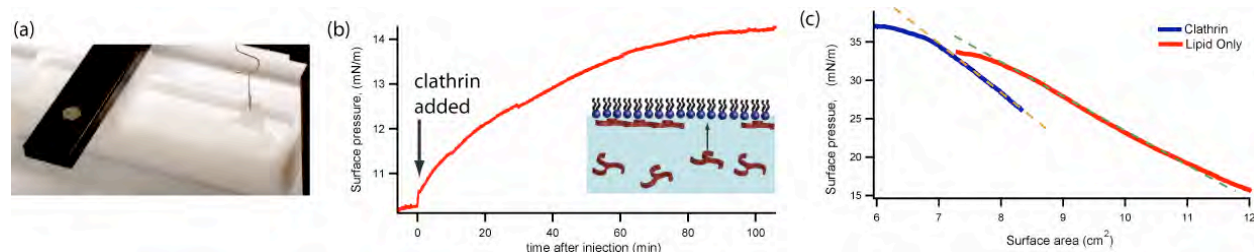


**Figure 6:** (a) A newly fabricated mini-Langmuir Blodgett trough with a total volume less than 2 mL. (b) Pressure increase in an 1:1:0.25 POPC:POPE:PIP2 lipid monolayer over time after  $0.45 \mu M$  clathrin is added to the subphase. (c) Pressure-Area isotherm ( $T=22.0^\circ C$ ) for POPG lipid alone, and after recruitment of clathrin.

### 5: Formed 3-D clathrin nanostructures.

Clathrin dissociates in buffers above pH 6.5 and will assemble below that value into various architectures including cages, cubes, and pyramids. To gain insight into the variables that control this process, assemblies of identical concentration of purified clathrin were formed by dialysis into buffers at pH 6.0 with a range of ionic strength. We find that at lower salt concentration (2 mM) pyramids can be formed, while cages of varying sizes form at higher salt concentrations (20, 50, and 100 mM), Fig. 7. Further experiments will inform and will also be guided by computational predictions based on the models described above as they develop into the third dimension.

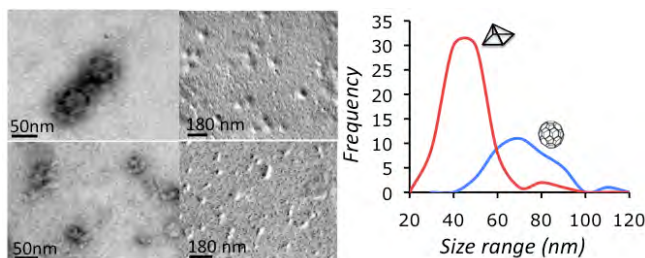


**Figure 7:** Clathrin cages (top) and pyramids (bottom) visualized by negative staining (left) and Pt shadow evaporation (right). Size distribution data for cages and pyramids is shown in the graph at right.

### 6: Decorated 3-D clathrin cages with gold nanoparticles.

Chimeric peptides have been designed to functionalize the clathrin molecules for interaction with inorganic molecules, specifically gold colloids and gold ions. The “clathrin box” peptide sequence, a region of sequence homology in many clathrin-binding proteins is fused upstream of sequences known to bind gold ions or nanoparticles, Fig. 8. The clathrin-binding motifs and the gold-binding motifs are joined with a linker sequence chosen to have minimal impact on secondary structure, charge, and hydrophobicity of the overall peptide.

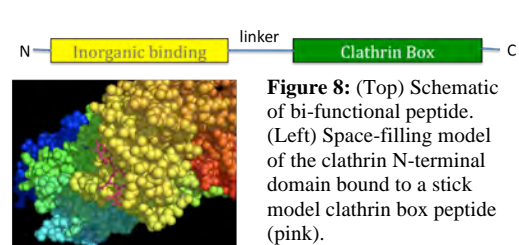


**Figure 8:** (Top) Schematic of bi-functional peptide. (Left) Space-filling model of the clathrin N-terminal domain bound to a stick model clathrin box peptide (pink).

By designing a family of bi-functional peptides to bind specific inorganic species, we can develop a flexible, modular system for biotemplating multiple inorganics onto a single protein template.

Colloidal gold particles (5 nm) were incubated with purified clathrin monomers or 3-D clathrin assemblies. High colloid densities correlate well to areas of staining on the grid, indicating interactions between the protein templates and the colloidal particles, Fig. 8. The addition of the bi-functional peptide that bridges gold colloids and clathrin increases the colloid density on stained areas in samples of monomeric clathrin, but not in samples of pre-assembled 3-D clathrin structures. It is possible that the peptide cannot access the clathrin binding site which is on the inside face of the protein structure when it is assembled. Future work will pursue bi-functional peptides with longer linkers and complexing clathrin monomers with peptide-bound colloids prior to assembly.

Purified clathrin monomers were also incubated with or without gold ion-binding bi-functional peptides in a solution of gold chloride. In samples containing bi-functional peptides, polydisperse gold particles (6-20 nm) formed on the clathrin templates. Evidence of gold nucleation was not observed in samples without the engineered bi-functional peptides. Upon addition of a reducing agent ( $\text{NaBH}_4$ ), the yellow-orange solution changed to a deep blue, indicating the formation of large or aggregated nanoparticles in both samples. TEM analysis shows areas of dense filamentous networks branching off of regions of staining. Further work will be done to develop these structures with long-range order and to template other inorganics by designing new bi-functional peptides.

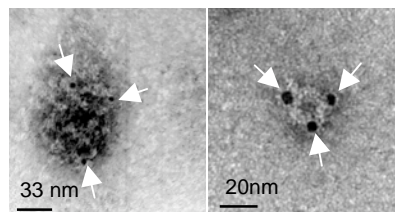


**Figure 9:** Gold colloid (white arrows) binding to two different clathrin assemblies via non-specific interactions.

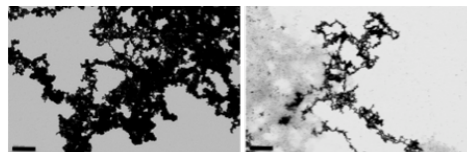


**Figure 9:** Filamentous networks formed upon reduction of gold chloride solution containing clathrin monomers (left) or clathrin monomers and bi-functional peptides (right). 200 nm scale bars.

## Molecularly Organized Nanostructural Materials

Jun Liu, Gregory J. Exarhos, Li-Qiong Wang, Yongsoon Shin,  
Maria Sushko, Praveen Thallapally, Donghai Wang

Pacific Northwest National Laboratory  
Richland, WA 99352

[Jun.liu@pnl.gov](mailto:Jun.liu@pnl.gov)

**Program Scope:** The overall goal of this project is to investigate a combination of self-assembly and controlled nucleation and growth approaches for synthesizing nanostructured materials with controlled three-dimensional architectures and desired stable crystalline phases of conductive or semiconducting metal oxides suitable for energy applications. Of importance is the understanding of crystallization in self-assembled materials in order to control both resident porosity and pore interconnectivity in these materials because these traits impart certain properties to the material that are underpinning for energy technologies including conversion and storage. The project contains the following components:

- Manipulation of the kinetics of competing self-assembly and precipitation reactions
- Use of molecular ligands to control nucleation and growth
- Multiscale modeling of the self-assembly process in solution
- *In situ* spectroscopic probes of structure-forming reactions and evolving porosity

**Recent Progress:** Biological systems abound with nanocomposites with well-controlled architectures based on multiscale and multifunctional building blocks. In contrast, traditional approaches for making such materials mostly rely on mechanical or chemical mixing which usually produces a random distribution of the constitutive phases. In the past, we and many other groups have performed extensive study of controlled nucleation and growth on functionalized surfaces based on the principles used in biomineralization. A wide range of metal oxides and polymers films have been prepared with controlled orientation, crystalline structures and systematic variations of the morphologies. However, this approach has been limited to thin films and supported two-dimensional structures, as well as single phase materials.

Under this project, we begin to explore a new strategy to extend the two-dimensionally controlled nucleation and growth method to three-dimensional functional nanocomposite materials. This strategy involves the integration of controlled nucleation and growth and three-dimensional self-assembly process. Rather than using a hard substrate or functionalized surface to make supported thin films and coating (Pathway 1 in Figure 1), we use other novel nanostructured materials as the molecular template as well as one of the critical component for forming the self-assembled materials. For example, we use molecularly dispersed graphene sheets as the template. The graphene sheets are dispersed in the hydrophobic domains of surfactant molecules or polymers. The functional groups on the absorbed surfactant surfaces controls the crystallization of metal oxide on the

graphene surfaces, forming a well-dispersed metal oxide and graphene nanocomposite that shows significantly better conductivity than conventional nanocomposites and carbon nanotube composite materials for energy storage.

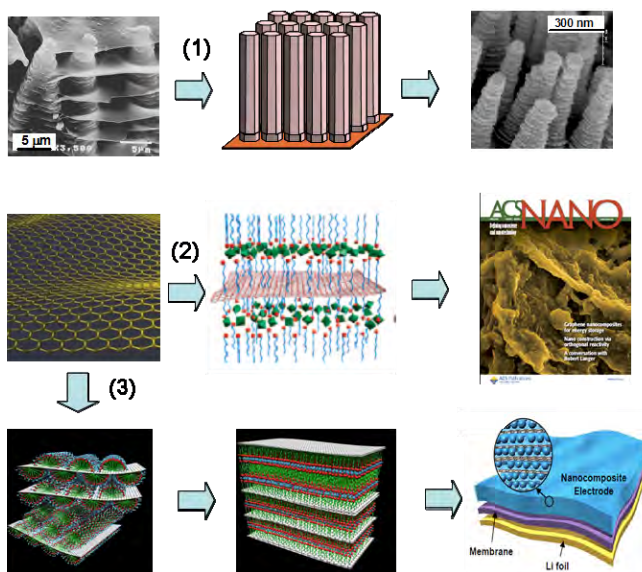


Figure 1. New pathways for three-dimensional self-assembly of metal oxide-carbon nanostructures using extended graphene molecular sheets as the template and the fundamental building block. Pathway 1: Conventional nucleation and growth of two-dimensional nanostructures supported on substrates based on lessons from biology. Pathway 2: Controlled nucleation and deposition of metal oxides on graphene sheets for novel metal oxide-graphene nanocomposite. Pathway 3: Self-assembly of ordered graphene-metal oxide nanocomposites.

Furthermore, we demonstrate that we can use the extended graphene sheets solubilized in the hydrophobic domains as the fundamental building blocks for the self-assembly of three-dimensionally ordered architectures (Pathway 3). The graphene sheets and metal oxide precursors self-assemble into ordered three-dimensional composite structures. The metal oxides are then crystallized between the graphene sheets as controlled by the functional head groups of the surfactants. This self-assembly method process produces a new class of nanocomposite materials with well-controlled architectures on the nano- and microscales. Such materials show much improved conductivity and mechanical stability. The self-assembly process can be further used to directly fabricate energy storage devices in one step.

In order to understand the origin of the improved properties, we used  $^{129}\text{Xe}$  NMR to probe the interconnectivity of micro- and nano-porosity, which plays an important role in the performance of porous materials. The pore geometry in most porous materials is complex with interconnected cages, channels and micropores. It is challenging to directly characterize the interconnectivity of the pores in nano or meso-porous materials. The techniques such as small angle x-ray or neutron scattering and gas absorption do not provide direct information on how channels and cages are connected.

Hyperpolarized (HP)  $^{129}\text{Xe}$  NMR is used to probe the porosity and interconnectivity of pores in highly crystalline mesoporous metal oxide ( $\text{TiO}_2$ ) and  $\text{TiO}_2$ -graphene nanocomposites. We have demonstrated that HP  $^{129}\text{Xe}$  NMR can be used to unambiguously differentiate between similar sized pores within different crystalline phases. Both anatase and rutile pores of 4 nm size were identified in mesoporous  $\text{TiO}_2$ . In contrast to other pore characterization methods, we are also able to probe interconnectivity between pores constrained to different phases. The cross peaks in 2D chemical shift exchange (EXSY) NMR spectra show exchange takes place between both types of pores with a

short mixing time of 5 ms, indicating that these two types of pores are well interconnected.

A small percentage of graphene in TiO<sub>2</sub> was found to greatly enhance ion transport rate in our recent study. HP <sup>129</sup>Xe NMR studies on TiO<sub>2</sub> with and without graphene help us to understand how the nanostructures of TiO<sub>2</sub>-graphene influence the ion transport. Comparative HP <sup>129</sup>Xe NMR studies of pure TiO<sub>2</sub> and TiO<sub>2</sub>-graphene show that TiO<sub>2</sub> and graphene are mixed uniformly on the nanoscale and the resulting hybrid nanostructure has better connected channels among different domains upon adding 1% graphene in TiO<sub>2</sub>. The better connected channels may be one of the factors that enhance the transport property of TiO<sub>2</sub>-graphene.

**Other Activities:** Uniform nanocarbon spheres from aqueous sugar solutions. We have developed a simple method to convert sugar like molecules into uniform nanocarbon spheres under mild hydrothermal conditions. We found that aqueous glucose or fructose solution dehydrates to form 5-hydroxymethyl-2-fufuraldehyde (HMF), which continues to polymerize and carbonize to form homogeneous carbon sphere (300-400 nm) in a closed system at 120-180 °C. The formation of the carbon spheres depends on dehydration, which is catalyzed by an intermediate product, levulinic acid (pKa = 4.53). The initial dehydration kinetics at different temperatures can be regarded as pseudo-first order and slopes are proportional to initial rate constants. The activation energy of forming HMF is 32.0-35.0 Kcal/mole, which is similar to that (32.4 Kcal/mole) of a typical acid-catalyzed dehydration. The sizes of the nanocarbon spheres can be controlled by choosing different carbon precursors which directly affect the reaction rates.

**Significance:** The recent progress on this project has the potential to bridge the gap of two-dimensional crystallization and three-dimensional self-assembly. In addition, in the past, self-assembled oxide materials are mostly limited to single phase materials and nanoparticle based systems. Our study points to a new direction for self-assembly using multiple phases and multilength building blocks. Currently many other building blocks are available besides graphene sheets, such as carbon nanotubes, nanowires and nanorods, and ceramic nanoplates. Similar principles should apply for such nanoscale building blocks and will lead to truly multifunctional composite materials with controlled architectures. The materials developed under this project already demonstrated superior kinetics and stability as compared with conventional composite materials.

**Future Plan:** We will focus on the fundamental understanding of the nature of the interactions between graphene sheets, the surfactant, and the metal oxides. High resolution electron microscopy, NMR and other spectroscopic techniques, as well as atomic force microscopy will be used to probe the nature of the chemical binding, and the kinetics of surface absorption and nucleation processes. We will also perform systematic studies of similar self-assembly and nucleation processes involving different nanoscale building blocks in order to develop the general guiding principles for a wide range of materials. Finally, we will develop multiscale modeling capabilities that can not only address the ternary self-assembly problems we encountered here, but also the transport properties in such materials.

## Publications:

1. Murugesan V., Kerisit S., Wang C., Nie Z., Rosso K.M., Yang Z., Graff G.L., Liu J. and Hu J. (2009) "Effect of chemical lithium insertion into rutile TiO<sub>2</sub> nanorods," *Journal of Physical Chemistry C* (in press), 2009.
2. Y. Shin, I.-T. Bae, G. J. Exarhos, "Green approach for self-assembly of platinum nanoparticles into nanowires in aqueous glucose solutions," *Colloids and Surfaces A* (in press), 2009.
3. C. M. Wang, Z. G. yang, S. Thevuthasan, J. Liu, D. R. Baere, D. Choi, D. wang, J. G. Zhang, L. Saraf, Z. Nie, "Crystal and electronic structure of lithiated nanosized rutile TiO<sub>2</sub> by electron diffraction and electron energy-loss spectroscopy," *Applied Phys. Lett*, 94, 233116, 2009.
4. D. Wang, D. Choi, J. Li, Z. Yang, Z. Nie, R. Kou, D. Hu, C. Wang, L. V. Saraf, J. Zhang, I. A. Aksay, J. Liu "Self-Assembled TiO<sub>2</sub>-Graphene Hybrid Nanostructures for Enhanced Li-Ion Insertion," *ACS Nano, cover article*, 3, 907-914, 2009.
5. L. -Q. Wang, D. Wang, J. Liu, G. J. Exarhos, S. Pawsey, I. Moudrakovski: "Probing Porosity and Pore Interconnectivity in Crystalline Mesoporous TiO<sub>2</sub> Using Hyperpolarized <sup>129</sup>Xe NMR," *J. Phys. Chem. C*, 2009, 113 (16), pp 6485-6490.
6. Wang D, D Choi, Z Yang, VV Viswanathan, Z Nie, CM Wang, Y Song, J Zhang, and J Liu. "Synthesis and Li-ion Insertion Properties of Highly Crystalline Mesoporous Rutile TiO<sub>2</sub>." *Chemistry of Materials* 20(10):3435-3442, 2008.
7. Jun Liu, Guozhong Cao, Zhenguo Yang, Donghai Wang, Dan Dubois, Xiaodong Zhou, Gordon L. Graff, Larry R. Pederson, and Ji-Guang Zhang, "Oriented Nanostructures for Energy Conversion and Storage," *ChemSusChem*, 1, 676-697. *Invited review, cover article*, 2008.
8. Y. Shin, L. -Q. Wang, I.-T. Bae, B. Arey, G. J. Exarhos, "Hydrothermal Syntheses of Colloidal Carbon Spheres from Cyclodextrins," *J. Phys. Chem. C* 112, 14236 (2008).9. I.-T. Bae. B. W. Arey, G. J. Exarhos. "Facile stabilization of gold-silver bimetallic nanoparticles on cellulose nanocrystal," Y. Shin, *J. Phys. Chem. C* 2008, 112, 4844-4848.
10. Y. Shin, G. E. Fryxell, C. A. Johnson II, M. M. Haley, "Templated synthesis of pyridine functionalized mesoporous carbons through the cyclotrimerization of diethynylpyridines," *Chem. Mater.* 2008, 20, 981-986.
11. Sounart T. L, J Liu, J A Voigt, M Huo, E D Spoerke, B Mckenzie, "Secondary Nucleation and Growth of ZnO," *Journal of the American Chemical Society*, 129,15786-15793, 2007.
12. L.-Q. Wang, X. -D. Zhou, C. Yao, G. J. Exarhos, C. F. Windisch Jr, L. R. Pederson, "Probing Proton Dynamics in ZnO Nanorods Quantified by *in situ* Solid-State <sup>1</sup>H Nuclear Magnetic Resonance Spectroscopy" *Applied Physics Letters*, 91, 173107 (2007).
13. C. Yao, Y. Shin, L.-Q. Wang, C. F. Windisch Jr, W. D. Samuels, B. W. Arey, C. Wang, W.M. Risen Jr., G. J. Exarhos, "Hydrothermal Dehydration of Aqueous Fructose Solutions in a Closed System," *J. of Physical Chemistry C*, 111, 15141 (2007).
14. C. F. Windisch Jr, G. J. Exarhos, C. Yao, L.-Q. Wang, "Raman Study of the Influence of Hydrogen on Defects in ZnO," *Journal of Applied Physics*, 101(12),123711 (2007).
15. L. -Q. Wang, S. Pawsey, I. Moudrakovski, G. J. Exarhos, J. Ripmeester, J. L. C. Rowsell and O. M. Yaghi "Hyperpolarized <sup>129</sup>Xe Nuclear Magnetic Resonance Studies of Isorecticular Metal-Organic Frameworks," *J. of Phys. Chem. C* 111, 6060, 2007.
16. Y. Shin, J. M. Blackwood, I.-T. Bae, B. W. Arey, G. J. Exarhos, "Synthesis and stabilization of selenium nanoparticles on cellulose nanocrystal," *Mater. Lett.* 2007, 61, 4297-4300.
17. Y. Shin, I. Bae, B. W. Arey, G. J. Exarhos, "Simple preparation and stabilization of nickel nanocrystals on cellulose nanocrystal," *Mater. Lett.* 2007, 61, 3215-3217.
18. Y. Shin, G. J. Exarhos, "Template synthesis of porous titania using cellulose nanocrystals," *Mater. Lett.* 2007, 61, 2594-2597.
19. Y. Shin, C. Wang, W. D. Samuels, G. J. Exarhos, "Synthesis of oriented SiC nanorods from bleached pulp, " *Mater. Lett.* 2007, 61, 2814-1817.
20. Y. Shin, G. J. Exarhos, "Replication of cellulose materials into hierarchically-structured," *ceramics. Cellulose* 2007, 14, 269-279.

## Bioinspired Materials

Surya Mallapragada, Mufit Akinc, George Kraus, Monica Lamm, Balaji Narasimhan, Marit Nilsen-Hamilton, Tanya Prozorov, Klaus Schmidt-Rohr, Alex Traveset, and David Vaknin  
Ames Laboratory, DMSE, 126 Metals Development, Ames, IA 50011; suryakm@iastate.edu

**Program Scope:** Synthesis and characterization of novel bioinspired hybrid materials that mimic living systems in their abilities to respond to the environment and self-assemble hierarchically. Use of organic templates coupled with mineralization proteins to direct biomineralization processes, and aptamers for achieving specificity of non-covalent binding, to facilitate a bottom-up approach to nanocomposite materials design. Understanding guiding mechanisms of assembly across multiple length scales through a combination of experimental techniques and computational methods. Advanced solid-state NMR and scattering techniques for investigating interactions of the organic templates with inorganic constituents.

**Recent Progress:** The three main thrusts of this program are  
*Development of multiscale self-assembling bioinspired hybrid materials using bottom-up approaches:* We have designed hierarchically self-assembling templates (synthetic polymers as well as peptide based templates), and have used bioinspired methods for synthesis of energy-relevant hybrid materials with hierarchical order that are difficult to synthesize otherwise.  
*Development of techniques to probe assembly at multiple length scales and properties of these nanocomposites:* We are using a combination of solid-state NMR, scattering and electron microscopy techniques to investigate the nanostructure and composition, and other characterization techniques to investigate the structure and properties of these hybrid materials.  
*Development of computational methods for understanding general design rules for self-assembled polymer nanocomposites:* We are developing and implementing molecular simulations as a powerful tool to understand the underlying principles of self-assembly of complex structures, and phase transformations between competing phases.

This work will yield a robust and modular method for developing bioinspired hierarchical materials, with control over the formation as well as placement of an inorganic phase in the nanocomposite structure. This, in turn, will lead to development of novel hybrid materials that are lightweight and energy efficient for fuel cells, spintronics, quantum computing, magnetic actuators, and other applications. Specific recent advances include:

*Template Design.* A family of self-assembling tri and pentablock copolymers with cationic, anionic, and zwitterionic groups was synthesized and used as templates for mineralization. The synthesis of the inorganic nanocrystals in the presence of the block copolymer viscous solution that thermoreversibly forms ordered gels allows for control of formation of the nanocrystals, as well as their placement within elastic polymer matrices. An alternative approach involving self-assembling diblock copolypeptides synthesized by Deming was pursued recently as these form gels at much lower concentrations, thereby increasing the inorganic content.

*Self-Assembling Nanocomposites.* Self-assembling thermo-reversibly gelling anionic and zwitterionic pentablock copolymers conjugated to hydroxyapatite (HAp) nucleating peptide sequence (DSKSDSSKSESDSS) were used as templates for precipitation of calcium phosphate nanostructures. The HAp particles in the nanocomposites produced using the block copolypeptides are constituted of thin elongated plate-like nanocrystals similar to bone (Fig 1a).

We have developed a novel, room temperature bioinspired (from magnetotactic bacteria) synthesis route to nanostructured magnetic materials, using the acidic recombinant protein, Mms6, and its synthetic C-terminal domain, containing 25 amino acids (c25-Mms6) to promote shape-specific magnetite growth. The peptides and proteins were attached to the ends of the synthetic polymer chains. We were able to template synthesis of more complex and highly magnetic nanocrystals

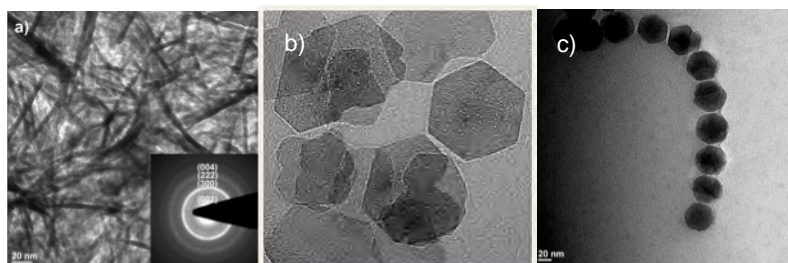


Fig.1 Nanocrystals of HAp, cobalt ferrite and Mn-doped magnetite

elucidate the mechanism of Mms6-assisted, shape-specific magnetite formation. We also succeeded in the synthesis of uniform complex ferrites like cobalt ferrite (Fig. 1b) *in vitro* and other complex ferrites containing Mn *in-vivo* using the same mineralization proteins (Fig 1c). “Doped” in such a way, magnetosomes exhibit changes in particle size, chemical composition, and shape that correlate with the observed changes in their magnetic properties.

**Techniques to probe structure/property relationships:** Several complementary techniques involving solid state NMR, TEM and scattering were developed and utilized to prove nanocomposite formation and to investigate the composition of the self-assembling nanocomposites. New solid state NMR techniques to probe these systems have been developed in the *Solid State NMR FWP*. Solid state NMR studies provided information about the composition of the inorganic phase. The formation of nanocomposites was proved by two-dimensional  $^1\text{H}$ - $^{31}\text{P}$  heteronuclear correlation NMR experiments with  $^1\text{H}$  spin diffusion. High resolution TEM analysis of the nanocomposites was used to image the inorganic phase. The nanocomposites were characterized with small angle x-ray scattering (SAXS) as well as small angle neutron scattering (SANS). For the nanocomposites templated by the block copolymers, proof of templating was obtained from the SAXS and SANS (At APS and IPNS at Argonne National Laboratory in collaboration with P. Thiyagarajan). The SAXS proved conclusively that the polymer templates the calcium phosphate structure to a significant extent. The thickness of the inorganic nanoparticles obtained from SAXS showed good agreement with values obtained using other techniques. The X-ray reflectivity studies at the air-water interface developed by Vaknin were used to investigate the mechanism by which the mineralization protein Mms6 leads to the formation of uniform magnetic nanocrystals. X-ray reflectivity and surface fluorescence studies of Mms6 at the air-water interface with iron ions in the aqueous solution showed a high surface density of Mms6 associated  $\text{Fe}^{3+}$  ions (Fig.2 ).

**Computational methods:** Molecular dynamics (MD) is an excellent tool to investigate ordered phases of these self-assembled nanocomposites systems. Our studies on polymer nanocomposites have been focused on establishing general conditions that allow successful self-assembly of inorganic components with block copolymers in solution. The results have shown that without specific affinity between inorganic components and polymers, phase separation preempts the formation of nanocomposites. We have demonstrated that if block copolymers are functionalized, that is, their end blocks

that do not occur in living organisms, using a developed bioinspired approach and by investigating a variety of magnetic ions for the synthesis. Block copolymers conjugated to Mms6 and c25-Mms6 yielded ~30 nm crystals resembling the magnetite particles produced *in vivo*. The concentration of protein used was varied in order to

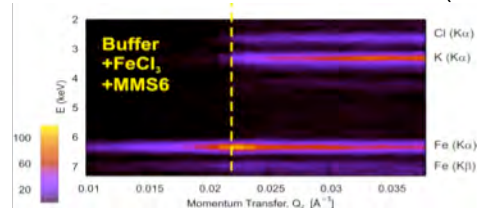


Fig. 2 Fluorescence spectra versus momentum transfer from Mms6 spread on  $\text{FeCl}_3$  solution. The  $\text{K}\alpha$  emission line from iron is below the critical angle (dashed line) indicates strong iron binding to Mms6.

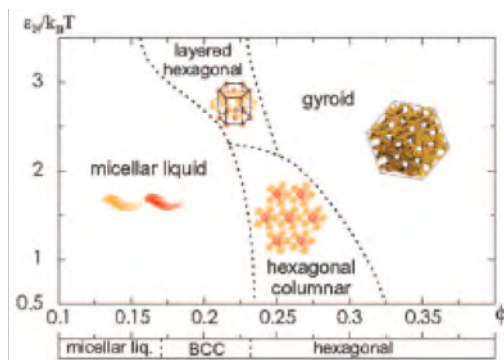


Fig. 3 Different self-assembled phases formed in solution

contain groups with specific affinity for the inorganic phase, a wealth of new nanocomposites, displaying novel phases and aggregations are found (Fig. 3). MD simulations are also being used to identify thrombin mimetic peptides that can bind to aptamers and result in reversible attachment of Mms6. It has recently become possible to make use of graphics processing units (GPUs) for scientific purposes, and more concretely for MD. Using these results, we have developed the first general purpose MD code, HOOMD (Highly Optimized Object-oriented MD), that runs entirely on GPUs. This code has been released under an open source license and is available for download at <http://www.ameslab.gov/HOOMD>. The computational power delivered by a simple inexpensive (less than \$500) GPU is equivalent to a cluster of over 40 cores.

**Future Plans:** Although HAp is an excellent example for biomimetic model experiments, for energy-related applications, other oxides and semiconductors will be targeted, using similar approaches. We are extending the knowledge gained from the HAp study into other oxide—in particular, Zirconia, which is of significance in solid oxide fuel cells. New solid-state NMR techniques have to be developed to investigate the zirconia nanocomposites. In addition, for reversible attachment of magnetic nanoparticles in the polymer matrix, the aptamer approach will be pursued. When the thrombin mimetic peptide is identified through simulations, we will link the multiblock copolymers with bacterial mineralization proteins that control magnetite nanocrystal growth using aptamers, to enable a reversible binding process. As a complementary approach to the aptamers, in collaboration of D. Tirrell's group at Caltech, we are developing an artificial polypeptide scaffold that could be used to synthesize nanocrystals on surfaces in different patterns with controlled architectures and specificity. The protein capture domain functions through the coiled-coil association of a leucine zipper pair. Here an elastin mimetic domain (ELF) with a para-azidophenylalanine group, that is UV-sensitive, is used for the surface anchorage, and the UV-sensitivity allows for patterning Mms6 on surfaces. The ELF peptides form gels similar to the block copolymer templates that we have investigated. We will also apply surface sensitive neutron and synchrotron x-ray scattering techniques to systematically investigate the assembly of complexes at vapor-aqueous interfaces, to investigate the mechanism of biomineralization. We will also investigate the origins of the different phases obtained, and develop analytical models to account for the phase diagrams computed from our MD studies. The overall impact of this effort is to create bioinspired self-assembled nanocomposites with controlled hierarchical structures ranging from the nanoscale to the macroscale.

#### **Publications (2007-09):**

1. "Self-assembled Calcium Phosphate Nanocomposites Using Block Copolypeptide Templates", Hu, Y., Yusufoglu, Y., Kanapathipillai, M., Yang, C.Y., Wu, Y., Thiyagarajan, P., Deming, T., Akinc, M., Schmidt-Rohr, K., Mallapragada, S.K., *Soft Matter* (2009); DOI: 10.1039/b904440j
2. "X-ray Fluorescence Spectroscopy from Ions at Charged Vapor/Water Interfaces", W. Bu, and D. Vaknin, *J. Appl. Phys.*, **105**, 084911 (2009).
3. "Preferential Affinity of Calcium Ions to Charged Phosphatidic Acid Surface from a Mixed Calcium/Barium Solution: X-Ray Reflectivity and Fluorescence Studies, W. Bu, K. Flores, J. Pleasants, and D. Vaknin, *Langmuir*, **25**, 1068 (2009)
4. "Synthesis and Characterization of Ionic Block Copolymer Templated Calcium Phosphate Nanocomposites", M. Kanapathipillai, Y. Yusufoglu, A. Rawal, Y.-Y. Hu, C.-T. Lo, P. Thiyagarajan, Y. Kalay, M. Akinc, S. Mallapragada, and K. Schmidt-Rohr, *Chem. Mater.*, **20**, 5922 (2008).
5. "Bioinspired Synthesis of Self-Assembled Calcium Phosphate Nanocomposites Using Block Copolymer-Peptide Conjugates", Y. Yusufoglu, Y. Hu, M. Kanapathipillai, Y. Wu, M.J. Kramer, P. Thiyagarajan, M.A. Akinc, K. Schmidt-Rohr, and S.K. Mallapragada, *J. Mater. Res. Special Issue on Biomimetics*, **23**, 3196 (2008).
6. "Temperature and pH-Dependent Phase Behavior of Cationic Pentablock Copolymers by Small Angle Neutron Scattering", M.D. Determan, C.-T. Lo, L. Guo, P. Thiyagarajan, and S.K. Mallapragada, *Phys. Rev E*, **78**, 021802 (2008).

7. "Micellar Crystals in Solution from Molecular Dynamics Simulations", J.A. Anderson, C.D. Lorenz, and A. Travesset, *J. Chem. Phys.*, **128**, 184906 (2008).
8. "General Purpose Molecular Dynamics Simulations Fully Implemented on Graphics Processing Units, J.A. Anderson, C.D. Lorenz, and A. Travesset, *J. Comput. Science*, **227**, 5342 (2008).
9. "Self-assembled Ordered Polymer Nanocomposites Directed by Attractive Particles", C.D. Knorowski, J.A. Anderson, and A. Travesset, *J. Chem. Phys.*, **128**, 164903 (2008).
10. "The Dispersion of Silicate in Tricalcium Phosphate Elucidated by Solid-State NMR", A. Rawal, X. Wei, M. Akinc, and K. Schmidt-Rohr, *Chem. Mater.*, **20**, 2583 (2008).
11. "Nanoparticle Ordering via Functionalized Block Copolymers in Solution", R. Sknepnek, J.A. Anderson, M.H. Lamm, J. Schmalian, and A. Travesset, *ACS Nano*, **2**, 1259 (2008).
12. "Effect of pH on the Carbonate Incorporation into the Hydroxyapatite Prepared by an Oxidative Decomposition of Calcium-EDTA Chelates", Y. Yusufoglu and M. Akinc, *J. Am. Ceram. Soc.*, **91**, 77 (2008).
13. "Deposition of Carbonated Hydroxyapatite (CO<sub>3</sub>HAp) on Poly (Methylmethacrylate) Surfaces by Decomposition of Calcium-EDTA Chelate", Y. Yusufoglu and M. Akinc, *J. Am. Ceram. Soc.*, **91**, 3147 (2008).
14. "Interfacial Restructuring of Ionic Liquids Determined by Sum-Frequency Generation Spectroscopy and X-Ray Reflectivity", Y. Jeon, J. Sung, W. Bu, D. Vaknin, Y. Ouchi, D. Kim, *J. Phys. Chem. C*, **112**, 19649 (2008).
15. "Direct Imaging of a Collapsed Langmuir Monolayer and Multilayer Formation", S. Seok, D. Kim, T. J. Kim, Y. D. Kim, and D. Vaknin, *J. Korean Phys. Soc.*, **53**, 1488 (2008).
16. "Extracting the Pair Distribution Function of Liquids and Liquid-vapor Surfaces by Grazing Incidence X-ray Diffraction Mode", D. Vaknin, W. Bu, and A. Travesset, *J. Chem. Phys.*, **129**, 044504 (2008).
17. "Synthesis and Characterization of Self-assembled Block Copolymer Templated Calcium Phosphate Nanocomposite Gels", D.R. Enlow, A. Rawal, M. Kanapathipillai, K. Schmidt-Rohr, S. Mallapragada, C.-T. Lo, P. Thiyagarajan, and M. Akinc, *J. Mater. Chem.*, **17**, 1570 (2007).
18. "Cobalt Ferrite Nanocrystals: Outperforming Magnetotactic Bacteria", T. Prozorov, L. Wang, P. Palo, M. Nilsen-Hamilton, D. Jones, D. Orr, S. Mallapragada, B. Narasimhan, and R. Prozorov, *ACS Nano*, **1**, 228 (2007).
19. "Ordering by Collapse: Formation of Bilayer and Trilayer Crystals by Folding Langmuir Monolayers", D. Vaknin, W. Bu, S.K. Satija, and A. Travesset, *Langmuir*, **23**, 1888 (2007).
20. "Thermoresponsive Behavior of Multistimuli Pluronic-based Pentablock Copolymers at the Air-Water Interface", S. Peleshanko, K. D. Anderson, M. Goodman, M.D. Determan, S.K. Mallapragada, and V. Tsukruk, *Langmuir*, **23**, 25-30 (2007).
21. "Synthesis and Characterization of Self-assembled Block Copolymer Templated Calcium Phosphate Nanocomposite Gels", D. Enlow, A. Rawal, M. Kanapathipillai, K. Schmidt-Rohr, S. Mallapragada, C.-T. Lo, P. Thiyagarajan, and M. Akinc, *J. Materials Chemistry*, **17**, 1570-78 (2007). Highlighted as a "hot" article.
22. "Hydrolysis of  $\alpha$ -Tricalcium Phosphate in Simulated Body Fluid and Dehydration Behavior During the Drying Process", X. Wei, O. Ugurlu, and M. Akinc, *J. Am. Ceram. Soc.*, **90**(8), 2315-2321, (2007).
23. "Crystal Structure Analysis of Si, Zn-Modified Tricalcium Phosphate by Neutron Powder Diffraction," X. Wei and M. Akinc, *J. Am. Ceram. Soc.*, **90**, 2709-2715 (2007).
24. "The many origins of charge inversion in electrolyte solutions: effects of discrete interfacial charges", J. Faraudo and A. Travesset, *J. Phys. Chem. C*, **111**, 987 (2007).
25. "Magnetic Irreversibility and Verwey Transition in Nano-crystalline Bacterial and Synthetic Magnetite", R. Prozorov, T. Prozorov, S. K. Mallapragada, B. Narasimhan, T.J. Williams, and D. Bazylinski, *D.*, *Phys. Rev. B.*, **76**, 054406 (2007).
26. "Protein-Mediated Synthesis of Superparamagnetic Magnetite Nanocrystals", T. Prozorov, S.K. Mallapragada, B. Narasimhan, M. Nilsen-Hamilton, T.J. Williams, D. Bazylinski, R. Prozorov, and P.C. Canfield, *Adv. Func. Mater.*, **17**, 951-57 (2007).

# DIRECTED ORGANIZATION OF FUNCTIONAL MATERIALS AT INORGANIC-MACROMOLECULAR INTERFACES

**PIs:** *Aleksandr Noy<sup>1</sup> and James J. De Yoreo<sup>2</sup>*  
**Contributors:** *Raymond W. Friddle<sup>1,2</sup>, Nipun Misra<sup>1</sup>, Julio Martinez<sup>1</sup>, George Gilmer<sup>1</sup>, Matt Francis<sup>2</sup>*

<sup>1</sup>*Physical and Life Sciences Directorate  
Lawrence Livermore National Laboratory,  
Livermore, CA*

<sup>2</sup>*The Molecular Foundry  
Lawrence Berkeley National Laboratory  
Berkeley, CA*

*noy1@llnl.gov  
jjdeyoreo@lbl.gov*

## **PROGRAM SCOPE:**

The goal for this project is to develop a quantitative physical picture of macromolecular organization and emergence of new functionality through templated assembly. We are exploring these topics using two systems. The first system utilizes phospholipid bilayers assembled on Si nanowire and carbon nanotubes surfaces, where the bilayer produces a barrier against solution species transport to the nanowire and provides an artificial environment for membrane proteins. We are studying the assembly and physical properties of these structures. We are also showing how we can use these assembly strategies to create novel bioelectronic circuits that combine biological functionality and building blocks with microelectronic scaffolds. The second system utilizes viruses adsorbed on the surface chemical templates defined by the dip-pen nanolithography. We are using a set of “designer” virus particles, including CPMV viruses and MS2 viruses modified to include light adsorbing centers that comprise FRET pairs as artificial light harvesting complexes.

## **RECENT PROGRESS.**

### **Bionanoelectronic Devices Based on 1D-Lipid Bilayers on Nanotube and Nanowire Templates.**

Biological molecules perform sophisticated functions in living systems with complexity often far exceeding most of man-made devices and objects. Direct integration of biological components with electronic circuits could drastically increase their efficiency, complexity, and capabilities and result in novel sensing and signaling architectures. Yet, one of the obstacles for this vision of a bionanoelectronic circuit is the absence of a versatile interface that facilitates communication between biomolecules and electronic

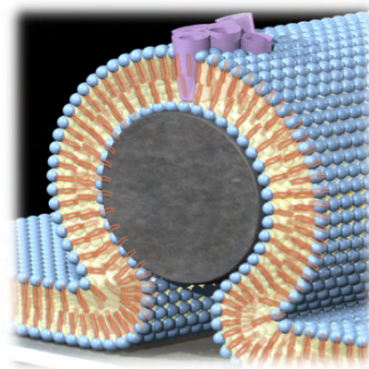


**Figure 1.** An illustration of nanowire coated with a lipid bilayer with an alamethicin cluster.

materials. We have been working on using templated self-assembly to build a platform that integrates membrane proteins with silicon nanowires. In our devices, nanowires are covered by a lipid bilayer that serves both as a universal membrane protein matrix and an insulating shield.

We recently used this platform to build prototype bionanoelectronic devices that use self-assembled passive peptide ion channels. For these experiments we have assembled the lipid bilayer shell on top of the silicon nanowire field-effect transistor. When these

“shielded” silicon nanowire transistors incorporated trans-membrane peptide pores Gramicidin A in the lipid bilayer, we showed that the ion flow through the pores can gate the nanowire transistor and perform ionic to electronic signal transduction. When the transistor incorporated the

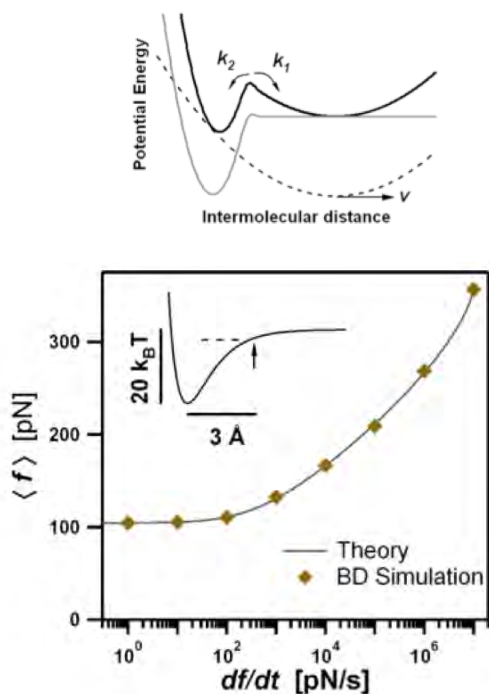


**Figure 3.** Reversible Force Spectroscopy. Upper panel: A two-state system is created by the harmonic probe used to break the bond. Lower panel: The derived two-state force spectrum against BD simulations of using a harmonic probe to force a particle out of the sketched Morse potential.

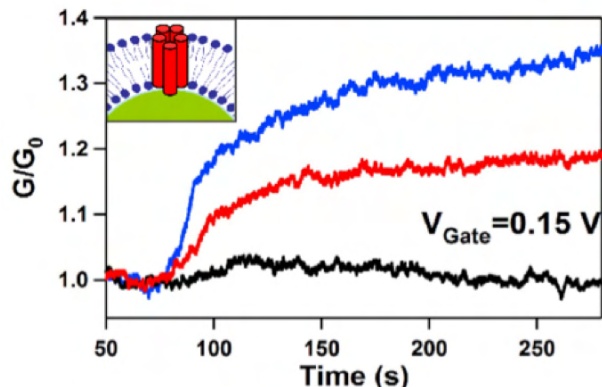


**Figure 2.** Time traces of the device conductance response to a change in solution pH in the fluid cell for bare nanowire (blue), lipid-coated nanowire (black) and lipid-coated nanowire incorporating Alamethicin protein (red). The device was biased to keep the protein pore open. From Misra, Noy, et. al., PNAS, 106, 13780 (2009)

voltage-gated peptide pore Alamethicin, we showed that the device can not only be gated by the ion flow through the pore, but also control the pore opening and closing.

### Probing the energies of macromolecule-template interactions with Single Molecule Force Spectroscopy

We have also made significant progress in interrogating single virus-substrate interactions by mechanical force. We have pursued an approach that combined experimental force spectroscopy measurements with development of a novel model for extracting quantitative thermodynamic and kinetic information from these measurements.

Bond rupture measurements can reveal a great deal of fundamental information about the bond energy and kinetic parameters. What makes these Dynamic Force Spectroscopy (DFS) measurements revealing is the dependence of the desorption rate on the applied force. If that applied force is increasing with time, then the rupture force will depend on the

loading rate (i.e. on how quickly the force is ramped). A plot of the rupture force vs. the loading rate creates a “force spectrum” of a bond that could be used to infer the bond kinetic and thermodynamic parameters.

The common theoretical interpretation of DFS assumes that bond rupture is irreversible. However, we have found the irreversible assumption to be invalid for general cases of bond rupture. Not only is reversibility observable in experiment, it also provides a critically important piece of information – the equilibrium free energy of adsorption. We have derived a unified model that describes both the non-equilibrium kinetic unbinding regime with the near-equilibrium unbinding. The low-force plateau in the spectrum is indicative of the linear-response regime of the system, which asymptotically approaches an equilibrium force as,

$$\langle f \rangle \approx \sqrt{2k\Delta G} + \frac{1}{k_{eq}} \frac{df}{dt} + \dots$$

where  $\Delta G$  is the equilibrium free energy change,  $k$  is the spring constant of the probe, and  $k_{eq}$  is the escape rate at the equilibrium force. The main advantage of this two-state model is that it can determine both the kinetic rates, pertinent over short timescales, and the equilibrium free energy, describing the long-time behavior, all from a single force spectrum.

We have tested our model against Brownian dynamics simulations (Fig 2) and the experimental measurements of rupturing His<sub>6</sub>-Ni-NTA complex. We designed the experiments to mimic our earlier studies of His-modified cowpea mosaic virus (CPMV) particles adsorbing to patterned lines of Ni-NTA on gold substrates (Cheung et al. JACS, 2006). We covalently linked His<sub>6</sub> peptides to the tip of an AFM cantilever and thiolated NTA molecules to a flat gold substrate. As expected, we find low, non-specific forces in solutions without Ni (Fig. 4, open squares). When Ni is introduced, rupture forces increase significantly (solid squares) and our two-state model fits the data nicely. In addition, we have compared our data with that of another laboratory, which measured interactions in a similar system (Fig. 4, solid circles). We find that our model is able to fit both data sets when we account for the differing force constants of the AFM probes used.

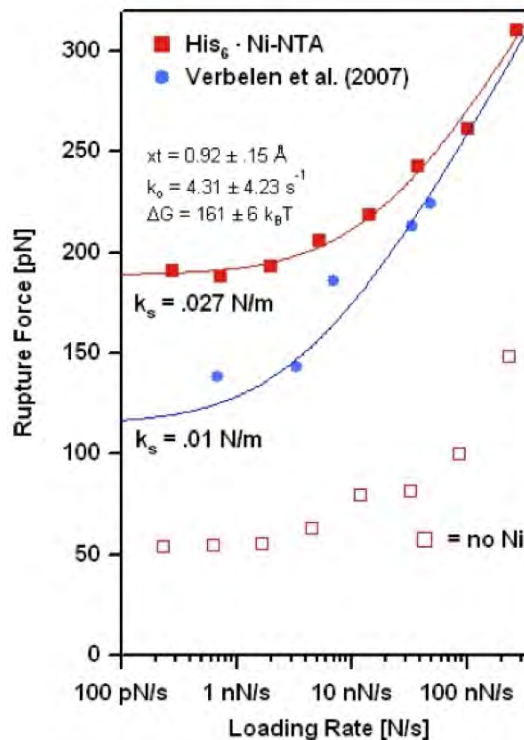


**Figure 4.** Force Spectra of the Ni-NTA/His<sub>6</sub> bond. Solid lines are fits to our analytical model, which accounts for rupture reversibility.

**Future Plans.** Our future plans center on studying the details of self-assembly in these system and on developing approaches for realizing an even more complicated functionality in these systems.

The future work in the lipid-nanowire centers on understanding the dynamics and organization of the lipid molecules on these one-dimensional inorganic templates, as well as on using these templated structures in device architectures that incorporate active biological components.

We will use single molecule force spectroscopy with tip-mounted virus particles for determining virus-template interactions; we will also compare these parameters with the bulk adsorption measurement results. We will then feed the results into the kinetic Monte-Carlo models and compare the results with the AFM images of the assembled viruses.

#### **PUBLICATIONS (2007-2009):**

N. Misra, J.A. Martinez, S.-C. J. Huang, Y. Wang, P. Stroeve, C.P. Grigoropoulos, A. Noy *Bioelectronic Silicon Nanowire Devices Utilizing Functional Membrane Proteins*, **Proc. Natl. Acad. Sci. USA**, v. 106 (33), p. 13780-13784 (2009)

J.A. Martinez, N. Misra, P. Stroeve, C.P. Grigoropoulos, A. Noy *Highly-efficient biocompatible single silicon nanowire electrodes with functional biological pore channels* **Nano Letters**, v. 9 (3), p. 1121-1126 (2009)

D. J. Sirbuly, N. O. Fisher, S.-C. J. Huang, J. B.-H. Tok, O. Bakajin, A. Noy *Biofunctional Subwavelength Optical Waveguides for Biodetection*, **ACS Nano**, v.2 (2), p. 255-262 (2008)

A. B. Artyukhin, M. Stadermann, P. Stroeve, O. Bakajin, A. Noy *Fabrication and Characterization of Suspended Carbon Nanotube Devices in Liquid*, **Int. J. Nanotechnology**, v.5(4/5), p. 488-496 (2008). **Invited article** for a special issue on *Nanosensors*

Friddle, R.W., "Unified Model of Dynamic Forced Barrier Crossing in Single Molecules", **Phys. Rev. Lett.** **100**, 138302 (2008).

Friddle, R.W., "Comment on "Experimental Free Energy Surface Reconstruction from Single-Molecule Force Spectroscopy Using Jarzynski's Equality" **Phys. Rev. Lett.** **100**, 019801 (2008).

Elhadj, S., Chernov, A.A., De Yoreo, J.J., "Solvent-mediated repair and patterning of surfaces by AFM" **Nanotechnology** **19**, 105304-105313 (2008).

S.-C. J. Huang, A. B. Artyukhin, J. A. Martinez, D. J. Sirbuly, Y. Wang, J.-W. Ju, P. Stroeve, A Noy *Formation, Stability, and Mobility of One-Dimensional Lipid Bilayers on Polysilicon Nanowires*, **Nano Letters**, v.7(11); p. 3355-3359 (2007)

R. W. Friddle, P. Podsiadlo, A. B. Artyukhin, A. Noy *Near-Equilibrium Chemical Force Microscopy*, **J. Phys. Chem. C**, **112** (13), p. 4986-4990 (2007)

A. Noy *Strength in numbers: Probing and understanding intermolecular bonding with Chemical Force Microscopy*, **Scanning**, **30** (2), p. 96-105. (2007). **Invited Article**

Chung, S.-W., Presley, A.D., Elhadj, S., Hok, S., Hah, S.-S., Chernov, A.A., Francis, M.B., Eaton, B.E., Feldheim, D.L. and J.J. De Yoreo, "Scanning probe-based fabrication of 3D nanostructures via affinity templates, functional RNA and meniscus-mediated surface remodeling." **Scanning** **30**, 159-171 (2007) **Invited Article**.

Lee, J.R.I., Han, Y., Willey, T.M., Wang, D., Muelenberg, R.W., Nilsson, J., Dove, P.M., Terminello, L.J., van Buuren, T. and De Yoreo, J.J., "Structural development of Mercaptophenol Self-Assembled Monolayers and the Overlying Mineral Phase During Templated CaCO<sub>3</sub> Crystallization from a Transient Amorphous Film" **J. Am. Chem. Soc.** **129**, 10370-10381 (2007).

## Directed Self-Assembly of Soft-Matter and Biomolecular Materials

Benjamin Ocko ([ocko@bnl.gov](mailto:ocko@bnl.gov)), Antonio Checco ([checco@bnl.gov](mailto:checco@bnl.gov))  
Masa Fukuto ([fukuto@bnl.gov](mailto:fukuto@bnl.gov)), and Lin Yang ([lyang@bnl.gov](mailto:lyang@bnl.gov))  
Brookhaven National Laboratory, Upton, NY 11973

**Program Scope:** The primary goal of the group is to understand the effects of nanoscale confinement and the role of self-assembly in soft materials through the use of patterned templates and well-defined interfaces. We use synchrotron x-ray scattering, scanning probe and optical microscopy techniques to study fundamental properties of complex fluids, simple liquids, macromolecular assemblies, liquid crystals, polymers, and biomolecular materials. The challenges are (1) to understand liquids under nano-confinement, (2) how templates and confinement can be used to direct the assembly of biomolecular materials and diblock copolymer thin films, (3) to understand the fundamental interactions which give rise to similar self-assembly behavior for a wide variety of systems, (4) how the order correlates with function. Understanding structural aspects of self-assembly and thin organic films underlies many emerging organic based devices and energy technologies. An important aspect of our approach is to use nanopatterned surfaces to confine liquids and complex fluids. To accomplish this, we are using polymer based self-assembly techniques and AFM based local-oxidation nanolithography. The program integrates experimentalists with a dedicated history of collaboration in liquids, wetting, biomaterials, and synchrotron-based structure characterization.

### Recent Progress:

**A. Biomolecular materials:** One of our main efforts is focused on lipid monolayer-mediated 2D assembly of biomolecular nanoparticles (BNPs) at liquid interfaces. A major challenge of nanoscience has been to identify and understand what physical parameters promote long-range order in the assemblies of nanoscale objects. Arrays of BNPs, i.e., proteins and virus particles, formed at the lipid membrane-aqueous solution interface are well suited to investigating ordered assembly in 2D because of the intrinsic monodispersity of BNPs as building blocks, the use of a fluid-phase lipid monolayer to promote the mobility of interface-confined BNPs, and the ability to tune the BNP-BNP and BNP-surface interactions through chemical compositions in the buffer and in the lipid membrane. Our recent progress in this research area includes

- *2D assembly of Tobacco Mosaic Virus (TMV) on cationic and zwitterionic lipid monolayers.* In-situ GISAXS, AFM, and optical microscopy measurements have been carried out at the substrate-liquid and liquid-vapor interfaces. The results demonstrate that the in-plane mobility of the interface-bound TMVs and the presence of divalent cations ( $\text{Ca}^{2+}$ ) are essential to developing structural order, consisting of close packing and alignment of these “nanorods” lying parallel to the interface. Quantitative analysis of the GISAXS data shows that the structure of the TMV arrays in the absence of  $\text{Ca}^{2+}$  is consistent with purely repulsive, electrostatic inter-particle interaction. By contrast, the structural order within  $\text{Ca}^{2+}$ -induced TMV assemblies is consistent with the behavior of a fluid of sticky rods, implying the presence of strong attraction between TMVs.
- *2D assembly of streptavidin (SA) on a Langmuir monolayer of biotin-bearing lipids.* The results of in-situ XR, GID, and optical microscopy measurements demonstrate that the adsorption and 2D crystallization of SA depend sensitively on the surface biotin density. The minimum biotin density required for the 2D crystallization of SA is found to be remarkably close to the density of the ligand-binding sites in the protein crystal. Moreover, the measured protein adsorption isotherm is consistent with the predominance of the doubly-bound SA over the singly-bound SA, both above and below the threshold biotin density. These results imply that even in the low-density noncrystalline phase, the bound proteins share a common, fixed orientation relative to the surface normal, and that dense packing of these already well-oriented proteins is the driving mechanism for the 2D crystallization of SA.

**B. Fundamental aspects of surface induced order at liquid interfaces:** Understanding interface-induced order is relevant to many fields including those used in molecular electronic and photovoltaic devices. We have had a long-standing program to understand interface-induced ordering of simple molecular and atomic systems. One of the most elegant examples is surface freezing in alkanes where a crystalline phase forms up to 3°C above the bulk melting transition. We have also investigated interfacial freezing in Langmuir-Gibbs films, surface freezing at the oil/water interface, surface induced ordering at the vapor interface of liquid metals and alloys. More recently we have investigated electrocapillary effects at the mercury/electrolyte interface, surface induced ordering of mercury, ionic liquids and long-chain alcohols at the sapphire interface. Two highlights of these studies are presented below:

- *Surface freezing of long-chain alcohols at the sapphire interface:* X-ray reflectivity measurements have been carried out to determine the structure of the deeply-buried interface between bulk alcohols (C<sub>n</sub>OH), for 12 ≤ n ≤ 20, and a solid surface, sapphire, (0001). Over a range of temperature (about 30 °C) above the freezing point of the alcohol an extremely well defined monolayer is stable at the solid interface, with surface-normal, rather than surface-parallel, molecules. After disordering the layer at higher temperature, the ordered layer is reformed by cooling. This reversible formation of an interfacial monolayer is reminiscent of surface freezing at the vapor interface where the much larger temperature range is consistent with the much stronger surface interaction. The interface between the interfacial monolayer and the molten alcohol exhibits strong electron depletion. After removing the sapphire crystal from the liquid, a well-defined SAM remains with a layer thickness identical to that of the original layer. Grazing incidence studies on these ex-situ samples show that the monolayer is crystalline and epitaxial with the underlying sapphire.
- *Thin-thick coexistence behavior of liquid crystalline films on silicon:* As the thickness of an adsorbed film is reduced the stresses within the films can lead to stable coexistence of thick and thin films on the surface. We have conducted optical and X-ray reflectivity measurements to study the effect of varying the thickness of 8CB liquid crystalline films on a flat silicon surface (with R. Garcia, Worcester Polytechnic Institute). Our measurements show the existence of a temperature-thickness phase diagram with a novel reentrant region. In this region, thick and thin films coexist on the silicon surface, consistent with the above hypothesis. Near the second-order smectic-A-to-nematic transition it is possible that fluctuation-induced forces contribute significantly to the unusual phase behavior.

**C. Nanoliquids:** A main research effort of the BNL's Soft Matter Group focuses on the study of the equilibrium and out-of-equilibrium wetting behavior of nanoscale liquids. Our unique experimental approach to the problem is based on the use of nanopatterned surfaces to confine liquids within nanometer-scale structures. The effects of confinement and long-range interactions between the liquid and the nanostructured substrate may lead to substantial deviations from the macroscopic wetting behavior. In situ X-ray scattering and AFM are then used to study the morphology of the confined nanoliquids which are then compared to recent theoretical models. Our recent progress in this research area includes:

- *Wetting of topologically nanopatterned surfaces.* Silicon surfaces were nanopatterned with an array of parallel, ~20 nm-wide trenches by using state of the art electron-beam lithography (Hitachi collaboration) or with hexagonal array of ~20 nm-sized parabolic cavities using diblock-copolymer lithography. The wetting of simple liquids (perfluoromethylcyclohexane, cyclohexane) on the nanopatterned surfaces was studied using transmission X-ray scattering measurements as a function of the chemical potential (temperature) difference between the substrate and a liquid reservoir contained in a hermetically sealed chamber. These measurements have provided the amount of liquid condensed in the nanocavities with unprecedented accuracy and therefore a stringent test for current theories of wetting on the nanoscale. Our results confirm the validity of continuum, mean field models with dispersive interaction potential for describing wetting phenomena at a ~10 nm length-scale.
- *Wetting of chemically nanopatterned surfaces.* We have studied the wetting of liquid

nanodrops of cyclohexane and ethanol on chemically nanopatterned stripes (50-1000 nm wide) prepared using oxidation nanolithography. The equilibrium shape of the nanodrops was investigated using non-contact AFM. The measured power law dependence of the height of the liquid drops versus the stripe width confirms the long-standing prediction that the shape of the drops is controlled by the dispersive (Van der Waals) potentials. These experiments were extended to the out-of-equilibrium conditions that occur when a non-volatile liquid spreads along the chemically patterned nanostructures. Results show that the liquid morphology of the spreading nanoliquid is truncated near the microscopic contact line due to the effect of long-range forces, in good quantitative agreement with mesoscale hydrodynamic theory.

- *Directed Assembly of Block Copolymers*: These same chemical patterns have also been used to direct the dewetting of polymer thin films into structures of complex shapes in order to study the effect of the lateral confinement on the spatial orientation of diblock copolymer microdomains, so called graphoepitaxy. The combined sectoring and self-assembly provides a unique route towards a guided self-assembly of BCP films with long-range order that may be used to fabricate sectored, high-density arrays of nanoscopic elements suitable as templates for device applications.
- *Deliquescence of model aerosol nanoparticles*. The wetting of nanoscale atmospheric aerosols by water is relevant to the accurate modeling of climate and climate changes. To gain insight into this phenomenon we have studied the hygroscopic growth of “model” aerosols particles (cubic NaCl crystals) deposited on a prepared hydrophobic surface using non-contact environmental atomic force microscopy (AFM). Results show that the nanoparticles (sized between 35 and 150 nm) reversibly adsorbed a 2–4 nm thick layer of water at values of relative humidity sensibly (~5%) below the deliquescence point (75.0% at 20C). These findings suggest that significant, but reversible, reorganization of mass near the interface of water and solid NaCl occurs at RH-values near 70%. Current physical models of the RH-dependent properties of some hygroscopic aerosols may therefore underestimate (i) particle size and (ii) salt-content of the liquid “shell” prior to deliquescence.

### **Future Plans:**

In addition to the projects discussed above, many of which are ongoing, we highlight some additional research plans below. In the area of biomolecular materials, we will extend the approach of the lipid-mediated 2D assembly to sphere-like virus particles, such as cowpea mosaic virus (CPMV), and explore the effects of the chemical environment, such as pH, ionic strength, type of ions, and lipid charge density. In the area of surface induced ordering, we intend to study the surface freezing of alcohols at the sapphire interface in mixtures, both of alcohols of different length and diols (two sided alcohols) with alcohols. At the vapor interface, we will investigate surface induced ordering of ionic liquids. In the area of nanoliquids, we will extend our studies of wetting phenomena to various chemically and topographically patterned surfaces with the aim of reducing the feature sizes so as to better test existing theories. The studies on the effect of lateral confinement on spreading will be extended to complex liquids (such as polymers and liquid crystals) where anomalous behavior is expected. We have started a program to improve our understanding of the structure and phase separation in organic electronic materials and organic photovoltaic devices. Specifically, we will extend our initial studies of temperature-dependent solvent annealing to include the effects of pressure, an important parameter in imprinting films to control the micro phase separation of the donor and acceptor components.

### **DOE Sponsored Publications (2008-2009)**

*Morphology and phase behavior of ethanol nanodrops condensed on chemically patterned surfaces*, A. Checco, and B.M. Ocko. Phys. Rev. E 77, 061601 (2008).

*Wetting, mixing and phase transitions in Langmuir-Gibbs films*, E. Sloutskin, Z. Sapir, C.D. Bain, Q. Lei, K.M. Wilkinson, L. Tamam, M. Deutsch, and B.M. Ocko. Phys. Rev. Lett. 99, 136102 (2007).

*Extended molecular layering of a pyrrolidinium-based ionic liquid at the sapphire(0001) surface*, M. Mezger, H. Schroeder, H. Reichert, S. Schramm, J. Okasinski, S. Schoeder, V. Honkimaki, M. Deutsch, B.M. Ocko, J. Ralston, and H. Dosch. *Science* **322**(5900), 424-428 (2008).

*In-Situ X-ray Reflectivity Studies on the Formation of Substrate-Supported Phospholipid Bilayers and Monolayers*, S. T. Wang, M. Fukuto, and L. Yang. *Phys. Rev. E* **77**, 031909 (2008).

*Thin-Thick Coexistence Behavior of 8CB Liquid Crystalline Films on Silicon*, R. Garcia, E. Subashi, and M. Fukuto. *Phys. Rev. Lett.* **100**, 197801 (2008).

*Comment on "How Water Meets a Hydrophobic Surface"*. B. M. Ocko, A. Dhinojwala, and J. Daillant. *Phys. Rev. Lett.* **101**, 039601 (2008).

*Post assembly chemical modification of a highly ordered organosilane multilayer: New insights into the structure, bonding, and dynamics of self-assembling silane monolayers*, K. Wen, R. Maoz, H. Cohen, J. Sagiv, A. Gibaud, A. Desert, and B.M. Ocko. *ACS Nano* **2**, 579-599 (2008).

*Dynamics and critical damping of capillary waves in an ionic liquid*, E. Sloutskin, P. Huber, M. Wolff, B.M. Ocko, A. Madsen, M. Sprung, V. Schon, J. Baumert, and M. Deutsch. *M. Phys. Rev. E* **77**, 060601 (2008).

*Wetting of Liquid-Crystal Surfaces and Induced Smectic Layering at a Nematic-Liquid Interface: An X-ray Reflectivity Study*, M. Fukuto, O. Gang, K. J. Alvine, B. M. Ocko, and P. S. Pershan. *Phys. Rev. E* **77**, 031607 (2008).

*Non-linear elasticity of a liquid contact line*. A. Checco. *Europhys. Lett.* **85**, 16002 (2009).

*Liquid spreading under nanoscale confinement*, A. Checco. *Phys. Rev. Lett.*, **102**, 106103 (2009)

*Lateral ordering of cylindrical microdomains under solvent vapor*. S. Park, B. Kim, J. Xu, T. Hofmann, B. Ocko, and T. Russell. *Macromolecules* **42**(4), 1278-1284 (2009).

*Equilibrating nanoparticle monolayers using wetting films*, D. Pontoni, K.J. Alvine, K.J., A. Checco, O. Gang, B.M. Ocko, and P.S. Pershan. *Phys. Rev. Lett.* **102**, 016101 (2009).

*Structure and Interaction in 2D Assemblies of Tobacco Mosaic Viruses*, L. Yang, S. T. Wang, M. Fukuto, A. Checco, Z. Niu, and Q. Wang. *Soft Matter* (accepted, August 2009).

*Effects of surface ligand density on lipid-monolayer-mediated 2D assembly of proteins*. M. Fukuto, S.T. Wang, M.A. Lohr, S. Kewalramani, and L. Yang. *Soft Matter* (submitted).

*Grazing incident small angle x-ray scattering: a metrology to probe nanopatterned surfaces*, T. Hofmann, E. Dobisz, and B. Ocko. *B. J. Vac. Sci. Technol.* (submitted).

*Formation and Collapse of Poly(n-Butyl Acrylate) Homopolymer Monolayers at the Air-Water Interface*, K. N. Witte, S. Kewalramani, I. Kuzmenko, W. Sun, M. Fukuto, and Y.-Y. Won. *Macromolecules* (submitted).

*Directed self-assembly of Block copolymers on 2D chemical patterns made by Electro-oxidation nanolithography*, J. Xu, S. Park, T.P. Russell, A. Checco, and B.M. Ocko. *Nanoletters* (submitted).

# Damage Tolerance in Biological Materials: Can This Be Mimicked in Engineering Structural Materials?

Robert O. Ritchie

Materials Sciences Division, Lawrence Berkeley National Laboratory  
and

Department of Materials Science & Engineering  
University of California, Berkeley, Berkeley, CA 94720

[roritchie@lbl.gov](mailto:roritchie@lbl.gov)

The structure of materials invariably defines their mechanical behavior. However, in most materials, specific mechanical properties are controlled by structure at widely differing length scales. Nowhere is this more apparent than with biological materials, which are invariably sophisticated composites whose unique combination of mechanical properties derives from an architectural design that spans nanoscale to macroscopic dimensions with precisely and carefully engineered interfaces. The fracture resistance of such materials originates from toughening mechanisms at almost every one of these dimensions. Few structural engineering materials have such a hierarchy of structure, yet the message from biology is clear – unique mechanical properties can be achieved through the combination of mechanisms acting at multiple length-scales. Nature has successfully used this approach over billions of years, yet despite intense interest by the scientific community, the biomimetic approach has yielded few real technological advances in the design of new synthetic *bulk* structural materials. Unlike engineering composites where properties are invariably governed by the “rule of mixtures”, the mechanical properties of many natural composite materials are generally far greater than their constituent phases. However, actually making such materials synthetically has proved to be extremely difficult, particularly in macroscopic form.

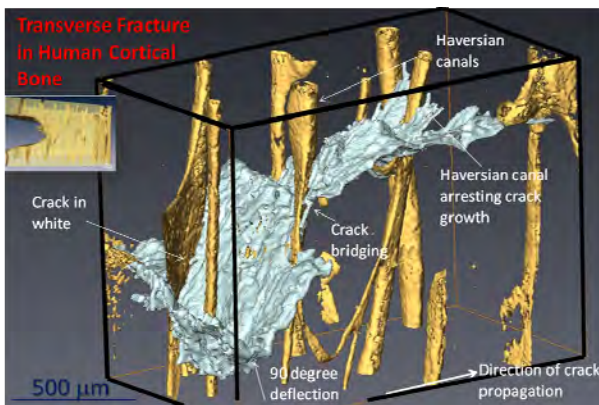


**Fig. 1:** Synchrotron x-ray computed tomography of toughening in human cortical bone by crack deflection and twist at cement lines (the interfaces of the osteons).

We first consider here how such biological materials, specifically bone, teeth and seashells, derive their strength (resistance to deformation) and toughness (resistance to fracture), *i.e.*, their *damage tolerance*, in terms of their hierarchical structural architecture over length-scales spanning nano to almost macro, and then in the case of bone and teeth describe how biological factors, such as aging, therapy and disease, can degrade these properties.<sup>1-3</sup> We then explore the notion of emulating in a

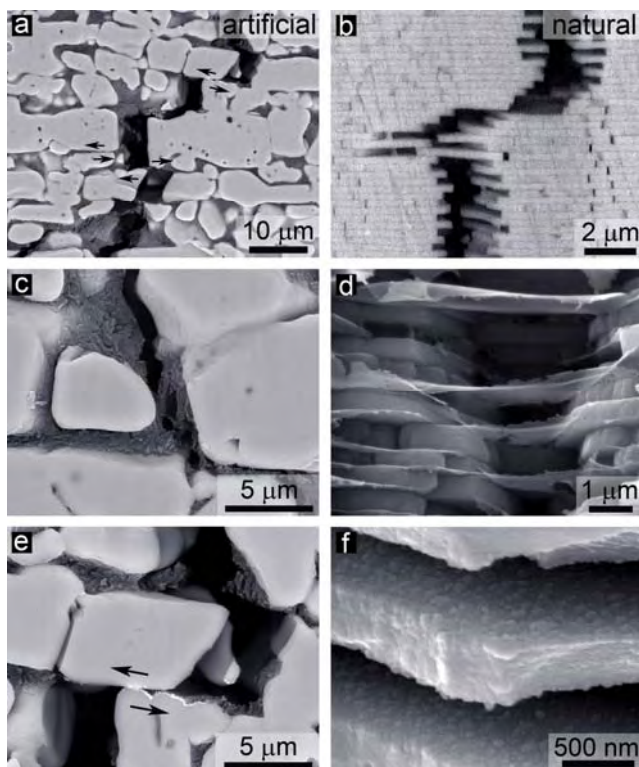


**Fig. 2:** Similarities between the toughening mechanisms acting in artificial ( $\text{Al}_2\text{O}_3/\text{PMMA}$ ) and natural nacre. Scanning electron micrographs taken during stable crack growth show the toughening mechanisms acting at multiple length scales: (a) “pull out” mechanisms similarly to that observed in (b) nacre, (c) polymer tearing and stretching over micrometer dimensions as also observed in the (d) organic phase of nacre, and (e) frictional sliding resisted by the interface roughness of the ceramic bricks as observed in (f) nacre.<sup>5,6</sup>

provides for strength but the polymer phase acts like a “lubricant” to relieve high stresses, much like plasticity in metals and microcracking in bone.

We believe that these model materials can be used to identify the key microstructural features that could guide the synthesis of more advanced Nature-inspired lightweight structural materials with unprecedented combinations of strength and toughness.

*Composites work supported by the Office of Science, Office of Basic Energy Sciences, Division of Materials Sciences and Engineering, of the U.S. Department of Energy under Contract No. DE-AC02-05CH11231.*

<sup>1</sup>RK Nalla, JH Kinney, RO Ritchie: *Nature Materials* **2**, 164 (March 2003).

<sup>2</sup>RK. Nalla, JJ Kruzic, JH Kinney, RO Ritchie: *Bone* **35**, 1240 (Dec. 2004).

<sup>3</sup>KJ Koester, JW Ager III, RO Ritchie: *Nature Materials* **7**, 672 (Aug. 2008).

<sup>4</sup>S Deville, E Saiz, RK Nalla, AP Tomsia: *Science* **311**, 515 (Jan 27, 2006).

<sup>5</sup>E Munch, ME Launey, DH Alsem, E Saiz, AP Tomsia, RO Ritchie: *Science* **322**, 1516 (Dec 5, 2008).

<sup>6</sup>ME Launey, E Munch, DH Alsem, HB Barth, E Saiz, AP Tomsia, RO Ritchie: *Acta Mater.* **57**, 2919 (June 2009).

synthetic material such natural toughening mechanisms to make bulk ceramic-polymer nacre- and bone-like hybrid structural materials with unprecedented strength and toughness properties. We employ a freeze-casting fabrication process<sup>4</sup> and utilize the combination of two ordinary compounds, specifically alumina and PMMA, with dopants of sugar, salt and alcohol, to make ice-templated structures whose toughness can be over 300 times (in energy terms) that of their constituents.<sup>5</sup> The final products are bulk lightweight hybrid ceramic materials whose high strength and fracture toughness ( $\sim 200$  MPa and  $\sim 30 \text{ MPa}\sqrt{\text{m}}$ ) provide specific properties in ceramic alumina that comparable to metallic aluminum alloys. These materials are probably the toughest ceramics ever produced, but must be made through careful control of structural size-scales at nano to macro-scales. Their exceptional toughness properties rely on the concept of the “lubricant phase”.<sup>5,6</sup> Specifically, they are unlike regular composites in that both phases are not load-bearing; the hard ceramic phase

## Adaptive and Reconfigurable Nanocomposites

### Molecular Nanocomposites Project - Subtask 1

Bruce C. Bunker ([bcbunke@sandia.gov](mailto:bcbunke@sandia.gov)), Todd M. Alam ([tmalam@sandia.gov](mailto:tmalam@sandia.gov)),  
David R. Wheeler ([drwheel@sandia.gov](mailto:drwheel@sandia.gov)), Dale L. Huber ([dlhuber@sandia.gov](mailto:dlhuber@sandia.gov)),  
Mark J. Stevens ([msteve@sandia.gov](mailto:msteve@sandia.gov)), Andrew M. Dattelbaum ([amdattel@lanl.gov](mailto:amdattel@lanl.gov)),  
Andrew P. Shreve ([shreve@lanl.gov](mailto:shreve@lanl.gov)), Darryl Y. Sasaki ([dysasak@sandia.gov](mailto:dysasak@sandia.gov))

Sandia National Laboratories, P.O. Box 969, Livermore, CA 94551  
& P.O. Box 5800 Albuquerque, NM 87185  
Los Alamos National Laboratory, P.O. Box 1663, Los Alamos, NM 87545

### Program Scope

This project explores the basic science associated with the development of responsive and addressable materials to create programmable and/or reconfigurable nanocomposites. As biological systems employ such schemes to intricately coordinate function in nanoscale self-organizing assemblies, we are exploring simplified versions of these nanomaterials to understand the molecular and supramolecular interactions that lead to dynamic component organization and integrated function. Similar to cellular systems, we impart in our systems with components that alter chemical, physical, or mechanical behavior in response to specific activators, such as heat, light, electric fields, and host-guest complex formation. Our activities include 1) synthesis of molecular building blocks with programmed function, 2) assembly of the building blocks into films and 3D structures, 3) stimulation and characterization of phase transitions and reconfigurations, and 4) modeling of component interactions to aid in the design and visualization of reconfigurable phenomena.

### Recent Progress

We have focused our research over the past few years on the development of self-assembling systems that alter shape, size, and supramolecular organization in 2D and 3D architectures in a reversible manner to temperature, pH, and binding events. Our research is driven by the need to understand the relationship between lateral tension, structural packing order, and bending energy of films and how we can influence these parameters by changing the interfacial molecular interactions and material asymmetry in a reversible manner. The materials are composed of lipids and amphiphiles that self-assemble into micellar and bilayer architectures. In this abstract we describe new amphiphilic molecules with polymeric headgroups that respond to temperature, or with affinity sites for protein capture. By changing the electrostatic and steric interactions between neighboring molecules we find that we can reversibly breakdown lipid vesicles, generate functionalized domains, create budding and tubulating structures (Fig. 1), and control nanoparticle assembly.



Figure 1. Curvature induced by steric interactions at the membrane surface.

### *Collapsing polymers – micelle to vesicle transformation*

In a study of steric interactions, we developed a surfactant that alters headgroup size upon small changes in temperature thereby dynamically modifying packing order and lateral tension. Several alkylated poly(N-isopropylacrylamide) [PNIPAM] surfactants were prepared and their behavior as micelles and incorporation into phosphatidylcholine lipid vesicles were studied as a function of temperature. PNIPAM has a distinct and reversible phase transition ( $T_g$ ) temperature at  $\sim 30$  °C, transitioning from a swollen hydrated state ( $< T_g$ ) to a collapsed dehydrated state ( $> T_g$ ). As the polymer transitions from hydrated state to the collapsed state the steric interactions at the membrane surface are expected to lead to changes in lateral tension and curvature.

When dispersed in water the PNIPAM surfactants formed micelles of defined size (e.g., 15 nm). A distinct temperature dependence on size was observed with an increase of nearly an order of magnitude above  $T_g$  (e.g., 120 nm). The size change was found to be completely reversible upon cooling. PNIPAM alone undergoes a similar reversibility in micellar size, but with a significant hysteresis. When incorporated into 1-palmitoyl-2-oleoylphosphatidylcholine (POPC) vesicles (10% mole fraction) the surfactant induces membrane budding near  $T_g$ , and then micelle formation with higher  $T$ . Remarkably, upon cooling the components of the micelles reversibly reorganize into vesicles. These single chain PNIPAM surfactants offer a facile and reversible system to study the role of steric effects and packing order on curvature in self-assembling films.

### *Microdomain formation*

The study of membrane curvature is essential for understanding budding and tubulation processes in cells that facilitate the packaging and transport of biomaterials. It is believed that biological membranes contain insoluble domains, which selectively partitions or attracts specific lipid and protein components. This selective partitioning may induce curvature of the domains. Understanding this process can aid in the development of functionally compartmentalized surfaces as coatings on macro and nanoscale materials. The issue is how do you reversibly form microdomains with the ability to attract membrane bending components?

We have developed a membrane system that reversibly forms domains on command via metal ion recognition. The domains form as a consequence of phase separation when  $\text{Cu}^{2+}$  ion binds to iminodiacetic acid (IDA) functionalized lipids. Metal ion binding neutralizes the negatively charged lipid and increases its phase transition temperature. As supported lipid bilayers the gel phase  $\text{Cu}^{2+}$ -IDA lipids formed microdomains (1 – 0.5  $\mu\text{m}$  dia.) in a fluid phase POPC membrane generating sites with high affinity for His-tagged proteins. We observed binding affinities of  $K > 10^8 \text{ M}^{-1}$  for 6-His-maltose binding protein. Additionally, the system showed complete reversibility with the addition of EDTA to remove  $\text{Cu}^{2+}$ .

### *Protein-induced membrane curvature and tubulation*

When uncoupled from solid substrates the microdomains of  $\text{Cu}^{2+}$ -IDA lipid coalesce into larger domains, observed microscopically with giant unilamellar vesicles (GUVs). These domains with sizes up to tens of microns in diameter exhibit the same selectivity and high

affinity for His-tagged proteins. However, due to the high concentration of bound proteins in a confined area the domain transforms from a planar 2D structure to a curved 3D bulge. Interestingly, depending on the matrix lipid the 3D structure can alter from buds to small tubular projections and even to stiff lipid nanotubes with lengths of tens of microns (Fig. 2). Our studies suggest that the change in structure is a product of steric interactions of bound proteins to the  $\text{Cu}^{2+}$ -IDA domains in conjunction with the line tension that develops at the domain boundary. Besides being a novel route towards self-assembling fluidic transport structures, the discovery sheds light on the role of steric crowding in confined space and binding energy of ligand-receptor interactions on membrane deformation.

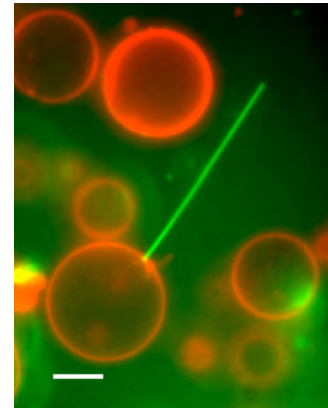


Figure 2. Membrane tubulation produced by binding of His-tagged GFP on  $\text{Cu}^{2+}$ -IDA lipid domain.

#### *pH sensitive gold nanorod assembly*

One of our goals has been the development of lipid bilayer coatings on nanoparticles via a facile process that yields asymmetric functionality that will ultimately enable directed assembly of structured materials. Metal and metal oxide nanoparticles are typically functionalized with chemically bound or electrostatically attached organic ligands to the particle surface. The functionalization process, however, can be inefficient and inhomogeneous providing less than full or stable coverage. As a consequence the coated nanoparticles are readily biofouled and offer poor biocompatibility.

We recently demonstrated the facile coating of gold nanorods with lipid bilayers using a simple surface adsorption process. The particle-membrane interaction was fully characterized using NMR, IR, and zeta-potential measurements. Although this simple construct is just the first step towards asymmetrically functionalized nanoparticles we demonstrated two unique properties: 1) distinct, reversible changes in nanoparticle organization through electrostatic interactions via solution pH, and 2) biocompatibility with cultured cells. These two properties indicate that the bilayer coating is structurally sound and stable to changes in chemistry at the membrane surface.

#### **Future Plans**

Our future goals are to further our understanding in the control of soft material architecture in two- and three-dimensions using physical, chemical, and mechanical stimuli to address specific regions in the material that facilitate dynamic processes. We shall continue to investigate the role of steric confinement to drive molecular aggregation and transformation of structural phase and dimensions. Of particular interest will be the development of asymmetrically functionalized nanoparticles and the possibilities of nanocomposite assemblies with unique optical and electrical functionality. Curved surfaces and structures offer a distinct and unique perspective in creating hierarchical nanostructures that are reconfigurable and rich in functional properties.

## Acknowledgements

This research was supported by the Division of Materials Science and Engineering in the Department of Energy Office of Basic Energy Sciences. Sandia is a multiprogram laboratory operated by Sandia Corporation, a Lockheed Martin Company, for the United States Department of Energy under Contract DE-AC04-94AL85000.

## Publications resulting from this subtask (2007 – 2009)

Stachowiak, J. S., Hayden, C. C., Sasaki, D. Y., “Membrane Budding and Tubulation through Steric Confinement of Proteins in Lipid Domains” to be submitted to *Proc. Nat. Acad. Sci.*

Lee, S. E., Sasaki, D. Y., Perroud, T. D., Yoo, D., Patel, K. D., Lee, L. P., “Biologically Functional Cationic Phospholipid-Gold Nanoplasmonic Carriers” *J. Am. Chem. Soc.*, *accepted*.

Orendorff, C. J., Huber, D. L., and Bunker, B. C., “Effects of Water and Temperature on Conformational Order in Model Nylon Thin Films,” *J. Phys. Chem. C.*, **2009**, *113*, 13723.

Orendorff, C. J., T. M. Alam, D. Y. Sasaki, B. C. Bunker, and J. A. Voigt. 2009. “Phospholipid-Gold Nanorod Composites” *ACS Nano*, **2009**, *3*, 971 - 983.

Hayden, C. C., J. S. Hwang, E. A. Abate, M. S. Kent, and D. Y. Sasaki. “Directed Formation of Lipid Membrane Microdomains as High Affinity Sites for His-Tagged Proteins” *J. Am. Chem. Soc.*, **2009**, *131*, 8728 - 8729.

Bunker, B. C., “Reversible switching of interfacial interactions” *Materials Science & Engineering, R: Reports*, **2008**, *R62(5)*, 157-173

Kent, M. S., H. Yim, J. K. Murton, D. Y. Sasaki, B. D. Polizzotti, M. B. Charati, K. L. Kiick, I. Kuzmenko, and S. Satija, “Synthetic Polypeptide Adsorption to Cu-IDA Containing Lipid Films: A Model for Protein-Membrane Interactions” *Langmuir*, **2008**, *24*, 932 - 942.

Alam, T. M. and McIntyre, S. K., "Self-Assembly and Magnetic Alignment in Cetyltrimethylammonium Bromide/Sodium Perfluorooctanoate Surfactant Mixtures Investigated Using <sup>2</sup>H Nuclear Magnetic Resonance Spectroscopy" *Langmuir*, **2008**, *24*, 13890-13896.

Satishkumar, B. C., Doorn, S. K., Baker, G. A., Dattelbaum, A. M., “Fluorescent single walled carbon nanotube/silica composite materials” *ACS Nano* **2008**, *2*, 2283-90.

Dattelbaum, A. M., Hicks, R. K., Shelly, J., Koppisch, A. T., Iyer, S., “Surface assisted laser desorption-ionization mass spectrometry on nanoporous silica thin films” *Micropor. Mesopor. Mater.*, **2008**, *114*, 193-200.

Bunker, B. C., Huber, D. L., Kushmerick, J. G., Dunbar, T., Kelly, M., Matzke, C., Cao, J., Jeppesen, J. O., Perkins, J., Flood, A. H., Stoddart, J. F., “Switching surface chemistry with supramolecular machines” *Langmuir*, **2007**, *23(1)*, 31 – 34.

## Program Title: Solid-State NMR of Complex Materials

**Principal Investigators:** Klaus Schmidt-Rohr, Ames Laboratory and Department of Chemistry, Iowa State University, Ames IA 50011. [srohr@iastate.edu](mailto:srohr@iastate.edu). E. M. Levin, Ames Laboratory and Department of Physics, Iowa State University, Ames IA 50011.

**Coworkers:** Ms. Yan-Yan Hu, Mr. Xueqian Kong

### Program Scope

We develop and apply solid-state NMR methods for studying complex materials. In the context of biomolecular materials, we analyze the structure and composition of organic-inorganic biomaterials on the nanometer scale. Other parts of this project involve studies of the nanostructure of the Nafion fuel-cell membrane and of complex thermoelectric tellurides.

In this Abstract, we will focus on the aspects of our program with bio-relevance. This work is tightly integrated with the FWP on bioinspired nanocomposites led by Dr. Surya Mallapragada.

### Recent Progress

#### NMR Characterization of Biological Nanocomposites

**The organic-inorganic interface in bone.** The load-bearing material in bone is a nanocomposite of ~ 3-nm thick apatite (calcium phosphate) platelets imbedded in a collagen matrix, with a volume ratio typically near 45:45 and the remaining 10% accounted for by water. Being a target for biomimetic materials synthesis, the structure of this nanocomposite needs to be known more accurately. Multinuclear ( $^{13}\text{C}$ ,  $^1\text{H}$ ,  $^{31}\text{P}$ ) NMR can characterize the composition of the organic and inorganic components. Most interestingly, it can selectively observe the signals of organic segments near the interface with the bioapatite nanocrystals, see Figure 1(b), to be compared to the reference spectrum of all carbons in Figure 1(a).

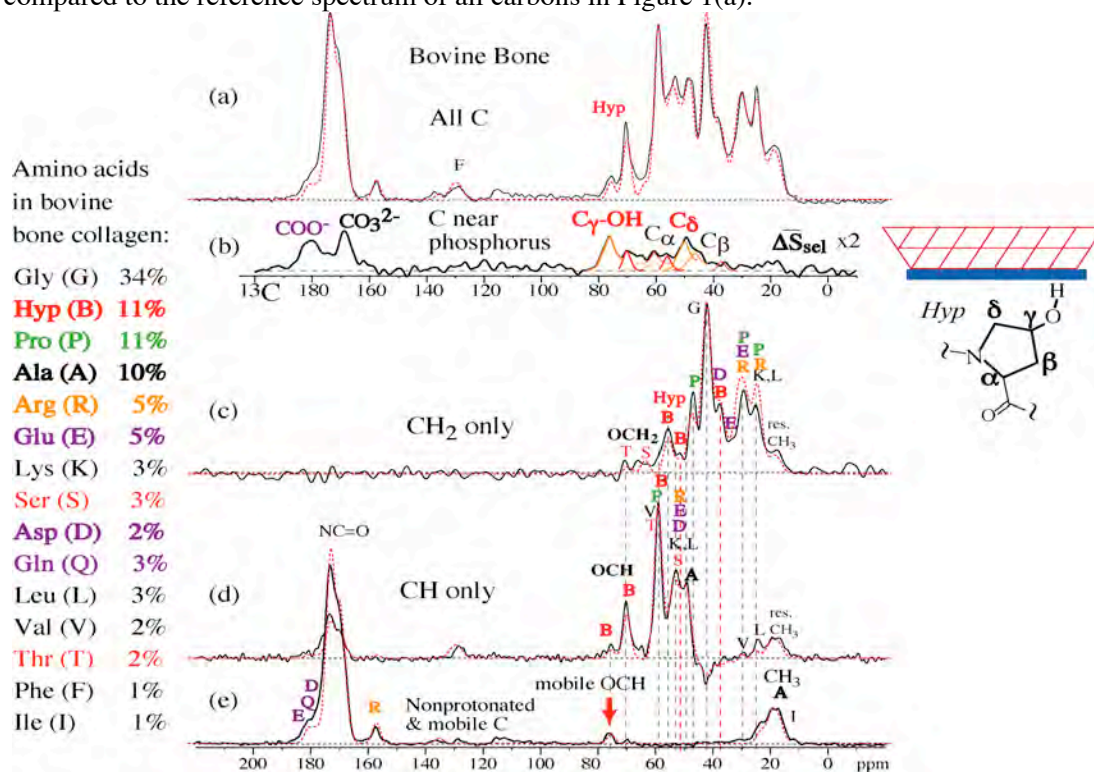


**Figure 1.**  $^{13}\text{C}$  NMR spectra of collagen in bovine bone. Simulated spectra, based on the known amino-acid composition of bovine-bone collagen as listed on the left, are shown by dashed red lines. (a) Full spectrum. (b) Spectrum of carbon near  $^{31}\text{P}$ , selected by  $^{31}\text{P}\{^{13}\text{C}\}$  REDOR. (c) Spectrum of methylene carbons. (d) Spectrum of methyne carbons. (e) Spectrum of nonprotonated carbons and mobile segments, which shows that the interfacial OCH groups resonating near 76 ppm exhibits large-amplitude mobility.

Based on such NMR data, it has been proposed that “The Organic-Mineral Interface in Bone Is Predominantly Polysaccharide”.<sup>1</sup> We will present evidence disputing that claim. For example, the <sup>13</sup>C NMR spectrum of bone in Figure 2(a,b) shows the absence of the O-C-O (anomeric-carbon) signals near 100 ppm that are characteristic of sugar rings, see Figure 2(c-e).

The assignment of the 76-ppm peak and of signals from other segments near the interface, e.g. the prominent resonance at 50 ppm in Figure 1b, does present some puzzles. The chemical shifts deviate from standard resonance positions of hydroxyproline residues by ~ 6 ppm. We propose that these signals are from hydroxyproline rings (see structure in Figure 1) in an unusual conformation. Alternatively, chemical modification (e.g. methylation) of hydroxyproline could be considered. To distinguish between frequency shifts from conformational and chemical changes, we have analyzed the spectra of demineralized bone, and of bone after separation of organic and inorganic components without removal of any material. The resonance of the mobile OCH segment at 76 ppm disappears upon separation of collagen and calcium phosphate, which again excludes the assignment to sugar, as well as to chemically modified (e.g. methylated) hydroxyproline. Rather, it supports the notion that the conformation of the hydroxyproline changes to a more regular one when it is not near the bioapatite surface.

As indicated in Figure 1, the pronounced peaks assigned to C $\gamma$  and C $\delta$  and the lack of a clear C $\beta$  signal in Figure 1(b) suggest that C $\gamma$  and C $\delta$  face the hydrated surface of the bioapatite nanocrystals. Using refocused detection for >3-fold signal enhancement as developed previously in this program, we have been able to show that the interfacial HCOH groups are closest to the layer of mobile water detected in our previous research, confirming its location at the organic-inorganic interface.

The organic segments near the interface also include COO groups, which resonate at 180 ppm (see left end of the spectra in Figures 1(a, b)). Our studies on demineralized bone indicate that these end up in the calcium-phosphate phase after separation from collagen, suggesting that they are due to soluble proteins other than collagen. This is consistent with the excess intensity in the experimental spectrum compared to that simulated from the collagen amino-acid composition, see left end of the spectra in Figure 1(a).

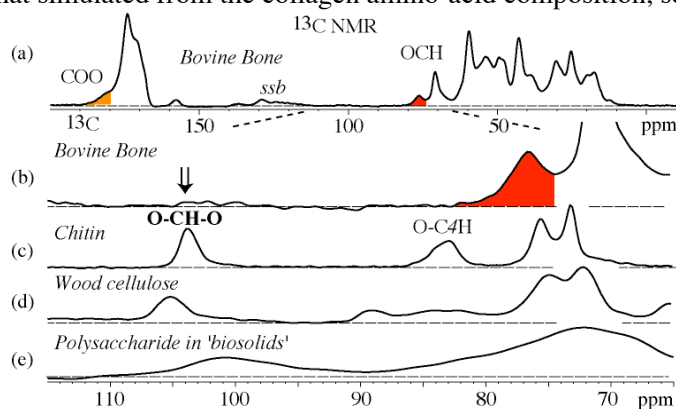


**Figure 2.** (a) <sup>13</sup>C NMR spectrum of bovine bone at 6.5 kHz MAS, with spinning-sideband suppression by TOSS. (b) Expanded 65 – 115 ppm region from (a). (c-e) Same spectral region as in (b) for (c) chitin, (d) cellulose in wood, (e) the hydrophilic high molecular weight fraction of biosolids in sludge.

**Supramolecular structure of diatom cell walls.** The cell walls of diatoms consist mostly of amorphous hydrated silica patterned on the submicron scale by the organic biomolecular machinery of these unicellular organisms. They have been shown to provide mechanical protection<sup>2</sup> and possibly act as photonic crystals directing sunlight to chlorophyll<sup>3</sup>. We are investigating the supramolecular structure of *T. pseudonana* diatoms isotopically labeled with <sup>13</sup>C, <sup>29</sup>Si, and <sup>15</sup>N at UC Santa Barbara (by M. Brzezinski et al.).<sup>4</sup> More than 8 distinct components have been identified and characterized by multinuclear NMR: Silica (<sup>29</sup>Si), protein (<sup>13</sup>C, <sup>15</sup>N), amines (<sup>13</sup>C, <sup>15</sup>N), casing polysaccharide (<sup>13</sup>C), disordered polysaccharide (<sup>13</sup>C, <sup>1</sup>H), two types of lipids (<sup>13</sup>C, <sup>1</sup>H), and inorganic hydrated phosphate (<sup>31</sup>P, <sup>1</sup>H). Their proximities on the 10-nm scale can be assessed most easily by <sup>1</sup>H-spin-diffusion mediated T<sub>1H</sub> relaxation, detected after cross polarization to various X-nuclei. This relaxation is particularly fast for polyamines and phosphates, apparently due to interactions with unpaired electrons. Figure 3 shows a plot of the T<sub>1H</sub> relaxation times for the various components of the diatoms. This provides information on their likely proximity, since components with significantly different T<sub>1H</sub> values cannot be close on the 10-nm scale of spin diffusion. In particular,

polyamines, which are believed to direct the assembly of the biosilica,<sup>5</sup> are not found close to silica in our samples. Rather, they appear to be associated with inorganic Ca/Mg phosphate deposited from the phosphate-rich growth medium. This phosphate, confirmed by scanning electron microscopy with energy-dispersive X-ray spectroscopy, forms a nanocomposite with polysaccharides and lipids of the diatom, as proven by <sup>1</sup>H-<sup>31</sup>P heteronuclear correlation spectra after spin diffusion.

Quantitative <sup>29</sup>Si NMR has revealed internal surfaces (Si-OH groups) in the >60-nm diameter silica structures. Some sharp <sup>1</sup>H signals are observed in spite of the amorphous nature of the silica, but <sup>13</sup>C-<sup>1</sup>H experiments showed that these are not from organic molecules. They are tentatively assigned to OH<sup>-</sup>.

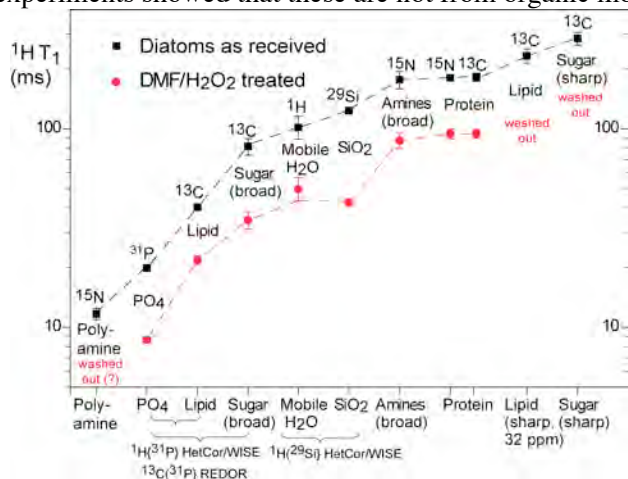


**Figure 4.** <sup>1</sup>H T<sub>1</sub> relaxation times, detected via various X-nuclei, of various components in regular (top) and dimethylformamide/H<sub>2</sub>O<sub>2</sub> treated diatoms. Components with significantly different relaxation times cannot be close on the 30-nm scale. The origin of the shorter relaxation times for the treated sample is not clear at this point. Proximities proved by multinuclear NMR are indicated at the bottom.

### Future plans

**Polyamines in diatoms.** It has been proposed that polyamine-rich, phosphorylated proteins direct the self-assembly of biosilica in diatoms.<sup>5</sup> Nevertheless, the polyamines have mostly escaped detection in two previous solid-state NMR studies of isotopically labeled diatoms.<sup>4,6</sup> This is due to their relatively small concentration and unfavorable relaxation properties. We have identified their signals in <sup>13</sup>C and <sup>15</sup>N NMR, determining conditions where they produce the dominant peaks in their spectral environment. On that basis, we plan to characterize their structure by two-dimensional <sup>13</sup>C-<sup>13</sup>C, <sup>1</sup>H-<sup>13</sup>C, and possibly <sup>13</sup>C-<sup>15</sup>N NMR. We will also try to elucidate the origin of the observed short relaxation times, which are most likely due to proximity to unpaired electrons of Fe ions.

**Phosphate on diatoms.** Unexpectedly, we found that our diatom samples contained more phosphate than silica, as determined by both NMR and SEM-EDX. Measurements of <sup>31</sup>P-<sup>31</sup>P dipolar couplings proved that this is mostly inorganic phosphate. While the large phosphate fraction is probably an artifact of the phosphate-rich growth conditions, the observation that the phosphate entrapped certain diatom biomolecules, possibly including polyamines, can provide insight into their location relative to the biosilica. In order to shed more light on these relations, we plan to measure the <sup>13</sup>C and <sup>31</sup>P NMR observables in the corresponding “normal” unlabeled diatoms for reference.

**Nanostructure of nacre.** The organic-inorganic composite of the nacre of the abalone shell, which consists of ~98 wt% calcium carbonate in the aragonite modification and ~2 wt% organic material, has a 3,000 times higher fracture resistance than pure aragonite. While a microlaminate “brick-and-mortar” structure, with ~500-nm thick single-crystalline aragonite “bricks” held together by organic “mortar”, has long been the accepted model of nacre, recently indications of organic matter within the “single-crystalline” platelets have been seen.<sup>7</sup> Nanograins ranging variously between 5 and 50 nm in thickness have been reported. Using <sup>13</sup>C{<sup>1</sup>H} long-range dipolar dephasing of carbonate signals, as successfully developed for carbonate in bone, we will look for organic-inorganic proximity in the nacre of green abalone.

### References

- 1 C. Jaeger, N. S. Groom, E. A. Bowe, A. Horner, M. E. Davies, R. C. Murray, and M. J. Duer, *Chem. Mat.* **17**, 3059 (2005); E. R. Wise, S. Maltsev, M. E. Davies, M. J. Duer, C. Jaeger, N. Loveridge, R. C. Murray, and D. G.

- Reid, *Chem. Mat.* **19**, 5055 (2007).
- <sup>2</sup> C. E. Hamm, R. Merkel, O. Springer, P. Jurkojc, C. Maier, K. Pechtel, V. Smetacek, *Nature* **421**, 841 (2003).
- <sup>3</sup> T. Fuhrmann, S. Landwehr, M. El Rharbi-Kucki, and M. Sumper, *Appl. Phys. B* **78**, 257 (2004).
- <sup>4</sup> S. C. Christiansen, N. Hedin, J. D. Epping, M. T. Janicke, Y. del Amo, M. Demarest, M. Brzezinski, and B. F. Chmelka, *Solid State NMR* **29**, 170 (2006).
- <sup>5</sup> M. Sumper and N. Kroeger, *J. Mater. Chem.* **14** (14), 2059 (2004).
- <sup>6</sup> B. Tesson, S. Masse, G. Laurent, J. Maquet, J. Livage, V. Martin-Jezequel, and T. Coradin, *Analyt. Bioanalyt. Chem.* **390**, 1889 (2008).
- <sup>7</sup> M. Rousseau, E. Lopez, P. Stempfle, M. Brendle, L. Franke, A. Guette, R. Naslain, and X. Bourrat, *Biomaterials* **26**, 6254 (2005); T. Sumitomo, H. Kakisawa, Y. Owaki, and Y. Kagawa, *Mater. Sci. Forum* **561-565**, 713 (2007).

### **Publications 2007-2009**

#### *Related to biomolecular systems:*

- K. Schmidt-Rohr, A. Rawal, X.-W. Fang, "A new NMR method for determining the particle thickness in nanocomposites, using  $T_{2,H}$ -selective  $X\{^1H\}$  recoupling", *J. Chem. Phys.* **126**, 054701-(1-16) (2007).
- K. Schmidt-Rohr, "Simulation of Small-Angle Scattering (SAXS or SANS) Curves by Numerical Fourier Transformation", *J. Appl. Cryst.* **40**, 16-25 (2007).
- D. Enlow, A. Rawal, M. Kanapathipillai, K. Schmidt-Rohr, S. Mallapragada, C.-T. Lo, P. Thiyagarajan, M. Akinc, "Synthesis and Characterization of Self-assembled Block Copolymer Templated Calcium Phosphate Nanocomposite Gels", *J. Mater. Chem.* **17**, 1570 – 1578 (2007).
- A. Rawal, X. Wei, M. Akinc, K. Schmidt-Rohr, "The Dispersion of Silicate in Tricalcium Phosphate Elucidated by Solid-State NMR", *Chem. Mat.* **20**, 2583-2591 (2008).
- M. Kanapathipillai, Y. Yusufoglu, A. Rawal, Y.-Y. Hu, C.-T. Lo, P. Thiyagarajan, Y.E. Kalay, M. Akinc, S. Mallapragada, K. Schmidt-Rohr, "Synthesis and characterization of ionic block copolymer templated calcium phosphate nanocomposites", *Chem. Mat.* **20**, 5922-5932 (2008).
- Y. Yusufoglu, Y.-Y. Hu, M. Kanapathipillai, M. Kramer, E. Kalay, P. Thiyagarajan, M. Akinc, K. Schmidt-Rohr, S. Mallapragada, "Bioinspired synthesis of self-assembled calcium phosphate nanocomposites using block copolymer-peptide conjugates", *J. Mater. Res.* **23**, 3196-3212 (2008).
- Y.-Y. Hu, K. Schmidt-Rohr, "Effects of L-spin Longitudinal Quadrupolar Relaxation in S{L} Heteronuclear Recoupling and S-spin Magic-Angle Spinning NMR", *J. Mag. Reson.* **197**, 193-207 (2009).
- Y.-Y. Hu, Y. Yusufoglu, M. Kanapathipillai, J. Yang, P. Thiyagarajan, T. Deming, M. Akinc, K. Schmidt-Rohr, S. Mallapragada, "Self-assembled calcium phosphate nanocomposites using block copolypeptide templates", *Soft Matter*, in press (2009).

#### *Other DOE-supported work:*

- E.M. Levin, S.L. Budko, J-D. Mao, Y. Huang, K. Schmidt-Rohr, "Effect of Magnetic Particles on NMR Spectra of Murchison Meteorite Organic Matter and Polymer-based Model Systems", *Solid State NMR* **31**, 63-71 (2007).
- Q. Chen, K. Schmidt-Rohr, "Backbone Dynamics of the Nafion Ionomer Studied by  $^{19}F$ - $^{13}C$  Solid-State NMR" *Macromol. Chem. Phys.* **208**, 2189-2203 (2007).
- K. Schmidt-Rohr, Q. Chen, "Parallel Cylindrical Water Nanochannels in Nafion Fuel Cell Membranes", *Nat. Mater.* **7**, 75-83 (2008).
- E. M. Levin, X. W. Fang, S.L. Budko, W. E. Straszheim, R. W. McCallum, K. Schmidt-Rohr, "The magnetization and  $^{13}C$  NMR spin-lattice relaxation of nanodiamonds", *Phys. Rev. B* **77**, 054418 (2008).
- X. Kong, K. Wadhwa, J. G. Verkade, K. Schmidt-Rohr, "Determination of the Structure of a Novel Anion Exchange Fuel Cell Membrane by Solid-State Nuclear Magnetic Resonance Spectroscopy", *Macromolecules* **42**, 1659-1664 (2009).
- Y.Y. Hu, E. L. Levin, K. Schmidt-Rohr, "Broadband "Infinite-Speed" Magic-Angle Spinning NMR Spectroscopy", *J. Am. Chem. Soc.* **131**, 8390 (2009).
- C. M. Jaworski, J. Tobola, E. M. Levin, K. Schmidt-Rohr, J. P. Heremans, "Antimony: an Amphoteric Dopant in Lead Telluride" *Phys. Rev. B*, in press (2009).
- E. M. Levin, B. A. Cook, M. G. Kanatzidis, K. Schmidt-Rohr, "Electronic Inhomogeneity and Ag:Sb Ratio in  $Ag_{1-x}Pb_{18}Sb_{1+y}Te_{20}$  High-Performance Thermoelectrics Elucidated by  $^{125}Te$  and  $^{207}Pb$  NMR" *Phys. Rev. B*, (2009).

## Molecularly Engineered Biomimetic Nanoassemblies

Andrew P. Shreve ([shreve@lanl.gov](mailto:shreve@lanl.gov)), Hsing-Lin Wang ([hwang@lanl.gov](mailto:hwang@lanl.gov)), Jennifer Martinez ([jenm@lanl.gov](mailto:jenm@lanl.gov)), Srinivas Iyer ([siyer@lanl.gov](mailto:siyer@lanl.gov)), Reginaldo Rocha ([rcrocha@lanl.gov](mailto:rcrocha@lanl.gov)),  
Los Alamos National Laboratory;  
James Brozik ([brozik@wsu.edu](mailto:brozik@wsu.edu)), Washington State University;  
Darryl Sasaki ([dysasak@sandia.gov](mailto:dysasak@sandia.gov)), Sandia National Laboratories;  
Atul N. Parikh ([anparikh@ucdavis.edu](mailto:anparikh@ucdavis.edu)), University of California, Davis;  
Sunil K. Sinha ([ssinha@physics.ucsd.edu](mailto:ssinha@physics.ucsd.edu)), University of California, San Diego.

### Program Scope

The program aims to develop self-assembly and biologically-assisted assembly methods for the control of functional responses in complex, multi-component materials. Relevant functions being explored are related to the control of energy flow and transduction, and include photophysical properties, charge-transfer processes, and manipulation of bioenergetic responses including those mediated by molecular recognition events. Focus on these functions and on use of a few active components, selected to represent several different classes of important nanomaterials, is intended to also provide improved general understanding of structure and performance of the assembly types under study. The approaches used include a combination of materials synthesis and fabrication, static and time-resolved spectroscopies, optical and scanning probe microscopies, structural characterization, and modeling and analysis. Our research team includes personnel with expertise in chemical and materials synthesis, self-assembly, electrochemistry, spectroscopy, molecular biology and biochemistry, and structural characterization.

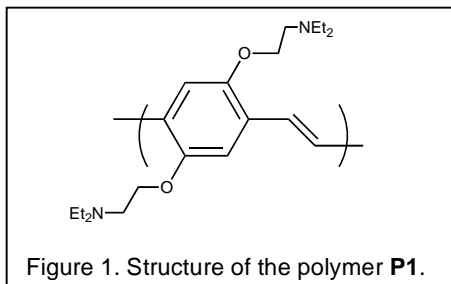
### Recent Progress

Our recent work has been largely targeted at: (i) the development of complex materials and assemblies that mediate the efficiency and performance of photophysical processes, and (ii) the development and characterization of model biological and biologically-inspired membrane-based systems that can be integrated with functional material components. An overall theme is the use of biologically-inspired assembly strategies, with examples including phospholipid membrane architectures and polyelectrolyte assemblies, and we apply a coordinated synthesis, characterization and modeling approach to explore the interplay of structure, dynamics and function in the materials.

*Tunable photophysical properties in assemblies.* A hallmark of biological systems is their ability to adapt and respond to changes in external environment or in a manner triggered by molecular recognition. In many cases, these responses arise from subtle changes that control the structure of multi-component assemblies. We are attempting to replicate some of these types of responses in synthetic material assemblies, particularly those that can be used for photophysical or photochemical processes.

A class of materials of recent interest is water-soluble conjugated polymers, where the water solubility is imparted by introducing a side chain on the conjugated backbone that is either charged or that can be charged in a tunable manner. For example, we have developed a PPV polymer derivatized with quaternary amine side chains (poly[2,5]-bis[3-(N,N,N-triethylammonium bromide)-1-oxapropyl]-1,4-phenylenevinylene), denoted as **P2**. This polymer demonstrates striking control of photophysical responses upon complexation and co-assembly with surfactants, phospholipids and biological polymers. These responses most likely reflect changes

in conformation induced by interactions of the polymer with its co-assembly components. For example, we have observed that forming nanocomposites of **P2** with liposomes of mixtures of 1,2-dipalmitoyl-phosphatidylcholine (DPCC) and 1,2-dipalmitoylphosphatidic acid (DPPA), in which interactions are mediated by electrostatic interactions, produce an enhancement of polymer fluorescence by 70%. Likewise, interaction with ss- or ds-DNA can result in over 400% increase in polymer fluorescence, and the luminescence can also be strongly mediated by surfactant interactions. Tunable responses can also be derived from changes in polymer-polymer interactions and polymer aggregate structures. As an example, the tertiary amine variant, **P1** (poly[2,5]-bis[3-(N,N-diethylamine)-1-oxapropyl]-1,4-phenylenevinylene), a precursor of **P2**, shows strong thermochromism in absorption and emission properties in solvents such as toluene. These responses can be understood as reflecting temperature-dependent variation in the structure and sizes of polymer aggregates.



Interest in photophysical behavior of conjugated polymers is driven in part by sensing applications, where environmental control of luminescence properties is a key element to improve performance. However, polymer incorporation into composite materials with photo-induced charge separation properties is also an important topic with energy relevance. To that end, we have synthesized water-soluble, negatively charged fullerene derivatives which can be co-assembled with charged conjugated polymers. The resulting composite assemblies, which in some cases can be produced as dispersible colloids, demonstrate near unit efficiency of charge-transfer quenching of polymer luminescence. We have also found that composite fullerene/conjugated polyelectrolyte assemblies can self assemble on surfaces in ordered structures over large areas. We have also used polyethylene-glycol based amphiphiles to solubilize and functionalize fullerenes, and have shown that this strategy can solubilize fullerenes into distinct assemblies with controllable aggregate size and surface chemistry. Likewise, fullerenes have been controllably solubilized using peptide amphiphiles having a specific molecular recognition head group. These strategies are anticipated to lead to means of integrating polymers and fullerenes into membrane assemblies or related structures.

Another class of biologically-inspired or templated materials with tunable photophysical behavior is noble element nanoclusters. These clusters consist of small numbers of metal atoms and exhibit strong size-dependent luminescence. Our team has synthesized gold and silver nanoclusters at physiological temperature using poly(amidoamine) dendrimers, conjugated polymers, small molecules, DNA and peptides as templates, and have used characterization methods such as fluorescence correlation spectroscopy to explore how the template size and chemical properties dictate the final complex size and performance. Because the cluster is produced in conjunction with the template, the incorporation of the clusters into complex assemblies can be developed using strategies such as electrostatic targeting, direct templating (as in conjugated polymer templates), or molecular recognition of DNA or peptides. These strategies to produce assemblies with higher-order control of cluster interactions are currently being explored.

*Model membrane assemblies.* In nature, phospholipid membranes can facilitate and mediate the assembly of functional multi-protein complexes. Inspired by many such examples, we are interested in the use of model membrane systems as synthetic materials, and to that end, are exploring fundamental aspects of model membrane structure and dynamics, the interaction of membranes with synthetic materials, and strategies for the stabilization of membranes. As noted

above, we have observed significant changes in functional behavior of nanomaterials upon interaction with phospholipid assemblies, and have been exploring strategies for the controlled delivery of components to membrane systems. In addition, we have studied some fundamental aspects of model membrane behavior. For example, we used a combination of chemically patterned surface geometries, self-assembly of substrate-supported lipid membranes, and optical microscopy to demonstrate that interaction of the lipid membrane with a charged silica substrate leads to a predictable, salt-concentration-dependent, redistribution of charged components in the membrane between the two leaflets of the bilayer. Being able to understand such redistribution processes of membrane components is an important aspect of reliably using membranes as a means of assembling materials. We have also explored the stabilization of substrate-supported membranes by the use of trehalose, which provides substantial protection against the effects of dehydration. Introducing such protection and improving the overall tolerance against environmental challenges also provides an important element needed for applying membrane assemblies in materials applications. We have also explored the assembly and function of membrane architectures on nanoporous substrates, both planar surfaces and spherical beads. In these cases, additional fluorescence reporting strategies can be incorporated directly into the substrate, thereby allowing, for example, optical reporting of protein- or peptide-mediated transmembrane ion transport. Further development of these and related strategies to provide sensitive probes of energy or signal transduction processes is envisioned.

### **Future Plans**

Our future work will build upon results to date that explore the development of optically and electronically active complex, multi-component assemblies. We aim for improvement in general understanding of assembly methods, particularly methods that can be extended to the generation of larger-scale assemblies. As active components, we will use representative members of different classes of nanomaterials that target functions involving control of charge and energy flow. Examples include carbon-based materials, conjugated polymers, metallic nanoclusters, and proteins. Characterization of assemblies and their functions using spectroscopic, scanning probe, electrochemical, imaging, and scattering methods will provide for improved understanding of how multi-scale and multi-component functional assemblies can be produced using the tools of self-assembly and biologically-assisted assembly.

### **Publications (2007-2009)**

Y. Gao, L. Wang, C.C. Wang and H.-L. Wang, "Conjugated polyelectrolytes with pH-dependent conformations and optical properties," *Langmuir* **23** (2007) 7760.

A.P. Shreve, E.H. Haroz, S.M. Bachilo, R.B. Weisman, S. Tretiak, S. Kilina, and S.K. Doorn, "Determination of exciton-phonon coupling elements in single-walled carbon nanotubes by Raman overtone analysis," *Phys. Rev. Lett.* **98** (2007) 037405.

Y. Bao, C. Zhong, D.M. Vu, J.P. Temirov, R.B. Dyer and J.S. Martinez, "Nanoparticle free synthesis of fluorescent gold nanoclusters at physiological temperature," *J. Phys. Chem. C* **111** (2007) 12194.

C. Zhong, Y. Bao, D.M. Vu, R.B. Dyer and J.S. Martinez, "Fabrication of fluorescent cellular probes: Hybrid dendrimer/gold nanoclusters," *Mater. Res. Soc. Symp. Proc.* **1007** (2007) 1007-S15-07

T.-H. Yang, C.K. Yee, M.L. Amweg, S. Singh, E.L. Kendall, A.M. Dattelbaum, A.P. Shreve, C.J. Brinker and A.N. Parikh, "Optical detection of ion-channel induced proton transport in supported phospholipid bilayers," *Nano Letters* **7** (2007) 2446.

Z. Tang, M.S. Johal, P. Scudder, N. Caculitan, R.J. Magyar, S. Tretiak and H.-L. Wang, "Study of the non-covalent interactions in Langmuir-Blodgett films: An interplay between  $\pi$ - $\pi$  and dipole-dipole interactions," *Thin Solid Films* **516** (2007) 58.

M.J. O'Connell, C.K. Chan, W. Li, R.K. Hicks, S.K. Doorn and H.-L. Wang, "Polyelectrolyte platform for sensitive detection of biological analytes via reversible fluorescence quenching," *Polymer* **48** (2007) 7582.

H.-L. Wang, W. Li., Q.X. Jia and E. Akhadov, "Tailoring conducting polymer chemistry for the chemical deposition of metal particles and clusters," *Chem. Mater.* **19** (2007) 520.

R.W. Davis, A. Flores, T.A. Barrick, J.M. Cox, S.M. Brozik, G.P. Lopez and J.A. Brozik, "Nanoporous microbead supported bilayers: Stability, physical characterization, and incorporation of functional transmembrane proteins," *Langmuir* **23** (2007) 3864.

A.E. Oliver, E.L. Kendall, M.C. Howland, B. Sani, A.P. Shreve and A.N. Parikh, "Protecting, patterning, and scaffolding supported lipid membranes using carbohydrate glasses," *Lab Chip* **8** (2008) 892.

P.L. Gourley, D.Y. Sasaki and R.K. Naviaux, "Nanolaser spectroscopy for studying novel biomaterials," (invited) *Proc. SPIE* **6859** (2008) 685914-1.

J.S. Treger, V.Y. Ma, Y. Gao, C.-C. Wang, H.-L. Wang and M.S. Johal, "Tuning the optical properties of a water-soluble cationic poly(p-phenylenevinylene): Surfactant complexation with a conjugated polyelectrolyte," *J. Phys. Chem. B* **112** (2008) 760.

A.N. Parikh, "Membrane-surface interface: Phospholipid assembly at chemically and topographically structured surfaces," *Biointerphases* **3** (2008) FA22.

J.S. Treger, V.Y. Ma, Y. Gao, C.-C. Wang, S. Jeon, J.M. Robinson, H.-L. Wang and M.S. Johal, "Controlling layer thickness and photostability of water-soluble cationic poly(p-phenylenevinylene) in multilayer thin films by surfactant complexation," *Langmuir* **24** (2008) 13127.

A.M. Dattelbaum, G.A. Montaño, A. Roco, A.P. Shreve, S. Iyer, "Myelin-mimetic lipid multilayers," *Proc. Nanotech* **2** (2008) Chapter 6, 480.

Y. Gao, C.-A. Chen, H.-M. Gau, J.A. Bailey, E. Akhadov, D. Williams and H.-L. Wang, "Facile synthesis of polyaniline-supported Pd nanoparticles and their catalytic properties toward selective hydrogenation of alkynes and cinnamaldehyde," *Chem. Mater.* **20** (2008) 2839.

A.P. Shreve, M.C. Howland, A.R. Sapuri-Butti, T.W. Allen and A.N. Parikh, "Evidence for leaflet-dependent redistribution of charged molecules in fluid supported phospholipid bilayers," *Langmuir* **24** (2008) 13250.

P.A. Chiarelli, D.-G. Liu, E.B. Watkins, F.R. Trouw, J. Majewski, J.L. Casson, Z. Tang, M.S. Johal, J.M. Robinson and H.-L. Wang, "Molecular order in Langmuir-Blodgett assembled films of an azobenzene amphiphile," *Thin Solid Films* **517** (2009) 4638.

H.-H. Shih, D. Williams, N.H. Mack and H.-L. Wang, "Conducting polymer-based electrodeless deposition of Pt nanoparticles and its catalytic properties for regioselective hydrosilylation reactions," *Macromolecules* **42** (2009) 14.

## Design Principles for Self-Assembly of Monomers into Tubules

Mark J. Stevens

Sandia National Laboratories  
Albuquerque, NM 87185  
msteve@sandia.gov

**Program Scope:** The work described here is a subtask on a large program entitled “Active Assembly of Dynamic and Adaptable Materials.” The goal of the overall program is to explore the extent to which energy-consuming proteins such as fiber-forming tubulin and motor proteins can be used for the active transport, assembly and reconfiguration of nanomaterials in artificial environments. Recently, a new activity was started in the program, which is entitled “Artificial Microtubules.” The goal of this task involves learning how to create artificial nanoscale ‘monomers’ that can be polymerized into objects such as tubular fibers via processes that mimic the dynamic instability phenomena observed in natural microtubules. This submission represents the theory and modeling component of the “Artificial Microtubules” effort. Here, our objective is to use molecular dynamics simulations to establish the design rules for polymeric nanoparticles, dendrimers and artificial peptides that are being prepared in the experimental component of the program.

**Recent Progress:** Biological materials often have a hierarchical structure which enables complex functionality. Some biopolymers such as microtubules and actin have monomers which are proteins. Having the monomer be a macromolecule enables a rich variety of features to be incorporated into the basic building block and a richer set of properties in the material. The complex behavior of subcellular systems arises in part because of the rich feature set of the basic natural components. In development of materials that mimic aspects of natural systems, we will need to develop basic building blocks that have a range of features. Even at the most basic feature set, just the assembly of particular geometric structures requires many elements.

From the perspective of materials science, proteins are nanoparticles. The complex surface chemistry of proteins distinguishes them from the nanoparticles that are presently synthesized. Proteins have nonuniform surfaces with a range of functional groups. Most functionalizations of nanoparticles are uniform coatings of a single molecule. Development of more complex functionalization is beginning (e.g. janus nanoparticles) and is a part of the experimental work in this program. From the modeling

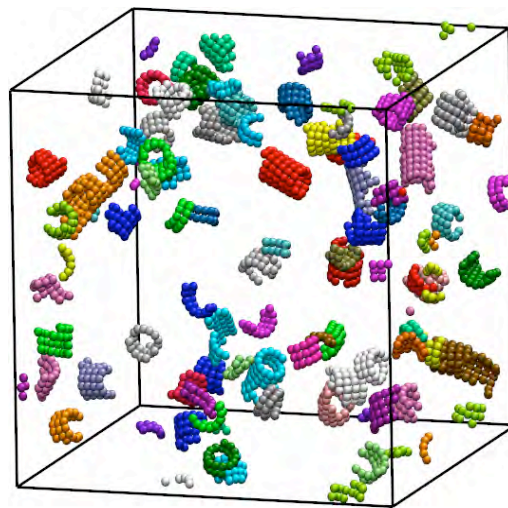


*Fig. 1 Fragments and full tubules formed in simulation of self-assembly process.*

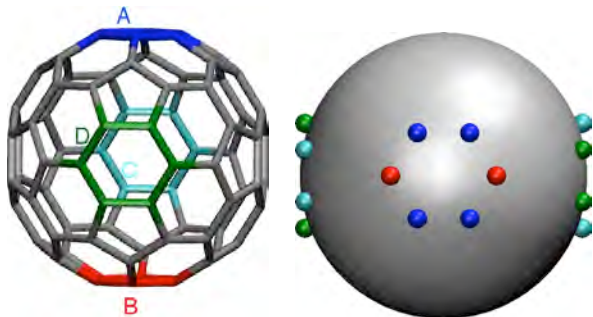


**Fig. 2.** Two models showing the attractive interactions sites (nongray). On the left (model I) the interaction sites for a representation of a spherical particle using C80 to define the locations. On the right is a revised version (model II). The A:B and C:D interactions are attractive. All other interactions are repulsive.

Recently, van Workum and Douglas have used Monte Carlo simulations to show that quadrupole potentials can self-assemble into sheets and in some cases tubules. We have produced similar results using molecular dynamics (MD) simulations and have further investigated the effects of nonspherical monomers on the self-assembly. We expect electrostatic interactions play an important role in assembly. Here, we will focus on results from the second model types, which treat the monomer as a nanoparticle with multiple interaction sites on the surface that define the binding between monomers. Figure 2 shows two model monomers. The basic idea is that two sets of sites on opposite surfaces will have attractive interactions and are the only attractive interactions. The attraction between A and B sites will produce the assembly of a linear chain of particles for sufficiently strong A:B interactions. Similarly attractive C:D interactions should form linear chains and the combination of all four should produce sheets.

Using model I, our simulations have already revealed an important requirement in the monomer design. The structures that form from model I do not form sheets as expected (see Fig. 3). This is because of the high degree of symmetry in the faces. For example, two particles can come together at complementary A and B faces, with 6 different orientations due to the hexagonal faces. Consequently the C-D axis is correspondingly oriented in 6 different directions. The clusters that form are a random collection of chains of particles that bond together with multiple orientations.

In order to limit the rotational symmetry, we altered the model as shown in Fig. 2 for model II. The geometry is set up such that rotation of the particles yield misalignment of the complementary matched sites and thus are not the low energy structures. With this model, simulations do yield sheets as can be seen in Figure 3. This figure shows multiple sheets that form in an MD simulation of model II particles. This is an important lesson in designing the interaction sites on a macromolecule that will self-assemble into well defined structures. The symmetry of the interacting local surfaces is very important. High symmetry allows multiple orientations for pairs of binding particles, which leads to a more random large scale structure.

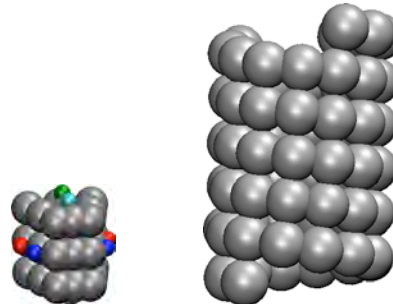
perspective we are working to understand the fewest and most fundamental features of the monomers that will yield the geometry and dynamic properties of interest. The initial focus of the modeling effort is determining design principles for assembly of tubular structures from monomers.

We are applying two types of models in this effort. One set of models is to use very simple potentials in a single particle to form sheets and tubes. Tubulin is known to be charged and have significant dipole moments. In general, it is known that dipole potentials will yield linear polymers.



**Fig. 3.** On the left is a large, random cluster that forms using the model I, and on the right is a set of sheets that form using model II.

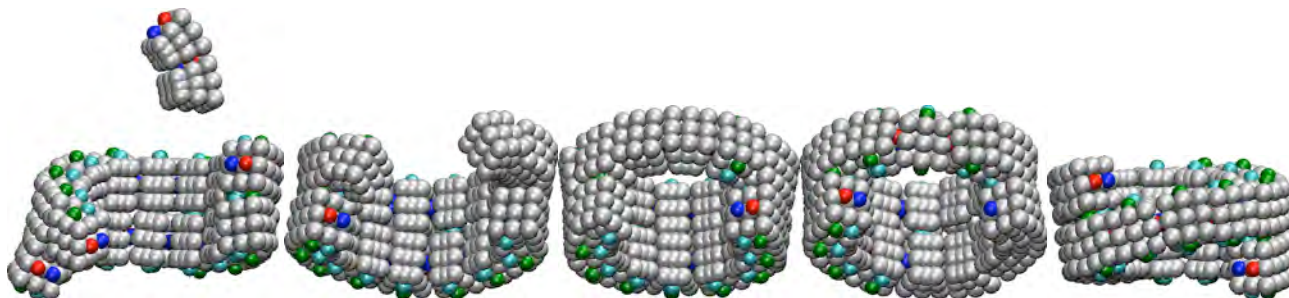
The local binding regions need to have low symmetry in order to drive specific geometry in the large scale self-assembly.



**Fig. 4.** Image of the wedge monomer with interaction sites and of a self-assembled helical tubule (each sphere represents a wedge).

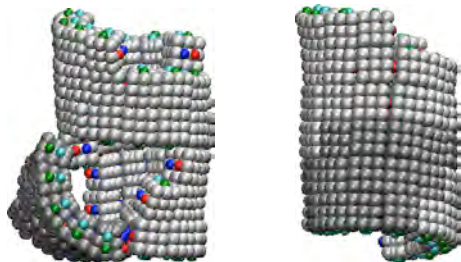
To form tubular structures, we have used a monomer with a wedge shape. Fig. 4 shows the geometry of the wedge monomers that are designed to form tubules with the red/blue interaction sites binding monomers to form rings of 13 monomers and the cyan/green sites binding monomers along the longitudinal axis. This design includes the low symmetry in the interaction sites that we discovered to be necessary from the above work. With this monomer we can readily form tubular structures. Surprisingly, the structures tend to be helical, which is not the structure designed to have the minimal energy (Fig. 4). However, calculations of the energy for helical and nonhelical tubules show that the energies are the same within thermal fluctuations. In addition, examination of the structures show helical structures have close contact between the interaction sites. We have examined the dynamics of the self-assembly for more than one helical structure. There is more than one pathway to forming the helical structure. Next we highlight an interesting example.

Figure 5 shows the sequence of structural events that ultimately lead to the formation of a helical structure. The assembly of monomers into a partial surface is quite common. For the interaction strengths used, there is considerable flexibility in these partial structures. This flexibility plays a role in the assembly process. The addition of a dimer allows the completion of



**Fig 5.** Sequence of structural transformations from forming a full ring to transforming to a helical structure. From left to right, the times are 52, 53, 54, 73, and 74 in units of 100,000 time steps.

a ring. This ring is planar as expected for the model. However thermal fluctuations destabilize this ring and a helical structure forms. This transformation shows that bonds between wedge monomers can break and reform. Other instances of bond reformation have been observed. The helical structure is stable and grows to more turns in subsequent dynamics.



**Fig. 6.** Well defined large, helical tubule (right) formed by merger of two clusters (left). The small cluster is denoted by dark gray spheres.

Even though we are at the early stages of the simulation work, well defined tubular structures have formed. Figure 6 shows a tubular structure that formed from the merged of two large clusters. The tubule has 5 full helical turns with 12 monomers per turn.

In summary, our simulations have revealed the importance of low symmetry in the self-assembly process. Our simulations yield helical structures prevalently even though monomer design is biased toward nonhelical

structure. Moreover, the simulations show that the formation dynamics is complex and that helical structures can form *after* nonhelical ring was first created.

## **Future Plans:**

In the short term, we will continue along the lines described above and obtaining a statistical picture of the self-assembly. We have found a set of interaction parameters that work well in producing self-assembly, but further investigation of the interaction strengths needs to be done, in order to study the relative importance of longitudinal vs. latitudinal growth, for example. In addition, we expect that combining the simple electrostatic models with the nanoparticle models will be an essential part of controlling self-assembly. We want to incorporate dynamical aspects of the assembly such as the polymerization-depolymerization of microtubules. In the natural system, a key part of this is the binding of small molecules (GTP in the case of tubulin). In terms of modeling, we need to incorporate the energetic effects of GTP into the dynamics. The main effect presently hypothesized is a conformational change in the tubulin dimers depending on whether GTP or GDP is bound. In the model system, the interface between two monomers will have to be flexible and depend on the energy state. The change in energy will be an event driven dynamics that alters the surface structure through changes in the spring constants, for example.

## **Publications 2007-2009:**

This task just started in August and thus there are no publications to date. For a list of publications from the other tasks in this program see the submission by Eric Spoerke and Bruce Bunker.

***UNIVERSITY GRANT  
PROJECTS***

# “Organic Heterojunction Devices: Structure, Composition, and Performance at Length Scales < 20 nm”

Harald W. Ade

Department of Physics  
North Carolina State University  
Raleigh, NC 27695  
harald\_ade@ncsu.edu

## Program scope:

The primary focus of this program is the use of special soft x-ray characterization tools to investigate and understand organic devices. This includes both organic light emitting diodes and organic photovoltaics. The methods utilized include scanning transmission x-ray microscopy, resonant scattering and resonant reflectivity. In call case, the rapid changes of the soft x-ray optical properties of organic matter near the carbon absorption edge are used to provide “bond” selective contrast. A secondary objective is the use of these *high and selective contrast* tools to explore their use for *biomaterials*.

## General background on NEXAFS microscopy and resonant scattering:

The combination of Near Edge X-ray Absorption Fine Structure (NEXAFS) spectroscopy with Scanning Transmission X-ray microscopy (STXM) provides high chemical and orientational sensitivity at a spatial resolution of ~35 nm. This unique combination, coupled will low radiation damage and the ability to investigate completely hydrated samples, facilitates the use of NEXAFS microscopy for a wide range of organic materials. However, NEXAFS microscopy is unable to characterize dilute systems and materials which have structures below the present resolution limit. Resonant Soft X-ray scattering (RSoXS) and Resonant Soft X-ray Reflectivity (RSoXR) are techniques that have contrast similar to NEXAFS microscopy, but that can provide information corresponding to much higher spatial resolution (albeit only for ensemble averages) and for low concentrations. RSoXS/RSoXR provides much higher scattering intensities than conventional hard x-ray scattering and improved compositional sensitivity (i.e. materials contrast) akin to deuteration in neutron scattering, albeit without the need to chemically modify the samples. Consequently, many present neutron or x-ray scattering studies of *biomaterials* might benefit from use of RSoXS/RSoXS.

## Recent progress:

RSoXS and NEXAFS microscopy was used to investigate the influence of annealing on intimately mixed blends of the conjugated polymers poly(9,9'-dioctylfluorene-co-bis-N,N'-(4-butylphenyl)-bis-N,N'-phenyl-1,4-phenylene-diamine) (PFB) and poly(9,9'-dioctylfluorene-co-benzothiadiazole) (F8BT). These blends are model systems for all-polymer solar cell devices. These PFB:F8BT devices are so-called bulk-heterojunctions in which the ideal morphology is an interpenetrating network with lateral structures of ~10 nm in size throughout a ~150-200 nm thick film. In addition, bilayer films of these two polymeric materials were characterized using RSoXR to investigate the influence of annealing upon the interfacial structure and device performance.

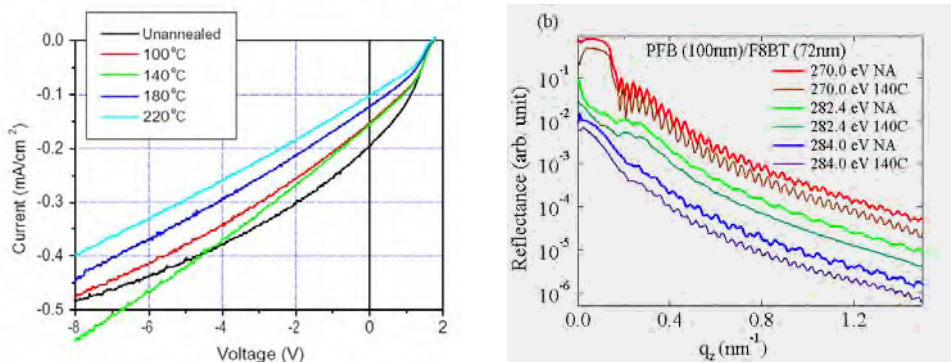
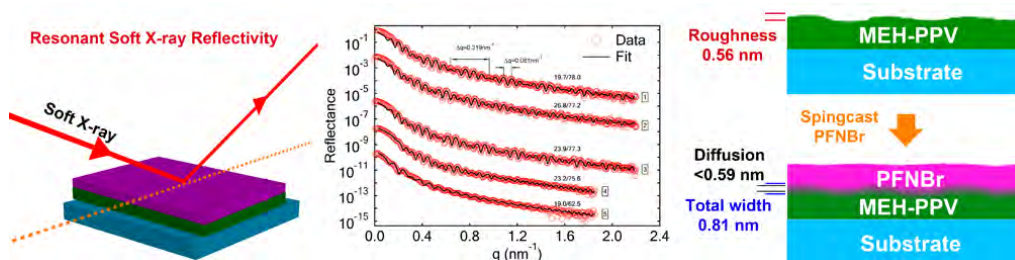


Figure 1. (a) Dark current subtracted I-V curves for PFB:F8BT bilayers (as cast and annealed at for 10 min at the temperature indicated) (Figure courtesy of McNeill, Cambrigid). (b) RSoXR for PFB/F8BT bilayer, as cast (NA) and annealed for 10 min at 140 °C at the photon energies indicated.

As seen from Fig. 1, the unannealed PFB:F8BT bilayer device performs best at short-circuit ( $V = 0V$ ), with device performance deteriorating at higher annealing temperatures. However at  $-6V$ , the  $140^{\circ}C$  device actually “performs better”. The voltage dependence of photocurrent, particularly the more curved shape of the unannealed device provides some interesting insight into the process of charge separation. The charge separation is easiest in the unannealed device, which has the sharpest interface. Monte-Carlo modeling of charge separation at the interface shows that having a diffuse interface makes charge separation more problematic. RSoXR (Fig. 1b) clearly shows that annealing is increasing the interfacial width (presumably due to roughening); quantitative fitting of the reflectance of the unannealed and  $140^{\circ}C$  annealed sample yield an interfacial width of  $\sim 0.6$  nm,  $2.0$  nm, respectively. For the case of the  $140^{\circ}C$  device at  $-6V$ , it seems that having a rougher interface can increase device performance (presumably through an increase interfacial area that provides exciton dissociation) but charge separation is harder (which is why it requires  $-6V$  to improve device collection yield over an unannealed device). We will shortly be performing photoluminescence measurements to provide more insight into how much exciton dissociation is enhanced.

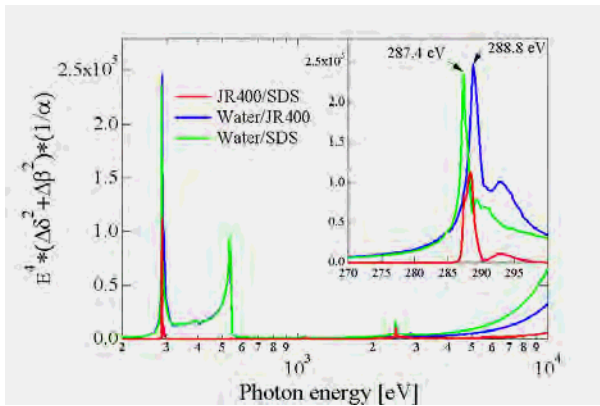


Similarly, the interfaces of conjugated polyelectrolyte (CPE)/poly[2-methoxy-5-(2'-ethylhexyloxy)-p-phenylene vinylene] (MEH-PPV) bilayers cast from differential solvents have been shown by RSoXR to be very smooth and sharp. The chemical interdiffusion due to casting is limited to less than  $0.6$  nm and the interface created is thus nearly “molecularly” sharp. These results demonstrate for the first time and with high precision that the non-polar MEH-PPV layer is not much disturbed by casting the CPE layer from a polar solvent. A baseline is established for understanding the role of interfacial structure in determining the performance of CPE-based polymer light emitting

diodes. Comparison to device performance in as-cast and annealed devices shows that the best devices are those with the sharpest interfaces.

**Other recent activities include:**

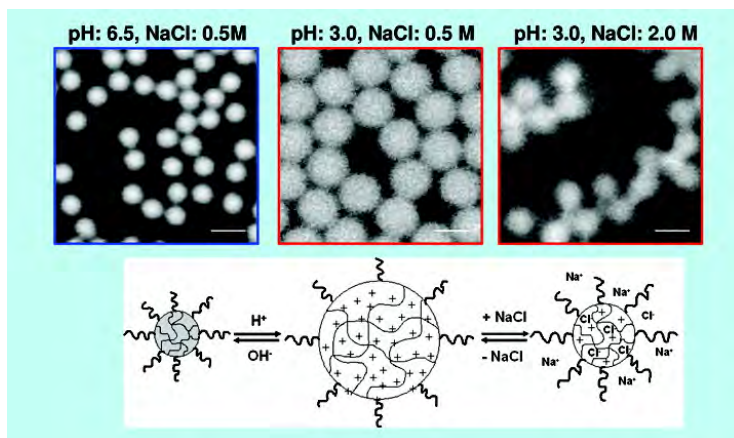
*Resonant scattering from dilute colloids (partially supported by Dow Chemical):* RSoXS should also be useful for the investigation of colloids. Figure 3 shows the calculated relative scattering for the cationic polymer hydroxyethylcellulose (JR400), the anionic surfactant sodium dodecyl sulphate (SDS) in water from 200 eV to 10,000 eV for the optimum sample thickness. Scattering in the soft X-ray region exceeds scattering at 10 keV by ~5x, thus leading to good sensitivity at photon energies near 288 eV and oxygen edge.



Investigations of very dilute solutions will be possible. Furthermore, selection of specific energies near the carbon edge or oxygen edge should allow strong differential and selective contrast to emphasize scattering from either the JR400 or from the SDS. Similar ability to selectively scatter from specific chemical constituents should be possible for many *biomaterials*.

Figure 3: Calculated relative scattering intensity for JR400/SDS, water/JR400 and water/SDS.

*In-situ NEXAFS microscopy of salt-screening in microgels:* Lightly cross-linked sterically stabilized poly(2-vinylpyridine) latexes exhibit pH-responsive behavior, undergoing a latex-to-microgel transition below pH 4.1 as a result of protonation of the pyridine pendent groups. We have examined both the latex and microgel states of such particles directly in aqueous solution using NEXAFS microscopy. Spectroscopic studies of individual particles confirm that the nitrogen atoms of the microgel particles are fully protonated at low pH. The addition of salt causes partial deswelling of these microgel particles, but spectroscopic analysis confirms the retention of their cationic character.



This is the first direct visualization of the effect of electrolyte screening on microgel dimensions in aqueous solution. In each case, the observed particle dimensions are consistent with dynamic light scattering characterization, especially when polydispersity effects are taken into consideration.

### Future plans:

Results of PFB/F8BT bilayer measurements point to an interesting strategy to disentangle the contributions of chemical interdiffusion and physical roughness in these devices. At a specific photon energy below the carbon edge (282.4 eV for PFB), the top layer has an index of reflection close to vacuum and reflects almost no x-rays. At the same time, total internal reflection at the PFB/F8BT polymer/polymer interface can be achieved. This will allow to study the in-plane structure of the buried polymer/polymer interface with diffuse scattering, yielding much improved structural information that can then be used to understand device performance in much greater detail.

Even more interesting is the prospect of combining the compositional sensitivity of resonant methods with photon correlation spectroscopy. This might open up the possibility to investigate fluctuations and dynamics in colloids and lipid rafts to be probed with micro-second time resolution if the newest synchrotron radiation facilities are used.

### List of publications (2008-2009 and selected earlier publications):<sup>1-13</sup>

1. C. Wang, T. Araki, and H. Ade, "Soft X-ray Resonant Reflectivity of low Z Material Thin Films", *Appl. Phys. Lett.* **87**, 214109 (2005).
2. S. Fujii, S. P. Armes, T. Araki, and H. Ade, "Direct Imaging and Spectroscopic Characterization of Stimulus-Responsive Microgels", *J. Am. Chem. Soc.* **127**, 16808 (2005).
3. T. Araki, H. Ade, J. M. Stubbs, D. C. Sundberg, G. Mitchell, K. J. and A. L. D. Kilcoyne, "Soft X-ray Resonant Scattering of Structured Polymer Nanoparticles", *Appl. Phys. Lett.* **89**, 124106 (2006).
4. C. R. McNeill, B. Watts, L. Thomsen, H. Ade, N. C. Greenham, and P. C. Dastoor, "X-ray Microscopy of Photovoltaic Polyfluorene Blends: Relating the Nanomorphology to Device Performance", *Macromolecules* **40**, 3263 (2007).
5. C. R. McNeill, B. Watts, L. Thomsen, W. Belcher, S. Swaraj, H. Ade, and P. C. Dastoor, "Evolution of the nanomorphology of photovoltaic polyfluorene blends: Sub-100 nm resolution with X-ray spectromicroscopy", *Nanotechnology* **19**, 424015 (2008).
6. H. Ade and A. P. Hitchcock, "NEXAFS microscopy, resonant scattering and resonant reflectivity: composition and orientation probed in real and reciprocal space", *Polymer* **49**, 643 (2008).
7. C. R. McNeill, B. Watts, L. Thomsen, W. J. Belcher, N. C. Greenham, P. C. Dastoor, and H. Ade, "Evolution of Laterally Phase-Separated Polyfluorene Blend Morphology Studied by X-ray Spectromicroscopy", *Macromolecules* **42**, 3347 (2009).
8. S. Swaraj, C. Wang, T. Araki, G. Mitchell, L. Liu, S. Gaynor, B. Deshmukh, H. Yan, C. R. McNeill, and H. Ade, "Extension of the utility of resonant soft x-ray scattering and reflectivity for nanoscale characterization of polymers", *Eur. Phys. J. Special Topics* **168**, 121 (2009).
9. K. B. Burke, W. J. Belcher, L. Thomsen, B. Watts, C. R. McNeill, H. Ade, and P. C. Dastoor, "Role of Solvent Trapping Effects in Determining the Structure and Morphology of Ternary Blend Organic Devices", *Macromolecules* **42**, 3098 (2009).
10. H. Ade and H. Stoll, "Near-edge X-ray absorption fine-structure microscopy of organic and magnetic materials", *Nature Materials* **8**, 281 (2009).
11. H. Ade, B. Watts, S. Swaraj, C. McNeill, L. Thomsen, W. Belcher, and P. C. Dastoor, "NEXAFS microscopy of polymeric materials: Successes and challenges encountered when characterizing organic devices", *Journal of Physics: Conference Series (IOP)*, (in press) (2009).
12. H. Ade, C. Wang, A. Hexemer, A. Garcia, T.-Q. Nguyen, G. C. Bazan, K. E. Sohn, and E. J. Kramer, "Characterization of multicomponent polymer trilayers with resonant soft x-ray reflectivity", *J. Polym. Sci., Part B: Polym. Phys.* **47**, 1291 (2009).
13. S. Fujii, D. Dupin, T. Araki, S. P. Armes, and H. Ade, "First Direct Imaging of Electrolyte-Induced Deswelling Behavior of pH-Responsive Microgels in Aqueous Media Using Scanning Transmission X-ray Microscopy", *Langmuir* **25**, 2588 (2009).

# Nanoscale organic hybrid materials (NOHMs)

Lynden A. Archer

School of Chemical & Biomolecular Engineering, Cornell University  
Ithaca, New York 14853-5201  
laa25@cornell.edu

**Program Scope:** The goals of this project are: (i) to design and synthesize tethered lubricant coatings comprised of an ordered self assembled monolayer (SAM) chemically tethered to a substrate, and an outer, *canopy* layer tethered to the SAM, and (ii) to characterize the interfacial friction properties of these coatings using a combination, micro- and macroscopic tribology measurement techniques, and theory. Our overall goal is to fundamentally understand the effect of the canopy layer structure, architecture, and dynamics on interfacial friction properties.

**Recent Progress:** Lubricants with dielectric properties that match those of the components they lubricate, and which possess large mechanical moduli and good thermal conductivity have long been known to be beneficial for high-performance machinery and aircraft. These requirements are currently met by dispersing conducting particles, typically  $\text{SiO}_2$ ,  $\text{TiO}_2$ ,  $\text{Al}_2\text{O}_3$ ,  $\text{Fe}_3\text{O}_4$ , Ag, Cu or graphite, in conventional organic lubricating oils and greases. There is an extensive literature showing that nanometer sized particles are preferred in these applications, but aggregation between the high surface-area particles remains an insurmountable challenge. In a continuum particle-fluid mixture, achieving good dispersion of the particle phase is a requirement for obtaining good lubrication properties.

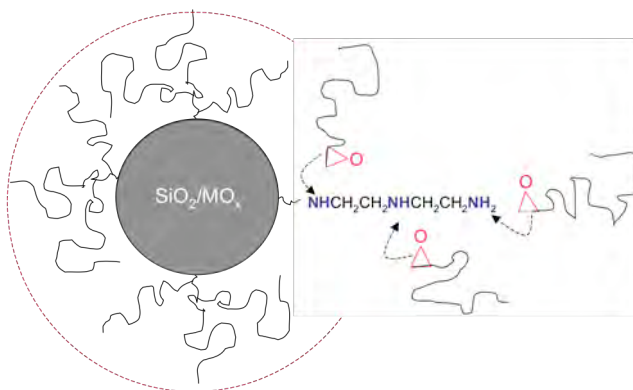


**Fig. 1** NOHMs based on epoxy-amine linkages.

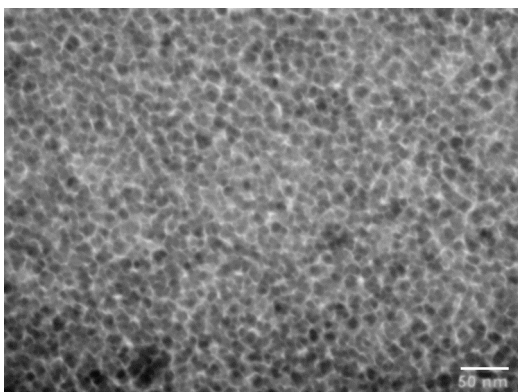
Building upon our earlier experimental and theoretical work,<sup>1-5</sup> which show how and why branched molecules densely tethered to a substrate yield superior lubrication properties to those obtained using the corresponding tethered or free linear chains, we recently discovered a family of nanoscale organic hybrid materials (NOHMs), which offer several exciting rheological and transport property attributes desirable in high-performance lubricants and lithium battery electrolytes. As illustrated in Fig. 1, NOHMs are star-branched organic polymers where the core of the star is a nanoparticle, and the corona is a low-molecular weight telomer (small polymer). By systematically changing the size and repeat unit chemistry of the telomer, the core particle size and mass distribution (e.g. hollow cores), the volume fraction,  $\phi$ , of the inorganic component can be

facilely adjusted to tune overall mechanical properties and conductivity of the hybrids. A particularly attractive class of NOHMs are materials in which  $\phi \geq 0.2$ . In these materials, the cores begin to percolate (i.e. exhibit connectivity/corporativity) up the macroscopic scale, but aggregation is prevented by the tethered polymeric corona. This means that unusual physical properties, e.g. large mechanical modulus, hardness, lithium intercalation efficiency, high refractive index, large heat capacity, and high



**Fig. 2** Liquid NOHMs based on PEG corona and 10 nm.  $\text{SiO}_2$  cores. The volume fraction of the core particles increases from right to left in the figure.

ionic/thermal conductivity, normally seen in inorganic materials, can exert measurable influence upon the behavior of the organic-inorganic hybrid. NOHMs in this category are also attractive because they combine desirable features of synthetic polymers (e.g. low density, low cost, and facile low-temperature processing) with unusual functionality (e.g. mechanical strength, high refractive index, lithium ion intercalation, thermal/electrical conductivity, photovoltaic properties, etc.) typical of inorganic materials.



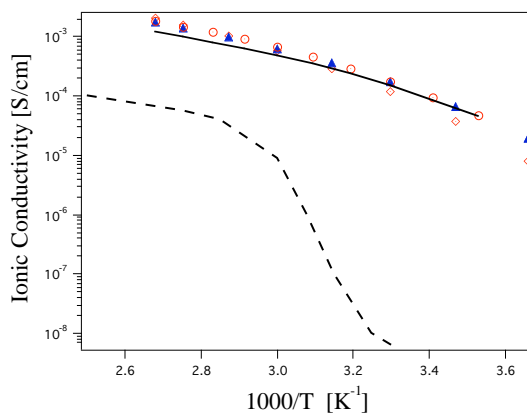
**Fig. 3** TEM micrograph for a representative PEO -SiO<sub>2</sub> liquid NOHM.

Fig. 2 are negligible. This feature makes them suitable for high temperature applications (e.g. lubricants, heat transfer liquids for solar thermal cells, and rechargeable battery electrolytes/electrodes), where colloidal suspensions either cannot be used or require specialized packaging to prevent solvent loss.

Figure 3 is a transmission electron micrograph (TEM) of a typical liquid NOHMs comprised of 10 nm. SiO<sub>2</sub> cores densely grafted (180 PEG chains/particle,  $v_{PEG} \approx 0.9$  chains/nm<sup>2</sup>) with an oligomeric ( $M_w = 700$  g/mol) polyethylene glycol (PEG) organic corona. It is clear from this figure that the SiO<sub>2</sub> particles are well dispersed in the corona material and an oligomeric ( $M_w = 700$  g/mol) polyethylene glycol (PEG) organic corona. The contrast in the figure is provided by the larger electron density of the SiO<sub>2</sub> cores. It is clear from this figure that the core particles are well dispersed in the corona material. This means that these liquid NOHMs are analogous to powders, except that the individual grains are of uniform, nanoscopic dimensions and of comparable size to the molecules that hold them together. This feature is important because it means that each NOHMs building block is in reality a star-branched polymer liquid comprised of an inorganic core and organic arms that can be manipulated to impart a broad spectrum of functionalities.

We will show that if the PEG corona is replaced by a polydimethyl siloxane or fluorine rich species (e.g. a fluorinated polyether), hybrid lubricants with unusual thermal and mechanical stability can be created. Figure 4 shows that even at high particle loadings, NOHMs constructed from hard, non-conducting inorganic particles and PEG corona doped with lithium salts (e.g. LiClO<sub>4</sub>, LiPF<sub>6</sub>, LiCF<sub>3</sub>SO<sub>3</sub>, LiAsF<sub>6</sub>, or LiN(CF<sub>3</sub>SO<sub>2</sub>)<sub>2</sub>) manifest temperature-dependent ionic conductivities almost identical to those of the oligomer corona (continuous line), and do not show

Because of their hybrid character, physical properties of liquid NOHMs can be manipulated over a surprisingly wide range by varying geometric and steric characteristics of the inorganic core particle and organic corona. On one end of the spectrum are materials with high core particle contents (Fig. 2, leftmost vial), which display properties similar to glasses, stiff waxes, and greases. At the opposite extreme are systems that spontaneously form particle-laden fluids (Fig. 2, rightmost vial), characterized by transport properties (viscosity, ionic conductivity) similar to simple Newtonian liquids comprised of molecular building-blocks. Importantly, because the effective solvent (the telomer) is chemically tethered to the core particle, the vapor pressures of all liquids in



**Fig. 4** Ionic conductivities of liquid NOHMs and polymer electrolytes as a function of reciprocal temperature. Circles  $\phi = 0.2$ , triangle  $\phi = 0.28$ , diamond  $\phi = 0.35$ .

any evidence of a crystalline transition (dashed line) that plague commercial PEG-based electrolytes. In the presentation, we will discuss how these features can be employed to create novel room-temperature liquid electrolytes capable of arresting harmful dendrite growth in high-capacity, rechargeable lithium metal batteries.

Figure 5 illustrates the effect of volume fraction of the core particle on rheological properties. Specifically, this figure plots the relative viscosity  $\eta_r \equiv \eta / \eta_s$ , where  $\eta$  and  $\eta_s$  are, respectively, the viscosities of the liquid NOHMs and the un-tethered corona. The lines in the figure are predictions of the Krieger-Dougherty model with the hard core radius of the SiO<sub>2</sub> NOHMS cores supplemented by an amount equal to twice the gyration radius of the attached PEG chains (i.e. close to the thickness of the tethered Alexander-deGennes brush).

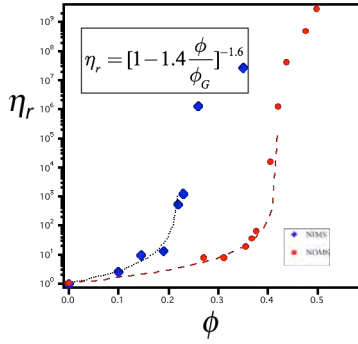


**Fig. 5** Relative viscosity of two families of NOHMs based on PEG corona and SiO<sub>2</sub> cores ( $d_c = 10$  nm. and 30 nm.) as a function of  $\phi$ .

Our ability to predict the relative viscosity of liquid NOHMs using this straightforward extension of the Krieger-Dougherty suspension model confirms that NOHMs are in reality self-suspended, suspensions of nanoparticles.

The molecular weight of the PEG corona chains provides a readily accessible handle for manipulating physical properties of the materials. Figure 6, for example, indicates that for PEGs with molecular weights in the range 1kg/mol - 18kg/mol the viscosity of a NOHMs liquid becomes lower, relative to that of the corona, as the un-tethered corona polymer molecular weight is increased (Fig. 6, squares). This observation is fundamentally different from what one would expect for a star-branched polymer, but is precisely what would be expected for a self-suspended suspension of particles as the volume fraction of the particles is lowered (Fig. 6, open circles).<sup>6</sup>

Figure 7 are strain-dependent dynamic storage,  $G'$ , and loss,  $G''$ , moduli for a PEG-SiO<sub>2</sub> NOHMs with  $\phi = 0.35$ . The results in the plot were obtained using oscillatory shear ( $\gamma(t) = \gamma \sin(\omega t)$ ) mechanical rheometry measurements at 28 °C. In the low-strain, *linear viscoelastic regime*, the elastic component of the shear modulus,  $G'$ , dominates the loss modulus  $G''$ , and both are independent of the imposed strain amplitude,  $\gamma$ , and only weakly dependent on frequency,  $\omega$ . This allows us to estimate the elastic modulus of the suspension,  $G_e \approx G'_{\lim \gamma \rightarrow 0} = 1MPa$ , which is much larger, by a factor of almost  $10^5$ , than the modulus of the unattached PEG oligomers; clearly showing that the hard silica cores provide strong mechanical reinforcement to the soft oligomer corona. At larger shear strains, in the so-called nonlinear shear regime, a crossover from solid (glass)-like,  $G'$ -dominant, to liquid-like  $G''$ -dominant, behavior is observed. The transition is characterized by the appearance of a pronounced maximum in  $G''(\gamma)$ , which is observed (inset) to grow as the measurement temperature is increased. The critical shear strain,  $\gamma_c$  at which the loss maximum occurs is, on the other hand, a weak function of temperature.

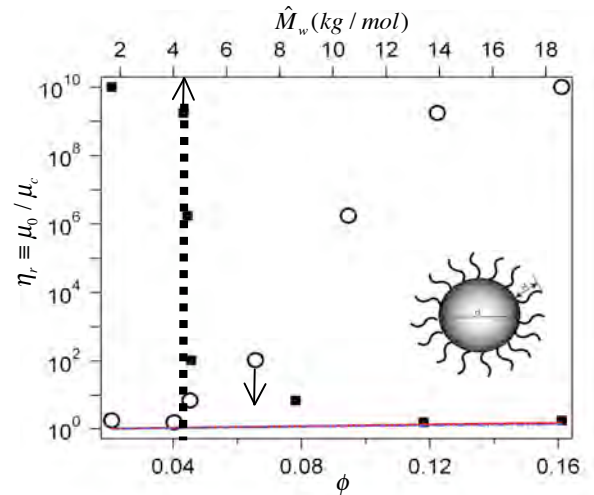


**Fig. 6** Relative viscosity of PEG-SiO<sub>2</sub> NOHMs vs. corona molecular weight (top) and core volume fraction (bottom axis).

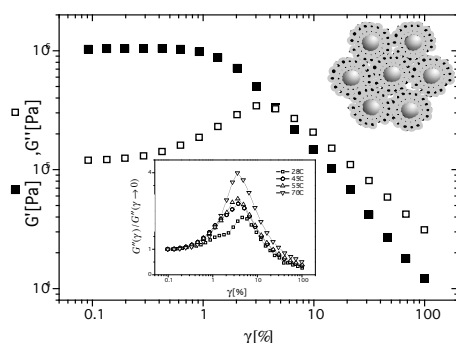


**Fig. 7** Strain-dependent elastic (filled symbols) and loss moduli (open symbols) of PEG-SiO<sub>2</sub> NOHMs. The cartoon (upper right inset) illustrates caging of the cores produced by neighboring particles.

plays the role of thermal energy. Yielding occurs in the SGR model when  $E_0 \approx k\gamma^2$ , and the cages break-apart under the action of the macroscopic deformation. This leads to a pronounced increase in viscous losses, which as in Fig. 7 manifests as a pronounced maximum in  $G''(\gamma)$ . Because the depth of the energy wells are substantially higher than the thermal energy  $kT$ , the critical strain at yield,  $\gamma_y$ , is not a function of temperature. All of these effects can be rationalized in terms of the greater levels of dissipation at break-up, which arises from enhanced penetration (crowding) and stretching of the tethered corona chains required to fill the intervening space between cores in a self-suspended suspension of nanoparticles.

**Future Plans:** (i) Develop NOHMs based on PEG-PDMS copolymer corona and investigate their temperature-dependent friction properties. Preliminary tribology studies performed in collaboration with an industrial partner indicate that PEG-based NOHMs can fill a critical need for high-performance biodegradable lubricants. Stribeck curves for these materials show that the friction coefficient is essentially independent of sliding speed and temperature down to the melting point of the PEG oligomer (-10 °C). NOHMs based on PEG-PDMS copolymers will allow us to extend this limit to -40 °C to meet current needs.

(ii) Synthesize NOHMs based on Ag and Cu nanocores and investigate the effect of core percolation and corona brush thickness on conductivity.

(iii) Investigate electrochemical stability of NOHMs electrolytes. Integrate NOHMs electrolytes into lithium batteries and determine their effect on capacity, power density, cyclability, and cell safety at high operating voltages.

### References Cited & Publications

- (1) Zhang, Q. and L.A. Archer, *J. Phys. Chem. B.* **107**, 13123 (2003)
- (2) Zhang, Q. and L.A. Archer, *Langmuir*, **21** 5405 (2005)
- (3) Zhang, Q. and L.A. Archer, *Langmuir* **22**, 717 (2006)
- (4) Zhang, Q. and L.A. Archer, *Langmuir* **23**, 7562 (2007)
- (5) Landherr, L.J.T., Zhang, Q., Cohen, C., and L.A. Archer, *J. Poly. Sci. B, Polym. Phys. Ed.* **46**, 1773 (2008)
- (6) Qi, H., Agarwal, P., and L.A. Archer, *Submitted* (2009)
- (7) P. Sollich *et al.*, *Phys. Rev. Lett.* **78**, 2020 (1997); S. M. Fielding, P. Sollich, and M. E. Cates, *J. Rheology* **44**, 323 (2000)

All of the rheological features manifested by PEG-SiO<sub>2</sub> NOHMs can be qualitatively retrieved in the framework of the Soft Glass Rheology (SGR) proposed by Sollich.<sup>6,7</sup> In this model, any soft glass is represented as a system of independent particles moving in response to a variable shear strain in a fixed energy landscape. The particles are trapped in energy wells (cages) of depth  $E(\gamma) \equiv E_0 - k\gamma^2$ , which at low shear strains are large in comparison to the thermal energy  $k_B T$ . At low strains, the escape probability from the wells is therefore small, proportional to  $\exp(-E_0/x)$  where  $x$  is designated the “effective temperature”, and

## Designing Colonies of Communicating Microcapsules that Exhibit Collective Behavior

Anna C. Balazs  
Chemical Engineering Department  
1248 Benedum Hall  
University of Pittsburgh  
Pittsburgh, PA 15261

**Program Scope:** Using theory and simulation, our goal is to design assemblies of active micro-scale structures that signal and communicate at the nano-scale and thereby collectively perform a large-scale, concerted function. Our fundamental microscopic units are polymeric microcapsules that encase nanoparticles. The microcapsules effectively communicate through the released nanoparticles, which bind to the underlying substrate and introduce adhesion gradients on the surface. Due to these gradients and hydrodynamic interactions with the surrounding solution, the microcapsules can undergo self-propelled motion. Building on this behavior, we will design *self-regulating colonies of microcapsules* that can interact, respond to external stimuli, and transduce energy to undergo a self-directed activity. Through these studies, we will devise non-living microscopic systems that exhibit unprecedented biomimetic behavior. Furthermore, we will be addressing two specific “grand challenges” for the DOE mission: 1) creating new technologies with “life-like” functionalities, and 2) controlling the behavior of systems far from equilibrium.

We focus on polymeric microcapsules as our fundamental structural unit because they are on the same size scale as biological cells and thus, *physical phenomena* that occur between living cells can potentially be made to occur between the capsules. Furthermore, the microcapsules can be readily fabricated and thus, design rules that emerge from our computational and theoretical studies could be implemented experimentally. The nanoparticles also constitute an important component of our system, enabling inter-capsule communication, and sustaining the collective dynamic behavior of the system. In effect, the nanoparticles provide a source of “fuel” for activating the microcapsules.

The nanoparticle-mediated interactions between the microcapsules involve complex couplings, feedback loops and noise. Thus, we anticipate that the *multiple, interacting* microcapsules will exhibit remarkable forms of collective activity. Furthermore the microcapsule colonies will provide an ideal “laboratory” for probing factors that give rise to non-linear, dynamical behavior and uncovering the fundamental physics that governs this behavior. As part of the proposed efforts, we will introduce chemo-responsive and light-sensitive elements into our microcapsules, as depicted schematically in Fig. 1. Additionally, we will utilize patterned substrates to facilitate the inter-capsule “communication” and effectively “steer” the motion of the capsules. Thus, the studies will also allow us to establish routes for controlling the dynamic self-assembly in non-equilibrium systems.

Ultimately, the findings could enable researchers to fabricate small-scale devices that “cooperate” to display effective forms of self-actuation, sensing, and sharing of information. For example, the findings could open the path to fabricating “intelligent” micro-scale delivery devices that corral their neighbors to localize at a specific site when the conditions are appropriate and thereby, deliver an increased dose of the encapsulated cargo. These micro-carriers would also stop delivery when the conditions have been changed and thus, introduce a useful feedback mechanism into the system.

Overall, by attempting to engineer a particular functionality, we actually learn a tremendous amount about the physical pathways that control that functionality. Since our efforts are focused on microcapsules that can be experimentally fabricated and our simulation parameters are matched to the

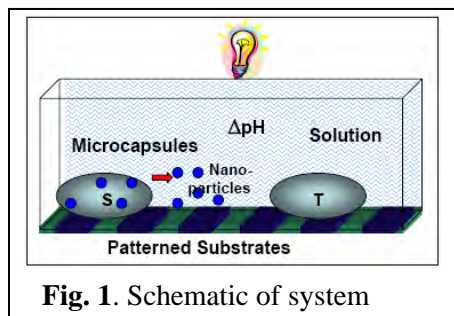


**Fig. 1.** Schematic of system

relevant experimental values, we can provide effective guidelines for converting these theoretical predictions into actual, working physical systems.

**Recent Progress:** Using theory and simulation, we demonstrated how nanoparticles can be harnessed to regulate the interaction between two initially stationary microcapsules on a surface [1]. Specifically, nanoparticles released from a “signaling” capsule modify the underlying substrate and thereby initiate the motion of the “target” capsule. The latter motion activates hydrodynamic interactions, which trigger the signaling capsule to follow the target. The continued release of the nanoparticles sustains the motion of both capsules along the surface. The process effectively mimics a unique scenario in cell signaling, where the signaling species can both send and receive directional cues.

We recently extended these studies by designing a “train” of  $N$  microcapsules that undergoes self-sustained, directed motion along an adhesive surface in solution [2]. The motion is initiated by the release of nanoparticles from a single signaling capsule at one end of the train of targets (see Fig. 2). The released nanoparticles can bind to the underlying surface and thereby induce an adhesion gradient on the substrate. Through the combined effects of the self-imposed adhesion gradient and hydrodynamic interactions, the  $N$  microcapsules autonomously move in a single file toward the region of greatest adhesion. At late times, this train reaches a steady-state velocity  $U$ , which decreases with train length as  $N^{-1/2}$ . We calculated the maximum

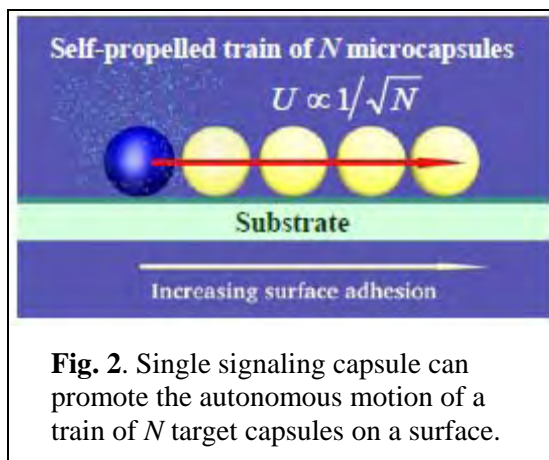


**Fig. 2.** Single signaling capsule can promote the autonomous motion of a train of  $N$  target capsules on a surface.

length for which the train maintains this cooperative, autonomous motion. While these simulations were carried out in two dimensions, the system can be realized experimentally by confining the three-dimensional microcapsules to a narrow groove or adhesive strip on a surface.

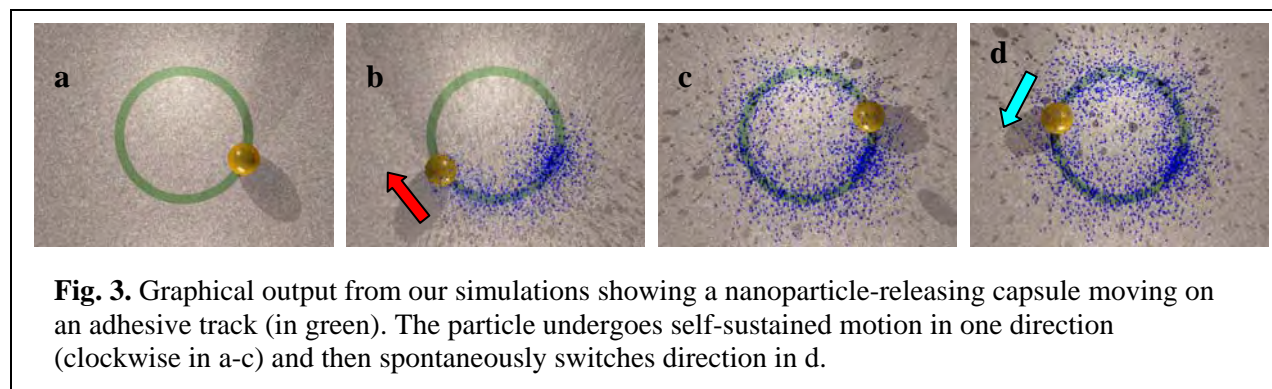


**Fig. 3.** Graphical output from our simulations showing a nanoparticle-releasing capsule moving on an adhesive track (in green). The particle undergoes self-sustained motion in one direction (clockwise in a-c) and then spontaneously switches direction in d.

We have expanded the simulations to 3D and are now in the process of uncovering the rich collective phenomenon that can emerge as the signaling and target microcapsules move on a plane. In carrying out these studies, we anticipate that the multi-capsule system will indeed exhibit distinct levels of complexity and for this reason, we will build our intuition about the behavior of the 3D assemblies by first considering smaller systems and then moving on to more complicated scenarios, which mimic certain biological processes (as described further below). Consequently, in the first set of 3D studies, we confined a single nanoparticle-filled microcapsule onto a circular adhesive track (as shown in Fig. 3) and already discovered intriguing behavior. Namely, the microcapsule first moves autonomously in a clockwise direction (in Figs. 3a-c) and then suddenly switches direction to undergo self-sustained motion in the counter-clockwise direction (Fig. 3d). Recall that nanoparticles released from the microcapsules can bind

to the surface and consequently make the surface less adhesive. Thus, the adsorbed nanoparticles introduce an adhesion gradient on the substrate. Due to the attractive interaction with the adhesive strip, the capsule moves towards the more “sticky” regions of the track. At the onset of the simulation, this sticky region lies ahead of the moving capsule and thus, the capsule moves in a clockwise motion. As the capsule returns to the starting point, the more adhesive region lies in the counter-clockwise direction, and hence, the capsule reverses its direction.

This behavior can be understood more clearly by examining the density distribution of the deposited nanoparticles in Fig. 4, where red marks the highest density of deposited nanoparticles and blue indicates the lowest density. The images in Fig. 4a-c are for the first traversal of the capsule around the circuit (Figs. 3a-c). As can be seen, when the capsule in Fig.

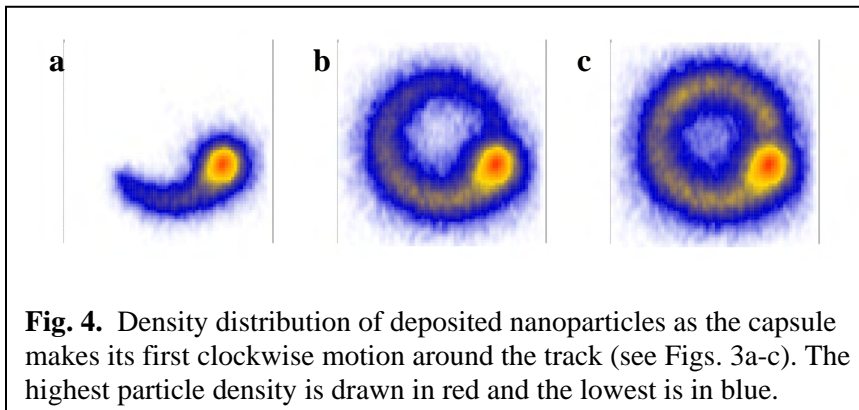


**Fig. 4.** Density distribution of deposited nanoparticles as the capsule makes its first clockwise motion around the track (see Figs. 3a-c). The highest particle density is drawn in red and the lowest is in blue.

3c reaches its initial starting point, it encounters a region of high particle density below it, corresponding to a less sticky surface. For enthalpic reasons, however, the capsule prefers the stickier region and consequently moves away from the large yellow “bump”, i.e., in the counter-clockwise direction. In future studies, involving multiple capsules and multiple tracks, we will use these “speed bumps” to regulate the trafficking of the capsules in more complicated circuits.

**Future Plans:** In biological cell signaling, “agonist” ligands bind to receptors on the surface of the cells and stimulate the production of signaling molecules. The agonists provide a means of amplifying the signaling process. We will introduce the analogue of this behavior into our synthetic system as illustrated in Fig. 5, where the “blue” nanoparticles in the solution play the role of the agonist. In this scenario, *both signaling and target capsules encapsulate nanoparticles; however, the nanoparticles in the respective carriers are chemically distinct*—the “blue” particles are encased in the signaling units and the “red” are housed in the targets. (Here, we neglect interactions between nanoparticles.)

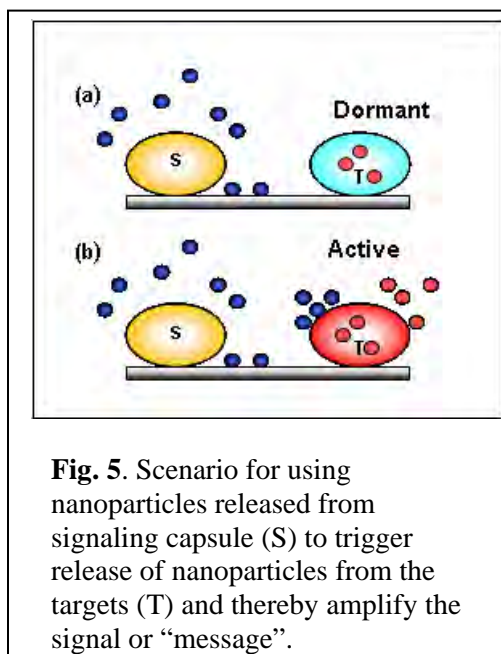


**Fig. 5.** Scenario for using nanoparticles released from signaling capsule (S) to trigger release of nanoparticles from the targets (T) and thereby amplify the signal or “message”.

The shells of the signaling and target carriers are also chemically distinct (drawn in yellow and cyan, respectively). At the onset of the simulations the target capsules are “dormant”—they do not release their cargo. The signaling capsules, however, are releasing blue nanoparticles that can impinge on the surface of the target capsules. Here, we assume that the target capsule’s shell is sensitive to the action of the released nanoparticles (e.g., to changes in pH produced by these nanoparticles) and if the concentration of impinging nanoparticles is sufficiently high, the “dormant” target capsule begins to release its own payload of red nanoparticles.

With more nanoparticles in the system, the dynamics at the surface (the deposition and the formation of the adhesion gradients) will be altered. Consequently, the dynamic interactions between the capsules will also be modified.

To realize this scenario computationally, we track the fraction of released blue nanoparticles that hit the surface of the target capsules. Once the latter number reaches a threshold value, the target capsules release their content. (Alternatively, the release rate of red nanoparticles can be dependent on the concentration of blue nanoparticles in the target’s vicinity.) Both the blue and red nanoparticles modify the surface properties; initially, we assume that they both contribute to making the surface less sticky. (In later studies, we will assume that the blue and red nanoparticles affect the surface in different ways.) In this manner, the signaling process will be amplified and thus, the collective behavior of the system could be modified.

Figure 6 below shows the output of simulations that incorporate the ideas described above; namely, the nanoparticles released from the central capsule not only modify the surface, but also activate the target capsules to release their own surface-modifying particles. The preliminary studies show that the system is capable of undergoing a primitive form of “quorum sensing”. In particular, the central capsule senses density variations in the number of neighboring capsules and moves in the direction of the higher concentration of neighbors. As shown below, the central signaling capsule moves to the right, since there are a higher number of spheres in that direction. The reason for this behavior is that the greater number of neighbors exerts a stronger hydrodynamic force, which effectively pulls the central capsule towards the group. In other words, the central capsule feels a greater tug from the larger population on the right and in that sense “feels” the relative size of the population.

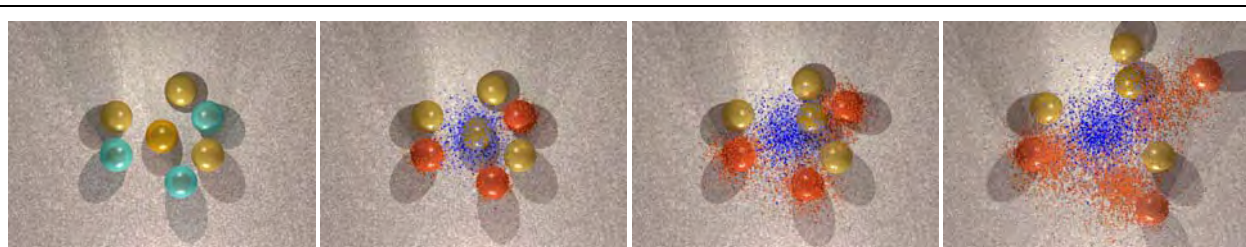


**Fig. 6.** Graphical output from our simulations showing that the central capsule autonomously moves towards the higher density of neighboring spheres. Time increases from the left to right

In future studies, we will exploit this behavior to design effective means of controlling the directionality of a transmitted signal. Along with controlling the direction in which the signal or “message” is passed between the capsules, we will establish means of maximizing the distance over which the signal is sent. In effect, our goal is evolving toward designing an “artificial cell”. Fortuitously, the most recent BESAC report targeted designing small-scale biomimetic devices and “artificial cells” using concepts inspired by nature as an important goal for DOE-based research. Excited by this convergence of ideas, we in turn were motivated by the report to consider some of the topics presented above (i.e., amplification of signaling and quorum sensing). Thus, our proposed research is quite timely in terms of addressing issues that are relevant to the DOE mission and due to our prior studies (summarized in [3]), we are well poised to contribute to this challenging research area.

#### References

1. Usta, B. O., Alexeev, A. Zhu, G. and Balazs, A. C. “Modeling Microcapsules that Communicate Through Nanoparticles to Undergo Self-propelled Motion”, *ACS Nano* 2 (2008) 471.
2. Bhattacharya, A. Usta, O.B., Yashin, V. V. and Balazs, A.C. “Self-sustained motion of a train of haptotactic microcapsules”, *Langmuir* 25 (2009) 9644.
3. Balazs, A. C. “New approaches for designing ‘programmable’ microfluidic devices”, *Polymer International*, 57 (2008) 669.

# High Efficiency Biomimetic Organic Solar Cells

Marc Baldo<sup>1</sup> and Troy Van Voorhis<sup>2</sup>

<sup>1</sup>Department of Electrical Engineering and Computer Science,

<sup>2</sup>Department of Chemistry

Massachusetts Institute of Technology

77 Massachusetts Av, Cambridge, MA 02139

[baldo@mit.edu](mailto:baldo@mit.edu)

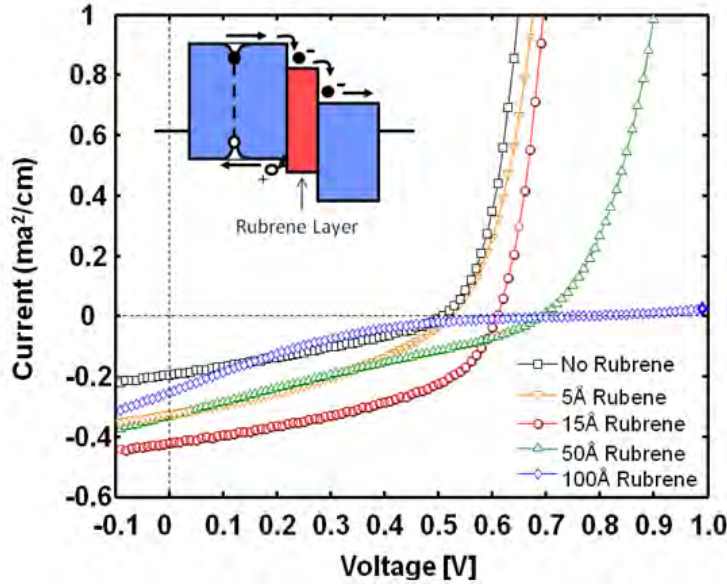
[tvan@mit.edu](mailto:tvan@mit.edu)

**Program Scope:** Organic solar cells exhibit higher charge recombination losses than their biological equivalents, photosynthetic reaction centers. Two measures of the importance of this loss in organic solar cells are the quantum efficiency of charge generation and the open circuit voltage, which is the internal electric field required to force recombination of the photogenerated charges. We are working to understand the mechanisms of charge recombination in small-molecular weight and polymeric organic cells, including the spin dependence of charge recombination, direct spectroscopy of charge transfer states, and engineering interfacial layers to block charge recombination. The latter approach is modeled on the multiple step charge dissociation process characteristic of photosynthetic reaction centers.

**Recent Progress:** Perhaps the key scientific question is the mechanism of exciton dissociation: Does successful exciton dissociation evolve through a bound charge transfer state? If bound charge transfer states are involved the likelihood of recombination may be significantly higher.

Our recent progress includes three experiments probing the presence of bound charge transfer state. We have obtained spectroscopic data demonstrating that photoexcitation of excitons is more likely to yield photocurrent than direct photoexcitation of bound charge transfer states. This suggests that the dissociation of excitons does not necessarily involve intermediate bound charge transfer states. To test this further, we have also investigated the spin dependence of charge recombination by selectively creating either singlet or triplet excitons. Comparisons of the open circuit voltage at constant short circuit current exhibit only a minimal dependence on spin. The longer lifetime expected from the triplet charge transfer state does not substantially reduce recombination losses, suggesting again that bound charge transfer states are not necessarily involved in photocurrent generation but that the formation of a bound charge transfer state will result in charge recombination. Finally, we demonstrate small molecular weight devices with a multiple step charge dissociation process at the donor-acceptor interface. We insert a material with energy levels positioned between those of the acceptor and donor. This destabilizes the charge transfer states at the donor-acceptor interface and we observe that about one monolayer of the intermediate material can substantially enhance both the short circuit current and the open circuit voltage by reducing recombination rates. However, we have

observed that the multistep dissociation process only benefits the quantum efficiency of certain material combinations.



Following the biological example, we reduce the recombination of separated electrons and holes at the exciton-dissociation interface by introducing an additional, thin, interfacial layer sandwiched between the active semiconductor layers. The interfacial layer in this architecture creates a cascade energy structure at the exciton-dissociation interface as shown in the inset of Figure 1.

**Fig. 1.** Current–Voltage characteristics for devices comprised of the acceptor MTDATA and donor PTCBI with and without a Rubrene interfacial layer. Devices with a thin layer of Rubrene at the exciton-dissociation interface exhibit increased short circuit current and increased open circuit voltage. However, at large interfacial layer thicknesses, the current decreases.

As illustrated in Figure 2, we find devices with too thin an interfacial layer demonstrate limited improvements in charge collection due to partial layer coverage. Devices with interfacial layers that are too thick suffer from carrier transport problems in the interfacial layers. Determining the optimal interfacial layer thickness promises to give greater insight into the physical mechanism of charge carrier recombination at the exciton dissociation interface in organic PVs.

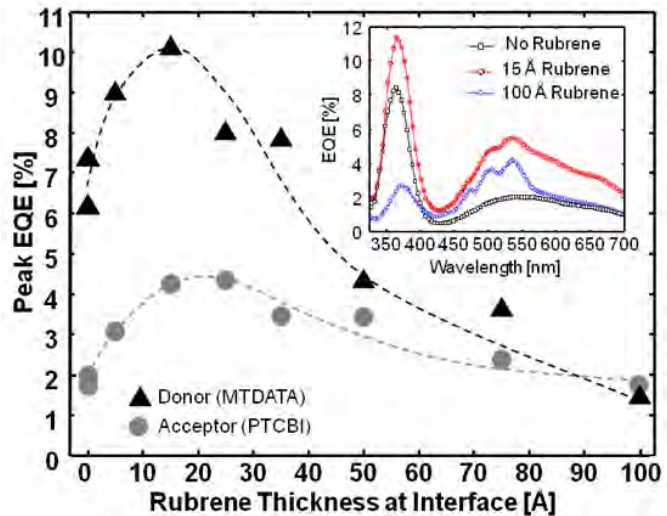


**Fig. 2.** Devices with thin interfacial layers exhibit higher external quantum efficiencies. The optimal layer thickness is approximately 15Å. The interfacial layer reduces recombination of separated charges at the exciton-dissociation interface.

In addition to being able to predict spectra, it is of pivotal importance that we be able to predict the rates at which different electronic states interconvert. The most pivotal such rate in solar cells is the rate of charge separation from an initial exciton state. At present, there is no meaningful way to predict this rate, primarily due to the fact that computing excited state wavefunctions is prohibitively difficult. We have developed a means of predicting the coupling between these states. These couplings lead to *avoided crossings* between the local excitons and charge separated CT states (See Figure 3). Putting these coupling together with the energies predicted from a QM/MM model, we will be in a position to derive kinetic equations for these processes without any adjustable parameters.

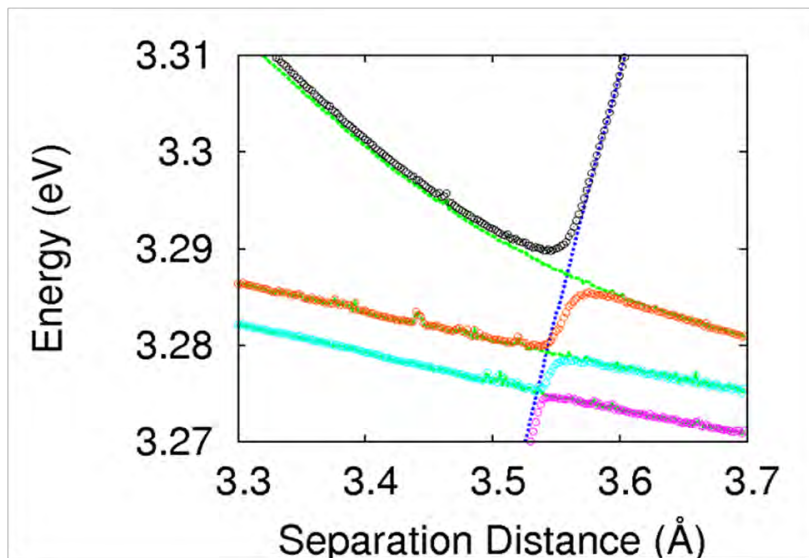


**Fig. 3.** A charge transfer state (blue dotted line) crosses three exciton states (green solid lines) to generate three avoided crossings (points) in a model donor-acceptor complex.

**Future Plans:** We have developed a very general procedure for modeling the electronic states present at disordered organic interfaces. At the coarsest level, the interface is described by a molecular force field, which yields information about the structure at the nanometer length scale. On a finer length scale, we use high level calculations to extract the electronic states accessible to the donor and acceptor molecules at the interface. A series of many such calculations leads to a prediction of the density of states in the heterogeneous structure. In the next twelve months, we plan to use this model to study the electronic states that operate in the multistep charge dissociation parts of this project.

We also intend to understand the origins of the material dependencies in the efficiency enhancements observed in some multistep devices. We have noted that the structure is most beneficial to the buckyball C60, typically more than doubling its quantum efficiency while leaving the efficiency of a donor material in the same device unaffected. This strongly suggests that the properties of the C60 exciton enhances the probability of charge recombination after exciton dissociation.

## **Publications 2007-2009:**

*On the Singlet-Triplet Splitting of Geminate Electron-Hole Pairs in Organic Semiconductors*, Difley, S., Beljonne, D. and Van Voorhis, T. *Journal of the American chemical Society* **130** 3420-3427 (2008).

*High-Efficiency Organic Solar Concentrators for Photovoltaics*, Currie, M. J., Mapel, J. K., Heidel, T. D., Goffri, S. & Baldo, M. A. *Science* **321**, 226-228 (2008)

*Luminescent Solar Concentrators Employing Phycobilisomes*, Mulder, C. L., Theogarajan, L., Currie, M., Mapel, J. K., Baldo, M. A., Vaughn, M., Willard, P., Bruce, B. D., Moss, M. W., McLain, C. E. & Morseman, J. P. *Advanced Materials* **21**, 1-5 (2009).

*High Efficiency Organic Multilayer Photodetectors based on Singlet Exciton Fission*, Lee, J., Jadhav, P., and Baldo, M.A., *Applied Physics Letters*, **95**, 033301 (2009).

# Self Assembling Biological Springs: Force Transducers on the Micron and Nanoscale

Natalia Kozlova<sup>a</sup>, Boris Khaykovich<sup>b</sup>, Aleksey Lomakin<sup>a</sup>,  
and George B. Benedek<sup>a,c</sup>

<sup>a</sup>Materials Processing Center, <sup>b</sup>Nuclear Reactor Laboratory, <sup>c</sup>Department of Physics,  
Massachusetts Institute of Technology, 77 Massachusetts Avenue, Cambridge, MA 02139

PI: George B. Benedek

## Program scope and definition:

We are developing a new system for measuring forces within and between nanoscale biological molecules based on mesoscopic springs made of cholesterol helical ribbons. These ribbons self-assemble in a wide variety of complex fluids containing sterol, a mixture of surfactants and water [1] and have spring constants in the range from 0.5 to 500 pN/nm [2]. To utilize these springs experimentally they must be tethered to biologically active binding tips, and to stationary suspension posts (Fig.1). In this way it should be possible to create mesoscale force transducers whose spring constants are well suited to probe quantitatively the forces acting in a wide variety of biological systems such as biopolymers, membranes, motile cells, protein-ligand pairs, and protein motors.

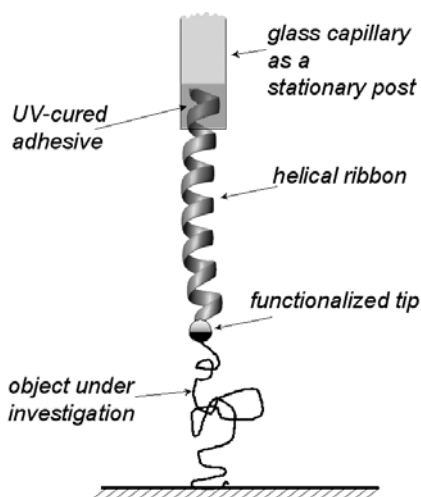


**Figure 1.** A schematic (not drawn to scale) showing the important components that would be associated with using the helical ribbons as force probes. The helix is attached at one end to a glass capillary that controls the extension by its connection to a micromanipulator, while the other end is attached to the biomolecule under investigation through the use of a functionalized latex sphere.

For practical use it is very important to be able to select from a polydisperse distribution a helical ribbon with a spring constant most suitable for the application in mind. Therefore the ability to easily determine the spring constants of individual helices from measurable geometric parameters is of crucial importance. Recently, we have established the relationship between the spring constant of the low-pitch cholesterol helical ribbon and its readily observable dimensions: width, radius and length. This relationship enables us to calculate spring constant for any ribbon in the suspension [3]. We are now working to reach the next goal of our proposal: to find a reliable way to tether helices to the stationary posts and to design a method of the attachment of biologically active binding tips to the opposite end of the helical ribbon.

## Recent progress

Our recent research has been focused on (1) studying the relationship between spring constants of helical ribbons and their external dimensions, and (2) designing practical methods for attaching helical ribbons to stationery posts and binding tips.

### (1) Understanding the relationship between spring constants of cholesterol helical ribbons and their observable geometric dimensions.

In order to use the helical ribbons as biological springs, it is crucially important to be able to predict their spring constants from external dimensions. Previously, we had proposed an anisotropic crystal model for the elasticity of cholesterol helical ribbons [2]. We recently proved their crystallinity experimentally by x-ray studies of individual helical ribbons [3]. In those studies, we established that each ribbon is in fact a curled single crystal with a structure very similar to that of cholesterol monohydrate. We have shown [2] that the spring constant  $K_{spring}$  of such a ribbon is determined by its width ( $w$ ), its contour length ( $s$ ), its radius ( $R$ ) and its effective bending modulus  $K_\alpha$  according to:

$$K_{spring} = \frac{8w}{R^2 s} K_\alpha, \quad (1)$$

According to beam-bending theory for solid ribbons, [4] we expect  $K_\alpha$  to be proportional to the cube of the thickness ( $t$ ) of the strip,  $K_\alpha \propto t^3$ . Our theoretical model also predicted a quadratic relationship between the thickness of the helical ribbon and its radius  $R \propto t^2$ . We have recently proved this last prediction experimentally, and confirmed that indeed there is a universal relationship, independent of solution conditions, between the thickness of the helical ribbon and its radius consistent with  $R \propto t^2$ , as shown in Fig.2. Measuring the thickness of helical ribbons was a challenging task since the thickness is less than 200 nm, which is below the diffraction-limited axial resolution of optical microscopes. Other techniques such as AFM and scanning electron microscopy require drying the helical ribbons on a flat surface, which was impractical due to the fragility of thin crystals. We have overcome these difficulties by using a novel optical methodology known as quantitative phase microscopy [5]. This method has capability to measure accurately the thickness of helical ribbons starting from 50 nm, and could be performed in solution, without any additional stress for the ribbon. This methodology has been developed in the MIT Spectroscopy Laboratory. We have collaborated with Prof. Michael Feld and Dr. Wonshik Choi of that laboratory to measure the radius of the ribbon as a function of thickness [6]. We have found that the ribbon radius varies quadratically with the thickness in the range from 0.06 to 0.18 microns (Fig.2).

Thus, a macroscopic measurement of the ribbon radius serves to determine a ribbon thickness. Since  $K_\alpha \propto t^3$ , this implies  $K_\alpha \propto R^{3/2}$ , hence we can eliminate  $K_\alpha$  in terms of  $R$ . From these measurements we have been able to deduce that the spring constant of any ribbon in a polydisperse distribution can be expressed solely in terms of the macroscopically measured quantities: ribbon width  $w$ , radius  $R$ , and contour length  $s$ :

$$K_{spring} = \kappa \frac{w}{R^{1/2} s},$$

where  $\kappa$  is a phenomenological constant independent of solution conditions with the value currently estimated as  $1.37 \cdot 10^{-6} \text{ N/m}^{1/2}$ .

The discovery of this formula now paves the way for the use of these mesoscopic springs to measure forces between nanoscale biological molecules.

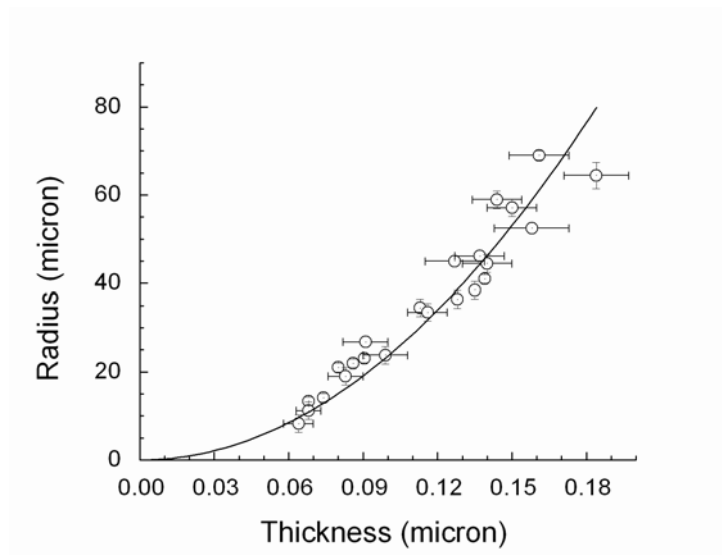


**Figure 2.** Radius ( $R$ ) vs thickness ( $t$ ) of cholesterol helical ribbons. The data is fitted according to  $R = ct^2$ . The fitting constant  $c = 3560 \pm 108$ . The radius is measured by standard bright field microscope; vertical error bars are due to uncertainty in the best focus position or slight deformation of the ribbons. The thickness was measured using quantitative phase microscopy.

## (2) Methodology for reliable attachment of helical ribbons to stationary posts and binding tips.

Using the helical ribbons as mesoscopic springs requires a reliable procedure for tethering their one end to a stationary post, while the other end is attached to a specific binding tip. We chose to use glass capillaries as stationary posts, and functionalized polystyrene spheres as binding tips. Due to the fragility of helical ribbon, which is a very thin solid crystal, rigid chemical bonding is inadvisable to use to attach it to a stationary post. A more practical approach appears to be encapsulating one end of the ribbon in a capillary filled with suitable adhesive. The selection of the adhesive has been the subject of our recent research. This adhesive should have following properties: low solubility in water, no effect on a ribbon structure, relatively low viscosity to enable insertion of the soft ribbon, and the ability to quickly set under an external stimulus without generating heat. After trying many different types of monomers, we have designed a polymer system containing an acrylic monomer, 3-[Tris(trimethylsiloxy)silyl]propyl methacrylate, and a UV-activated free radical initiator. The resulting silicone-like polymer appears to meet all of the requirements. We are now optimizing and testing this system.

Also we have designed and built two-micromanipulator system, which enables us to choose a helical ribbon with desired spring constant and then hold the chosen ribbon and a stationary post together during polymerization of the acrylic monomer.

Another important issue is to be able to hold the chosen ribbon and the stationary post together during the polymerization. We accomplished this last task by designing and building a two-micromanipulator system.

#### Future plans:

The groundwork summarized above should enable us to complete the development of the technique for tethering the helical ribbons to stationary posts in the near future. This adhesive may also be useful for attaching binding tips to other end of the helical ribbon. Another approach to attachment of a binding tip to a helical ribbon is to introduce chemically active groups on the surface of the ribbon. We are now studying the incorporation of Thiocholesterol molecules onto a surface of helical ribbons. This should provide the surface of the helical ribbon with highly active binding sites.

#### **References:**

- [1] Y. V. Zastavker, N. Asherie, A. Lomakin, J. Pande, J. M. Donovan, J.M. Schnur, G. B. Benedek "Self-assembly of helical ribbons", *Proc. Natl. Acad. Sci. USA* **96**, pp. 7883-7887 (1999).
- [2] B. Smith, Y.V. Zastavker, G.B. Benedek, "Tension-induced straightening transition of self-assembled helical ribbons", *Phys. Rev. Lett.* **87**, pp. 278101-278104 (2001).
- [3] B. Khaykovich, C. Hossain, J. J. McManus, A. Lomakin, D. E. Moncton, and G. B. Benedek, "Structure of cholesterol helical ribbons and self-assembling biological springs", *Proc. Natl. Acad. Sci. U. S. A.* **104**, 9656 (2007).
- [4] L. D. Landau and E. M. Lifshitz, *Theory of elasticity* (Pergamon Press, New York, 1986).
- [5] W. Choi, C. Fang-Yen, K. Badizadegan, S. Oh, N. Lue, R. R. Dasari, M. S. Feld "Tomographic phase microscopy", *Nature Methods*, **4**, pp. 717-719, (2007).
- [6] B. Khaykovich, N. Kozlova, W. Choi, A. Lomakin, C. Hossain, Y. Sung, R.R. Dasari, M.S. Feld, and G.B. Benedek "Thickness-radius relationship and spring constant of cholesterol helical ribbons." *Proc. Natl. Acad. Sci. USA* published online before print August 26, 2009, doi:10.1073/pnas.0907795106.

#### **DOE Sponsored Publications in 2007-2009:**

- 1) B. Khaykovich, C. Hossain, J. J. McManus, A. Lomakin, D. E. Moncton, and G. B. Benedek, "Structure of cholesterol helical ribbons and self-assembling biological springs" , *Proc. Natl. Acad. Sci. USA* **104**, 9656 (2007).
- 2) B. Khaykovich, N. Kozlova, W. Choi, A. Lomakin, C. Hossain, Y. Sung, R.R. Dasari, M.S. Feld, and G.B. Benedek "Thickness-radius relationship and spring constant of cholesterol helical ribbons." *Proc. Natl. Acad. Sci. USA* published online before print August 26, 2009, doi:10.1073/pnas.0907795106.

Program Title: Design, Synthesis & Characterization of Novel Electronic & Photonic BioMolecular Materials

Principal Investigators: J.K. Blasie (lead-P.I.), W.F. DeGrado, J.G. Saven & M.J. Therien

Mailing Address: Department of Chemistry, University of Pennsylvania,  
231 South 34<sup>th</sup> Street, Philadelphia, PA 19104-6323

Email: [jkblasie@sas.upenn.edu](mailto:jkblasie@sas.upenn.edu)

Program Scope:

Linearly extended conjugated chromophores can now be designed to possess an electron donor-bridge-acceptor motif, and thereby exhibit efficient light-induced electric charge separation over large nano-scale distances. Closely related chromophores can be designed to also modulate their HOMO-LUMO bandgap and thereby optimize their molecular non-linear optical polarizability. These exceptional microscopic properties can be exploited to result in novel macroscopic electro-optical materials if the following can be controlled and thereby optimized: a) the positional & orientational ordering of the chromophores in a 2-D or 3-D ensemble, b) the conformation & symmetry of the chromophore within the ensemble, and c) the interaction among the chromophores in the ensemble. Exceptionally stable, artificial  $\alpha$ -helical peptides based on n-helix bundle structural motifs (e.g., n=2-6) can now be computationally designed to achieve these three key goals. The interior of the bundle can be designed to control the local environment, conformation and vectorial orientation of the chromophore within the bundle. The exterior can be designed to control the vectorial orientation and ordering of the peptide-chromophore complexes within both 2-D and 3-D ensembles. Importantly, incorporation of the chromophore into the core of the bundle with its exterior controlling the nature of the ordering of the complex in the ensemble provides for the additional control over chromophore-chromophore interactions within the ensemble. For example, in non-linear optics, the lack of control of interactions between chromophores is thought to be responsible for the inability of chromophore ensembles to achieve their predicted material properties. In the case of light-induced electric charge separation, the inability to achieve purely uni-directional charge separation over large nano-scale distances is thought to contribute substantially to their relatively low efficiencies. The n-helix bundle structural motifs are chosen for the artificial peptides because of their significantly higher stability compared to natural proteins. However, the interior of the bundle scaffold may not be so stable to the supramolecular assembly process required to form a sufficiently ordered material. Thus, it is important to monitor structurally the various stages of the self-assembly process starting from the designed peptide, e.g. a particular n-helix bundle, to the incorporation of the extended conjugated chromophore, through to the supramolecular assembly of the peptide-chromophore complexes into an ensemble material ordered on a macroscopic scale. Since the desired material properties need not require long-range periodic order, as opposed to orientational order, in two or three dimensions, structural determination in the absence of such "crystallinity" is essential. As a result, the research program necessarily involves a strong coupling of chromophore design and peptide design, with essential structural and functional characterization at the microscopic level of the isolated chromophore-peptide complex, as well as at both the microscopic and macroscopic levels within the 2-D & 3-D ensembles. These essential structural and functional characterizations can then provide important feedback to the chromophore and peptide design process to result in the desired optimization of the macroscopic material properties of the ensemble. Thus, the research program described can only be accomplished via a highly collaborative multi-investigator approach.

### Selected Recent Accomplishments:

#### 1) *Novel cofactor design for non-linear optical susceptibility:*

A new class of NLO chromophores have been developed and characterized that possess many key properties that have heretofore been without precedent in single chromophoric entities. These include microsecond excited-state lifetimes, highly polarized low energy excited states, and extremely large excited-state molar absorption over large, technologically important wavelength windows.

#### 2) *Novel peptide design for the incorporation of such novel electro-optic cofactors:*

A new water-soluble, 108-residue protein has been designed *de novo*, expressed and characterized that binds and encapsulates a nonbiological cofactor (an ethyne-bridged Zn-porphyrin polypyridyl-Ru “push-pull” chromophore) with a large molecular hyperpolarizability at telecommunications wavelengths. The linear and non-linear optical properties of the cofactor-peptide complex have been investigated in aqueous solution, via transient spectroscopy and hyper-Rayleigh scattering, respectively. A mutant of this protein has been utilized to form a densely-packed, vectorially-oriented single monolayer of the peptide-cofactor complex on the alkylated surface of an inorganic substrate via self-assembly.

A novel  $\alpha$ -helical bundle protein has been computationally designed that crystallizes into a targeted space group, P6, having parallel orientation of the bundles throughout the macroscopic 3-D crystal. This is a critical first step toward the development of protein-cofactor assemblies that spontaneously self-order into vectorially ordered arrays in two- and three-dimensions.

#### 3) *Novel peptide design for long-range electric charge separation:*

The first example of a fully artificial and functionally active membrane protein has been computationally designed. The protein is a transmembrane 4-helix bundle protein based on an anti-parallel  $D_2$  symmetric coiled-coil backbone, with one His residue per chain. In the tetramer, the four His residues align along the membrane normal axis to form two coordination sites for the non-biological iron porphyrins separated by a theoretical distance of 12.7Å, allowing edge-to-edge contact of the rings (3.9Å). The peptide exhibits cooperative assembly in detergent micelles and binding of diphenyl-porphyrin with the expected 4:2 stoichiometry. The protein catalyzes electron transfer across lipid bilayers 2-orders of magnitude faster relative to the iron(III) porphyrin alone embedded in the lipid bilayer.

#### 4) *Structural & dynamical characterization of peptide-cofactor complexes at interfaces:*

Non-resonance x-ray reflectivity and grazing-incidence x-ray diffraction were previously used to localize the NLO cofactor RuPZn (an ethyne-bridged Zn-porphyrin polypyridyl-Ru) within the amphiphilic 4-helix bundle peptide AP0, vectorially-oriented at the water-gas interface. Resonance x-ray reflectivity, dramatically enhanced via interferometry employing an adjacent multilayer reference structure, has now been successfully utilized to localize the metal atoms

associated with this RuPZn cofactor along the core of the vectorially-oriented amphiphilic 4-helix bundle peptide.

The polarization-dependence of resonant SHG (840nm fundamental) from single monolayer ensembles of the vectorially-oriented RuPZn/AP0 complex has been measured both in transmission and reflection geometries. The single monolayer ensembles covalently attached to the smooth surface of fused silica were also characterized by polarized linear absorption spectroscopy and x-ray interferometry prior to the SHG measurements. Importantly, the large molecular hyperpolarizability of the cofactor was found to be preserved in the densely-packed 2-D ensembles of the complex as the incoherent sum in the macroscopic 2<sup>nd</sup>-order response for cofactor-helix mole ratios up to ~1:1. The average orientation of the long-axis of the chromophore, parallel to the bundle axis of the amphiphilic 4-helix bundle AP0 peptide, was found to be perpendicular to the plane of the monolayer. The molecular hyperpolarizability of the RuPZn cofactor vectorially-oriented within the core of the detergent-solubilized amphiphilic 4-helix bundle peptide AP0 has also been measured via hyper-Rayleigh scattering at the telecommunications relevant wavelength of 1300nm. This value at 1300nm was found to be 30x greater than that at 840nm via SHG described above.

#### Future Plans:

*Non-Linear Optics:* Prior work has shown that we can utilize computational design to control the inter-helical crossing angle in coiled-coil  $\alpha$ -helical bundles. This designed coiled-coil structure of the bundle has been shown to control the twist of extended linear multi-metalloporphyrin or metalloporphyrin-metallopolypyridyl chromophores incorporated with vectorial specificity into the core of the bundle. In addition, prior work has shown that the exterior of the bundle can be designed to facilitate the formation of ordered 2-D arrays of the vectorially-oriented peptide-chromophore complex at interfaces, e.g., solid-liquid & solid-gas. We plan to utilize this approach to create densely-packed, ordered 2-D arrays of chiral chromophores vectorially-oriented on inorganic surfaces, whose non-linear optical response is anticipated to be exceptionally large, for potential applications in electro-optic modulation.

*Light-Induced Electric Charge Separation:* Recent work has shown that cofactors possessing a donor-spacer-acceptor motif, exhibiting efficient light-induced electric charge separation *through bonds* over nano-scale distances, can be incorporated vectorially into the core of 4-helix bundle peptides. The exterior of the bundles has been designed to vectorially-orient the cofactor-peptide complex in densely-packed 2-D ensembles at interfaces, e.g., liquid-gas and solid-gas. Recent work has also shown that the separation of non-bonded cofactors along the core of such  $\alpha$ -helical bundles can be controlled by design thereby effecting vectorial electric charge separation *through space* over nano-scale distances. We plan to pursue both approaches to effectively control efficient, vectorial light-induced electric charge transport between metal/semiconductor nanoparticles and semiconductor/metal electrode surfaces.

*Crystallization in 2-D to 3-D:* Recent work has demonstrated that computational design can be employed to generate 2-D and 3-D arrays of  $\alpha$ -helical bundle proteins of macroscopic extent with long-range periodic order. The next challenge is to design these to vectorially incorporate cofactors exhibiting nano-scale electric charge separation or exceptional non-linear optical response. This approach may be a key step toward the development of protein-cofactor assemblies that spontaneously self-order into vectorially ordered arrays in two- and three-dimensions. Such highly ordered arrays of these

complexes would be essential to any coherent (as opposed to incoherent) superposition of their microscopic properties in the macroscopic response of the ensemble.

Publications 2007-2009 (Principal Investigators in **boldface**):

1. Duncan, T.V., Ishizuka, T. and **Therien**, M.J. (2007) Molecular Engineering of Intensely Near-Infrared Absorbing Excited-States in Highly Conjugated Oligo(Porphinato)Zinc-(Polypyridyl)Metal(II) Supermolecules. *J. Am. Chem. Soc.* 129: 9691-9703.
2. Bender, G.M., Lehmann, A., Zou, H., Cheng, H., Fry, H.C., Engel, D., **Therien**, M.J., **Blasie**, J.K., Roder, H., **Saven**, J.G. and **DeGrado**, W.F. (2007) De Novo Design of a Single Chain Diphenylporphyrin Metalloprotein. *J. Am. Chem. Soc.* 129: 10732-10740.
3. Zou, H., Strzalka, J., Xu, T., Tronin, A. and **Blasie**, J.K. (2007) 3-D Structure and Dynamics via Molecular Dynamics Simulation of a de novo Designed, Amphiphilic Heme Protein Maquette at Soft Interfaces. *Phys. Chem. B* 111: 1823-1833.
4. Nikiforov, M., Zerwek, U., Milde, P., Loppacher, C., Park, T-H., Uyeda, H.T., **Therien**, M.J., Eng, L. and Bonnell, D. (2008) The Effect of Molecular Orientation on the Potential of Porphyrin-Metal Contacts. *Nano Lett.* 8: 110-113.
5. Lehmann, A. and **Saven**, J.G. (2008) Computational Design of Four-Helix Bundle Proteins That Bind Nonbiological Cofactors. *Biotechnol. Prog.* 24: 74 -79.
6. **Saven**, J.G. (2008) Computational aspects of protein design. Chapter in Computational Structural Biology (eds. Manuel C. Peitsch and Torsten Schwede).
7. **Saven**, J.G. (2008) Computational approaches to protein engineering. Chapter in Protein Engineering Handbook, (ed. Stefan Lutz and Uwe Bornscheuer, John Wiley).
8. Lehmann, A., Lanci, C.J., Petty II, T.J., Kang, S.-G. and **Saven**, J.G. (2008) Computational Protein Design. Chapter in Protein Folding and Misfolding (ed. V. Munoz; Royal Society of Chemistry).
9. McAllister, K.A., Zou, H., Cochran, F.V., Bender, G.M., Senes, A., Fry, C.F., Nanda, V., Keenan, P.A., Lear, J.D., **Saven**, J.G., **Therien**, M.J., **Blasie**, J.K, and **DeGrado**, W.F. (2008) Using  $\alpha$ -Helical Coiled-Coils to Design Nanostructured Metalloporphyrin Arrays. *J. Am. Chem. Soc.* 130 (36): 11921-11927.
10. Zou, H., **Therien**, M.J. and **Blasie**, J.K. (2008) Structure & Dynamics of an Extended Conjugated NLO Chromophore within an Amphiphilic 4-Helix Bundle Peptide by Molecular Dynamics Simulation. *J. Phys. Chem. B* 112(5): 1350-1357.
11. Duncan, T. V., Song, K., Hung, S.-T., Miloradovic, I., Persoons, ., A., Verbiest, T., **Therien**, M. J. and Clays, K. (2008) Molecular Symmetry and Solution Phase Structure Interrogated by Hyper-Raleigh Depolarization Measurements: Insights for Elaborating Highly Hyperpolarizable D2 – Symmetric Chromophores. *Angew. Chemie, Int. Ed. Engl.* 47: 2978-2981.
12. Tronin, A., Krishnan, V., Strzalka, J., Kuzmenko, I., Gog, T., Fry, C., **Therien**, M.J. and **Blasie**, J.K. (2009) Portable UV-VIS spectrometer for measuring absorbance and dichroism of Langmuir monolayers. *Rev. Sci. Instru.* 80(3): 033102-1-7.
13. **Saven**, J.G. (2009) Computational protein design: advances in the design and redesign of biomolecular nanostructures. *Current Opinion in Colloid and Interface Science*, in press.

# Hyperbranched Conjugated Polymers and Their Nanodot Composites

Uwe Bunz and Vincent M. Rotello

Georgia Institute of Technology, School of Chemistry and Biochemistry,  
901 Atlantic Drive, Atlanta GA 30332

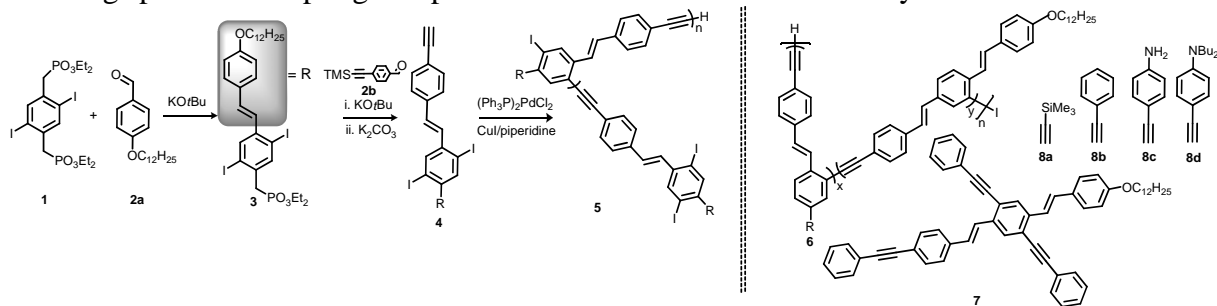
University of Massachusetts, Department of Chemistry  
501 N. Pleasant Street, Amherst MA 01003

[Uwe.bunz@chemistry.gatech.edu](mailto:Uwe.bunz@chemistry.gatech.edu)

[rotello@chem.umass.edu](mailto:rotello@chem.umass.edu)

**Program Scope:** The goals of this project are to address the synthesis and property evaluation of novel hyperbranched conjugated polymers and their self-assembly with gold nanoparticles and semiconductor quantum dots such as cadmium selenide. We are interested in the mechanisms and the control of the factors that govern the electronic interaction between nanoparticles and conjugated polymers to give bioinspired hybrid materials that combine the desired properties of the quantum dots and nanoparticles with those of organic conjugated polymers.

**Recent Progress:** *Hyperbranched Polymers.* We successfully synthesized a hyperbranched conjugated polymer, **5**; this material contains one aryl iodide group per repeat unit, which allows it to be postfunctionalized using Pd-catalyzed couplings to alkynes. We have used the four alkynes **8a-d** to prepare the polymers **9a-d** (Fig. 1) in high yield. Fig. 2 displays the emission colors of **9a-d**, and **5-7**. The polymeric iodide, **5** is almost non-fluorescent, due to the heavy atom effect allowing spin orbit coupling and promotes efficient nonradiative decay.



Scheme 1. Synthesis of the hyperbranched polymer **5**.

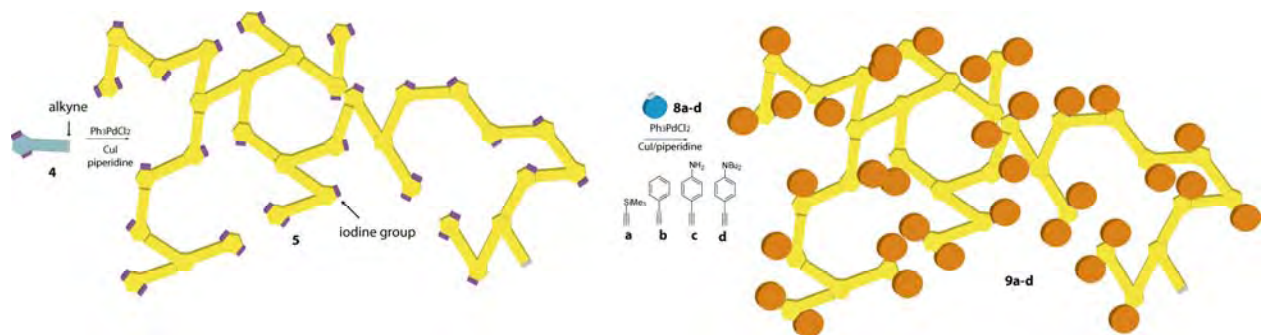


Fig 1. Synthesis of the hyperbranched polymer **9a-d**.

We have expanded the number of alkynes that we have coupled to the core **5** to give a series of other hyperbranched functionalized polymers (Fig. 3). The colors behind the structures are photographs of their emission, which can be varied from green to yellow-orange. As the molecular weight of the hyperbranched polymers is only modest, we found that **5** can be post-crosslinked by addition of 5-10% of a diethynylbenzene derivative to give polymer of significantly enhanced molecular weight. Upon addition of 10 mol% diyne  $M_n$  increases from  $1.7 \times 10^4$  to  $4.2 \times 10^4$ , and the polydispersity ( $M_w/M_n$ ) increases slightly from 1.9 to 2.3. The optical properties, i.e. absorption and emission of the crosslinked materials are also changed and the emission wavelength shifts from 501 to 515 nm. When more crosslinker is added, the materials are insoluble and form tough, solvent-swollen gels. We are currently reacting the polymer **5** with tetraalkynes to see if we can obtain soluble materials of higher molecular weight.

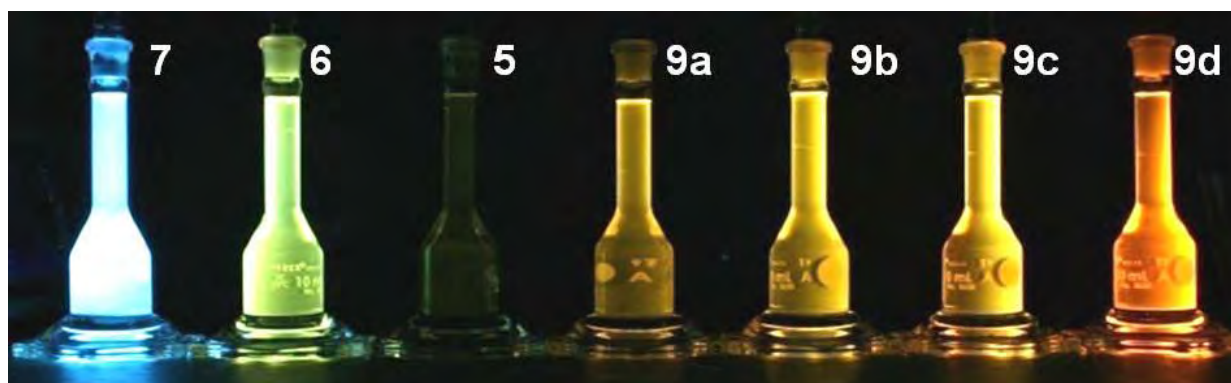


Fig 2. Photograph of solutions of **5-7** and **9a-d** in dichloromethane under a hand-held blacklight (365 nm).

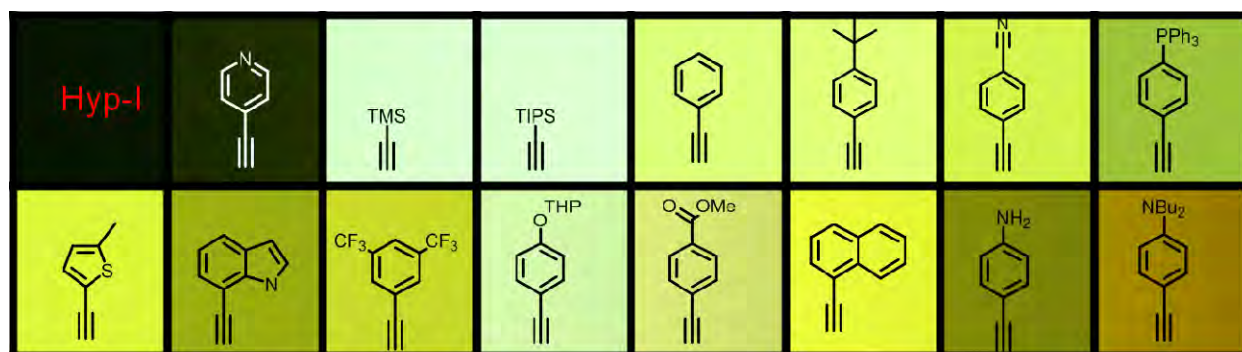


Fig 3. Photographs of solutions of further postfunctionalized

*Oxide-Nanoparticle PPE Constructs:* Nanoparticle/conjugated polymer constructs display a host of useful properties that combine the particles' properties with those of the conjugated polymer. In this case a polycarboxylated PPE. The PPE is fluorescent in water, but is quenched upon addition of 10 nm cobalt ferrite spinel NPs ( $\text{CoFe}_2\text{O}_4$ )<sub>x</sub>. This nonfluorescent construct is very effective in detecting phosphate and diphosphate-based anions, as these bind strongly to the oxide nanoparticle surface and release the bound conjugated polymer from the nanoparticles. As a consequence, the fluorescence turns on in a strongly analyte-dependent fashion. This system

can detect diphosphate in the presence of phosphate and should be of interest in potential biomedical applications to detect excess or lack of diphosphate in dialysis patients with kidney disease.

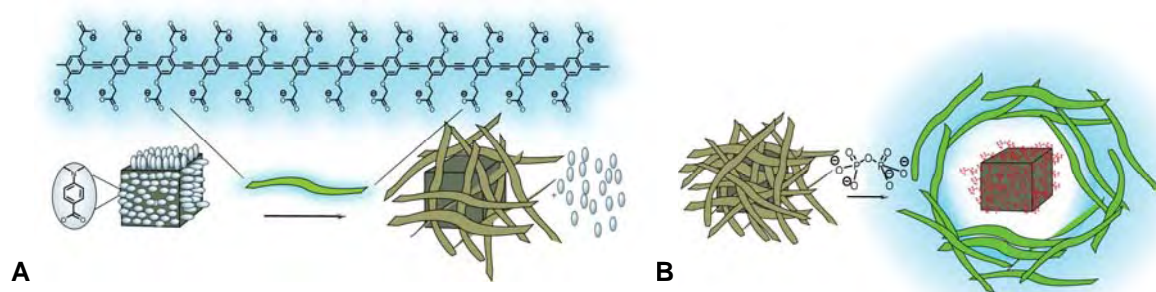


Fig. 4. a) Schematic representation for the PPE-NP construct and fluorescence quenching with conjugated polymers. A. Displacement of the DMAB by carboxylate PPE into a non-fluorescent construct. b) Working principle of the nanoparticle based displacement assay. On the left hand side is the quenched PPE-NP construct, and on the right hand side is the now pyrophosphate-decorated NP and the displaced and now fluorescent PPE.

*PPEs and gold nanoparticles:* We have investigated a series of carboxylated PPEs and their gold nanoparticle (NP) constructs and investigated the quenching ability of the gold NPs in dependence of their ligand sphere. In electrolyte free water, NPs that feature aromatic ammonium head groups bind strongest to the carboxylate substituted PPEs, while in the presence of increasing amounts of sodium chloride, cyclohexyl end capped NPs bind strongest to the PPEs.

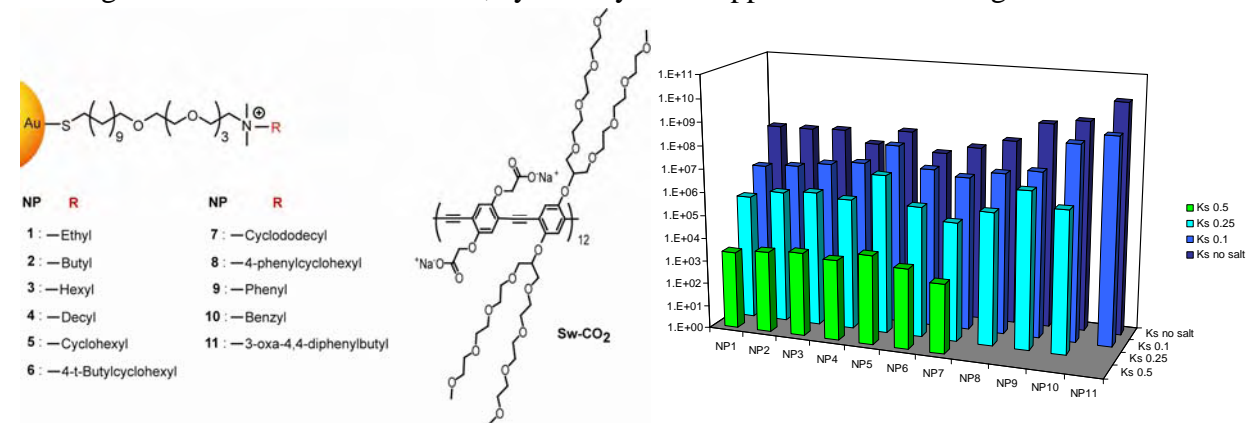


Fig. 5. Logarithmic plot of binding constants between NP1-NP11 and Sw-CO<sub>2</sub> in the presence of different concentrations of sodium chloride.

**Future Plans:** We will expand our chemistry of hyperbranched conjugated polymers and introduce specific oligoethyleneglycol groups into the supporting part of the monomer that will impart both water solubility as well increased quantum yield (in water). These monomers will be polymerized and post-functionalized with alkynes that carry groups that can interact with gold nanoparticles. We will use carboxylated alkynes that are attached in a similar fashion as shown in Fig. 5, but also nitrile and trimethylammonium substituted head groups that can interact with

neutral or anionically charged gold nanoparticles. Positively charged hyperbranched polymers can be used in connection with CdSe and CdTe nanoparticles to give novel energy transfer materials. In addition, we will investigate neutron diffraction of the gold NP polymer constructs to obtain structural information how these assembled materials order in liquid and solid phases as a consequence of their concentration.

#### **Publications 2007-2009:**

1. Detection and differentiation of normal, cancerous, and metastatic cells using nanoparticle-polymer sensor arrays, Bajaj A, Miranda OR, Kim IB, Phillips RL, Jerry DJ, Bunz UHF, Rotello VM *Proc. Nat. Acad. Sci.* 106, 10912-10916, 2009
2. Hyperbranched: A universal conjugated polymer platform, Tolosa J, Kub C, Bunz UHF *Angew. Chem.* 48, 4610-4612, 2009
3. Gold nanoparticle-PPE constructs as biomolecular material mimics: understanding the electrostatic and hydrophobic interactions, Phillips RL, Miranda OR, Mortenson DE, Subramani C, Rotello VM, Bunz UHF, *Soft Matter* 5, 607-612, 2009
4. Nano-conjugate fluorescence probe for the discrimination of phosphate and pyrophosphate, Kim IB, Han MH, Phillips RL, Samanta B, Rotello VM, Zhang ZJ, Bunz UHF, *Chem. Eur. J.* 15, 449-456, 2009
5. Sugar-substituted poly(p-phenyleneethynylene)s: Sensitivity enhancement toward lectins and bacteria, Phillips RL, Kim IB, Carson BE, Tidbeck B, Bai Y, Lowary TL, Tolbert LM, Bunz UHF, *Macromolecules* 41, 7316-7320, 2008
6. Molecular recognition based on low-affinity polyvalent interactions: Selective binding of a carboxylated polymer to fibronectin fibrils of live fibroblast cells, Mcrae RL, Phillips RL, Kim IB, Bunz UHF, Fahrni CJ *J. Am. Chem. Soc.* 130, 7851-7852, 2008
7. Fluorescence self-quenching of a mannosylated poly(p-phenyleneethynylene) induced by Concanavalin A, Phillips RL, Kim IB, Tolbert LM, Bunz UHF *J. Am. Chem. Soc.* 130 Issue: 22 6952-6954, 2008
8. Rapid and efficient identification of bacteria using gold-nanoparticle - Poly(para-phenyleneethynylene) constructs, Phillips RL, Miranda OR, You CC, Rotello VM, Bunz UHF *Angew. Chem.* 47, 2590-2594, 2008.
9. Array-based sensing of proteins using conjugated polymers, Miranda, OR, You CC, Phillips R, Kim IB, Ghosh PS, Bunz UHF, Rotello VM *J. Am. Chem. Soc.* 129, 9856-9857, 2007
10. Carboxylate group side-chain density modulates the pH-dependent optical properties of PPEs. Kim IB, Phillips R, Bunz UHF *Macromolecules* 40, 5290-5293, 2007
11. Use of a folate-PPE conjugate to image cancer cells in vitro, Kim IB, Shin H, Garcia AJ, Bunz UHF *Bioconjugate Chem.* 18, 815-820, 2007
12. Detection and identification of proteins using nanoparticle-fluorescent polymer 'chemical nose' sensors, You CC, Miranda OR, Gider B, Ghosh PS, Kim IB, Erdogan B, Krovi SA, Bunz UHF, Rotello VM *Nature Nanotechnology* 2, 318-323, 2007

## Protein Architecture for Photo-catalytic Hydrogen Production

Trevor Douglas, Mark Young, John Peters  
Montana State University  
Department of Chemistry and Biochemistry  
Bozeman, MT 59717  
[tdouglas@chemistry.montana.edu](mailto:tdouglas@chemistry.montana.edu)

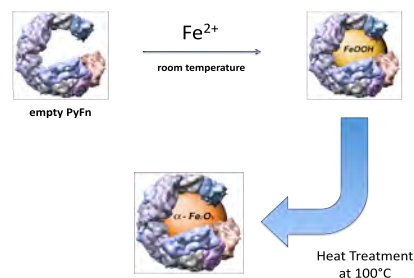
**Program Scope:** The goals of this project are to develop protein-based templates for materials synthesis towards coupled light harvesting and hydrogen formation. The focus is on utilizing hydrogenase and synthetic hydrogenase mimics for the reduction of  $H^+$  to  $H_2$  using sacrificial reductants, coupled to efficient light harvesting systems as well as the synthesis of inorganic light harvesting and catalytic materials using biomimetic methods.

**Recent Progress:** The exposed surfaces of the protein-based systems (both the hydrogenase and synthetic protein cage systems) provide a rich template for a wide range of attachment chemistries including molecular, colloidal, or solid surfaces for enhanced materials synthesis. The overall goal is to maximize the light harvesting capacity of each self-assembled protein-based catalyst for optimized and directed electron transfer to the protein-based catalysts.

*Protein cage encapsulated semiconductors:*

*Biomimetic  $TiO_2$  synthesis.* We have developed a technique that involves complexed anionic Ti(IV) bis-(ammonium lactato)-dihydroxide (Ti-BALDHI) salts which undergo conversion to nanoparticulate  $TiO_2$  within a viral protein cage template. The resultant nanoparticles, 20-24 nm in diameter, are size and shape constrained by the interior surface of the viral capsid. The Ti-BALDHI reaction product had a diffraction pattern that could be indexed to  $\beta$ - $TiO_2$  and the structure was determined using the PDF (pair distribution function) method from high-energy X-ray scattering collected at beamline 11-ID-B at the Advanced Photon Source at Argonne National Laboratories. These materials are photoactive and we have measured their photocurrent using a coupled electrochemical system, in ethanol (as sacrificial reductant) and methyl viologen as electron transfer mediator, with a transparent ITO working electrode, and ITO counter electrode and a Ag pseudo reference.

*Protein cage mediated synthesis of  $\alpha$ - $Fe_2O_3$ .* We have demonstrated that a remarkably thermal stable ferritin protein from *Pyrococcus furiosus* ( $\alpha$  hyperthermophilic archaeon) can successfully be used to synthesize uniform inorganic



Cartoon schematic for the conversion of a disordered iron oxide to an ordered photoactive iron oxide.

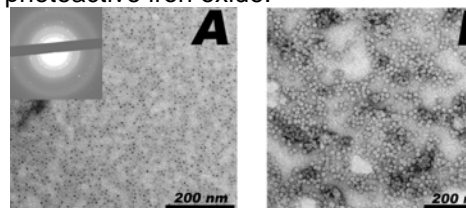


**Figure 1.** Transmission electron micrographs of (A) unstained and (B) stained refluxed Pf-Fn. The dark electron dense cores in (A) have an electron diffraction pattern (insert) consistent with  $\alpha$ - $Fe_2O_3$ .

nanoparticles under extreme synthetic conditions (**Figure 1**). The conversion of ferrihydrite (a disordered iron oxide) to hematite (ordered iron oxide) was also demonstrated at elevated temperature ( $\sim 100^\circ\text{C}$ , 1-5 days) within this protein cage template. The hematite samples exhibited behavior indicative of a visible band gap semiconductor making them of interest for energy production. Photocurrents have been measured using a coupled electrochemical system, in ethanol (as sacrificial reductant) and methyl viologen as electron transfer mediator (**Figure 2**). The ability to reduce  $\text{MV}^{2+}$  under these conditions indicates that we can couple this system to the hydrogenase to drive  $\text{H}_2$  formation.

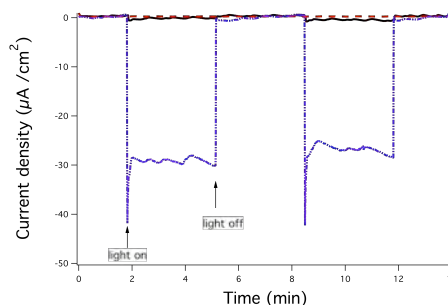


**Figure 2.** Photocurrent generated upon exposure of hematite in Pf\_Fn with methyl viologen (blue dash-dotted), ferrihydrite in Pf\_Fn (red dashed), and methyl viologen (black solid) to a high intensity LED light.

#### *Protein cage mediated synthesis of ZnSe and CdSe nanoparticles.*

Horse spleen ferritin was used as a template for the synthesis of CdSe and ZnSe nanoparticles under mild biomimetic conditions. Photocatalytic activity towards the reduction of methyl viologen ( $\text{MV}^{2+}$ ), with sodium sulfite ( $\text{Na}_2\text{SO}_3$ ) as a reductant was tested and both the Cd- and ZnSe particles were able to reduce  $\text{MV}^{2+}$  to the characteristic blue  $\text{MV}^{+}$ , demonstrating their semiconductor activity.

#### *Synthetic Coupling of Light harvesting complexes to Hydrogenase*

Covalent attachment to hydrogenase enzymes is limited by difficulties in producing heterologously expressed enzymes. We have used a two pronged approach involving pilot work targeted at providing insight into the effects of coupling model light harvesting complexes to both [NiFe]- and [FeFe]-hydrogenases that are the targets of our studies and in parallel improving the means to express hydrogenase enzymes and engineering modification sites in an informed manner.

Our initial studies on covalent attachment have used the [NiFe]-hydrogenase from *Thiocapsa roseopersicina* as a model system because it is highly stable in comparison with other [NiFe]-hydrogenases. In our pilot work the enhanced stability of this enzyme allows it to retain a significantly larger percentage of activity that other [NiFe]-hydrogenase or [FeFe]-hydrogenases upon labeling. The photocatalytic ruthenium complex ( $[\text{Ru}(\text{bpy})_2(5\text{-NH}_2\text{-phen})]^{2+}$ ) has been covalently attached to stable [NiFe]-hydrogenase from *T. roseopersicina* using 1-ethyl-3-(3-dimethylaminopropyl carbodiimide (EDC) for amide bond coupling. We have optimized the conditions for the light depended hydrogen production by the covalently modified protein with the Ru(II) complex (**Figure 3**) and have shown that labeled *T. roseopersicina* hydrogenase retains  $\sim 50\%$  of its activity after labeling. Highest activities are observed at pH 5.0 under a nitrogen atmosphere and irradiated by Xe-arc lamp. The light dependent reaction by labeled

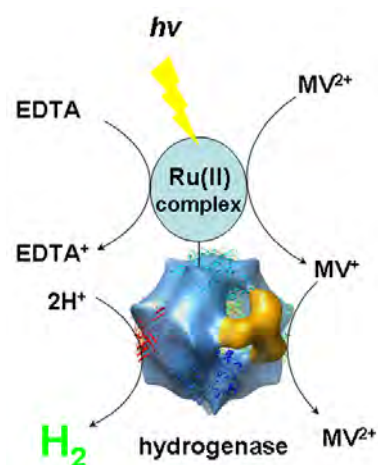


**Figure 3.** Scheme of hydrogen production by *T. roseopersicina* hydrogenase labeled with Ru(II)-complex.

hydrogenase requires an electron carrier however we have found that attachment of the Ru(II) complex to the hydrogenase greatly enhances light dependent hydrogenase activity (22X) over that of the equivalent Ru(II) complex concentrations in solution.

We will extend these studies to targeted modifications adjacent to the [NiFe] active site to facilitate direct electron transfer and eliminate the need for a redox mediator in the reaction. Structural information is not available for stable *T. roseopersicina* hydrogenase and we are therefore working toward this using both high resolution electron microscopy and x-ray crystallography. At high protein concentration (~10 mg/ml) this enzyme forms a supermolecular complex of six dimers, organized in D3 hexamer with molecular weight ~650 kDa and this supermolecular assembly is key to the observed enhanced stability of the enzyme. We have completed the structural characterization of this hydrogenase revealing the nature of the supermolecular assembly. Through this work we have been able to determine that the extended C-terminus of the small subunit is key to stability of the supermolecular complex but we have not been able to obtain a reliable enough reconstruction of the assembly based on the existing [NiFe]-hydrogenase structures to place surface exposed regions of the protein with any degree of confidence. We have however been able to implicate a specific role of the small subunit extended C-terminus in stabilizing the assembly and we are currently examining this possibility by site-specific modification studies using an over-expression system for the enzyme.

#### Other recent activities:

##### Light harvesting metal coordination polymers (bulk and protein cage encapsulated)

We have used a click chemistry approach to make protein cage encapsulated polymers and have recently made metal containing coordination polymers with control by using preformed coordination complexes and then linking them together using a ligand-ligand coupling reaction under mild conditions. We have created a series of metal-organic polymers with this approach, which includes both Fe(II) and, Ru(II) based phenanthroline complexes bearing either alkyne or azide functional groups which can then be 'clicked' together to form either a bulk polymer or a protein cage constrained polymer (**Figure 4**). These materials have high porosity, are rigidly held together and constitute a very dense arrangement of light harvesting ligands.

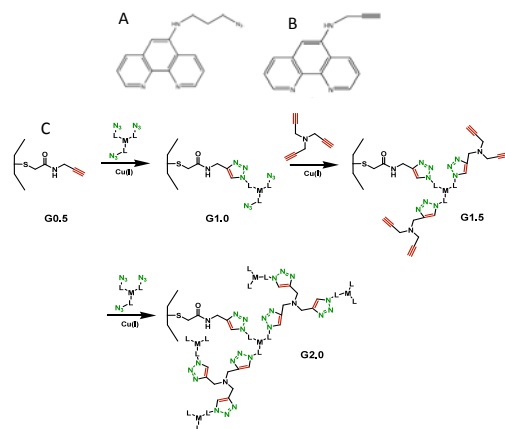


**Figure 4.** Phenanthroline ligands bearing (A) azide and (B) alkyne functionalities that can participate in the Cu(I) catalyzed click reaction (C) to form an extended porous polymer network.

#### Future Plans:

- Couple light harvesting  $\text{Fe}_2\text{O}_3$  with Hydrogenase (either the [FeFe] or the [FeNi]) to drive  $\text{H}_2$  production.
- Expand the heterologous expression of recombinant [FeFe] hydrogenase

- Complete the structural characterization of the *T. roseopersicina* hydrogenase and couple to nanoparticulate light harvesting systems.
- Expand the coordination polymers comprising light harvesting molecules and couple them to H<sub>2</sub> generating catalyst systems.

#### Publications:

1. P. Suci, M. Klem, M. Young, T. Douglas "Signal amplification using nanoplatfrom cluster formation" *Soft Matter* (2008), 4, 2519 - 2523.
2. M. Klem, J. Mosolf, M. Young, T. Douglas "Synthesis of Protein Encapsulated Nanomaterials by Photoreduction" *Inorg Chem* (2008) 47, 2237-2239.
3. Z. Varpness, C. Shoopman, J. Peters, M. Young, T. Douglas "H<sub>2</sub> catalysis by Pt nanoparticles in Ferritin" *ACS Symposium Series* (2008) 986, 263- 272.
4. M. Klem, M. Young, T. Douglas "Biomimetic Synthesis of β-TiO<sub>2</sub> Inside a Viral Capsid" *J. Materials Chem* (2008) 18, 3821-3823.
5. Sebyung Kang, Janice Lucon, Zachary B. Varpness, Lars Liepold, Masaki Uchida, Debbie Willits, Mark J. Young, and Trevor Douglas "Monitoring Biomimetic Platinum Nanocluster Formation using Non-covalent Mass Spectrometry and Cluster Dependent H<sub>2</sub> Production" *Angewandte Chemie* (2008) 47, 7845 – 7848.
6. M. Young, D. Willits, M. Uchida, T. Douglas "Plant Viruses as Biotemplates for Materials and Their Use in Nanotechnology" *Annual Reviews in Phytopathology* (2008) 46, 361-368.
7. Sebyung Kang, Luke M. Oltrogge, Chris C. Broomell, Lars O. Liepold, Peter E. Prevelige, Mark Young, and Trevor Douglas "Controlled Assembly of Bifunctional Chimeric Protein Cages and Composition Analysis using Non-covalent Mass Spectrometry" *J. Amer. Chem. Soc.* (2008) 130, 16527-16529.
8. Lars O. Liepold, Luke M. Oltrogge, Peter Suci, Trevor Douglas, Mark J. Young "Accurate Mass Assignment of Noncovalent Complexes by Electrospray Mass Spectrometry" *J. Amer. Society for Mass Spec.* (2009) 20 435-442.
9. M. Klem, P. Suci, D. Britt, M. Young, T. Douglas "In plane ordering of CCMV" *Journal of Adhesion* (2009) 85, 69-77.
10. Sebyung Kang, Craig C. Jolley, Lars O. Liepold, Mark Young, and Trevor Douglas, "From Metal Binding to Core Formation; Monitoring Biomimetic Iron Oxide Synthesis within Protein Cages using Mass Spectrometry", *Angew. Chemie.* (2009) 48, 1-6.
11. Sebyung Kang, Peter A. Suci, Chris C. Broomell, Ichiro Yamashita, Mark Young, and Trevor Douglas "Janus-like Protein Cages; Spatially Controlled Dual-functional Surface Modifications of Protein Cages" *Nano Letters* (2009), 6, 2360-2366
12. Oleg A. Zadvorny, Susan K. Brumfield, Trevor Douglas, Nikolay A. Zorin, and John W. Peters "Hydrogen Enhances Ni Ion Tolerance of Purple Sulfur Bacterium *Thiocapsa roseopersicina*" *Environmental Science & Technology* (2009) *submitted*.
13. Michael Klem, Mark Young, Trevor Douglas "Biomimetic synthesis of photoactive α-Fe<sub>2</sub>O<sub>3</sub> templated by the hyperthermophilic ferritin from *Pyrococcus furiosus*" *Advanced Materials* (2009) *submitted*.

## In situ studies of nucleation and assembly at soft-hard interfaces

Pulak Dutta

Dept. of Physics & Astronomy, Northwestern University  
2145 Sheridan Road, Evanston, IL 60208  
pducta@northwestern.edu

### Program scope

Many soft materials (whether thin films or living organisms) use hard materials for support and for added functionality, and many physical, chemical and biological processes take place at the soft-hard interface. Although traditional surface science has largely focused on hard surfaces and interfaces, the same techniques (in particular, synchrotron X-ray scattering) can be very useful for studies of soft surfaces and soft-hard interfaces.

The objective of this project is the in situ study of mineral nucleation and growth at organic surfaces. We want to learn what controls crystal orientation, shape and morphology, and to observe the surface and bulk structures and dynamics during growth. We are interested in both biology and materials science----we seek bioinspired ways to make crystalline materials using organic templates, and we also seek insights into how living organisms grow shells, bones, etc.

### Recent progress

When the subphase of a Langmuir monolayer is a supersaturated solution, crystals will nucleate preferentially under the organic monolayer, and will have specific structures (in materials where more than one crystal structure is possible), crystal orientations and morphologies. We follow this process using X-ray scattering, which averages over a large footprint and thus gives statistically significant information. We also study the finished product using optical microscopy SEM, etc..

*Calcium carbonate*: Highly oriented calcite crystals are found in shells where they provide mechanical strength, in trilobite eyes where they are used as optical elements, etc.. Biogenic calcite nucleation and growth are presumably governed in some way by the organic matrices that are found within the biomineral. These consist of macromolecules rich in acidic peptides such as aspartic acid, and sulfated polysaccharides. Therefore, ordered organic monolayers (Langmuir films) floating on supersaturated calcium carbonate aqueous solutions have been used to simulate the biological process of oriented calcite nucleation. Selected crystals have been harvested and used as evidence of templated growth,<sup>1</sup> but crystals can reorient during harvesting, there is no statistical averaging, and there is no information about the actual template structure. In situ X-ray scattering addresses all these problems.

---

<sup>1</sup> e.g. S. Mann, *Biomineralization: Principles and Concepts in Bioinorganic Materials Chemistry*, Oxford University Press, Oxford, 2001.

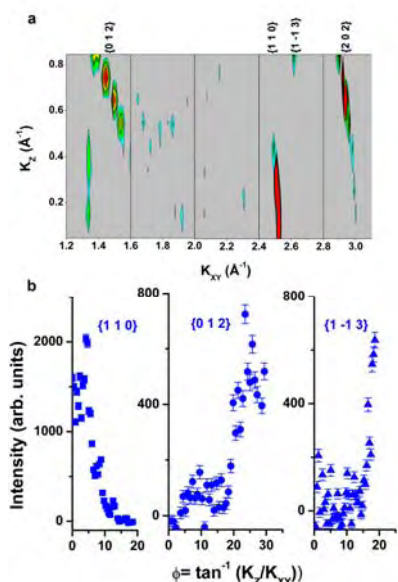


Fig. 1 Calcite structure during growth under a sulfate monolayer. (a) Contour plots derived from scattering data showing diffraction peaks from (0 0 1) oriented calcite crystals. (b) “Debye” ring scans (equivalent to rocking curves). These data indicate that calcite is (0 0 1) oriented, with a misorientation of  $\sim\pm 5^\circ$  FWHM.

There have been many reports of oriented calcium carbonate growth under fatty acid monolayers, but recent in situ studies<sup>2</sup> clearly show that there is no average preferential alignment when calcite is grown under carboxylate monolayers: the nucleate is a powder. Calcite will also nucleate under Langmuir monolayers of alkyl sulfates.<sup>3</sup> We have used in-situ grazing incidence diffraction (GID) to study the nucleation of calcite under floating arachydl sulfate monolayers. GID scans show clearly that in this case there is oriented growth in the (0 0 1) direction  $\pm 5^\circ$ . The (0 0 1) orientation is often observed in biological minerals, even though it is not stable *in vacuo*. Thus sulfate monolayers, unlike acid monolayers, can biomimetically nucleate calcite. We also see that arachydl sulfate forms a stable hexagonal monolayer structure that is precisely commensurate with the calcite (0 0 1) plane—the Ca-Ca distance on this plane and the intermolecular distance in the sulfate monolayer are both 4.99 Å, i.e. there is a 1:1 commensurate relationship.

These results have specific implications for mineral nucleation in biological systems. It is quite possible for the sulfated polysaccharide molecules found within biominerals to adopt a conformation such that the sulfates match the calcium ion positions and stabilize the (0 0 1) crystal face.

Thus, sulfate groups in biological systems may not only drive the calcium ions to the nucleation sites, but also determine the orientation of the nucleating crystal.

We also investigated the growth of calcium carbonate crystals under Langmuir monolayers in the presence of chitosan, a soluble derivative of chitin added to the subphase to better simulate the polyelectrolyte-containing *in vivo* environment. Chitosan does not change the orientation of the growing calcite crystals, and X-ray scattering shows no apparent effect. However, microscopy shows that chitosan causes dramatic concentration-dependent changes in the orientation, shape and morphology of the calcite crystals nucleating under acid and sulfate monolayers. Our results suggest that polyelectrolytes can and perhaps do play major roles in controlling the growth of biogenic calcite crystals. Curiously, the sequence of crystal shapes we saw closely tracked those seen by Pokroy and Aizenberg<sup>4</sup> as a function of self-assembled template spacing. In that paper it was postulated that increasing lattice mismatch caused increasing



<sup>2</sup> E. Dimasi, M. J. Olszta, V. M. Patel and L. B. Gower, *CrystEngComm*, **5**, 346 (2003); J. Kmetko, C.-J. Yu, G. Evmenenko, S. Kewalramani and P. Dutta, *Phys. Rev. B* **68**, 085415 (2003)

<sup>3</sup> e.g. S. Mann, *Biomineralization: Principles and Concepts in Bioinorganic Materials Chemistry*, Oxford University Press, Oxford, 2001.

<sup>4</sup> B. Pokroy and J. Aizenberg, *Crystengcomm*, **9**, 1219 (2007)

strain, which led to each of these shapes being sequentially favored. In our experiments we have no rigid substrate to which the template molecules are tethered. However, these results can still be related to those by postulating that the driving force is the organic-inorganic interface tension (energy).

*Barium chloride and fluoride:* Our earlier studies<sup>5</sup> had established that barium and strontium fluoride grow oriented crystals under heneicosanoic acid Langmuir monolayers, and that this happens because there is epitaxy. In the case of BaF<sub>2</sub>, supersaturated solutions are prepared by mixing BaCl<sub>2</sub> and HF, but the compound BaFCl, which has low solubility, doesn't nucleate. The interface selects not just a specific orientation but also a specific mineral. The bulk BaClF (001) square unit face has exactly half the area of the BaF<sub>2</sub> (100) square unit face. Thus geometric match alone cannot explain the preferential nucleation of BaF<sub>2</sub>. When the pH is lowered to ~5.8, we see that *both* materials grow oriented crystals at the interface. From these studies we are learning more about how crystal growth can be directed.

*Self-assembled monolayers and multilayers:* We have been collaborating with the van der Boom group at the Weizmann Institute, Israel to develop strategies for self-assembling organic structures and to establish the success of these techniques through X-ray studies. For example, we have demonstrated the optical detection of parts-per-million (ppm) levels of CO by a structurally well-defined monolayer consisting of bimetallic rhodium complexes on glass substrates. Multilayer assemblies with molecular-level organization based on organic chromophores and a bimetallic palladium complex have been assembled using a layer-by-layer strategy on quartz and silicon substrates functionalized with a covalently-bound template layer. The long-range order of the system is determined by the structure of the chromophores and by the square-planar geometry of the metal centers. We have also collaborated with the group of Tobin Marks, Chemistry Department, Northwestern University on the use of self-assembled electroactive monolayers as a way to measure the electroactive coverage and electron transfer rate of various transparent oxides (ITO, CdO, ZITO).

## Future plans

*Template-directed nucleation:* Since a Langmuir monolayer is 'soft', its structure are easily changed. It is reasonable to expect that different phases may nucleate different compounds (subject to the available ingredients) or polymorphs, or at least different crystal faces. We propose to explore this possibility in detail. We also plan to study biominerals other than calcium carbonate. Specifically, calcium oxalate (used in plants, and also appearing as kidney stones); calcium phosphate (hydroxyapatite, the primary constituent of bone), and iron oxide (magnetite, used by many organisms for navigation) will be studied.

*From superlattice to crystal:* When fatty acid monolayers are spread on dilute solutions of various salts, a large number of in-plane diffraction peaks appears, and these can be indexed as a two-dimensional supercells of the Langmuir monolayer structure. This is a mystery: the ions are not large enough to justify such a large unit cell, and no such structures have been seen in bulk

---

<sup>5</sup> J. Kmetko, C. Yu, G. Evmenenko, S. Kewalramani and P. Dutta, *Phys. Rev. Lett.* **89**, 186102 (2002); J. Kmetko, C.-J. Yu, G. Evmenenko, S. Kewalramani and P. Dutta, *Phys. Rev. B* **68**, 085415 (2003)

crystals of these materials. We plan to follow the evolution of the metal-ion structure from a monolayer to the bulk crystal, by varying subphase concentration.

*Organic deposition at inorganic surfaces:* We would like to look at sulfate monolayers transferred by the LB method to clean calcite surfaces, to see what order is induced in the organic film. We would also like to study organic deposition from aqueous solutions. Organic and inorganic components are interleaved within biominerals, so although this proposal is primarily focused on hard-material deposition at soft surfaces, the reverse process is also of interest. Such deposition may have environmental/geochemical relevance as well.

### **DOE-supported publications, 2007-present**

“Pathways for oriented assembly of inorganic crystals at organic surfaces”, Sumit Kewalramani, Jan Kmetko, Geoffrey Dommett, Kyungil Kim, Guennadi Evmenenko, Haiding Mo, and Pulak Dutta, *Thin Solid Films* **515**, 5627 (2007)

“Mechanisms for species-selective oriented crystal growth at organic templates”. Sumit Kewalramani, Kyungil Kim, Guennadi Evmenenko, Paul Zschack, Evguenia Karapetrova, Jianming Bai and Pulak Dutta, *J. Mat. Res.*, **22**, 2785 (2007)

“Observation of an organic-inorganic lattice match (templating) during biomimetic growth of (0 0 1)-oriented calcite crystals under floating sulfate monolayers”, Sumit Kewalramani, Kyungil Kim, Benjamin Stripe, Guennadi Evmenenko, Geoffrey H. B. Dommett and Pulak Dutta, *Langmuir* **24**, 10579 (2008)

"Self-Propagating Assembly of a Molecular-Based Multilayer", L.Motiei, M.Altman, T.Gupta, F.Lupo, A.Gulino, G.Evmenenko, P.Dutta, M.E. van der Boom, *J. Am. Chem. Soc.***130**, 8913 (2008)

"Molecular assembly of a 3D-ordered multilayer", M.Altman, O.Zenkina, G.Evmenenko, P.Dutta, M.E. van der Boom, *J. Am. Chem. Soc.* **130**,5040 (2008)

"Selective monitoring of parts per million levels of CO by covalently immobilized metal complexes on glass", Antonino Gulino, Tarkeshwar Gupta, Marc Altman, Sandra Lo Schiavo, Placido G. Mineo, Ignazio L. Fragalà, Guennadi Evmenenko, Pulak Dutta and Milko E. van der Boom, *Chem. Commun.* **25**, 2900 (2008)

"Characterization of transparent conducting oxide surfaces using self-assembled electroactive monolayers", J.Li, L.Wang, J.Liu, G.Evmenenko, P.Dutta, T.J.Marks, *Langmuir* **24**, 5755 (2008)

“Effects of chitosan on the morphology and alignment of calcite crystals nucleating under Langmuir monolayers”, Kyungil Kim, Ahmet Uysal, Sumit Kewalramani, Benjamin Stripe and Pulak Dutta, *CrystEngComm*, **11**, 130 (2009)

“Positive Constructs: Charges Localized on Surface-Confined Organometallic Oligomers”, Marc Altman, Olena Zenkina, Takahito Ichiki, Mark Iron, Guennadi Evmenenko, Pulak Dutta, Milko Van der Boom, *Chem. Mater.*, accepted for publication

# Modular Designed Protein Constructions for Solar Generated H<sub>2</sub> from Water

P. Leslie Dutton

University of Pennsylvania  
Department of Biochemistry and Biophysics  
Philadelphia PA 19104  
[dutton@mail.med.upenn.edu](mailto:dutton@mail.med.upenn.edu)

**Program Scope:** We aim to design and engineer artificial proteins equipped to promote light-activated charge separation and concomitant generation of stable strongly oxidizing and reducing cofactors. We intend to couple separated oxidizing and reducing power via electron tunneling chains to sites catalyzing bond-breaking/forming redox chemistry. A principle challenge is to split water into its elements, oxygen and hydrogen.

## Recent progress:

We are developing the practical understanding of protein as a material for construction and as a medium for electron tunneling over nanometer distances, electron tunneling coupled to protons and activation of redox chemistry in the confines of a catalytic site. Despite the apparent complexity of natural protein structures revealed by x-ray crystallography, we have found that artificial protein (maquette) as a material does not require a high degree of structural precision for ligand binding and activity. We have also found that simply constructed artificial proteins are rather easily supplied with sufficient dynamics for activity associated with catalysis, and that simple principles such

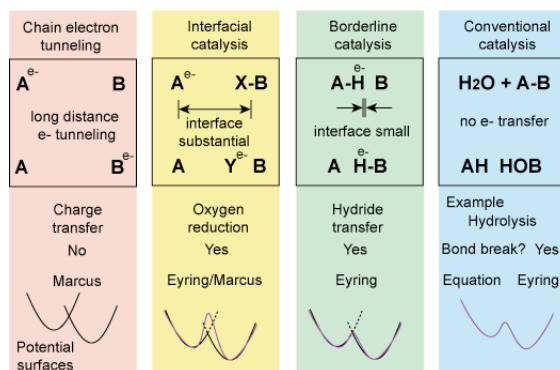


Figure 1

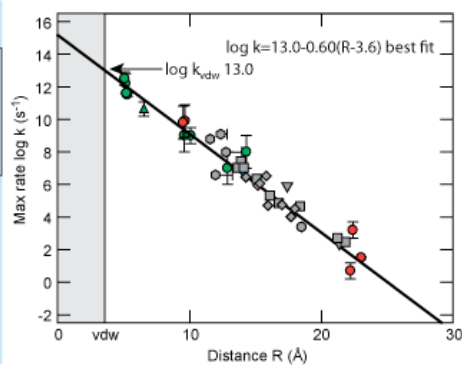


Figure 2

as strain can be built into the maquette protein frameworks. Furthermore, we have found that it is possible to control the dielectric and proton availability of maquette interiors that are important in the design of buried catalytic sites. The progress from the well-understood engineering of electron tunneling between one- electron redox centers in

proteins to the engineering of multi-electron catalytic sites goes through 4 stages (Figure 1).

We described our latest understanding of long distance, chain one-electron tunneling (column 1 of figure 1) in a recent report (ref 2) that focused on the important metric of distance. We find a remarkable superposition of rate-distance tunneling data of Gray from ruthenated redox proteins and our own data from photosynthetic reaction centers (Figure 2). With this strengthened generality of our empirical tunneling expressions, we have recently (C.C Moser, L.N.R. Anderson and P.L. Dutton *Biochim Biophys Acta*) merged Marcus electron tunneling theory with Eyring's general chemical catalysis (columns 2 and 3). We introduce a second kappa related to electron tunneling through the insulating protein medium that profoundly modulates the prefactor ( $\kappa k_B T / h$ ) in Eyring's transition state theory absolute rate expression. This allows us to separate out electron tunneling energetics from adiabatic bond making and breaking energetics. Moreover we have mapped out the energetic boundaries of the transition between sequential two-electron ( $H^+$ ) transfer and the concerted hydride transfer common for  $NAD^+/NADH$ , important in the engineering of strongly reducing electron transfer (column 3).

We have also made use of the resulting empirical tunneling expression tools to appraise natural redox enzymes. We can now see in quantitative terms that Nature does not evolve enzymes to be perfect or optimal but instead to be adequate with plenty of leeway for structural and environmental variance. Natural proteins are generally built to standards of adequacy, accompanied by broad engineering tolerances. This may explain why there is such a range of functional enzymatic variations on any particular catalytic theme in Nature. Despite deliberate efforts in multiple laboratories to alter the catalytic characteristics of enzymes, success has been relatively limited. As we have recently discussed (ref 3), we consider the trouble to be that evolution tends to develop strong, irreversible interdependencies between amino acids in a nature protein, analogous to that described in genetic systems by Muller. Interdependencies also arise simply because amino acids typically serve multiple functions and utilities in a way analogous to the organism scale description by Darwin. These interdependencies between amino acids both adjacent and non-adjacent are a common root of complexity in proteins that can be expected to deeply compromise efforts to re-engineer natural protein for new purposes as well as efforts to reproduce exacting mimics of enzyme catalytic sites in new scaffolds.

However common it may be in nature, we maintain that complexity is not an essential feature of protein as material for construction or enzyme activity. This strengthening view is the foundation of this grant aiming to design and create simple artificial working proteins (called maquettes) that support catalytic functions familiar in nature. While we recognize that complexity cannot be entirely avoided in any designed protein, management of the Muller/Darwinian sources is crucial (ref 3). This leads us to build maquettes from scratch: we commence with the simplest amino acid sequences, avoid natural selection and minimize amino acid multiple utility. Maquettes under development display redox functional characteristics that are within the tolerances of structure and engineering that we identified in natural redox enzymes.

Recent developments toward the creation of new proteins with tailored functionalities include:

**Design and engineering of an O<sub>2</sub> transport protein (Ref 2).** This paper validates our approach sharply contrasting it with other protein design or redesign methods in maintaining the simplicity and minimizing complexity typical of native proteins. Thus we started from a functionally featureless peptide comprising just three different amino acids with a length and sequence selected to ensure association as a water-soluble, molten globular four- $\alpha$ -helical bundle, to produce a heme-containing protein maquette with native-like tertiary structure that performs the myoglobin-like function of dioxygen binding to the ferrous heme. Two critical elements are included. One created a strained bis-histidine-heme ligation sufficient to support oxygen displacement of a histidine and binding. Another element was introduced to restrict inter-helix motion and renders the oxyferrous-heme state stable at 16°C. Restriction of this motion is crucial as water penetration is minimized for stable oxyferrous-heme formation. This demonstration represents a major step forward for the engineering of catalytic new proteins.

**Covalently linked and non-natural redox and light excitable cofactors (refs 1, 4, 5).** Incorporation of covalently linked redox cofactors (natural and non-natural) to the protein brings greater choice in positioning the cofactors in or on the protein, alternative possibilities to confer higher stability to the functionalized protein as well as new chemical functions. As Figure 3 shows this includes the di-iron hydrogenase catalytic unit (non active; ref 1), a naphthoquinone amino acid (Naq; ref. 4) and flavins (see ref 5) and most recently to successful expression in *E. coli* of an iron-porphyrin thiolate-linked (heme C) to a single chain protein variant of the protein used as an O<sub>2</sub> transporter. Its anaerobic E<sub>m8</sub> value is higher than most of its di-vinyl heme B counterparts in the O<sub>2</sub> transporter protein. But like its heme B counterparts, it also forms a stable ferrous oxy state, implying little or no disruption to the structure. We are at the present working to exchange the central Fe atom of the porphyrin for a Zn in order to create the first covalently linked Zn-porphyrin for light-activation in an artificial protein. The production and initial characterization of this artificial cytochrome *c* will be described in an upcoming paper to be submitted to Proc. Natl. Acad. Sci. USA, authored by Ross Anderson, Bruce Lichtenstein, Tammer Farid, Chris Moser and Leslie Dutton

**Single-chain four-helix bundles:** The achievement of single chain 4-helix bundle proteins escapes the restrictions of the symmetric structures we have used so far, opening up design options. Work on single chain bundles, as indicated with the *E. coli* expressed covalent heme C expression mentioned above, are well on their way. The work on and the intein extensions required by the inclusion of Naq are also proceeding well.

**Amphiphilic maquettes:** We have synthesized a new set of amphiphilic maquettes (AP6 series). These assemble as four helix bundles in detergent and membrane and ligate up to six ferric hemes B. The AP maquettes co-solubilize with synthetic diblock copolymers or lipids at an air-water interface, where they compress to a specific surface pressure for transfer to highly ordered pyrolytic graphite surfaces by Langmuir-Blodgett techniques. We are currently testing several scanning probe microscopy techniques that allow measurement of the electrical properties of the films. This work describing the assembly and electrochemical characterization of biomolecular electronic interfaces from redox-active protein maquettes incorporated into lipid monolayers is a collaboration with Prof. Dawn Bonnell at the Department of Materials Science and Engineering at Penn and it

will be submitted to Nano Letters: M.P. Nikiforov, D.A. Bonnell, P.L. Dutton, B.M. Discher.

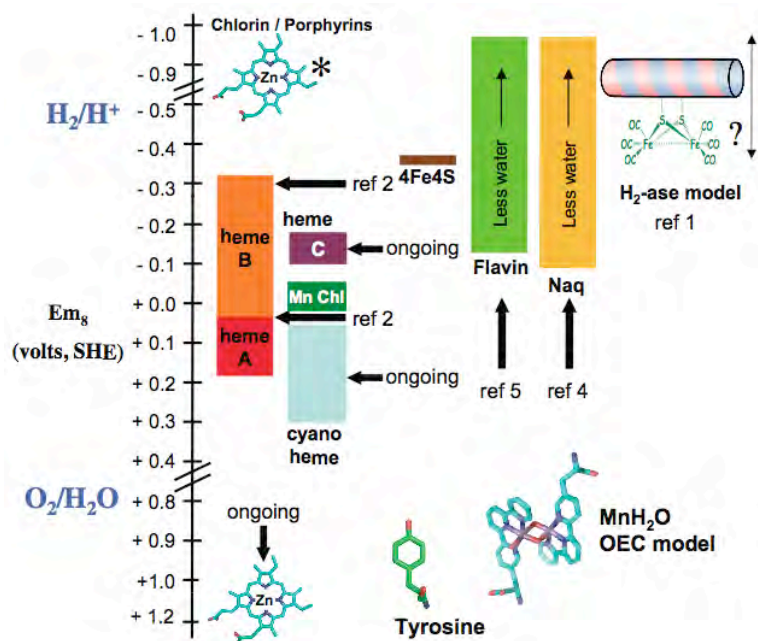


**Figure 3** Summary of redox potentials of cofactors incorporated or under development for incorporation in maquette proteins. The rectangles represent the range of redox midpoint potential values encountered for the hemes/porphyrins in other maquettes. The heme C potential was obtained from an expressed single chain four helix bundle as our ongoing work. The ranges seen for flavin and quinone are dependent on water content. The irons of hemes (Fe porphyrins) exchange their Fe for Zn and 5-coordinate ligation

### DOE-BES Bibliography 2007-2009

1. *Synthetic Hydrogenases: Incorporation of an Iron Carbonyl Thiolate into a Designed Peptide*. Jones, A.K., Lichtenstein, B.R., Dutta, A., Gordon, G. and Dutton, P.L. J. Am. Chem. Soc. (Communication).
2. *Distance Metrics for Heme Protein Electron Tunneling*. Moser, C.C., Chobot, S.E., Page, C.C. and Dutton, P. L. Biochem. Biophys. Acta, 1777: 1032-1037, 2008.
3. *Design and Engineering of an O<sub>2</sub> Transport Protein* Koder, R.L., Anderson, J.L.R., Solomon, L.A. Reddy, K.S., Moser, C.C. and Dutton, P.L., Nature, 458, 305-309, 2009
4. *Reversible Proton Coupled Electron Transfer in a Peptide-incorporated Naphthoquinone Amino Acid*. Lichtenstein, B.R., Cerda, J.F., Koder, R.L., and Dutton, P.L. The Royal Society of Chemistry, Chemical Communication, 170, 168-170, 2008.
5. *Hydrogen Bond-Free Flavin Redox Properties: Managing Flavins in Extreme Aprotic Solvents*. Cerda, J. F., Koder, R. L., Lichtenstein, R.R., Moser, C. C. Miller, A-F, and Dutton, P. L. Organic and Biomolecular Chemistry, 6, 2204-2212, 2008.

# Material lessons of biology: Structure-function studies of protein sequences involved in inorganic - organic composite material formation.

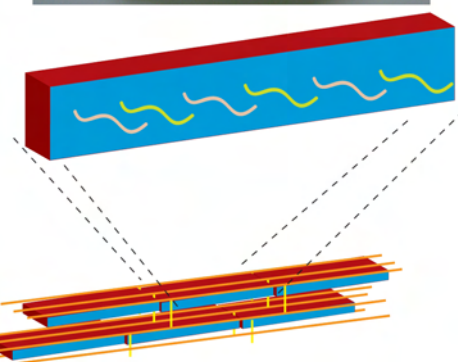
John Spencer Evans

New York University  
Laboratory for Chemical Physics  
345 E. 24<sup>th</sup> Street, Room 1007 NY, NY 10010  
jse1@nyu.edu

**Program Scope:** The goals of this project are to determine the molecular mechanisms of protein-mediated mollusk shell nacre layer fracture resistance and inorganic polymorph selection.

**Recent Progress:** The mollusk shell is a true biocomposite that is comprised of two physically distinct layers of calcium carbonate that co-exist with a series of biomacromolecules. The nacre layer of the shell (Figure 1) is comprised of the calcium carbonate polymorph, aragonite, which is thermodynamically unstable. Moreover, the nacre layer is fracture-resistant (3000 x > pure aragonite) and exhibits crack deflection and energy dissipation. These properties arise from the presence of proteins which either inhabit the aragonite crystals (intercalation) or the space surrounding these crystals.

**Figure 1:** Mollusk shell nacre layer (*H. rufescens*). TOP: Macroscopic view of shell layer. BOTTOM: Cartoon microscopic view of aragonite crystals (blue) coated with protein biofilm (red) and polysaccharide (orange). Intracrystalline proteins within aragonite are represented as squiggles.



How do biomacromolecules impart fracture resistance to the nacre and achieve phase stabilization? Recent studies suggest that some nacre proteins provide adhesion and elasticity between aragonite crystals thus allowing deformation and nanograin rotation under force and the resultant dissipation of energy. Moreover, there are other nacre proteins which are entrapped or occluded within aragonite crystals leading to anisotropic distortions in the crystal lattice, which in turn change the bulk properties of these crystals. The stabilization of the thermodynamically unstable aragonite polymorph also is controlled by these proteins.

Our working hypothesis is that fracture resistance, nucleation, and polymorph selection are controlled, in part, by the structural features of these nacre proteins. Perhaps the biggest breakthrough in this area came with the realization that the unfolded, conformationally labile structures of nacre protein sequences share some common features with another set of important proteins known as intrinsically disordered or unfolded proteins (IDP). IDPs are

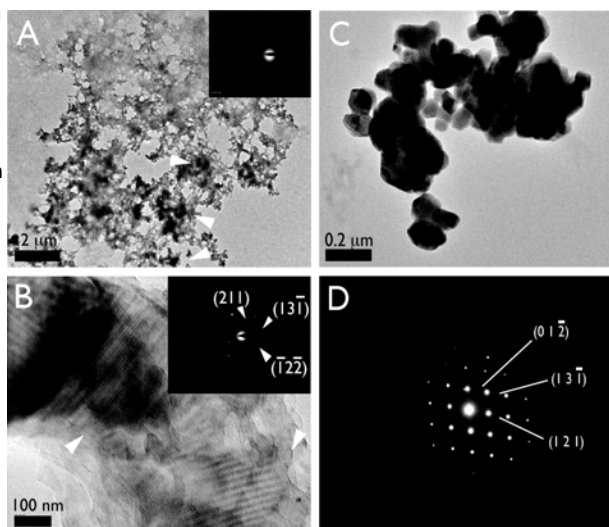
associated with many intracellular regulation processes including transcription, protein assembly, and protein activation or deactivation. These proteins have a unique amino acid composition that favors disorder-promoting residues (E, D, K, R, G, M, Q, S, P) and minimizes the inclusion of order-promoting residues (W, Y, H, T, F, C, I, L, N). A key concept in the IDP story is that unfolded sequences offer extreme adaptability to a number of potential targets (e.g., proteins, cell receptors, ligands, etc.) and often undergo disorder-to-order conformational transformations upon binding to these targets. Given this new twist to structural biology, our group began to realize that many biomineralization protein sequences that we've worked with fall into the IDP category. We now believe that nacre fracture resistance and inorganic phase stabilization are controlled by the intrinsic disorder of nacre proteins.

## Recent Activities

**Identifying and characterizing nacre IDP sequences.** Our group identified that the mineral-interactive 30 AA N-terminal sequences of aragonite-associated proteins AP7, AP24, nI6N are intrinsically disordered. We named these N-terminal sequences AP7N, AP24N, and nI6N, respectively. Subsequently, we established that the 66 AA AP7 protein is partially disordered and contains a Cys, His - Zn (II) binding C-RING protein-protein interaction domain found in a number of intracellular proteins. We investigated the nacre-associated ACC binding protein (ACCBP) of *P. fucata* which is homologous (30% conserved) to acetylcholine binding proteins. Sequence homology modeling prediction methods tell us that ACCBP adopts an acetylcholine receptor-like folded structure, yet possesses several short sequence regions that are intrinsically disordered. We confirmed these predictions by chemically synthesizing one of the predicted ACCBP disordered regions, namely, the 50 AA mature N-terminal sequence hereafter referred to as ACCN. The ACCN domain exists in a partially disordered conformation that includes random coil and some percentage of alpha-helix.

**Phase stabilization by nacre protein sequences.** For several years we have utilized Kevlar threads as nucleation sites for evaluating *in vitro* calcium carbonate crystal growth. Recently, we shifted

**Figure 2:** AP7-induced mineralized assemblies. (A) Type "A", amorphous-appearing, no diffraction pattern observed (inset); (B) Type "B", organized mineralized plates, aragonite diffraction observed (inset); (C) another Type "B", featuring hexagonal platelet clusters that give rise to (D) aragonite diffraction pattern.<sup>4</sup> Note that these assemblies do not form under negative control conditions.



our focus to nucleation in solution. What we found was quite surprising: in all three cases we detected the presence of supramolecular assemblies that contain either aragonite or amorphous calcium carbonate (ACC). These types of assemblies do not form in negative control assays (no peptide added). Given the discovery of protein films and silk fibroin gels

within the mollusk nacre layer, our findings support the hypothesis that protein assemblies are the key to phase stabilization processes. Here's a summary of our findings:

**AP7:** Three types of supramolecular assemblies were identified: an amorphous type (Figure 2A) and two crystalline types which contain aragonite in either as polycrystalline oriented multiple platelets (Figure 2B) or as clusters of single crystals (Figure 2C), both of which possess anisotropic lattice distortions arising from protein occlusion.

**nI6N:** We observed nI6N mineralized films to “coat” Kevlar-templated calcite crystals (Figure 3A-C). XANES measurements confirm that this deposited film is *stabilized ACC* (Figure 3D).

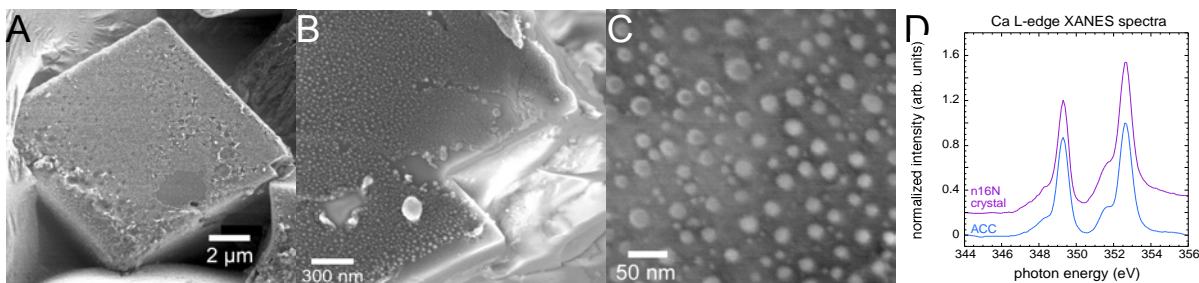
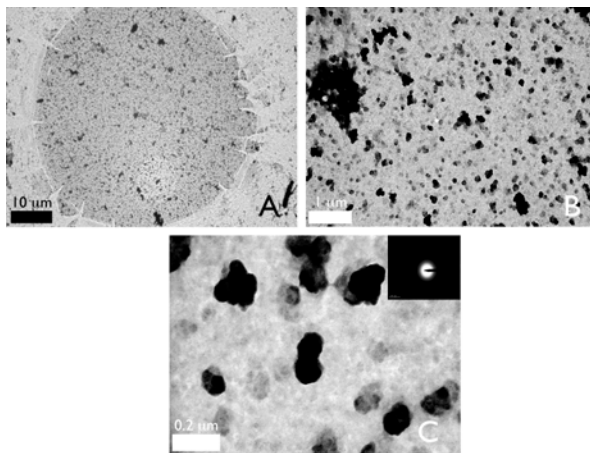


**Figure 3:** SEM images of a calcite crystal grown in the presence of the nI6N peptide. (A) Note roughened surface layer on the exposed (104) face. (B, C) Higher magnification of the same crystal, showing the film-coated surface. (D) Surface-sensitive Ca XANES spectrum from the same crystal, compared to synthetic amorphous calcium carbonate (ACC). The spectrum from the film-coated crystal is very similar to ACC.

**ACCN:** The ACCBP protein modifies calcite morphologies and stabilizes ACC but does not generate a crystalline mineral phase. In our lab, the trend is similar: ACCN forms mineralized supramolecular assemblies that contain electron dense spherical particles that do not give rise to a detectable electron diffraction pattern (Figure 4). Hence, we believe that the ACCN peptide mimics the activity of ACCBP, i.e., stabilizes an amorphous phase without further phase transformation.

**Figure 4:** TEM images of supramolecular aggregates formed by ACCN (100 micromolar) *in vitro*. (A) Low magnification image of representative aggregate that deposited onto grids. (B), (C) Higher magnification images showing numerous spherical or clustered spherical electron dense deposits suspended within the aggregate; inset image in (C) amorphous diffraction pattern taken of representative electron dense particles.<sup>3</sup>



The fact that mineralized protein supramolecular assemblies have also been identified in biomineralization systems such as silicates, calcium carbonates, calcium phosphates, and now calcium carbonates suggests that protein assemblies plays an important role in biocomposite inorganic material formation in Nature and may prove to be important models for the formation of new materials or nanodevices with energy applications.

**Future plans:** We will establish the mechanisms involved in nacre protein self-assembly, how polypeptides stabilize ACC versus aragonite, and whether or not ACC serves as a precursor for aragonite.

### **Publications from DOE funding (2007-2009)**

- (1) Keene, E.C., Evans, J.S., Estroff, L.A. (2009) Phase stabilization by a nacre polypeptide associated with a chitin polysaccharide framework. *Langmuir*, in press.
- (2) Metzler, R.A., Evans, J.S., Zhou, D., Appathurai, N.P., Coppersmith, S.N., Gilbert, P.U.P.A. (2009) Lamellar self-assembly and aragonite polymorph selection by a single intrinsically disordered protein fragment. *JACS*, in press.
- (3) Amos, F.F, Ndao, M., Evans, J.S. (2009) Evidence of mineralization activity and supramolecular assembly by the N-terminal region of ACCBP, a biomineralization protein that is homologous to the acetylcholine binding protein family. *Biomacromolecules*, in press.
- (4) Amos, F.F, Evans, J.S. (2009) AP7, a partially disordered pseudo C-RING protein, is capable of forming stabilized aragonite *in vitro*. *Biochemistry* 48, 1332-1339.
- (5) Evans, J.S., (2008) "Tuning in" to mollusk shell nacre- and prismatic-associated protein terminal sequences. Implications for biomineralization and the construction of high performance inorganic-organic composites. *Chem. Rev.* 108, 4455-4462.
- (6) Collino, S., Evans, J.S., (2008) The molecular specifications of a mineral modulation sequence derived from the aragonite-promoting protein, n16. *Biomacromolecules* 9, 1909-1918.
- (7) Collino, S., Kim, I.W., Evans, J.S. (2008) Identification and structural characterization of an unusual RING-like sequence within an extracellular biomineralization protein, AP7. *Biochemistry* 47, 3745-3755.
- (8) Metzler, R.A., Kim, I.W., Delak, K, Evans, J.S., Zhou, D., Beniash, E., Wilt, F., Abrecht, M, Chiou, J-W, Guo, J, Coppersmith, S.N., Gilbert, P.U.P.A. (2008) Probing the organic-mineral interface (OMI) at the molecular level in model biominerals. *Langmuir* 24, 2680-2687.
- (9) Collino, S., Evans, J.S. (2007) Structural features that distinguish kinetically distinct biomineralization polypeptides. *Biomacromolecules* 8, 1686-1694.
- (10) Delak, K, Collino, S, Evans, JS (2007) Expected and unexpected effects of amino acid substitutions on polypeptide – directed crystal growth. *Langmuir* 23, 11951-11955.
- (11) Kulp, JL III, Minamisawa, T, Shiba, K, Evans, JS (2007) Conformational properties of an artificial protein that regulates the nucleation of inorganic and organic crystals. *Langmuir* 23, 3857-3863.

# In Vitro Evolution of Catalysts for the Production and Utilization of Alternative Fuels

Dan Feldheim and Bruce Eaton  
Department of Chemistry and Biochemistry  
University of Colorado  
Boulder, CO 80309  
Daniel.Feldheim@Colorado.edu  
Bruce.Eaton@Colorado.edu

## Program Scope

The extraordinary materials found in our biosphere have inspired a growing research effort in which biomolecules are used to synthesize and assemble materials in the laboratory. Peptides, nucleotides, RNA, DNA, and proteins have all been shown to be capable of mediating the formation of nanoscale materials with atypical morphologies, crystal structures, and sizes that have resulted in some instances in unexpected properties. In addition to potentially affording more environmentally benign routes to novel inorganic materials, the highly selective recognition capabilities of biomolecules are proving to be useful in the assembly of nanoscale materials into more complex functional assemblies and devices.

The central premise of this project is that biological macromolecules can evolve in vitro in response to selection pressures to synthesize materials with desired catalytic activities. Prior results from our labs have shown that RNA has the remarkable ability to

catalyze and/or mediate the formation of a variety of inorganic nanoparticles and control nanoparticle size, shape, and physical properties. Our recent work has focused on understanding how the selected sequences function and developing new methods for exploiting these biomolecules in the assembly of novel photocatalyst systems.

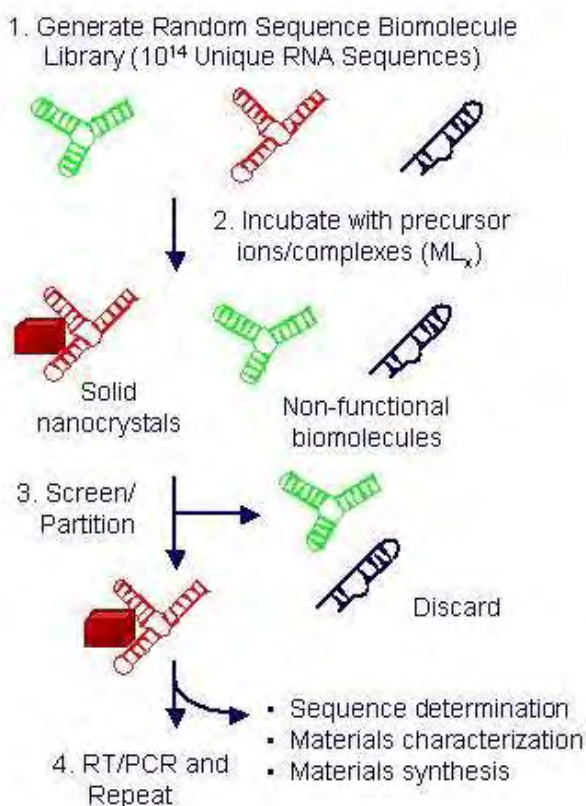


Figure 1. The RNA in vitro selection cycle for discovering new materials.

## Recent Progress

*RNA In Vitro Selection in Materials Discovery.* The RNA in vitro evolution approach to catalyst discovery begins by synthesizing a library of  $10^{14}$  unique RNA sequences (Figure 1). We are not limited to the native RNA bases when generating the RNA library because the Eaton lab has developed novel methods for modifying uridine with >30 different functional groups. When incorporated into RNA these moieties can aid in the formation of inorganic materials. The RNA library is then exposed to an array of different solutions containing

inorganic precursors (e.g., metal salts and organometallic complexes), resulting in nucleation and inorganic cluster growth on the functional RNA sequences. However, because each RNA sequence in the initial mixture differs in primary sequence and 3D structure, many different inorganic crystal types are possible. In fact, our expectation is that different sequences will mediate the formation of nanocrystals that differ in size, shape, or physical properties; of course many of the initial  $10^{14}$  RNA sequences will also be incapable of nucleating a crystal. A separation is then performed to isolate the desired particles. For example, in “selection cycle 1” RNA sequences not bound to a crystal are easily removed by centrifugation. These sequences are said to be “selected” out; that is, only those sequences that grow crystals survive and are carried forward to the second cycle. The RNA that is carried forward may constitute a minor fraction of the overall sample. However, it can be reverse transcribed into cDNA, amplified using the polymerase chain reaction (PCR), and converted back into RNA for the next cycle. In subsequent cycles, more stringent selection pressures may be imposed. It may be possible to select for RNA that grows crystals possessing a certain catalytic, electronic, photophysical, magnetic, etc. property. After several cycles (typically around 10), the initial RNA pool of  $10^{14}$  sequences is narrowed to a much smaller pool (hundreds) containing families of sequences that grow crystals with the desired property.

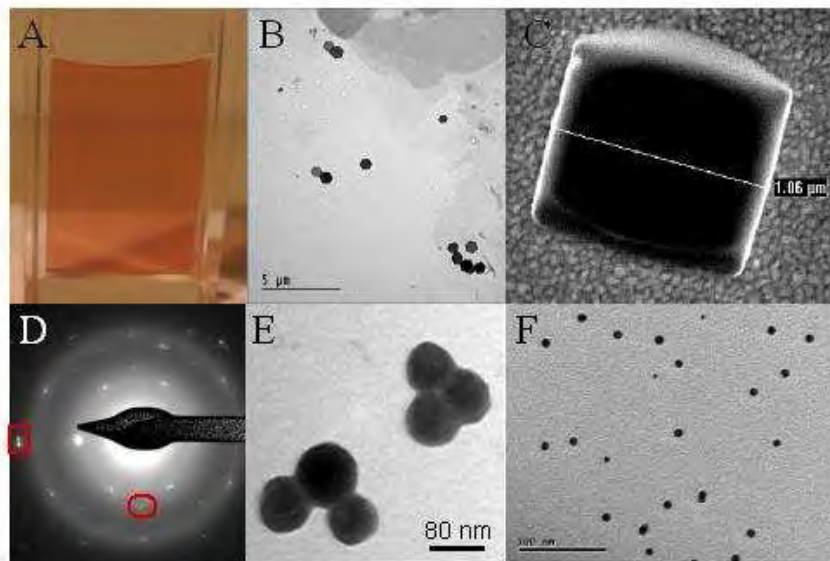


Figure 2. (A) Photograph of an aqueous solution containing 10 % THF and  $400 \mu\text{M}$   $[\text{Pd}_2(\text{DBA})_3]$  prior to the addition of RNA. No solid material is evident by eye or when the solution is examined by electron microscopy. (B) and (C) are examples of RNA sequence-dependent nanoparticle shape control. One sequence controls the formation of hexagonal Pd nanoparticles when incubated with aqueous solutions of  $[\text{Pd}_2(\text{DBA})_3]$ . Another sequence mediates the formation of Pd cubes. Both sequences were isolated from the same RNA in vitro selection experiment (see Figure 1). (D) Electron diffraction pattern of a hexagonal nanoparticle synthesized with RNA. Circled is the formally forbidden  $1/3(422)$  reflection characteristic of thin fcc Pd plates. Square shows the  $(220)$  reflection. (E) Transmission electron microscope image of Pt nanoparticles synthesized using an RNA sequence isolated via in vitro selection. (F) Iron oxide nanoparticles synthesized at  $25^\circ\text{C}$  and pH 7 water using an RNA catalyst.

Our initial hypothesis has now been supported by several experiments. In three separate in vitro selections, our labs have isolated RNA sequences that mediate the formation of Pd, Pt, and iron oxide nanoparticles (Figure 2). The former two selections were based upon nanoparticle size. A combination of filters and polyacrylamide gels were used to isolate the metal nanoparticles and RNA sequences bound to those particles. The latter selection was based upon a physical property. A magnetic field was used to isolate sequences that assembled magnet-responsive particles. Sequences that were incapable of assembling magnetic nanoparticles were discarded. These experiments have taught

us that RNA sequences can be found that catalyze inorganic reactions and control the size and shape of the resulting materials. Figures 2B and 2C, for example, show

hexagonal and cubic Pd nanoparticles synthesized using the same Pd source ( $[\text{Pd}_2(\text{DBA})_3]$  where DBA is dibenzylideneacetone), but two different RNA sequences. Figure 2D shows iron oxide nanoparticles synthesized at 25 °C and neutral pH. The iron oxide nanoparticles formed in the presence of the selected RNA sequences in 10 min at room temperature and neutral pH. In the absence of RNA, nanocrystals of this type are reported to form under these conditions with a half-life of ~1 year.

*Use of Selected RNA Sequences in Assembling Photocatalyst Materials.* The photocatalytic splitting of water using visible light is an essential reaction for sustainable hydrogen production that has yet to be achieved with great efficiency. Experiments reported here suggest that the reduction of water to hydrogen has been achieved through visible light photoreduction by a nanoscale RNA Pt/CdS catalyst (see Figure 3). Our photocatalyst is an assembly of biomolecule-templated materials suspended in water at pH 7. DNA-passivated cadmium sulfide (CdS) quantum dots (QDs) are combined with RNA mediated platinum nanoparticles<sup>2</sup> to assemble a single substrate suitable for the reduction of water to  $\text{H}_2$ . Upon visible light irradiation, electrons excited into the conduction band of CdS are injected into the Pt substrate and generate metal hydrides at their surface. To date, we have focused on the proton reduction half reaction at the Pt surface. To study this we have developed a novel and highly sensitive small molecule assay for the detection of metal hydride formation. We monitor subsequent  $\text{H}_2$  production using the compound N-[p-(2-benzimidazolyl)phenyl]maleimide (BIPM) as it becomes highly fluorescent upon reduction by  $\text{H}_2$ . Using this  $\text{H}_2$  fluorescence detection assay and our RNA-Pt/CdS catalyst the effects of light vs no light have been studied.

Each water splitting reaction contains the RNA-Pt/CdS catalyst, BIPM (50uM) and  $\text{dH}_2\text{O}$  (pH 7). The samples are irradiated under a solar simulator designed by our lab consisting of a 250 W tungsten filament bulb and filters that prevent wavelengths outside the visible spectrum. The reactions run over a 60-hour time course and the data is plotted as a function of signal intensity versus time (Figure 4). Parallel reactions

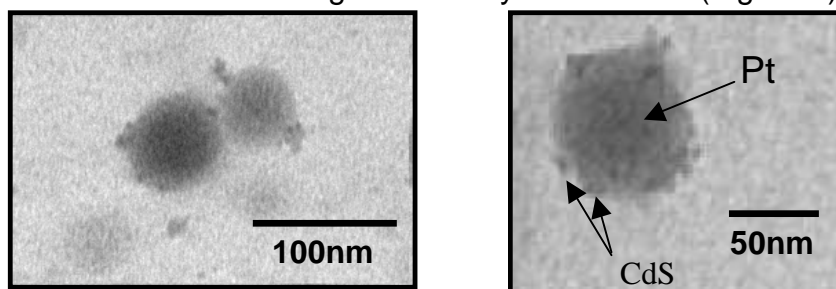


Figure 3. Transmission Electron Micrograph of RNA Pt/CdS photocatalysts constructed from individual RNA mediated Pt nanoparticles and DNA passivated CdS quantum dots.

are run simultaneously; one sample is irradiated under visible light while the other is kept in the dark for the entire time course.

The water splitting reactions conducted thus far have shown the efficiency of BIPM reduction to the hydrogenated product by the RNA Pt/CdS catalyst to be between 5-10%. Considering the extremely small concentration of catalyst (~250nM if one assumes 1RNA molecule per Pt nanoparticle - an over estimation) the rate of BIPM turnover is significant. The catalyst's ability to function under a low intensity visible light source is also encouraging. Moving away from UV light requirements helps meet the practical energy requirement for an effective water splitting catalyst. Efforts to scale up this reaction and characterize the hydrogenated BIPM product are currently underway.

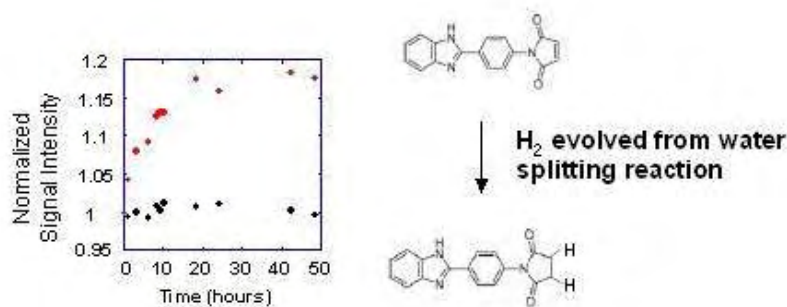


Figure 4. (Left) Effect of visible light (red) vs. no light (black) on the fluorescence of BIPM when in the presence of water and the RNA Pt/CdS photocatalyst. (Right) Reduction of BIPM by H<sub>2</sub> results in a highly fluorescent reduced product.

Overall our system offers multiple advantages including easy-to-prepare catalyst components and a new form of hydrogen detection at the surface of a nanoscale metal surface. Finally, in addition to the advantages of nanoscale material synthesis by the RNA, the biocompatibility with aqueous solutions and the construction of a two-part catalyst involving

transition metal and semiconductor components offers a promising first step towards the RNA driven assembly of functional nanostructures.

### Future Plans

Our experiments to date have shown that RNA is capable of catalyzing the formation of metal and metal oxide nanoparticles, and that a diversity in biomolecule sequence space leads to a diversity in particle size, shape, and composition. Such versatility is important in finding new heterogeneous catalysts for reactions of interest in alternative energy schemes because catalytic activity depends very sensitively on these parameters. We have also shown that RNA is capable of further assembling inorganic nanoparticles on surfaces or into metal/quantum dot heterostructures. In the coming months we plan to further quantify the catalytic activity of Pt/CdS nanoparticle heterostructures in the production of H<sub>2</sub> from H<sub>2</sub>O and visible light. New RNA in vitro selections are also in progress that are designed to test the limits of surface recognition and nanoparticle shape control by RNA.

### DOE Publications 2007-2009

C. J. Carter, M. Dolska, C. J. Ackerson, B. E. Eaton, Daniel L. Feldheim "In Vitro Selection of RNA Sequences Capable of Mediating the Formation of Iron Oxide Nanoparticles" *J. Mater. Chem.*, **2009** In Press.

S. Kim, J. J. DeYoreo, Bruce E. Eaton, Daniel L. Feldheim, et al. "Scanning Probe-Based Fabrication of 3D Nanostructures Via Affinity Templates, Functional RNA, and Meniscus-Mediated Surface Remodeling" *Scanning*, **2008**, 30, 159.

Daniel L. Feldheim, Bruce E. Eaton "Selection of Biomolecules Capable of Mediating the Formation of Materials" *ACS Nano*, **2007**, 1, 154.

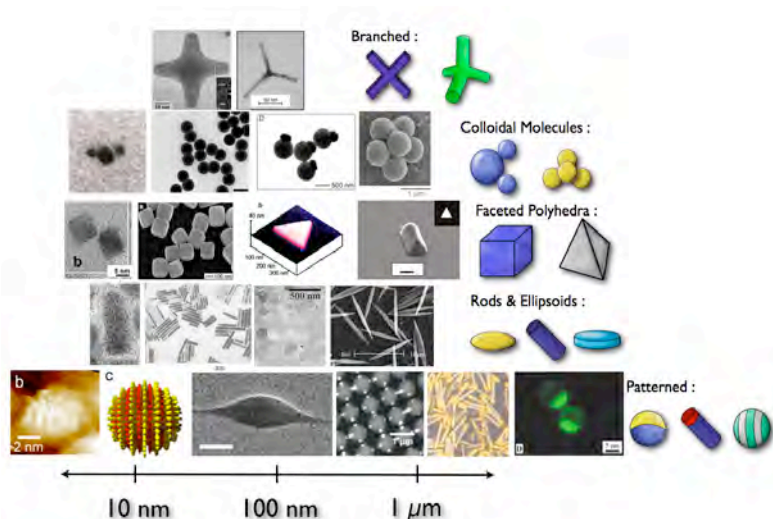
**Strategies for self-assembly:  
Simulation studies and design of tethered nanoparticle “shape amphiphiles”  
as building blocks for next-generation materials**

Extended Abstract

**Sharon C. Glotzer**

Department of Chemical Engineering and Department of Materials Science & Engineering,  
University of Michigan, Ann Arbor 48109-2136  
[sglotzer@umich.edu](mailto:sglotzer@umich.edu)

Self-assembly is a governing principle for the formation of material structures from elementary building blocks such as atoms, molecules, polymers and colloids. Today, the extent to which



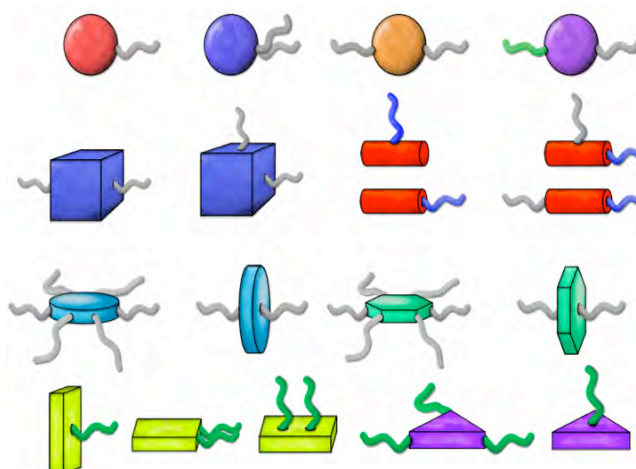
Examples of nano and colloidal building blocks reported in the literature. See article for original image references. From S.C. Glotzer and M.J. Solomon, *Nature Materials*, 2007.

materials building blocks can be engineered has undergone a quantum leap. We are on the verge of a materials revolution in which entirely new classes of particulate building blocks will be designed and fabricated with desired features, including programmable instructions for assembly. A rich diversity of nanoparticle shapes can be easily fabricated, and numerous demonstrations exist in the literature. These shapes can be further modified with anisotropic interactions due to asymmetric surface patterning with atoms and

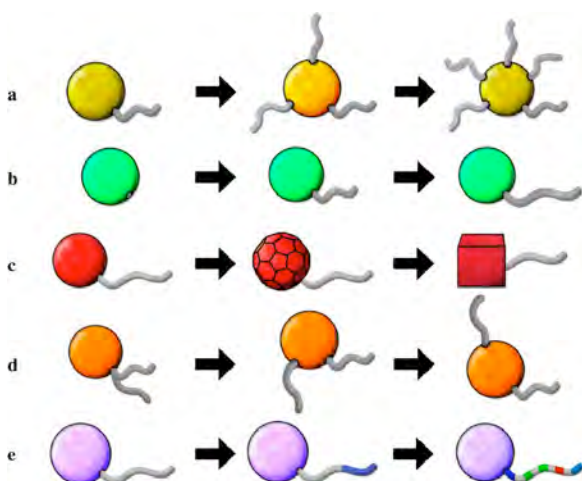
molecules, and even functionalization by organic “tethers”. In this way, it is now possible to create nanoparticle “shape amphiphiles” for self-assembly that combine key features of surfactants, block copolymers, colloids and liquid crystals in wholly new ways. This approach to nanoparticle assembly exploits the use of soft matter to organize nanoparticles into structures that would not spontaneously form from the nanoparticles alone.

In contrast to traditional materials, little is known about how to control the self-assembly of nanoparticles, nor about the assembly tendencies for these new amphiphilic building blocks. Without this knowledge and its formulation into a predictive theoretical framework, we remain far from realizing the ability to synthesize arbitrary building blocks designed to precisely assemble into target structures that exhibit an application-specific property or perform a desired function. Because of the complexity of nanoparticle shape amphiphiles, the available parameter

space that can be exploited for assembly is large. Computer simulation is therefore a critical tool to help understand the governing principles of self-assembly in these systems. We are using simulation to elucidate the nature of the forces controlling assembly, predict the asymmetries in building blocks that lead to desired target structures, and intelligently explore the vast parameter space available to the assembly of nanoparticle shape amphiphiles. Our simulations are providing critical design rules for pursuing strategies for encoding instructions for assembly into elementary nanoparticle building units based on purposeful changes in their symmetry.



Examples of tethered nanoparticle “shape amphiphiles”, many of which we have studied via simulation.



Classification of tethered nanoparticle shape amphiphile anisotropy. Left: Various building blocks are classified in homologous series according to particular measures of anisotropy: (A) Number of tethers. (B) Length of tether. (C) Number of nanocrystal vertices. (D) Relative location of tethers. (E) Tether specificity. Many additional “axes” are not shown. More complex anisotropy can be described as combinations of these measures. From Glotzer, et al. *Current Opinions in Colloid Science*, 2005.

under various thermodynamic conditions, and we are reverse-engineering tethered nanoparticles that will self-assemble into particular target structures.

The motivation behind our work lies in the fact that experimental advances are driving new approaches to nanoparticle assembly, yet we still lack a comprehensive, fundamental understanding of assembly that allows even a qualitative prediction of the structures that will form from a given building block. We have developed and validated strategies for modeling and simulating patchy and tethered nanoparticles, and carried out systematic and detailed investigations of their assembly behavior. Building on this work, we are extending the complexity of the systems we study by combining building block anisotropies in new ways to achieve more complex, and potentially more useful, self-assembled structures. We are exploring the role of particle shape, size and polydispersity, as well as tether length, rigidity, number, and placement, as well as solvent selectivity, all of which we expect to profoundly impact the assembled phases. We are investigating what a given judiciously chosen nano building block or set of building blocks will form

In this talk we present examples from our recent work, including the self assembly of end-tethered and laterally-tethered nanorods, mono- and di-tethered nanospheres, and tethered nanoparticles of more unusual shape. We map phase diagrams for these systems and show and explain the formation of various unique self-assembled structures, including perforated layers with ordered perforations, double gyroids, chiral cylinders, bilayer sheets and scrolls, quasiperiodically ordered micelles, diamond structures, and ionic crystal structures.

We also present new methods for characterizing self-assembled systems, including a new Voronoi tessellation method to characterize soft matter structures containing multiple domains.

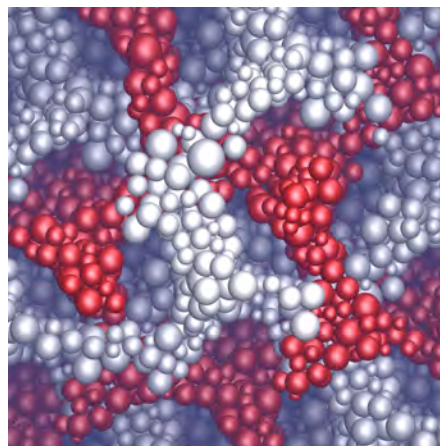


Image of a simulated double gyroid from mono-tethered nanospheres with polydisperse sphere size distribution. From C.L. Phillips, et al, preprint.

Z.L. Zhang, M.A. Horsch, M.H. Lamm, and S.C. Glotzer, 'Tethered nano building blocks: Toward a conceptual framework for nanoparticle self-assembly,' *Nano Letters* **3**, 1341 (2003).

S.C. Glotzer, M.A. Horsch, C.R. Iacovella, Z.L. Zhang, E.R. Chan, and X. Zhang, 'Self-assembly of anisotropic tethered nanoparticle shape amphiphiles,' *Current Opinion in Colloid & Interface Science* **10**, 287 (2005).

C.R. Iacovella, M.A. Horsch, Z.L. Zhang, and S.C. Glotzer, 'Self-assembly of mono-tethered spheres: comparison to surfactants,' *Langmuir (Letter)* **10**, 9488 (2005).

E.R. Chan, X. Zhang, C.Y. Lee, M. Neurock, and S.C. Glotzer, 'Simulations of tetra-tethered organic/inorganic nanocube-polymer assemblies,' *Macromolecules* **38**, 6168 (2005).

M.A. Horsch, Z.L. Zhang, and S.C. Glotzer, 'Self-assembly of polymer-tethered nanorods,' *Phys. Rev. Lett.* **95**, 056105 (2005).

M.A. Horsch, Z. Zhang, and S.C. Glotzer, 'Self-assembly of laterally-tethered nanorods,' *Nano Letters* **6**, 2406 (2006).

E.R. Chan, L.C. Ho, and S.C. Glotzer, 'Computer simulations of block copolymer tethered nanoparticle self-assembly,' *J. Chem. Phys.* **125**, (2006).

M.A. Horsch, Z.L. Zhang, and S.C. Glotzer, 'Simulation studies of self-assembly of end-tethered nanorods in solution and role of rod aspect ratio and tether length,' *J. Chem. Phys.* **125**, (2006).

S.C. Glotzer, and M.J. Solomon, 'Anisotropy of building blocks and their assembly into complex structures,' *Nature Materials* **6**, 557 (2007).

X. Zhang, Z.L. Zhang, and S.C. Glotzer, 'Simulation study of cyclic-tethered nanocube self-assemblies: effect of tethered nanocube architectures,' *Nanotechnology* **18**, (2007).

C.R. Iacovella, A.S. Keys, M.A. Horsch, and S.C. Glotzer, 'Icosahedral packing of polymer-tethered nanospheres and stabilization of the gyroid phase,' *Physical Review E* **75**, 040801 (R) (2007).

T.D. Nguyen, Z.L. Zhang and S.C. Glotzer, "Molecular simulation study of self-assembly of tethered V-shaped nanoparticles," *J. Chem. Phys.*, **129**, 244903 (2008).

T.D. Nguyen and S.C. Glotzer, "Switchable helical structures formed by the hierarchical self-assembly of laterally-tethered nanorods," *Small*, published online May 28, 2009. DOI: 10.1002/sml.200900168

D-J Hong, E. Lee, H. Jeong, J-k Lee, W-C Zin, T.D. Nguyen, S.C. Glotzer, and M. Lee, "Solid state scrolls from hierarchical self-assembly of T-shaped rod-coil molecules," *Angewandte Chemie*, **48**(9), 1664-1668 (2009).

C.R. Iacovella and S.C. Glotzer, "Phase behavior of ditethered nanospheres," *Soft Matter*, in press.

C.R. Iacovella and S.C. Glotzer, "Complex crystal structures formed by the self assembly of di-tethered nanospheres," *Nano Letters* **9**(3), 1206-1211(2009).

C.L. Phillips, C.R. Iacovella and S.C. Glotzer, "Stability of the double gyroid phase to nanoparticle polydispersity in polymer-tethered nanosphere systems," preprint.

M.A. Horsch, Z-L Zhang and S.C. Glotzer, "Self-Assembly of End-Tethered Nanorods in a Neat System and Role of Block Fractions and Aspect Ratio," preprint.

C.R. Iacovella, A.S. Keys and S.C. Glotzer, "Quasicrystals in tethered nanoparticle systems," preprint.

*Work funded by the U.S. Department of Energy, grant no. DE-FG02-02ER46000.*

# A PS I-molecular wire-H<sub>2</sub>ase Construct for Light-Induced H<sub>2</sub> Generation

John H. Golbeck<sup>1,2</sup> and Donald A. Bryant<sup>1</sup>

<sup>1</sup>Department of Biochemistry and Molecular Biology

<sup>2</sup>Department of Chemistry

The Pennsylvania State University

University Park, PA 16802 USA

[jhg5@psu.edu](mailto:jhg5@psu.edu)

[dab14@psu.edu](mailto:dab14@psu.edu)

**Program Scope:** The goal of this project is to design, assemble, characterize, and optimize a hybrid biological/organic photochemical half-cell for light-induced generation of H<sub>2</sub>. The device couples Photosystem I (PS I), which captures and stores energy derived from sunlight, with an [FeFe]-hydrogenase (H<sub>2</sub>ase), which can generate a high rate of H<sub>2</sub> evolution with an input of electrons. The key design feature is a covalently bonded molecular wire that directly connects the F<sub>B</sub> iron-sulfur cluster of PS I to the distal iron-sulfur cluster of the H<sub>2</sub>ase so as to transfer electrons without loss to potentiate high rates of photo-hydrogen production.

**Recent Progress:** *PS I — molecular wire — Pt nanoparticle bioconjugate*

We demonstrated proof-of-principle by first constructing a PS I-molecular wire-Pt nanoparticle bioconjugate. This system, which employed PS I from the cyanobacterium *Synechococcus* sp. PCC 7002, 1,6-hexane dithiol as the molecular wire, and a platinum nanoparticle, generated light-induced H<sub>2</sub> production at a rate of 49.3 μmol H<sub>2</sub> mg Chl<sup>-1</sup> h<sup>-1</sup> (1.17 mol H<sub>2</sub> mol PS I<sup>-1</sup> s<sup>-1</sup>). Over the course of the last year, we carried out an in depth study to optimize the rate of H<sub>2</sub> production. The affect of the solution pH and ionic concentration, the cross-linking of plastocyanin, the molecular wire length and bond saturation, and the light intensity were varied systematically. Only ~3 nm Pt nanoparticles were used in this study as they were shown to be more effective for the heterogeneous catalysis of H<sub>2</sub> than Au nanoparticles. Additionally, PS I isolated from commercially available baby spinach was used in place of the cyanobacterial PS I, because we found the electron transfer throughput to be approximately 2-times higher. The enhanced electron throughput rates of spinach PS I are related mostly to the organization and conformation of the isolated protein complexes and the specificity of its interactions with the native electron donating protein in spinach, plastocyanin. Faster electron throughput rates for PS I allow for the

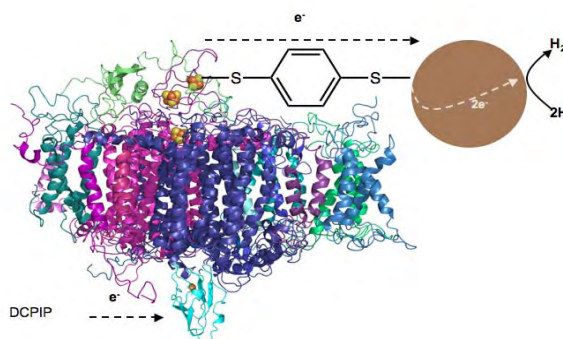


**Figure 1.** H<sub>2</sub> production rates were maximized by constructing a bioconjugate that consisted of plastocyanin cross-linked PS I, 1,4-benzenedithiol as the molecular wire, and Pt nanoparticles.

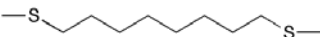
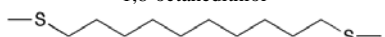
possibility of higher H<sub>2</sub> production rates. The bioconjugates with conjugated bonds have higher rates of H<sub>2</sub> generation than do bioconjugates with aliphatic molecular wires of similar length. For aliphatic dithiols, the rate of H<sub>2</sub> production decreased as the length of the molecular wire increased. A notable exception to this trend was observed in the H<sub>2</sub> production rates for bioconjugates constructed with 1,3-propanedithiol for which the light-induced H<sub>2</sub> generation rate was considerably lower than expected. The length of 1,3-propanedithiol may not be sufficient to allow efficient covalent linkage between PS I and the Pt nanoparticle. Additionally, as the length of the carbon chain decreased, the effectiveness for shielding proteins from denaturation on metal surfaces also decreased. Because

the carbon chain in the 1,3-propanedithiol is so short, if the PS I and the Pt nanoparticle were successfully linked by the molecular wire, some protein denaturation might occur. Depending on the degree of denaturation, the electron transfer capabilities of PS I may be reduced or lost and H<sub>2</sub> production rates would therefore be lower. By combining the optimal conditions for H<sub>2</sub> production for each iterative change to the system, a bioconjugate was constructed utilizing plastocyanin cross-linked to rebuilt spinach PS I and 1,4-benzenedithiol as the molecular wire to connect PS I to the Pt nanoparticle (Figure 1). Illumination of this bioconjugate at a light intensity of 70 μE m<sup>-2</sup> s<sup>-1</sup> generated H<sub>2</sub> at a rate of 312 μmol H<sub>2</sub> mg Chl<sup>-1</sup> h<sup>-1</sup> (11.2 mol H<sub>2</sub> mol PS I<sup>-1</sup> s<sup>-1</sup>). If the light intensity were extrapolated to saturation, the rate of H<sub>2</sub> production would be about 600 μmoles H<sub>2</sub> mg Chl<sup>-1</sup> h<sup>-1</sup>. To put this number into further perspective, a green plant evolves about 400 μmol O<sub>2</sub> mg Chl<sup>-1</sup> h<sup>-1</sup>. The 300-fold increase in the activity of our bioconjugate can be attributed to the efficiency of the molecular wire in transferring electrons from PS I directly to the Pt nanoparticle. In other words, the core idea of using a molecular wire to transfer electrons efficiently from PS I to an acceptor has been validated.

#### Assembly of the PS I — molecular wire — [FeFe]-hydrogenase construct

PS I, which was rebuilt using the C13G/C33S variant of PsaC, was connected to the C98G HydA variant of the [FeFe]-hydrogenase from *Clostridium acetobutylicum* (heterologously expressed in *E. coli*) using a 1,6-hexanedithiol molecular wire. Cytochrome (Cyt) *c*<sub>6</sub> and ascorbate were added to the solution to function as soluble electron donors to PS I (The two proteins were not cross-linked in this study.). Upon illumination of the construct in a sealed Ar-purged vial for 8 to 15 hours, H<sub>2</sub> was produced at rates ranging from 0.3 to 2.1 μmol H<sub>2</sub> mg Chl<sup>-1</sup> h<sup>-1</sup>, depending on the sample. After a rough optimization of solution conditions, the rate increased approximately two-fold to 3.9 μmol H<sub>2</sub> mg Chl<sup>-1</sup> h<sup>-1</sup>. Control experiments were performed to verify light-induced H<sub>2</sub> production. The controls involved the absence of the following substrates: light, rebuilt PS I with

**Table 1.** Molecular wire length and bond saturation affect the rate of H<sub>2</sub> production by plastocyanin cross-linked rebuilt spinach PS I/dithiol molecular wire/Pt nanoparticle bioconjugates.

Molecular wire	Rate of H <sub>2</sub> production (μmol H <sub>2</sub> mg Chl <sup>-1</sup> h <sup>-1</sup> )	Rate of H <sub>2</sub> production (mol H <sub>2</sub> mol PS I <sup>-1</sup> s <sup>-1</sup> )
 1,3-propanedithiol	2.54	0.09
 1,6-hexanedithiol	98.57	3.52
 1,8-octanedithiol	49.03	1.75
 1,10-decanedithiol	16.09	0.57
 1,4-benzenedithiol	150.47	5.37
4,4'-biphenyldithiol	92.53	3.31

variant PsaC, variant [FeFe]-H<sub>2</sub>ase, and 1,6-hexanedithiol; as well as the substitution of wild-type PS I or wild-type [FeFe]-H<sub>2</sub>ase. As expected, all of the controls failed to generate H<sub>2</sub>. Because the rates of H<sub>2</sub> production were lower than expected based on the Pt nanoparticle bioconjugate, characterization of the enzymatic activity of the H<sub>2</sub>ase was undertaken. Following an accepted protocol, the wild-type HydA and its C98G variant were mixed with methyl viologen and dithionite in a sealed Ar purged vial. H<sub>2</sub> production was assayed by gas chromatography over time. Initial rates (5 to 10 min) of H<sub>2</sub> production were found to be 418 μmol H<sub>2</sub> mg H<sub>2</sub>ase<sup>-1</sup> h<sup>-1</sup> and 808 μmol H<sub>2</sub> mg H<sub>2</sub>ase<sup>-1</sup> h<sup>-1</sup> for WT and the C98G variant H<sub>2</sub>ases, respectively. By comparison to the literature, this WT hydrogenase, when derived from the native organism, should be able to produce 4512 μmol H<sub>2</sub> mg H<sub>2</sub>ase<sup>-1</sup> h<sup>-1</sup>. It thus became clear that the heterologous expression system does not produce H<sub>2</sub>ases with consistently high activities. We have recently begun working with Prof. Thomas Hoppe (U. of Bochum, Germany), who has developed a hydrogenase expression system for variant enzymes within *C. acetobutylicum*. Using the C98G HydA expressed in this organism, we were able to achieve a ten-fold increase in the rate of light-induced H<sub>2</sub> generation to 30.3 μmol H<sub>2</sub> mg Chl<sup>-1</sup> h<sup>-1</sup>. This is nearly the same rate that we initially published for our PS I-molecular wire-Pt nanoparticle bioconjugate. Initial long term stability studies have shown the PS I-molecular wire-H<sub>2</sub>ase construct to be stable and active for approximately 56 days at room temperature in the light. These results suggest that the ability of the organism to insert the metallocofactors efficiently into the H<sub>2</sub>ase will likely be the most important factor for obtaining highly active hydrogenase, and thus is the rate-limiting step to increased light-induced H<sub>2</sub> generation.

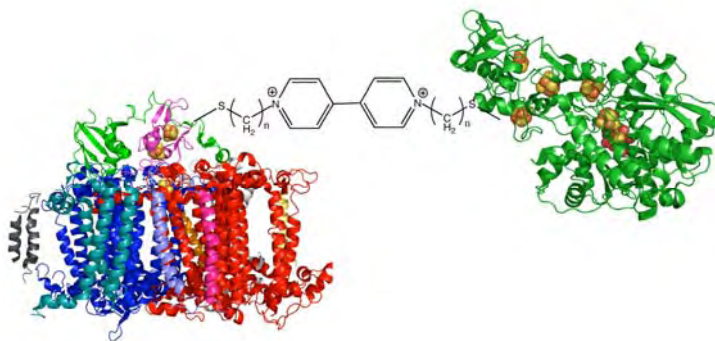


**Figure 2.** Design of the PS I-molecular wire-H<sub>2</sub>ase construct. We are currently using 1,6-hexanedithiol as the molecular wire for proof-of-concept. The best rate of light-induced H<sub>2</sub> generation to-date is 30.3 μmol H<sub>2</sub> mg Chl<sup>-1</sup> h<sup>-1</sup>.

## Future Plans:

### *Overproduction of H<sub>2</sub>ase in Shewanella oneidensis MR-1*

Based on the H<sub>2</sub> evolution assays, it appears that the specific activity of recombinant HydA is lower than expected, even though the *hydE*, *hydF* and *hydG* genes were coexpressed with the *hydA* gene in *E. coli* for maturation of this [FeFe]-hydrogenase. It has been shown that the HydE, HydF and HydG proteins play important roles in H-cluster maturation in the [FeFe]-hydrogenase (King *et al.*, J. Bacteriol. 188:2163-2172 (2006)). However, the details of the maturation of the [FeFe]-hydrogenase are still not well understood, and thus manipulation of assembly in heterologous systems remains trial and error. Recent reports suggest that the facultative anaerobe, *Shewanella oneidensis*, might be a more efficient system for heterologous expression and maturation of [FeFe]-hydrogenases. To obtain [FeFe]-hydrogenase with higher specific activity, we have been exploring the overproduction of the *C. acetobutylicum* [FeFe]-hydrogenase in *S. oneidensis* MR-1. With assistance from Dr. Alexander Beliaev at Pacific

Northwest National Laboratory, we are using a *hydB* deletion strain and the *hydB* and *hydB* double deletion mutant strain of *S. oneidensis* MR-1 (Marshall *et al.*, Environ. Microbiol. 10:125-136 (2008)) as the host strains for heterologous expression of the *C. acetobutylicum* [FeFe]-hydrogenase. This system relies on the endogenous [FeFe]-hydrogenase maturation system of *Shewanella oneidensis*. For this purpose, the *C. acetobutylicum hydB* gene (with addition of a C-terminal Strep-tag) was cloned into the pJBC2 vector that has been shown to be an efficient overexpression vector in *S. oneidensis*. This *hydB* expression construct, pJBC2HydA, has been introduced into the *Shewanella oneidensis* MR-1  $\Delta hydA\Delta hydB$  cells through conjugation using DAP-dependent *E. coli* strain WM3064. The pETductHydAE (pET expression vector with *C. acetobutylicum hydB* and *hydE* genes) and pAQ1ExHydA (a construct for overexpression of the *C. acetobutylicum hydB* gene in the cyanobacterium *Synechococcus* sp. PCC 7002, Yu, Shen and Bryant, unpublished results) have also been successfully introduced into the *Shewanella oneidensis* MR-1  $\Delta hydA\Delta hydB$  host cells. Higher expression level of HydA has been achieved with the pJBC2hydA construct, as examined by immunodetection using the HydA antibody and also by measuring the H<sub>2</sub> evolution rate in *Shewanella oneidensis* MR-1  $\Delta hydA\Delta hydB$  cells expressing the *C. acetobutylicum hydB* gene. Using the bioreactors of the Penn State fermentation facility, we have been optimizing the overproduction and purification of a stable, more active [FeFe]-hydrogenase for reconstitution of the PSI-HydA supercomplex.

#### *Attachment of the PS I-molecular wire-H<sub>2</sub>ase construct to a Gold Electrode*

The design of a practical device that effectively and efficiently converts solar energy into hydrogen gas depends on the attachment of our PSI-molecular wire-H<sub>2</sub>ase construct to an electrode surface. It has been demonstrated that PS I can be directly attached to the surface of a nanoporous gold leaf electrode and still retain its photoactivity (Ciesielski *et al.*, ACS Nano. 2:2465-2472 (2008)). We are currently initiating a collaboration with Drs. G. Kane Jennings and David Cliffel to attach our PS I-molecular wire-H<sub>2</sub>ase construct to an electrode in order to study the photoelectrochemical effects. H<sub>2</sub> production will be measured to provide a determination of the efficiency of the construct.

#### **Publications 2007-2009:**

- Antonkine, M. L., Maes, E. M., Czernuszewicz, R. S., Breitenstein, C., Bill, E., Falzone, C. J., Balasubramanian, R., Lubner, C., Bryant, D. A., and Golbeck, J. H. (2007) Chemical Rescue of a Site-Modified Ligand to a [4Fe-4S] cluster in PsaC, a Bacterial-Like Dicluster Ferredoxin Bound to Photosystem I, *Biochim Biophys Acta*, **1267**, 712-724.
- Grimme, R. A., Lubner, C. E., Bryant, D. A., and Golbeck, J. H. (2008) Photosystem I/molecular wire/metal nanoparticle bioconjugates for the photocatalytic production of H<sub>2</sub>, *J Am Chem Soc* **130**, 6308-6309.
- Grimme, R. and Golbeck, J. H. (2008) "A biologically-inspired electrochemical half-cell for the light-driven generation of H<sub>2</sub>", *Material Matters* **3**, 78-83.
- Grimme, R., Lubner, C. E. and Golbeck, J. H. (2009) "Maximizing H<sub>2</sub> production in Photosystem I/dithiol molecular wire/platinum nanoparticle bioconjugates" *Dalton Trans.* (in press).

## Structured, Stabilized Phospholipid Vesicles

Steve Granick

University of Illinois  
Department of Materials Science and Engineering  
1304 West Green St.  
Urbana, IL 61801  
[sgranick@uiuc.edu](mailto:sgranick@uiuc.edu)

**Program Scope:** It is a grand challenge in material science to form structure that is not frozen in place but instead robustly responds adaptively to its environment. Phospholipid vesicles hold promise to achieve this but the needed integrated, predictive understanding does not yet exist, the current field being dominated by cellular and biosensor perspectives. This project addresses the biomolecular science and engineering of nanoparticle-phospholipid constructs. The methods involve integrated imaging and spectroscopic study.

**Recent Progress:** A focus of activity this year was to understand what determines the mobility of particles and vesicles when they diffuse. This led to a breakthrough in understanding the nature of Brownian motion in biomolecular environments. A schematic diagram of the two systems that we studied is shown in Fig. 1.

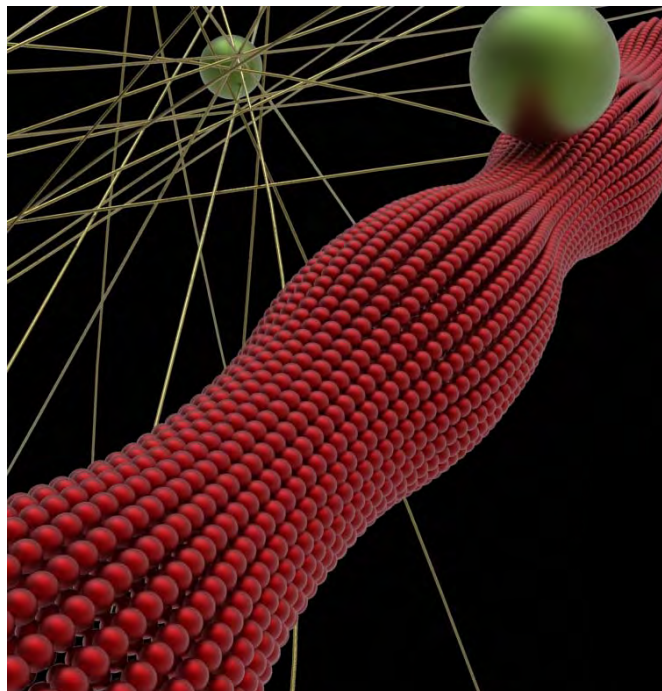
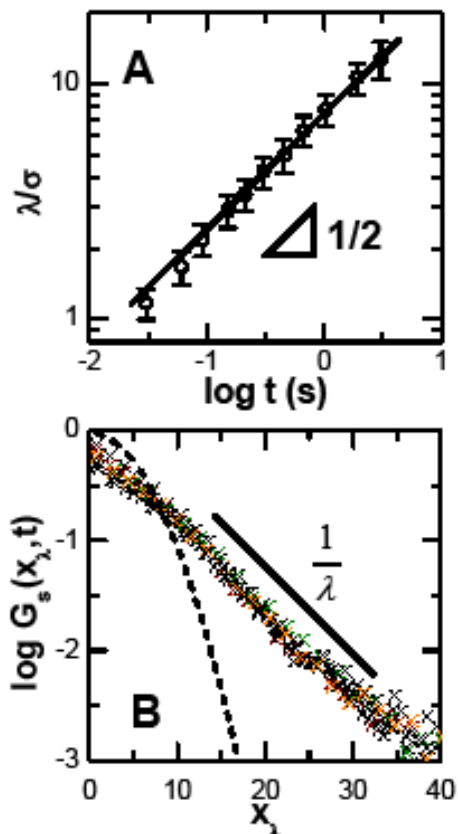


*Fig. 1. Schematic diagram of a submicron-sized particle diffusing on a phospholipid tubule (red) or through a tightly entangled actin network (green fibers). The nanoparticle diameter was varied over a wide range and also the degree of entanglement.*

These experiments used single-particle tracking and discovered that mean-square displacement is simply proportional to time (Fickian) yet the distribution of displacement probability is not Gaussian as should be expected of a classical random walk, but instead is decidedly exponential for large displacements, the decay length of the exponential being proportional to the square root of time. The first example is when colloidal beads diffuse along linear

phospholipid bilayer tubes whose radius is the same as that of the beads. The second is when beads diffuse through entangled F-actin networks, bead radius being less than one-fifth of the actin network mesh size. We explore the relevance to dynamic heterogeneity in trajectory space, which has been extensively discussed regarding glassy systems. Data for the second system might suggest activated diffusion between pores in the entangled F-actin networks, in the same spirit as activated diffusion and exponential tails observed in glassy systems. But the first system

shows exceptionally rapid diffusion, nearly as rapid as for identical colloids in free suspension, yet still displaying an exponential probability distribution as in the second system. Thus while the exponential tail is reminiscent of glassy systems, in fact these dynamics are exceptionally rapid. We also compare to particle trajectories that are at first subdiffusive but Fickian at the



longest measurement times, finding that displacement probability distributions fall onto the same master curve in both regimes. Looking to the future, these experiments and their analysis emphasize the promise of additional experiments, theory, and computer simulation to allow definitive interpretation of this simple and clean exponential probability distribution, as the simpler Gaussian distribution would have been expected from conventional wisdom.

*Fig. 2. (A) The decay length  $\lambda(t)$ , plotted versus delay time on log-log scales, shows a square root power law. (B) Master curve obtained by normalizing the probability distribution by the square root of the time step,  $x_\lambda = x(t)/\sqrt{t}$ , with delay times ranging from 30 ms to 1 s. The solid line, a guide to the eye, shows semilogarithmic behavior. The dotted line shows Gaussian behavior with the same diffusion coefficient. This data, showing fewer short steps and more large steps than enter into conventional ideas of diffusion, is expected to modify diffusion-limited chemical reactions.*

Other recent activities include:

- *Supported lipid bilayers.* We compared the association of an ortho-substituted and a planar PCB (polychlorinated biphenyls PCB-52 and PCB-77, respectively) with single-component phospholipid bilayers terminated with phosphocholine headgroups. First, fluorescence correlation spectroscopy (FCS) studies of diffusion on supported fluid-phase DLPC showed that the ortho-substituted PCB diffuses more slowly, indicating either complex formation or obstructed diffusion. Differential scanning calorimetry (DSC) of vesicles formed from DMPC showed that the gel-to-fluid phase transition temperature is lower for vesicles containing this ortho-substituted PCB. Atomic force microscopy (AFM) showed that whereas supported bilayers of DMPC containing this ortho-substituted PCB display two melting points, bilayers containing the coplanar PCB display just a single melting point. A model was proposed in which the ortho-substituted PCB resides within the lipid tails of these phospholipid bilayers but the coplanar PCB associates preferentially with the headgroups. This is consistent with the known membrane disruptive ability of the ortho substituted isomer.

- *Friction and lubrication.* An invited review in the Proc. Roy. Soc. B. examined several instrumental developments that reveal the spectroscopic response of molecularly-thin fluids confined between mica sheets. They are predicated on using a redesigned surface forces apparatus, developed during prior funding by this program, whereby dielectric coatings, transparent to light at needed optical wavelengths, retain the ability to measure interferometric thickness at other optical wavelengths. Examples of recent measurements were demonstrated using confocal laser Raman spectroscopy to evaluate how molecules orient as well as to perform chemical imaging. Other examples were developed using confocal fluorescence recovery after photobleaching (FRAP) to evaluate translational diffusion of confined polymer melts. The method to separate apparatus from sample contributions is stressed. From this work, we learned the advantage of separating the mechanical average (force and friction) from direct information about structure and mobility at the molecular level.
- *Electric charge on a weak polyelectrolyte.* Fluorescence measurements with single-molecule sensitivity were used to measure the hydrodynamic size and local pH of a weak polyelectrolyte, poly 2-vinyl pyridine end-labeled with pH-sensitive dye, the polyelectrolyte having concentration so low (nM) that molecular properties are resolvable only from fluorescence experiments and cannot be accessed by light scattering. We found that the local pH near the dye, inferred from its brightness, is consistently 3 orders of magnitude higher than the bulk pH. Upon varying the bulk pH, we measured the collapse point at which hydrophobic attraction overwhelms electrostatic repulsion between charged elements along the chain, and concluded that adding monovalent salt shifts this coil-to-globule collapse to higher pH than in the absence of salt. The influence of salt appears to be to shift the ionization equilibrium of this weak polyelectrolyte in the direction of the chain possessing enhanced electric charge at a given pH. This is opposite to the case for strong polyelectrolytes although the mechanism differs.
- *Single particle tracking.* A computationally rapid image analysis method, weighted over-determined regression, was presented for two dimensional (2D) Gaussian fitting of particle location with sub-pixel resolution from a pixelized image of light intensity. Compared to least-squares Gaussian iterative fitting, which is most exact but prohibitively slow for large data sets, the precision of this new method is equivalent when the signal-to-noise ratio is high and approaches it when the signal-to-noise ratio is low, while enjoying a more than hundred-fold improvement in computational time. Compared to another widely-used approximation method, 9-point regression, we showed that precision and speed are both improved. Additionally, weighted regression runs nearly as fast and with greatly improved precision compared to the simplest method, the moment method, which despite its limited precision is frequently employed due to its speed. Quantitative comparisons were presented for both circular and elliptical Gaussian intensity distributions. This new image analysis method may be useful when dealing with large data sets such as frequently met in astronomy or in single-particle and single-molecule tracking using microscopy and may facilitate advances such as real-time quantification of microscopy images.

**Future Plans:** This is the final year of this 3-year grant.

## Publications 2007-2009:

1. Yan Yu, Stephen M. Anthony, Liangfang Zhang, Sun Chul Bae, and Steve Granick, "Cationic Nanoparticles Stabilize Zwitterionic Liposomes Better than Anionic Ones," *J. Phys. Chem. C* 111, 2833-2836 (2007).
2. L. Zhang, K. Dammann, S. C. Bae, and S. Granick, "Ligand-Receptor Binding on Nanoparticle-Stabilized Liposome Surfaces," *Soft Matter* 3, 551-553 (2007).
3. L. Zhang and S. Granick, "Inter-Leaflet Diffusion Coupling when Polymer Adsorbs onto One Sole Leaflet of a Supported Phospholipid Bilayer," *Macromolecules* 40, 1366-1368 (2007).
4. S. Granick and S. C. Bae, "Molecular Motion at Soft and Hard Interfaces: from Phospholipid Bilayers to Polymers and Lubricants", *Annu. Rev. Phys. Chem.* 58, 353-374 (2007).
5. H. Tu, L. Hong, S. Anthony, P. V. Braun, S. Granick, "Brush-Sheathed Particles Diffusing at Brush-Coated Surfaces in the Thermally-Responsive PNIPAAm System", *Langmuir* 23, 2322-2325 (2007).
6. Shengqin Wang, Steve Granick, and Jiang Zhao, "Charge on a Weak Polyelectrolyte," *J. Chem. Phys.* 129, 241102 (2008).
7. Steve Granick and Sung Chul Bae, "A Curious Antipathy for Water" (Perspective), *Science* 322, 1477-1478 (2008).
8. Bo Wang, Liangfang Zhang, Sung Chul Bae, and Steve Granick, "Nanoparticle-Induced Surface Reconstruction of Phospholipid Membranes," *Proc. Nat. Acad. Sci. USA.* 105, 18171-18175 (2008).
9. Andrew S. Campbell, Yan Yu, Steve Granick, and Andrew A. Gewirth, "PCB Association with Model Phospholipid Bilayers," *Environmental Sci. and Tech.* 42, 7496-7501 (2008).
10. Sung Chul Bae, Janet S. Wong, Minsu Kim, Shan Jiang, Liang Hong, and Steve Granick, "Using Light to Study Boundary Lubrication: Spectroscopic Study of Confined Fluids," *Phil. Trans. Roy. Soc. A*, 366, 1443-1454 (2008).
11. Stephen M. Anthony, and Steve Granick, "Image Analysis with Rapid and Accurate 2D Gaussian Fitting," *Langmuir* 25, 8152 (2009).
12. Yan Yu, Stephen M. Anthony, Sung Chul Bae, Erik Luijten, and Steve Granick, "Biomolecular Science of Liposome-Nanoparticle Constructs," *Mol. Cryst. Liq. Cryst.* (2009) in press.
13. Bo Wang, Stephen M. Anthony, Sung Chul Bae, and Steve Granick, "Anomalous but Brownian," *Proc. Nat. Acad. Sci. USA* (2009). DOI:10.1073/pnas.0903554106.

# Biomimetic 3D Network Polymers Containing Reversibly Unfoldable Modules (RUMs) for Strong and Tough Materials

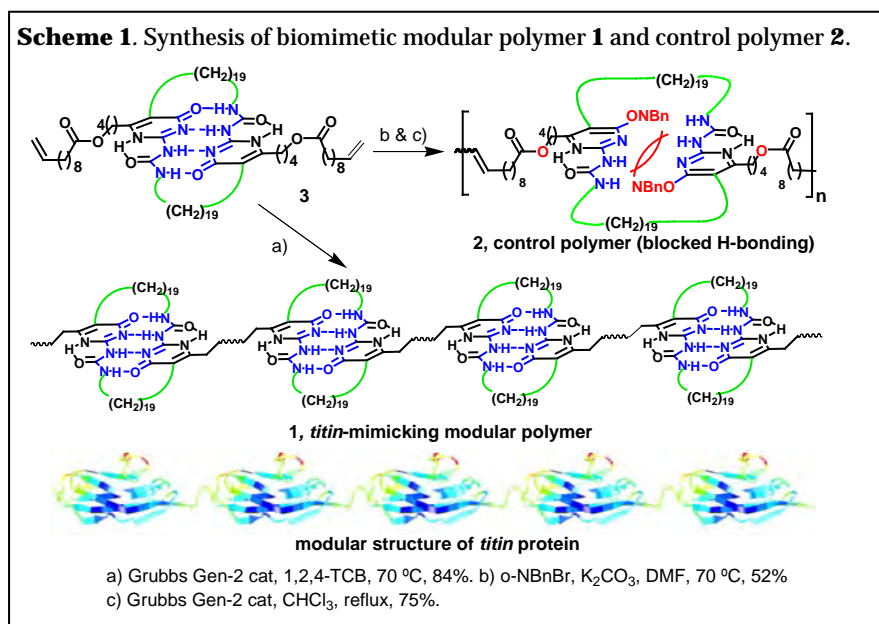
Zhibin Guan

Department of Chemistry and Biomedical Engineering  
1102 Natural Sciences II  
University of California  
Irvine, CA 92697-2025  
[zguan@uci.edu](mailto:zguan@uci.edu)

**Program Scope:** The goal of this project is to develop biomimetic modular polymers that have a combination of mechanical strength, toughness, elasticity, and adaptive properties. Our biomimetic approach is to program weak non-covalent molecular forces into strong covalent polymers to combine these orthogonal properties.

**Recent Progress:** In this funding period, we have made significant progress both in design and synthesis of biomimetic modular polymers and fundamental structure-property studies of these biomimetic systems at single molecule and bulk scales. Following the modular design of skeletal muscle protein *titin*, we have synthesized a linear modular polymer showing the combination of high modulus, toughness, resilience, and self-healing, stimuli-responsive properties. The modular polymer **1** was synthesized by acyclic diene metathesis (ADMET) polymerization of monomer **3** using the Grubbs Gen-2 catalyst (Scheme 1) ( $M_n = 18.0$  kDa, PDI = 1.7). As a control, monomer **3** was protected with *ortho*-nitrobenzyl (NBn) group to block H-bonding of 4-ureido-2-pyrimidone (UPy), then polymerized to yield polymer **2**. The control polymer is identical to the real sample except that the protected UPy units cannot form dimers.

While the control polymer **2** is brittle and fractures at 7% strain, the modular polymer **1** exhibits high modulus (~450 MPa) and undergoes large deformation with maximal strain > 100% (Figure 2A). After yielding at ~5% strain, it shows a strikingly large deformation with relatively a small increase in stress, a consequence of sequential unfolding of the folded modules which results in the absorption of a large amount



of energy and making the polymer tough. Whereas large deformation of traditional thermoplastic polymers is usually accomplished through crazing or necking leading to permanent damage, neither necking nor crazing was observed in our modular polymer.

In further studies, we observed interesting “self healing” and “shape-memory” properties for polymer **1**.<sup>3</sup> After ten strain cycles, the material was temporarily “damaged” and set at ~135% of its original length. With time this sample gradually regains its shape and property, recovering to 87% of its original dimension after 18 hr at r.t. (Figure 1A). To further explore this adaptive property, we investigated the temperature dependence of the self-healing process and observed an interesting shape-memory behavior. After heating to 80 °C, the sample was extended to 250% strain, then cooled to 5°C to freeze the shape. The stress was then released and the temperature was ramped up gradually. After reaching ~27°C, the sample specimen began to retract and then quickly recovered to its original dimension upon further heating, with both shape-fixity and recovery approaching 100% (Figure 1B).

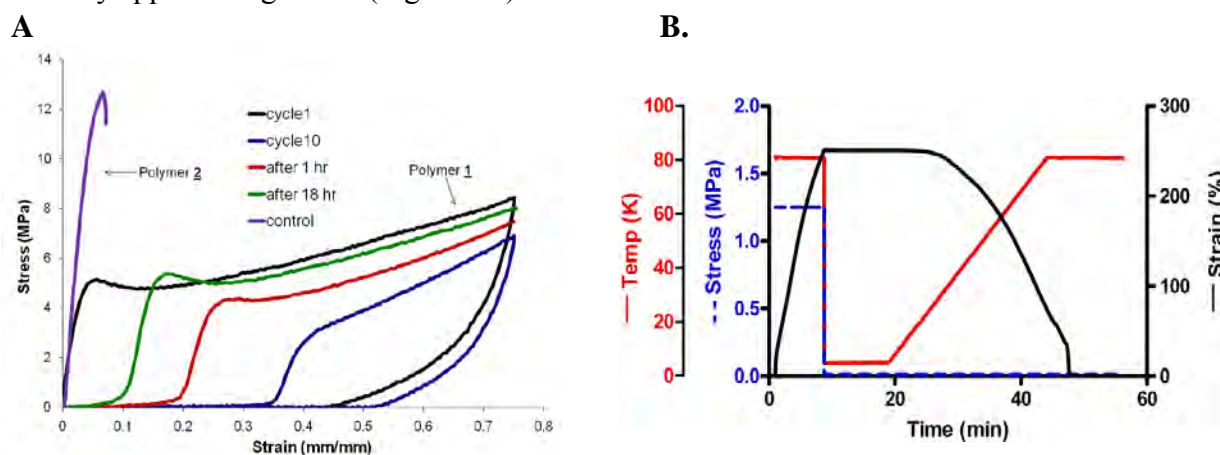


**Figure 1.** (A) Stress-strain curves for the biomimetic modular polymer **1** and control polymer **2**. For the modular polymer sample, multiple cycles of stress-strain were applied as indicated in the legend; (B) Shape-memory cycle for polymer **1** (color code: red – temperature, blue – stress, and black – strain).

Following successful demonstration of our biomimetic modular concept using organic model systems, we recently also developed peptide-based polymers with folded secondary structures. In previous year, we have demonstrated the application of Cu-catalyzed alkyne-azide cycloaddition (CuAAC, or the so-called “click” chemistry) to efficiently construct a  $\beta$ -turn mimic. Upon mixing two peptides derivatized with terminal azide and alkyne in presence of a Cu(I) catalyst, the two strands are ligated by formation of triazole ring which induces the formation of  $\beta$ -turn. We recently have successfully applied this methodology to the polymerization of a peptide module which induces the formation of extended  $\beta$ -sheet nanofibrils (Figure 2). A protected alanyl-glycine (AG)<sub>3</sub> monomer **4** having terminal alkyne and azide was efficiently polymerized into high polymer via CuAAC reaction. Upon deprotection of the 2,4-dimethoxybenzyl (DMB) group, the polymer folds into antiparallel  $\beta$ -sheet conformation and further self-assemble into hierarchical amyloid-like nanofibrils. The antiparallel  $\beta$ -sheet structure is confirmed by FTIR, CD and powder X-ray diffraction. TEM and AFM micrographs prove the formation of

hierarchical amyloid-like nanofibrils (Figure 2, right). To our knowledge, this represents the first example of polymerization-induced folding of a polymer into extensive  $\beta$ -sheets.

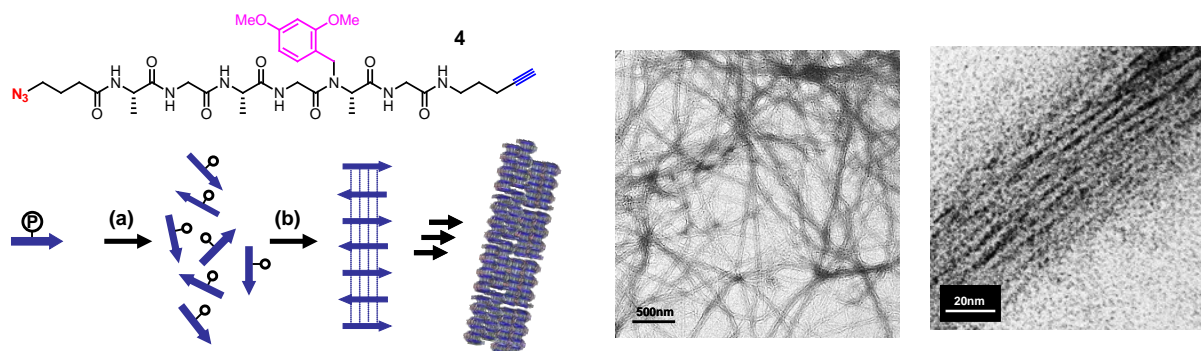


**Figure 2.** *Left:* Concept of cycloaddition-induced folding and self-assembly: (a) [2+3] cycloaddition polymerization of a protected peptide monomer; (b) upon deprotection polypeptides fold into well-defined antiparallel  $\beta$ -strands; (c) self-assembly of multiple  $\beta$ -sheets forms hierarchical nanofibrils. Chemical structure of the peptide monomer **4** is shown on top; *Right:* TEM image of nanofibrils at different magnification. The high resolution TEM image clearly shows the hierarchical assembly of the  $\beta$ -sheet peptide polymer.

**Future Plan:** We will continue our biomimetic modular polymer synthesis and investigations. For the linear array of modular polymers, we will conduct single molecule force studies and continue exploring their novel properties. We will continue our design and investigation of 3D network polymers containing reversibly unfolding modules. We have attempted synthesis of 3D networks using Diels-Alder reactions but encountered some technical difficulties. We will revise the design and try new routes in this coming year. For the “click” polymerization for induction of  $\beta$ -sheet polymers, we will expand the synthesis to polymers with other secondary structures. Eventually, our goal is to develop an efficient synthesis of silk-like polymers with exceptional strength and toughness. Finally, we plan to further investigate dynamic polymers with adaptive and self-healing properties.

### Publications 2007-2009:

1. “Biomimetic Design of Reversibly Unfolding Cross-linker to Enhance Mechanical Properties of 3D Network Polymers” Kushner, A. M.; Gabuchian, V.; Johnson, E. G. Guan, Zhibin. *J. Am. Chem. Soc.* **2007**, *129*, 14110.
2. “Supramolecular Design In Biopolymers And Biomimetic Polymers for Advanced Mechanical Properties” Guan, Zhibin. *Polymer International* **2007**, *56*, 467-473.

3. “Mechanical stability of peptidomimetic  $\beta$ -sheets revealed by steered molecular dynamics simulations” Guzman, Dora L.; Roland, Jason T.; Guan, Zhibin; Keer, Harindar; Ritz, Thorsten. *PMSE Preprints* **2007**, 97, 545.
4. “Biomimetic modular design for high-strength, high-toughness materials” Kushner, Aaron; Roland, Jason T.; Gabuchian, Vahe; Johnson, Evan; Guan, Zhibin. *PMSE Preprints* **2007**, 97, 334.
5. “Using Steered Molecular Dynamic Simulation and Single-molecule Force Spectroscopy to Guide the Rational Design of Biomimetic Modular Polymeric Materials” Guzmán, D. L.; Roland, J. T.; Keer, H.; Kong, Y. P.; Ritz, R.; Yee, A.; Guan, Zhibin. *Polymer* **2008**, 49, 3892.
6. “Bio-Inspired Supramolecular Design in Polymers for Advanced Mechanical Properties” Guan, Zhibin; Book chapter in “Molecular Recognition and Polymers: Control of Polymer Structure and Self-Assembly” Editors: Rotello, V. and Thayumanavan, S.; Wiley & Sons, **2008**.
7. Cycloaddition-Promoted Self-Assembly of a Polymer into Well-Defined  $\beta$ -Sheets and Hierarchical Nanofibrils” Ting-Bin Yu, Jane Z. Bai and Zhibin Guan. *Angew. Chem., Int. Ed.* **2009**, 48, 1097 –1101 [*highlighted by Angew. Chem. and SYNFACTS as high impact paper*].
8. “Biomimetic Modular Polymer with Unique Combination and Adaptive Mechanical Properties” Kushner, A.; Vossler, J.; Williams, G.; Guan, Zhibin. *J. Am. Chem. Soc.* **2009**, 131, 8766-8768 [*highlighted by C&EN News and Nature Chemistry*].
9. “Computational and single-molecule force studies of a macro domain protein reveal a key molecular determinant for mechanical stability” Guzmán, D.; Randall, A.; Baldi, P.; Guan, Zhibin. *Proc. Natl. Acad. Sci. USA*, in revision.

# Protein-Templated Synthesis and Assembly of Nanostructures for Efficient Hydrogen Production Using Visible Light

Arunava Gupta<sup>(a)</sup> and Peter E. Prevelige<sup>(b)</sup>

<sup>(a)</sup> University of Alabama, Tuscaloosa, AL 35487

<sup>(b)</sup> University of Alabama, Birmingham, AL 35294

[agupta@mint.ua.edu](mailto:agupta@mint.ua.edu)

[prevelig@uab.edu](mailto:prevelig@uab.edu)

**Program Scope:** The primary goal of the project is to develop some general protein-templated approaches for the synthesis and directed assembly of semiconductor nanomaterials and dyes that are efficient for visible light absorption and hydrogen production. We have successfully synthesized a variety of sulfide nanomaterials with controlled size, phase structure, and three-dimensional architectures, using *E.coli* bacteria and genetically engineered virus (P22) as affinity bio-templates. Some of the synthesized nanomaterials exhibit efficient photocatalytic hydrogen production under simulated sunlight of global AM 1.5 illumination. In particular, photoelectrodes fabricated using hexagonal structured CdS nanoporous hollow microrods using *E.coli* bacteria exhibit excellent performance for photocatalytic hydrogen production, with a photoconversion efficiency of up to 4.1 %. This is significantly better than the 1.34 % efficiency obtained using CdS nanoparticles synthesized utilizing the same procedure in the absence of *E. coli*. We are also investigating the ability of icosahedral structures as scaffolds for energy harvesting via Förster resonance energy transfer (FRET). For this purpose, we are using a form of the P22 capsid in which a cysteine residue replaces tryptophan 182 in the flexible loop region to conjugate Oregon Green and AlexaFluor 594 to P22 capsids.

**Recent Progress:** Cadmium sulfide (CdS) has a narrow band gap with a valence band at relatively negative potential, which is attractive for visible-light-active photocatalysis. By introducing a cheap sacrificial electron-donor, such as  $S^{2-}$  and  $SO_3^{2-}$ , with a redox potential higher than the anodic decomposition potential of CdS, the photo-electrochemically unstable CdS can be stabilized kinetically. For good photocatalytic activity, the material should have large surface area, good dispersity, and efficient electron transfer property. Thus, nanoporous hollow nanostructures are attractive since they can avoid the agglomeration problem of nanocrystals, with reduced bulk/interface electron/hole recombination. However, it is a challenge to assemble nanoparticles into highly ordered hollow nanostructures.

Hollow structures have recently attracted attention for a variety of applications, and are commonly fabricated on pre-synthesized templates such as polystyrene, silica spheres, etc. A number of microbiological organisms, including proteins, nucleic acids, phage, bacteria, and complex multicellular systems have also been investigated as templates. Using such biological systems, a number of inorganic nanomaterials have been synthesized with precisely controlled size, shape, structure, and functionality. These nanomaterials can be further assembled into more complex functional structures and devices. We are interested in investigating microbiological organisms, such as *Escherichia coli* bacteria and bacteriophage P22, as templates for the synthesis of hollow CdS and other inorganic nanostructures as photocatalysts.

Bacterial systems, including *Clostridium*, *Klebsiella aerogenes*, and *Escherichia coli* (*E. coli*), have been used to biosynthesize CdS nanocrystals. *E. coli* is of particular interest, since the genetic tools and cellular metabolisms associated with this bacterium are well understood. Using *E. coli*, intracellular hexagonal CdS nanocrystals have been produced with a size distribution of 2-5 nm when the bacteria are incubated in a solution containing cadmium chloride and sodium sulfide. However, the low permeability of cell envelope and efflux pump inhibition of the bacteria prevents nucleation of the inorganic throughout the cell envelope.

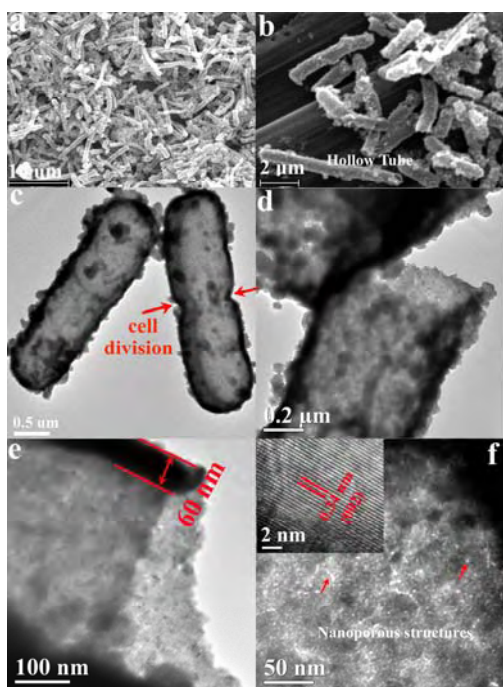


**Figure 1:** (a, b) SEM and (c-f) TEM images of *E. coli*-templated nanoporous hollow CdS microrods.

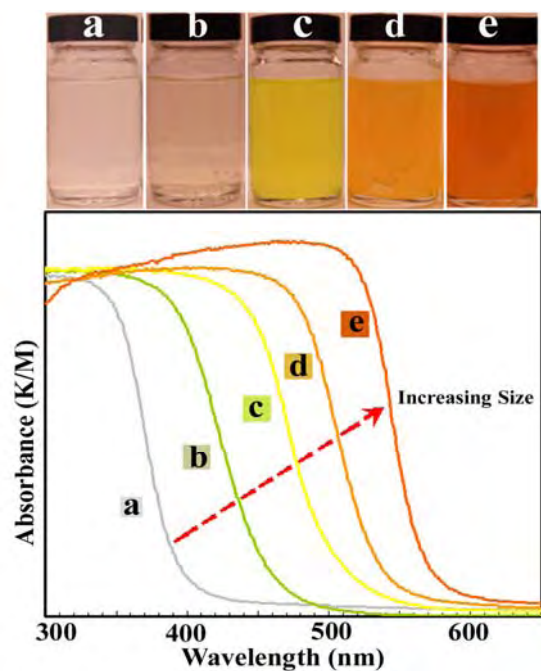


**Figure 2:** Optical images and UV-Vis spectra *E. coli*-templated CdS nanostructures in solution after (a) 0 min, (b) 1, (c) 10, (d) 120, and (e) 240 min of reaction.

We have developed a simple sonochemical route for the synthesis and assembly of CdS nanostructure with high yield under mild ambient conditions by exploiting the chemical characteristics and structure of permeabilized *E. coli* bacteria. The cell permeability is enhanced by ethanol treatment in order to enable  $\text{Cd}^{2+}$  adsorption and reaction throughout the cell envelope, and not just on the surface. Therby, by simply varying the reaction time, CdS nanostructures in the form of monodisperse quantum dots, near monodisperse nanocrystals, and nanoporous hollow microrods can be controllably formed throughout the whole cell envelope of the *E. coli* using cadmium acetate and thioacetamide as reactants. Figure 1 shows the typical morphology and structure of as-synthesized *E. coli*-templated nanoporous hollow CdS microrods obtained after a reaction time of 4 h. We have additionally fabricated novel structures consisting of CdS nanorod antennas attached to nanoporous hollow microrods by using the *E. coli* pili as templates. As expected, the synthesized CdS show a distinct red shift with increasing size of the nanostructures (Fig. 2). In addition to varying the morphology, we are able to precisely control the crystal phase of CdS products from cubic, mixture of cubic and hexagonal, to pure hexagonal by simply adjusting the sulfur/cadmium molar ratio of the reactants. Photoelectrodes fabricated using the hexagonal structure CdS nanoporous hollow microrods exhibit excellent performance

for photocatalytic hydrogen production, with a photoconversion efficiency as high as 4.1 % under global AM 1.5 illumination (Fig. 3). This is significantly better than the 1.34 % efficiency obtained using CdS nanoparticles synthesized using the same procedure in the absence of *E. coli*. Use of mixed chalcogenide nanostructures can potentially lead to further improvements in the photoconversion efficiency. The bacterial synthesis approach has been extended to the synthesis and assembly of other sulfides, including PbS, ZnS, and HgS.

Phage display techniques have been successfully utilized by the pharmaceutical industry for quite some time for the rapid identification, selection and evolution of peptide sequences against organic targets. In recent years, genetic engineering of phages has also provided unprecedented opportunities for the synthesis and assembly of a variety of nanostructured inorganic materials in the form of nanowires, quantum dots, nanoparticles, *etc.*, and in building

complex nano-architectures. Proteins that have an affinity to bind to technologically important materials can be rapidly screened and selected by biopanning techniques. In a number of systems, the unique recognition peptides of the genetically engineered phage can then be used to control the nucleation and growth of the desired material in the nanometer-scale, with specific crystal type and orientation, using simple solution chemistry methods that can be carried out under ambient conditions. While, the filamentous bacteriophage M13 has been investigated in some detail for materials synthesis, there has so far been no reported work using the icosahedral bacteriophage P22. The bacteriophage P22 is ~ 60 nm in diameter and the outer icosahedral procapsid shell is composed of 420 chemically identical subunits arranged on a symmetric T=7 sub-triangulated lattice. The procapsid form contains an internal scaffold composed of approximately 300 molecules of scaffolding protein anchored to the inner surface of the procapsid shell via a C-terminal helix-loop-helix binding motif. These scaffolding proteins can diffuse into or out of the procapsid shell, which offers the potential for both internal and external display of nanostructured inorganic materials.

Ongoing activities related to engineered bacteriophage P22 include:

- Nucleation of CdS crystal formation in P22 procapsids – P22 scaffolding protein carrying an N-terminal dodecapeptide sequence reported to nucleate CdS formation was introduced into the interior cavity of the 60 nm P22 capsid. The particles were purified and used to seed the nucleation of CdS crystal formation. Electron microscopic examination suggested the nucleation of multiple crystals within each procapsid.
- Synthesis of ZnS hollow nanospheres on P22 procapsid shells – Engineered P22 capsid shells have been used as template for the synthesis of hollow ZnS nanoballs under

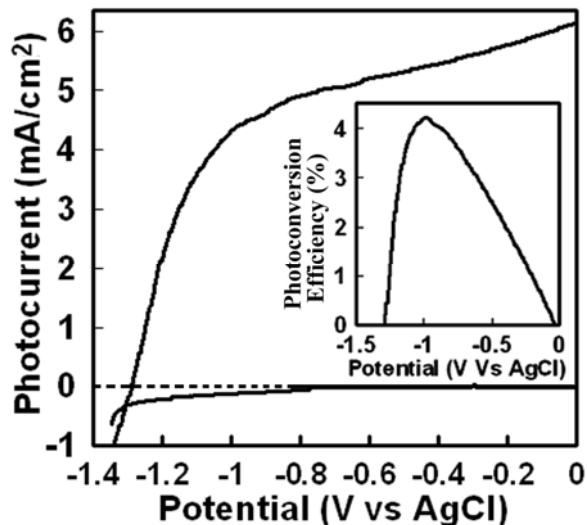


**Figure 3:** Photocurrent density and photoconversion efficiency (inset) of a photoelectrode fabricated using the *E. coli*-templated nanoporous CdS hollow microrods.

ambient conditions. The optimum peptide sequences for target ZnS inorganic material was determined by standard biopanning technique. The determined peptide sequences were then genetically engineered for specific proteins to help direct the spatially selective nucleation and growth of inorganic materials.

- Introduction of reactive cysteine residues in P22 procapsids – Based on a high resolution cryo-electron micrographic reconstruction of P22 procapsids six internally facing amino acids were targeted for cys replacement. Five of the six mutant capsids were capable of assembly and two of the six were readily chemically reactive to a variety of cysteine modifying reagents.
- FRET studies on labeled P22 procapsid shells – To ascertain the utility of icosahedral structures as scaffolds for energy harvesting various densities of donor (Oregon green) and acceptor (Alexa-Fluor 594) dyes were introduced into a unique cysteine on the surface of the T=7 P22 procapsids. At high donor concentrations donor self-quenching was observed and was unmitigated by increased acceptor density. Under optimal conditions an antenna effect of approximately 2 was observed. Modeling of the distance distribution between dyes at various loading concentrations provided theoretical insights into the extent of antenna effect observed.

**Future Plans:** In the coming year we will assay the ability of the constructed mutant P22 capsids to bind CdS, ZnS, PbS, TiO<sub>2</sub>, etc. We will also assay the ability of the full length and deleted scaffolding protein to bind the same materials and either re-enter the capsids or promote de novo assembly. These studies will center on altering the density of the scaffolding molecules as well as the fraction of the central cavity occupied by the scaffolding molecules. The number and size of the CdS crystals will be correlated with changes in the scaffolding content. The engineered P22 bacteriophages fused with the specific peptide sequences responsible for binding to Cd(Pb)S will be used to prepare porous hollow nanoballs. We will optimize the synthetic conditions for the best control of the shell thickness, the size of nanocrystal subunits, and the assembly of heterogeneous components. Photocatalytic activity and photoconversion efficiency of the obtained heterogeneous nanostructures will be evaluated. We will also continue the FRET studies on labeled P22 procapsids. Based on the distance distribution analysis, FRET pairs with longer Förster constants will be used to try and increase the antenna effect. Modifications to both the interior and exterior of the capsid will also be used in an effort to increase the antenna effect. In addition, spherical P22 shells homogeneously labeled with either donor or acceptor will be packed into close packed arrays by centrifugation. The ability of the close packed spheres to transfer will be determined as a function of the label density.

**Publication 2008-2009:**

*E.coli Bacteria-Templated Synthesis of Nanoporous Cadmium Sulfide Hollow Microrods for Efficient Photocatalytic Hydrogen Production*, L. Shen, N. Z. Bao, P. E. Prevelige and A. Gupta, submitted.

## VIRUS ASSEMBLIES AS TEMPLATES FOR NANOCIRCUITS

Michael T. Harris<sup>1</sup> and James N Culver<sup>2</sup>

<sup>1</sup>School of Chemical Engineering, Purdue University, West Lafayette, IN 47907

<sup>2</sup>Center for Biosystems Research, University of Maryland Biotechnology Institute,  
College Park, MD 20742-4450

[mtharris@ecn.purdue.edu](mailto:mtharris@ecn.purdue.edu)

[jculver@umd.edu](mailto:jculver@umd.edu)

### Program Scope:

The goals of this project are to develop the approaches and understandings needed to integrate biological and inorganic components for the creation of novel energy reactive materials. The chemistry of life encodes an incredible array of reaction mechanisms and functionalities. Increasingly, these life-based mechanisms are being investigated as potential cost effective methods to produce or enhance energy production and storage. Specific efforts in this project focus on the use of a well-defined plant virus, *Tobacco mosaic virus* (TMV) to identify fundamental understandings of bio-interface mineralization that enable the development of strategies for the assembly, patterning and functionalization of nanoscale surface features and devices. We anticipate that the processes developed in this study will have broad application for the engineering of a diverse array of biologically derived templates.

### Recent Progress:

Using TMV as a model system we have developed novel biotemplates and inorganic coating methodologies for the patterning of nanoparticles, wires and tubes onto numerous device surfaces. This work involves a multidisciplinary team with expertise in biology/protein engineering (Dr. Culver, University of Maryland Biotechnology Institute) and chemical engineering/nanophase structures (Dr. Harris, Purdue University). Ongoing efforts are focused on developing biological patterning methods that promote the self-assembly of virus templates into novel three-dimensional materials as well as understanding the fundamental biosorption properties regulating inorganic deposition onto a biologic template. Recent activities include:

Pd(II) ion biosorption on genetically engineered TMV. A major obstacle in the mineralization of metal onto biologically derived templates is the lack of fundamental information pertaining to the relationship between metal ion loading and overall metal deposition onto the biotemplate. A series of experiments have been conducted that focuses on Pd(II) biosorption on the model biological template TMV. Metal ion [Pd(II)] loading on the TMV template was measured as a function of the equilibrium concentration of Pd(II) ions in solution at several temperatures. Also, the Pd(II) loading on the unmodified TMV wild type template and a genetically modified TMV1cys template were compared to estimate the improvement of metal ion loading via the addition of novel cysteine residues to the virus template. The Pd(II) ion loading on the TMV1cys template was found to be twice that of its loading on the TMV wild-type template. Palladium coatings on the TMV1Cys were prepared at various metal ion loadings. Results show, for a range of metal ion loadings, a positive correlation between

the loading of the metal ions on the TMV and the coating density of the metals deposited on the virus surface.

Development of a reducing agent free method for enhanced biomineralization. The use of an external reducing agent can result in the inability to control the thickness of the metal deposition on the biotemplate due to the nucleation and growth of large metal particles or clusters in the solution and the subsequent deposition of these nonproductive particles onto the surface of the biotemplate. Improved palladium mineralization on TMV was achieved without the use of an external reducing chemical (Fig. 1). The Pd(II) ions were most probably reduced during the reaction of -PdCl and HOPd- groups and the subsequent oxidation of the Cl from -1 to a +1 oxidation state. The surface nucleated Pd nanoclusters on the amine/thiol surface groups formed an ~10 nm thick palladium layer with polycrystalline structure. The thickness of the palladium layer is potentially tunable in the nanometer scale by repeating the coating cycle. X-ray diffraction (XRD), electron energy loss spectroscopy (EELS), and high-resolution TEM analyses confirm the FCC crystal form of the Pd metal coatings. The results also suggest the formation of palladium or palladium hydride on the TMV biotemplate.

Virus assembled high aspect ratio platinum surfaces. Another area of recent progress involves the development of direct coating methodologies for metals that previously failed to coat virus assembled surfaces. In particular, we focused on platinum as a catalytic metal for use in hydrogen based fuel cells. Previous attempts to coat surface assembled viruses with Pt via standard electroless plating methods destabilized the biotemplate. Our analysis indicated that Pt ion equilibrium concentration, similar to the Pd loadings described above, was critical to achieving a uniform loading of Pt ions prior to metal reduction. Thus, by limiting initial Pt concentrations in the electroless plating solution it was possible to produce uniform Pt shells up to 30nm in thickness (Fig. 2). We have recently combined these coating methodologies with viruses genetically modified to bind “Nafion” membranes, the polymer most commonly used as a fuel cell electrolyte. Results indicated Pt coated virus assembled surfaces yield a >80 fold increase in active surface area. Ongoing studies are investigating the ability to tune Pt particles sizes, either directly on the virus or on silica-coated virus templates with the aim of creating high aspect ratio Pt surfaces for characterization in fuel cell applications.

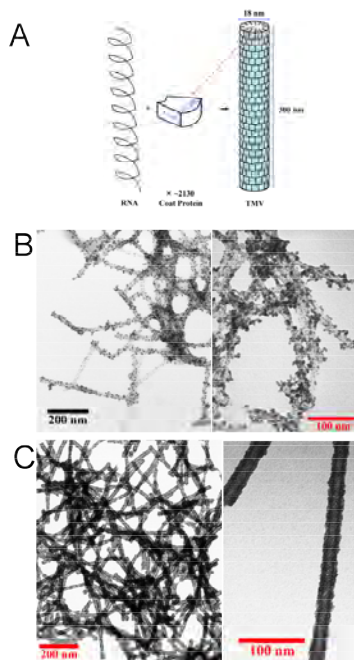


Figure 1. Improved metal deposition in the absence of a chemical reducing agent. A, Schematic diagram of TMV structure. B, Palladium nanocluster coatings on TMV1Cys (cysteine mutant TMV) via dimethylamine borane reduction. C, TMV1Cys templated palladium nanowire via a reducing agent free process.

Silica stabilized TMV templates for the production of metal and layered nanoparticles.

Biologically derived nanotemplates hold the potential to produce novel nanostructures of unique size, shape, and function. However, the inherent instabilities in these templates that give flexibility also inhibits their use in a diverse array of coating strategies, thus limiting their application. We have developed a silica coating strategy that promotes not only the stability of the bio-template but also its affinity for metal ions. The silica

provides a surface with well-known chemistry that is readily adaptable to mineralization strategies through the use of tin or crosslinking molecules. Enhanced bio-template stability was achieved using an aniline polymerization step prior to silica coating. This aniline step serves to neutralize protein charge and hydrophobic features that likely interfered with silica shell formation. Once encased in silica, the TMV bio-templates provided a highly stable and robust platform with several unique attributes that include; the deposition of metals at high densities, stability for long term storage, and resistance to sonication, organic solvents, and drying effects. Besides producing a robust bio-template for the production of nanoparticles, this silica shell process also allows the multi-layering of materials over the bio-template to create novel composites. We are currently investigating the enhanced solvent stability conferred via this process to develop virus assembled nanostructured catalytic surfaces for use in methanol based fuel cell applications.

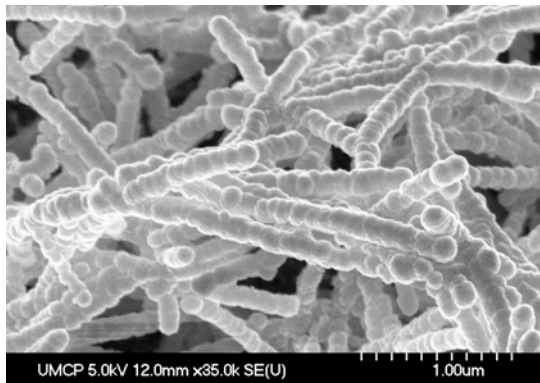


Figure 2. Silica coated surface assembled TMV.

**Future Plans:**

One area of future research is to develop theoretical models for the loading of metal ions on the surface of TMV. However, such a model requires a detailed understanding of the interaction of the metal ions and its complexes with functional groups on the surface of the TMV. To ascertain the interaction of the metal ions with a specific functional group, experiments will be done using silica particles that display specific functional groups found on the TMV surface to determine the interaction of the metal ion precursors and to obtain equilibrium constants for the model. Additionally, real time observations elucidating surface nucleation and biomineralization processes using *in situ* equipped TEM is under development. As an initial step, we are investigating the effect of *in situ* palladium hydrogenation on morphological changes in the metal structure. Combined, resulting knowledge from these efforts should be directly applicable toward the rational design of novel biotemplates for use in a variety of applications.

Another area of future research focuses on nucleic acid hybridization methods to assemble simple TMV based structures and circuits. We have recently designed a DNA based tiling system for the assembly of organized virus grids with defined spacings. Initial computational and experimental studies indicate that rigidity of the grid network is

an important factor in assembling virus arrays. Based on these findings we have designed a double-stranded DNA grid system for virus assembly at 50nm intervals. Testing of this grid system is currently in progress. Our long term goals are to develop methods to surface mount DNA grid patterns for subsequent hybridization with the virus template. Surface mounted grid assemblies will be tested for their ability to be coated with various reactive metals (Ni, Co, and Pt) with the aim of assembling patterned three-dimensional nano-featured surfaces. Ultimately, we envision utilizing the nucleic acid hybridization methods developed in this project to control the assembly of differentially functionalized nanoparticle templates, allowing us for the first time to precisely control the assembly of anodic, cathodic or catalytic materials on a nanoscale level.

#### **Publications in 2007-2009:**

Royston ES, Brown AD, Harris MT, Culver JN. 2009 Preparation of silica stabilized Tobacco mosaic virus templates for the production of metal and layered nanoparticles. *J. Colloid Interface Sci.* 332, 402-407.

Gerasopoulos K, McCarthy M, Royston E, Culver JN, Ghodssi R. 2008. Nanostructured Nickel Electrodes using the Tobacco Mosaic Virus for Microbattery Applications, *Journal of Micromechanics and Microengineering*, 18(10):1-8.

Lee SY, Lim JS, Culver JN, Harris MT. 2008. Coagulation of tobacco mosaic virus in alcohol-water-LiCl solutions. *J Colloid Interface Sci.* 324:92-98.

Royston, E, Ghosh, A, Kofinas P, Harris MT, Culver JN. 2008. Self-assembly of virus structured high surface area nano-materials and their application as battery electrodes. *Langmuir* 24:906-912.

Widjaja E, Harris MT. 2008 Numerical Study of Vapor Phase-Diffusion Driven Sessile Drop Evaporation. *Computers & Chemical Engineering*, **32**, 2169-2178.

Widjaja E, Harris MT. 2008. Particle Deposition Study during Sessile Drop Evaporation. *AIChE J*, **54**, 2250-2260 (2008).

Yi H, Rubloff, GW, Culver, JN. 2007. TMV Microarrays: Hybridization-based assembly of DNA-programmed viral nanotemplates. *Langmuir*, 23:2663-2667. Widjaja E, Liu NC, Li M, Harris MT. 2007. Dynamics of Sessile Droplet Evaporation: A Comparison of the Spine and the Elliptic Mesh Generation Methods. *Computers in Chemical Engineering*, 31:219-232.

## Designing Two-Level Biomimetic Fibrillar Interfaces

Anand Jagota\* ([anj6@lehigh.edu](mailto:anj6@lehigh.edu)) and Chung-Yuen Hui<sup>&</sup> ([ch45@cornell.edu](mailto:ch45@cornell.edu))

\* Department of Chemical Engineering & Bioengineering Program, Lehigh University, Bethlehem PA 18017

<sup>&</sup> Department of Theoretical and Applied Mechanics, Cornell University, Ithaca, NY 14853

**Program Scope:** Our aims are to study two-level biomimetic fibrillar structures, to achieve interesting surface properties such as enhanced adhesion, friction, and contact compliance. Our work combines bioinspired design of architecture, fabrication of these fibrillar architectures, measurement of their properties, and the development of detailed quantitative models. We have studied two systems:

1. A polymeric strip with a layer of fibrils terminated by a continuous thin film. Most of our work on fabrication, testing, and modeling has been on this structure, which exhibits greatly enhanced adhesion, compliance, and friction (Figure 1a).
2. A model core-shell fiber (Figure 1b). We have explored whether such a structure can result in self-forming compliant terminal elements that enhance adhesion.

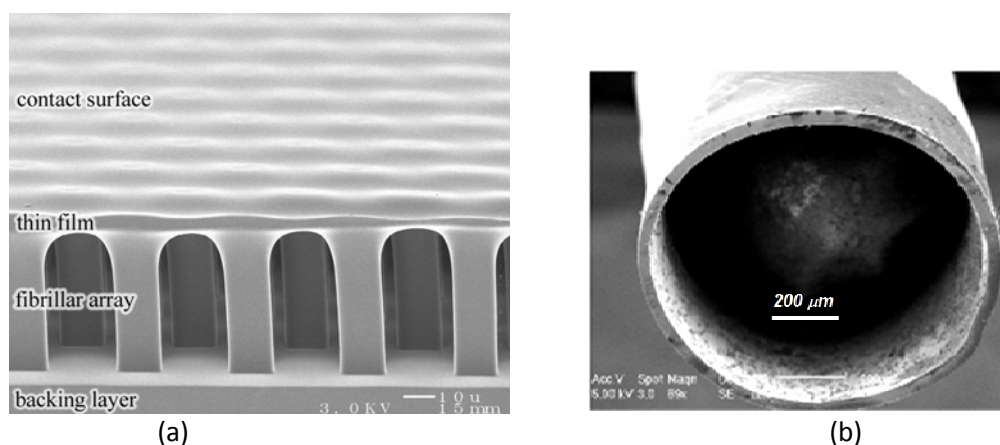


**Figure 1.** (a) Scanning electron micrograph of a film-terminated fibrillar interface. We can vary the fibril width, spacing, length, and terminal film thickness. (b) Scanning electron micrograph of a coated, partially etched, and trimmed core-shell fiber with shell thickness of about 25 microns.

**Recent Progress:** Our main accomplishments are

1. *The film-terminated fibrillar architecture (Figure 1(a)) results in strongly enhanced static friction, greater than a flat control sample by up to a factor of ten [1].* Figure 2 shows a few examples of shear force between a spherical indenter and a sample as the two are slid relative to each other. Notice the prominent “static” friction peak, which is much larger than the sliding friction force. The peak increases with fibril spacing; this allows one to control static friction by manipulating architecture. We have studied this phenomenon in detail since it also sheds light on the more fundamental question of the relationship between adhesion and friction. Figure 3 shows an image of the contact region from which we can directly measure the deformation of each individual fibril. This has allowed us to

develop a mechanistic model for how frictional force develops. Another very interesting feature we discovered was that the structure has essentially no influence on the sliding friction. Thus, surprisingly, our architecture allows one to *adjust static friction strongly without altering the sliding friction*. An advantage of our structure is that it is resistant to buckling during shear. Fibrils under shear buckle easily, thus, shearing a fibril array under normal load often cause the array to collapse, resulting in low static friction. We have demonstrated experimentally and theoretically that the continuous thin film in our structure can support the normal compressive load. In fact, fibrils in our experiments are in tension [3, 14] despite the fact that the applied load is compressive.

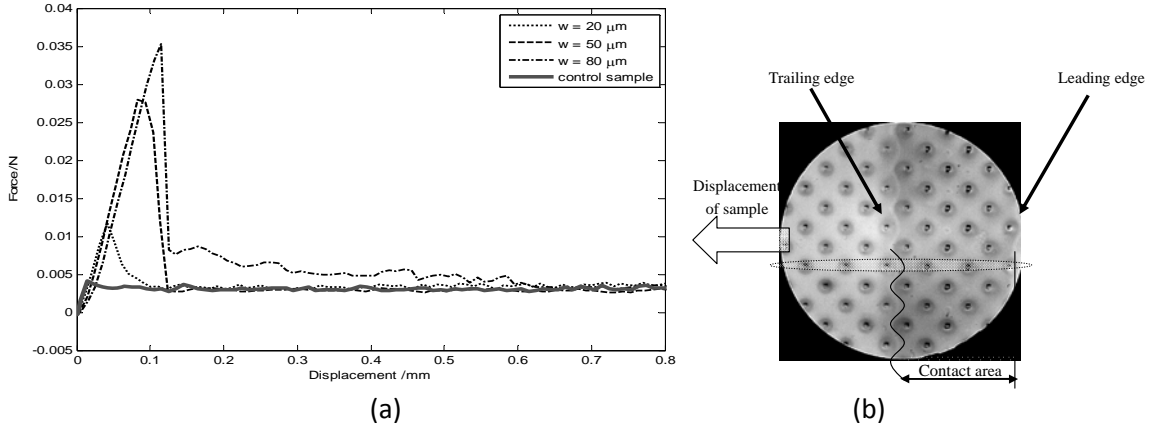


**Figure 2** (a) Shear force as a function of shear displacement for fibrillar samples with spacing of 20, 50 and 80  $\mu\text{m}$ , and for a flat control sample. Notice the strongly enhanced “static” friction peak. Notice also that sliding friction force remains substantially unchanged. (b) Optical micrograph of contact region prior to initiation of sliding. [1,10].

2. *Understanding the mechanism of static and sliding friction in the film-terminated architecture.* We have established that static friction enhancement is by crack trapping [6,12]. We have additionally studied rate effects [12], details of the sliding friction mechanism [10], and adhesion under water and against rough surfaces [13]. Specifically, we have demonstrated that both adhesion and static friction increases with shear displacement rate [12]. However, sliding friction is approximately independent of rate. We have discovered that the rate and crack trapping mechanisms are coupled to each other multiplicatively [12]. Thus, the architectural enhancement of adhesion operates *independently* of any chemical enhancement of adhesion. We have demonstrated that the presence of water gives rise to additional enhancement in adhesion [13]. A unique strength of our work is the tight quantitative coupling between experiments and theory.
3. *Model-independent extraction of works of adhesion from indentation experiments.* We have found indentation to be an excellent probe of compliance, adhesion, and frictional properties. This technique is used very widely in the field as well because of its ease of use, ease of sample preparation, and its ability to measure properties quickly and in a spatially resolved manner. Quantitative interpretation of measurements, for example, extraction of the adhesion energy from force-displacement-contact area data, typically requires one to use a theory such as the well-known Johnson-Kendall-Roberts model for adhesive contact. However, any small complexity, such as variable thickness, inhomogeneities, or complex architecture, invalidate the theory and there has been no method available to interpret

indentation experiments in terms of adhesion energy. Motivated by the needs of our own research, we have developed a method by which adhesion energy can be extracted directly from experimental measurements of force, displacement, and contact area *without the assumption of or need for a theory* [4].

4. *Core-shell architecture appears to be a promising design for separated terminal spatulae.* It is clear that a compliant (usually film-like) terminal element is a crucial element in all natural fibrillar structures. We have conducted a preliminary study to explore the possibility that such a structure can be fabricated using a core-shell approach (Fig. 1b). We have fabricated a terminal thin shell by selectively etching the aluminum core wire coated with an elastomer (PDMS). We find that the resulting structure exhibits greatly enhanced and pressure-sensitive adhesion in shear when pressed against a substrate [7]. Figure 3i shows measured shear and normal forces during an experiment in which the fibril is pressed against a glass substrate and then dragged in shear. We find that shear is accommodated by a stick-slip mechanism (Fig. 3ii).

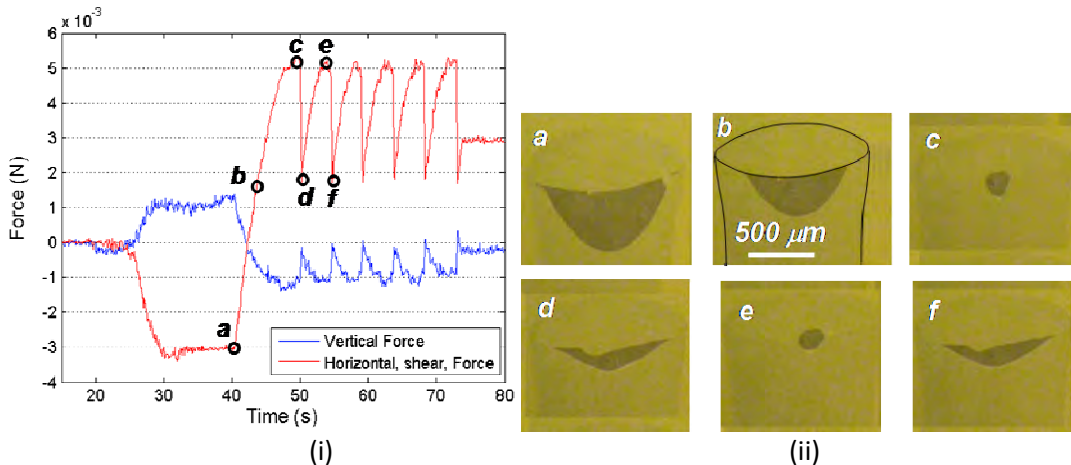


**Figure 3.** (i) Measured horizontal (shear) and vertical forces during a typical experiment. After an initial transition, the force traces are periodic, corresponding to stick-slip behavior. (ii) Optical micrographs of the contact region at selected points. In Figure *b* we have added lines to indicate sample edges which image poorly compared to the contact region.

5. *Mechanics of adhesion with large deformations.* Soft materials, such as those we are using, undergo large deformations during processes of interfacial separation. However, there are very few fundamental studies of the mechanics of adhesion under conditions of large deformation. We have conducted detailed analyses of adhesion problems under large deformations that address the physics of the detachment processes near stress concentrators such as the edge of indenters and cracks [8,9]. In the friction test, micro-fibrils are subjected to very large shear deformation. Therefore, the shear force acting on these fibrils cannot be captured by linear theory. We have developed a nonlinear rod model to characterize the normal and shear forces acting these fibers [3].

### Future Plans

- *Friction in Compliant Materials.* Our work has shown some new possibilities for friction that have not been understood in much detail. In this context, we will study the role of frictional mechanisms such as sliding, stick-slip, and Schallamach waves from the point of view of understanding their mechanics.

- *Complementary Surfaces*. We are opening a new direction in our research by developing architectures that generate pressure-sensitive adhesion only against one type of complementary surface.
- *Active control of properties* Most work in this field (ours and others') has been on design of passive structures. A second new direction that these enable is active control of properties by changing architecture in response to a mechanical stimulus such as pressure or strain, which we plan to investigate.
- *Demonstrate core-shell architecture using multiple fibrils*. We are continuing to work on large-scale fabrication of the promising single-fibril demonstration of a core-shell structure into an array of core-shell fibers.

### **Publications (2007-09)**

1. Lulin Shen, N.J. Glassmaker, A. Jagota and C.-Y. Hui, "Strongly Enhanced Static Friction Using a Film-Terminated Fibrillar Interface", *Soft Matter*, **4**, 618-625, (2008).
2. P. Pankaj and C.Y. Hui, "Strength statistics of adhesive contact between a fibrillar structure and a rough substrate, *Journal of the Royal Society, Interface*, vol. 5, 21,441-448 (2008).
3. Jingzhou Liu, Chung-Yuen Hui, Lulin Shen and Anand Jagota, "Compliance of a Micro-Fibril subjected to Shear and Normal loads", *Journal of the Royal Society, Interface*, **5**, 1087-1097, (2008).
4. S. Vajpayee, C.Y. Hui and A. Jagota, "Model-independent Extraction of adhesion energy from indentation experiments," *Langmuir*, **24** (17), 9401-9409, (2008).
5. Rong Long, Chung-Yuen Hui, Seok Kim and Metin Sitti, "Modeling the Soft Backing Layer Thickness, Effect on Adhesion of Elastic Microfiber Arrays", **104**, 044301, *J. of Applied Physics*, (2008).
6. Lulin Shen, Chung-Yuen Hui, and Anand Jagota, "A two-dimensional model for enhanced adhesion of film-terminated fibrillar interfaces by crack trapping", **104**,123506, *J. of Applied Physics*, (2008).
7. Matthew B. Havener, Vincent Sica, Tian Tang, Anand Jagota, "Biomimetic core-shell fibril for enhanced adhesion," *Langmuir*, **24** (12), 6182-6188, (2008).
8. V. R. Krishnan, C.Y. Hui and R. Long, "Finite Strain Crack Tip Fields in Soft Incompressible Elastic Solids", *Langmuir*, **2008**, **24** (24), pp 14245-14253.
9. V. R. Krishnan and C.Y. Hui, "Large deformation of soft elastic materials in adhesive contact with a rigid cylindrical flat punch", **4**, 1909-1915 *Soft matter*, (2008).
10. Lulin Shen, Anand Jagota, Chung-Yuen Hui, "Mechanism of Sliding Friction on a Film-Terminated Fibrillar Interface", *Langmuir*, **25** (5) 2772-2780 (2009).
11. R. Long and C.Y. Hui, "The effect of preload on the pull-off force in indentation test of micro-fibre arrays", *Proc. R. Soc. A.*, **465**, 961-981 (2009).
12. Shilpi Vajpayee, Rong Long, Lulin Shen, Anand Jagota and Chung-Yuen Hui, "Effect of rate on adhesion and static friction of a film-terminated fibrillar interface," *Langmuir*, **25** (5) 2765-2771 (2009).
13. Shilpi Vajpayee, Anand Jagota, Chung-Yuen Hui, "Adhesion of a Fibrillar Interface on Wet and Rough Surfaces," *Journal of Adhesion*, accepted (2009).
14. Jingzhou Liu, C.Y. Hui, A. Jagota, L. Shen, "A model for static friction in a film-terminated micro-fibril array," *Journal of Applied Physics*, accepted (2009).
15. Jingzhou Liu, C.-Y. Hui, A. Jagota, "Effect of fibril arrangement on crack trapping in a film-terminated fibrillar interface," *Journal of Polymer Science Part B: Polymer Physics* accepted (2009).

## (Bio)Chemical Tailoring of Biogenic 3-D Nanopatterned Templates with Energy-relevant Functionalities

Nils Kröger, Kenneth H. Sandhage  
School of Chemistry and Biochemistry  
School of materials Science and Engineering  
Georgia Institute of Technology  
901 Atlantic Dr. NW  
Atlanta, GA 30332  
[nils.kroger@chemistry.gatech.edu](mailto:nils.kroger@chemistry.gatech.edu)  
[ken.sandhage@chemistry.gatech.edu](mailto:ken.sandhage@chemistry.gatech.edu)

**Program Scope:** The goal of this project is to obtain fundamental understanding of methodologies for the (bio)chemical functionalization of the 3-D nanopatterned biosilica architectures produced by diatoms. The mechanisms of two completely different methodologies will be studied: (1) *in vivo* functionalization of diatom biosilica through molecular genetic engineering, and (2) *in vitro* functionalization through shape-preserving chemical conversion of diatom biosilica into high surface area silicon replicas. Understanding of these methodologies will be explored to establish methods for the incorporation of energy-relevant enzymes (hydrolases, oxidoreductases) into diatom biosilica and onto diatom biosilica-derived silicon replicas.

**Recent Progress:** The program is scheduled to start in September 2009. Therefore no recent progress can be reported yet.

**Future Plans:** A strong technological demand exists to develop the next generation of efficient, long cycle life, electrochemical energy storage/conversion devices (e.g., solid oxide fuel cells) and highly-active, recyclable, heterogeneous catalyst systems for the high yield processing of energy-relevant biomass. Dramatic improvements in the efficiency/yield and cycle life of such devices, while maintaining competitive costs, will require the development of inexpensive processes for mass producing robust, functional, three-dimensional (3-D) inorganic components with well-controlled nanostructures and tailored chemistries. Nature provides impressive examples of organisms that self-assemble intricate inorganic structures. A stunning variety of nanopatterned 3-D silica-based cell walls (frustules) are formed by diatoms (Figure 1).

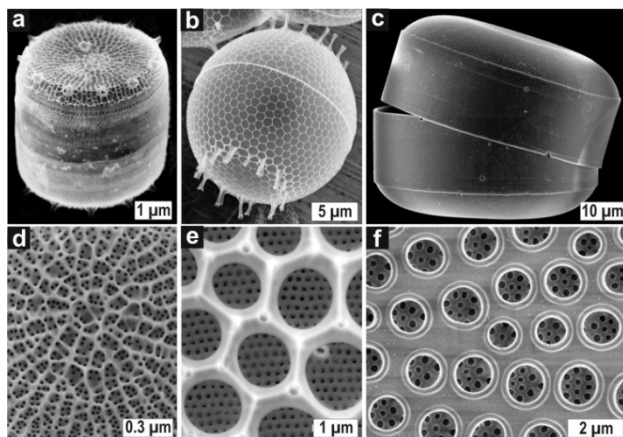


**Figure 1. SEM images of diatom silica.** Overviews and details of silica produced by different diatom species. *Thalassiosira pseudonana* (a, d), *Stephanosira turris* (b, e), and *Coscinodiscus granii* (c, d).

Diatoms are a large group of single-celled algae that are ubiquitously present in nearly all water habitats. Each of the tens of thousands of extant diatom species forms a frustule with a particular microscale shape and with nanoscale features that are reproduced with genetically-controlled fidelity from generation to generation. Hence, sustained reproduction of diatoms can yield enormous numbers of morphologically identical frustules. Such direct, precise 3-D assembly and massively-parallel reproduction under ambient conditions are highly attractive characteristics with no man-made analog. The well-controlled hierarchical (micro-to-nanoscale) morphologies of diatom frustules endow such structures with mechanical properties and mass transport characteristics that can be attractive for a number of applications, including filters or supports for macromolecular separations or catalysis. However, the native biochemistry and inorganic chemistry of diatom frustules have severely limited the range of applications for such biogenic structures. Recent work by the groups of Kröger and Sandhage has provided new capabilities for the (bio)chemical tailoring of diatom frustules for energy-related applications. Kröger's group has established a novel, genetic engineering-based method that enables functionalization of diatom silica *in vivo*, thereby opening a direct and sustainable route for the production of active silica-based nanomaterials. The Sandhage group has developed (and patented) gas/solid reaction methods for the shape-preserving chemical conversion of diatom silica *in vitro* into other inorganic materials (e.g., MgO, TiO<sub>2</sub>, ZrO<sub>2</sub>, Si), which enables unprecedented opportunities for the syntheses of chemically-diverse (silica-independent) functional devices with desired 3-D diatom nano- and micro-morphologies. While these breakthroughs provide necessary capabilities for the (bio)chemical engineering of diatom frustules, fundamental mechanisms associated with such genetic engineering and chemical modification are not well understood. Such basic understanding is needed in order to fully integrate and exploit the potential of these two novel processes for energy-relevant applications.

This interdisciplinary research program aimed at:

- ▶ *investigating the **biochemical mechanism** that enables functionalization of diatom biosilica *in vivo**
- ▶ *developing an understanding of the fundamental **mechanism of shape-preserving chemical conversion** of diatom biosilica into high surface area silicon replicas *in vitro**
- ▶ *applying *in vivo* and *in vitro* (bio)chemical methods to synthesize **active diatom-derived materials with energy-relevant functionalities***

The results from this research will **provide a novel paradigm for biologically-enabled syntheses of (bio)chemically-tailored, 3-D, energy-relevant nanostructured assemblies**. The program is divided into three interrelated Thrusts:

- Thrust 1:** *Mechanistic analysis of *in vivo* immobilization of proteins in diatom biosilica*
- Thrust 2:** *Mechanistic analysis of shape-preserving reactive conversion of diatom biosilica into high-surface area silicon replicas*
- Thrust 3:** *Immobilization of energy-relevant enzymes in diatom biosilica and onto diatom biosilica-derived silicon replicas*

**Thrust 1** is directed towards elucidating the fundamental mechanism underlying the cellular process of *in vivo* immobilization of proteins in diatom silica. This is essential for optimizing this

approach for the incorporation into diatom biosilica of highly active enzymes for energy-relevant applications (see Thrust 3). **Thrust 2** aims to understand the fundamental mechanism of shape preservation and nanostructure evolution associated with the reactive conversion of diatom biosilica templates into high surface area silicon replicas. The knowledge gained from research in Thrust 2 is expected to allow for enhanced control over the pore size distributions and surface areas of the silicon replicas which, in turn, will enable the tailoring of these replicas for use as critical components of electrochemical energy storage/conversion devices and applications in catalysis. **Thrust 3** will utilize results from the research activities in both Thrust 1 and 2 to explore strategies for *in vivo* and *in vitro* immobilization of enzymes (hydrolases, oxidoreductases) in diatom biosilica and diatom biosilica-derived silicon replicas, respectively. In this Thrust, we aim to synthesize novel biocatalytic materials of relevance for the chemical processing of biomass, and the production of biofuel cells.

### Relevant Previous Publications:

Z. Bao, E. M. Ernst, S. Yoo, K. H. Sandhage (2009) Syntheses of Porous Self-Supporting Metal Nanoparticle Assemblies with 3-D Morphologies Inherited from Biosilica Templates (Diatom Frustules). **Adv. Mater.** 21 [4] 474-478.

N. Kröger, N. Poulsen (2008) Diatoms- from cell wall biogenesis to nanotechnology. **Annu. Rev. Genet.** 42, 83-107.

R. F. Shepherd, P. Panda, Z. Bao, K. H. Sandhage, J. A. Lewis, P. S. Doyle (2008) Stop-Flow Lithography of Colloidal, Glass, and Silicon Microcomponents. **Adv. Mater.** 20 [24] 4734-4739.

N. Kröger (2007) Prescribing diatom morphology: toward genetic engineering of biological nanomaterials. **Cur. Opin. Chem. Biol.** 11, 662-669.

N. Poulsen, C. Berne, J. Spain, N. Kröger, N. (2007) Silica immobilization of an enzyme via genetic engineering of the diatom *Thalassiosira pseudonana*. **Angew. Chem. Int. Ed.** 46, 1843-1846.

Z. Bao, M. R. Weatherspoon, Y. Cai, S. Shian, P. D. Graham, S. M. Allan, G. Ahmad, M. B. Dickerson, B. C. Church, Z. Kang, C. J. Summers, H. W. Abernathy, III, M. Liu, K. H. Sandhage (2007) Shape-preserving Reduction of Silica Micro-Assemblies into Microporous Silicon Replicas. **Nature** 446 [3] 172-175.

N. Kröger, N. Poulsen (2007) Diatom Silica Biomineralization: Biochemistry and Molecular Genetics. In: **Handbook of Biomineralization: Biological aspects and structure formation.** (E. Baeuerlein, ed.) Weinheim: Wiley-VCH.

N. Kröger, M. B. Dickerson, G. Ahmad, Y. Cai, M. S. Haluska, K. H. Sandhage, N. Poulsen, V. C. Sheppard (2006) Bio-enabled synthesis of Rutile (TiO<sub>2</sub>) at ambient temperature and neutral pH. **Angew. Chem. Int. Ed.** 45, 7239-7243.

- N. Poulsen, P. M. Chesley, N. Kröger (2006) Molecular genetic manipulation of the diatom *Thalassiosira pseudonana* (Bacillariophyceae). **J. Phycol.** 42, 1059-1065.
- S. Shian, Y. Cai, M. R. Weatherspoon, S. M. Allan, K. H. Sandhage (2006) Three-Dimensional Assemblies of Zirconia Nanocrystals Via Shape-preserving Reactive Conversion of Diatom Microshells. **J. Am. Ceram. Soc.** 89 [2] 694-698.
- M. S. Haluska, R. L. Snyder, K. H. Sandhage, S. T. Mixture (2005) A Closed, Heated Reaction Chamber Design for Dynamic High-Temperature X-ray Diffraction Analyses of Gas/Solid Displacement Reactions. **Rev. Sci. Instr.** 76, 126101-1 - 126101-4.
- Y. Cai, S. M. Allan, F. M. Zalar, K. H. Sandhage (2005) Three-dimensional Magnesia-based Nanocrystal Assemblies via Low-Temperature Magnesiothermic Reaction of Diatom Microshells. **J. Am. Ceram. Soc.** 88 [7] 2005-2010.
- R. R. Unocic, F. M. Zalar, P. M. Sarosi, Y. Cai, K. H. Sandhage (2004) Anatase Assemblies from Algae: Coupling Biological Self-assembly of 3-D Nanoparticle Structures with Synthetic Reaction Chemistry. **Chem. Comm.**, [7] 795-796.
- K. H. Sandhage, M. B. Dickerson, P. M. Huseman, M. A. Caranna, J. D. Clifton, T. A. Bull, T. J. Heibel, W. R. Overton, M. E. A. Schoenwaelder (2002) Novel, Bioclastic Route to Self-Assembled, 3D, Chemically Tailored Meso/Nanostructures: Shape-Preserving Reactive Conversion of Biosilica (Diatom) Microshells. **Adv. Mater.** 14 [6] 429-433.

# Structure-Property Relationships of Polymer Brushes in Restricted Geometries and their Utilization as Ultra-Low Lubricants.

Tonya L. Kuhl and Roland Faller  
University of California-Davis  
Department of Chemical Engineering and Materials Science  
One Shields Avenue  
Davis, CA 95616

[tlkuhl@ucdavis.edu](mailto:tlkuhl@ucdavis.edu)

[rfaller@ucdavis.edu](mailto:rfaller@ucdavis.edu)

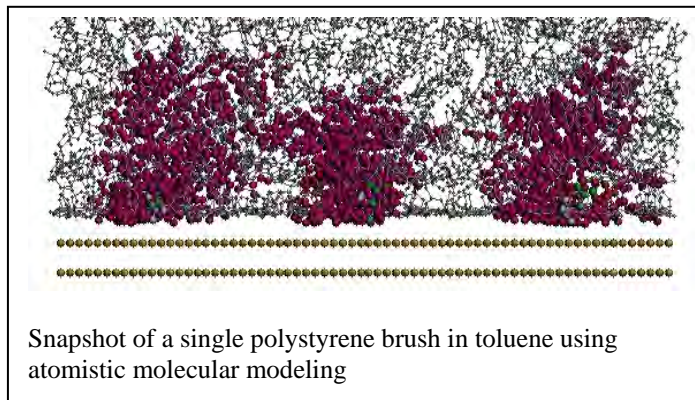
**Program Scope:** The goals of this project are to obtain a thorough understanding at the molecular level of high density polymer brushes under confinement. To this end an integrated experimental and computational project has been developed to elucidate the behavior of soft materials at interfaces in restricted geometries. We use neutron scattering in tandem with molecular simulations to elucidate the thin film structure and combine this with Surface Force Apparatus measurements to address the interactions. The studies also address the performance and response of thin films under shear.

Polymer molecules at solid or fluid interfaces have an enormous spectrum of applications in a wide variety of technologies from lubrication of mechanical surfaces to the synthesis of biocompatible interfaces. Over the past decade, neutron reflectivity measurements and molecular simulations have become powerful tools for measuring and predicting the conformations of ultra-thin polymer layers at interfaces, however the structure of polymer thin-films under confinement and/or shear has remained elusive due to the inherent difficulties in measuring and simulating thin-film properties under these conditions. To produce more effective lubricants requires a thorough understanding at the molecular level of surface interactions and the confined lubricant film's properties under load and shear. Towards this end, we have developed a novel apparatus – Neutron Confinement Shear Cell (NCSC), which enables the surface separation (<100nm) between aligned substrates to be controlled while simultaneously conducting in-situ structural characterization of the intervening material with neutron reflectivity measurements under static and dynamic shear conditions. By coupling these experimental measurements with molecular simulations we obtain a precise understanding of how the materials respond and are developing predictive models that can be used to design more effective lubricants.

Progress towards elucidating the structure of thin polymer films and ultimately their lubrication behavior has been made by several intertwined studies discussed below.

## Recent Progress:

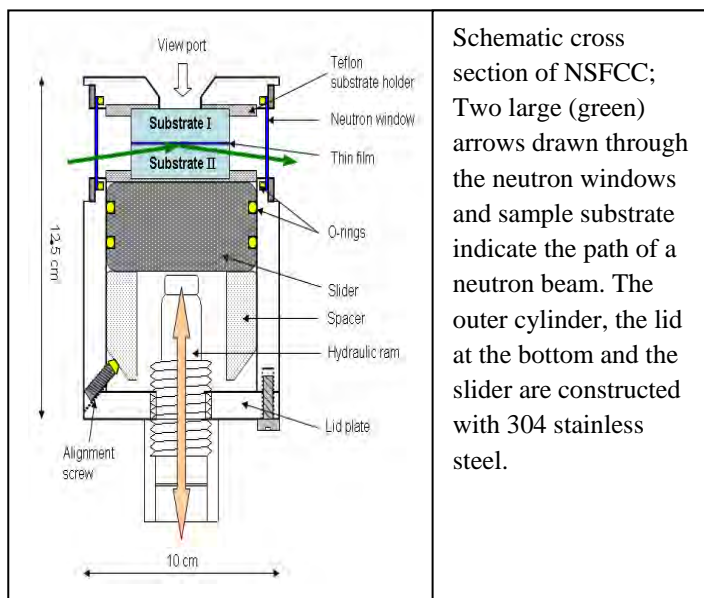
- Atomistic Molecular modeling** We have carried out extensive studies on the behavior of polystyrene brushes either dry or under good solvent conditions as a function of grafting density via detailed atomistic molecular dynamics simulations. We considered



- individual brushes as well as double layers of opposing brushes. The structural properties of single and double brushes were found to be similar. Using radial distribution functions and corresponding structure factors we are in a position to perform direct comparison with experimental investigations, and can thereby serve as a reference for scattering experiments. Additionally, we observe the formation of up to three ordered layers of toluene at the base of the grafted chains irrespective of the grafting density, similar to polymer depletion layers previously found close to the grafting surface. Information from simulations are currently being integrated into models to interpret the scattering experiments.
- Coarse Grained Modeling** To extend the simulations to longer chains and increase computational efficiency, coarse grained models have been developed. These molecular dynamics simulation studies have, so far, been used to study a single polymer brush system under static conditions. The initial model was developed for a polar polymer in polar solvent. We found that chain extension was heavily influenced by temperature, with large chain extensions from the surface at high temperature while surface adsorption dominated at low temperature. Increasing grafting density also increased chain extension due to excluded volume effects under all conditions. Polymer depletion regions were observed near the surface indicating an initial chain orientation normal to the surface. The exact details of the grafting pattern have not been found to affect the overall brush configuration, as grafting point effects were not significant beyond the first few monomers of each chain.
  - Neutron Scattering Characterization of ATRP Grown Brushes** The development of well controlled synthetic schemes for growing polymer brushes directly from surfaces has recently enabled very high polymer grafting densities to be explored. Here, we performed a study on the structure of polystyrene brushes as a function of molecular weight. The brushes were prepared by atom transfer radical polymerization (ATRP) at a high grafting density of  $0.44 \text{ chains/nm}^2$ . The dry film thickness scaled linearly with chain molecular weight. Under good solvent conditions, strongly stretched brushes of moderate molecular weight were found to maintain a parabolic density distribution consistent with theoretical predictions. Anomalous behavior was observed for higher

molecular weights suggesting that entanglements are much more pronounced in “grafted from” systems. As entanglements in thin films are far from understood this opens up an important new line of research.

- Development of Neutron surface force confinement cell** We constructed a new neutron surface force confinement cell (NSFCC). The NSFCC is equipped with hydraulically powered in situ, temporally stable, force control system for simultaneous neutron reflectometry studies of nanoconfined complex fluid systems. Test measurements with deuterated toluene confined between two opposing diblock copolymer (polystyrene+poly 2-vinylpyridine) coated quartz substrates demonstrated the capabilities of the NSFCC. With increasing hydraulically applied force, a series of well-defined decreasing separations were observed from neutron reflectivity measurements. No noticeable changes in the hydraulic pressure used for controlling the surface separation were observed during the measurements, demonstrating the high stability of the apparatus. This newly designed NSFCC introduces a higher level of control for studies of confinement and consequent finite size effects on nanoscale structure in a variety of complex fluid and soft condensed matter systems



**Future Plans:** Our experimental and simulational developments allow us now to co-analyze the data and obtain significant new insights by modeling directly the systems we are studying experimentally. We are starting to model large scale systems not available before which are reaching into length scales relevant for experiments. At the same time we are studying a wider range of confinement scenarios (distances) as well as chain lengths. We will systematically study the entanglement effects and for the first time determine entanglement lengths under confinement.

### Publications 2007-2009:

Cho, J.-H. J., Smith, G. S., Hamilton, W. A., Mulder, D. J., Kuhl, T. L., and Mays, J. “Neutron surface force confinement cell for neutron reflectometry studies of complex fluid under nano-confinement,” *Rev. Sci. Instruments* 79:103908 7pgs (2008).

Jayeeta Ghosh and Roland Faller: Comparing the density of states of binary Lennard Jones glasses in bulk and film J Chem Phys 128(12) 124509 (2008)

Petra T. Träskelin, Florence R. Pon, Qi Sun, and Roland Faller Multiscale modeling of polystyrene dynamics in different environments Proceedings of ESAT 2008, Cannes, France, ISBN 2-905267-59-3, pages 593-596

Jayeeta Ghosh, Masaomi Hatakeyama, Petra Träskelin, Chenyue Xing and Roland Faller: Molecular Modeling in confined polymer and biomembrane systems Songklanakarin J Sci Tech 31(2) 167-173 (2009)

# Structure and Dynamics of Vesicles in Solution

Erik Luijten

Department of Materials Science and Engineering  
Department of Engineering Sciences and Applied Mathematics  
Northwestern University  
2220 Campus Dr  
Evanston, IL 60208  
[luijten@northwestern.edu](mailto:luijten@northwestern.edu)

**Program Scope:** This project aims to elucidate the structure and dynamics of multicomponent mixtures of lipid vesicles, polyelectrolytes, and colloidal particles. Through the combination of different building blocks with individually designed properties, aggregation and self-assembly behavior in these solutions can be controlled and exploited to create functional materials. It is our goal to address the fundamental questions underlying this challenge by means of new computational strategies.

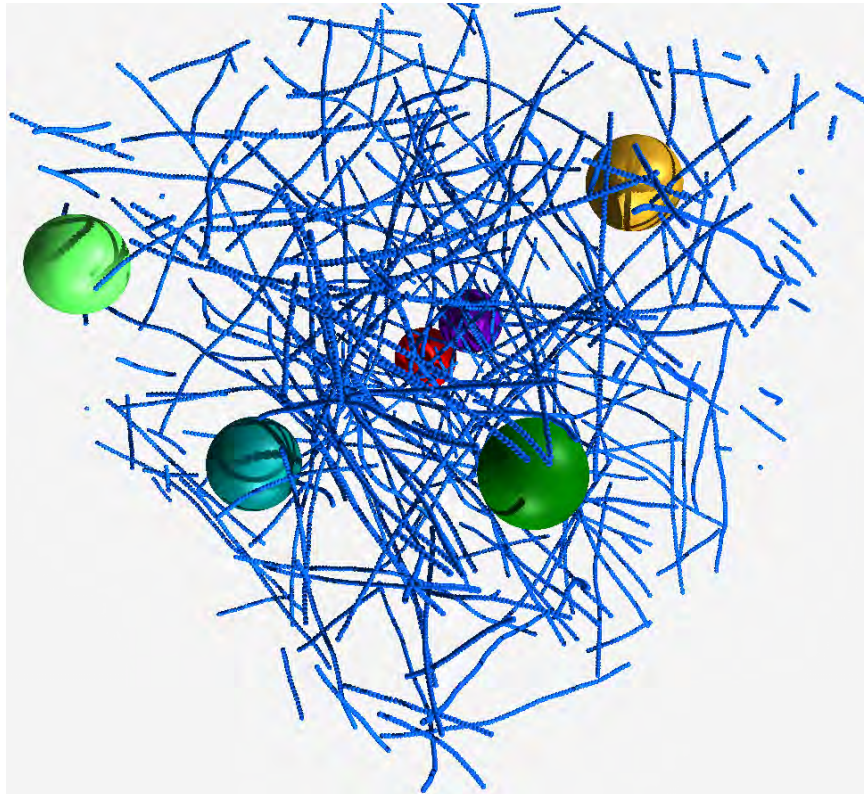


*Figure 1: Typical configuration obtained in a molecular dynamics simulation of deformable vesicles diffusing through a network of actin filaments.*

**Recent Progress:** The idea of creating functional materials through self-assembly of properly designed colloidal building blocks is being pursued by a considerable number of experimental groups. Many of these efforts concentrate on combinations of biological and synthetic components. Whereas such systems hold considerable promise, the use of multiple components results in a daunting parameter space. It is our aim to provide predictive capabilities, through the development of modeling tools that permit an efficient exploration of the effects of composition and particle dimensions and charge. We typically employ coarse-grained models that capture the essential properties of the original systems.

An important factor that must be considered in the study of self-assembly is the notion of phase separation. The phase behavior of multicomponent systems is not only notoriously complex, but also difficult to access by means of molecular dynamics simulations, as these simulations often do not operate in the appropriate thermodynamic ensemble. Thus, we specialize in grand-canonical Monte Carlo methods to elucidate the phase diagrams that frequently provide crucial insights in the driving forces for experimentally observed aggregation phenomena.

Concrete examples of recent achievements include:

- We have investigated the diffusion of vesicles through a network of actin filaments (see Fig. 1). In this situation, the deformability of the vesicles plays an important role once the mesh size is comparable to the vesicle diameter (see Fig. 2). In addition, the motion of the filaments must be incorporated in the simulations.

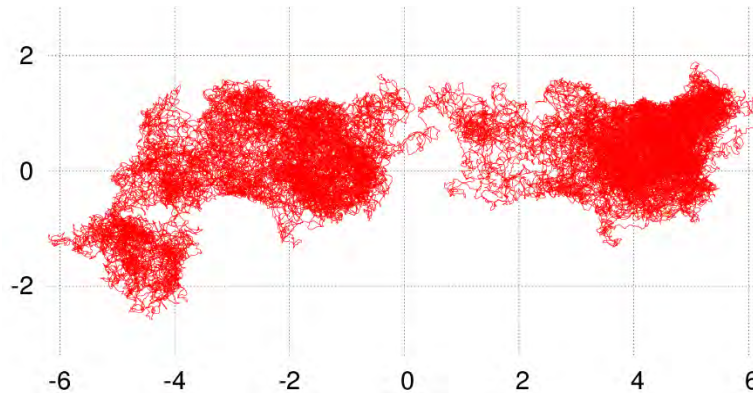


*Figure 2: Trajectory of a vesicle through an actin network with a mesh size of 150 nm, equal to ~70% of the vesicle diameter. The vesicle diffusion is highly localized.*

- We have demonstrated and quantified how small, rod-like particles can act as extremely efficient depletion agents, leading to strong aggregation behavior of colloidal particles at concentrations much smaller than those typically employed for polymeric depletants. This work could be realized through extending existing cluster Monte Carlo algorithms to systems with anisotropic components.

**Future Plans:** In many self-assembled materials the interactions between different building blocks are strong enough to lead to kinetically trapped states. Thus, proper prediction of these long-lived states requires knowledge of the system's time evolution, which in turn makes it important to include hydrodynamic effects as well as Brownian behavior. We have just completed the implementation of dynamic simulations that incorporate these effects. In particular, we are able to vary the slip coefficient of particles, and can even incorporate areas with different slip lengths on a single particle. While these capabilities are already sufficient to address questions that were hitherto inaccessible to simulations, we now intend to expand our modeling work to systems with both hydrodynamic and electrostatic effects.

# Room-Temperature Synthesis of Semiconductor Nanowires by Templating Collagen Triple Helices and Their Precise Assembly into Electrical Circuits by Biomolecular Recognition

PI: Hiroshi Matsui

695 Park Ave., Dept. of Chemistry, City University of New York, Hunter College, New York, NY 10065, hmatsui@hunter.cuny.edu

## I. Program Scope

The collagen triple helix is made of three polypeptide chains tightly twisted and bundled together to form a rigid, rod-shaped molecule. Collagen triple helices are monodisperse in length and diameter, which can be genetically designed and amplified by using the recombinant technology, and these triple helices can be mineralized with metals and semiconductors and can, thus, be applied as rigid biomolecular templates for electronic nanowire fabrications. The production of the triple helix can be cost-effective when the *E. coli* expression system is optimized for the amplification. The overall hypothesis is that collagen triple helices can be converted to multifunctional nanowires incorporating both antibodies and “mineralizing peptides”. Specificity of the biomolecular recognition of antibody enables us to immobilize multiple types of triple helices at desired positions respectively, based on logic circuit designs. By using enzymatic functions of the peptides, semiconductor nanoparticles are grown on triple helices at room temperature. The specificity of peptide sequence and conformation will enable us to mineralize these nanoparticles on the triple helices in the controlled size, shape, and inter-particle distance, which ultimately tunes the conductivity of resulting triple helices.

The outcome of proposed researches will have broad impacts in basic sciences and applied engineering because this peptide-templated material synthesis method has potential to create new nanomaterials possessing novel physical, structural, and catalytic properties with no synthetic counterparts. Development of methodology to produce materials at room temperature, which currently require high temperature to synthesize, will become a significant intellectual merit for manufacturing industries since it will reduce the production cost, the facility size (such as cooling systems), and the manpower in the facility.

## II. Recent Progress

### i) Electronic property of metal NP-coated peptide nanowires

When a Au mineralizing peptide, D-Y-F-S-S-P-Y-Y-E-Q-L-F, was incorporated on the surface of peptide nanowires, Au NPs were grown on the nanowire surfaces between pH 7 and pH 12. While CD spectra showed the conformational change of the peptide between pH 7 and pH 10, this conformational change of peptide did not induce the size change of Au NPs and the average size was 6 nm in both conditions. However, the density of Au NP was quite different between pH 7 and pH 10 samples. The density of Au NPs on peptide nanowires is very high when they are grown at pH 10 (Figure 1-(a)), while at pH 7 Au NPs are less dense on the peptide nanowire as

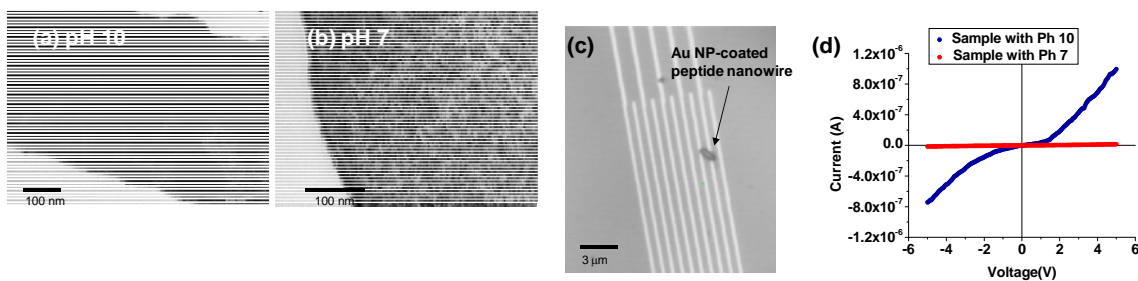


**Figure 1.** (a) TEM image of Au NPs on the peptide nanowire at pH 10. (b) TEM image of Au NPs on the peptide nanowire at pH 7. (c) SEM image of the interdigitated array of electrodes (1  $\mu\text{m}$  spacing) fabricated by electron beam lithography. The Au-coated peptide nanowire was shown by an arrow. (d) I-V curves of peptide nanowires of (a) and (b).

compared to the pH10 sample (Figure 1-(b)). When we measured resistance of these nanowires on interdigitated electrodes (Figure 1-(c)), the peptide nanowires with high-density Au NP coating has much lower resistance (25 M ohm) as compared to the low-density Au NP-coated nanowires (80 G ohm) as shown in Figure 1-(d). This result indicates that the density of Au NP on peptide nanowires is influenced by the peptide conformation and this morphology change is responsible to tune the conductivity, an important feature for future electric applications.

When the same Au biomineralization took place at pH 12, peptide nanowires tended to be bundled with the similarly dense Au NP coatings. These bundled nanowires possess a modest conductivity (resistance = 700 M ohm), however at this pH the bundled nanowires showed a hysteresis effect in Figure 2-(a) which indicates that there could be some oxygen absorption on the peptide nanowire where charges become trapped, similarly observed by single walled carbon nanotube (SWNT). Another possibility for the hysteresis is that the peptides on the nanowires behave as ligands and the peptide-capped Au NPs could create charge traps. When gate voltage was applied at a fixed bias voltage of 1.5 volts on these bundled nanowires (Figure 2-(b)), the  $I-V_{gate}$  plot shows approximately an order of magnitude change in the current when the back gate voltage becomes more negative indicating *p-type* FET behavior (Figure 2-(c)). We also calculated the electron mobility from this figure using the equation,  $\mu = (dI/dV_g) \cdot (L_2/V_{bias} C_G)$  where  $L = 1 \mu\text{m}$  is the length of the channel,  $C_G = 2\pi\epsilon\epsilon_0 L / \ln(2t/r)$ ,  $t = 250 \text{ nm}$  is the thickness of the oxide, and  $r = 250 \text{ nm}$  is the radius of the wire. From this calculation, we obtain a value of  $\mu \sim$

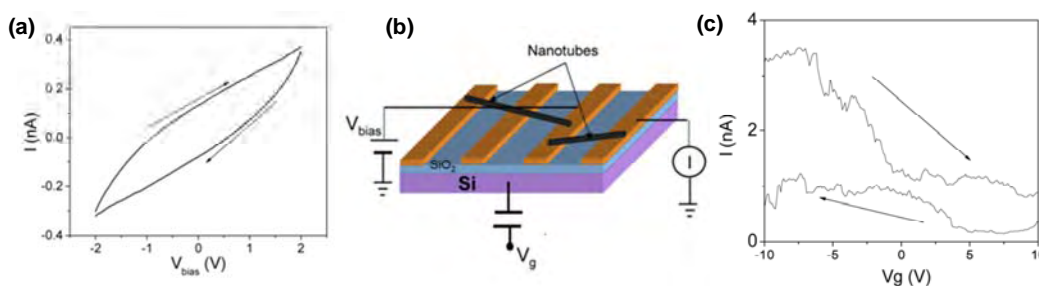


**Figure 2.** (a) Current vs. source drain voltage showing hysteresis from forward and reverse sweeps. (b) Schematic of the FET device and measurement setup with Au-coated peptide nanowires. (c) Current versus gate voltage for the lower resistance peptide nanowire ( $\sim 700 \text{ Gohm}$ ) that gives  $\mu \sim 0.03 \text{ cm}^2/\text{V}_s$ .

$0.03 \text{ cm}^2/\text{V}_s$  for the bundled Au-coated peptide nanowires.

ii) *Newly developed biomineralization nanolithography technique: Combination of bottom-up and top-down fabrications to grow arrays of monodisperse metal nanoparticles (NPs) along peptide lines on substrates*

Superior and distinguished physical properties of nanomaterials have attracted investigators to construct complex architectures in device configurations in nanometer-scale. For these

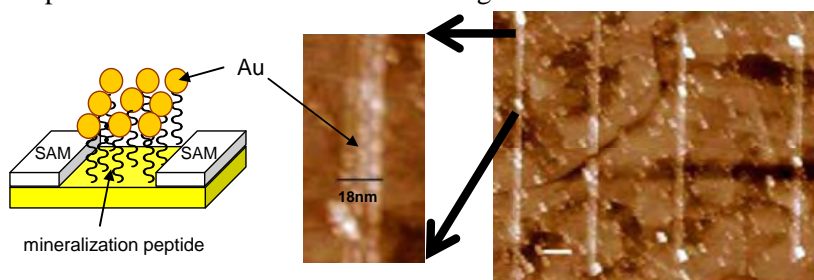


**Figure 3.** (left) Scheme of growth of the nanowire of Au nanoparticles on Au substrate by mineralizing Au nanoparticles on underlying HRE peptide array (AHHAHHAAD). (middle) Magnified AFM image of Au nanoparticles grown in the 18 nm width-trenches filled with HRE peptide. Three lines of Au NPs were aligned inside the trench in parallel to form Au nanowires (right) AFM image of four nanowires of the three-lined Au NPs grown on the HRE peptide array. [N. Nuraje, S. Mohammed, L. Yang, and H. Matsui, *Angew. Chem. Intl. Ed.*, **48**, 2546 (2009)]

fabrications, two major approaches have been applied; top-down and bottom-up assemblies, which have own strength and weakness. Here we combine the top-down and the bottom-up fabrications to grow arrays of monodisperse Au nanoparticles (Au-NPs) on peptide lines patterned on substrates (Figure 3). The part for the top-down came from the patterning of peptides which can effectively mineralize Au-NPs. Then the bottom-up fabrications were applied to grow Au-NPs on underlying peptide lines to produce the array of Au-NP lines. This biomineralization nanolithography yielded monodisperse Au-NPs in the line-array due to the mineralization function of peptide. Another advantage for our integrated technique is the simplicity to design the number of Au-NP lines on substrates; the number of lines of close-packed Au-NPs could be increased proportionally as the lines of the mineralizing peptides were patterned wider. This is one of the simplest methods to fabricate large-scaled arrays of monodisperse nanoparticles whose line width is less than 10 nm. The writing of Au-NP lines via nanolithography could be applied to wire electronic components in the complicated designs of logic gates, and the fabrication of line-arrays of the monodisperse nanoparticles could be useful in the fabrication of advanced photonic devices. The combination of biomineralization and nanolithography has a unique advantage to create the complex device geometries, and the types of nanoparticles can be expanded to semiconducting nanomaterials because recently various peptides were reported to behave as nanoreactors and they could catalyze semiconductor nanoparticle growths at room temperature. This result was published in *Angewandte Chem. Intl. Ed.*, (48, 2546 (2009)), and this paper was selected as a hot paper in 2009.

### **III. Future Plan**

Previously, we have developed a technique to immobilize antibody-conjugated peptide nanowires at desired locations by anchoring them at the positions where the complimentary antigens were marked. This antibody recognition-based nanowire assembly technique is suitable to establish the complex circuit fabrication requiring the multiple nanowire attachment at respective areas. In the last year's plan, we proposed to examine the nanowire alignment via dielectrophoresis as an alternative technique. We had preliminary results that the dielectrophoretic assembly of peptide nanowires on the electrodes is very robust and the strong interaction pulls nanowires instantaneously onto the desired location on the electrodes where AC field is applied. In addition to this finding, we observed that there is a correlation between the AC frequency of dielectrophoresis and the size of immobilized peptide nanowire. This is consistent with the dielectric difference between large and small peptide nanowires, whose dielectric constants are related to the size of peptide nanowire. We are very excited to find this phenomenon since it means that the dielectrophoresis approach could select the size of peptide nanowires and immobilize the only selected size of the nanowire onto desired substrate location. In the 3<sup>rd</sup> year of funding term, we would like to complete this new and sophisticated immobilization technique for the complex device fabrication.

In the 3<sup>rd</sup> year, we will also grow ZnO, CdSe, and PbSe on the peptide nanowires in various morphologies by changing size and density of the particle domain with the peptide functionality, and we will apply these semiconductor NP-coated peptide nanowires for the fabrication of field effect transistor (FET). During the 2<sup>nd</sup> year of our funding term, we accomplished the Au and ZnO nanowire fabrications by growing them on the peptide nanowires; The conformation and the charge distribution of the mineralizing peptides on the nanowires could control the morphology of the NP coatings, and the size of NP on the nanowires could sensitively tune the conductivity of the resulting nanowires as shown in the previous section. In the 3<sup>rd</sup> year, we will develop ZnO-, CdSe-, or PbSe-coated peptide nanowires featuring the field effect and assemble them into the simple transistors. We will also examine the reproducibility of *p-type* behavior of the bundled Au-NP-coated peptide nanowires (Figure 3-(c)) and investigate the origin of this property. The tunability of electric properties of the nanowires by changing the morphologies of ZnO, CdSe, and PbSe NP domains will also be examined. In addition to the peptide nanowire-based FET, the

bridging peptide nanowire in the gate structure of Figure 3-(b) will be replaced by the peptide nano-line written with our new biomineralization lithography technique (section 1-(i)), and the FET behavior of this semiconductor-grown peptide nano-line will also be investigated.

#### **IV. DOE-sponsored publications in 2007-2009**

1. "Single-Cell Pathogen Detection with a Reverse-Phase Immunoassay on Impedimetric Transducers", R. de la Rica, A. Baldi, C. Fernández-Sánchez, and H. Matsui, *Anal. Chem.*, **81**, in print (2009). (selected as a highlight paper in 2009)
2. "Long Electron-Hole Separation of ZnO-CdS Core-Shell Quantum Dots", F. Xu, V. Volkov, Y. Zhu, H. Bai, A. Rea, N.V. Valappil, X. Gao, I.L. Kuskovsky, and H. Matsui, *J. Phys. Chem. C*, **113**, accepted (2009).
3. "Selective detection of live pathogens via surface-confined electric field perturbation on interdigitated silicon transducer", R. de la Rica, A. Baldi, C. Fernández-Sánchez, and H. Matsui, *Anal. Chem.*, **81**, 3830 (2009).
4. "Biomineralization Nanolithography: Combination of Bottom-Up and Top-Down Fabrications to Grow Arrays of Monodisperse Au Nanoparticles along Peptide Lines on Substrates", N. Nuraje, S. Mohammed, L. Yang, and H. Matsui, *Angew. Chem. Intl. Ed.*, **48**, 2546 (2009). (selected as a hot paper in 2009)
5. "Low temperature synthesis of ZnO nanowire by using a genetically modified collagen-like triple helix as a catalytic template", H. Bai, F. Xu, L. Anjia, and H. Matsui, *Soft Matter*, **5**, 966 (2009).
6. "Label-Free Pathogen Detection with Peptide Nanotube-Assembled Sensor Chips", R. de la Rica, E. Mendoza, L.M. Lechuga, and H. Matsui, *Angew. Chem. Intl. Ed.*, **47**, 9752 (2008).
7. "Enzyme Urease as Nano-Reactor to Grow Crystalline ZnO Nanoshells at Room Temperature", R. de la Rica and H. Matsui, *Angew. Chem. Intl. Ed.*, **47**, 5415 (2008).
8. "Comparison of Electrical Properties of Viruses Studied by AC Capacitance Scanning Probe Microscopy", R.I. MacCuspie, N. Nuraje, S-Y. Lee, A. Runge, and H. Matsui, *J. Am. Chem. Soc.*, **130**, 887 (2008).
9. "Liquid/liquid interfacial epitaxial polymerization to grow single crystalline nanoneedles of various conducting polymers", N. Nuraje, S. Kai, N.L. Yang and H. Matsui, *ACS Nano*, **2**, 502 (2008).
10. "Virus Assay Using Antibody-Functionalized Peptide Nanotubes", R.I. MacCuspie, I.A. Banerjee, S. Gummalla, H.S. Mostowski, P.R. Krause, and H. Matsui, *Soft Matter*, **4**, 833 (2008).
11. "Crossbar Assembly of Antibody-Functionalized Peptide Nanotubes via Biomimetic Molecular Recognition", L. Yang, N. Nuraje, H. Bai, H. Matsui, *J. Pep. Sci.*, **14**, 203 (2008).
12. "Fabrication of Au nanowire of uniform length and diameter using a new monodisperse and rigid biomolecular template, collagen-like triple helix", H. Bai, K. Xu, Y. Xu, and H. Matsui, *Angew. Chem. Intl. Ed.*, **46**, 3319 (2007). (selected as a hot paper in 2007)
13. "Catalytic growth of silica nanoparticles in controlled shapes at planar liquid/liquid interfaces", N. Nuraje, K. Su, and H. Matsui, *New J. Chem.*, **31**, 1895 (2007).
14. "Biomimetic and Aggregation-Driven Crystallization Route for Room-Temperature Material Synthesis: Growth of  $\beta$ -Ga<sub>2</sub>O<sub>3</sub> Nanoparticles Using Peptide Assemblies as Nanoreactors", S.Y. Lee, X. Gao, H. Matsui, *J. Am. Chem. Soc.*, **129**, 2954 (2007).
15. "Single crystalline nanoneedles with fast conductance switching properties from an interfacial polymerization-crystallization of 3, 4-ethylenedioxythiophene", K. Su, N. Nuraje, L. Zhang, I.W. Chu, R.M. Peetz, H. Matsui, and N-L. Yang, *Adv. Mater.*, **19**, 669 (2007).
16. "Mineralization of semiconductor nanocrystals on peptide-coated bionanotubes and their pH-dependent morphology changes", I.A. Banerjee, G. Muniz, S-Y. Lee, and H. Matsui, *J. Nanosci. Nanotechnol.*, **7**, 2287 (2007).
17. "Highly Accurate Immobilization of Antibody Nanotubes on Protein-Patterned Arrays with Their Biological Recognition by Tuning Their Ligand-Receptor Interactions", Z. Zhao, H. Matsui, *Small*, **3**, 1390 (2007).

## **Biological and Biomimetic Low-Temperature Routes to Materials for Energy Applications**

Daniel E. Morse

Institute for Collaborative Biotechnologies  
University of California, Santa Barbara, CA 93106-5100 USA  
d\_morse@lifesci.ucsb.edu

### **Program Scope**

Biological systems fabricate multifunctional, high-performance materials at low temperatures and near-neutral pH with a precision of three-dimensional nanostructural control that exceeds the capabilities of present human engineering. Our analyses of the proteins, genes and molecular mechanisms governing the formation of silica in a marine sponge have revealed a unique mechanism of synthesis with industrial applicability for the low-temperature manufacture of nanostructured materials with compositions and structures that were not previously attainable. Advantages of these novel materials for applications in energy generation, transduction and storage are under investigation.

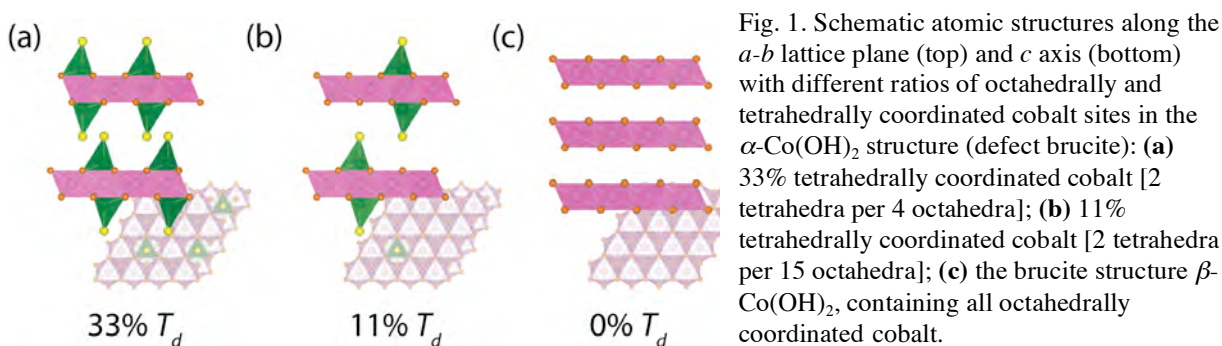
### **Recent Progress**

**1. Summary:** We discovered the mechanism governing the nanofabrication of silica in a marine sponge, and translated this mechanism to develop a generic bio-inspired low-temperature route for the kinetically controlled catalytic synthesis of a wide range of nanostructured semiconductor thin films and nanoparticles. We learned that the silicateins - proteins we found occluded in the glass skeletal elements of a sponge, self assemble via a previously unsuspected pathway to form macroscopic, crystallographically ordered filaments, and that these filaments can enzymatically catalyze and template the synthesis of silica and a wide variety of silsesquioxanes and metal oxide semiconductors from the corresponding molecular precursors at low temperature and near-neutral pH. The molecular mechanism of action of the silicateins was revealed by genetic and molecular analyses and confirmed with a series of biomimetic, synthetic analogs and catalytic self-assembled monolayers that mimic the catalytic and templating features of the natural protein.

From this information, we developed a generic new, biologically inspired low-temperature route for the kinetically controlled catalytic synthesis of a wide range of nanostructured metal oxide, -hydroxide, -phosphate and bimetallic perovskite semiconductor thin films and nanoparticles without the use of organic templates. Post-synthesis conversion to the nitrides and sulfides has been demonstrated. Because no organics are used, this new biologically inspired synthesis method yields high purity inorganic semiconductors, and thus is potentially integrable with MOCVD, CMOS and other conventional manufacturing methods. Employing gentle catalysis at low temperature, this method yields a wide range of nanostructured materials that exhibit unique combinations of structures and properties not readily attainable by conventional high-temperature processes; these exhibit potential advantages now under investigation for improved energy conversion and storage, ferroelectric random access memory, infrared and piezoelectric detectors, optoelectronics and flexible displays. The novel pathway of silicatein self-assembly additionally suggests a powerful new design principle for synthetic materials and structures.

**2, Harnessing the lessons from biological nanofabrication: low-temperature, kinetically controlled catalysis:** We employ vapor diffusion of a catalyst through a gas-liquid interface to provide kinetically and vectorially controlled catalysis, at low-temperature, of synthesis from molecular precursors that require hydrolysis prior to polycondensation. The method relies on the integrated tuning of molecular precursors and vectorially controlled catalysis, utilizing only chemical physics and highly purifiable inorganic components, *with no biochemicals, biologicals or organic materials*. The use of the molecular precursor and its vectorially controlled catalytic hydrolysis provide coordinate kinetic and directional control of semiconductor growth not afforded by conventional high-temperature approaches.

Using the kinetic control afforded by our synthetic method to control the crystal chemistry and the development of structure of the layered cobalt hydroxides, we found that we can control the relative proportions of octahedrally and tetrahedrally coordinated cobalt in the final product by carefully regulating the rate of hydrolysis of the precursor:



We are using this ability to kinetically control the structures of these materials to investigate the structural dependence of the photovoltaic and photomagnetic properties and magnetic ordering we have discovered in these materials. (See James Neilson's poster for details.)

We also have taken advantage of the kinetic control of nanocrystal growth afforded by this low temperature method to make the smallest (2 nm) nanocrystalline particles of cerium oxide yet reported. These offer a wide range of potential advantages for applications ranging from catalysis and water splitting to wafer planarization as a consequence of their unique reactivity with oxygen.

**3. Proof of principle applications for energy harvesting and storage:** In collaboration Jean Fréchet and his colleagues at LBL's Molecular Foundry, we fabricated a prototype hybrid solar cell based on the high surface area nanostructured cobalt hydroxide thin film described in the previous section. This proof-of-principle represented the first bio-inspired energy-harvesting device made with no biological or biomolecular components.

A powerful advantage of the gentle, low-temperature, biologically inspired synthesis method described above is the ability to preserve the inter-metallic structure of bimetallic precursors to produce high quality nanostructured ferroelectric perovskites such as  $\text{BaTiO}_3$  with very high purity and crystallinity and no detectable phase segregation. We scaled-up this method to routinely make >100 gram quantities of 6 nm  $\text{BaTiO}_3$  nanoparticles in high yield (99%) and purity. When doped and sintered, the resulting fine-grained nanocrystalline ceramic exhibits a strong positive thermal coefficient of resistivity (PTCR) with a sharp increase of resistance of

10,000-fold when heated above the Curie temperature of ca. 130 °C. We are optimizing this material for use as an internal protectant against thermal runaway in Li ion batteries.

We also have used the method described above for the kinetically controlled catalytic synthesis of a novel composite of Sn particles homogeneously dispersed throughout the resilient and conductive matrix of graphite microparticles. This advantageous distribution results from the growth of the metal nanoparticles *in situ* within the porous graphite matrix, while preserving the high crystallinity of the graphite. Used as an anode for Li ion batteries, this composite exhibits 30% greater specific electrochemical capacity than that of present commercial graphite anodes, with exceptionally stable cyclability through multiple cycles of charge and discharge, under conditions in which a composite with comparable content of Sn fabricated by conventional procedures exhibits rapid deterioration and loss of capacity. Nanocrystalline vanadium oxide fabricated by this method exhibits 70% greater specific electrochemical capacity than that of present commercial cathodes for Li batteries, also with exceptionally stable cyclability.

**4. Extension to other modes of catalysis:** As an extension of the studies described above - that all are based on the chemistry of kinetically controlled *catalysis of hydrolysis* - we discovered an enzyme that catalyzes the low-temperature transfer of nitrogen for the direct synthesis of nanocrystalline gallium nitride. This new discovery opens the path to low-temperature catalytic nanofabrication of the valuable nitride-based semiconductors, and even more significantly, extends the proof-of-concept that biological mechanisms of materials synthesis can lead to the development of innovative methods for low-temperature nanofabrication of a wide range of materials important for energy applications.

### **Future Plans**

We plan to extend the investigations summarized above. We will further investigate the use of our biologically inspired low-temperature catalytic system for the kinetically controlled synthesis of layered metal oxides, hydroxides and perovskites to predictively control (or “tune”) chemical structure and physical (electronic, optical and magnetic) properties important for energy applications.

We also plan a deeper genetic and biophysical investigation of the semiconductor-producing silicatein proteins that we discovered self-assemble to yield hierarchically structured filaments capable of catalytically synthesizing and structurally directing the low-temperature formation of silica and various semiconductors, to better understand the path to genetically encoded trajectories to different, specific self-assembly outcomes. The objective of this work, extending our two recent discoveries and publications based on this system, is to better understand the mathematical potential that can be written to describe this trajectory for a given protein, and to identify the sensitive parameters comprising that potential that can be predictively manipulated to obtain a different outcome. (E.g., how can we change the silicatein subunits so that they self-assemble to yield a sheet, rather than a filament – and can we then use that protein sheet to catalytically template the formation of a thin-film of semiconductor?)

We will continue to build on our ongoing collaborations with research leaders at DOE facilities, including LBL’s Molecular Foundry, Stanford’s SSRL and ORNL’s CNMS.

### DOE-Sponsored Publications, 2007-2009:

- Weaver, J.C., J. Aizenberg, G. E. Fantner, D. Kisailus, A. Woesz, P. Allen, K. Fields, M. J. Porter, F. W. Zok, P.K. Hansma, P. Fratzl and D. E. Morse. 2007. Hierarchical Assembly of the Siliceous Skeletal Lattice of the Hexactinellid Sponge *Euplectella aspergillum*. J. Structural Biology 158: 93-106 (+ cover).
- Gomm, J.R., B.Schwenzer and D. E. Morse. 2007. Textured films of chromium phosphate synthesized by low-temperature vapor diffusion catalysis. Solid State Science 9: 429-431.
- Adamson, D.H., D.M. Dabbs, C. Pancheco, M.V. Giotto, D.E. Morse and I.A. Aksay. 2007. Non-peptide polymeric silicatein alpha mimic for neutral pH catalysis of silica condensation. Macromolecules 40 5710-5717.
- Gayathri, S., R. Lakshminarayanan, J. C. Weaver, D.E. Morse, R M. Kini and S. Valiyaveetil. 2007. In vitro study of magnesium-calcite biomineralization in the skeletal materials of the seastar, *Pisaster giganteus*. Chemistry- A European Journal 13: 3262-3268.
- Schwenzer, B. and D. E. Morse, 2008. Biologically inspired synthesis route to three-dimensionally structured inorganic thin films. Journal of Nanomaterials, vol. 2008, Article ID 352871, 6 pages, 2008. doi:10.1155/2008/352871.
- Brutchey, R. L., G. Cheng, Q. Gu, and D. E. Morse. 2008. Positive temperature coefficient of resistivity in donor-doped BaTiO<sub>3</sub> ceramics derived from nanocrystals synthesized at low temperature, Adv. Mater. 20: 1029-1033.
- Miserez, A., J. C. Weaver, P. J. Thurner, J. Aizenberg, Y. Dauphin, P. Fratzl, D. E. Morse and F. W. Zok. 2008. Effects of laminate architecture on fracture resistance of sponge biosilica: Lessons from nature. Adv. Func. Mater. 18: 1241-1248 + cover.
- Morse, D.E. and R.L. Brutchey. 2008. Very low-temperature, gram-scale synthesis of monodisperse BaTiO<sub>3</sub> nanocrystals via an interfacial hydrolysis reaction. Materials Research Society Proceedings 2008: 1-7.
- Brutchey, R. L. and D. E. Morse, 2008. Silicatein and the translation of its molecular mechanism of biosilicification into low temperature nanofabrication methods. Chem. Revs. 108: 4915-4934.
- Schwenzer, B., L. Pop, J. Neilson, T. B. Sbardellati and D.E. Morse. 2009. Nanostructured ZnS and CdS films synthesized using layered double hydroxide films as precursor and template. Inorganic Chemistry 48(4), 1542-1550.
- Murr, M.M., G. S. Thakur, Y.-L. Li, H. Tsuruta, I. Mezić and D. E. Morse. 2009. New pathway for hierarchical self assembly and emergent properties. 2009. Nano Today 4: 116-124.
- P. O'Leary, C.A. v.-Walree, N. C. Mehendale, J. Sumerel, D. E. Morse, W. C. Kaska,\* G. v.-Koten and R. J.M. K. Gebbink. 2009. Enzymatic immobilization of organometallic species: Biosilification of NCN- and PCP-pincer metal species using demosponge axial filaments. Dalton Transactions 22: 4289-4291
- Schwenzer, B., J.R. Neilson, K. Sivula, C. Woo, J. M. J. Fréchet and D. E. 2009. Nanostructured *p*-type cobalt hydroxide thin film infilled with a conductive polymer yields an inexpensive bulk heterojunction photovoltaic cell. Thin Solid Films 517: 5722-5727.
- F. Qian, M. Baum, Q. Gu and D. E. Morse. 2009. A 1.5 mL microbial fuel cell for on-chip bioelectricity generation. Lab on a Chip. (in press.)
- Zhang, H.-L. and D.E. Morse. 2009. Vapor-diffusion catalysis and *in situ* carbothermal reduction yields high performance Sn@C anode materials for lithium ion batteries. J. Mater. Chem. (submitted).

## Observation and Simulations of Transport of Molecules and Ions Across Model Membranes

Sohail Murad and Cynthia Jameson ([murad@uic.edu](mailto:murad@uic.edu); [cjames@uic.edu](mailto:cjames@uic.edu))

University of Illinois at Chicago  
Department of Chemical Engineering  
Chicago IL 60607

**Program Scope:** The goals of the project are to understand the molecular mechanism of transport of molecules and ions through phospholipid bilayer membranes. These studies will include a modeling component using the methods of coarse grained molecular dynamics and experiments using nuclear magnetic resonance (NMR) and magnetic resonance imaging (MRI).

**Recent Progress:** There is an urgent need to understand basic permeation functions of a biomembrane, since many important biological processes are dependent on such permeation. We have carried out molecular dynamics simulations using dipalmitoylphosphatidylcholine (DPPC)

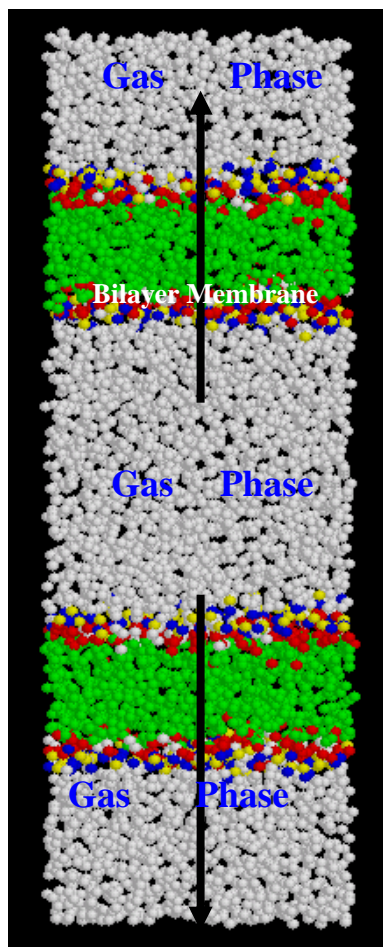
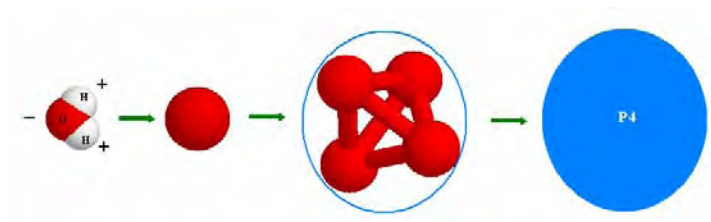


Figure 1. Two bilayers of DPPC bounded above and below by bulk water containing dissolved gas.

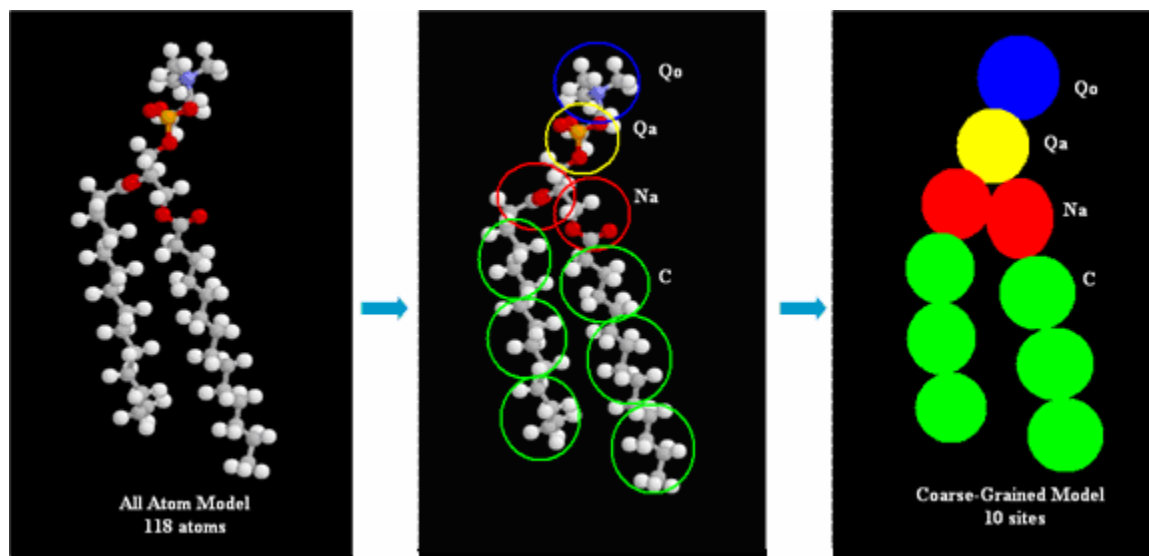
as the bilayer membrane (see Fig. 1). Using coarse grained molecular dynamics and our unique arrangement of the membranes and bulk phases, we were able to show for the first time the entire permeation process of small gases such as Xe, O<sub>2</sub> and CO<sub>2</sub> from the bulk gas phase through the lipid bilayers to another bulk phase as shown in the figure. Our results showed that by using coarse grained MD which allows us to have access to much larger time scales, we were able to realistically model the entire process. Our results were validated by comparisons both qualitative and quantitative with a range of experimental results such as density, diffusion rates, and membrane permeability. This work was presented at the Annual Meeting of the American Institute of Chemical Engineers, where it was the session kickoff presentation. In addition it will appear as an invited paper in a special issue of Molecular Simulation

In our simulations we studied three lipid structures with various tail lengths. We used the 4:1 mapping technique using the Martini CG force field. This then led to a coarse grained model that allowed us to study the larger length and time scales needed in our simulations. We were able to compare our results with experimental data to validate our models. For example we were able to calculate the permeability of oxygen in our system and compare it with the experimental results obtained by Tamimi et al. These comparisons as well as our simulation strategy are shown below. Nuclear magnetic resonance (NMR) and magnetic resonance imaging (MRI) afford the greatest analytical potential for experimentally examining transport speciation and associated molecular dynamics of biomembrane permeation. The experimental challenge is complicated because commercial NMR/MRI probe vendors have not developed a probe capable of

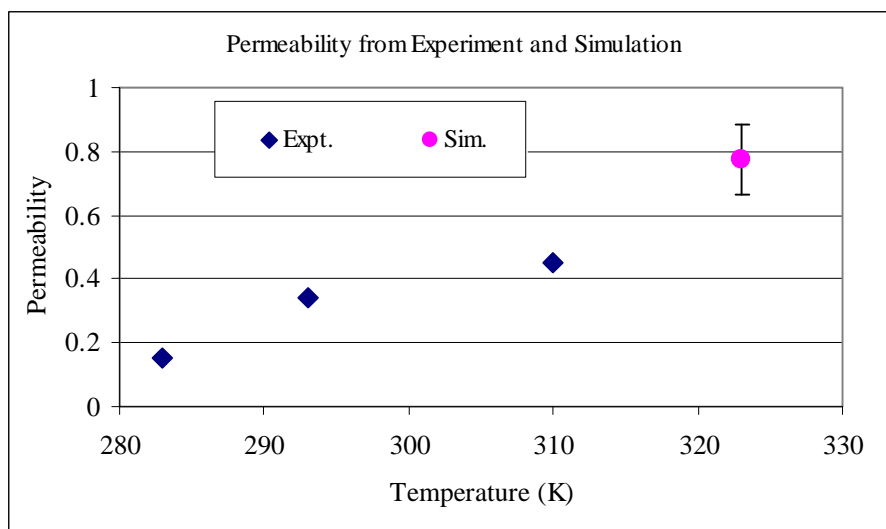
supporting a biomembrane and the ancillary components needed to introduce a transportable permeate.



Coarse-grain mapping strategy for water



Coarse-grain mapping strategy for a DMPC molecule



Comparison of permeability of oxygen in biomembrane (expt.) and our model membrane (simulations)

However, we have modified a novel NMR imaging probe invented at Argonne National Laboratory for the purpose of supporting a single contiguous bilayer membrane approximately  $2\text{ cm}^2$  in total area. This novel probe shown in Fig. 2 is based on the near electrode imager, which takes advantage of the inverse-distance dependence of the radiofrequency magnetic field to record one-dimensional radial concentration profiles of samples placed on or near the central conductor rod. As a first test of the probe, we wrapped a thin film of the proton permeable membrane Nafion on the cylindrical inductor rod. In a cylindrical coordinate system, the NMR imager provides a one-dimensional image along the radial coordinate composed of sequential NMR spectra recorded for concentric shells spatially ordered from the volume on the outside of the membrane (containing the permeate), through the membrane interior, and into the volume on the inside of the membrane. We observed images for the first time that detailed the variations in chemical shifts of water protons as the membrane was hydrated from the outer surface inward. We also were able to monitor changes in the chemical shift and spatial disposition of the bulk water on the surface and in the interior of the membrane as the membrane was hydrated (see Fig. 3). Our results were presented in the NMR Symposium at the latest annual Rocky Mountain Conference on Analytical Chemistry.



Figure 2. TCD NMR probe. Aluminum rod with thin porous oxide coating is shown partially wrapped with Teflon tape.

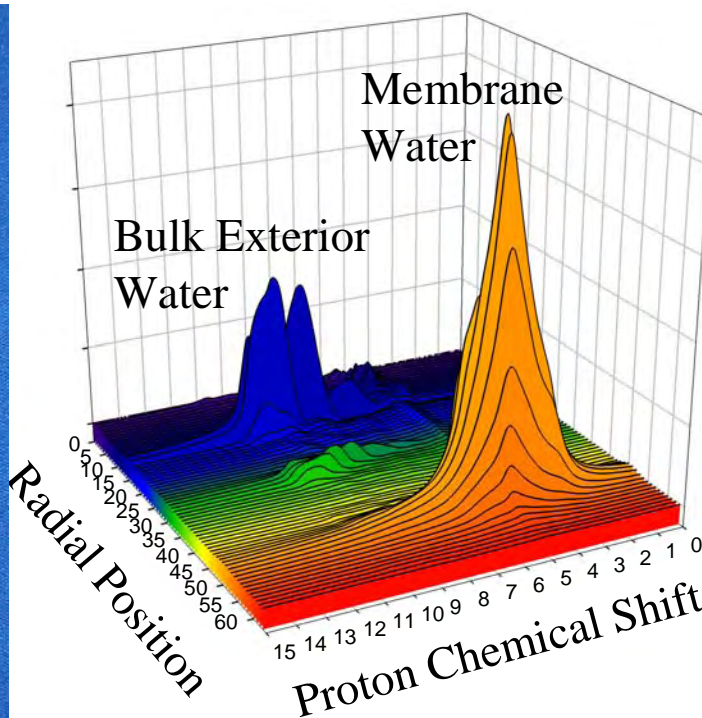


Figure 3. One-dimensional radial proton NMR image of a thin membrane wrapped on the surface of the aluminum rod NMR detector. The orange peaks measure the free water profile across the thickness of the membrane. The blue peaks reveal excess water near the detector that was used to hydrate the membrane.

**Future Plans:** We plan to carry out bilayer synthesis using equipment that is unavailable to us at the University but is available at ANL. This request was approved by ANL in May '09. CNM equipment will be used to modify and characterize our AAO substrate, deposit L-B and large unilamellar vesicle (LUV) bilayers, and characterize the AAO-supported bilayers. For these purposes we will use the JEOL FE-SEM for characterization of AAO surface uniformity and the tapping-mode AFM for probing the existence of pore-spanning bilayers. We also requested the use of the gold sputtering tool (Kurt- Lesker) for growing gold films, which will be used for phospholipid anchors. We have access to a SEM at the Research Resource Center (RRC) at the University of Illinois; however, we do not have access to a tapping-mode AFM and a high-quality gold sputtering tool. Importantly, careful gold sputtering must be performed so as not to seal over the pores. The gold-sputtered AAO surface will undergo a chemical reaction with mercaptopropionic acid, which is used to anchor the bilayers. The tapping-mode AFM will allow us to maintain our bilayer intact after initial characterization. The CNM will be an ideal location to both prepare and characterize the bilayer film before sealing the sample in the TCD NMR probe. We have initiated preliminary efforts to synthesize large unilamellar vesicles prepared by the extrusion technique (LUVET). The target LUVETs typically range in diameter from 100 to 200 nm, sizes that are larger than the AAO pore diameters. The technique is used to form vesicles from an aqueous lipid solution by passing the solution through a membrane extruder positioned between two syringes that are maintained at an elevated temperature. Once formed, these vesicles may be directly placed on the gold-modified AAO substrate. This process creates an attraction between the positive polar phospholipid head groups and negatively charged mercaptopropionic acid anchor points (deprotonated under basic conditions) on the substrate.

Our future theoretical studies of lipid membrane will include investigating the transport of water molecules and dissolved ions assisted by the transmembrane proteins such as OmpA - a porin from Escherichia coli with a small pore size and high stability. We will compare the molecular transport across with and without the assistance of transmembrane channels. MD simulation studies in such assisted transport will then also be compared with available experimental data. The information obtained from this study will lead to better understanding of proteins and advance the use of OmpA for the development of biochips and drug delivery systems. We also plan to investigate the adsorption characteristics of water, chemical toxins such as sarin on a range of phospholipid membranes. To describe the solution behavior correctly, we will use a mixed atomic and coarse grain scheme. The solution will be modeled atomistically, while keeping the coarse grained scheme for the lipid.

### **Publications (2008-9)**

Huajun Yuan, Cynthia Jameson and Sohail Murad, “**Exploring Gas Permeability of Lipid Membranes Using Coarse Grained Molecular Dynamics**”, *Molecular Simulation*, **35**, 953-61(2009).

### **Selected Presentations (2008- 9)**

Malerie Wolke, Cynthia J. Jameson<sup>1</sup>, Rex E. Gerald II, Sohail Murad, Huajun Yuan, “**Development of a Toroid Cavity Detector NMR Probe for Measuring the Transport of Molecules and Ions Across Model Membranes**”, 2008 Rocky Mountain Conference Solid State NMR Symposium, Breckenridge, Colorado, July 2008,

Huajun Yuan, Cynthia Jameson, Sohail Murad, “**Exploring the Gas Permeability of a Lipid Bilayer Membrane Using Course Grained Molecular Dynamics**”, AICHE Annual Meeting, Philadelphia, PA, November 2008.

## Electrostatic Driven Self-Assembly Design of Functional Nanostructures

Graziano Vernizzi, Samuel I. Stupp, Michael J. Bedzyk and Monica Olvera de la Cruz

Northwestern University

Departments of Materials Science and Engineering, Physics and Chemistry

[m-olvera@northwestern.edu](mailto:m-olvera@northwestern.edu), [g-vernizzi@northwestern.edu](mailto:g-vernizzi@northwestern.edu), [bedzyk@northwestern.edu](mailto:bedzyk@northwestern.edu).

**Program Scope:** We aim to understand how to control the functionality of charged molecules by modifying the electrostatic environment and by designing molecules with specific charge densities and configurations. Gaining this understanding offers the possibility of designing the assembly at the nanoscale of complex molecules for specific functions. Electrostatic interactions are able to drive the spontaneous formation of highly organized structures. By using biocompatible cationic and anionic amphiphiles we will generate closed shapes such as spheres and polyhedrons, and cylindrical assemblies with specific surface heterogeneities, which will render them specific functionalities. Moreover, ionic materials can be assembled and disassembled by changing the ionic concentrations. The global structure of co-assembled cationic and anionic molecules depends on their microscopic architecture, specific interactions, charged densities and concentrations. In this proposal we explore the molecular structure and external conditions for designing the co-assembly of cationic and anionic peptide amphiphiles into vesicles, that can form polyhedral shapes including the icosahedral shape of large viral capsids. The outcomes of the proposed work are:

- 1) The guidelines to design amphiphilic molecules of opposite charges that will co-assemble into vesicles of different shapes and sizes.
- 2) The analysis of the shape of the aggregates, and in particular, the parameters that determine the buckling of vesicles into different polyhedrons.
- 3) The understanding of the stability of the aggregates in different ionic conditions and the characterization of the structures.

**Recent Progress:** We have demonstrated theoretically and experimentally that vesicles composed of a mixture of +3 cationic and -1 anionic surfactants (catanionic vesicles) are capable of buckling into faceted shapes [1]. A new mechanism by which charged molecules, including molecules with biological motifs, organize in closed shells faceted due to ionic lateral correlations was recently discovered by the group [2]. The work illuminates the question of how molecules that are assembled in a liquid state can form shapes expected for elastic membranes, such as faceted vesicles, which are observed in many biological ionic assemblies including viruses. Our theoretical and experimental results show that the supramolecular shape, which has its roots in intermolecular interactions, generates non-spherical structures. We have demonstrated that anionic and cationic amphiphiles of unequal charge can co-assemble into small buckled vesicles, and provided a physical argument to explain this phenomenon. The strong electrostatic interaction between the +3 and -1 head groups increases the cohesion energy of the amphiphiles and favors the formation of two-dimensional, flat ionic domains on the vesicle surface, resulting in edges and a buckled shape, as shown in Fig. 1. The amphiphilic molecules used in this study consists of a +3 charged amino acid sequence covalently attached to an alkyl acid containing a diacetylene moiety, and a diacetylenic fatty acid. Diacetylenes can undergo a 1,4-addition polymerization when exposed to UV light. Importantly, this topochemical polymerization requires the positions of the atoms to be at specific distances, and higher degrees of polymerization can only occur if the fatty acid tails are locally ordered.

The supramolecular structures of the amphiphiles were characterized by quick-freeze deep-etch (QFDE) transmission electron microscopy (TEM). QFDE is a sample preparation technique that allows high-resolution imaging of hydrated structures while minimizing disruption of the sample due to fixation or processing. Solutions of the single 3+ were composed of micelles with an average diameter of ~10 nm (Fig.1). In contrast, solutions of a mixture of 3+ and 1- contained vesicles with an average diameter of ~200 nm. Some vesicles appear to buckle on all sides, whereas others have both flat and rounded domains in the same structure.

To determine whether these buckled vesicles could be polymerized, we irradiated at 254 nm samples of the 3+ alone, 1- alone, and the catanionic mixture. The samples of the 3+ and of 1- alone did not polymerize. In contrast, the mixed sample turned blue upon irradiation and showed the characteristic trace of polymerized diacetylene. When the amphiphiles were dissolved together in 1 M NaCl no polymerization was observed, indicating that the salt inhibited the formation of the ordered lattice necessary for polymerization. Furthermore, these solutions do not contain buckled vesicles. However, we find that adding NaCl *after mixing* the cation and anion in water does not inhibit their ability to polymerize or to form buckled vesicles. The coassembly also polymerized in the presence of KCl and phosphate buffered saline, but little or no polymerization was observed in solutions of NaI, NaClO<sub>4</sub>, or LiCl, consistent with the Hofmeister series of protein solubilization for anions and cations. That is, only the mixed systems had sufficient *internal order* to support polymerization.

We analyzed the elastic properties of vesicles with different stoichiometric ratios. The buckling transition of a vesicle can be effectively described by a single parameter, the Föppl–von Kármán number  $\gamma = YR^2/\kappa$ , where  $Y$  is the two-dimensional Young modulus,  $R$  is the linear size of the vesicle, and  $\kappa$  is the bending rigidity of the membrane. More precisely, when  $\gamma$  is greater than a critical value, the membrane buckles by condensing its curvature energy into conical vertices and edges while flat domains grow over the surface. Clearly, strategies for increasing the value of  $\gamma$  include: increasing  $Y$ , increasing  $R$  (larger vesicles), or decreasing  $\kappa$ . We showed that increasing the stoichiometric charge ratio of the headgroups produces a larger effective two-dimensional Young modulus because of the stronger local correlations between charged components over the vesicle surface. It is important to note that the structure of the vesicle surface does not have to be a perfectly ordered long-range ionic lattice in order to develop a non-vanishing Young modulus. The length scale  $L$  of the local correlations must be such that  $L < \xi$ , where  $\xi$  is the screening length induced by salt in the solution (which effectively screens electrostatic interactions), where  $L$  is the average distance between multivalent headgroups. Furthermore, in the particular case for a 3:1 stoichiometric ratio of charges, we computed the effect of a screening length  $\xi$  on the Young modulus, by using a screened potential  $V(r) \sim \text{Exp}[-r/\xi]/r$  plus a Lennard-Jones potential. The Young modulus has been obtained by analyzing small deformations of the lattice around the equilibrium configuration  $E_c$ , and evaluating the energy  $E = E_c + c_{ijlm} \epsilon_{ij} \epsilon_{lm} / 2$ , where  $\epsilon_{ij}$  is the strain tensor and  $c_{ijlm}$  is the stiffness elastic tensor, from which we can extract the Young modulus. We showed that the electrostatic contribution to the Young modulus grows linearly with the ratio  $l_B/\sigma$ , at large  $l_B/\sigma$ , and that the screening effect of salt in the solution decreases the stiffness of the ionic surface. The residual stiffness ( $Y$  at  $l_B/\sigma=0$ ) is induced by the Lennard-Jones short range interactions.

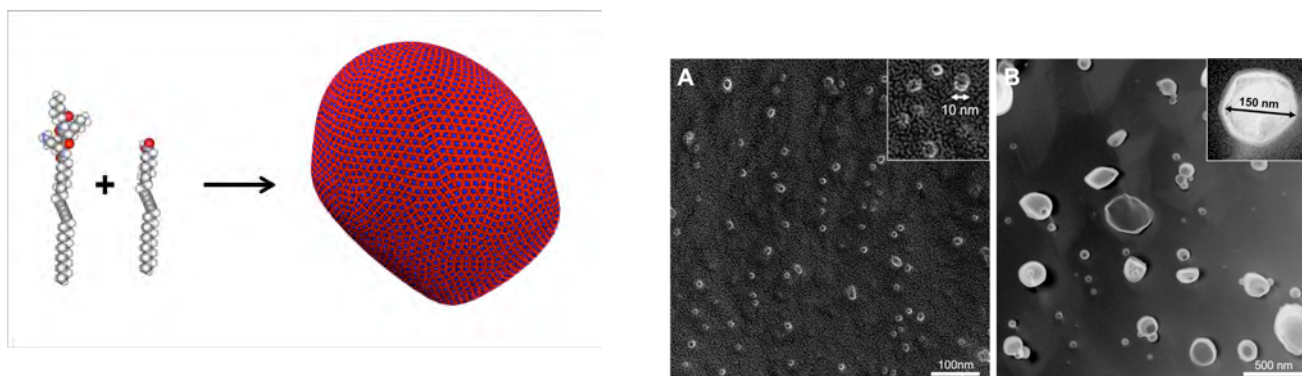


**Fig. 1.** Schematic diagram of the co-assembly 3+ and 1- of biocompatible amphiphile molecules into vesicles (left). Quick-freeze deep-etch TEM microscopy (left) of (a) micelles formed from 1 and (b) larger buckled vesicles from 1 and 2 in water.

The bending rigidity of the membrane is also affected by electrostatic interactions among charged head-groups. We have explored the effect of different stoichiometric charge ratios on the membrane's bending rigidity  $\kappa_{\text{tot}} = \kappa + \Delta\kappa$ , where  $\kappa$  is the rigidity induced by the Lennard-Jones short range interactions and  $\Delta\kappa$  is the contribution of the electrostatic interactions only. We considered only the effect on one-dimensional system of positive (+q) and negative (-1) charges. We are interested in particular at the large- $R$  asymptotic expansion of the electrostatic energy  $E = E_0 + E_1 / R^2 + O(1/R^4)$ . The physical meaning of the coefficient  $E_1$  is precisely the contribution of electrostatics to the bending rigidity, that is  $E_1 = \Delta\kappa$ . This also provides a handle for testing how much the softening effect depends on the long-range nature of electrostatic interactions versus short-range correlation effects. We performed all the calculations for different stoichiometric ratios 1:1, 2:1, 3:1, 4:1. We found that the decreasing value of the bending rigidity with increasing stoichiometric charge ratio increases the value of the Föppl-von Kármán number since they are inversely proportional. Second, at very small screening lengths (where the electrostatic effects are weaker) the correction to the bending rigidity vanishes ( $\Delta\kappa$  goes to zero), as expected. Importantly, at any finite value of the screening length the correction is non-zero and negative. This result confirms that short-range electrostatic correlations are sufficient for affecting the elastic properties of the membrane and do not have to extend up to infinity as in the case of unscreened long-range interactions. Our results demonstrate that high stoichiometric ratios yield smaller bending rigidities ( $\Delta\kappa$  is more negative), and larger Young moduli, supporting vesicle buckling at small radii.

We have also analyzed charged patterns on fibers [3,4] and showed that electrostatic interactions alone are capable of generating helical structures. We have extended the work to include the effect of the different dielectric constant and salt concentrations inside and outside by generating a formalism based on Green's Functions. This offers a unique opportunity to design surface charged patterns.

The effective interactions among suspended nano-particles have been extensively studied with models that ignore the molecular structure of the supporting electrolyte, which ignore the permittivities inside and outside the nanoparticles. The group applied a model developed to introduce the molecular structure of the solvent to show that the negatively charged nano-particles are effectively less charged than the positive ones, and the degree of asymmetry depends on the size and the bare charge of the nano-particles [5]. Their results suggest that in the absence of short-range attractions among nano-particles, positively charged nano-particles have larger solubility than negatively charged nano-particles. These findings agree with recent experiments in the group of Prof. Jay Groves. These new results have consequences in protein solubility and many self-assembled structures, including adsorbed proteins on oppositely charge membranes, which also form ionic lateral patterns and lead to buckling. The group has initiated studies on effective interactions in water to address this type of buckling including effective potentials in water.

We believe that the observed buckling of the vesicles composed of a mixture of +3 cationic and -1 anionic surfactants (catanionic vesicles) is the direct result of the ionic lattice of the cationic and anionic headgroups on the vesicle's surface. We are interested in using X-ray scattering to investigate the size and shape of these buckled vesicles and WAXS to investigate the ordering of the cationic and anionic headgroups on the vesicle's surface. During our first set of X-ray experiments our goal was to determine the optimal testing parameters and optimize samples preparation to achieve the best data from our low contrast catanionic vesicles. It is important to note that all our mixed cationic and anionic mixtures should be composed of the buckled vesicles, as well as small cation-only micelles. First and foremost, our preliminary data, that are shown in Fig. 2, indicates that with the high intensity Argonne X-ray source we have sufficient scattering for X-ray analysis. Although the data has not been fit to a detailed model yet, we believe the -2 slope in the low  $q$ -range corresponds the flat plat-like structure of the vesicles' surface and the peak at  $\sim 0.1$  corresponds to either the thickness of the vesicle's bilayer membrane or the diameter of the cationic micelles. The WAXS data contains two sharp peaks, which correspond to  $d$ -spacings of  $\sim 4.5\text{\AA}$  and  $3.9\text{\AA}$ . We believe these distances correspond to the hexagonal packing of the cationic and anionic molecules in the vesicle bilayer.

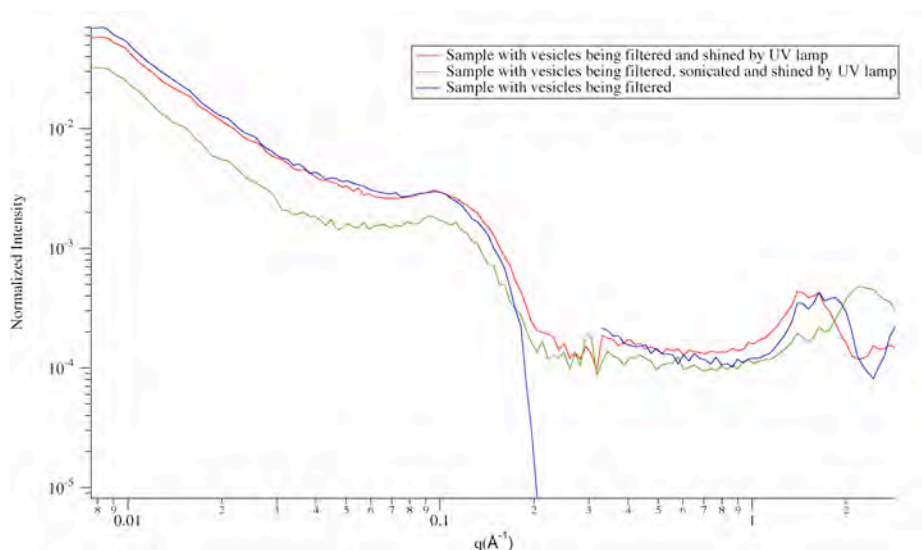


**Fig. 3.** The X-Ray intensity  $I$  versus wave vector  $q$  for samples of ionically co-assembled vesicles of peptides of 3+ and 1-.

**Future Plans:** The following new developments will be pursued:

1. In our next round of X-ray experiments we will modify the experiments to maximize our ability to confirm the predicted hexagonal ionic lattice structure on vesicles of co-assembled biocompatible 3+ and 1- amphiphiles. To do so, we will be increasing the accessible  $q$ -range by decreasing the distance of the WAXS detector to the sample and will be increasing the sample concentration. Furthermore, we will extend our investigation to include how these peaks change when different salts are added to the solvent. Our previous work suggests that some salts increase the lattice spacing, while others may decrease it. To collaborate this finding we will form vesicles in a variety of salt solutions and then monitor how the WAXS peaks change with the type of salt added to the vesicle solution. We anticipate that our X-ray experiments will allow us to confirm the presence of the hexagonal ionic lattice that drives the buckling of these vesicles.
2. We will extend the Green's function new description of fibers with ionic domains on their surfaces to vesicles with surface charge lateral ionic correlations to include the different dielectric constants inside and outside the vesicle and possible different salt concentrations.
3. We will continue our computational studies of heterogeneous vesicles with rafts of elastic ionic regions embedded in liquid domains including also the different bending rigidities of the domains. We aim to determine also the correlations of finite ionic rafts occurring on the surface of lipids with raft forming on the inner membrane of the vesicles. Electrostatic interactions are capable of providing **communication** between the outer and inner layers of a membrane given that the electrostatic fields propagate in three dimensions and the dielectric constant in the middle of the membranes is much lower than that of the water, allowing important interactions between the ionic raft in the outer and inner layers.

**Publications 2007-2009:**

1. M. A. Greenfield, L. C. Palmer, G. Vernizzi, M. Olvera de la Cruz, and S. I. Stupp *J. Am. Chem. Soc.*, 131 (34), 12030–12031 (2009).
2. G.Vernizzi and M. Olvera de la Cruz, *Proc. Natl. Acad. Sci. USA*, 104 (47) 18382-86 (2007).
3. G.Vernizzi, K.L. Kohlstedt and M. Olvera de la Cruz *Soft Matter* 5, 736 (2009).
4. K.L. Kohlstedt, G.Vernizzi and M. Olvera de la Cruz “**Surface patterning of low-dimensional systems: the chirality of charged fibres**” *Journal of Physics: Condensed Matter* (*in press*, 2009).
5. P. Gonzalez-Mozuelos and M. Olvera de la Cruz, *Phys. Rev. E* 79, 31901, (2009).

**Dynamic Self-Assembly:  
Structure-Dynamics-Function Relations in Heterogeneous Phospholipid Bilayers**

Atul N. Parikh<sup>1</sup> and Sunil K. Sinha<sup>2</sup>

<sup>1</sup>Department of Applied Science and Biophysics Graduate Group  
University of California, Davis, CA 95616  
[anparikh@ucdavis.edu](mailto:anparikh@ucdavis.edu)

<sup>2</sup> Department of Physics  
University of California, San Diego  
La Jolla CA 92093  
[ssinha@physics.ucsd.edu](mailto:ssinha@physics.ucsd.edu)

**Program Scope.** The use of self-assembly processes to date has focused on developing static structures. But dynamic self-assembling systems widely prevalent in nature – those that develop local temporal organizations to perform time-dependent tasks – offer a tremendous opportunity to devise entirely new classes of complex functional materials with dynamic properties. Within this framework, we are investigating formation-structure-dynamics-function relations in organized phospholipid bilayers that underscore dynamic self-assembly. Specifically, we are focused on how structured interfaces, differences in affinities among membrane components, and curvatures allow bilayers to spatially organize and reorganize their components and hence functions. Our primary material system of choice include substrate-supported bilayer configurations. Support surfaces also exhibit pre-determined spatial patterns of topological (e.g., curvature) physical (e.g., wetting) and electrostatic properties. We have adapted and developed applications of optical and fluorescence based techniques for characterization of spatial and temporal dynamics in bilayers over a range of length- and timescales. In particular, quantitative applications of fluorescence photobleach recovery, Forster resonance energy transfer, total internal reflection fluorescence, and time-resolved aqueous phase imaging ellipsometry provide diffraction-limited spatial resolutions. Smaller spatial resolutions are achieved by adapting X-ray (and neutron) reflectivity, off-specular measurements, and x-ray photocorrelation methods. Our specific projects currently address how chemically and topographically structured surfaces template (a) surface dynamics, namely, rupture, spreading, and self-healing; (b) intra-membrane dynamics including micro-phase separation and mesoscopic domain ordering; and (c) curvature-dependent membrane functions. A tight synergy between these themes affords a parallel investigation.

**Recent Progress.** We have several exciting developments from the work performed over the past-two years. Below, we highlight three such accomplishments.

*First, we have obtained an experimental evidence toward what may be characterized as configuration-induced structural transition in fluid lipid bilayers.* Topological defects and discontinuities are rarely encountered in uniform lipid microphases which form via self-assembly in water. Rather aqueous suspensions of these amphiphiles reveal a rich variety of closed shapes and configurations (e.g., spheres, tubules, ellipsoids) via so-called hydrophobic effect. The formation of such defect-free, dynamic lipid aggregates reflects the preponderance of the - which relates to energetic penalties of exposing the hydrophobic lipid-tails to the aqueous environment - and high edge-energies associated with molecular reorganization and elastic deformations caused by such defects. Appearance of defects in lipid bilayers require the reduction in line tension via reorganization of boundary lipid molecules in response to the hydrophobic penalty they face. Here, the polar head-groups of the bilayer are envisioned to rearrange in a molecularly-tight curved geometry connecting the two constituent leaflets of the bilayer. This hairpin geometry constrains the acyl chains in the hemi-spherical or hemi-cylindrical configuration (Fig. 1).

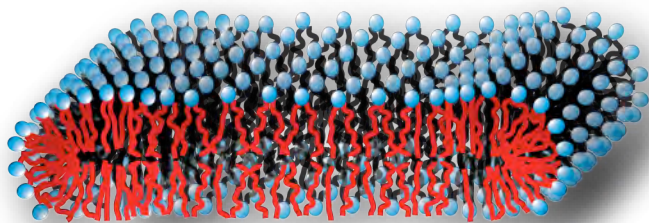


Fig. 1 | Lipids in the vicinity of an edge are more ordered and display higher effective transition temperature than the bulk of the bilayer.

We have obtained an experimental evidence for the emergence of an ordered lipid state in the vicinity of the edge of a single lipid bilayer. Using

well-controlled patches of fluid supported lipid bilayers including POPC and DMPC in conjunction with temperature-programmed fluorescence recovery experiments, we demonstrated that the lipid organization near the edge of a fluid, supported lipid bilayer is characterized by a net increase in chain-order, reduced effective lateral mobility, and a distinctly higher local, effective transition temperatures. Together, these features signal a novel configuration-induced, phase change nucleated by the edge geometry. Analyzing these structural details within the chain-conformational model derived in a recent molecular simulations for micellar organization suggests that the edge structure reflects the dominance of head-group interactions and the hydrophobic effect — jamming the acyl tails within the three-dimensional micellar interior. Furthermore, this dense “glassy” structure near the membrane edge displays a continuous and gradual (spatial) evolution from the micellar to the lamellar motif— suggesting a spatial display of a gel-fluid “critical point” at which the distinction between the fluid and gel-like phase becomes indistinguishable.

*Second, we have been developing a suite of experimental methods to characterize lateral phase separation spanning nanometer to micrometer length scales in raft-mimetic multicomponent lipid bilayers.* Physical-chemical basis for micro-phase separation in multicomponent bilayers remain a poorly-understood issue. Depending on the topological and dimensional constraints of the model system used, broad variations in the degree of phase separation has been reported. Because these phase-separated states suggest structural self-assembly processes within the bilayer milieu, developing a fundamental understanding of their formation mechanism is critical. We have been developing applications of specular reflectivity, grazing incidence diffraction, and off-specular diffuse scattering measurements (Advanced Photon Source (APS), beamline 8-ID) to characterize presence of nanoscale domains in bilayers containing single lipid components and raft-forming mixtures consisting of unsaturated lipids, cholesterol, and sphingolipid. For the pure systems we have obtained diffuse scattering results, which correspond to natural undulations of fluid bilayers and yield the bending modulus and surface tension. For the mixed lipid bilayers, we have (for various concentrations) observed peaks in the diffuse scattering indicating the formation of nanometer scale domains. The scattering has been analyzed in terms of a model for islands on a film and yields an inter-domain average spacing, which varies from 30 to 100 microns, increasing and then saturating with cholesterol concentration. ***We believe this is the first time the formation of these nanometer scale domains in mixed lipid bilayers have been observed with GISAXS.*** Additional temperature dependent GID measurements using monolayer models (at an air-water interface) yielded consistent results revealing the presence of both sharp peaks indicating long-range order as well as broad peaks indicating liquid-like order depending on the relative concentration of the raft forming lipids.

For large-area and large-scale phase separation processes, we have been developing a label-free imaging using optical ellipsometry. In a recent study, we have examined thermally induced dynamical reorganization in lipid bilayers. In particular, *via* imaging ellipsometry, we studied the microstructure evolution during phase transition induced by selective gelation of one component in a binary supported phospholipids bilayer.

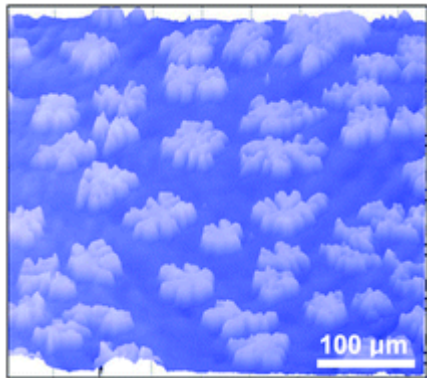
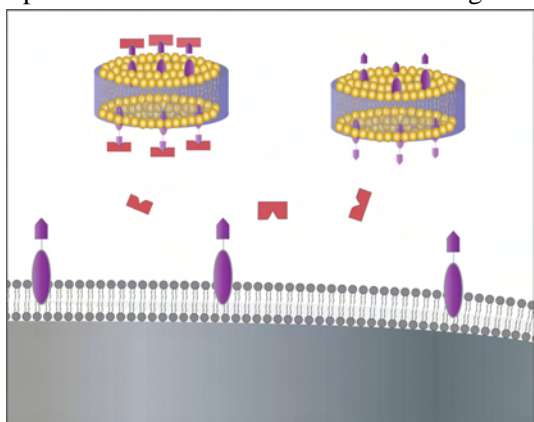


Fig. 2 | Imaging ellipsometry derived topographic map for a binary bilayer consisting of a fluid, DLPC, and a gel-forming, galactosylceramide, lipids.

We found the modulation of two attendant morphological features: emergence of extended defect chains due to a net change in the molecular areas and fractal-like domains suggesting weak line tension. A time-lapse analysis of the ellipsometric images revealed the cluster size of 4–20 molecules undergoing gelation indicating weak cooperativity and importance of interfacial interactions. These results

demonstrated the use of ellipsometry for *in situ*, label-free, non-contact, and large-area imaging of dynamics in interfacial biomolecular fluids.

**Receptor Clustering**, a dynamic self-assembly within the membrane, plays a critical role in controlling many protein recognition processes. Thus, from a biomolecular materials perspective, an ability to produce biomimetic nanostructures that can bind to proteins more efficiently can provide a physical-chemical basis for developing synthetic “decoys”. We have recently shown that biosynthetic lipidic nanostructures that resemble high-density lipoproteins, provide a molecular environment that



promotes interaction between cholera toxin, a bacterial protein, and its native receptor, ganglioside GM1, thus opening a possibility for the design and development of decoys to manipulate receptor-protein interactions at the membrane level.

Fig. 3. | Depiction of decoy protective process. Toxin molecules (*red*) bind with higher affinity to receptors (*purple*) embedded in synthetic lipid nanostructures than those present at the whole cell membranes or vesicles (*gray*).

Other activities include studies of (1) role of substrate structure and interface properties, including spatial patterns of wettability and curvature, in modulating membrane self-assembly (molecular sorting and phase separation) and dynamics (in-plane and undulatory) (2) dynamic and static influences of curvatures on molecular distributions and dynamics in lipid bilayers; and (3) reaction-diffusion dynamics in lipid membranes following selective chemical (or oxidative) transformation of membrane components.

**Future Plans.** Building on these studies, our future studies will continue the focus on how lateral compartmentalization, curvature, interface properties, and selective chemical reactions regulate organization (and dynamic reorganization) of membrane components in multicomponent mixtures. Specifically, we will elaborate our studies of how raft-forming and related multicomponent bilayers undergo dynamic reorganizations in response to static and dynamically presented topological, chemical, and interfacial cues. The latter include nanoscale curvatures, enzymatic actions (e.g., acid sphingomyelinase which hydrolyzes sphingomyelin), and membrane organization at soft and dynamic interfaces.

## References (2007-2009)

1. *Evidence for Interleaflet Slip During Spreading of Single Lipid Bilayers at Hydrophilic Solids* B. Sanii, K. Nguyen, J. O. Rädler and A. N. Parikh, **ChemPhysChem** (Dedicated to Erich Sackmann on the occasion of his 75th Birthday), in press, 2009.
2. *Nanofiber Supported Phospholipid Bilayers*, F. Yi, J. Xu, A. M. Smith, A. N. Parikh, D. A. LaVan, **Soft Matter**, in press 2009.
3. *Cell Attachment Behavior on Solid and Fluid Substrates Exhibiting Spatial Patterns of Physical Properties*, A. E. Oliver, V. Ngassam, P. Dang, B. Sanii, H. Wu, C. K. Yee, Y. Yeh, A. N. Parikh **Langmuir** 25, 6992-6996, 2009.
4. *Early stages of oxidative stress-induced membrane permeabilization: a neutron reflectometry study* H. Smith, M. Howland, A. Szmodis, Q. Li, D. Luke, A. N. Parikh, J. Majewski, **J. Amer. Chem. Soc.** 131, 3631–3638, 2009.
5. *Evidence for Leaflet-Dependent Redistribution of Charged Molecules in Fluid Supported Phospholipid Bilayers*, A. P. Shreve, M. C. Howland, A. R. S. Butti, T. W. Allen, A. N. Parikh, **Langmuir** 24, 13250-13253 (Letter) 2008.
6. *Bridging Across Length Scales: Multi-Scale Ordering of Supported Lipid Bilayers via Lipoprotein Self-assembly and Surface Patterning*, M. Vinchurkar, D. Bricarello, J. Lagerstedt, J. P. Buban, H. Stahlberg, M. Oda, J. Voss, A. N. Parikh, **J. Amer. Chem. Soc.** 130, 11164-11169, 2008.
7. *Direct Visualization of Phase Transition Dynamics in Supported Lipid Bilayers Using Imaging Ellipsometry*, A. W. Szmodis, C. D. Blanchette, A. Levchenko, A. Navrotsky, M. L. Longo, C. A. Orme, A. N. Parikh, **Soft Matter** 4, 1161 - 1164, DOI: 10.1039/b801390j, 2008.
8. *Membrane-Substrate interface: Phospholipid Assembly at Chemically and Topographically Structured Surfaces*, A. N. Parikh, **Biointerphases** 3, FA22-FA32 (DOI: 10.1116/1.2889055) , 2008
9. *Bending Membranes on Demand: Fluid Phospholipid Bilayers on Topographically Deformable Substrates*, B. Sanii, A. M. Smith, R. Butti, A. M. Brozell, A. N. Parikh, **Nano Letters** 8, 866 - 871, 2008.
10. *Patterning Fluid and Elastomeric Surfaces Using Short-wavelength UV Radiation and Photo-generated Reactive Oxygen Species*, B. Sanii and A. N. Parikh, **Ann. Rev. Phys. Chem.** 59, 411-432, 2008.
11. *Patterned when Wet: Environment-dependent Multifunctional Patterns in Amphiphilic Colloidal Crystals*, A. M. Brozell, M. A. Muha, A. Adel-Amoli, D. Bricarello, and A. N. Parikh, **Nano Letters** 7, 3822-3826, 2007.
12. *Structural Characterization of Supported Membranes on Topographically Patterned Polymeric Elastomers and Their Applications in Micro-Contact Printing*, A. R. S. Butti, R. Butti, A. N. Parikh, **Langmuir**, 23, 12645-12654, 2007.
13. *Surface Energy Dependent Spreading of Lipid Monolayers and Bilayers*, Babak Sanii and Atul N. Parikh, **Soft Matter** 3, 974-977, 2007. (ISSUE COVER)
14. *Dynamic Recompartmentalization of Supported Lipid Bilayers Using Focused Femtosecond Laser Pulses* Andreia M. Smith, Thomas Huser, and Atul N. Parikh, **J. Amer. Chem. Soc.** 129, 2422-2423, 2007
15. *Characterization of Physical Properties of Supported Phospholipid Membranes Using Imaging Ellipsometry at Optical Wavelengths*, Michael C. Howland\*, Alan W. Szmodis\*, Babak Sanii, Atul N. Parikh, **Biophys J.** 92, 1306-1317, 2007. (ISSUE COVER)

## Development of New Methods for Studying Nanostructures using Neutron Scattering

Roger Pynn

Indiana University  
Department of Physics  
Swain Hall West, 3<sup>rd</sup> Street  
Bloomington, IN 47405  
[rpynn@indiana.edu](mailto:rpynn@indiana.edu)

**Program Scope:** The goal of this project is to develop a new technique that overcomes some of the limitations of neutron scattering in the study of nanostructures. Traditional neutron diffraction techniques use monochromatic, collimated beams to achieve good momentum-transfer ( $Q$ ) resolution. This method leads to a rapid decrease in neutron signal as momentum-transfer resolution improves and as larger spatial scales are accessed. This makes measurement of structure on length scales beyond a few 10's of nm challenging when scattering is weak (e.g. for small samples or for samples with weak scattering contrast). Our goal is to develop an interferometric technique that makes use of the neutron spin to overcome these limitations and allows the benefits of neutron scattering (such as isotopic sensitivity) to be applied to a wider range of nano-materials. The new method, dubbed Spin Echo Scattering Angle Measurement (SESAME) should be particularly useful for measuring structural correlations in complex fluids and at surfaces and interfaces.

**Recent Progress:** About 200 years ago, a British chemist named William Wollaston showed that the two polarization states of light could be split by a pair of birefringent prisms that now bear his name. The action of Wollaston's device is shown in Figure 1a. A pair of Wollaston prisms, combined with an optical polarizer can be used to produce two, spatially-separated, polarized light rays which are coherent with one another and which have a well defined relative phase,  $\psi$ , as shown in Figure 1b. An equivalent device, such as those shown in Figures 2b and 2c can be built for neutrons by using triangular regions of magnetic field rather than calcite prisms.

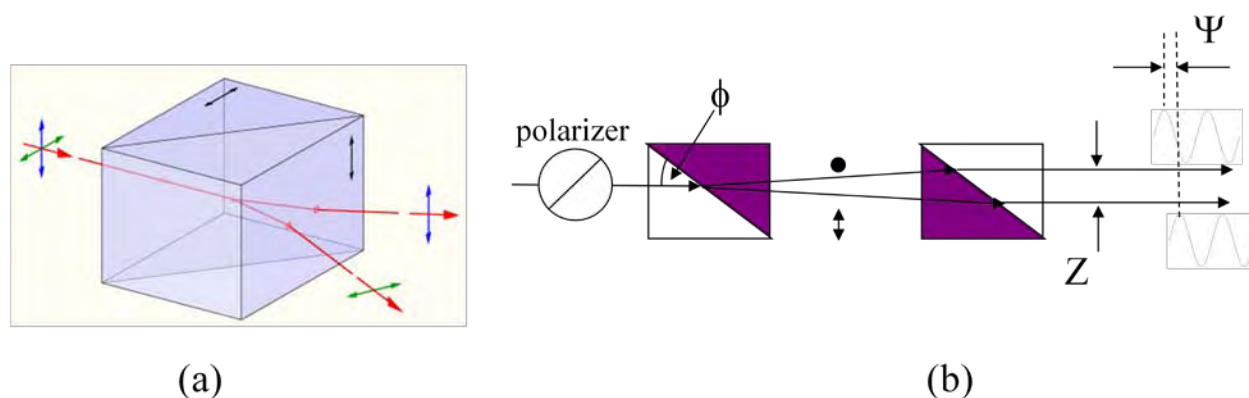


Figure 1: (a) A Wollaston prism made from two pieces of calcite with perpendicular optic axes; (b) A pair of such prisms produces two separated parallel rays with orthogonal polarizations indicated by a dot and a diamond. If the light incident on the first prism is plane polarized at  $45^\circ$  to the optic axis of either calcite crystal, as indicated by the circle with a  $45^\circ$  line to the left of the first Wollaston prism, the two parallel rays will be coherent and separated by a phase angle  $\Psi$ .

Our use of neutron Wollaston prisms is quite analogous to that of optical Wollaston prisms in differential interference contrast microscopy. Two neutron Wollaston prisms are used to spatially separate the spin eigenstates of a neutron and another pair of such prisms is used to bring those two states back together again, as shown in Figure 2a. The distance probed in the sample turns out to be equal to the separation of the spin states at the sample position and can range from a few nanometers to several microns for reasonably achievable magnetic fields. The measured neutron polarization turns out to be the Fourier transform of the slit-smeared neutron scattering function which, in turn, is the Abel transform of the density-density correlation function of the sample.

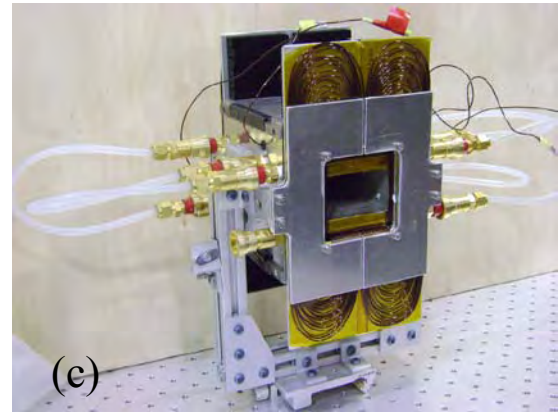
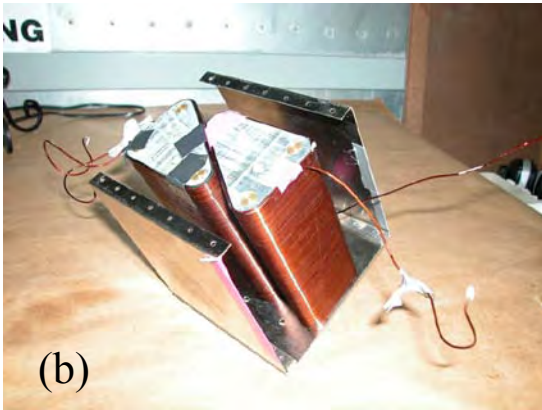
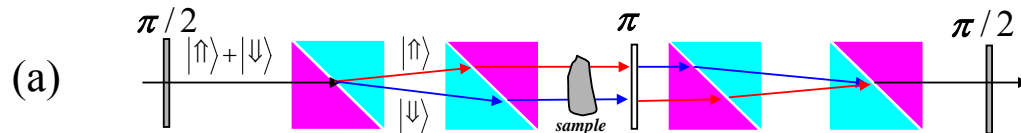


Figure 2: (a) the combination of neutron Wollaston prisms used in our experiments showing the separation of the two neutron spin eigenstates at the sample position; (b) an early version of a neutron Wollaston prism wound using aluminum wire (transparent to neutrons) showing the partially disassembled mu-metal magnetic flux return box; (c) a more recent neutron Wollaston device with water cooling.

Our recent results include:

- (a) *Development of neutron Wollaston prisms with smooth magnetic field transitions.* An essential difference between Wollaston prisms for light and neutrons is that it is easy to embed the former in a medium that is not birefringent for light (e.g. air) and which does not therefore interfere with the phase relationship between the polarization states. This is harder to do for neutrons because the birefringent medium is a magnetic field so the Wollaston prisms either have to be placed in a constant field that is parallel to the field inside the prisms or in zero field. Neither is easy to achieve. We have resolved this problem by building prisms with gaps for neutrons to enter and exit (Fig 2c). The magnetic field “leaks out” of the gaps but, because of the symmetry of the arrangement in Fig 2a, the effects of this leakage on the overall neutron polarization cancel one another almost completely. This effect, in which symmetry is used to

cancel aberrations in measurement instruments is a principle that we are trying to employ systematically.

- (b) *Measurement of large in-plane length scales using neutron reflectometry.* To test the ability of SESAME to interrogate relatively long length scales (50 nm – 500 nm) within a surface, we used it to measure scattering from a simple silicon diffraction grating with a rectangular profile of period 140 nm. This would be a hard measurement with Grazing Incidence Small Angle Neutron Scattering (GISANS) because the neutron beam would have to be collimated strongly to achieve the desired in-plane resolution, causing the scattered intensity to be severely depressed. We were able to make the measurement very quickly using SESAME. Interpreting it was less straightforward. The normalized neutron polarization measures a quantity which is approximately equal to the height-height correlation function of the grating. We developed a dynamical scattering theory that fit the data without any adjustable parameters (cf Figure 3a), providing confidence that we understand what the new technique measures.
- (c) *In collaboration with colleagues in Europe and from Argonne national Laboratory, we demonstrated that the new technique could be used to measure correlations in bulk samples.* For example, we examined correlations in a nanoporous alumina sample using regular Small Angle Neutron Scattering (SANS) and SESAME. The latter clearly shows the range of density correlations in real space as shown in Figure 3c while the resolution of the former (Figure 3b) turns out to be insufficient to draw such conclusions.

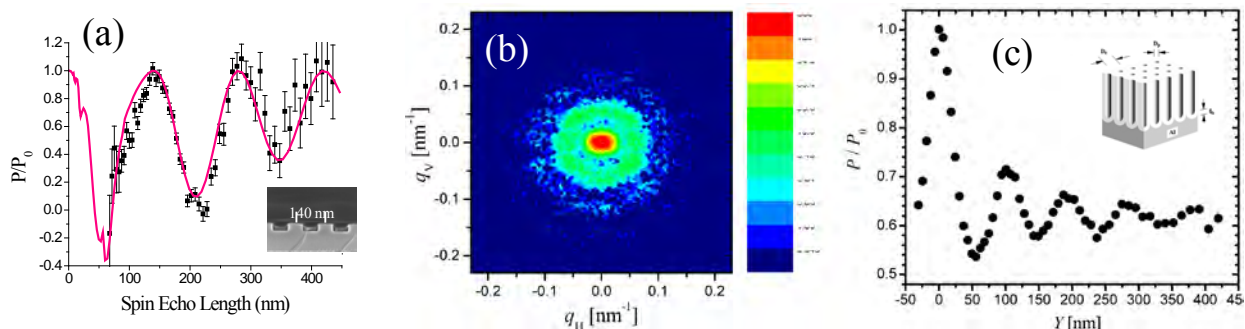


Figure 3: (a) Normalized neutron polarization measured from a diffraction grating whose profile, measured by TEM, is shown in the insert; (b) SANS measurement of the porous alumina sample sketched as the insert in part (c); (c) SESANS measurement of the same alumina sample showing real space density correlations extending up to 450 nm.

**Future Plans:** We plan to apply SESAME to a number of complex-fluid systems in the near future. For example, Dr. W-R Chen at Oak Ridge National Laboratory has shown that it should be possible to use the method to study short range correlations in colloidal suspensions and to obtain accurate forms for the interparticle potential. For various technical reasons, the approach is expected to give much more accurate results than standard SANS or light scattering and we will use it to determine the effect on interparticle potentials of “entropic crowding” due to smaller molecules. We also plan to examine the ordering of block copolymers that is driven by physical and chemical patterning of surfaces and the height correlations in stacks of membranes.

**Publications 2007-2009:**

*The Use of Symmetry to Correct Larmor Phase Aberrations in Spin Echo Scattering Angle Measurement*; Roger Pynn, Wai-Tung Hal Lee, Paul Stonaha, Shah Valloppilly, Adam Washington, Brian Kirby, Brian Maranville, and Charles Majkrzak; *Rev. Sci. Instrum.* **79**, 063901 (2008)

*Spin Echo Scattering Angle Measurement at a Pulsed Neutron Source*; Roger Pynn, M. R. Fitzsimmons, W. T. Lee, V. R. Shah, A. L. Washington, P. Stonaha, and K. Littrell; *J. Appl. Cryst.*, **41**, 897 (2008)

*Pulsed Neutron Beam Control using a Magnetic Multiplet Lens*; T. Oku, T. Shinohara, J. Suzuki, R. Pynn, H. M. Shimizu; *Nuclear Instruments and Methods* **A600**, 1, 100-102 (2009)

*Birefringent Neutron Prisms for Spin Echo Scattering Angle Measurement*; Roger Pynn, M. R. Fitzsimmons, W. T. Lee, P. Stonaha, V. R. Shah, A. L. Washington, B. J. Kirby, C. F. Majkrzak, and B. B. Maranville; *Physica B* **404**, 2582–2584 (2009)

*A Spin Echo Resolved Grazing Incidence Scattering (SERGIS) set-up for Neutron Interrogation of Buried Nanostructures*; J. Major, A. Vorobiev, G. P. Felcher, P. Falus, T. Keller and R. Pynn, (submitted to *Rev. Sci. Instrum.*, 2009)

## WET INTERFACES: DEVELOPING A MOLECULAR FRAMEWORK FOR UNDERSTANDING THE BEHAVIOR OF MATERIALS IN AQUEOUS SOLUTIONS

*Geraldine L. Richmond*  
*Department of Chemistry*  
*1253 University of Oregon*  
*Eugene, Oregon 97403-1253*  
[richmond@uoregon.edu](mailto:richmond@uoregon.edu)

### *Program Scope and Motivation*

There has been a rapid growth in interest in surface and interfacial phenomena in recent years. This field continues to be an exciting and challenging area of research, with the focus progressing from simple systems, e.g. the adsorption of gases at inert surfaces, to more complex systems such as the liquid–gas or solid–liquid interfaces. Mineral–water interfaces are a particular challenge because of the often-strong solid–liquid interaction and the microscopically heterogeneous nature of many minerals. Preferential dissolution and hydration of surface ions, chemical modification of the surface and pH all affect the often-delicate balance of forces at the mineral–water boundary. In a subset of our current and future planned studies we are examining (1) the molecular and ionic factors that control the adsorption and assembly of molecular monolayers at charged mineral surfaces in aqueous media and (2) the dynamics of molecular and assembly at these interfaces. Our approach is one that closely couples experiment with computation. Surface vibrational sum frequency spectroscopy (VSFS) is used to probe the molecular properties in-situ in addition to using other traditional surface characterization methods. These studies are intimately coupled to our increasing expertise in molecular dynamics simulations. This combination of experiment and simulation provides us with powerful capabilities for understanding the molecular complexity of these important interfacial systems.

### *Recent Progress on Project: Carboxylate Adsorption at Mineral/Aqueous Interfaces*

In the past two years we have been examining the interaction of mineral surfaces with low molecular weight carboxylates. Carboxylate ions can govern dissolution processes, regulate the biological availability of nutrients, and are a determining factor for the environmental transport cycle of various metals, including the bioretention of chromium and other toxic pollutants. In industry, the adsorption of carboxylate ions onto particles is a common mechanism for growth inhibition and impurity inclusion during product crystallization (e.g., in the Bayer process, a key step in the production of aluminum). Carboxylates have also found a variety of applications from surface modifying agents to the size-controlled synthesis of nanoparticles and can act as an intermediate layer for the interaction of surfaces with other organic materials, which is crucial for promising innovations like dye-sensitized solar cells. Even with their widespread use, little is known on a fundamental level about the molecular behavior that underlies these applications. In these studies we examine the adsorption of formate, acetate, and propionate at the  $\text{CaF}_2/\text{H}_2\text{O}$  interface with VSFS. Our focus is on the molecular structure of the carboxylate adsorbates, the water structure and hydrogen

bonding before and during adsorption and the effect of pH on the interfacial properties and carboxylate adsorption.

The first set of studies have involved detailed measurements of the vibrational spectrum of the adsorbed carboxylates in order to assign particular vibrational modes to the VSF observed bands. The bands associated with the carboxylate head group ( $\sim 1350$   $\text{cm}^{-1}$  for formate,  $\sim 1450$   $\text{cm}^{-1}$  for other carboxylates), often described only as a symmetrical  $\nu\text{CO}$  group mode, also contain contributions from  $\text{CH}_2$  and  $\text{CH}_3$  vibrations. For formate and propionate, we find that both types of bands are separated well enough to allow for at least a semi-quantitative analysis. In all cases we measure a steady increase in the sum-frequency response from these modes with increasing bulk concentration, up to the highest concentration studied,  $\sim 333$  mM. Use of carboxylate ions with selected deuteration has assisted in this analysis. For example, by deuteration of propionate adsorbed on fluorite, the strong coupling of the carboxylate resonances with CH deformation modes could be removed, allowing more definitive assignment of spectral features (Figure 1). In Figure 1(a), two distinctive bands are visible for hydrogenated propionate. For the compounds with the terminal methyl group deuterated (Figures 1(b) and (d)), the band at  $\sim 1477$   $\text{cm}^{-1}$  disappears, indicating that this peak corresponds to the  $\delta\text{CH}_3$  mode. The loss of the  $\delta\text{CH}_3$  mode contribution also results in a shift in the  $\sim 1450$   $\text{cm}^{-1}$  resonance due to the changing of the  $\nu\text{CH}$  contributions to the carboxylate resonance. For acetate, the CH bending modes and carboxylate vibrations overlap too much to separate, obscuring details of the headgroup resonances. Consequently, for acetate ions, the combined amplitude of carboxylate and  $\text{CH}_3$  deformation bands were used to quantify acetate adsorption at this interface.

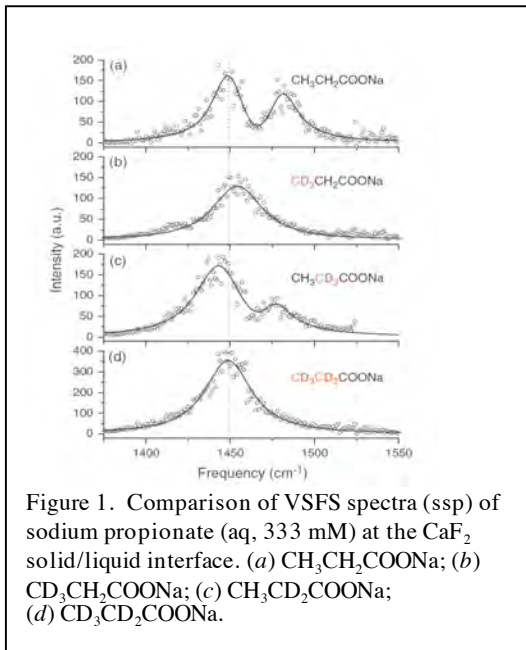


Figure 1. Comparison of VSFS spectra (ssp) of sodium propionate (aq, 333 mM) at the  $\text{CaF}_2$  solid/liquid interface. (a)  $\text{CH}_3\text{CH}_2\text{COONa}$ ; (b)  $\text{CD}_3\text{CH}_2\text{COONa}$ ; (c)  $\text{CH}_3\text{CD}_2\text{COONa}$ ; (d)  $\text{CD}_3\text{CD}_2\text{COONa}$ .

The other spectral region of interest for these studies ( $2700$ – $3800$   $\text{cm}^{-1}$ ) covers the signatures of interfacial water molecules and of  $\text{CH}_2/\text{CH}_3$  stretch resonances. The amplitudes of the main water modes located at  $\sim 3200$  (highly coordinated water - tetrahedral) and  $\sim 3450$   $\text{cm}^{-1}$  (more asymmetrically bonded water) are found to undergo a notable decrease in amplitude with increasing acetate concentration. Furthermore, the relative abundance of tetrahedrally coordinated water molecules is shifted in favor of more asymmetrically bonded water species. These observations were attributed to the presence of acetate ions at the interface, shielding the surface charge. Consequently, fewer water molecules experience an aligning interfacial electrical field. Furthermore, unfavourable interactions between water molecules and the methyl groups of acetate ions reduce the number of tetrahedrally coordinated water molecules with a net orientation towards the interface. Even at high acetate concentrations (333 mM) where adsorbed acetate works to neutralize the mineral surface charge, the interface remains positively charged, and the residual water response still amounts to over 60% of its original

amplitude. From this and other evidence it was concluded that orientation of water molecules extends well beyond the first molecular layer of adsorbed carboxylate. We conclude that the adsorbate layer of short-chain carboxylates is not dense enough to cause complete screening of the surface charge, nor do the carboxylate substrate interactions alone lead to complete charge neutralization or even overcharging of the interface. The relative weakness of carboxylate-fluorite bonding in the absence of other effects which stabilize the adsorbate layer is also evident from the full reversibility of the adsorption process and the rapid dynamic equilibrium between bulk and adsorbed acetate molecules.

The mainly coulombic nature of the interaction of short-chain carboxylates with the fluorite substrate has also been demonstrated by a study of the pH dependence of acetate adsorption. As the surface speciation undergoes pH-controlled changes, the amount of acetate detected at the interface varies considerably: the surface charge is increasingly positive below the isoelectric point (IEP) when the pH is lowered, because more positively charged protonated  $\text{OH}_2^+$  surface species are generated. Only at pH values below the  $\text{pK}_a$  of acetic acid does protonation of acetate ions lead to a rapid decrease of acetate adsorption. At  $\text{pH} > \text{IEP}$ , acetate adsorption is rendered electrostatically unfavourable by the prevalence of

negatively charged surface species. From the analysis of pH-dependent energy shifts of carboxylate resonances, we show that adsorbate–adsorbate interactions are weak for fluorite-adsorbed acetate ions. The corresponding shifts of the water bands, albeit small, are noticeable and indicate that hydrogen-bonding strength of interfacial water molecules is modulated by the bulk pH. A schematic view of the acetate(aq)/fluoride interface at an intermediate  $\text{pH}$  is given in Figure 2. Although no strict separation should be implied, we conclude from a series of experiments that tetrahedrally coordinated (dark blue, region (b)) molecules reside further away from the interface, while more disordered molecules are predominantly located closer to the surface (light blue, region (a)). The amplitude of the latter increases markedly with decreasing  $\text{pH}$  due to a higher degree of orientational alignment caused by a stronger electrical field at the interface. The water molecules interspersed in the ion layers close to the interface thus act as probes for the electrical field at the interface. As the ion layer balancing the surface charge becomes more diffuse further from the interface, the number of tetrahedrally coordinated water molecules oriented by the interfacial field increases. Over a broad range of pH values, the orienting field in this region appears to be remarkably constant due to the charge-compensating action of the electrical double layer and the adsorbed acetate, and only increases when acetate adsorption becomes unfavourable at low  $\text{pH}$ .

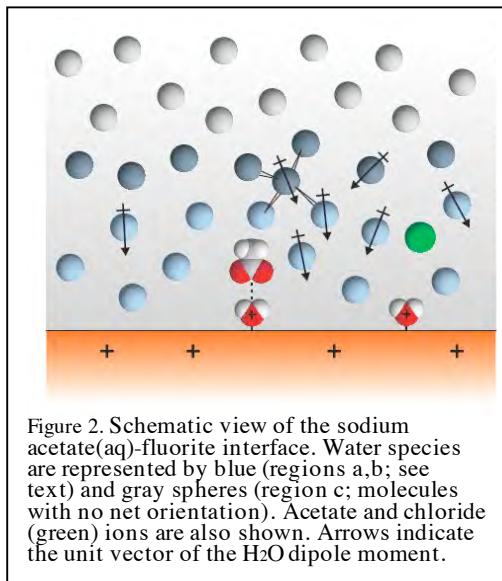


Figure 2. Schematic view of the sodium acetate(aq)-fluorite interface. Water species are represented by blue (regions a,b; see text) and gray spheres (region c; molecules with no net orientation). Acetate and chloride (green) ions are also shown. Arrows indicate the unit vector of the  $\text{H}_2\text{O}$  dipole moment.

#### *Ongoing and Near-Future Plans*

1. Our ongoing studies of adsorption and molecular assembly at the solid-liquid interface include:

- measuring the molecular structure and bonding of charged surfactants as they assemble at the surface of charged mineral surfaces and aluminum oxides surfaces in solution and exploring how the interfacial water plays a role in the assembly these surfactants
- determining how surface-adsorbate interactions and the assembly process vary with the composition of the aqueous phase (i.e. inorganic salt, pH, ionic strength etc.).
- conducting time-resolved spectroscopic measurements of the assembly process to determine the rates of adsorption and desorption of monomers, the dynamic behavior of interfacial water, and the effect of ions, solutes and surface composition on these rates.
- measuring the structure and bonding of water and solutes at fluorinated polymers and fluorocarbon monolayer assemblies, and comparing them with their hydrocarbon counterparts.
- conducting computational studies that calculate the VSF spectrum using MD simulations, determining from these calculations the best model(s) to use to accurately describe the system by comparison with experiment, and extracting additional molecular information from the results to complement and augment the understanding derived from the experimental studies.

### *Publications*

1. "In-situ Investigation of Carboxylate Adsorption at the Fluorite/Water Interface by Sum Frequency Spectroscopy", S. Schrödle, F.G. Moore and G.L. Richmond, *J. Phys. Chem. C.*, 111, (8050-8059) 2007.
2. "Surface Speciation at Solid/Liquid Interfaces: A Vibrational Sum-Frequency Study of Acetate at the Fluorite/Water Interface", S. Schrödle, F.G. Moore and G.L. Richmond, *J. Phys. Chem. C*, 111 (10088-10094) 2007.
3. "Layered Organic Structure at the Carbon Tetrachloride–Water Interface" D. Hore, D. Walker and G. Richmond, *J. Amer. Chem. Soc.*, 129 (752-753) 2007.
4. "Molecular Structure of the Chloroform-Water and Dichloromethane-Water Interfaces", D. K. Hore, D.S.Walker, L.MacKinnon and G.L.Richmond, *J.Phys.Chem.C*,111 (8832-42) 2007.
5. "Depth Profiling of Water Molecules at the Liquid-Liquid Interface using a Combined Surface Vibrational Spectroscopy and Molecular Dynamics Approach", D. S. Walker and G.L. Richmond, *J. Amer. Chem. Soc.*, 129 (9446-9451) 2007.
6. "Monomer Exchange Dynamics of Self-Assembled Surfactant Monolayers at the Solid-Liquid Interface", S. Schrödle and G.L. Richmond, *Chem. Phys. Chem.*, 8 (2315-2317) 2007.
7. "In-situ Nonlinear Spectroscopic Approaches to Understanding Adsorption at Mineral-Water Interfaces", S. Schrödle and G. L. Richmond, *J. of Phys. D: Appl. Phys.*, 41 (1-14) 2008.
8. "Sequential Wavelength Tuning: Dynamics at Interfaces Investigated by Vibrational Sum Frequency Spectroscopy", S. Schrödle and G. L. Richmond, *Appl. Spec.*, 62 (389-393) 2008.
9. "Equilibrium and Non-Equilibrium Kinetics of Self-Assembled Surfactant Monolayers: A Vibrational Sum-Frequency Study of Dodecanoate at the Fluorite-Water Interface", S. Schrödle and G. L. Richmond, *J. Amer. Chem. Soc.*, 130 (5072-5085) 2008.

Program Title:  
Programming Function Via Soft Materials

Principal Investigator:  
John A. Rogers  
University of Illinois  
Materials Research Laboratory  
403 North Goodwin Avenue  
Urbana, IL 61801  
jrogers@illinois.edu

Program Scope/Definition:

Electronic/optoelectronic systems that involve transistors, solar cells, light emitting diodes (LEDs) and other components on thin plastic or rubber substrates offer mechanical properties (e.g. stretchability) and other features (e.g. curvilinear shapes) that cannot be achieved with conventional approaches. Application possibilities include devices that use biologically inspired designs (e.g. eyeball cameras) and those that require intimate integration with the human body (e.g. health monitors). This program seeks to develop means to create, assemble and integrate inorganic micro/nanomaterials into systems that offer the performance of state-of-the-art, wafer-based technologies but with the mechanical properties of a rubber band, in planar or curvilinear layouts and in two or three dimensional configurations.

Recent Progress:

We have developed approaches to fabricate large-scale collections of microscale inorganic devices, including transistors, solar cells and LEDs. Figure 1 shows examples of silicon nanoribbons, and nanowires of gallium arsenide, gallium nitride and indium phosphide, created from high quality, semiconductor wafers or films of these materials. Deterministic assembly methods that use these devices as solid 'inks' with soft, elastomeric 'stamps' provide a route to their integration into heterogeneous functional systems on diverse substrates, ranging from plates of glass to sheets of plastic and slabs of

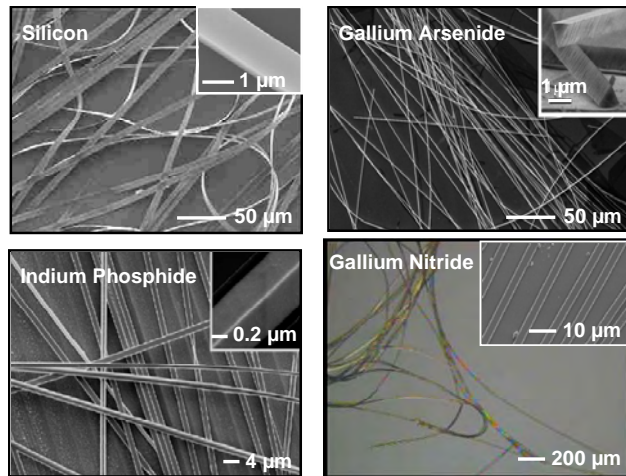
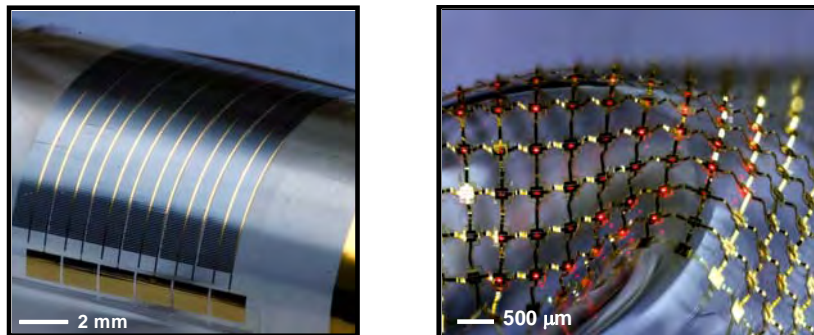


**Figure 1.** Scanning electron and optical micrographs of micro/nanoscale wires and ribbons of inorganic semiconductors created from bulk wafers or thin films of these materials.

**Figure 2.** Flexible photovoltaic module (left) and stretchable lighting system (right) formed with printed assemblies of micro/nanoscale inorganic material structures.



rubber, in two dimensional arrangements or three dimensional multilayer stacks. Figure 2 provides examples of a flexible photovoltaic module based on arrays of silicon microbar solar cells and a stretchable lighting system that integrates collections of microscale AlInGaP LEDs.

#### Future Plans:

We are exploring ways to assemble active devices and passive structures from solution phase suspensions, as a more versatile mode for integration compared to the printing based assembly techniques used to achieve the systems shown in Fig. 2. Such strategies have the potential to add dynamic reconfigurability for enhanced functionality, e.g. concentrator optics in microcell photovoltaic modules that can track the sun, without overall mechanical motion; lighting systems that incorporate reconfigurable collections of microscale LEDs to adapt to user needs.

#### References (selected; 2007-2009)

S.-I. Park, Y. Xiong, R.-H. Kim, P. Elvikis, M. Meitl, D.-H. Kim, J. Wu, J. Yoon, C.-J. Yu, Z. Liu, Y. Huang, K.-C. Hwang, P. Ferreira, X. Li, K. Choquette and J.A. Rogers, "Printed Assemblies of Inorganic Light-Emitting Diodes for Deformable and Semitransparent Displays," *Science* 325, 977-981 (2009).

M.C. George, E.C. Nelson, J.A. Rogers, and P.V. Braun, "Direct Fabrication of 3D Periodic Inorganic Microstructures Using Conformal Phase Masks," *Angewandte Chemie International Edition* 48, 144 –148 (2009).

D. Shir, E.C. Nelson, Y.C. Chen, A. Brzezinski, H. Liao, P.V. Braun, P. Wiltzius, K.H.A. Bogart and J.A. Rogers, "Three Dimensional Silicon Photonic Crystals Fabricated by Two Photon Phase Mask Lithography," *Applied Physics Letters* 94, 011101 (2009).

Q. Cao and J.A. Rogers, "Ultrathin Films of Single-Walled Carbon Nanotubes for Electronics and Sensors: A Review of Fundamental and Applied Aspects," *Advanced Materials* 21, 29-53 (2008). (invited)

D.-H. Kim, J. Song, W.M. Choi, H.-S. Kim, R.-H. Kim, Z. Liu, Y.Y. Huang, K.-C. Hwang, Y. Zhang and J.A. Rogers, "Materials and noncoplanar mesh designs for integrated circuits with linear elastic responses to extreme mechanical deformations," *Proceedings of the National Academy of Sciences USA* 105(48), 18675–18680 (2008). (cover feature article)

D.-H. Kim and J.A. Rogers, "Stretchable Electronics: Materials Strategies and Devices," *Advanced Materials* 20(24), 4887-4892 (2008). (invited)

J. Yoon, A.J. Baca, S.-I. Park, P. Elvikis, J.B. Geddes, L. Li, R.H. Kim, J. Xiao, S. Wang, T.H. Kim, M.J. Motala, B.Y. Ahn, E.B. Duoss, J.A. Lewis, R.G. Nuzzo, P.M. Ferreira, Y. Huang, A. Rockett and J.A. Rogers, "Ultrathin Silicon Solar Microcells for Semitransparent, Mechanically Flexible and Microconcentrator Module Designs," *Nature Materials* 7, 907-915 (2008). (cover feature article)

S.-I. Park, J.-H. Ahn, X. Feng, S. Wang, Y. Huang and J.A. Rogers, "Theoretical and Experimental Studies of Bending of Inorganic Electronic Materials on Plastic Substrates," *Advanced Functional Materials* 18, 2673–2684 (2008).

- J.-H. Ahn, Z. Zhu, S.-I. Park, J. Xiao, Y. Huang and J.A. Rogers, "Defect Tolerance and Nanomechanics in Transistors that Use Semiconductor Nanomaterials and Ultrathin Dielectrics," *Advanced Functional Materials* 18, 2535-2540 (2008). (cover feature article)
- D. Shir, H. Liao, S. Jeon, D. Xiao, H.T. Johnson, G.R. Bogart, K.H.A. Bogart and J.A. Rogers, "Three-Dimensional Nanostructures Formed by Single Step, Two-Photon Exposures through Elastomeric Penrose Quasicrystal Phase Masks," *Nano Letters* 8(8), 2236-2244 (2008).
- H.C. Ko, M.P. Stoykovich, J. Song, V. Malyarchuk, W.M. Choi, C.-J. Yu, J.B. Geddes, J. Xiao, S. Wang, Y. Huang and J.A. Rogers, "A Hemispherical Electronic Eye Camera Based on Compressible Silicon Optoelectronics," *Nature* 454, 748-753 (2008). (cover feature article)
- D.-H. Kim, W.M. Choi, J.-H. Ahn, H.-S. Kim, J. Song, Y. Huang, Z. Liu, C. Lu, C.G. Koh and J.A. Rogers, "Complementary Metal Oxide Silicon Integrated Circuits Incorporating Monolithically Integrated Stretchable Wavy Interconnects," *Applied Physics Letters* 93, 044102 (2008).
- Q. Cao, H.-S. Kim, N. Pimparkar, J.P. Kulkarni, C. Wang, M. Shim, K. Roy, M.A. Alam and J.A. Rogers, "Medium-Scale Carbon Nanotube Thin-Film Integrated Circuits on Flexible Plastic Substrates," *Nature* 454, 495-500 (2008).
- A.J. Baca, J.-H. Ahn, Y. Sun, M.A. Meitl, E. Menard, H.-S. Kim, W.M. Choi, D.-H. Kim, Y. Huang and J.A. Rogers, "Semiconductor Wires and Ribbons for High-Performance Flexible Electronics," *Angewandte Chemie International Edition* 47, 5524 – 5542 (2008).
- J. Yao, M.E. Stewart, J. Maria, T.-W. Lee, S.K. Gray, J.A. Rogers and R.G. Nuzzo, "Seeing Molecules by Eye: Surface Plasmon Resonance Imaging at Visible Wavelengths with High Spatial Resolution and Submonolayer Sensitivity," *Angewandte Chemie International Edition* 47, 5013-5017 (2008).
- M.J. Schultz, X. Zhang, S. Unarunotai, D.-Y. Khang, Q. Cao, C. Wang, C. Lei, S. MacLaren, J.A.N.T. Soares, I. Petrov, J.S. Moore and J.A. Rogers, "Synthesis of Linked Carbon Monolayers: Films, Balloons, Tubes, and Pleated Sheets," *Proceedings of the National Academy of Sciences USA* 105(21), 7353-7358 (2008).
- D.-H. Kim, J.-H. Ahn, W.-M. Choi, H.-S. Kim, T.-H. Kim, J. Song, Y.Y. Huang, L. Zhuangjian, L. Chun and J.A. Rogers, "Stretchable and Foldable Silicon Integrated Circuits," *Science* 320, 507-511 (2008).
- M.E. Stewart, C.R. Anderton, L.B. Thompson, J. Maria, S.K. Gray, J.A. Rogers and R.G. Nuzzo, "Nanostructured Plasmonic Sensors," *Chemical Reviews* 108, 494-521 (2008). (invited)
- C. Kocabas, H.-S. Kim, T. Banks, J.A. Rogers, A.A. Pesetski, J.E. Baumgardner, S. V. Krishnaswamy and H. Zhang, "Radio Frequency Analog Electronics Based on Carbon Nanotube Transistors," *Proceedings of the National Academy of Sciences USA* 105(5), 1405-1409 (2008).
- D.-H. Kim, J.-H. Ahn, H.-S. Kim, K.J. Lee, T.-H. Kim, C.-J. Yu, R.G. Nuzzo and J.A. Rogers, "Complementary Logic Gates and Ring Oscillators on Plastic Substrates by Use of Printed Ribbons of Single-Crystalline Silicon," *IEEE Transactions on Electron Devices* 29(1), 73-76 (2008). (George Smith Award – best paper for 2008)

- A.J. Baca, M.A. Meitl, H.C. Ko, S. Mack, H.-S. Kim, J. Dong, P.M. Ferreira and J.A. Rogers, "Printable Single-Crystal Silicon Micro/Nanoscale Ribbons, Platelets and Bars Generated from Bulk Wafers," *Advanced Functional Materials* 17, 3051–3062 (2007).
- D.J. Shir, S. Jeon, H. Liao, M. Highland, D.G. Cahill, M.F. Su, I.F. El-Kady, C.G. Christodoulou, G.R. Bogart, A.V. Hamza and J.A. Rogers, "Three-Dimensional Nanofabrication with Elastomeric Phase Masks," *Journal of Physical Chemistry B* 111, 12945-12958 (2007). (cover feature article)
- N.H. Mack, J.W. Wackerly, V. Malyarchuk, J.A. Rogers, J.S. Moore, R.G. Nuzzo, "Optical Transduction of Chemical Forces," *Nano Letters* 7(3), 733-737 (2007).
- J.-H. Ahn, H.-S. Kim, E. Menard, K.J. Lee, Z. Zhu, D.-H. Kim, R.G. Nuzzo J.A. Rogers, I. Amlani, V. Kushner, S.G. Thomas and T. Duenas, "Bendable Integrated Circuits on Plastic Substrates by Use of Printed Ribbons of Single-Crystalline Silicon," *Applied Physics Letters* 90, 213501 (2007). (cover feature article)
- V. Malyarchuk, M.E. Stewart, R.G. Nuzzo and J.A. Rogers, "Spatially Resolved Biosensing with a Molded Plasmonic Crystal," *Applied Physics Letters* 90, 203113 (2007).
- S. Jeon, D.J. Shir, Y.S. Nam, R. Nidetz, M. Highland, D.G. Cahill, J.A. Rogers, M.F. Su, I.F. El-Kady, C.G. Christodoulou and G.R. Bogart, "Molded Transparent Photopolymers and Phase Shift Optics for Fabricating Three Dimensional Nanostructures," *Optics Express* 15(10), 6358-6366 (2007).
- C. Kocabas, N. Pimparkar, O. Yesilyurt, S. J. Kang, M. A. Alam and J.A. Rogers, "Experimental and Theoretical Studies of Transport through Large Scale, Partially Aligned Arrays of Single-Walled Carbon Nanotubes in Thin Film Type Transistors," *Nano Letters*, 7(5) 1195-1202 (2007).
- S.J. Kang, C. Kocabas, T. Ozel, M. Shim, N. Pimparkar, M.A. Alam, S.V. Rotkin and J.A. Rogers, "High-performance electronics using dense, perfectly aligned arrays of single-walled carbon nanotubes," *Nature Nanotechnology* 2, 230-236 (2007). (cover feature article)
- T.T. Truong, R. Lin, S. Jeon, H.H. Lee, J. Maria, A. Gaur, F. Hua, I. Meinel and J.A. Rogers, "Soft Lithography Using Acryloxy Perfluoropolyether Composite Stamps," *Langmuir* 23, 2898-2905 (2007).
- Y. Sun and J.A. Rogers, "Structural Forms of Single Crystal Semiconductor Nanoribbons for High-Performance Stretchable Electronics," *Journal of Materials Chemistry* 17, 832-840 (2007). (Invited cover feature article.)
- Y. Sun and J.A. Rogers, "Inorganic Semiconductors for Flexible Electronics," *Advanced Materials* 19, 1897-1916 (2007).

# Nanomanipulation and Optical Nanotomography of Anisotropic Fluids

Charles Rosenblatt

Department of Physics  
Case Western Reserve University  
Cleveland, Ohio 44106-7079  
[rosenblatt@case.edu](mailto:rosenblatt@case.edu)

**Program Scope:** The physical properties of anisotropic fluids can be manipulated on very short length scales of 100 nm or less by appropriate treatment of the confining substrate(s). Our goal is to control and image in 3D with high resolution the fluid's molecular orientation profile and to understand the fluid's behavior within  $\sim 500$  nm of a substrate. To accomplish these tasks we have developed and implemented both an AFM-based surface control technique and a subwavelength aperture optical fiber imaging approach that we call "Optical Nanotomography" (ONT). These methods are applicable to a variety of soft systems. Here we apply these techniques to the investigation of liquid crystal behavior within  $\sim 500$  nm of a patterned substrate.

**Recent Progress:** Liquid crystal orientation may be controlled on nanoscopic length scales by manipulating the stylus of an atomic force microscope (AFM) to scribe nanoscopic patterns into polymer-coated or surfactant-coated substrates. Figure 1 shows a polyimide-coated substrate that was scribed with a very large force to create nanoscopic grooves. The liquid crystal subsequently is deposited onto the substrate and aligns parallel to the scribing direction *via* two primary mechanisms: elastic interactions in the LC that favor alignment parallel rather than perpendicular to the grooves, as well as epitaxial growth of LC alignment from the aligned polyimide backbone due to anisotropic dispersive and other interactions. Although Fig. 1 shows a uniform alignment pattern, we also can vary the scribing direction in the plane of the substrate on length scales of a few nm, with a concomitant variation of the preferred liquid crystal alignment direction over the substrate (Fig. 2). In regions where the "easy axis" (scribing direction) changes abruptly, a nematic liquid crystal is unable to follow the easy axis due to elastic forces. The trade-off between elastic and surface interactions results in an "extrapolation length"  $L$  over which the LC orientation undergoes a direction change. In the smectic-A phase, the layered structure actually undergoes a melting into the nematic phase in regions of high distortion, in analogy with the breakdown of the Meissner effect in a type I superconductor that is subjected to a strong magnetic field.

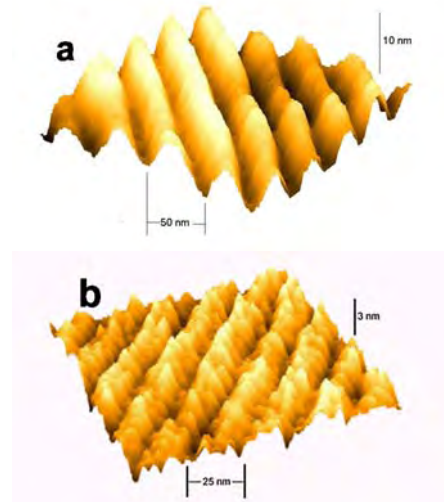


**Fig. 1** AFM-scribed polyimide. The polyimide layer was scribed with a large force using the AFM stylus in "contact mode," and the image of the grooved surface then was created by the same stylus in non-contact ("tapping") mode. a) Grooves scribed 50 nm apart on smooth surface. b) Grooves spaced 25 nm on a topographically rough surface.

Owing to diffraction limitations, high resolution 3D imaging of the liquid crystal's molecular orientation profile has been beyond the reach of extant optical techniques. Instead, we have developed a powerful new imaging approach (“Optical Nanotomography”), which is based on the use of polarized light emitted from a tapered optical fiber immersed in an anisotropic medium and collected in the far field. As there are no significant scattering sources due to dielectric inhomogeneities, the near field light does not scatter in the customary manner, but instead decays exponentially with distance and is not detected downstream. Instead, the light that reaches the detector from the fiber aperture consists of low spatial Fourier components, and is optically retarded by a phase  $\delta$  as it propagates through the continuous birefringent fluid medium. By performing in-plane ( $xy$ ) scans *inside* the sample at a series of heights  $z_i$  above the surface, we obtain intensity matrix slices, from which we extract information about the fluid's local optical — and therefore orientational — properties.

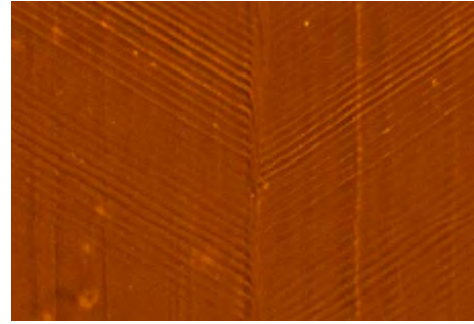


**Fig. 2** AFM image of chevron-scribed pattern, with rub lines spaced approximately 80 nm apart.

As an example of ONT we examined a nematic liquid crystal, whose molecular orientation is controlled by a nanoscopic pattern scribed into the underlying polymer-coated substrate. We have selected this system as an ideal test bed for validation of our high resolution imaging technique because there exist theoretical predictions about the liquid crystal's behavior, even though extant experimental techniques are unable to examine these small length scales. Images based upon the total optical retardation of the liquid crystal from the fiber aperture to the substrate were obtained at up to 17 heights above the substrate, out to 480 nm (Fig. 3). We empirically found that: i) the lateral resolution of our ONT method is as small as 100 nm and vertical resolution  $\sim 2$  nm, and ii) the fiber's perturbation of the fluid structure is small and does not significantly affect the signal. From these images we were able to visualize for the first time and measure the extrapolation length  $L \sim 200$  nm over which the molecular orientation relaxes due to the liquid crystal's elastic forces. Moreover, the “fingers” at the right in each of the images in Fig. 3 are due to the topography of the substrate created by the AFM-scribing. From the relative contrast in each image, a peak-to-peak surface height variation of  $17 \pm 3$  nm was determined, in excellent

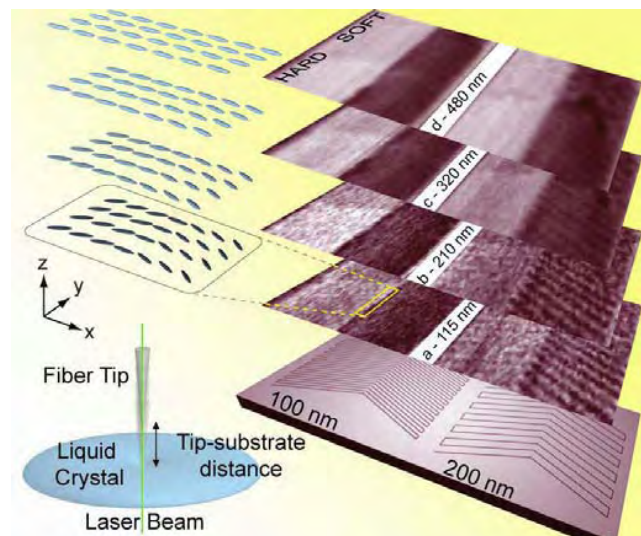


**Fig. 3** Optical Nanotomography images at different heights  $h$ . A series of images created from the intensity data matrix collected at heights (a) 115 nm, (b) 210 nm, (c) 320 nm, and (d) 480 nm above the polymer coated substrate, with an uncertainty of  $\pm 10$  nm. The scan dimension is approximately  $15 \times 9 \mu\text{m}$ . Polarizer makes an angle  $\beta$  nominally equal to  $7.5^\circ$  and  $37.5^\circ$  with respect to the easy axes. Note the “fingers” in the images on the right.

agreement with the value of 18 nm determined by a non-contact AFM topographical measurement.

We also have applied a variation of ONT to examine surface-induced orientational order in the isotropic liquid crystal phase on cooling toward the nematic- isotropic transition temperature  $T_{NI}$ . For more than 30 years the conventional wisdom had been that surface-induced orientational order involves a delta-function (*i.e.*, a highly localized) interaction potential between the substrate and liquid crystal, which induces nonzero nematic order  $S_0$  at the substrate above  $T_{NI}$ . For sufficiently weak  $S_0$  the order supposedly decays approximately exponentially into the bulk, although for stronger surface order the higher order terms — proportional to  $S^3$  and  $S^4$  in the Landau expansion of the free energy — need to be included and can give rise to prewetting and capillary condensation phenomena. In this experiment we treated the substrate for weak planar order by means of weak rubbing. We then used a variation on our ONT technique by keeping the optical fiber fixed in the  $x,y$ -plane but varying its height  $h$  above the substrate in 1 nm steps and measuring the intensity  $I(h)$  downstream. In the present experimental configuration the intensity  $I$  is proportional to the integrated nematic order parameter  $S(z)$  from the substrate to the fiber's aperture at height  $h$ . Thus the quantity  $dI/dh$  allows us to extract  $S(z)$  with resolution  $< 2$  nm normal to the interface (Fig. 4). The most important result is that  $S(z)$  does *not* decay exponentially with  $z$ , but rather falls off slowly for the first 5 – 8 nm, and then decays rapidly further away from the substrate. This behavior is contrary to all extant results, both theoretical and experimental, in which a delta-function surface potential and exponential decay have been *assumed*. Instead, we have proposed that the behavior is due to a combination of non-local interactions near the surface, as well as short range order correlations.

Similarities between the superconducting and the smectic-A phases were noted by DeGennes in 1972. In particular, he showed that twist and bend deformations are expelled in the smectic-A

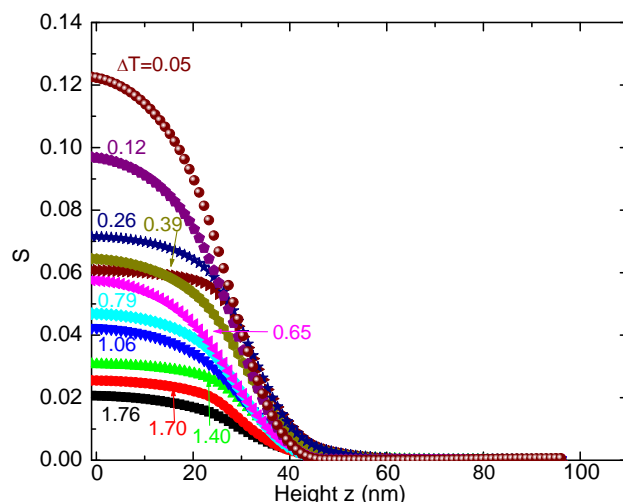


**Fig. 4** Nematic order parameter  $S(z)$  vs.  $z$  as a function of  $\Delta T = T - T_{NI}$ .

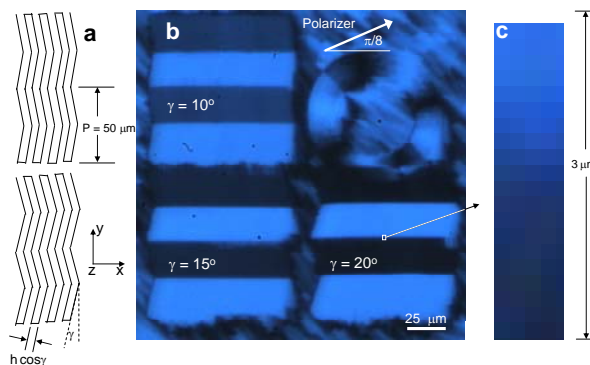


**Fig. 5** a) Schematic representation of rubbing pattern for  $\gamma=10^\circ$  (top) and  $\gamma=15^\circ$  (bottom). Period  $P=50 \mu\text{m}$ . b) Polarized micrograph of sample, showing three herringbone patterns and the spiral (upper right). The tiny square in the  $\gamma=20^\circ$  pattern is enlarged in panel c), which shows the intensity variation across the pixel interface, allowing us to determine  $W$ .

phase, in analogy with the superconducting Meissner effect in which a magnetic field is expelled completely for a type I superconductor. For sufficiently large bend deformation the smectic-A phase melts into the nematic phase, analogous to the superconducting-to-normal transition in a strong magnetic field. In this experiment we AFM-scribed a large bend distortion into a substrate (Fig. 5), and measured the width  $W$  of the nematic (melted) region at temperatures below the bulk nematic – smectic-A phase transition temperature  $T_{NA}$ .  $W$  was found to increase with increasing temperature toward  $T_{NA}$ , and was several  $\mu\text{m}$  in extent for  $T_{NA} - T \sim 10 \text{ mK}$ . The results were in excellent agreement with our scaling model based on DeGennes' theory for the width of the melted nematic region for a type I smectic.

**Future Plans:** We will continue refinement of our ONT technique in order to be able to extract 3D orientational profiles of topological defects, liquid crystalline order around colloids, and surface-induced orientational order. In particular, we intend to examine the physical phenomena associated with the initial slow spatial decay of orientational order near the substrate above the nematic – isotropic transition temperature. As improvements are made, we intend to expand the range of applicability of ONT to include a variety of other soft materials.

#### **DOE-Sponsored Publications:**

- “Bend expulsion from the smectic-A phase: Analogy to type-I superconductor,” R. Wang, I.M. Syed, G. Carbone, R.G. Petschek, and C. Rosenblatt, **Phys. Rev. Lett.** *97*, 167802 (2006)
- “Continuous control of liquid crystal pretilt angle from homeotropic to planar,” K. Vaughn, M. Sousa, D. Kang, and C. Rosenblatt, **Appl. Phys. Lett.** *90*, 194102 (2007)
- “Optical Nanotomography of anisotropic fluids,” Antonio De Luca, Valentin Barna, T.J. Atherton, G.i Carbone, M.E. Sousa, and C. Rosenblatt, **Nature Physics** *4*, 869 (2008)
- “Nanoscale anisotropic patterning for alignment of a birefringent fluid and nanoimaging of its optical phase retardation,” V. Barna, A. De Luca, and C. Rosenblatt, **Nanotechnology** *19*, 325709 (2008)
- “Diverging Elasticity and Director Uniformation in a Nanopatterned Cell near the Nematic - Smectic-A Phase Transition,” T.J. Atherton, R. Wang, and C. Rosenblatt, **Phys. Rev. E** *77*, 061702 (2008)
- “Full control of nematic pretilt angle using spatially homogeneous mixtures of two polyimide alignment materials,” J.-H. Lee, D. Kang, C.M. Clarke, and C. Rosenblatt, **J. Appl. Phys.** *105*, 023508 (2009)
- “Direct measurement of surface-induced orientational order parameter profile above the nematic -- isotropic phase transition temperature,” Ji-Hoon Lee, Timothy J. Atherton, Valentin Barna, Antonio De Luca, Emanuala Bruno, Rolfe G. Petschek, and Charles Rosenblatt, **Phys. Rev. Lett.** *102*, 167801 (2009)

## **Program Title: Miniaturized Hybrid Materials Inspired by Nature**

**Principle Investigator: C. R. Safinya; Co-PIs: Y. Li and K. Ewert**

**Mailing Address: Materials Department, University of California at Santa Barbara  
Santa Barbara, CA 93111**

**E-mail: safinya@mrl.ucsb.edu**

### **Program Scope**

The goals of the program are to develop a fundamental understanding of the mechanisms underlying lipid and protein based nanometer scale assembly. The understanding should lead to the development of nanometer scale materials, which are scientifically and technologically important. Nanometer scale tubes and rods and their assemblies are of interest as miniaturized materials with diverse applications as circuitry components, enzyme encapsulation systems and biosensors, vehicles for chemical delivery, and as templates for hierarchical nanostructures.

The main strategy that we use to achieve our goals consists of learning from, and building upon, the many illuminating examples of assembly occurring in vivo far from equilibrium. For example, the nerve cell cytoskeleton provides a rich variety of assembled bundles and networks of filamentous actin, microtubules (MT), and neurofilaments, where the nature of their interactions leading to their hierarchical structures, and the structure-function correlations are not understood [1-4,6]. In earlier work (including DOE supported work dating back to 2007) in far simpler protein systems (using a combination of synchrotron x-ray diffraction, electron microscopy, and optical imaging data), we have demonstrated how (i) MTs (model nanotubes) may be assembled in distinct structures (e.g. 2D versus 3D bundles) through a competition between short-range attractions and longer-ranged repulsions, and (ii) isolated MTs may be used as templates to form lipid-protein nanotubes with open and closed ends and varying inner diameters [2]. In more recent work we have discovered an entirely new mechanism, using custom synthesized curvature stabilizing lipids, to develop lipid bio-nanotubes and bio-nanorods. The nanorods and nanotubes are a result of the formation of block liposomes [5]; a new class of liposomes, with the blocks consisting of distinctly shaped nanoscale spheres, tubes, or rods. Indeed, similar membrane shape changes, occurring in vivo for the purpose of specific cellular functions, are often induced by curvature generating/stabilizing proteins through their interactions with cellular membranes [7]. For example, in endocytosis, which requires vesicle budding, the (curvature stabilizing) protein dynamin is recruited and assembled into stacks of rings in the negative curvature region of the invaginated membrane vesicle forcing dynamical lipid shape changes where a transient tubular neck formation is followed by membrane fission.

The projects involve both custom synthesis of novel lipids, peptide-lipids, and PEG-lipids with or without functional end groups, and purification of biological molecules [8,9]. In some instances the enhanced stability of the lipid assemblies will be achieved by lipids with polymerizable chains. The higher order assembly of the building blocks will be achieved via competing interactions, where end-functionalized PEG-lipids may play an important role.

The projects utilize the broad spectrum of expertise of the group members in biomolecular self-assembling methods, synchrotron x-ray scattering and diffraction, electron and optical microscopy characterization techniques.

## Recent Progress

Block Liposomes consisting of Distinctly Shaped and Connected Nanotubes, -rods or –spheres: Membrane Shape Evolution in Response to Incorporation of Curvature Generating Charged Lipids [Reference 5].

### BACKGROUND

Lipids – one of the main building blocks of life – and their assemblies (e.g. membranes and liposomes) play a major role in numerous cellular processes including compartmentalization, macromolecular transport, and signal/energy transduction. A distinguishing feature of membranes in vivo, enabling their function, is the evolution in their shapes. Thus, understanding the mechanisms by which membranes undergo shape changes remains a major scientific challenge. Indeed, much effort has been expended to elucidate membrane shapes in the context of their interactions with membrane-associated, curvature generating proteins. Such curvature generating proteins play a key role in vesicle budding, which is required in receptor-mediated endocytosis, in inter-organelle trafficking and at synaptic junctions recycling vesicles. In our work described below we are interested in elucidating the key parameters; for example, charge and steric shape of the curvature generating lipid molecule, involved in membrane shape evolution in relatively simple model systems.

Discussion of Findings In exploring the properties of curvature forming/stabilizing lipids on membrane shape evolution (a simple mimic of the more complicated process occurring *in vivo* via curvature stabilizing proteins) we have discovered *block liposomes*, an entirely new class of liposomes, with the blocks consisting of distinctly shaped nanoscale spheres, tubes, or rods (see Figs. 1 and 2) [5]. The block liposomes resulted from membrane shape evolution in response to the incorporation of a custom synthesized charged lipid (the cone-shaped MVLBG2, shown schematically in FIG. 2) to giant vesicles with  $\approx$  zero curvature. Cryogenic-TEM revealed the blocks to consist of distinctly shaped nanoscale spheres, tubes, or rods. Diblock (sphere-rod) liposomes were found to contain micellar nanorods  $\approx$  4 nm in diameter and several  $\mu$ m in length, analogous to cytoskeletal filaments of eukaryotic cells (FIG. 1).



FIG. 1 An example of a block liposome induced in response to the incorporation of a highly charged curvature-generating dendritic lipid MVLBG2 to a vesicle of neutral lipid DOPC as revealed by cryogenic TEM. Block liposomes (BL) are a new class of liposomes, consisting of distinctly shaped, yet connected, nanoscale spheres, tubes, or rods. Within a BL shapes are separated on the nanoscale. The image shows a diblock (sphere-rod) consisting of a spherical vesicle connected to a cylindrical micelle (rod). The rod diameter is the thickness of a lipid bilayer (4 nm, the hydrophobic core with high contrast in cryo-TEM). The schematic illustrates an arrangement of lipid molecules within this diblock (sphere-rod) with a higher concentration of the curvature-generating MVLBG2 (green) in the high curvature micellar region as opposed to the spherical part where more DOPC (white) resides. See reference 5 for more detail (A. Zidovska et al, Langmuir 2009, 25, 2979.)

Coexisting with sphere-rod block liposomes are diblock (sphere-tube) and triblock (sphere-tube-sphere) liposomes, which contain nanotubes with inner lumen diameter in the range between 10-50 nm (FIG. 2).

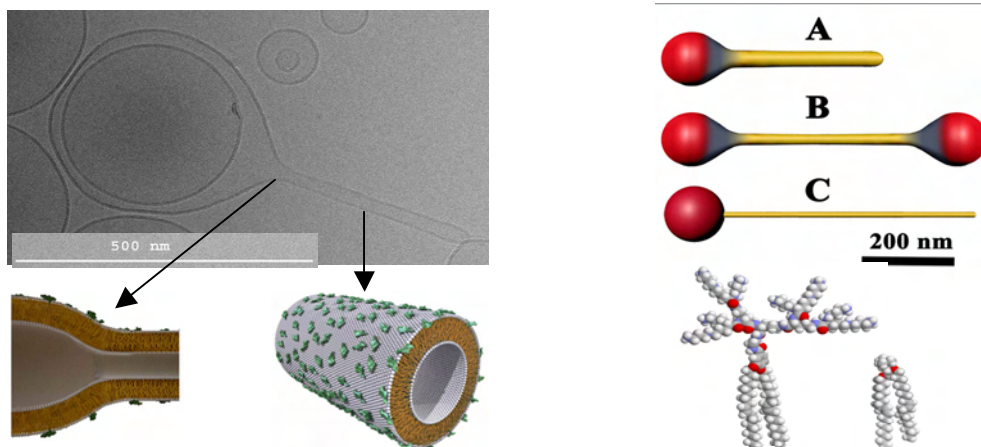


FIG. 2 (**LEFT**) Example of a diblock (sphere-tube) liposome as seen by cryogenic TEM. Bottom schematics showing the intersection region between the sphere and tube and a section of the tube. The schematic shows an arrangement of lipid molecules with a higher concentration of the curvature-stabilizing MVLBG2 (green) in the outer monolayer as opposed to the inner monolayer, which has a higher concentration of neutral DOPC (white) lipids. (**RIGHT**) Top: schematics of the different nanoscale Block Liposomes revealed by Cryo-TEM: (**A**) diblock (sphere-tube) liposome seen in the left TEM image, (**B**) triblock (sphere-tube-sphere) and (**C**) diblock (sphere-rod) liposome seen in FIG. 1. The color coding represents different membrane Gaussian curvature: positive (red), negative (blue) and zero (yellow). Bottom: Molecular models of neutral DOPC (right) and hexadecavalent MVLBG2 (left). (Adapted from reference 5, A. Zidovska; et al. Langmuir 2009, 25, 2979-2985.)

Importance of findings both from experimental and theoretical perspectives: While a large variety of micron scale vesicle shapes including spheres, ellipsoids and oblates, tori, and discocytes has been described previously, the discovery of block liposomes presents a major challenge to the current understanding of membrane shapes at equilibrium. Current theories, based on the widely accepted Helfrich elastic free energy of membranes, predict macroscopically phase separated distinctly shaped liposomes. In contrast, shapes are connected and separated on the nanometer scale in block liposomes (see Figures 1 and 2). New theories of charged membranes are required to account for block liposomes. Broadly speaking, nano-tubes and nano-rods are indispensable components in the development of future miniaturized materials. They have applications in diverse areas from uses as chemical encapsulation vehicles, to biosensors and circuitry components. Thus, an area of intense current research in nanoscience is in elucidating the key parameters, which control the self-assembling properties of nanometer scale tubes and rods. Block liposomes may find a range of applications in chemical and nucleic acid delivery and as building blocks in the design of templates for hierarchical structures and for nanostructures such as wires or needles.

## Future Plans

### (1) Towards the Development of Sterically Stabilized Block Liposomes

To date, we have only observed block liposome formation in charged membrane systems. We have planned a series of experiments to address the important question of whether long-range electrostatic interactions are needed for BL formation or is the cone-shape of the lipid (which may be achieved through steric considerations alone) sufficient for BL formation. The systematic experiments should differentiate between the separate contributions of steric shape

and charge of the lipid molecules to block liposome (BL) formation. In one set of pH studies we will explore whether very weakly charged lipids (e.g. at sufficiently high pH  $\approx$  pKa values of primary/secondary amines of MVLBG2) might still form BLs entirely due to the fact that their relatively large steric lipid headgroups would still result in a cone-shaped lipid. In another set of experiments we plan to selectively neutralize the membrane charge by replacing cationic sections of MVLBG2's headgroup (see Fig. 2) with uncharged short-PEG units. This will allow us to decrease the charge to zero while simultaneously maintaining the large lipid headgroup entirely through steric interactions (e.g. by increasing the number of ethylene-oxide units). These planned experiments, which involve new synthesis should enable us to develop sterically stabilized block liposomes, which would inherently be more stable than their charged counterparts and thus more suitable in future applications. The studies involving systematic variations in the shape, size and charge of the curvature-stabilizing lipid should lead to optimal control of the tubule diameter distribution.

## (2) Nanotubes from Proteins undergoing Conformational Transitions

We have recently discovered a novel biomolecule, which acts as a switch between two configurational states of tubulin oligomers (which are used in assembling microtubules). This conformation transition is observed to "effectively" invert one nanotube state into another. We are currently studying the relevant parameters, which (i) control the rate of transitions between the nanotube structures and (ii) control the reversibility of the switching between the nanostructures.

## **References (which acknowledge DOE support)**

1. Molecular scale imaging of F-actin assemblies immobilized on a photopolymer surface T. Ikawa, F. Hoshino, O. Watanabe, Y. Li, P. Pincus, C. R. Safinya, *Physical Review Letters* **98** (1): 018101, (2007)
2. Microtubule Protofilament Number is Modulated in a Stepwise Fashion by the Charge Density of an Enveloping Layer. U. Raviv, T. Nguyen, R. Ghafouri, D. J. Needleman, Y. Li, H. P. Miller, L. Wilson, R. F. Bruinsma, C. R. Safinya, *Biophysical Journal* **92** (1): 278-287, (2007)
3. Hesse, H. C.; Beck, R.; Ding, C.; Jones, J. B.; Deek, J.; MacDonald, N. C.; Li, Y.; Safinya, C. R.: Direct Imaging of Aligned Neurofilament Networks Assembled Using In Situ Dialysis in Microchannels. *Langmuir* 2008, **24**, 8397-8401 (Cover of August 19, 2008 issue).
4. Jones, J. B.; Safinya, C. R., Interplay between Liquid Crystalline and Isotropic Gels in Self-Assembled Neurofilament Networks. *Biophysical J.* 2008, **95**, 823-825.
5. Zidovska, A.; Ewert, K. K.; Quispe, J.; Carragher, B.; Potter, C. S.; Safinya, C. R., Block Liposomes from Curvature-Stabilizing Lipids: Connected Nanotubes, -rods or -spheres. *Langmuir* 2009, **25**, 2979-2985 (Cover image of March 3, 2009 issue).
6. Choi, M.C., Raviv, U., Miller, H. P., Gaylord, M. R., Kiris, E., Ventimiglia, D., Needleman, D. J., Kim, M.W., Wilson, L., Feinstein, S. C., Safinya, C. R.: Human Microtubule-Associated-Protein Tau Regulates the Number of Protofilaments in Microtubules: A Synchrotron X-ray Scattering Study. *Biophysical Journal*, **97** (2), 519-527 (2009). (Cover of July 22, 2009 issue)

## **Other References**

7. McMahon, H. T. & Gallop, J. L. Membrane curvature and mechanisms of dynamic cell membrane remodelling. *Nature* **438**, 590-596 (2005).
8. A Columnar Phase of Dendritic Lipid-Based Cationic Liposome-DNA Complexes for Gene Delivery: Hexagonally Ordered Cylindrical Micelles embedded in a DNA Honeycomb Lattice. K. Ewert, H. Evans, A. Zidovska, N. F. Buxsein, A. Ahmad, C. R. Safinya, *J. Am. Chem. Soc.* **128**, 3998-4006 (2006)
9. Dendritic Cationic Lipids with Highly Charged Headgroups for Efficient Gene Delivery. K. Ewert, H. Evans, C. R. Safinya, *Bioconjugate Chemistry*, **17** (4), 877-888 (2006).

## Bio-gating a Physical Nanosystem by Metabolic Activity of Microorganisms

Ravi F. Saraf, University of Nebraska-Lincoln; [rsaraf@unlnotes.unl.edu](mailto:rsaraf@unlnotes.unl.edu)

### Scope of the project

Coupling physical electronics with *live* cells or microorganism opens the possibility of leveraging the highly sophisticated functions of biological system, such as memory, adaptability, and multitasking, to create novel logic circuits, sensors, and new sources of power. Typically, in a cell, the energy required to fuel endergonic biochemical reactions by exergonic processes (such as hydrolysis of ATP to ADP) is in tens of KJ/mole. Per molecule, at room temperature, this energy corresponds to hundreds of meV, which is in the 4-10 kT range at room temperature (where k is Boltzmann constant and T is temperature). An interesting question becomes, is it possible to couple these (redox) biochemical processes in cells to drive a physical system? More tangibly, *can a stimuli (such as food, toxin, or drug) given to a cell, for example, flip an electronic switch from OFF to ON?* The goal of this research is to take the first step towards developing these systems—created with microorganisms (or cells) coupled to an electronically active physical structure. The project will have three basic studies:

- (a) Design and study of a physical electronic system sensitive to single electron charge modulation and the active area of the system  $>5 \mu\text{m}$  to couple cells.
- (b) Develop a scanning probe method to map electronic activity on cell surface, such as, modulation of charge, ion-flux and pH, as the cell is chemically stimulated.
- (c) Design and study electronic coupling (strategies) between the cell and the physical electronic system.

### Electronic System sensitive to Single Electron Charging

The key to making a successful hybrid system, is conceiving an electronic switch sensitive to single electron charge that can operate at room temperature. Due to its low capacitance, C, the potential of an isolated nanoparticle is substantially increased by a single electron charging to cause a Coulomb blockade of the second electron from flowing through the particle. As a result, the isolated particle behaves as an electronic switch that turns ON/OFF depending on the (single electron) charge state of the nanoparticle.<sup>1</sup> The key parameter of the device is the Coulomb blockade voltage,  $V_T = e/2C$  (where e is charge of the electron) above which the current suddenly begins to increase (i.e., turns ON).<sup>1</sup> Because, for a typical 10 nm Au particle, the switching energy barrier,  $e^2/2C$  is only  $\sim 3kT$  at room temperature, cryogenic temperatures are required to observe robust switching due to Coulomb blockade. Coulomb blockades at room temperature can be obtained by a single particle  $<1 \text{ nm}$ ; however, quantum noise and charge fluctuation make the devices very noisy.<sup>2</sup>

The switching voltage,  $V_T$ , and the corresponding switching barrier energy,  $eV_T$ , can be enhanced by over an order of magnitude using a two-dimensional (2D) array of nanoparticles. In recent years, based on theoretical predictions,<sup>3</sup> 2D arrays of nanoparticles that are easy to interconnect with electrical circuits have been demonstrated to exhibit single-electron (charging) switching behavior<sup>4</sup> with robust  $V_T$  above 1 V. Unfortunately, unlike in single isolated nanoparticle, the  $V_T$  depends on temperature. Thus, the over tenfold enhancement compared to a single nanoparticle observed at

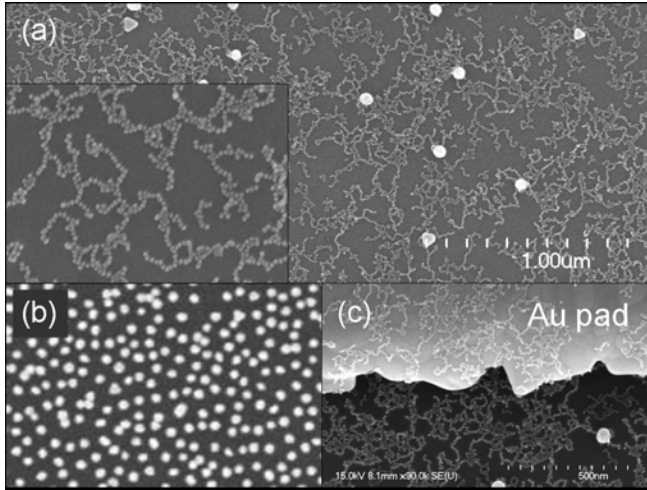


Fig. 1 Field Emission Scanning Electron Microscope (FESEM) image of the network deposited on a SiO<sub>2</sub>/Si chip. (a) The necklace deposition after exposing the chip to the solution for ~24 hours. (b) Deposition of pure 10 nm particles from the pH 7 solution. (c) The deposition of the necklace on the Au pad leading to a robust interconnection with the array. Inset (a) A higher magnification image of the nanoparticle necklace.

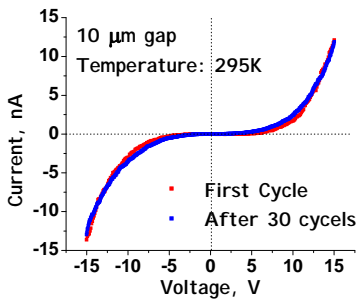


Fig. 2: I-V behavior of 2D network of 1D necklace of 10 nm Au particles between electrodes 10 μm apart.

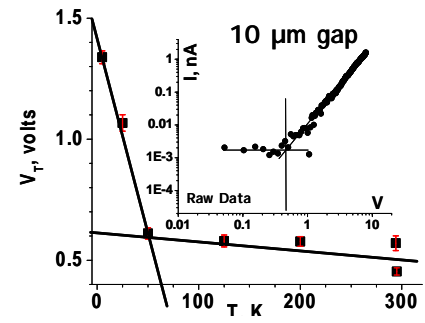


Fig. 3:  $V_T$  as a function of  $T$

cryogenic temperature vanishes at room temperature because  $V_T$  decreases (linearly) as  $T$  increases.<sup>4</sup>

We have recently developed a process to “polymerize” 10 nm Au particles in solution to form one dimensional (1D) necklaces. In this process, the pH of negatively charged Au nanoparticles (due to citrate) is gradually decreased from 7 to 3.5 to form linear necklaces of particles. The formation of necklace is observed as change in color from red to blue, attributed to delocalization surface plasmon electrons reported in the literature.<sup>5</sup> The polymerization occurs due to partial neutralization of the negative charge by  $H^+$  to form electric dipoles in the particle that attract each other to form linear chains. Subsequently,

the necklaces are deposited on SiO<sub>2</sub>/Si surface with Au electrodes (10 μm apart), to form a 2D network (Fig. 1). On applying a bias,  $V$  between the electrodes, the current,  $I$  exhibits a robust Coulomb blockade effect (Fig. 2). The I-V behavior is symmetric and reproducible for at least 30 cycles.

For isolated 10 nm Au particle surrounded with insulating media of dielectric constant,  $\epsilon$ ,  $V_T \sim e/(4\pi\epsilon\epsilon_0d)$ , where  $\epsilon_0$  is permittivity in vacuum and  $d$  is diameter of the particle. Thus,  $V_T$  is independent of temperature, and for 10 nm Au particle, with  $\epsilon \sim 4$ ,  $V_T$  is  $\sim 70$  mV that is too small to exhibit an effect at room temperature because Coulomb

blockade barrier energy is only  $\sim 3kT$ . Qualitatively, the I-V behavior at room temperature in Fig. 2, exhibits large non-linearity and blockade behavior (semi-log plot in inset of Fig. 3 shows the threshold behavior more conspicuously). The enhancement in  $V_T$  in 2D array is due to trapped single electron charge in few particles distributed randomly over that array.<sup>3,6</sup> The random charge distribution (usually referred to as “quenched charge distribution”<sup>3,6</sup>) is fixed as the sample is cycled over the bias cycle (as experimentally observed in Fig. 3). These multiple

barricades cause a larger effective switching barrier. The barricades are “isolated” nanoparticles in the percolating path that are separated by surrounding particle with a

tunneling barrier significantly larger than  $kT$ . In a 2D array, the current can circumvent the charge center due to co-ordination number in 4 to 5 range. However, the topology of the percolating path in necklace network with co-ordination number  $\sim 2$ , the “isolated” nanoparticle effectively barricades the electron transport. As a result,  $V_T$  above 50K is regulated by only single isolated particle and below 50K clusters larger than single isolated particle will commence to contribute to the blockade. Thus, a sharp transition in  $V_T$  is observed at 50K followed by a steeper slope at lower  $T$  due to increase in number of clusters contributing to the barricades (Fig. 3). Importantly, the significantly small slope above 50K leads to a finite  $V_T$  of  $\sim 0.45V$  at room temperature. This is the first observation, to our knowledge, where a Coulomb blockade is observed at room temperature for 10-20  $\mu m$  long array.

### **Hybrid Bio-Nano System” Bio-gating**

Owing to  $V_T$  of 0.45 V at room temperature, we explore the electronic coupling between living cells and the nanoparticle necklace, i.e., a “living” bio-transistor. The electrochemical coupling between the metabolic process of the living cell, *Pichia pastoris* (yeast), and the necklace is obtained by simply seeding the cells on the device. The  $\sim 2 \mu m$  diameter yeast cell, *P. pastoris*, can survive in air for approximately 14 hours, as long as humidity is maintained above  $\sim 70\%$ . The cells are grown in media containing methanol as a carbon source for 24 hours. About 200 yeast cells are then deposited on an  $\sim 1$  mm wide nanoparticle necklace network (Fig. 4a, Inset).

First, we consider the effect on the I-V behavior in the yeast-network coupling due to metabolism in the cell. The I-V after deposition of the cells does not change significantly. Upon exposure to methanol vapors, the cell utilizes the methanol to produce formaldehyde.<sup>7</sup> At an appropriate potential, the formaldehyde undergoes oxidation on the nanoparticle network (electrode) to form CO,  $H^+$  and releases an electron per molecule of HCOH. Analogous to cyclic voltametry, the electron production leads to a maxima at  $\sim 2$  V attributed to (diffusion limited) oxidation current (Fig. 4a). During the “down” cycle, from 10 to 0 V, no reduction-current is observed at  $\sim 2$  V as the product, CO, is a gas. However, the current is higher than “no yeast” due to variation in the quenched charge distribution due to redox electrons. In the reverse bias, the formaldehyde reduces to methanol leading to a redox peak at  $\sim -3$  V. In contrast, the device without the yeast cells shows an I-V behavior similar to Fig. 2 as seen in Fig. 4a (“no yeast”). Because, the reactions are in solid state with no reference electrode, the redox potentials are not thermodynamic quantities. The methanol exposure is performed by simply placing the device in a small sealed bell jar with a reservoir of methanol. The high currents are because the width of the network is  $\sim 1$  mm (in contrast to  $\sim 100 \mu m$  for the device in Fig. 3) to ensure deposition of adequate yeast cells on the network.

To demonstrate bio-gating, a constant bias of 4 V is applied to the cell-network device; and the current is monitored as the system is exposed to methanol (Fig. 4b). A gain of approximately fivefold is observed on exposure to methanol. After a couple of cycles, the yeast-network device is left at zero bias for  $\sim 12$  hours in a humid environment. On subsequent methanol exposure, the gain reduces; and the rise time further slows down from  $\sim 20$  to over 30 minutes. The slow rise is due to the response of the cell which is consistent with metabolic kinetics. At fixed bias of 4V, the current modulation of approximately fivefold observed in Fig. 4b is consistent with Fig. 4a, i.e., an increase

from A to B. The observed bio-gating behavior in Fig. 4b is explained as follows. Upon exposure to methanol, the electron, due to oxidation, alters the quenched charge distribution of the network, thereby modulating the current, similar to gating by a physical third electrode. We note that (unfortunately) because the redox current quickly becomes inhibited by diffusion, the current gain to C (in Fig. 4(a)) does not occur (during bio-gating). The gain is due to the switching, *i.e.*, bio-gating, caused only by the redistribution of quenched charge distribution, *i.e.*, from A to B (in Fig. 4(a)).

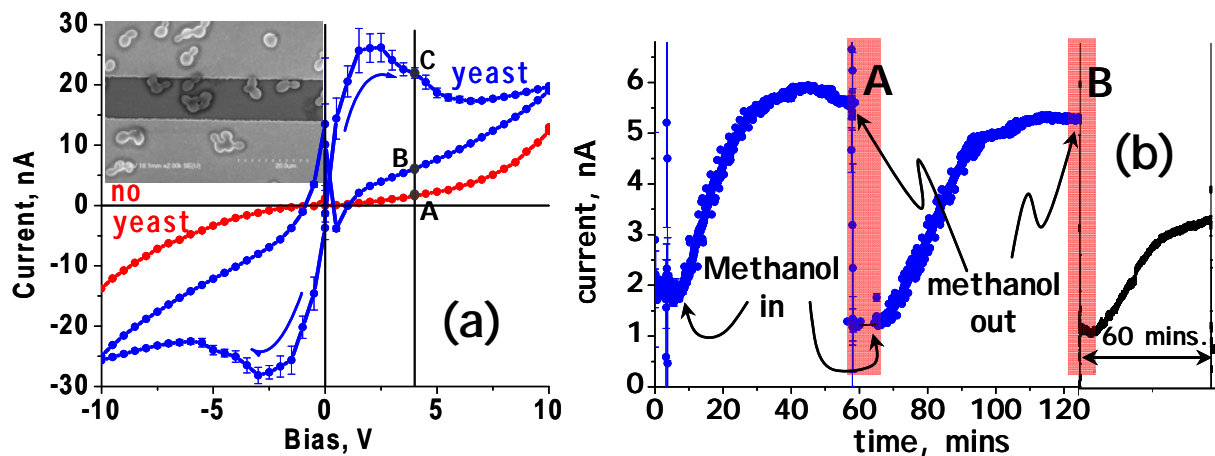


Fig. 4. Bio-gating of the nanoparticle necklace device with the metabolism of living microorganism cells. (a) The I-V behavior of the necklace network on exposure to methanol. The two curves correspond to the network as is and with discreet yeast cell deposition. The inset shows an FESEM image of yeast cells on the network between 10  $\mu\text{m}$  spaced Au electrodes. (b) The modulation of device current at 4 V as the yeast cell is exposed to methanol. At A and B, the methanol is removed.

### Future Plans

At the initiation of the project all the three studies mentioned in “Scope of the Project” will be pursued.

### References

1. Likharev, K.K. Single-Electron Devices and Their Applications. *Proceedings of the IEEE* **1999**, *87*, 606-632.
2. Berven, C.A.; Wybourne, M.N.; Clarke, L.; Longstreth, L.; Hutchison, J.E.; Mooster, J.L. Background Charge Fluctuations and the Transport Properties of Biopolymer-Gold Nanoparticle Complexes. *J. Appl. Phys.* **2002**, *92*, 4513-4517.
3. Middleton, A.A.; Wingreen, N.S. Collective Transport in Arrays of Small Metallic Dots. *Phys. Rev. Lett.* **1993**, *71*, 3198-3201.
4. Parthasarathy, R.; Lin, X.M.; Elteto, K.; Rosenbaum, T.F.; Jaeger, H.M. Percolating Through Networks of Random Thresholds: Finite Temperature Electron Tunneling in Metal Nanocrystal Arrays. *Phys. Rev. Lett.* **2004**, *92* (7).
5. Shipway, A.N.; Lahav, M.; Gabai, R.; Willner, I. Investigations into the Electrostatically Induced Aggregation of Au Nanoparticles. *Langmuir* **2000**, *16*, 8789-8795.
6. Shipway, A.N.; Lahav, M.; Gabai, R.; Willner, I. Investigations into the Electrostatically Induced Aggregation of Au Nanoparticles. *Langmuir* **2000**, *16*, 8789-8795.
7. Sibirny, A.A.; Titorenko, V.I.; Gonchar, M.V.; Ubiyvovk, V.M.; Ksheminskaya, G.P.; Vitvitskaya, O.P. Genetic Control of Methanol Utilization in Yeasts. *J. Basic Microbiology.* **1988**, *28*, 293-319.

## Biopolymers Containing Unnatural Amino Acids

Peter G. Schultz

The Scripps Research Institute  
Department of Chemistry  
10550 North Torrey Pines Road  
La Jolla, CA 92037  
[schultz@scripps.edu](mailto:schultz@scripps.edu)

**Program Scope:** In our own work we ask the question whether our molecular level understanding and chemical/biological tools are sophisticated enough to begin to manipulate the genetic code itself, i.e., generate organisms that genetically encode 21 or more amino acids. Although the genetic codes of all known organisms specify the same 20 amino acids (with the rare exceptions of selenocysteine and pyrrolysine), it is clear that many proteins require additional chemistries associated with cofactors and post-translational modifications to carry out their natural functions. Therefore, although the functional groups contained in the 20 amino acid code might be sufficient for life, they might not be optimal. Consequently, the development of a general method that allows us to genetically encode additional amino acids beyond the canonical 20 might facilitate the evolution of proteins, or even entire organisms, with new or enhanced properties. Moreover, the ability to incorporate amino acids with defined steric/electronic properties and chemical reactivity at unique sites in proteins should provide powerful new tools for exploring protein structure and function, much the same way physical organic chemists use synthesis to understand the chemical reactivity of organic molecules. In particular, our recent efforts have focused on genetically encoding metal ion binding amino acids to generate new catalytic functions and structural motifs, photoreactive amino acids to activate protein function in a spatially and temporally controlled fashion, chemically reactive amino acids to selectively modify and/or immobilize proteins with a high degree of control over structure, and a number of biophysical probes of protein structure and function.

### Recent Progress:

#### Metal ion binding proteins

Metal ions play important roles in the structure and function of many proteins: they serve as important structural elements, regulate biological activity, and act as cofactors in a wide array of catalytic and electron-transfer processes. Accordingly, there is considerable interest in the rational design of metalloproteins. However, it remains a challenge to engineer a cluster of precisely oriented inner- and outer-shell residues that selectively coordinate a metal ion at a defined site in a protein. The ability to genetically encode multidentate, metal-binding amino acids would simplify the design of metalloproteins by reducing the number of residues required to bind a desired metal ion. One such amino acid (2,2'-bipyridin-5-yl)alanine (BpyAla) bears an  $N,N'$ -bidentate side chain that strongly chelates transition-metal ions such as  $\text{Fe}^{2+/3+}$ ,  $\text{Cu}^{2+}$ ,  $\text{Co}^{2+/3+}$ , and  $\text{Ru}^{2+/3+}$  and is able to form dimeric or trimeric metal ion complexes. To this end, we have cotranslationally incorporated BpyAla into proteins in *E. coli* in response to an amber nonsense codon with excellent fidelity and yield. The structural basis for selective recognition of this novel amino acid by its cognate aminoacyl-tRNA synthetase (aaRS) has also been determined by x-ray crystallography. Moreover, we have shown that by incorporating this amino acid into the DNA binding protein CAP that one can generate redox activity that leads to cleavage of the DNA backbone by reactive oxygen species. We have also genetically encoded metal binding amino acids with metallocene and 8-hydroxyquinoline side chains and shown that the latter can be used to introduce heavy atoms into proteins to facilitate x-ray structure determination.



Stoke's shift, and sensitivity to both pH and polarity, this amino acid should provide a useful probe of protein localization and trafficking, protein conformation changes, and protein-protein interactions. The unnatural amino acid *p*-nitrophenylalanine (pNO<sub>2</sub>-Phe) has also been genetically introduced into proteins in *E. coli*. It was shown that pNO<sub>2</sub>-Phe efficiently quenches the intrinsic fluorescence of Trp in a distance-dependent manner in a model GCN4 basic region leucine zipper (bZIP) protein. Thus, the pNO<sub>2</sub>-Phe/Trp pair should be a useful biophysical probe of protein structure and function. We have also developed a general strategy for the site-specific dual-labeling of proteins for single-molecule fluorescence resonance energy transfer experiments. A genetically encoded unnatural ketone amino acid was labeled with a hydroxylamine-containing fluorophore with high yield (>95%) and specificity. This methodology was used to construct dual-labeled T4 lysozyme variants, allowing the study of T4 lysozyme folding at single-molecule resolution and should be generally applicable to other proteins. Finally, an orthogonal tRNA/aminoacyl-tRNA synthetase pair has been evolved that makes it possible to selectively and efficiently incorporate *para*-cyanophenylalanine (pCNPhe) into proteins in *E. coli*. Substitution of pCNPhe for histidine-64 in myoglobin (Mb) affords a sensitive vibrational probe of ligand binding. This methodology provides a useful infrared reporter of protein structure, biomolecular interactions, and conformational changes.

#### Chemically reactive amino acids

The selective chemical modification of proteins remains a challenge. Electrophilic reagents in general react with multiple nucleophilic residues in proteins and thiol specific reagents can be problematic when there are multiple cysteine residues or they are involved in folding. To overcome this challenge, we have genetically encoded a series of amino acids with unique chemical reactivity relative to the common twenty amino acids. These include diketo amino acids, boronate containing amino acids, dehydroalanine and amino acids with long chain thiol side chains. We have demonstrated the utility of these amino acids for the affinity purification of proteins and in the modification of proteins with a number of biophysical probes. We are currently attempting to use the unique reactivity of these amino acids to selectively immobilize proteins and to introduce inter- and intraprotein crosslinks.

#### Methodology improvement

We have further improved and extended the unnatural amino acid mutagenesis methodology by: (1) developing a *Pichia pastoris* system for the high level expression of mutant proteins; (2) developing rapid two step selection systems that can be used to evolve aminoacyl-tRNA synthetases with unique specificities; and (2) improved bacterial expression systems in which promoter, copy number, tRNA sequences, etc. were optimized.

#### **Future Plans:**

- Rationally engineer metal ion binding sites into proteins to create new catalytic and electron transfer activities and structural motifs
- Modify soluble proteins or cell surface proteins selectively to begin to develop engineered protein or cellular arrays, respectively
- Attempt the DNA-templated ribosomal synthesis of polymers composed entirely of unnatural building blocks in bacteria
- Continue efforts toward a codon deleted host strain to directly encode additional unnatural amino acids
- Develop and apply selection strategies (phage display and bacteria selection schemes) to evolve proteins with unique chemical reactivity (Schiff base formation, metal ion binding, nucleophilic, etc.) which act as selective catalysts or receptors

#### **Publications:**

- Ryu, Y., Schultz, P.G. "An improved system for the incorporation of unnatural amino acids into proteins in *Escherichia coli*." *Nature Methods*, 3(4):263-5, **2006**.
- Deiters, A., Groff, D., Ryu, Y., Xie, J., Schultz, P.G. "A Genetically Encoded Photocaged Tyrosine." *Angew. Chemie*, 45(17):2728-2731, **2006**.
- Turner, J.M., Graziano, J., Spraggon, G., Schultz, P.G. "Structural plasticity of an aminoacyl-tRNA synthetase active site." *Proc. Natl. Acad. Sci.*, 103(17):6483-8, **2006**.
- Tsao, M.L., Summerer, D., Ryu, Y., Schultz, P.G. "The genetic incorporation of a distance probe into proteins in *Escherichia coli*." *J. Am. Chem. Soc.*, 128(14):4572-3, **2006**.
- Wang, J., Xie, J., Schultz, P.G. "A Genetically Encoded Fluorescent Amino Acid." *J. Am. Chem. Soc.*, 128(27):8738-9, **2006**.
- Schultz, K.C., Supekova, L., Ryu, Y., Xie, J., Perera, R., Schultz, P.G. "A Genetically Encoded Infrared Probe of Protein Structure." *J. Am. Chem. Soc.*, 128(43):13984-5, **2006**.
- Xie, J., Liu, W., Schultz, P.G. "A Genetically Encoded Bidentate, Metal-binding Amino Acid." *Angew. Chem.*, 46(48):9239-9242, **2007**.
- Lemke, E.A., Summerer, D., Geierstanger, B.H., Brittain, S.M., Schultz, P.G. "Activation of a kinase pathway using a genetically encoded, photocaged amino acid and visible light." *Nature Chem. Biol.*, 3(12):769-772, **2007**.
- Guo, J., Wang, J., Anderson, J.C., Schultz, P.G. "Addition of an Alpha Hydroxy Acid to the Genetic Code of Bacteria." *Angew. Chem.*, 47(4):722-725, **2007**.
- Guo, J., Wang, J., Lee, J.-S., Schultz, P.G. "Site-Specific Incorporation of Methyl- and Acetyl-Lysine Analogues into Recombinant Proteins." *Angew. Chem.*, 47(34):6399-401, **2008**.
- Brustad, E., Bushey, M.L., Brock, A., Chittuluru, J., Schultz, P.G. "A Promiscuous Aminoacyl-tRNA Synthetase that Incorporates Cysteine, Methionine, and Alanine Homologues into Proteins." *Bioorg. Med. Chem. Lett.*, 18(22):6004-6, **2008**.
- Brustad, E.M., Lemke, E., Schultz, P.G., Deniz, A.A. "A General and Efficient Method for the Site-Specific Dual Labeling of Proteins for Single Molecule FRET." *J. Am. Chem. Soc.*, 130(52):17664-5, **2008**.
- Young, T.S., Ahmad, I., Brock, A., Schultz, P.G. "Expanding the Genetic Repertoire of the Methylophilic Yeast, *Pichia pastoris*." *Biochemistry*, 48(12):2643-2653, **2009**.
- Chen, P.R., Groff, D., Guo, J., Ou, W., Geierstanger, B., Schultz, P.G. "A Facile System for Encoding Unnatural Amino Acids in Mammalian Cells." *Angew. Chem.*, 48(22):4052-4055, **2009**.
- Young, T.S., Ahmad, I., Schultz, P.G. "An enhanced system for unnatural amino acid incorporation in *E. coli*." *J. Mol. Biol.*, *submitted*, **2009**.

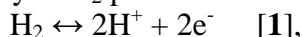
## Theoretical Research Program on Bio-inspired Inorganic Hydrogen Generating Catalysts and Electrodes.

Annabella Selloni (PI), Roberto Car

Department of Chemistry, Princeton University, Princeton, NJ 08544

[aselloni@princeton.edu](mailto:aselloni@princeton.edu), Tel: 609- 258- 3837; [rcar@princeton.edu](mailto:rcar@princeton.edu), Tel 609-258-2534

**Program Scope:** The overall goal of this project is to establish theoretically the feasibility of efficient electrocatalytic H<sub>2</sub> production from water,



by abiotic catalysts derived from the di-iron subsite [FeFe]<sub>H</sub> of the active site of Fe-only hydrogenases and attached to the surface of an FeS<sub>2</sub> electrode.

We focus on the [FeFe]<sub>H</sub> cluster because of the established high efficiency of di-iron hydrogenases in the hydrogen evolution reaction [1]. The choice of pyrite as the electrode material is motivated by the central role of the iron sulfur bonding in the enzyme's active site, as well as by the important role of this material in many redox geochemical and biogeochemical processes, and by its potential role as photovoltaic semiconductor for solar energy conversion.

**Recent Progress:** There has been a growing interest in photochemical H<sub>2</sub> production with hydrogenases over the last years. A particularly attractive goal in this context would be the design of a device for H<sub>2</sub> production in which the bare active center of the enzyme would be immersed in acidified water (the proton supply for [1]) and linked to the cathode of a photovoltaic device (the electron supply for [1]). If the [FeFe]<sub>H</sub> cluster of the active site of the di-iron hydrogenases so employed were to retain its high activity for H<sub>2</sub> production when naked in water, it would offer the advantage of higher surface density when linked to the electrode than possible with the entire enzyme as well as facile electron transfer from the electrode. In fact, hydrogen production by a hydrogenase enzyme on an electrode surface (Reisner, et al *Chem. Commun.* **2009**, 550) and by a model of an isolated active site in a solvent (Felton, et al. *J. Am. Chem. Soc.* **2007**, 129, 12521) has already been demonstrated experimentally.

To explore this possibility, we have used First-Principles Molecular-Dynamics (FPMD) simulations and static Density Functional Theory (DFT) calculations to investigate the H<sub>2</sub> production cycle by the [FeFe]<sub>H</sub> cluster, first in vacuo and more recently in acidified water, both in the absence and in the presence of a supporting FeS<sub>2</sub> surface electrode.

Unsupported [FeFe]<sub>H</sub> cluster in vacuo. In agreement with other theoretical studies, we found that in vacuo there are at least two stable or metastable configurations of the [FeFe]<sub>H</sub> cluster: CO-bridging (μ-CO) and CO-terminal (CO<sub>T</sub>). The μ-CO configuration can produce hydrogen molecules via reaction [1], through a low activation-energy pathway in vacuo. However, it cannot function as an efficient hydrogen-production catalyst in vacuo because the CO<sub>T</sub> configuration is slightly more stable and would effectively stop catalytic action.

Unsupported [FeFe]<sub>H</sub> cluster in water. To understand the effects of the water environment on the cluster stability and reactivity, we have performed FPMD simulations of the [FeFe]<sub>H</sub> cluster immersed in water containing hydronium ions, the first *ab initio* study of a cluster derived from the [FeFe]<sub>H</sub> active center in which *all* the water molecules are treated at the quantum mechanical level.

The first conclusion of this study is that the bridging and terminal isomers have overlapping energy distributions at RT, indicating that both are present in the equilibrium. Interconversion between some  $\mu$ -CO and CO<sub>T</sub> isomers occurs in a few picoseconds (see Fig. 1), indicating that there is no significant activation energy involved.

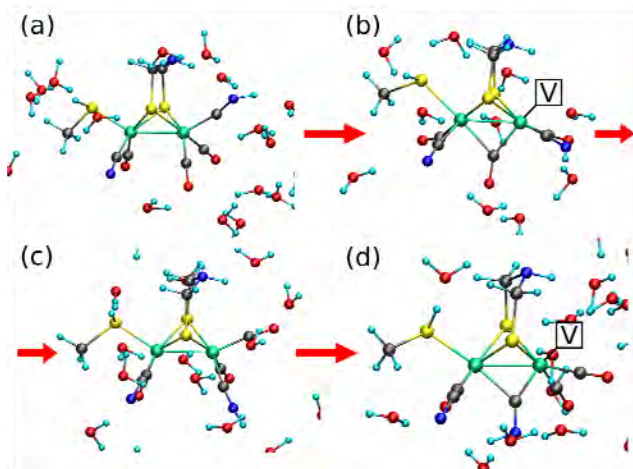


**Fig. 1** Snapshots from a FPMD simulation showing the evolution of the negatively (-1) charged CO<sub>T</sub> with the CN<sub>d</sub> and methyl-thiol groups both protonated (a). This CO<sub>T</sub> cluster is not stable in vacuo or in water; at RT it transforms to (b)  $\mu$ -CO, V-up. At T=300-350 K the latter doubly-protonated  $\mu$ -CO is also not kinetically stable, converting into the (c) CO<sub>T</sub> with CO<sub>d</sub>-up, CN<sub>d</sub>-down *cis* in less than 2.0 ps and subsequently to (d), an unusual structure with the protonated CN<sub>d</sub> bridging the two Fe-atoms and V-up, obtained dynamically in water only.

The above result raises the issue of whether protonation of the terminal configuration would poison the catalytic cycle of the cluster. We found that it does not, since a strong local hydrophobicity of the bridging region in CO<sub>T</sub> prevents the formation of the bridging  $\mu$ -H isomer, the occurrence of which would poison the cluster. We infer that while both  $\mu$ -CO and CO<sub>T</sub> are present at equilibrium, the latter is inert so that its presence does not prevent H<sub>2</sub> production. Conversely, we found that the bridging configuration *is* catalytically active in dense water. More specifically, we have identified three catalytic cycles for H<sub>2</sub> production by the bridging configuration via a sequential protonation of Fe<sub>d</sub> only or of both Fe<sub>d</sub> and DTMA. The first protonation of Fe<sub>d</sub> is the bottleneck during the reaction, due to the strong competition between proton transfer to the deprotonated Fe<sub>d</sub> (energetically favorable) and proton diffusion in water (entropically favored). Unlike the first protonation of Fe<sub>d</sub>, the protonation of Fe<sub>d</sub>-H is much faster, occurring spontaneously without constraints. The difference is that the H on Fe<sub>d</sub> is a hydride negatively charged and exposed. DTMA is easily and rapidly protonated, but cannot accept a second proton. Once Fe<sub>d</sub> is protonated facile transfer of a second proton from DTMA-H or from the H<sub>2</sub>O environment occurs with associated H<sub>2</sub> production.

The overall conclusion of this study is that the active site of the [FeFe]<sub>H</sub> hydrogenases, extracted from the enzyme and immersed in acidified water, can be an efficient catalyst for hydrogen production provided that electrons are transferred to the cluster. In a practical device, however, the electrons must be supplied by a cathode or photocathode surface functionalized with the cluster. Accordingly, our most recent work is focused on H<sub>2</sub> production by [FeFe]<sub>H</sub> attached to the FeS<sub>2</sub>(100) surface in a water environment.

[FeFe]<sub>H</sub> cluster attached to the (100) surface of FeS<sub>2</sub> in water.

In analogy with the enzyme, we can link the catalyst to the FeS<sub>2</sub>(100) surface via a bridging sulfur atom connecting the Fe<sub>p</sub> to one of the Fe atoms on the surface. We found however that there are configurations in which the Fe<sub>p</sub>-S bond is weak and can break. Instead, a stable link is formed by removing the SCH<sub>3</sub> group from the [FeFe]<sub>H</sub> cluster and connecting the Fe<sub>p</sub> directly to a sulfur atom on the pyrite surface; this link is also stabilized by the interaction between the N atom of (CN)<sub>p</sub>-H and one Fe atom on the surface. Moreover, an additional modification of the cluster, cf. Fig. 2, inspired by the results of our simulations of the unsupported cluster in water, allows us to stabilize a bridging configuration, which is catalytically active towards H<sub>2</sub> production.

Investigation of the H<sub>2</sub> evolution reaction by this modified [FeFe]<sub>H</sub> cluster attached to the FeS<sub>2</sub>(100) surface has already been carried out both in vacuo and in acidified water, and a manuscript reporting these results is in preparation.

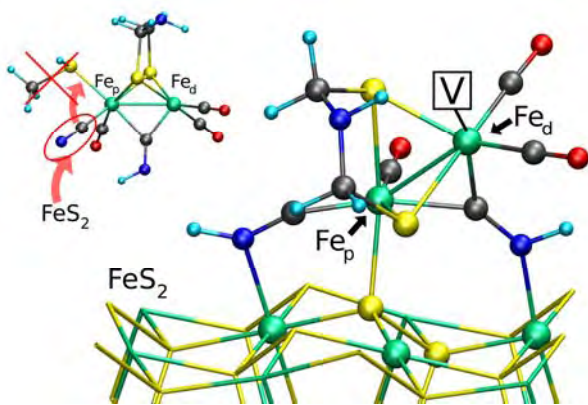


**Figure 2.** Optimized geometry of a modified [FeFe]<sub>H</sub> cluster in which (CN)<sub>d</sub>-H bridges the two iron atoms of the cluster, while its N atom forms a dative bond with a surface Fe. (CN)<sub>p</sub>-H is bonded to a surface Fe atom as well. In order to link both (CN)<sub>d</sub> and Fe<sub>p</sub> to the surface, the position of (CN)<sub>p</sub> has been exchanged, as indicated by the red arrows in the inset. Fe<sub>p</sub> is linked to a S atom of the surface and the dative bond between the μ-(CN)<sub>d</sub>-H and the surface stabilize the bridging configuration with V-up. The isomer in the inset was obtained during a FPMD simulation (see Fig. 1d) on the unsupported cluster in water.

Methodological advance Another recent activity funded under the current grant is the theoretical development and implementation of a new order-N approach for calculating the exact (Hartree-Fock) exchange in extended systems. DFT calculations based on the local density approximation (LDA) or the generalized gradient approximation (GGA) are known to suffer from the self-interaction error. These difficulties can be mitigated by the use of hybrid functionals in which some exact exchange energy is mixed into the DFT exchange-correlation functional. While the considerable computational cost of evaluating the exact exchange energy has generally limited the use of hybrid functionals to relatively small systems, especially in FPMD simulations, with our new approach, the exact exchange energy and potential can be accurately and efficiently computed for large molecules and extended insulating systems. This methodological advance is important for the H<sub>2</sub> production studies discussed above. In H<sub>2</sub> production, proton transfer between the catalyst and the enveloping H<sub>2</sub>O play major multiple roles; the new method allows for more accurate calculation of the relevant portions of the energy surface. Using this method we have already found a substantial improvement in the description of pure water, a prerequisite to using it in our hydrogen evolution studies.

**Future Plans:** While providing evidence of the feasibility of efficient H<sub>2</sub> production from water, our study on the modified [FeFe]<sub>H</sub> cluster attached to the FeS<sub>2</sub> (100) surface shows that a few stability issues are still present. In particular, we found that there are configurations in which the bond between Fe<sub>p</sub> and one of the S atoms of the cluster's bridging dithiolate group is weak and can break. To overcome this difficulty, promising studies of further cluster modifications are in progress.

Building on these results, the future directions of our planned research will be described in our renewal proposal, currently in preparation.

**Publications:**

1. C. Sbraccia, F. Zipoli, R. Car, M.H. Cohen, G.C. Dismukes, A. Selloni, Mechanisms of H<sub>2</sub> production by the [FeFe]<sub>H</sub> Subcluster of Di-iron hydrogenases: implications for abiotic catalysts, *J. Phys. Chem. B* **2008**, *112*, 13381
2. X. Wu, A. Selloni, R. Car, Order-N implementation of exact-exchange in extended systems, *Phys Rev. B* **2009**, *79*, 085102 **Editors' Suggestion**
3. F. Zipoli, R. Car, M.H. Cohen, A. Selloni, Hydrogen Production by the Naked Active Site of the Di-Iron Hydrogenases in Water, *J. Phys. Chem. B* **2009**, accepted (in press).
4. X. Wu, E.J. Walter, A.M. Rappe, R. Car, A. Selloni, Hybrid density functional calculation of the band gap of Ga<sub>x</sub>In<sub>1-x</sub>N, *Phys Rev B* **2009**, accepted (in press)
5. W. Chen, X. Wu, R. Car, X-ray absorption spectra of water: a first principles study with the GW method, submitted.
6. F. Zipoli, R. Car, M.H. Cohen, A. Selloni, Hydrogen production by the active site of the di-Iron hydrogenases attached to the (100) surface of FeS<sub>2</sub>, manuscript in preparation.

**Collaborators:** Dr Federico Zipoli (Post-Doctoral Fellow), Department of Chemistry, Princeton University; Dr. Xifan Wu, (Post-Doctoral Fellow, 50%), Department of Chemistry, Princeton University; Dr Morrel H. Cohen (Senior Research Staff), Dept. of Chemistry, Princeton University, and Department of Physics and Astronomy, Rutgers University, Piscataway, New Jersey

## Photoelectrochemical Complexes for Solar Energy Conversion that Chemically and Autonomously Regenerate

**Michael S. Strano**  
66-566 MIT  
77 Massachusetts Avenue  
Cambridge, MA 02139  
strano@mit.edu

**Stephen G. Sligar**  
23 Morrill Hall UIUC  
505 S. Goodwin Ave  
Urbana, IL 61801  
s-sligar@illinois.edu

**Colin A. Wraight**  
160 Davenport, B4 UIUC  
600 S. Mathews  
Urbana, IL 61801  
cwraight@illinois.edu

### Project Scope

Naturally occurring photosynthetic systems in plants are supported by elaborate pathways of self-repair that limit the impact of photo-damage and degradation. Despite advantages in stability and fault tolerance, synthetic photoelectrochemical systems have to date been invariably static. Herein, we demonstrate a complex consisting of two recombinant proteins, phospholipid and a carbon nanotube that reversibly assembles into a particular configuration, forming an array of 4 nm lipid bilayers housing light-converting proteins orientated perpendicular such that the hole conducting site is in close proximity to the nanotube conductor. The complex can reversibly self-assemble into this configuration, and disassemble upon the addition of sodium cholate, over an indefinite number of cycles. The assembly is thermodynamically meta-stable and can only transition reversibly between free components and assembled state if the rate of surfactant removal exceeds about  $10^{-5} \text{ sec}^{-1}$ . In the assembled state only, the complexes exhibit high photoelectrochemical activity using a dual  $\text{Fe}(\text{CN})_6^{3-}$ /ubiquinone mediator with external efficiencies near 40%. We demonstrate a regeneration cycle that utilizes only surfactant to signal between assembly and disassembly that increases photo-conversion efficiency more than 300% over 168 hours, and extends the lifetime indefinitely.

### Recent Progress

In this work, we extend the concepts of self assembly to develop the first synthetic photoelectrochemical complex capable of mimicking key elements of this self-repair cycle<sup>1,2</sup>. To develop such a complex, we examined the use of phospholipid-based light-harvesting nanostructures. Phospholipids have been used to disperse single- and multi-walled carbon nanotubes,<sup>3</sup> and the dialysis of phospholipids such as 1,2-dimyristoyl-sn-glycero-3-phosphocholine (DMPC) in the presence of a membrane scaffold protein (MSP) creates a lipid bilayer nanodisc (ND) approximately 10 nm in diameter and 5 nm high, as shown previously.<sup>4</sup> Such discs assemble onto a single-walled carbon nanotube (SWNT) such that the diameter is parallel to a nanotube, creating a platform for attaching membrane proteins (Fig. 1a). One protein used for photoelectrochemical conversion is the photosynthetic reaction center (RC) isolated from the purple bacterium, *Rhodobacter sphaeroides*.<sup>5</sup> This bacterial RC is a protein complex composed of 4 bacteriochlorophylls, 2 bacteriopheophytins, and primary and secondary ubiquinones ( $\text{Q}_A$  and  $\text{Q}_B$ ). Upon photoabsorption, the complex acts as a photoconverter, shuttling the formed exciton to the Bchl dimer (called the primary donor, P) where charge is separated, with the hole remaining ( $\text{P}^+$ ) and the electron transferred to the  $\text{Q}_B$  site on the other side of the RC via electron transfer reaction.<sup>6</sup> The incorporation of the RC into the ND places the hole injection site ( $\text{P}^+$ ) directly facing the carbon nanotube, which may act as a hole conducting wire. We find that this ordered assembly of lipids, MSP, RC, and SWNT forms spontaneously when a sodium cholate-suspended mixture of the components is dialyzed to remove the surfactant. Control experiments confirm that all components are necessary to form the structure. The complexes are broken apart upon the re-introduction of 2 wt% sodium cholate in a cycle that can be repeated indefinitely with no irreversible degradation of the photoelectrochemical properties

of the assembled state, as described below. We confirmed the parallel arrangement of the ND along the nanotube surface using atomic force microscopy (AFM) and small-angle neutron scattering (SANS). Typical AFM image shown in Fig. 1b reveals either free ND stacks or ND assembled along the nanotube axis. The height profile (Fig. 1c) along the nanotube, which indicates a height of  $8\pm 0.4$  nm, is consistent with a bilayer stack on either side of the nanotube. The specific orientation of the discs is confirmed by SANS. Figures 1d and 1e show the scattering intensity versus reciprocal lattice vector for ND (red, Fig. 1d) and ND-SWNT (red, Fig. 1e) described by the best fit model of an isotropic suspension of monodisperse 8 nm diameter by 4 nm high discs (blue, Fig. 1d) and a series of parallel discs in linear arrangement (black, Fig. 1e), respectively. The parallel arrangement leads to a maximum in scattering at  $q = 2\pi/(2R)$ , where R is the radius. In contrast, the blue curve in Fig. 1e compares the same data to that of an isotropic dispersion, highlighting the difference. We used density gradient centrifugation to isolate the complexes from background components and further verify their structure.<sup>7</sup>

Surprisingly, once formed, this dynamically-assembled RC-ND-SWNT complex has a large photoelectrochemical activity only in the assembled state. We monitored the photoresponse of the system using a double mediator scheme containing ferrocyanide/ferricyanide (70  $\mu$ M) and ubiquinone/ubiquinol (70  $\mu$ M) redox couples in a photoelectrochemical cell with a transparent bottom mounted on an inverted microscope (Fig. 2a). A SWNT film cast on a glass substrate was utilized as the transparent electrode<sup>8,9</sup> as it was found that it produced a root mean square (rms) value of 1 nA for noise, reduced by a factor of 50 over ITO. A 700 nM RC-ND-SWNT solution in standard Tris buffer produces, under open-circuit conditions, a current that saturates at 20 nA and upon 20 mW laser illumination at 785 nm, as shown in Fig. 2b. When the light is turned off, the current consistently returns to the baseline.

The reaction scheme is that ferrocyanide donates an electron to the SWNT which shuttles it to the photo-reduced P site on the RC ( $P^+ + e^- \rightarrow P$ ). The assembly described above places this P site in close proximity to the nanotube. After electron transfer, ferricyanide travels to the working electrode where it is reduced ( $Fe(CN)_6^{3-} + e^- \rightarrow Fe(CN)_6^{4-}$ ). On the opposite side of the RC, ubiquinone reduces to ubiquinol by accepting two electrons from the  $Q_A$  site in sequential turnovers of the RC, shuttling the electrons to the anode.<sup>10-12</sup> Some interaction between the redox couples may also take place under these conditions.<sup>12</sup> We find that the photoresponse is enhanced with this dual mediator system compared to a single the ubiquinone mediator.

The complex is photoelectrochemically active in free solution, as the saturation current does not change upon illumination of the electrodes or bulk solution only. This current of 20 nA translates into an external quantum efficiency of  $8.0 \times 10^{-5}\%$  for a solution containing  $8.4 \times 10^{12}$  RC-ND-SWNT complexes. For an isotropic solution, the fraction near the electrode area for electron transfer is  $2.0 \times 10^{-6}$ , yielding an external efficiency estimate of 40% in our system. Such extracted value is in good agreement with measurements on isolated RC complexes, which approach unity. Increasing the overall efficiency of the cell requires increasing the density of RC-ND-SWNT complexes, and is the subject of future work. Several promising techniques demonstrated to date are embedding into  $Al_2O_3$  gels<sup>13</sup> and polymer composites.<sup>14</sup>

The complex enables the construction of a photoelectrochemical cell where a regeneration cycle can be prompted using a chemical signal, sodium cholate addition or removal, alone. Figure 2c outlines the cell with two re-circulating membrane dialyzers: one 1000 kDa and the other 12–14 kDa for disassembly and reassembly, respectively. All components except the nanotube scaffold (damaged RC, lipids, and MSP) can permeate the former when sodium cholate addition signals disassembly. The sodium cholate is then removed via the latter dialyzer, and the

remaining lipids and proteins, supplemented from outside of the loop, re-form the complexes. Without the regeneration cycle, the photocurrent falls off rapidly to 50% after 5 hours, and to 20% after 32 hours (Fig. 2d). Such deactivation rate constants are comparable to similar cells, as illustrated by recent measurements on quasi-solid-state dye-sensitized solar cells (DSSC) showing deactivation to zero photocurrent after 60 hours.<sup>15</sup> Immediately following each regeneration cycle, which is initiated every 32 hours, the photocurrent is restored to the previous maximum followed by a similar deactivation curve. Repeated regeneration appears to extend the lifetime of the device for over 168 hours (Fig 3d), and increases the photo-conversion efficiency by more than 300%. The increase is limited by the frequency of regeneration steps, which we arbitrarily set at  $8.7 \times 10^{-6}$  Hz, and the length of the regeneration cycle (8 hours). More efficient dialyzers and mass transfer, such as those encountered in a microfluidic platform, would shorten both times. In theory, the device could regenerate just as easily from biological components derived from waste biomass,<sup>16-18</sup> or by coupling directly to conventional biosynthesis in a manner similar to natural chloroplast operation.<sup>19-21</sup>

### Future Work

We need to improve the efficiency in the current photoelectrochemical cells based on RC complexes. To do this, we will increase the amount of RC per nanotube or the surface area of the working electrode through 3-dimensional architecture of the nanotubes while keeping the colloidal stability of the complexes. In addition, we have developed the technique for separation of carbon nanotubes, and have explored the enrichment of metallic or semiconducting carbon nanotubes. We will utilize separated carbon nanotubes to improve the electron transfer. Second, we will develop a two-terminal device where the nanotube tethers on one side of the RC and the metal contacts on opposing side of the RC. To make an efficient RC-based device, the potential difference between the nanotube and the metal such as Al or Ag will be optimized. Another advancement on this work includes the development of a chloroplast-based photoelectrochemical cell. For these cells, nanotubes will be interfaced to chloroplasts instead of RCs, which would facilitate biomass separation. Additionally, isolation of chloroplasts would introduce advantages in system stability, robustness, and possible increased efficiency.

### References

1. Ham, M.H., Choi, J.H., Boghossian, A.A., Jeng, E.S., Graff, R.A., Heller, D.A., Chang, A.C., Mattis, A., Bayburt, T.H., Grinkova, Y.V., Zeiger, A.S., Van Vliet, K., Hobbie, E.K., Sligar, S.G., Wraight, C.A., Strano, M.S. Synthetic photoelectrochemical complexes that self-regenerate. *Submitted to Nature*.
2. Boghossian, A.A., Ham, M.H., Choi, J.H., Strano, M.S. Kinetic Modeling of Nanotube-Based Photoelectrochemical Complexes Capable of Reversible Self-Assembly. *In preparation*.
3. Richard, C., et. al. *Science* **300**, 775-778 (2003).
4. Bayburt, T. H., et. al. *Biochim. Biophys. Acta-Bioenerg.* **1143**, 113-134 (1993).
6. Hoff, A. J., et. al. *Phys. Rep.-Rev. Sec. Phys. Lett.* **287**, 1-247 (1997).
7. Arnold, M. S., et. al. *Nat. Nanotechnol.* **1**, 60-65 (2006).
8. Hu, L., et. al. *Nano Lett.* **4**, 2513-2517 (2004).
9. Ham, M. H., et. al. *Phys. Rev. Lett.* **102**, 047402 (2009).
10. Agostiano, A., et. al. *Electrochim. Acta* **45**, 1821-1828 (2000).
11. Trammell, S. A., et. al. *Biosens. Bioelectron.* **21**, 1023-1028 (2006).
12. Trammell, S. A., et. al. *Biosens. Bioelectron.* **19**, 1649-1655 (2004).
13. Zhao, J. Q., et. al. *J. Photochem. Photobiol. A-Chem.* **152**, 53-60 (2002).

14. Kalabina, N. A., *et al. Biochim. Biophys. Acta-Biomembr.* **1284**, 138-142 (1996).
15. Biancardo, M., *et al. Photochem. Photobiol. A-Chem.* **187**, 395-401 (2007).
16. Kermasha, S., *et al. Biotechnol. Appl. Biochem.* **15**, 142-159 (1992).
17. Voronin, P. Y. *Russ. J. Plant Physiol.* **44**, 23-29 (1997).
18. Melis, A., *et al. In: Zaborsky, O. R. (ed) BioHydrogen* (Plenum Press, New York, 1998).
19. Dawson, T. L. *Color. Technol.* **125**, 61-73 (2009).
20. Moser, S., *et al. Eur. J. Org. Chem.* **2009**, 21-31 (2009).
21. Vasilikiotis, C., *et al. Photosynth. Res.* **45**, 147-155 (1995).

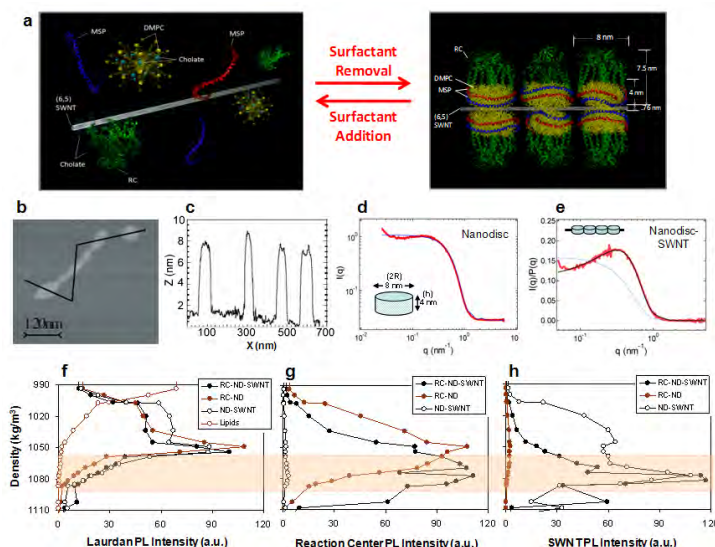


Figure 1. Schematic and structural characterizations of self-assembled photoelectrochemical complexes. (a) Molecular model of self-assembly process of carbon nanotubes before (left) and after (right) surfactant removal (b) AFM image showing a ND-SWNT and (c) height profile indicating that these nanostructures are ~8 nm high. SANS measurements are shown in red for ND (d) and ND-SWNT (e). Fluorescence intensity distributions of Laurdan (f), RC (g), and SWNT (h) of the self-assembled complexes as a function of density after ultracentrifugation.

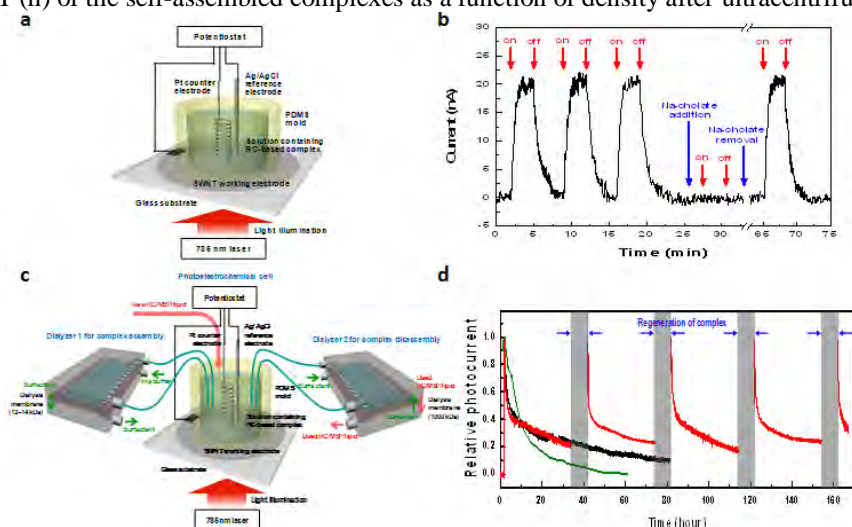


Figure 2. Photoelectrochemical activity of a RC-ND-SWNT complex that autonomously regenerates. (a) Schematic of the photoelectrochemical measurement apparatus. (b) Photoresponse of RC-ND-SWNT complex solution illustrating activity only in the assembled state. (c) Schematic of the photoelectrochemical system consisting of a photoelectrochemical cell with two re-circulating membrane dialyzers. (d) Photoresponse of the RC-ND-SWNT with (red) and without (black) regeneration. Compared to deactivation of a DSSC published in the literature (green).<sup>15</sup> With regeneration, efficiency is increased over 300% over 168 hours.

# Electrostatically Self-assembled Amphiphiles

Helmut H. Strey and Vesna Stanic  
Department of Biomedical Engineering  
Stony Brook University, Stony Brook, NY 11794  
Helmut.Strey@stonybrook.edu  
Vesna.Stanic@stonybrook.edu

**Program Scope:** In this project we study the electrostatic self-assembly of amphiphiles made from polyelectrolytes, oppositely charged surfactants, neutral cosurfactants, oil and water (Fig.1). Such complexes are fascinating because they spontaneously precipitate after mixing of the components in water to form long-range ordered materials. The main focus of this proposal is to gain a basic understanding of their phase diagrams, their material properties and mechanism of self-assembly. In particular we are proposing to study (1) the role of counterion release in polyelectrolyte induced attraction, (2) the phase diagram as function of surfactant type, polyelectrolyte charge density, cosurfactant type, oil and cosurfactant concentration, and salt concentration. To enable the daunting task of measuring phase diagrams of a system with multiple components we have developed a setup for combinatorial x-ray scattering at beamline X6B at Brookhaven National Laboratories (Upton, NY) capable of determining the structure of thousands of structures per day. We envision future applications of these materials for bioseparation, oil-recovery and water cleanup, and fuel cell membranes.

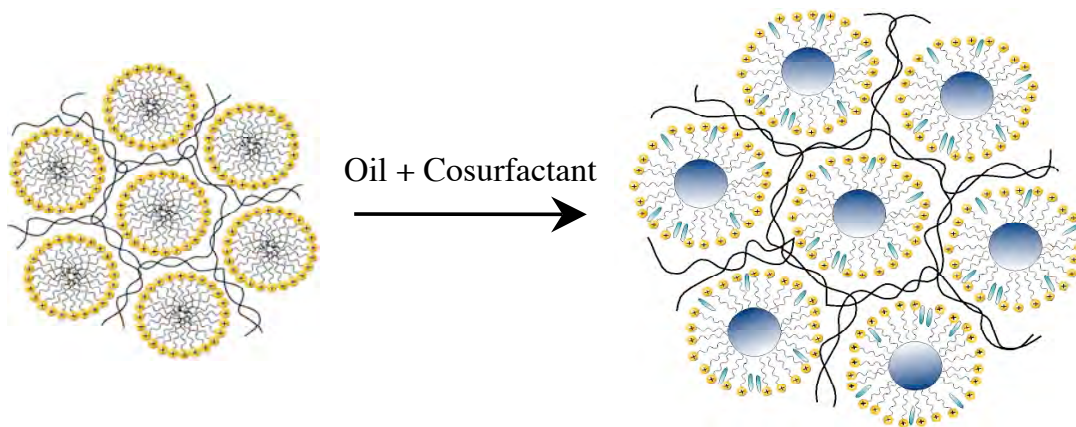


Fig.1: Schematic of a polyelectrolyte-surfactant complex that is swollen with oil and cosurfactant.

## Recent Progress

### 1. Design and construction of a combinatorial material science X-ray scattering beamline at NSLS

Our amphiphile system and also many soft matter materials (e.g. personal care products, detergents, emulsions) consist of many different components. In order to optimize the structure and performance of these materials for specific applications the phase diagram has to be scanned as a function of composition. The difficulty with this approach is that, because of the enormity of the available phase space, often many thousand samples with varying compositions have to be investigated.

One possible solution to this problem is to scan through phase space using a combinatorial approach. This approach has been successfully employed in molecular biology, drug discovery

and recently in material science. In collaboration with Elaine DiMasi from Brookhaven National Labs, we have developed a combinatorial material science X-ray scattering setup at the National Synchrotron Light source (NSLS) located at Brookhaven National Labs (BNL) for structure determination in soft matter systems. The development consists of a robotic liquid handling system commonly used in molecular biology using 96 or 384 well plates for the preparation of samples with varying composition.

We designed a motorized stage that can hold up to 3 well plates and that will allow us in an automated fashion collect X-ray scattering data of up to 1152 individual samples in one run. For samples that contain organic molecules that are incompatible with standard plastic well plates we developed 96-well plates made from Teflon whose top and bottom can be pressure sealed using mylar sheets.

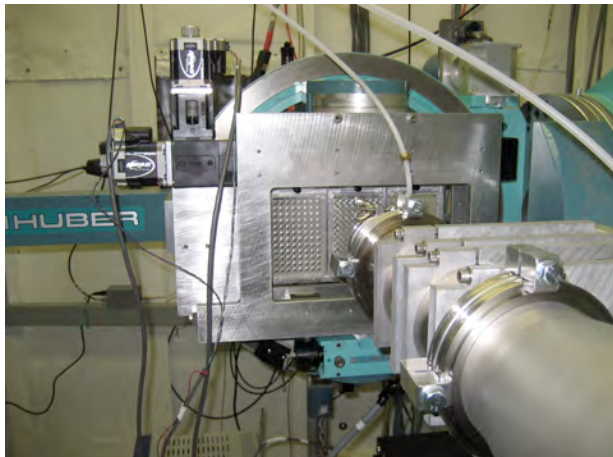


Fig. 2: NSLS X-ray scattering setup to test our sample preparation procedures. Using a x-y translation stage X-ray scattering pictures were obtained for samples in different wells. Using this setup, we successfully determined phase diagrams of ESAs as a function of composition.

We developed software that aids in the design of experiments to determine phase diagrams of a mixture of multiple liquid components. For that we chose to use “Python” as a programming language because it is open-source and will allow us to create an open analysis platform for other X-ray scattering users. We wrote “Python” scripts that allow the user to enter the number of components, their physical parameters such as specific density and concentration, and the range over which each component should be varied in the phase diagram. The scripts are then designing the plate layouts taking into consideration the resulting sample thickness (to optimize scattering intensity), patterns that minimize the number of individual pipetting steps for multi-pipettors. In addition to the plate layout, the scripts also create XML files that contain the sample position, plate number and composition in each well. That allows to later automate X-ray scattering data analysis and construction of phase diagrams.

## 2. Polyelectrolyte – oppositely charged surfactant – cosurfactant – oil complexes

As model system we are studying microemulsions formed from copolymers of poly (acrylic acid – acrylamide), cethyltrimethylammonium chloride, alcohols of different chain length (1-pentanol, 1-octanol), and dodecane. We have studied this system as function of composition (ratio between polyelectrolyte and surfactant is fixed by charge neutrality: for each surfactant charge there is one charged group on the polyelectrolyte chain), polyelectrolyte charge density, and salt concentration.

Fig. 3 shows the phase diagrams of PAA, CTACl, Dodecane and Pentanol at 100mM, 300mM and 500mM NaCl. We find phases with lamellar, hexagonal and cubic structures and phase coexistence of those. Interestingly, we found long-range orderd cubic and hexagonal order at high oil content. To our knowledge, this is the first time that such high oil content was observed for hexagonal or cubic phases (usually long-range order is only found for oil contents below

20%). This finding is crucial for applications in which the oil phase is solidified by cross-linking to fabricate solid nanoporous membranes for use in filtration and possibly fuel cells.

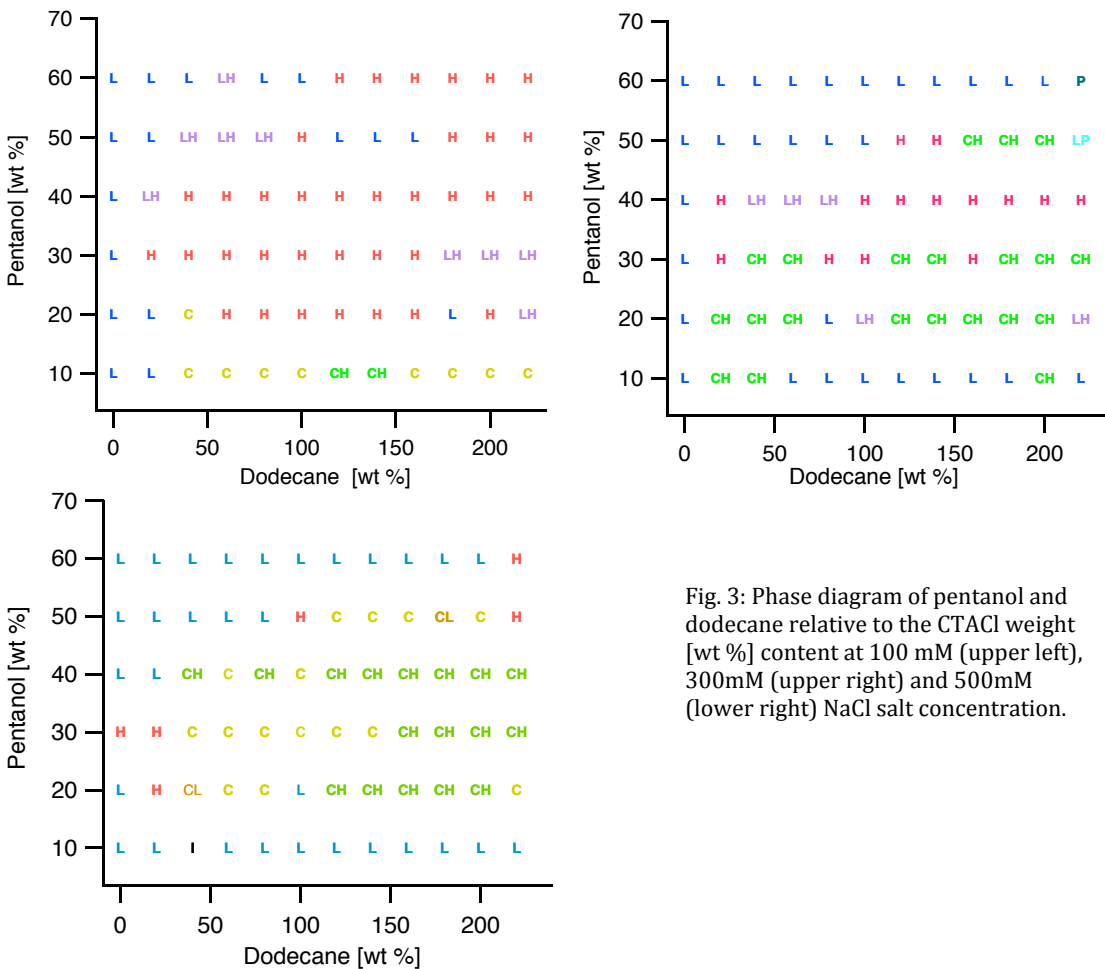


Fig. 3: Phase diagram of pentanol and dodecane relative to the CTACl weight [wt %] content at 100 mM (upper left), 300mM (upper right) and 500mM (lower right) NaCl salt concentration.

In general, at a given pentanol concentration the phase sequence is dominated by lamellar – hexagonal – cubic with increasing dodecane concentration. Such a phase sequence is similar to what is observed in a diblock copolymer system when starting from a 50:50 diblock and increasing one monomer relative to the other.

We also observed a swelling of the unit cell of each phase as the dodecane concentration is increased. The unit cell parameter  $a$ , for the hexagonal phase increase from 68.3 °Å to 108.2 °Å, for the lamellar phase increase from 42.3°Å to 54.5 °Å, while for the cubic phase increase from 142.6 °Å to 164.1 °Å.

### 3. Cross-linking of ESAs using a polymerizable oil

In recent years, tremendous progress has been made in the synthesis of solid nanoporous materials taking advantage of molecular self-assembly. The research on such materials is motivated by the promise as optical materials, catalyst support and filter membranes. Successful synthesis of mesoporous silica and block copolymer materials has resulted in materials and membranes of exquisite order and uniformity.

We are pursuing a slightly different strategy using ESAs. In this project, ESAs serve as templates for solid nanoporous structures with tunable pore size. Similar strategies have been reported in

the literature resulting in solid lamellar structures. We believe that by our choice of monomer and templating system we will have access to a larger variety of structures that are reproduced with higher fidelity. In order to fabricate solid nanoporous materials we are forming ESAs in which the oil is replaced by a polymerizable monomer.

For our monomer we chose dicyclopentadiene (DCPD) with added 2.8% of 5-ethylidene 2-norbornene to make the monomer liquid at room temperature. The advantage of this monomer is that the bulk density of the polymerized material is identical to the bulk density before polymerization. This avoids the common problem of breakup of the material after polymerization that is caused by residual stresses resulting from shrinkage. Dicyclopentadiene is often used in the reaction injection molding manufacture of such large-scale parts as golf cart bodies, sports equipment, and for high-temperature chemically resistant pipes.

During this period, we have mapped out ESA phase diagram with dicyclopentadiene as the oil component in order to identify desirable structures (e.g. bicontinuous cubic phases) for separation materials. We have measured phase diagrams of CTACl, PAA, dicyclopentadiene with various cosurfactants (pentanol, octanol, Brij 52, Brij 56, Brij 76, Dimethyldioctadecylammonium chloride, SPAN 80) at 300mM NaCl to explore for hexagonal and cubic phases with high incorporation of monomer.

We then polymerized some of those samples using ring-opening metathesis polymerization (ROMP) using Second-generation Grubbs' catalysts at a 1:2500 ratio catalyst/DCPD. Second generation Grubbs' catalyst, compared to other metal-catalyst systems, is more tolerant to water and ions and has been successfully used in emulsion and microemulsion polymerization.



Fig. 4: Polymerized samples of various compositions placed in a 96-well plate for X-ray measurements.

**Future Plans:** We will characterize our samples using TEM to elucidate their global structure and to find out why cubic structures refuse to polymerize. We will also investigate phase diagrams of DCPD, charged surfactant, cosurfactant and water to polymerize long-range ordered solid structures for fuel cell membrane applications. This system should lead to solid structure with narrow water channels suited for charge transport of small ions. We are also planning of incorporating polymerizable surfactants into such structures.

## Self-Assembly of Hierarchical Structures: Filaments, Artificial Cells, and Hybrids

Samuel I. Stupp

Departments of Chemistry, Materials Science and Engineering, and Medicine  
Northwestern University

Hierarchical structures are pervasive in biology, formed by highly dynamic processes of self-assembly and in some cases accompanied by mineralization templated within ordered matrices. Interesting examples are found in the extracellular matrices of mammalian biology, for example cartilage and bone. In articular cartilage, collagen fibrils composed of associated triple helices change orientation in space in contiguous layers in order to optimize the required physical properties. Parallel fibrils on surfaces can generate a matrix with low coefficients of friction, whereas radial orientations in other layers of fibrils optimize the distribution of load. In bone, the temporal and spatial control of hydroxyapatite crystal formation within a collagen matrix hosting cells yields a hybrid material, which is extremely tough and has adaptive and self-repairing capacity (1,2). Artificial molecular systems that acquire through self-assembly functional hierarchical structure and dynamic properties would be of great interest in materials chemistry. Most work on self-assembly over the past few decades has focused on the formation and characterization of structures at or close to thermodynamic equilibrium (3,4). Many examples of static molecular self-assembly have been reported with particular interest on ordering of molecules at interfaces or formation of nanoscale supramolecular aggregates. After several decades of strong interest in self-assembly, our understanding of this bioinspired phenomenon remains in its early stages. Mechanisms, pathways, kinetics, and particularly dynamic processes of self-assembly are still wide open topics in the field. This lecture will describe recently discovered systems with hierarchical structure, based on peptides and biopolymers (4), peptides alone (5,6), and conjugated molecules functionalized to create hybrid structures with inorganic oxides (7).

One system to be described involves formation of a membrane in millisecond time scales at the interface of two aqueous solutions, one containing a positively charged peptide amphiphile and the other a negatively charged biopolymer such as hyaluronic acid, alginate, and others. Contact between the two liquid droplets containing oppositely charged molecules yields macroscopic sacs (see figure 1) and membranes of arbitrary shape. The resulting macroscopic structures have a highly ordered architecture in which fairly uniform nanofiber bundles self-align and switch orientation by nearly 90 degrees as the membrane grows. The formation of a diffusion barrier consisting of fibrils contained within the plane of initial contact of the two liquids prevents the chaotic mixing of "reactants" in this self-assembly process. The growth of the membrane is driven by a dynamic synergy between osmotic pressure of ions and static self-assembly. Also, the mechanically robust sac structures engulf the biopolymer solution and have the capacity to self-heal large defects by contact with oppositely charged small molecules. These systems have a broad range of potential applications, which include the encapsulation of cells, the design of sophisticated membranes, and microencapsulation by self-assembly. We have recently miniaturized the liquid-liquid contact process using microfluidic systems and generated a viable method to create "artificial cells" with hierarchical structures and widely varying morphologies.



Figure 1. Macroscopic sac formed after contact between two aqueous solutions. The sac membrane grows through a process of dynamic self-assembly and contains various layers, its blue color is due to the use of a diacetylene peptide amphiphile as the positively charged component.

We investigated the microstructure of the sac membranes as a function of time using electron microscopy. In the early stages of liquid-liquid contact, scanning electron micrographs reveal an amorphous layer directly adjacent to a layer of parallel fibers on the PA solution side. What follows after early contact is a remarkable ordered growth of nanofibers oriented perpendicular to the interface and forming a layer which measures  $\sim 1.5$  microns after 30 minutes and  $\sim 20$  microns after 4 days of initial contact (see Figure 2).



Figure 2. Scanning electron micrograph showing the dominant structure of the membrane containing a remarkable array of vertically oriented fibrils formed by small peptides and biopolymer. The magnification bar equals 5 microns.

We have reported earlier on the self-assembly of one-dimensional cylindrical nanostructures using peptide amphiphiles (10). These nanostructures are composed of  $\beta$ -sheets that collapse into uniaxially symmetric filaments due to hydrophobic interactions among the alkyl segments grafted at one terminus of short peptides. A number of hierarchical structures have been recently observed in these systems, and our understanding of their formation is work in progress. In one example, the cylindrical nanostructures can lose all curvature and become giant nanobelts composed of bilayer assemblies when certain alternating sequences of hydrophobic and charged amino acids are used (6). By lowering concentration, we find that the flat structures with widths on the order of 100 nanometers tend to break up into twisted filaments. In another recent example, substituents on the nitrogen of the amide bond in a single amino acid were found to transform the 1D nanostructures into highly structured quadruple helices (7). These helices revert back to the well known canonical cylinders when UV light is used to remove the photolabile substituent.

A different direction in hierarchical materials to be discussed in the lecture is the formation of hybrid structures, which can be designed for efficient charge transport. Highly-ordered nanostructured organic/inorganic hybrid materials offer chemical tunability, novel functionalities, and enhanced performance over their individual components. Hybrids consisting of complementary p-type organic and n-type inorganic components have attracted widespread interest in optoelectronic devices, such as photoconductors and photovoltaics. Molecular self-assembly offers a strategy to circumvent complex and expensive fabrication techniques by generating highly ordered functional nanostructures as the active layer of a device from liquid precursors. We recently demonstrate the self-assembly of a lamellar hybrid material with electronically active organic and inorganic components directly onto an electrode surface. The hybrid material contains periodic and alternating 1-nm thick sheets of polycrystalline ZnO separated by 2-3 nm thick layers of conjugated organic surfactants (see Figure 3). Initially the inorganic component is electrodeposited as  $\text{Zn(OH)}_2$  sheets, but strong  $\pi$ - $\pi$  interactions among conjugated molecules stabilize synergistically the periodic lamellar structure as it converts to the semiconductor ZnO at 150 °C. When non-conjugated insulating surfactants are used, we find that structures collapse losing all their lamellar hierarchical architecture. The new materials have been integrated into photoconductor devices and selective excitation of the organic component at 500nm, exhibited detectivities that are among the highest measured for organic, hybrid, and even amorphous silicon devices.

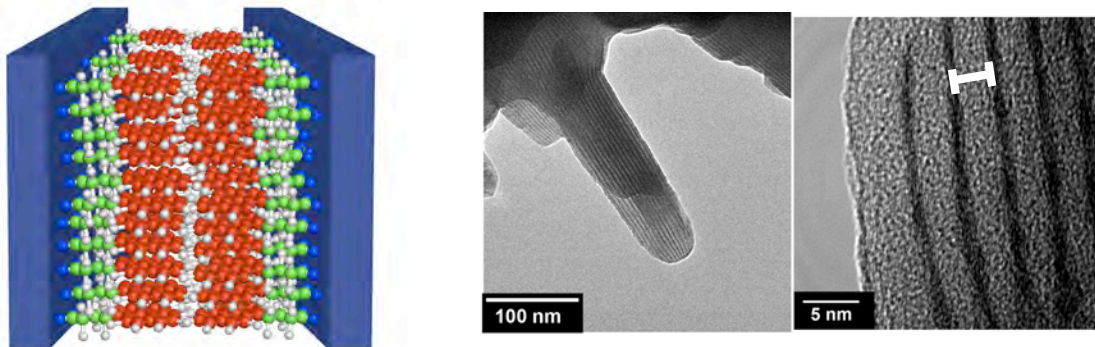


Figure 3. Schematic representation of the lamellar structure consisting of inorganic two-dimensional structures separated by assemblies of organic molecules (left). Transmission electron micrographs of the lamellar material, showing ZnO nanolayers (dark regions) separated by organic nanolayers of self-assembling conjugated molecules.

## References

1. Palmer, L. C.; Newcomb, C.; Kaltz, S. R.; Spoerke, E. D.; Stupp, S. I., "Biomimetic Systems for Hydroxyapatite Mineralization Inspired By Bone and Enamel" *Chemical Reviews* **2008**, 108 (11), 4754-4783.
2. Spoerke, E. D.; Anthony, S. G.; Stupp, S. I., "Enzyme Directed Templating of Artificial Bone Mineral" *Advanced Materials* **2009**, 21(4), 425-430.
3. Palmer, L. C.; Velichko, Y. S.; de la Cruz, M. O.; Stupp, S. I., "Supramolecular Self-Assembly Codes for Functional Structures" *Phil. Trans. R. Soc. A* **2007**, 365, 1417-1433.
4. Palmer, L. C.; Stupp, S. I., "Molecular Self-Assembly into One-Dimensional Nanostructures" *Accounts of Chemical Research* **2008**, 41(12), 1674-1684.
5. Capito, R.; Azevedo, H.; Velichko, Y. R.; Mata, A.; Stupp, S. I., "Self-Assembly of Large and Small Molecules Into Hierarchically Ordered Sacs and Membranes" *Science* **2008**, 319(5871), 1812-1816.
6. Cui, H.; Muroaka, T.; Cheetham, A.; Stupp, S. I., "Self-Assembly of Giant Peptide Nanobelts" *Nano Letters*, **2009**, 9(3), 945-951.
7. Muraoka, T.; Cui, H.; Stupp, S. I., "Quadruple Helix Formation of a Photoresponsive Amphiphile and Its Light-Triggered Dissociation into Single Fibers" *J. Am. Chem. Soc.* **2008**, 130(10), 2946-2947.
8. Sofos, M.; Goldberger, J.; Stone, D. A.; Allen, J. E.; Ma, Q.; Herman, D. J.; Tsai, W-W.; Lauhon, L. J.; Stupp, S. I., "A Synergistic Assembly of Nanoscale Lamellar Photoconductor Hybrids" *Nature Materials* **2009**, 8(1), 68-75.
9. Stone, D. A.; Hsu, L.; Stupp, S. I., "Self-Assembling Quinquethiophene-Oligopeptide Hydrogelators" *Soft Matter* **2009**, 5, 1990-1993.
10. Hartgerink, J. D.; Beniash, E.; Stupp, S. I., "Self-Assembly and Mineralization of Peptide-Amphiphile Nanofibers" *Science* **2001**, 294, 1684-1688.

# Water-Immersed Polymer Interfaces and the Roles of Their Materials Properties on Biolubrication

PI: Y. Elaine Zhu

Department of Chemical and Biomolecular Engineering  
182 Fitzpatrick Hall, University of Notre Dame,  
Notre Dame, IN 46556  
Email: [yzhu3@nd.edu](mailto:yzhu3@nd.edu)

## Program Scope

The broad aim of this project is to fundamentally understand the roles of the structure and interfacial interactions of biological fluids-immersed polymer thin films on biolubrication. The understanding also leads us to the development of tunable and functional polymeric surfaces for improved biolubrication properties. The experimental methods involve integrated imaging, laser spectroscopic study and interfacial force measurement. The project also involves the expertise in the PI's group in polymer synthesis and surface modification to molecular design and synthesis of smooth and homogeneous "smart" polymer thin films for single-molecule experiments.

## Recent Progress

### *1. Molecular design, synthesis and characterization of smooth, responsive polymer brush-like surfaces of tunable surface properties.*

We have recently developed a new and facile method by combining Langmuir-Blodgett (LB) deposition and surface-initiated atomic transfer radical polymerization (SI-ATRP) to synthesize smooth, stimuli-responsive polymer brushes with variable grafting density and thickness. Our facile, grafting-from method allows us to graft molecularly smooth and chemical homogeneous polymer brushes or hybrid brushes of varied chain make-up from different solid substrates, by which the problems of polymer segregation, high surface roughness and limited selection of substrates reported in other surface-initiated polymerization methods have been all successfully prevented. We employed this method to grow thermo- and pH-responsive poly-N-isopropylacrylamide (PNIPAM) brushes from smooth quartz or silicon substrate to control the adsorption and surface diffusion of proteins at PNIPAM aqueous interfaces. We synthesize and use the active initiator mixed with its tailor-made inert spacer, two of which have the same chemical structure except the end-functional groups, to vary the brush grafting density to form smooth initiator monolayers of varied active initiator coverage on smooth quartz or silicon wafer by LB, which minimizes the problems of mixed monolayer segregation and reduced initiator reactivity by the self-assembly method. Polymer brushes, such as PNIPAM brushes, can be subsequently grafted from smooth initiator monolayers with controllable brush thickness by SI-ATRP under optimized reaction conditions. It is demonstrated that our new method can be applied to graft a variety of hydrophilic and hydrophobic polymer brushes, including polyelectrolytes and block copolymers, from different solid surfaces such as quartz and indium tin oxide surface, to produce functional non-fouling coating and lubricious thin films. We are also investigating the control of

monomer concentration and LB-deposition speed to design and produce polymer brushes with a continuous gradient in grafting density on a single substrate.

## 2. Single protein dynamics at responsive polymer brush surfaces.

With molecularly smooth and homogeneous PNIPAM brush thin films prepared by our LB-ATRP method, we have examined the microscopic friction of single protein molecules moving past PNIPAM surfaces of varied interfacial interactions. The effect of protein-PNIPAM interfacial interactions on protein dynamics is examined by using fluorescence correlation spectroscopy (FCS) combined with temperature-controlled fluidic cell. We find out that the measured surface diffusion coefficient of fluorescence-labeled human serum albumin (HSA) strongly depends on protein-PNIPAM interfacial interactions that is tunable by varying temperature ( $T$ ) across the lower critical solution temperature (LCST) of PNIPAM brush surfaces: Strong hydrophobic attraction between HSA protein and PNIPAM at  $T > \text{LCST} \sim 32^\circ\text{C}$ , when PNIPAM surface is hydrophilic, results in much more sluggish dynamics of HSA than that at hydrophilic PNIPAM interface at  $T < 25^\circ\text{C}$ ; the dependence of HSA surface diffusion on interfacial interaction is quantitatively obtained at varied  $T$  across LCST, where PNIPAM surfaces gradually change from a non-adsorbing hydrophilic surface to a strong-adsorbing, hydrophobic surface to protein. We further examine the effect of surface interaction on local friction of interfacial protein aggregates with added hyaluronic acid (HA), a key lubricating component in natural synovial fluids. The protein-HA aggregation, possibly due to H-bonding, lead to the further reduction in measured surface diffusion of interfacial biomolecular at PNIPAM surfaces with increased HA concentration. The conformational structure of surface-bound protein and its aggregates is under current investigation by AFM and single-molecule imaging to further determine the protein-surface interactions and their effect on local friction. To examine the coupling of protein dynamic and viscoelasticity of polymer surface, the dependence of protein surface diffusion on brush thickness and grafting density of PNIPAM brush thin films is under current investigation.

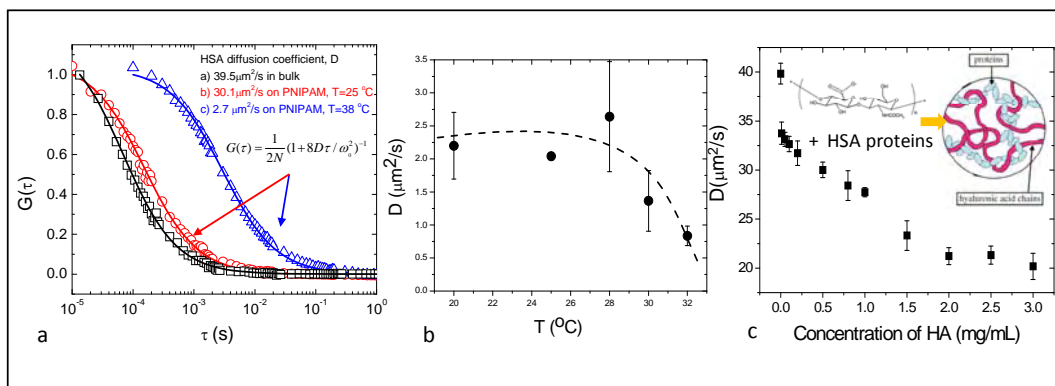


Fig. 1. (a) Auto-correlation functions of fluorescent labeled HSA protein in bulk buffer solution (squares) and at methyl-terminated self-assembled monolayer surface against lag time. (b) Measured diffusion coefficients of HAS added with HA of increased concentration in the buffer solution. Inset: autocorrelation functions at increased HA concentrations.

## 3. Biomacromolecular manipulation and assembly under AC-electric fields.

We strive for not only understanding dynamic interfacial interactions of protein and other macromolecules at polymer surfaces, polymeric materials, but also actively tuning

their structure and dynamics in a rapid and controlled fashion. There is also emerging interest in employing AC-electrokinetics to effectively manipulate and assemble supramolecular aggregates, such as AC-field induced protein crystallization and DNA hybridization. Recently, we have explored the AC-induced conformational transition of both synthetic and biological polyelectrolytes under AC-fields of varied frequency and amplitude. We have examined a model weak polyelectrolyte, poly (2-vinyl pyridine) (PVP), which exhibits a first-order coil-to-globule conformational transition in bulk solution by varying pH and ionic strength. In response to *uniform* AC-fields between two extended, parallel electrode surfaces, where the effect of imposed DEP forces on PVP conformations is strategically avoided and the PVP concentration is kept constant in the focal volume at varied AC-frequency and voltage, PVP is observed to undergo a gradual coil-to-globule transition of PVP as decreasing AC-frequency when a threshold AC-voltage is exceeded; additionally, curious hysteresis is observed with AC-frequency sweep. We have developed a theoretical model based on stochastic resonance due to applied AC-fields of varied frequency to tune the energy landscape near two conformational states of a weak polyelectrolyte. The scaling of AC-field activated polyelectrolyte conformational transition with molecular weight and ionic solution parameters is under current investigation.

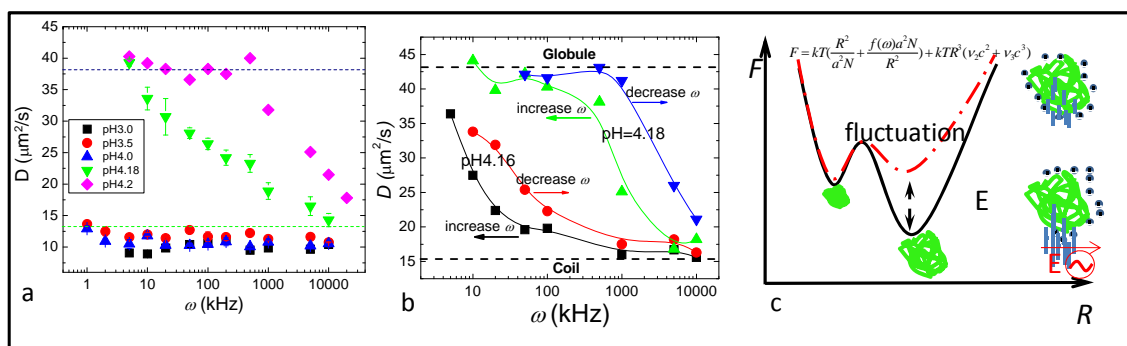


Fig. 2. (a) AC-field frequency dependence of measured PVP dynamics in response to uniform AC-fields, indicating the AC-induced coil-to-globule transition of PVP near its transition pH, (b) observed hysteresis in PVP conformational transition upon frequency sweep repeatedly, (c) a model based on stochastic resonance to predict the modulated free-chain energy landscape by AC-polarization.

### Future plan:

The exciting new research development described above will be further pursued. Our overarching goal is an improved understanding, at a single-molecule level, of the interplay of protein interfacial interactions and structural dynamics at polymer biointerfaces that underlies soft lubrication in biological fluids. One major experimental task is to examine how the viscoelasticity of deformable polymer thin films inversely affect the local sliding friction of interfacial molecules in relative motion with sheared polymer interfaces. We will investigate the effect of PNIPAM brush thickness and grafting density on surface diffusion of single protein at rest and under varied oscillatory shear. With polyelectrolyte brush thin films, this concept will also be extended to use electric and ionic stimuli to modify the conformational structure and surface chemistry of polymer chains to effectively tune protein-polymer interfacial interactions. Beyond the fundamental understanding, we will explore varied external forcing fields, particularly AC-electric fields, integrated in microfluidic devices, to regulate the conformational

structure of biomacromolecules and control their assembly to develop new functional materials for lubrication, non-fouling coating and other applications.

#### **DoE sponsored publications in 2007-2009**

- 1) P. Sarangapani and Y. Zhu, "Impeded structural relaxation of confined hard-sphere colloidal suspension under confinement," *Phys. Rev. E* 77, 010501(R) (2008).
- 2) P. Hoffman and Y. Zhu, "Double-layer effects on low frequency dielectrophoresis-induced colloidal assembly," *Appl. Phys. Lett.*, 92, 224103 (2008).
- 3) P. Sarangapani, Y. Yu, J. Zhao and Y. Zhu, "Direct visualization of colloidal gelation under confinement," *Phys. Rev. E*, 77, 061406 (2008).
- 4) P. Sarangapani, J. Zhao and Y. Zhu, "How does sensitivity to dynamical heterogeneity in supercooled colloidal liquids depend on tracer size?" *J. Chem. Phys.*, 129, 104514 (2008).
- 5) P. Hoffman, P. Sarangapani and Y. Zhu, "Dielectrophoresis and AC-induced assembly in binary colloidal suspensions," *Langmuir*, 24, 12164-12171 (2008).
- 6) V. Froude and Y. Zhu, "Dielectrophoresis of lipid unilamellar vesicles (liposomes) of contrasting surface constructs," *J. Phys. Chem. B*, 113, 1552-1558 (2009).
- 7) Lu Zhang and Y. Zhu, "Electrostatically tuned DNA adsorption and clustering on functionalized colloidal particles," *Soft Matter*, DOI: 10.1039/b910082b (2009).
- 8) B. Jing, Y. Zhu and J. Zhao, "Surface hopping and sliding polymer chains under electric fields," *J. Polymer Sci. B*, in press (2009).
- 9) I-Fang Cheng, V. Froude, Y. Zhu, H.-C. Chang, H.-C. Chang, A continuous high-throughput bioparticle sorter based on 3D traveling wave dielectrophoresis, Lab on a Chip, in press (2009).
- 10) S. Wang and Y. Zhu, "A facile method to grow smooth polymer brushes with varied grafting density by combining Langmuir-Blodgett deposition and atomic transfer radical polymerization," *Langmuir*, in press (2009).

## Dynamic Self-Assembly, Emergence and Complexity

George M. Whitesides

Harvard University

Department of Chemistry and Chemical Biology

Cambridge, MA 02138

617-495-9430

617-495-9857 (FAX)

[gwhitesides@gmwgroup.harvard.edu](mailto:gwhitesides@gmwgroup.harvard.edu)

**Program Scope:** The broad objectives of this research are to examine systems that are complex, and that show emergent behavior. Our emphasis is increasingly on the “emergent” aspects of these systems: “emergent”, in this context, mean “unexpected”: whether unexpected because there is genuinely new physics and chemistry underlying the experimental observations, or unexpected in the sense that the science already exists but we did not *predict* the behavior, is irrelevant to us: the study of these systems has become a kind of engine for discovery of new phenomena. Our approach is *constructionist*, rather than *deconstructionist*: that is, we *design and synthesize/assemble* complex systems to study their behavior, rather than picking apart already existing systems. Our procedure is to design components, and the interactions between them, to be as simple as possible, to put them in motion by allowing a flux of energy through them, and to observe the resulting behaviors of the components as they interact.

**Recent Progress:** Work in the last year has focused on these themes:

**a. Bubbles and Droplets.** We continued to work with bubbles and droplets inside microchannels using the so-called “flow-focusing” system. These particulate systems remain a very attractive for observing dynamic behavior in dissipative systems involving interacting components. We investigated systems that show the stability required to encrypt and to decrypt information, and we used the flow-focusing systems to generate more complex patterns of drops and bubbles.

**b. Electrostatic charging and self-assembly.** Electrostatic charging by contact electrification is one of the first manifestations of electric and magnetic interactions ever observed, yet we don’t have a good scientific understanding of this complex phenomenon. Our recent work aims at understanding the fundamental physics and chemistry of contact electrification and at creating a molecular model (beads on a string) that self-assembles based on electrostatic interactions.

i). Our experimental work from this past year has supported our model that the transfer of ions causes contact electrification, and that dielectric breakdown of the surrounding medium sets the maximal charge density an object can have. We have expanded our set of tools for studying these phenomena by characterizing the dynamics of contact charging and discharging in real time.

ii). We developed a physical model for the study of polymers folding in two dimensions (Figure 1). The model that we developed is based on a simple theoretical model for polymers,

the “beads-on-a-string” model. We made a “beads-on-a-string” model by threading sequences of spherical Nylon-6,6 and Teflon beads on a thin Nylon-6,6 string. Upon contact, these beads develop net charges at similar rates but with opposite electrical polarities.

We constructed a random motion generator that moved the surface under the strings (and consequently the strings) randomly. This realizes a simple physical simulator of the random motion of polymers in solution. In order to model folding with realistic length scales that corresponds with real polymers like proteins or polynucleic acids, we worked with large sequences, up to 50 beads long. We are currently investigating what are the stable conformations of this system and the kinetics of string folding.

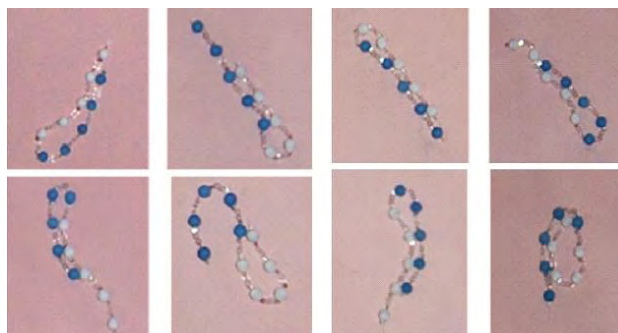


Figure 1. Conformations observed for sequences composed of 10 beads with alternating sets of 5 Nylon-6,6 beads and 5 Teflon beads after 110 minutes of agitation.

#### **c. Nucleation of freezing in drops of water.**

We continued to develop our microfluidic system for the study of ice nucleation on statistically large ensembles of water droplets.

We can measure now with good precision (better than 0.5 °C) the temperatures at which an ice nucleation event occurs in a droplet. The number of events we can investigate is very large (>10000 in a typical experimental run). We acquired large data sets for the nucleation of ice in pure water (homogenous nucleation). We are currently processing and validating these data, which should provide one of the most accurate measurements of the homogenous ice nucleation rates in pure water.

**d. Flames.** We have succeeded in producing patterns of small flames that oscillate at 20 Hz for several minutes. In addition we have characterized several modes of complex, coupled patterns of flames in more complex patterns. These accomplishments have imparted a measure of predictive power to our system that needs to be explored, and has enabled some control over the direction and coupling of flames. For example, we observed coupled circles that alternate clock-wise or counter clock-wise rotation depending on the spacing of the holes.

**Future Plans:** In the next year, we will:

- **Develop methods to synchronize formation of bubbles and droplets** by combining multiple flow-focusing generators in parallel and allowing them to interact via the fluctuation of fluidic resistance.
- **Investigate the interaction between the nematode *C. elegans*** and its physical environment, using microfabrication to produce fluidic microenvironments for the worm of well-defined geometries, in order to probe how physical environment affects behavior and lifespan.

- **Use interactions between charged particles** to build new complex systems that respond to environmental parameters (relative humidity, dielectric strength of atmosphere, etc.) and simple physical models for the electrostatic interactions between biologically relevant molecules such as proteins and polynucleic acids.
- **Measure homogenous and heterogeneous ice nucleation rates** in pure water, and in water containing well-defined ice nucleation agents, such as monodisperse silver iodide nanoparticles.
- **Characterize the modal behavior of flames** and create systems that are coupled in a predictable way and operate at frequencies that are stable over long periods of time.

## Publications (2007-2009)

### BUBBLES AND DROPLETS

1. "Coding/decoding and reversibility of droplet trains in microfluidic networks", Fuerstman, M. J., Garstecki, P. and Whitesides, G. M., *Science*, **2007**, *315*, 828-832.
2. "The pressure drop along rectangular microchannels containing bubbles", Fuerstman, M. J., Lai A., Thurlow M.E., Shevkoplyas S.S., Stone H.A. and Whitesides G.M., *Lab Chip*, **2007**, *7*, 1479-1489.
3. "Synthesis of composite emulsions and complex foams with the use of microfluidic flow-focusing devices", Hashimoto M., Garstecki P. and Whitesides, G. M., *Small*, **2007**, *3*, 1792-1802.
4. "Interfacial instabilities in a microfluidic Hele-Shaw cell", Hashimoto M., Garstecki P., Stone H.A. and Whitesides, G. M., *Soft Matter*, **2008**, *4*, 1403-1413..
5. "Emulsification in a microfluidic flow-focusing device: effect of the viscosities of the liquids", Nie Z., Seo MS., Xu S., Lewis P.C., Mok M., Kumacheva E., Whitesides G.M., Garstecki P. and Stone H.A., *Microfluid Nanofluid.*, **2008**, *5*, 585-594.
6. "Formation of Bubbles and Droplets in Parallel, Coupled Flow-Focusing Geometries", Hashimoto, M., Shevkoplyas, S. S., Zasońska, B., Szyborski, T., Garstecki, P. and Whitesides, G. M., *Small*, **2008**, *4*, 1795-1805.
7. "Independent Control of Drop Size and Velocity in Microfluidic Flow-Focusing Generators Using Variable Temperature and Flow Rate", Stan, C. A., Tang, S. K. Y. and Whitesides, G. M., *Anal. Chem.*, **2009**, *81*, 2399-2402.
8. "Preparation of Monodisperse Biodegradable Polymer Microparticles Using a Microfluidic Flow-Focusing Device Controlled Drug-Delivery", Xu, Q., Hashimoto, M., Dang, T. T., Hoare, T., Kohane, D. S., Whitesides, G. M., Langer, R. and Anderson, D. G., *Small*, **2009**, *5*, 1575-1581.
9. "A Microfluidic Apparatus for the Study of Ice Nucleation in Supercooled Water Drops", Stan, C. A., Schneider, G. F., Shevkoplyas, S. S., Hashimoto, M., Ibanescu, M., Wiley, B. J. and Whitesides, G. M., *Lab Chip*, **2009**, *9*, 2293-2305.
10. "Formation of Bubbles in a Multi-Section Flow-Focusing Junctions", Hashimoto, M. and Whitesides, G. M., *Small*, **submitted 2009**,
11. "Dynamically reconfigurable liquid-core liquid-cladding lens in a microfluidic channel", Tang S.K.Y., Stan C.A. and Whitesides G.M., *LabChip*, **2008**, *8*, 395-401.

### WORMS AND MICROORGANISMS

12. "A microfabricated array of clamps for immobilizing and imaging C-elegans", Hulme S.E., Shevkoplyas S.S., Apfeld J., Fontana W. and Whitesides, G. M., *LabChip*, **2008**, *7*, 1515-1523.

13. "Using Ratchets and Sorters to Fractionate Motile Cells of *Escherichia coli* by Length", Hulme, S. E., DiLuzio, W. R., Shevkoplyas, S. S., Turner, L., Mayer, M., Berg, H. C. and Whitesides, G. M., *Lab Chip*, **2008**, *8*, 1888-1895.

#### ELECTROSTATIC CHARGING AND SELF-ASSEMBLY

14. " Patterns of electrostatic charge and discharge in contact electrification ", Weibel, Thomas S.W., Vella S.L., Kaufman G.K. and Whitesides, G. M., *Angew. Chem. Int. Ed.*, **2008**, *47*, 6654-6656.

15. "Phase Separation of 2D Coulombic Crystals of Meso-scale Dipolar Particles from Meso-scale Polarizable "Solvent"", Kaufman, G. K., Reches, M., Thomas, S. W., Feng, J., Shaw, B. F. and Whitesides, G. M., *Appl. Phys. Lett.*, **2009**, *94*, 044102-1 - 3.

16. "Phase Separation of 2D Meso-Scale Coulombic Crystals from Meso-Scale Polarizable "Solvent"", Kaufman, G. K., Thomas, S. W. R., M, Shaw, B. F., Feng, J. and Whitesides, G. M., *Soft Matter*, **2009**, *5*, 1188-1191.

17. "Folding of Electrostatically Charged Beads-on-a-String: An Experimental Realization of a Theoretical Model", Reches, M., Snyder, P. W. and Whitesides, G. M., *Proc. Natl. Acad. Sci. USA*, in press 2009,

#### OTHER

18. "Laterally Ordered Bulk Heterojunction of Conjugated Polymers: Nanoskiving a Jelly Roll", Lipomi, D. J., Chiechi, R. C., Reus, W. F. and Whitesides, G. M., *Adv. Funct. Mater.*, **2008**, *18*, 3469-3477.

19. "Propulsion of Flexible Polymer Structures in a Rotating Magnetic Field", Garstecki, P., Teirno, P., Weibel, D. B., Sagués, F. and Whitesides, G. M., *JPCM*, **2009**, *21*, 204110+ 0.

20. "Green Nanofabrication: Unconventional Approaches for the Conservation Use of Energy", Lipomi, D. J., Weiss, E. and Whitesides, G. M., in *Nanotechnology for the Energy Challenge*, , J. Garcia-Martinez, Ed., Wiley-VCH, Alicante, Spain, in press 2009,

# *INVITED TALKS*

## Single molecule nanopore analysis of nucleic acids, exonucleases and polymerases

David Deamer and Mark Akeson  
Department of Biomolecular Engineering  
University of California, Santa Cruz  
Santa Cruz CA 95064  
[deamer@soe.ucsc.edu](mailto:deamer@soe.ucsc.edu)  
[makeson@soe.ucsc.edu](mailto:makeson@soe.ucsc.edu)

### Program scope.

The goal of our research is to use nanopore-based devices to provide information about single molecules of nucleic acids in solution, including base sequence.

### Background

In the 1970s, it was discovered that electrophoresis in gels is a powerful tool for separating long polyanions like nucleic acids. A typical agarose or polyacrylamide gel is a porous material, so a nucleic acid strand moving through the gel must find its way through a maze-like matrix of nanoscopic pores. The velocity at which a nucleic acid strand moves through the gel is a function of its length, such that molecules up to several hundred nucleotides in length can be separated with single base resolution (see Brody and Kern, 2004, for a review of gel electrophoresis and sequencing methods). Instead of a matrix of nanoscopic pores in a gel, it is also possible to produce a single pore in an otherwise impermeable membrane and then use electrophoresis to drive single molecules of a nucleic acid through the pore. The term nanopore came into general use as a descriptive term for nano-scale pores that can capture linear polymers of nucleic acids when an electrical field is generated in the pore by an applied voltage. The voltage also generates an ionic current through the pore, typically composed of potassium and chloride ions in the medium, which is markedly affected by the presence of the anionic polymer that occupies the pore. Modulations of the ionic current provide information about the nature of the polymer and can resolve its dynamic motions on time scales of tens of microseconds.

The  $\alpha$ -hemolysin ( $\alpha$ -HL) channel was the first to be used as a nanopore detector of nucleic acids in solution. Kasianowicz, Brandin, Branton and Deamer published initial results which confirmed that ssDNA molecules, but not dsDNA, were translocated through the pore by single molecule electrophoresis (Kasianowicz et al. 1996). As each strand entered the pore, it produced a marked blockade of ionic current, typically between 85 to 90 percent of the open channel current. The capture of a nucleic acid strand from solution required a minimal voltage in the range of 80 mV, and the duration of the signal and translocation velocity was a function of the length of the nucleic acid strand. Because each strand passed through the nanopore in strict single file, it was proposed that a nanopore could provide sequence information if individual bases produced base-specific modulations of ionic current during translocation. When it was measured, the velocity of translocation was such that individual bases in the strand passed through the pore in a few microseconds. This was slower than expected from typical rates of diffusion, which suggested that some form of molecular friction was acting between the strand and the side of the pore.

Akeson et al. (1999) demonstrated that the  $\alpha$ -HL nanopore had sufficient resolution to distinguish between RNA homopolymers of cytidylic acid and adenylic acid during translocation. Furthermore, if the strands were synthetic 100mers containing segments of 70 cytosine bases followed by 30 adenine bases, the ionic current blockade showed a demarcation that reflected the difference between the cytosine and adenine segments. Although this difference arose from secondary structures adopted by the two homopolymers, rather than the nucleotide bases themselves, the result established that, in principle, it was possible to capture sequence information from a single molecule during translocation.

## Recent progress

*A nanopore can monitor functioning DNA-processing enzymes.*

The velocity at which ssDNA strands pass through the pore under a driving voltage of 120 mV is too fast to discriminate between individual bases, which transit the pore in ~2 microseconds. To give a perspective on this limitation, consider that during a translocation event, the ionic current is typically reduced to ~10 pA, equivalent to 60 million ions per second. It follows that in 2 microseconds just 120 ions per base would be available to establish the identity of the base. The actual number is even smaller, because on average there is only a 2 pA difference between purine and pyrimidine homopolymers occupying the pore. The miniscule number of ions cannot provide sufficient signal-to-noise to identify a single base in transit on microsecond time scales.

In a typical nanopore device, sampling is carried out at 10 kHz, producing approximately 10 data points per millisecond. It follows that translocation time must be slowed from microsecond to millisecond time scales to allow signal averaging sufficient to resolve current differences of a few picoamperes that distinguish purine from pyrimidine bases. One way to do this is to use a DNA processing enzyme to slow translocation, which would then be limited to the turnover time of the enzyme. The enzyme would bind to ssDNA in solution and then be drawn to the pore as an enzyme-substrate complex. As the enzyme processed its DNA substrate, the strand would be drawn through the pore in stepwise fashion on a time scale of tens of milliseconds.

DNA polymerase I of *E. coli* catalyzes both DNA repair and lagging strand synthesis during replication (see Friedberg, 2006, for an interesting history of this discovery). When treated with subtilisin, a smaller fragment is produced that lacks the 5'-3' exonuclease activity of the complete enzyme but retains the 5'-3' polymerase activity (Klenow and Hennington, 1970). The interaction between the Klenow fragment and its substrate DNA was investigated by Benner et al. (2007). The Klenow fragment, like other polymerases, requires a primer that is complementary to a template strand in order to initiate polymerization. It also requires four deoxynucleotide triphosphates (dNTPs) and magnesium. This system is more complicated than a simple exonuclease activity, because signals could reflect the primer-template itself, the primer-template with bound enzyme, or the primer-template-enzyme complex in the presence of an NTP substrate. Despite the complexity, three distinct blockade could be distinguished that represent each of the three components of the system. The primer-template signal was short, ranging from 0.2 to 7 ms with a mean duration of about 1 ms. The mean duration with bound Klenow fragment was 2 - 3 ms, but when the correct NTP was present the mean duration increased to 200 ms. (The process was limited to a single binding event by using a dideoxy end group on the primer.) As expected, the duration increment occurred only if the correct nucleotide was present, showing that the signals were related to a functional enzyme and its binding site.

These results were encouraging that an enzyme could be used to control nucleic acid translocation for sequencing purposes. Cockcroft et al. (2008) used DNA polymerase to add single bases to a DNA strand that was tethered to the  $\alpha$ -HL nanopore. The substrates were extremely dilute so that only occasionally was a base added to the DNA by the polymerase. After each addition, the strand was drawn into the pore by appropriately adjusting the voltage, and the current was measured. It was observed that each of the four bases produced a distinct increment in blockade resistance to ionic current, so that the order of bases in the template strand could be established. This result demonstrated that in principle, an enzyme-controlled addition of nucleotides to a DNA strand could provide sequence information.

## Future prospects for nanopore sequencing

Despite the advantages inherent in  $\alpha$ -HL nanopores, their utility for DNA sequencing analysis has been limited by the spatial and temporal demands inherent in single nucleotide discrimination within individual DNA strands. In the last two years, several breakthroughs have substantially increased the likelihood that nanopore sequencing will become a viable alternative to Sanger-based sequencing. The Bayley group at Oxford has significantly improved the sensitivity of the  $\alpha$ -HL pore by site directed mutagenesis and cyclodextrin adapters (Astier et al., 2006). Furthermore, although  $\alpha$ -HL has served as a work horse in developing nanopore sequencing technology, there is no guarantee that it is the best possible protein nanopore. Its main limitation is that the stem is more of a tunnel than a pore, so that ~ten nucleobases contribute to the overall modulation of ionic current. Significantly, an alternative nanopore has recently emerged that in large part may resolve this limitation. Gundlach and co-workers (2008) have modified a bacterial porin called MspA by site-directed mutagenesis. The pore geometry resembles a funnel rather than a mushroom, and its limiting aperture has dimensions approximately that of a single nucleotide.

The advances described here suggest that nanopore DNA sequencing is feasible, but a remaining question concerns how competitive it will be with other sequencing methods. Nanopore sequencing has four major advantages: Minimal preparation of samples, very small samples are required, the promise of long read lengths, and inexpensive, portable hardware. We note that Oxford Nanopore Technologies was incorporated in 2005 to bring a nanopore sequencing technology to market. Their approach uses a processive exonuclease to present mononucleotides in sequential order to a modified  $\alpha$ -HL pore, with the expectation that each nucleotide can be identified by its characteristic modulation of ionic current through the pore. The working principles of this method were recently described by Clarke et al (2009).

A critical unresolved issue concerns the length of DNA fragments that can be reproducibly captured, controlled and processed at single nucleotide precision by nanopores. If this length substantially exceeds the read length of state-of-the-art second generation sequencing devices (~400 nt for 454/Roche technology), then nanopore sequencing is likely to be a competitive third generation sequencing platform. Nanopore sequencing of intact DNA templates also will require precise single nucleotide spatial register if a base is to be accurately identified. For DNA-polymerase-controlled translocation this would be in the range of 1 to 100 milliseconds per measurement. At low voltages that are likely to permit polymerase catalysis, it is unclear whether registry can be maintained. Extending read length and maintaining registry are the primary focus of current research related to nanopore sequencing.

## References

- Akeson, M., D. Branton, J.J. Kasianowicz, E. Brandin, and D.W. Deamer. 1999. Microsecond time-scale discrimination among polycytidylic acid, polyadenylic acid, and polyuridylic acid as homopolymers or as segments within single RNA molecules. *Biophys. J.* 77: 3227-3233.
- Astier Y, Braha O, Bayley H. 2006. Toward single molecule DNA sequencing: direct identification of ribonucleoside and deoxyribonucleoside 5'-monophosphates by using an engineered protein nanopore equipped with a molecular adapter. *J Am Chem Soc.* 128:1705-10.
- Benner S, Chen RJ, Wilson NA, Abu-Shumays R, Hurt N, Lieberman KR, Deamer DW, Dunbar WB, Akeson M. 2007 Sequence-specific detection of individual DNA polymerase complexes in real time using a nanopore. *Nat Nanotechnol.* 2:718-24.
- Brody J. R., Kern S. E. History and principles of conductive media for standard DNA electrophoresis. 2004. *Anal. Biochem.* 333:1-13.
- Clarke J, Wu HC, Jayasinghe L, Patel A, Reid S, Bayley H. 2009. Continuous base identification for single-molecule nanopore DNA sequencing. *Nat Nanotechnol.* 4:265-70.

Cockroft SL, Chu J, Amarin M, Ghadiri MR. 2008. A single molecule-molecule nanopore device detects DNA polymerase activity with single-nucleotide resolution. *J Am Chem Soc.* 130:818-20.

Friedberg EC 2006. The eureka enzyme: the discovery of DNA polymerase. *Nature Reviews Molecular Cell Biology* 7: 143–7.

Gijs G, Smith S Young M, David Keller D Bustamante C. 2000. Single-molecule studies of the effect of template tension on T7 DNA polymerase activity. *Nature* 404: 103-106

Gundlach JH. 2008. Single-molecule DNA detection with an engineered MspA protein nanopore. *Proc Natl Acad Sci U S A.* 105:20647-52.

Hornblower B, Coombs A, Whitaker RD, Kolomeisky A, Picone SJ, Meller A, Akeson M. 2007. Single-molecule analysis of DNA-protein complexes using nanopores. *Nat Methods.*4:315-7.

Hurt N, Wang H, Akeson M, Lieberman KR. 2009. Specific nucleotide binding and rebinding to individual DNA polymerase complexes captured on a nanopore. *J Am Chem Soc.* 131:3772-8.

Kasianowicz, J., E. Brandin, D. Branton and D.W. Deamer. 1996. Characterization of individual polynucleotide molecules using a membrane channel. *Proc. Natl. Acad. Sci. USA* 93:13770-13773.

Klenow H and Henningsen I. 1970. Selective elimination of the exonuclease activity of the deoxyribonucleic acid polymerase from *Escherichia coli* B by limited proteolysis.

Vercoutere, W., S. Winters-Hilt, H. Olsen, D.W. Deamer, D. Haussler, and M. Akeson. 2001. Rapid discrimination among individual DNA molecules at single nucleotide resolution using a nanopore instrument. *Nature Biotechnology* 19: 248-250.

Wilson NA, Abu-Shumays R, Gyarfás B, Wang H, Lieberman KR, Akeson M, Dunbar WB. 2009, Electronic control of DNA polymerase binding and unbinding to single DNA molecules. *NanoLetters* 3:995-1003.

## **Artificial Cells and Cytomimetic Environments**

Christine D. Keating, *Department of Chemistry, Pennsylvania State University, University Park, PA 16802.*

Single cells can be considered the fundamental unit of life, and have much to teach us about materials science. Cells are complex assemblies that can interact with their environments and perform numerous functions tailored to the needs of the organism. The synthesis and characterization of artificial cells and cell-like environments can provide new insight into how biological systems exert exquisite control over processes such as complex multistep chemical reactions, mineral formation, energy harvesting, and response to external stimuli. Artificial cells are nonliving assemblies meant to mimic their living biological counterparts structurally and/or functionally. They are often based on micron-scale lipid or polymer vesicles that encapsulate an aqueous solution of biomolecules. Cell-like environments are also of interest; these mimic one or more aspects of the intracellular milieu but need not be encapsulated within microscopic volumes. Examples include (1) addition of polymers as volume excluders to enhance intermolecular associations, (2) compartmentalization to increase local concentrations and affect reaction rates, or (3) the use of scaffolds to organize biomolecules in relation to each other.

## **Unscientific America**

Sheril Kirshenbaum, *Duke University*

The vast majority of Americans do not see the ways in which science holds relevance in their lives, and too many scientists are unable to explain why our work matters.

Meanwhile, partisan politics, a new media environment, and religious ideologies have magnified the growing rift between science and mainstream American culture. Science should be a value shared by all, but it will take far more than political will to bridge what C.P. Snow once described as a “vast gulf of mutual incomprehension” between scientists and everyone else. The scientific community must find new ways of reaching out or we will fail to influence the public, inform the decision-making process, and rise to meet the greatest challenges of the 21st century.

What is a quorum in the “real world”? Chemical, physical, and biological parameters that influence quorum sensing in *Pseudomonas aeruginosa*.

Matthew R Parsek

Bacterial quorum sensing is a means by which bacteria can coordinate gene expression as a group. There are various chemical signals used by different quorum sensing species of bacteria. The traditional way to study quorum sensing in the laboratory is in shaken liquid batch culture where a quorum sensing response occurs at a specific point in the growth curve, coinciding with a threshold concentration of signal. However, unlike closed systems such as batch cultures where only gaseous exchange occurs, most, if not all, structured communities grow in open systems in which exchange occurs between the community and the surrounding liquid. Volume is fixed in a culture flask and signal molecules produced by bacteria generally increase in concentration over time (unless they are degraded). In an open, flowing system, signals may be “washed” away by the overlying fluid. In open systems, the concentration of signal molecules within structured communities is primarily a function of 1) the signal production rate, 2) the degradation rate or half-life of the signal, 3) the diffusion properties of the signal, and 4) the external hydrodynamic or mass transfer conditions. The prevailing environmental conditions and resident biology are important for each of these processes to varying degrees.

One of the most common quorum sensing systems is the acyl homoserine lactone (AHL)-based quorum sensing used by many Gram-negative bacterial species. In 1993, *P. aeruginosa* was shown to utilize acyl-homoserine lactone (AHL)-based quorum sensing to regulate the expression of virulence factors. Currently, *P. aeruginosa* is now known to have two primary AHL systems, *las* and *rhl*. Each system has its own AHL synthase (LasI and RhII), an AHL-responsive, DNA-binding regulator (LasR and RhIR), and AHL signal (3-oxo-dodecanoyl homoserine lactone and butyryl homoserine lactone). In my presentation I will review how the physical and chemical environment has been shown to impact quorum sensing in this species and address important issues such as “what is a quorum?” in different important biological contexts.

## Dynamical Quorum Sensing and Synchronization in Populations of Excitable and Oscillatory Catalytic Particles

Kenneth Showalter\*

C. Eugene Bennett Department of Chemistry  
West Virginia University, Morgantown, WV

From the periodic firing of neurons to the flashing of fireflies, the synchronization of rhythmic activity plays a vital role in the functioning of biological systems. Synchronization often occurs by global coupling, where each oscillator is connected to every other oscillator through a common mean field. With this mechanism, oscillators are regulated by the average activity of the population (the mean field) and a collective rhythm emerges above a critical coupling strength. A distinctly different type of transition to synchronized oscillatory behavior has been observed in suspensions of yeast cells. Relaxation experiments demonstrate that, slightly below the critical cell density, the system is made up of a collection of quiescent cells rather than unsynchronized oscillatory cells, whereas slightly above the critical density, the cells oscillate in nearly complete synchrony. This type of transition is much like quorum-sensing transitions in bacteria populations, where each member of a population undergoes a sudden change in behavior with a supercritical increase in the concentration of a signaling molecule (autoinducer) in the extracellular solution. We have studied large, heterogeneous populations of discrete chemical oscillators (~100,000) with well-defined kinetics to characterize the two different types of density-dependent transitions to synchronized oscillatory behavior. For different chemical exchange rates between the oscillators and the surrounding solution, we find with increasing oscillator density (1) the gradual synchronization of oscillatory activity or (2) the quorum-sensing-like "switching on" of synchronized oscillatory activity. We analyze the roles of oscillator density and exchange rate of signaling species in these transitions with a model of interacting chemical oscillators.

Many types of unicellular organisms are able to switch from individual to collective behavior in spatially distributed groups in response to increasing cell numbers. For example, in certain bacteria a suprathreshold increase of an autoinducer species in the extracellular solution triggers a positive feedback for cellular autoinducer production and synchronous gene expression. We have studied spatially distributed groups of particles loaded with the catalyst of the Belousov-Zhabotinsky reaction that are immersed in unstirred catalyst-free reaction mixtures. The particles diffusively exchange activator and inhibitor species with the surrounding solution. All particles are nonoscillatory when separated from the other particles; however, target and spiral waves spontaneously appear in sufficiently large groups. A cellular model of the particle system also exhibits transitions from excitable steady state behavior to spatiotemporal wave activity with increasing group size. We find the transition to be associated with a decrease in the loss rate of activator in groups of locally coupled excitable particles.

\*In collaboration with Annette F. Taylor, Mark R. Tinsley, Fang Wang, and Zhaoyang Huang

A. F. Taylor, M. R. Tinsley, F. Wang, Z. Huang, and K. Showalter, *Science* **323**, 614 (2009).  
M. R. Tinsley, A. F. Taylor, Z. Huang, and K. Showalter, *Phys. Rev. Lett.* **102**, 158301 (2009).



***AUTHOR INDEX***  
***AND***  
***PARTICIPANT LIST***

## Author Index

Ade, H. W. ....	88	Golbeck, J. H. ....	140	Prevelige, P. E. ....	152
Akeson, M. ....	247	Goldstein, R. E. ....	4	Prozorov, T. ....	58
Akinc, M. ....	58	Granick, S. ....	144	Pynn, R. ....	195
Alam, T. M. ....	72	Green, O. ....	27	Reinhard, B. ....	1
Alivisatos, P. ....	1	Groves, J. T. ....	47	Richmond, G. L. ....	199
Archer, L. A. ....	92	Grubjesic, S. ....	27	Ritchie, R. O. ....	70
Aronson, I. S. ....	4	Guan, Z. ....	148	Rocha, R. ....	80
Ashley, C. ....	15	Gupta, A. ....	152	Rogers, J. A. ....	203
Bachand, G. ....	8, 23	Harris, M. T. ....	156	Rosenblatt, C. ....	207
Bachand, M. ....	8	Heilshorn, S. ....	50	Rotello, V. M. ....	112
Balazs, A. C. ....	96	Hendricks, J. ....	23	Safinya, C. R. ....	211
Baldo, M. ....	100	Hu, Y.-Y. ....	76	Sandhage, K. H. ....	164
Becht, G. ....	27	Huber, D. L. ....	72	Saraf, R. F. ....	215
Bedzyk, M. J. ....	187	Hui, C.-Y. ....	160	Sasaki, D. Y. ....	72, 80
Benedek, G. B. ....	104	Iyer, S. ....	80	Saven, J. G. ....	108
Bertozzi, C. R. ....	12, 47	Jagota, A. ....	160	Schmidt-Rohr, K. ....	58, 76
Blasie, J. K. ....	108	Jameson, C. ....	183	Schultz, P. G. ....	219
Boal, A. ....	23	Jun, Y. ....	1	Selloni, A. ....	223
Brinker, C. J. ....	15	Keating, C. D. ....	251	Sheikholeslami, S. ....	1
Browning, N. D. ....	19	Khaykovich, B. ....	104	Shin, Y. ....	54
Brozik, J. ....	80	Kirshenbaum, S. ....	252	Showalter, K. ....	254
Bryant, D. A. ....	140	Kong, X. ....	76	Shreve, A. P. ....	72, 80
Bunker, B. C. ....	8, 23, 72	Kozlova, N. ....	104	Sinha, S. K. ....	80, 191
Bunz, U. ....	112	Kraus, G. ....	58	Sligar, S. G. ....	227
Car, R. ....	223	Kröger, N. ....	164	Spakowitz, A. ....	50
Carnes, E. C. ....	15	Kuhl, T. L. ....	168	Spoerke, E. ....	8, 23
Checco, A. ....	66	Laible, P. D. ....	27	Stanic, V. ....	231
Claridge, S. ....	1	Lamm, M. ....	58	Stevens, M. J. ....	72, 84
Culver, J. N. ....	156	Lee, S. ....	27	Strano, M. S. ....	227
Dattelbaum, A. M. ....	72	Levin, E. M. ....	76	Strey, H. H. ....	231
Deamer, D. ....	247	Li, Y. ....	211	Stupp, S. I. ....	187, 235
DeGrado, W. F. ....	108	Liu, H. ....	8	Sushko, M. ....	54
DeYoreo, J. J. ....	19, 62	Liu, J. ....	54	Thallapally, P. ....	54
Doniach, S. ....	50	Lohmueller, T. ....	47	Therien, M. J. ....	108
Douglas, T. ....	116	Lomakin, A. ....	104	Travesset, A. ....	58
Dutta, P. ....	120	Luijten, E. ....	172	Vaknin, D. ....	58
Dutton, P. L. ....	124	Mallapragada, S. ....	58	van der Lelie, D. ....	39
Eaton, B. ....	132	Martinez, Jennifer ....	80	Van Voorhis, T. ....	100
Evans, J. S. ....	128	Martinez, Julio ....	62	Vernizzi, G. ....	187
Ewert, K. ....	211	Mastroianni, A. ....	1	Wang, D. ....	54
Exarhos, G. J. ....	54	Matsui, H. ....	175	Wang, H.-L. ....	80
Faller, R. ....	68	Melosh, N. ....	50	Wang, L.-Q. ....	54
Feldheim, D. ....	132	Misra, N. ....	62	Wheeler, D. R. ....	72
Firestone, M. A. ....	27	Morse, D. E. ....	179	Whitesides, G. M. ....	243
Francis, M. B. ....	31, 47, 62	Murad, S. ....	183	Wraight, C. A. ....	227
Fréchet, J. M. J. ....	35	Narasimhan, B. ....	58	Yang, L. ....	66
Friddle, R. W. ....	62	Nilsen-Hamilton, M. ....	58	Young, M. ....	116
Fukuto, M. ....	66	Noy, A. ....	62	Zhu, Y. E. ....	239
Gang, O. ....	39	Ocko, B. ....	66		
Geissler, P. ....	43, 47	Olvera de la Cruz, M. ....	187		
Gilmer, G. ....	62	Parikh, A. N. ....	80, 191		
Glotzer, S. C. ....	136	Parsek, M. R. ....	253		
Godula, K. ....	12	Peters, J. ....	116		

## Biomolecular Materials Contractors' Meeting -- 2009 Participants

<u>Last Name</u>	<u>First Name</u>	<u>Organization</u>	<u>Phone</u>	<u>Email</u>
Ade	Harald	North Carolina State University		harald_ade@ncsu.edu
Alper	Mark	Lawrence Berkeley National Laboratory	510-486-6581	JLEdgar@lbl.gov
Archer	Lynden	Cornell University	607-254-8825	laa25@cornell.edu
Aronson	Igor	Argonne National Laboratory	630-252-9725	aronson@anl.gov
Ashton	Christie	U.S. Department of Energy, BES	301-903-0511	christie.ashton@science.doe.gov
Bachand	George	Sandia National Laboratories	505-321-1047	gdbachand@gmail.com
Balazs	Anna	University of Pittsburgh	412-648-9250	balazs@pitt.edu
Baldo	Marc	Massachusetts Institute of Technology	617-452-5132	baldo@mit.edu
Becht	Gregory	Argonne National Laboratory	630-252-6494	becht@anl.gov
Blasie	J. Kent	University of Pennsylvania	215-898-6208	jkblasie@sas.upenn.edu
Bricarello	Daniel	University of California, Davis	530-754-7098	dbricare@ucdavis.edu
Brinker	Jeff	Sandia National Labs/University of New Mexico	505-272-7627	cjbrink@sandia.gov
Browning	Nigel	Lawrence Livermore National Laboratory	925-424-5563	browning20@llnl.gov
Bunker	Bruce	Sandia National Laboratories	505-284-6892	bcbunke@sandia.gov
Bunz	Uwe	Georgia Institute of Technology	404-510-2443	uwe.bunz@chemistry.gatech.edu
Checco	Antonio	Brookhaven National Laboratory	631-344-3319	checco@bnl.gov
Chen	Gang	University of California, San Diego	858-534-8434	gchen@physics.ucsd.edu
Cui	Honggang	Northwestern University	302-562-6796	cuihonggang@gmail.com
Culver	James	University of Maryland Biotechnology Institute	301-405-2912	jculver@umd.edu

Dattelbaum	Andrew	Los Alamos National Lab	505-665-0142	amdattel@lanl.gov
Deamer	David	University of California, Santa Cruz	831-459-5158	deamer@soe.ucsc.edu
DeYoreo	James	Molecular Foundry, Lawrence Berkeley National Laboratory	510-486-5259	jjdeyoreo@lbl.gov
Douglas	Trevor	Montana State University	406-994-6566	tdouglas@chemistry.montana.edu
Dutta	Pulak	Northwestern University	847-491-5465	pdutta@northwestern.edu
Dutton	P. Leslie	University of Pennsylvania	215-898-0991	dutton@mail.med.upenn.edu
Eaton	Bruce	University of Colorado at Boulder	303-735-1002	bruce.eaton@colorado.edu
Evans	James	UC Davis / Lawrence Livermore National Laboratory	530-752-8282	JEEvans@ucdavis.edu
Evans	John Spencer	New York University	212-998-9605	jse1@nyu.edu
Exarhos	Gregory	Pacific Northwest National Laboratory	509-371-6243	greg.exarhos@pnl.gov
Faller	Roland	University of California, Davis	530-752-5839	rfaller@ucdavis.edu
Feldheim	Dan	University of Colorado	303-492-7907	Daniel.Feldheim@Colorado.edu
Firestone	Millicent	Argonne National Laboratory	630-252-8298	firestone@anl.gov
Francis	Matthew	University of California, Berkeley	510-643-9915	francis@cchem.berkeley.edu
Fréchet	Jean	Lawrence Berkeley National Laboratory	510-643-3077	frechet@berkeley.edu
Fukuto	Masafumi	Brookhaven National Laboratory	631-344-5256	fukuto@bnl.gov
Galvin	Mary	U.S. Department of Energy, BES	301-903-8334	Mary.Galvin@science.doe.gov
Gang	Oleg	Brookhaven National Laboratory	631-344-3645	ogang@bnl.gov
Geissler	Phillip L.	Lawrence Berkeley National Laboratory/UC Berkeley	510-642-8716	geissler@cchem.berkeley.edu
Gersten	Bonnie	U.S. Department of Energy, BES	301-903-0002	Bonnie.Gersten@science.doe.gov
Glotzer	Sharon	University of Michigan	734-615-6296	sglotzer@umich.edu

Godula	Kamil	University of California, Berkeley and the Molecular Foundry, the Lawrence Berkeley National Lab	510-495-2514	kgodula@lbl.gov
Golbeck	John H.	The Pennsylvania State University	814-865-1163	jhg5@psu.edu
Gopalan	Padma	University of Wisconsin-Madison	608-265-4258	pgopalan@wisc.edu
Gorey	Kerry	U.S. Department of Energy, BES	301-903-7661	kerry.gorey@science.doe.gov
Granick	Steve	University of Illinois	217-333-5720	sgranick@uiuc.edu
Guan	Zhibin	University of California, Irvine	949-824-5172	zguan@uci.edu
Gupta	Arunava	University of Alabama	205-348-3822	agupta@mint.ua.edu
Harris	Michael	Purdue University	765-494-0963	mtharris@purdue.edu
Hayden	Steven	Georgia Institute of Technology	404-358-5523	steven.hayden@gatech.edu
Heilshorn	Sarah	SLAC/Stanford University	650-796-9525	heilshorn@stanford.edu
Horton	Linda	U.S. Department of Energy, BES	301-903-7506	linda.horton@science.doe.gov
Hu	Yan-Yan	Ames Laboratory	515-451-2525	huyy06@iastate.edu
Hui	Herbert C. Y.	Cornell University	607-255-3428	ch45@cornell.edu
Jagota	Anand	Lehigh University	610-758-4396	anj6@lehigh.edu
Kaehr	Bryan	Sandia National Laboratories	505-272-7665	bjkaehr@sandia.gov
Kane	Ravi	RPI	518-276-2536	kaner@rpi.edu
Keating	Christine	Pennsylvania State University	814-863-7832	keating@chem.psu.edu
Kelley	Richard (Dick)	U.S. Department of Energy, BES	301-903-6051	richard.kelley@science.doe.gov
Kini	Aravinda	U.S. Department of Energy, BES	301-903-3565	a.kini@science.doe.gov
Kirshenbaum	Sheril	Duke University	914-552-2584	sheril.kirshenbaum@duke.edu
Kitts	Sophia	Oak Ridge Associated Universities	865-241-5650	Sophia.Kitts@ornl.gov

Kozlova	Natalia	Massachusetts Institute of Technology	617-253-4826	kozlova@mit.edu
Kröger	Nils	Georgia Institute of Technology	404-894-4228	nils.kroger@chemistry.gatech.edu
Laible	Philip	Argonne National Laboratory	630-252-4875	laible@anl.gov
Lewis	Jennifer	University of Illinois	217-244-4973	jalewis@illinois.edu
Lim	Jung-Sun	Purdue University	765-714-9834	lim14@purdue.edu
Liu	Jun	Pacific Northwest National Laboratory	509-275-5743	jun.liu@pnl.gov
Lohmueller	Theobald	University of California, Berkeley	510-666-3604	tlohmueller@gmail.com
Lucon	Janice	Montana State University	406-994-6855	jerader@hotmail.com
Luijten	Erik	Northwestern University	847-491-4097	luijten@northwestern.edu
Mallapragada	Surya	Ames Laboratory	515-294-7407	suryakm@iastate.edu
Markowitz	Michael	U.S. Department of Energy, BES	301-903-6779	mike.markowitz@science.doe.gov
Matsui	Hiroshi	City University of New York - Hunter College	212-650-3918	hmatsui@hunter.cuny.edu
Miranda	Oscar R.	University of Massachusetts at Amherst	413-54-54865	omiranda@chem.umass.edu
Morse	Daniel	University of California, Santa Barbara	805-893-7442	d_morse@lifesci.ucsb.edu
Murad	Sohail	University of Illinois at Chicago	312-996-5593	murad@uic.edu
Neilson	James	University of California, Santa Barbara	805-893-3416	neilson@lifesci.ucsb.edu
Noy	Aleksandr	Lawrence Livermore National Laboratory	925-424-6203	noy1@llnl.gov
Ocko	Benjamin	Brookhaven National Laboratory	631-344-4299	ocko@bnl.gov
O'Neal	Joreé	Oak Ridge Institute for Science and Education	865-576-7434	Joree.ONeal@orise.orau.gov
Parikh	Atul	University of California, Davis	530-304-7523	anparikh@ucdavis.edu
Parsek	Matthew	University of Washington	206-221-7871	parsem@u.washington.edu
Parsons	Lisa	CBR/UMBI	301-641-4848	parsons@umbi.umd.edu

Prevelige	Peter	Univ. Alabama at Birmingham	205-975-5327	prevelig@uab.edu
Pynn	Roger	Indiana University	505-670-9708	rpynn@indiana.edu
Richmond	Geraldine	University of Oregon	541-346-4635	richmond@oregon.uoregon.edu
Ritchie	Robert	University of California, Berkeley Lawrence Berkeley National Laboratory	510-409-1779	roritchie@lbl.gov
Rogers	John	University of Illinois	217-244-4979	jrogers@illinois.edu
Rosenblatt	Charles	Case Western Reserve University	216-368-4125	rosenblatt@case.edu
Rotello	Vincent	University of Massachusetts	413-545-2058	rotello@chem.umass.edu
Rouge	Jessica	University of Colorado at Boulder	303-735-1617	jessica.rouge@colorado.edu
Safinya	Cyrus	University of California, Santa Barbara	805-893-8635	safinya@mrl.ucsb.edu
Sandhage	Ken	Georgia Institute of Technology	404-894-6882	ken.sandhage@mse.gatech.edu
Saraf	Ravi	University of Nebraska - Lincoln	402-472-8284	rsaraf@unlnotes.unl.edu
Sasaki	Darryl	Sandia National Laboratory	925-294-2922	dysasak@sandia.gov
Schaffer	David	University of California, Berkeley	510-643-5963	schaffer@berkeley.edu
Schmidt-Rohr	Klaus	Ames Laboratory	515-294-6105	srohr@iastate.edu
Schultz	Peter	The Scripps Research Institute	858-784-9300	schultz@scripps.edu
Selloni	Annabella	Princeton University	609-258-3837	aselloni@princeton.edu
Sheikholeslami	Sassan	Lawrence Berkeley National Laboratory	510-642-2148	sassan@berkeley.edu
Showalter	Kenneth	West Virginia University	304-293-3435 x6428	kshowlt@wvu.edu
Shreve	Andrew	Los Alamos National Laboratory	505-667-6933	shreve@lanl.gov
Sinha	Sunil	University of California, San Diego	858-822-5537	ssinha@physics.ucsd.edu
Sknepnek	Rastko	Northwestern University	847-467-2130	r-sknepnek@northwestern.edu
Spakowitz	Andrew	Stanford University	650-796-9445	ajspakow@stanford.edu

Spoerke	Erik	Sandia National Laboratories	505-284-1932	edspoer@sandia.gov
Stanic	Vesna	SUNY Stony Brook	516-380-2028	vstanic@notes.cc.sunysb.edu
Stevens	Mark	Sandia National Laboratories	505-844-1937	msteve@sandia.gov
Strano	Michael	Massachusetts Institute of Technology	617-324-4323	strano@mit.edu
Strey	Helmut	Stony Brook University	631-632-1957	Helmut.Strey@stonybrook.edu
Stupp	Samuel I.	Northwestern University	847-492-3002	j-wrubleski@northwestern.edu
Sushko	Maria	Pacific Northwest National Laboratory	509-371-7286	maria.sushko@pnl.gov
Talley	Lee-Ann	Oak Ridge Institute for Science and Education	865-576-2077	Lee-Ann.Talley@orise.ornl.gov
Thiyagarajan	Thiyaga P.	U.S. Department of Energy, BES	301-903-9706	P.Thiyagarajan@science.doe.gov
Tolosa	Juan	Georgia Institute of Technology	404-578-3996	juan.tolosa@chemistry.gatech.edu
Travesset	Alex	Ames Laboratory	515-292-0808	trvsst@ameslab.gov
Vaknin	David	Ames Laboratory, Iowa State University	515-294-6023	vaknin@ameslab.gov
Vernizzi	Graziano	Northwestern University	847-467-2130	g-vernizzi@northwestern.edu
Wang	Hsing-Lin	Los Alamos National Laboratory	505-667-9944	hwang@lanl.gov
Wang	Lijun	Ames Laboratory	515-441-0861	wlj@iastate.edu
Whitesides	George	Harvard University	617-495-9830	smart@chemistry.harvard.edu
Zhu	Y. Elaine	University of Notre Dame	574-631-2667	yzhu3@nd.edu
Zipoli	Federico	Princeton University	609-258-0116	fzipoli@Princeton.edu